A THREE DIMENSIONAL MATHEMATICAL MODEL OF THE HUMAN KNEE

by

PAPAIOANNOU GEORGE

A Thesis submitted in partial fulfillment
of the requirements for the Award of
the Degree of Doctor of Philosophy

Bioengineering Unit
University of Strathclyde
Glasgow

August 1999

Abstract

Muscle and joint force during locomotion is estimated according to available formulations consistent with available methods of solving the indeterminate problem. In the case of the knee joint direct comparisons of results between several optimization methods proposed in the literature presents difficulties due to largely varying model formulation, input data, algorithms and other issues. The application presented here introduces a new optimization program which includes linear and non-linear techniques allowing greater flexibility in problem formulation. It also increases the variety of cost functions under a unified solution which allows for direct evaluation of factors such as optimization criteria and constraints. The method demonstrates that nonlinear solutions lead to more synergistic activity and in contrast to linear formulations, allows antagonistic activity. Nonlinearity also improves concurrence of EMG activity and predicted forces. Higher joint force predictions are resulting as expected from improved predictions of synergistic-antagonistic activity. The formulation allows for relaxation of the requirement that muscles resolve the entire intersegmental moment which in turn maintains muscle synergism in the nonlinear formulation while relieving muscle antagonism and reducing the predicted joint contact force. These methods allow for more possibilities for exploring new optimization formulations and in comparing the solutions to previously reported formulation. The present study based its input data on healthy subjects volunteering for a variety of walking tasks involving normal walking and turning during walking. Muscle and joint contact forces agree with other published results and the lateral:medial bony contact force distribution is calculated as 1:2.5.

Contents

Blank Page

List of Figures

List of Tables

To my Mother Olga

ACKNOWLEDGEMENTS

This work was carried out in the Bioengineering Unit, University of Strathclyde. I am most grateful to Professor J.P. Paul for offering me a place in the MSc. in Bioengineering course of 1992 and for his guidance, constructive criticism and advice throughout the work. I appreciate the valuable supervision of Dr. A.C. Nicol who provided suggestions and final corrections to the thesis. I also thank Mrs. S. Nicol for her help with the modifications of the programs.

A very special thank you to the subjects who volunteered for the tests. The computational work owns its final tunning to Mr. Don Evans of the Srtathclyde University Computer Centre.

I must also express my appreciation to the help of Professor Arora J.S. of University of Iowa, Professor Delp S.L. of Northwestern University, and Loan P. of Musculo-Graphics. Thanks also to Professor Maglavera D. of Auth University of Thessaloniki and the COMMET programs for the financial support.

A special thank you is due also to Professor Spaepen A. of K.U. Leuven, for invitating me to work in his team -at the last stages of my thesis (CAMARN Program)-, giving me, therefore, the opportunity to continue my work.

At last I want to express my gratitude to my beloved mother, Olga, for her support and sense of direction in life.

ABREVIATIONS:

HS:HEEL STRIKE

TO:TOE-OFF

MS:MID-STANCE

IC: INITIAL CONTACT

GT: GREATER TROCHANTER

HC:HIP CENTER

KC:KNEE CENTER

EMG:Electromyography

Muscles, ligaments and their abreviations as they appear in the OPTIMISATION PART OF THE TEXT:

Biceps femoris (BF),

Gracilis (GRA),

Rectus femoris (RF),

Sartorious (SART),

Semimembranosus (SEMIM),

Semitendinosus (SEMIT),

Tensor fasciae latae (TFL),

Gastrocnemius medial head (GASM),

Gastrocnemius lateral head (GASL),

Biceps femoris short head (BFS),

Vastus intermedius (VI),

Vastus interalis (VL)

and Vastus medialis (VM).

Anterior medial collateral ligament (AMC),

deep medial collateral ligament (DMC),

posterior medial collateral ligament (PMC),

oblique medial capsular ligament (OMC),

medial posterior capsular ligament (MPC),

lateral posterior capsular ligament (LPC),

oblique lateral capsular ligament (OLC),

lateral collateral ligament (LC),

deep lateral collateral ligament (DLC),

anterior anterior cruciate ligament (AAC),
posterior anterior cruciate ligament (PAC),
anterior posterior cruciate ligament (APC)
and posterior posterior cruciate ligament (PPC).

Muscles and their abreviations as they appear in the SIMM documentation and the additional programs.

GMED1 gluteus medius (anterior compartment)
GMED2 gluteus medius (middle compartment)
GMED3 gluteus medius (posterior compartment)
GMIN1 gluteus minimus (anterior compartment)
GMIN2 gluteus minimus (middle compartment)
GMIN3 gluteus minimus (posterior compartment)
SEMIMEM semimembranosus

SEMITEN semitendinosus
BIFEMLH biceps femoris (long head)
BIFEMSH biceps femoris (short head)
SAR sartorius
ADDLONG adductor longus
ADDBREV adductor brevis
AMAG1 adductor magnus (superior component)
AMAG2 adductor magnus (middle component)
AMAG3 adductor magnus (inferior component)
TFL tensor faciae latae
PECT pectineus
GRA gracilis
GMAX1 gluteus maximus (superior component)
GMAX2 gluteus maximus (middle component)
GMAX3 gluteus maximus (inferior component)

ILIACUS Iliacus
PSOAS

QUADFEM quadatus femoris

GEM gemelli

PERI periformis

RF rectus femoris

VASMED vastus medialis

VASINT vastus intermedius

VASLAT vastus lateralis

MEDGAS gastrocnemius (medial head) LATGAS gastrocnemius (medial head)

SOL soleus

SOLSTIF soleus with stiff tendon

FLEXDIG flexor digitorus longus

TIBPOST tibialis posterior

FLEXHAL flexor hallucis longus

TIBANT tibialis anterior

PERBREV peroneus brevis

PERLONG peroneus longus

PERTERT peroneus tertius

EXTDIG extensor digitorum longus

EXTHAL extensor hallucis longus

Chapter 1

Prolegomena

1.1 Introduction

The knee joint (see figure 2.1 on page 11 and 2.2 on page 15) is the largest and arguably the most complex in the body (Nordin and Frankel,1980) Pope et al. [1976], and therefore the reasons for choosing to model its behaviour must be persuasive. The primary function of the knee is to provide locomotion and in doing so to support the weight of the body, to aid in the conservation of momentum of the lower extremity and to transmit loads through the lower limbs. The knee's functions and its position between some of the longest bones in the body, i.e. femur and tibia, subject it to high forces and moments, making it prone to injury. Current techniques for clinical assessment and treatment consist of the quantification of injury extent. It is well recognised by orthopaedic surgeons that such an approach is not efficient enough for the diagnosis of injuries other than complete ligamentous tears. Current medical visualization systems allow manipulation of computer representations of anatomical structures of interest for visual purposes but they provide insufficient and often no quantitative analysis of these structures and reduced information about behaviour and interaction with the immediate environment. As a result, complex structures such as joints cannot be fully assessed. This lack of quantitative assessment tools is responsible for the direction of research towards computer-based models of the joints with the long term aim of increased patient specification simulation, quantitative assessment of the normal joint (motion behaviour) and the trauma. Integration of disciplines such as biomedical modelling, physically based modelling and computer graphics, with an aim to construct biomechanical simulator systems of the musculoskeletal system, although

still treated with some concern by the medical community as was the case for early computer-based imaging technologies, have much to offer to both the clinician and the surgeon. Perigraphically, four key areas of application can be identified for an interactive graphical environment:

a)improvement of the functional anatomy information and the study of the cause and effects of pathology,

b)training related to clinical examination and surgical procedures or for introducing established procedures to students,

c)the evaluation and optimisation of treatment with the use of preoperative simulation of surgical procedures, as well as postoperative analysis of the treatment results,

d)The design, development and evaluation of prostheses.

1.1.1 Scope of Dissertation

1.2 Statement of Purpose

The overall purpose of this investigation is to devise a new iterative procedure for solving the load distribution problem at the knee using optimization techniques based on parallel working algorithms, and to compare the results obtained using this new method to those previously reported in the literature. We aim to combine firstly the visualization tools that enhance lower limb 3D model development in terms of reduction of time and ease of model manipulation with clinical relevance with secondly the advanced engineering algorithms that will be provided in a user friendly environment (X-windows based). A new user friendly environment ought to allow faster and easier creation of models and model libraries, robust optimum control algorithms that do not require extensive learning curves, no additional post-processing of the optimization data and easy to comprehend results for its possible clinical applications. It is a generally accepted view that user friendly applications that support advanced engineering solutions in the "background" of the actual environment tend to improve the bridging of the gap between clinical and engineering approaches to problem solving.

Pursuit of this overall purpose involves the completion of the following five tasks in two parts.

PART 1. 1. Analysis of the walking pattern of a number of normal subjects during normal walking and during walking and turning. This will allow us to study the effect

of certain parameters (speed, footwear) on the kinetic and kinematic characteristics of gait and moreover to be able to chose a representative sample of the population in order to study the behaviour of the muscles , ligaments and bony contact forces and the effects of these parameters on the sensitivity of the final model.

PART 2. 1. Identification of a suitably detailed mechanical model of the musculoskeletal system in the neighborhood of the human knee, including all major muscles, ligaments and bony contact forces.

2. Construction of the corresponding joint equilibrium equations, together with appropriate constraints on the forces transmitted by individual joint structures.

3. development of a new iterative solution algorithm to solve the associated joint distribution problem using non-linear optimization of muscle force at the typical instant during a normal human gait cycle.

4. Implementation of this method of solution and comparison of the results obtained with those previously reported in the literature.

This dissertation is organized into ten chapters. Following an introductory Chapter, chapter 1, Chapter 2 describes the support and movement systems related to the knee joint. In Chapter 3 the knee anatomical and behavioural characteristics are presented with attention to both active and passive tissues. Chapter 4 is a review of the knee modelling literature with reference to studies of similar nature to the present study as well as a description of alternative attempts to model the knee joint. Chapters 5 and 6 describe the rationale of the methodology used in the knee model, its anatomic structures, the method of collecting kinetic and kinematic data, model properties and model input. In Chapter 7 more detailed explanation of the mechanical model of the knee detailed model properties and model input is attempted. Joint equilibrium equations and constraints are formulated and discussed. In Chapter 8 a new iterative solution algorithm is described and explained. The cost function to be used in the optimization models of the new algorithm is determined, and a few solutions are obtained to present comparisons with some results available in the literature. Finally, a discussion of the assumptions and limitations of the model algorithm is presented.

Chapter 9 contains complete results and their sensitivity to variations of selected parameters of the knee model. An envelope of the intersegment loads during turning in level walking is presented and discussed.

Finally chapter 10 presents a discussion of the model algorithm, the recommenda-

tions for future study and conclusions.

Chapter 2

Anatomy of the Knee

The knee is a synovial joint in which the joint cavity is partially divided into parts by the presence of two fibrocartilaginous articular disks, known as menisci. The joint is formed where the distal end of the femur and the proximal end of the tibia meet. Figures 2.1 on page 11, 2.2 on page 14, and 2.3 on page 15, show the anatomy of the knee. The femoral condyles, the tibial plateau and the patella form the osseous components of the joint. In the absence of articular cartilage their surfaces are incongruent.

2.1 BONE GEOMETRY

2.1.1 FEMORAL CONDYLES

The lateral condyle protrudes less than the medial condyle along the longitudinal axis of the femur but is broader in the antero-posterior and transverse directions. Viewing anteriorly, both condyles become less rounded in extension and more rounded in flexion. Viewing laterally they become more curved posteriorly with the curvature of the lateral condyle increasing from anterior to posterior more quickly than that of the medial condyle, Evans [1986], Al-Turaiki [1986], Gray [1993]. The anterior surface between the femoral condyles forms a slight groove, extending down into the intercondylar norch and articulates with the patella.

2.1.2 TIBIAL plateau

The plateau are each formed from two smooth concave surfaces located laterally and medially. The medial plateau is bi-concave in shape an is longer in the anterior-

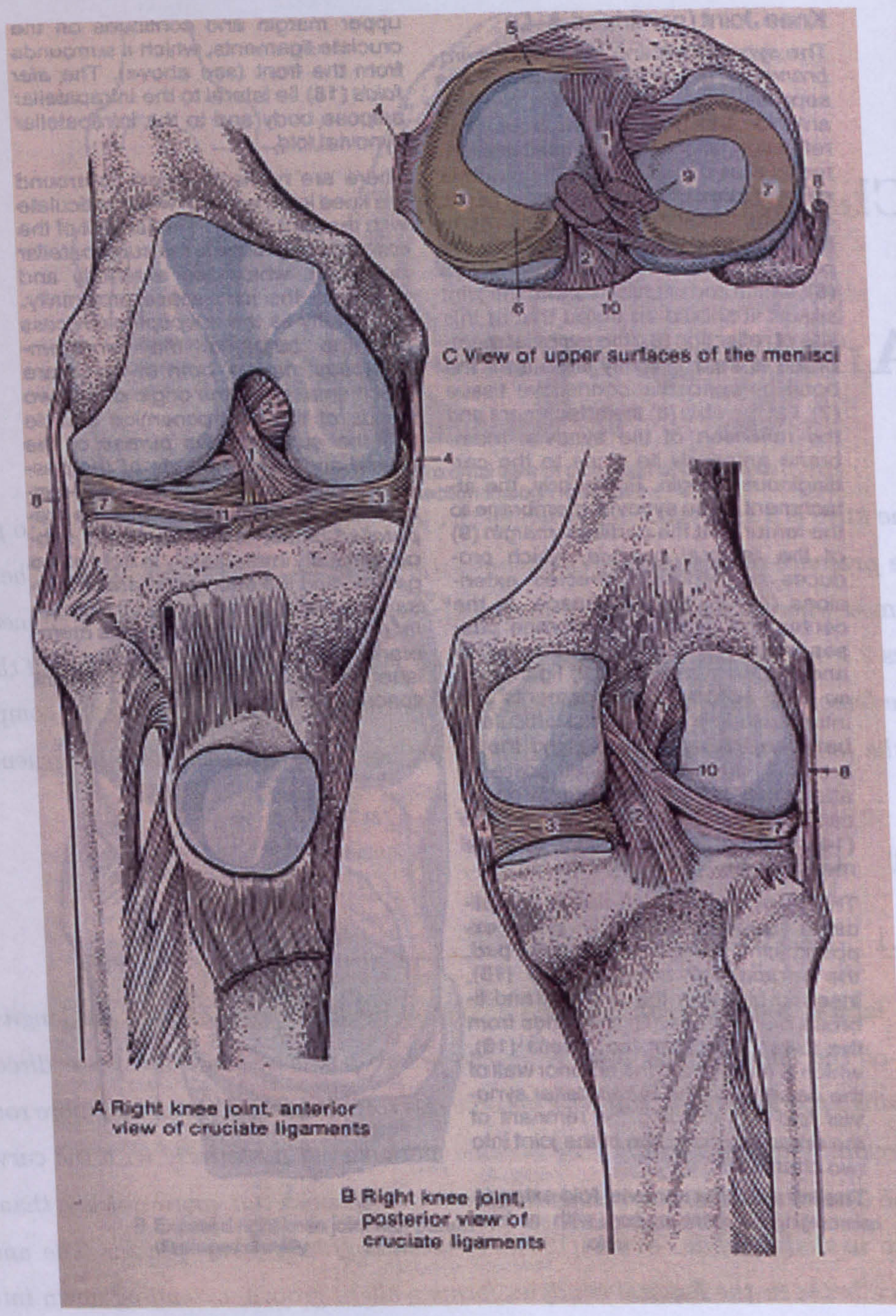

Figure 2.1: The KNEE JOINT.(1)anterior cruciate ligament, (2) posterior cruciate ligament, (3) medial meniscus, (4) tibial collateral ligament, (5)anterior crus, (6)posterior crus, (7) lateral meniscus,(8) fibular collateral ligament,(9) anterior meniscofemoral ligament, (10) posterior meniscofemoral ligament, from Platzer [1986]

posterior direction than the lateral plateau. In contrast, the lateral plateau is saddle-shaped, more circular and broader than the medial plateau. In general, the medial plateau is larger than the lateral and consequently is thought to bear more. Articulation between the femoral condyles and the tibial plateau forms the tibial-femoral joint - the main joint within the knee.

2.1.3 PATELLA

The patella is a flat triangular bone situated in the anterior part of the knee within the tendon of the quadriceps extensor muscle. The posterior surface is smooth and oval-shaped consisting of medial and lateral facets divided by a vertically running ridge. Articulation with the femur occurs with this ridge "sitting" in the groove on the trochlear surface of the femur forming the patello-femoral joint. The function of the patella is two fold, first it lengthens the lever arm of the quadriceps musle force by displacing the quadriceps tendon anteriorly and second, it offers a larger contact area between the patellar tendon and femur thus reducing contact stress between the two Nordin et al. [1989].

2.1.4 HYALINE ARTICULAR CARTILAGE

Hyaline articular cartilage forms a layer on the femoral condyles, the tibial plateau and the posterior surface of the patella. On the tibial plateau it is usually found to be thicker on the areas where the menisci are not effective and the bones are in direct contact. Nordin et al. [1989] reported that it is three times thicker on the medial plateau, further suggesting that greater weight is carried on this surface. As stated in an earlier section (section 2.3) the main functions of the cartilage are to protect the subchondral bone from mechanical damage, to prevent abrasive wear between bone extremities and to lower the friction of the bearing surfaces. Prevention against mechanical damage is achieved in the three ways outlined by Kempson [1980]:

a)by reducing the contact stresses at the joint. Freeman et al. [1975] showed that cartilage protects subchondral bone of the hip joint from mechanical damage due to fatigue. Weightman et al. [1979] reported that cartilage reduces the maximum contact stress by up to 50%. b)by reducing the maximum dynamic forces across the joint. c) by reducing the energy transmitted across the joint. This energy is important as a system can only store a maximum amount of energy before it fails. Since for elastic

behaviour the energy is proportional to the maximum transmitted force the energy transmitted is reduced by the presence of cartilage.

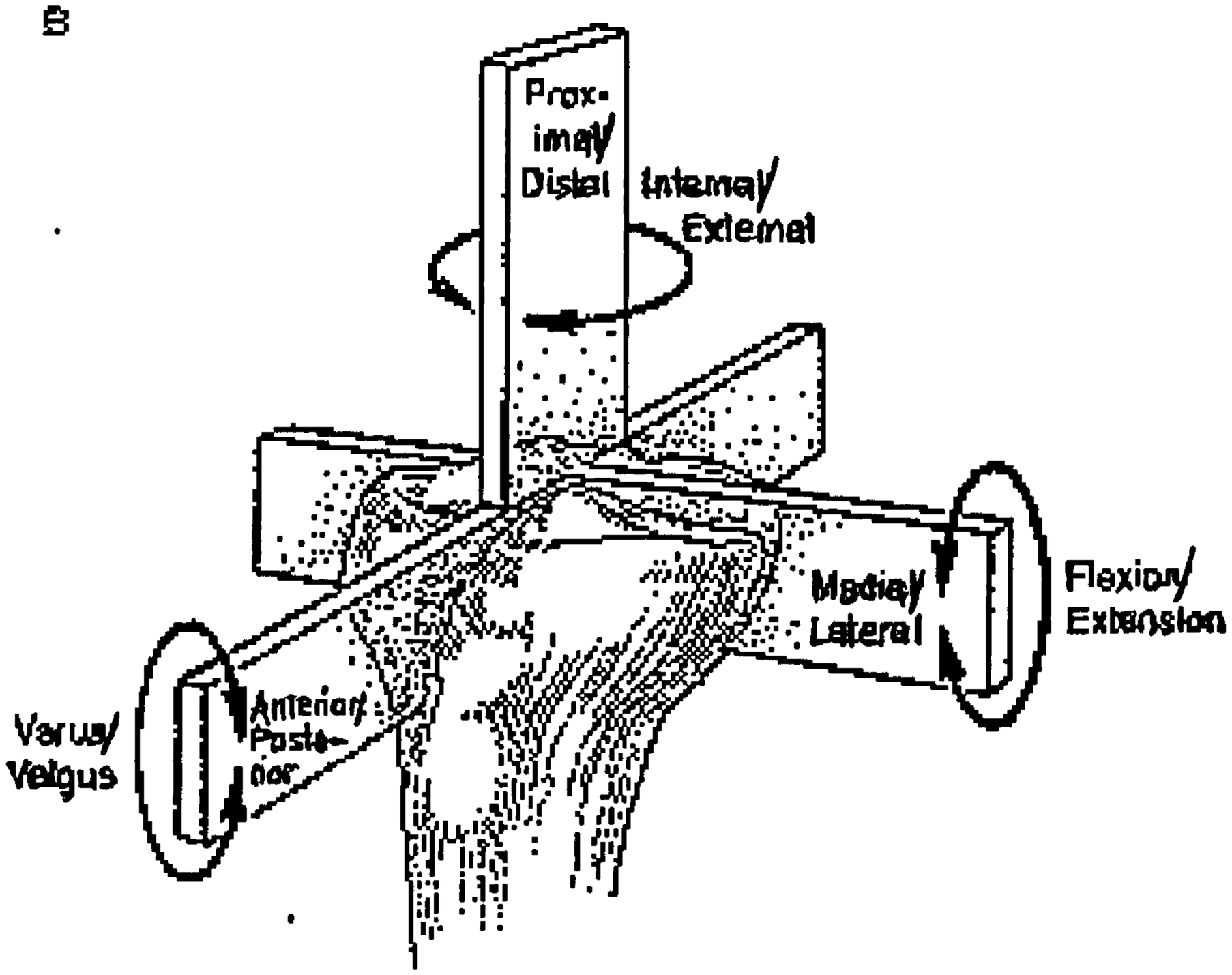

Figure 2.2: Six degrees of freedom at the knee joint (After Scott, 1994)

2.1.5 MENISCI

The menisci are fibrocartilaginous semilunar structures, wedge-shaped in cross-section, and are formed by collagen fibres running circumferentially which results in giving them high resistance to lateral shearing forces (Bullogh et al. [1970], Aspden [1985]). They are sandwiched between the tibia and femoral condyles, both on the medial and lateral plateau in such a way that only a small direct tibial-femoral contact area exists. The morphological differences reflect the different motional behaviour that occurs in the medial and lateral compartments Evans [1986]. They are attached to the tibial plateau on the central sagital line by their anterior and posterior horns and are attached indirectly to the femur and tibia via the joint capsule at their outer peripheries. The flexibility of the menisci enables them to move posteriorly and anteriorly across the plateau about their horn attachments (Figure 2.1 on page 11).

Although there is some controversy on the role of the menisci in knee joint function the following characteristics are believed to describe menisci's behaviour: a)Shock absorption to protect the articular surface, a similar functional charactreristic to the articular cartilage. b)Elimination of the direct tibial-femoral contact while increasing the area of surface contact in the joint to include almost the whole of the tibial plateau, thus reducing the contact stresses and distributing them more uniformly.

c) The increased congruity improves the stability and thus enlarges the range of flexion.

2.1.6 LIGAMENTS

There are four main types of ligaments which are categorised according to their location in the knee structure as patellar, capsular, extracapsular and cruciate.

2.1.7 PATELLA LIGAMENTS

Termed the patellar retinaculum they stabilise the patella and are formed by layers of vertical fibres from the quatriceps interleaving with oblique fibres between the patella and the femur Evans [1986].

2.1.8 CAPSULAR AND EXTRACAPSULAR LIGAMENTS

The ligaments of the capsule can be divided into the deep layer ligaments and the major capsular ligaments. Both the capsular and extracapsular ligament locations are shown in Figure 2.1 on page 11.

The mechanical properties properties of capsular ligaments have been investigated by Rastegar [1977] and the properties of the collateral ligaments have been investigated in canines by Laros et al. [1971], in rats by Weisman et al. [1979], and in human specimens by Kennedy et al. [1976] and Weisman et al. [1979]. The functional properties of some of the ligaments have been the focus of mush research. The properties of the medial collateral ligament have been investigated by Edwards et al. [1970], Wang et al. [1973],

Warren et al. [1974], Trent et al. [1976], and Crowninshield et al. [1976]; of the lateral collateral ligament by Edwards et al. [1970], Wang et al. [1973] and

Trent et al. [1976]; of the menisco-femoral ligaments by Girgis et al. [1975]. Wilson [1981] studied the lengthening of the collaterals during walking. Limitations of space

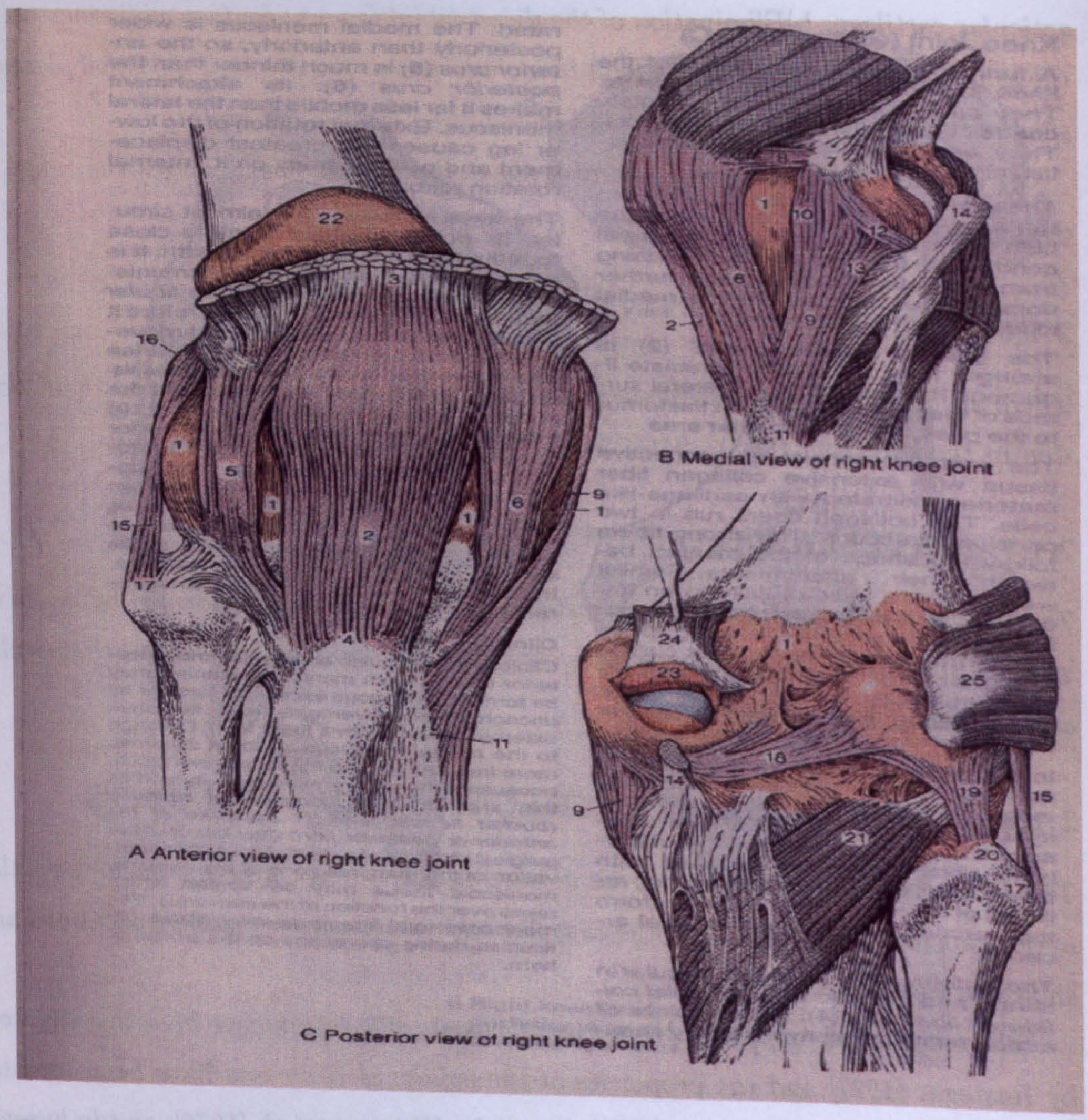

Figure 2.3: The KNEE JOINT: (1) capsule, (2) patellar ligament, (3) quadriceps tendon, (4) tibial tuberocity, (5) lateral patelar retinaculum, (6) medial patelar retinaculum, (7) medial epicondyle, (8) transverse fibers, (9) tibial collateral ligament, (10) anterior long fibers, (11) medial margin of the tibia , (12) short upper posterior fibers, (13) inferior posterior fibers, (14) semimembranosus muscle, (15)fibular collateral ligament , (16) lateral epicondyle, (17) head of the fibula , (18) oblique popliteal ligament, (19) arcuate popliteal ligament, (20) apex of the head of the fibula, (21) popliteus muscle, (22) suprapatellar bursa, (23) subtendineal bursa of the medial gastrocnemious muscle, (24) medial head of the gastrocnemious muscle, (25) lateral head of the gastrocnemious muscle, from Platzer [1986]

do not allow descriptions of individual ligaments and their specific femoral and tibial insertion points here so the reader is referred to the texts of Evans [1986], Al-Turaiki [1986], Gray [1993] and to the research literature referenced in the remaining part of this section.

2.1.9 CRUCIATE LIGAMENTS

Two cruciate ligaments are located in the intercondylar notch of the knee. The anterior cruciate ligament (ACL) has its tibial attachment on the anterior area of the medial tibial spine and passes backwards, laterally and upwards to its femoral attachment point on the posterior part of the medial surface of the lateral femoral condyle Evans [1986], Girgis et al. [1975]. The mechanical properties of this ligament have been the subject of study of Viidik [1966] and Viidik [1968], Gupta et al. [1969], Noyes et al. [1974] and Noyes et al. [1976], Bingham et al. [1976], Kennedy et al. [1976] and Bonnel et al. [1988]. The functional properties were also investigated by a series of scientific teams

Robichon et al. [1968], Edwards et al. [1970], Smillie [1970],

Kennedy et al. [1974], Detenbeck [1974], Wang et al. [1974], Wang et al. [1973], Girgis et al. [1975], and Trent et al. [1976]. The posterior cruciate ligament (PCL) has its tibial attachment on the posterior edge between the articular upper surfaces of the tibia and passes anteriorly, upwards and medially to the ACL and has its femoral attachment on the posterior part of the lateral surface of the medial condyle Evans [1986], Girgis et al. [1975]. The mechanical properties have been investigated by Viidik [1966], Gupta et al. [1969], Bingham et al. [1976] an the functional properties by Brantigan et al. [1941], Kennedy et al. [1976], Edwards et al. [1970], Wang et al. [1973], Wang et al. [1974], Trent et al. [1976] and Girgis et al. [1975]. The specific functions of the cruciate ligaments cannot be covered with the space available here so the the following section summarizes the ligaments' role in the knee joint.

2.1.10 FUNCTION OF LIGAMENTS

An early review of the contributions of the different ligaments to knee function was reported by Brantigan et al. [1941]. They suggested that the integrity of the knee joint depends on the muscles and tendons around the knee, the articular capsule, the intrinsic ligaments and the bone architecture of the femur and tibia. They concluded

the following which are supported by recent work as shown from the references.

a) Varus rotation in extension is controlled by the lateral collateral ligament (LCL), the cruciate ligaments (CL's) and the capsule. In flexion it is controlled by the CL's and the capsule. Supported by Grood et al. [1981] and Seering et al. [1980].

b) Valgus rotation in extension is controlled by the medial collateral ligament (MCL) and the capsule, and in flexion by the CL's and the capsule. Supported by Warren et al. [1974], Seering et al. [1980], Grood et al. [1981], Crowninshield et al. [1976] and Kennedy et al. [1971].

c) Rotary motion in extension is controlled by the capsule, the MCL and LCL, and the CL's and in flexion is controlled by the capsule, the MCL and the CL's. Supported by Seering et al. [1980], Girgis et al. [1975], Wang et al. [1974].

d) Forward motion of the tibia is controlled by the ACL. Supported by Girgis et al. [1975] and Piziali et al. [1980].

e) Backward motion of the tibia is controled by the PCL. Supported by Kennedy et al. [1957], Girgis et al. [1975] and Piziali et al. [1980]. f) Medial and lateral glidings of the tibia are controlled by the tibial intercondyloid eminence, the femoral condyles and all the ligaments. Supported by Piziali et al. [1980].

g) Hyperextension of the knee is controlled by the MCL and LCL, the CL's, the menisci, the anterior aspect of the posterior capsule, the oblique popliteal and architecture of the femoral condyles. Supported by Kennedy et al. [1957], Girgis et al. [1975], Hughston et al. [1965].

h) Hyperflexion of the knee is contolled by the CL's,the menisci, the posterior aspect of the anterior capsule, the bone structure of the femur and tibia and the femoral attachments of the gastrocnemius muscle. This latter argument is not supported by any recent experimental literature.

2.2 ACTIVE TISSUE

The muscles of the lower limb may be conveniently considered in the following groups (Gray's Anatomy, Gray [1993]): I: Muscles of the iliac region. II: Muscles of the femoral and gluteal regions. III: Muscles of the leg. IV: Muscles of the foot. The following figures provide the name and locations of the most important muscles to be encountered in a 3-dimensional model of the knee as well as their origin and insertion

positions (Figures 2.3 on page 17, 2.2 on page 18 2.4 on page 19 2.2 on page 19 2.2 on page 20).

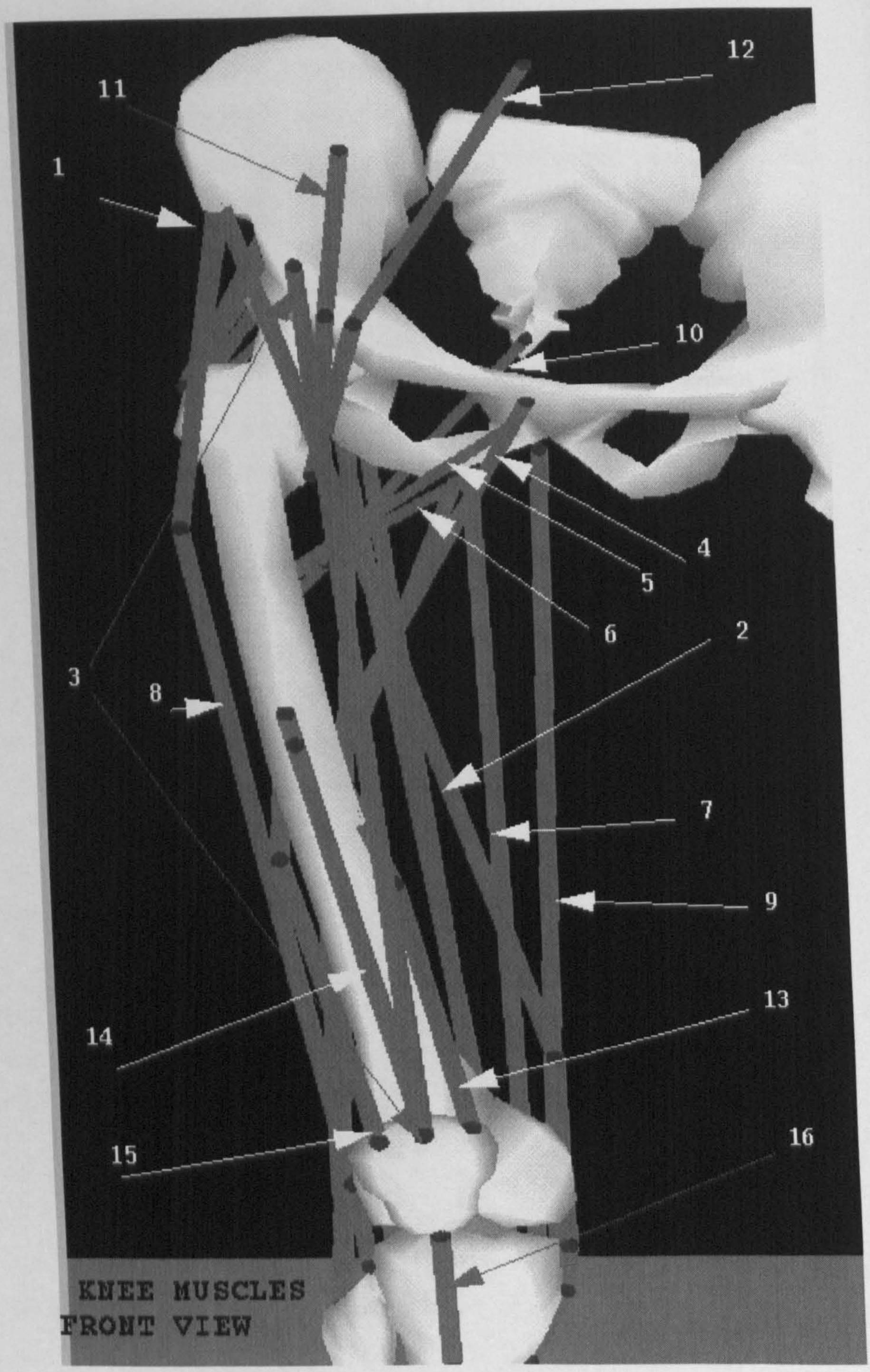

Figure 2.3: 1 GLUTEUS MEDIUS1, 2 Sartorius, 3 Rectus femoris, 4 Adductor Longus, 5 Adductor Brevi
6 Adductor Magnus1, 7 Adductor Magnus3, 8 Tensor Fascia latae, 9 Gracilius, 10 GLUTEUS MAXIMUS
11 Iliacus, 12 Psoas, 13 Vastus Medialis, 14 Vastus Intermedius, 15 Vastus Lateralis, 16 Patellar Ligament

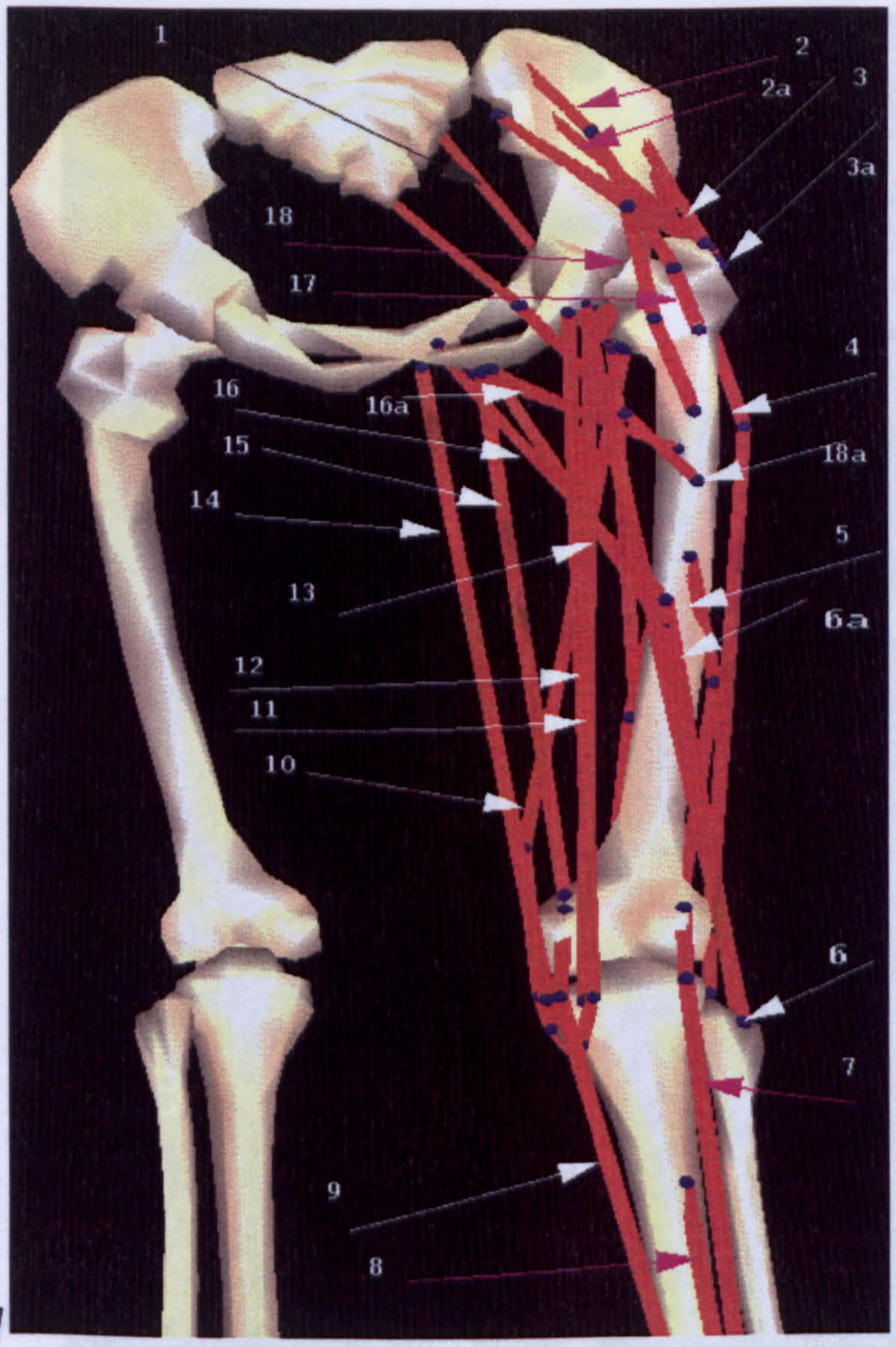

[H] ***1=Psoas 2 and 17 =GLUTEUS MAXIMUS1 2a=GLUTEUS MEDIUS2 3a=GLUTEUS MEDIUS1 4=Tensor Fascia latae 5=Vastus Lateralis 6=Biceps Femoris LONG HEAD 6a=Biceps Femoris short HEAD 7=Lateral Gastrognemius 8=Soleus 9=Medial Gastrognemius 10=Sartorius 11=Semimembranosus 12=Semitendinosus 13=Adductor Magnus2 14=Gracilius 15=Adductor Magnus3 16=Adductor Longus 16a=Adductor Magnus1 18=GLUTEUS MAXIMUS2 18a=GLUTEUS MAXIMUS3***

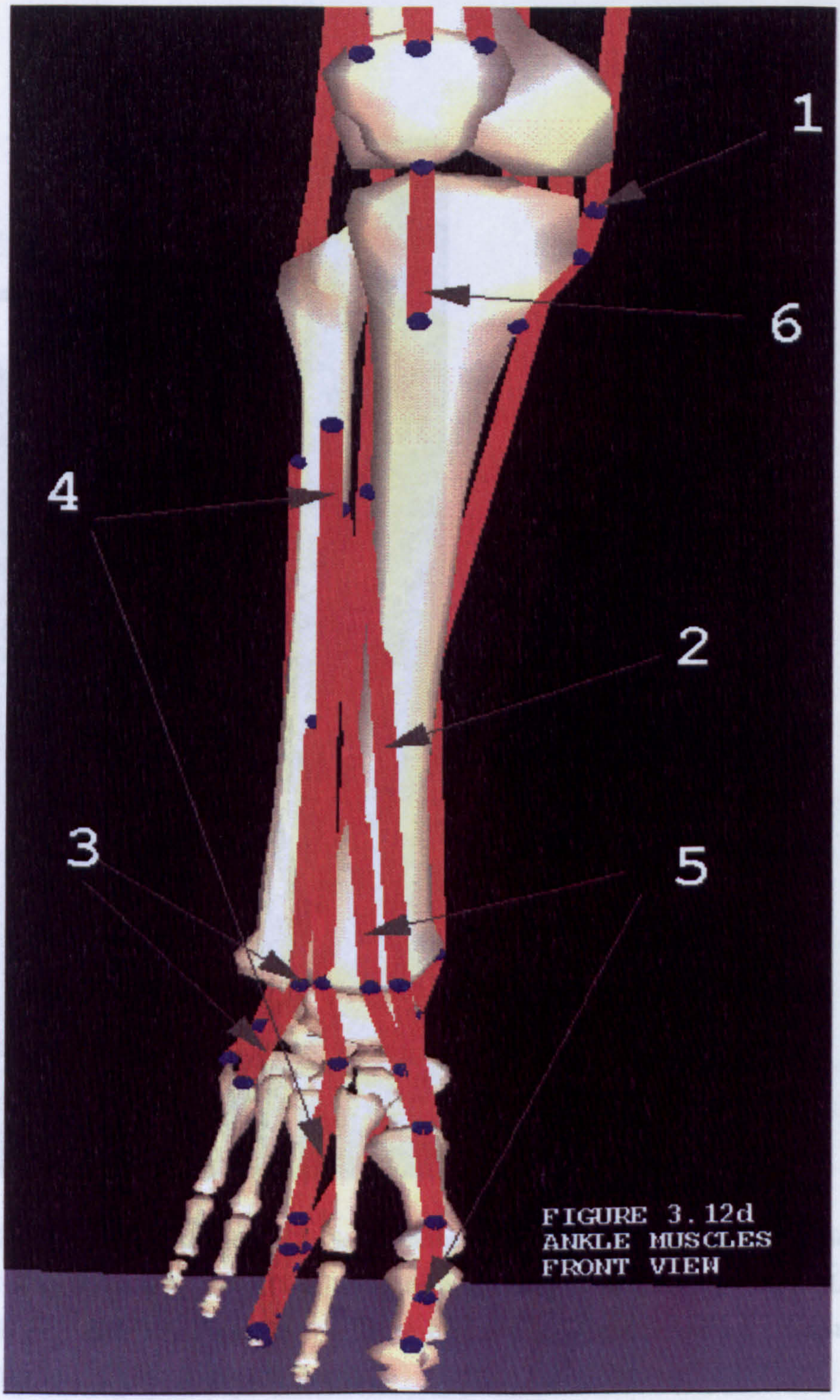

Figure 2.6: 1=Sartorius 2=Tibialis Anterior 3=PerTert 4=Extensor Digitalis 5=Extensor Hallusis 6=Patelar Ligament

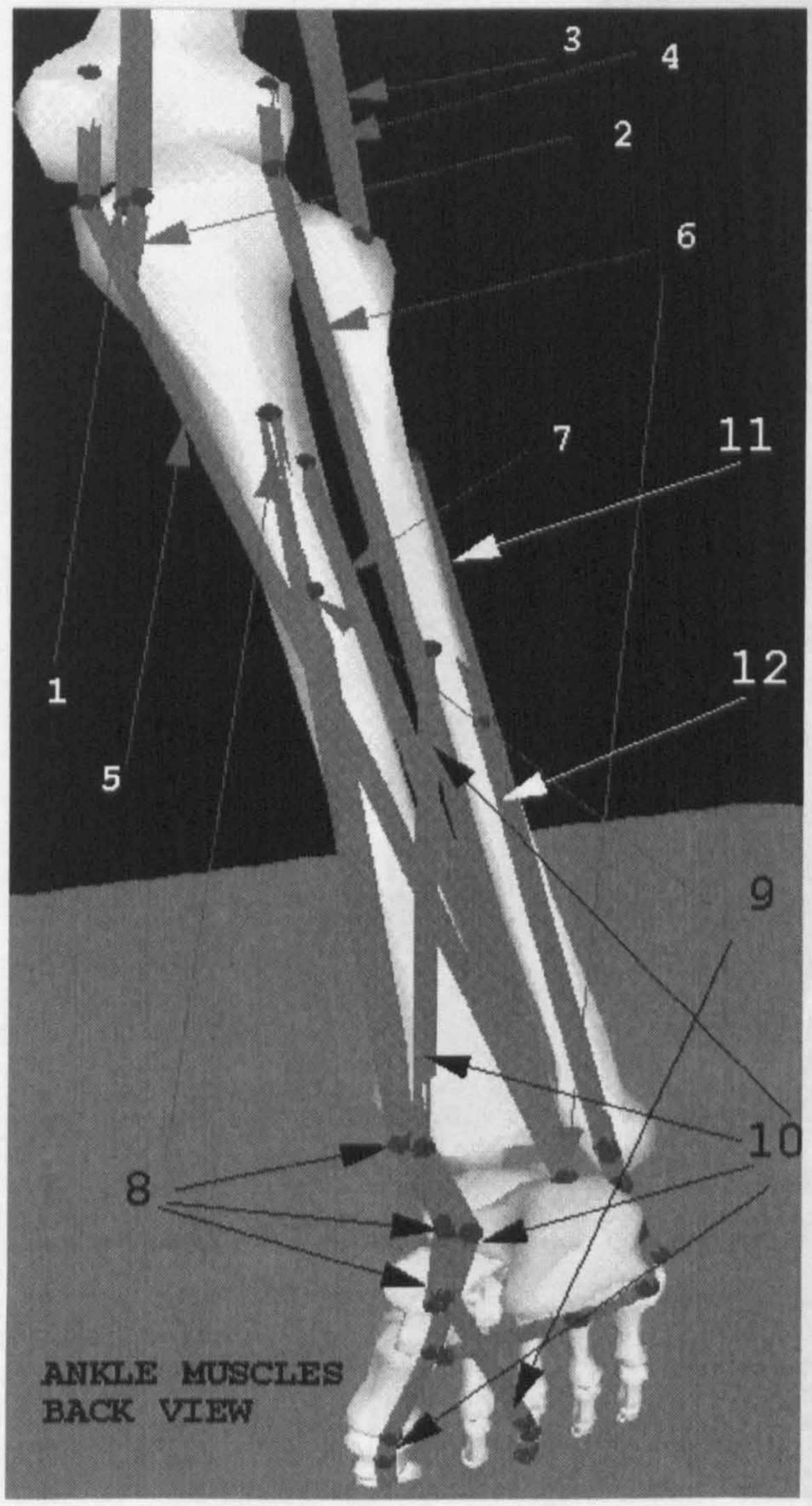

Figure 2.7: 1=Semimembranosus 2=Semitendinosus 3=Biceps Femoris Short Head 4=Biceps Femoris Long Head 5=Gastrognemius Medial 6=Gastrognemius Lateral 7=Soleus 8=Tibialis Posterior 9=Flexor Digitorum Longus 10=Flexor Hallusis 11=Peronius Longus 12=Peronius Brevis

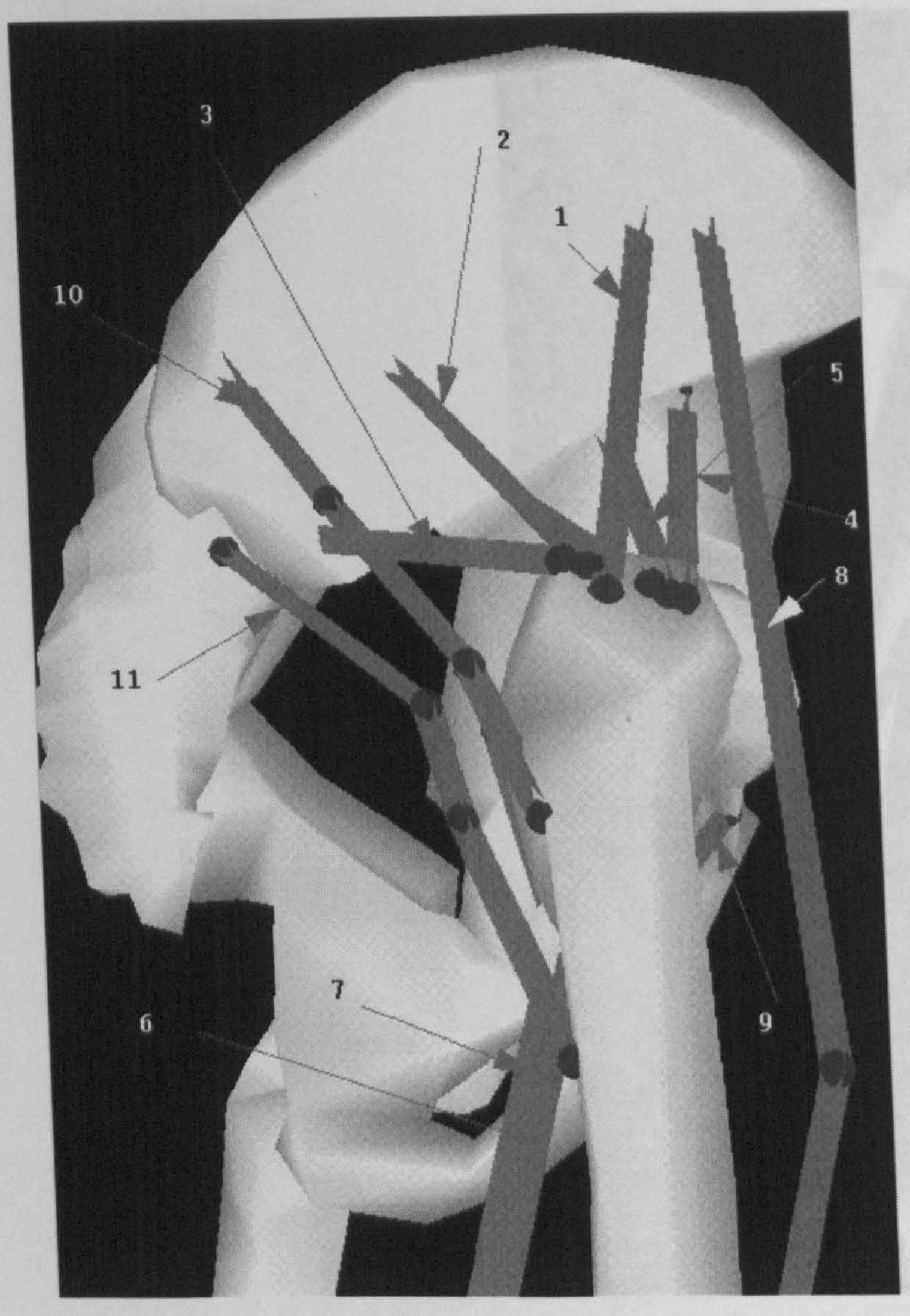

Figure 2.8: 1= GLUTEUS MEDIUS1 2= GLUTEUS MEDIUS2, 3= GLUTEUS MEDIUS3, 4= GLUTEUS MINIMUS1, 5= GLUTEUS MINIMUS2, 6=Semimembranosus, 7=Semitendinosus, 8=Tensor Fascia latae, 9=Pectineus, 10=Gluteus MAXIMUS1, 11=Gluteus MAXIMUS2

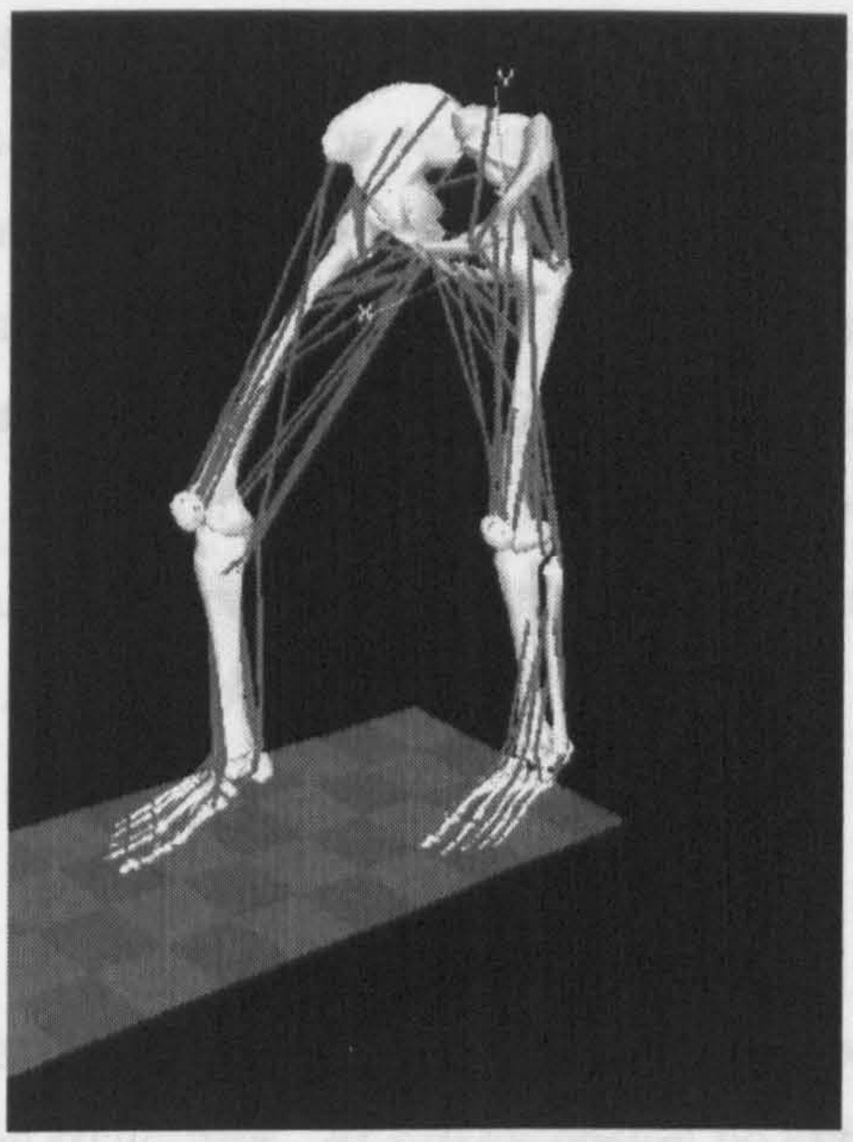

Figure 2.5: 3D Graphics based modelling of the KNEE JOINT with muscle wrapping (SIMM) Delp et al. [1996b]

2.3 KNEE JOINT MOVEMENT

The movements of the knee joint can be described as either active, conjunct or passive Evans [1986]. Active joint motion is voluntary. Physiological movements in flexion-extension and medial-lateral rotation are active. Conjunct movements are the consce-quence of other movements and are due to the geometry of the articulating surfaces and the presence of surrounding ligamentous structures. The musculature contributes nothing to such movements. If the foot is free, then as the knee goes from flexion to extension the tibia rotates externally about its longitudinal axis. In extension to flex-ion it rotates internally. Passive movements are those that an examiner may perform and thus may include active movements. Motion occurs in all three body reference planes, shown in Figure 2.1.4 on page 14), but is largest in the sagittal plane due to the flexion-extension movement.

2.3.1 FLEXION-EXTENSION

Full extension generally occurs at a joint angle of 0 degrees, full flexion at 140 degrees, and the average limit of hyperextension is 5 degrees. In full flexion the posterior, more

curved surfaces of the femoral condyles are located towards the posterior periphery of the tibial plateau. As the joint moves from flexion to extension the femoral condyles roll forwards or slide in the menisci as the menisci themselves slide across the tibial plateau until full extension is reached. In full extension the flats of the femoral condyles are located at the anterior edge of the tibial plateau. During this flexion-extension movement the position of the axis of motion varies from one instant to the next. For full flexion to full extension the final displacements of the tibial contact locations are larger on the lateral side than the medial side.

2.3.2 MEDIAL-LATERAL ROTATION

As flexion proceeds the medial-lateral rotation of the tibia or femur decreases due to the restrictions of surrounding tissue structures. At full extension no external/internal rotation can occur due to the close-pack condition. The range of medial-lateral motion is largest at 90 degrees flexion, where internal rotation has 0-30 degrees of motion and external rotation has 0-45 degrees of motion.

2.3.3 CONJUNCT ROTATION

From full extension to 20 degrees flexion the lateral contact moves in an arc with the centre located in vicinity of the medial meniscus, the lateral meniscus sliding over the tibial as the femur both rolls and slides upon it. Due to its proximity to the arc centre the medial condyle mainly slides without moving far and thus the medial meniscus moves little also. These two motions result in the

conjunct rotation of the tibia about an axis parallel to its longitudinal axis if the foot is free or the conjunct rotation of the femur, again about an axis parallel to its longitudinal axis if the foot is fixed. Between 20 degrees flexion and full extension the point of articulation on the medial tibial plateau moves back thus accelerating the conjunct rotation resulting in the final screw home motion and close-pack condition of the joint Evans [1986].

According to Trent et al. [1976] there exists up to 40 degrees of conjunct rotation throughout the full range of flexion with 20 degrees of this occuring within 15 degrees of full extension. During normal gait this conjunct motion is substantially reduced to approximately 8 degrees in the stance phase.

2.3.4 PASSIVE MOTION

At full extension and hence, in the close-pack condition, no passive movements can be produced. At 10-15 degrees of flexion approximately 10 degrees of valgus-varus rotation can be produced and passive rotations of the order 25-30 degrees can be obtained. As Evans [1986] points out the drawer movement tests are rather more subjective and are usually evaluated qualitatively by comparison with the opposite side.

Chapter 3

Modelling of the Knee Joint

Much attention has been devoted to the solution to what has become known as the general joint distribution problem. The problem of estimating the in vivo forces transmitted by the individual anatomical structures in the joint neighborhood during some activity of interest Paul [1966], Paul [1976] , Barbenel [1972]. The prediction of forces in joint structures has many applications Seireg et al. [1973], Seireg et al. [1975].
In the field of medicine, these predictions are useful for obtaining a better understanding of muscle and ligament function, mechanical environment within which prosthetic components must operate, and mechanical effects of musculoskeletal diseases Poulson [1973], Rohrle et al. [1984]. In the realm of sport biomechanics, these predictions are useful for better understanding of the kinetic demands, performance constraints, and mechanisms for improving athletic performance. Industrial applications include the optimization of occupational performance and safety considerations. Although the general techniques for predicting forces in joint structures may be used throughout this broad range of applications, the particular method of choice and the details of the analysis depend upon the application Penrod et al. [1972], Pedotti et al. [1978], Crowninshield et al. [1981].

3.1 The general Force Distribution Problem

The general force distribution problem normally arises in the following way. The musculoskeletal system or a relevant portion thereof is modeled as a mechanical system consisting of a number of essentially rigid elements (body segments) subjected to forces due to the presence of a gravitational field, and segmental contact with external

objects, neighboring segments, and soft tissue structures that produce and constrain system motion. The associated inverse dynamics problem is then formulated and solved to determine the variable intersegmental (joint) force and moment resultants during the activity of interest. The joint resultants are abstract kinetic quantities that represent the net effect of all the forces transmitted by the anatomic structures crossing the joint. At a typical joint, these forces normally include the forces transmitted by the muscles, ligaments, and articular (bony) contact surfaces.

The unknown forces transmitted by the joint structure are next related to the known intersegmental resultants by writing the joint equilibrium equations. These equations express the fact that the vector sum of all the forces in the individual anatomic structures, and the vector sum of all the moments about the joint centre produced by those forces, are equal to the intersegmental resultant force and moment, respectively. Assuming that all joint geometry (point of application and orientation of forces) is known and that these two independent vector equations (or six independent scalar equations) involve as unknowns the M muscle and L Ligament forces, together with the 3C scalar components of the C bony contact forces, these joint equilibrium equations are indeterminate whenever the sum (M + L + 3C) of the unknown forces exceeds six. Thus, if the system model includes only one bony contact force (C=1) and more than three muscle and/or ligament forces (M + L > 3), the corresponding joint distribution problem will be indeterminate and therefore have an infinite number of solutions.

Finally the joint resultants are decomposed or distributed to the individual joint structures at each instant of interest during the activity, using some appropriate solution methodology.

The general joint distribution problem may thus be stated in the following way. At any instant of time when the joint resultants are known, the forces transmitted by the individual joint structures are determined such that the equilibrium equations, and all relevant constraints on the forces in the individual joint structures, are simultaneously satisfied. The classical studies of joint distribution problems use essentially two different methods to solve the indeterminate joint distribution problem: the reduction method, and the optimization method, both of which are reviewed in the following chapters.

The mathematical modelling of human anatomy and its functions has been influenced by two main simulation approaches or philosophies. In the first the joint

structures are of no importance in the mathematical modelling while in the second simulation of the geometry and structural relationships of the joint components in addition to their behavioural properties are the main tasks. Hefzy et al. [1988] categorised these different approaches as phenomenological and anatomical respectively.

3.2 PHENOMENOLOGICAL MODELS

The phenomenological models include two groups: the rheological models and the advanced figure animation models.

The rheological models analyse the dynamic behaviour of a system by treating it as viscoelastic, being composed of springs and dampers. However, the non-correspondence of these components to the structure of the components in the knee leads to no structural information in the model output Viidik et al. [1968], Viidik [1968], Moffatt et al. [1969].

The advanced figure animation models provide information on body dynamics by taking into account body segment dimensions, masses, moments of inertia, etc, but do not model the detailed geometry of joints Crowninshield et al. [1976], Pope et al. [1976]. The model of Delp et al. [1990], Delp et al. [1993], Delp et al. [1992], Delp et al. [1996a] Delp et al. [1994], involved simulation of the muscoloskeletal system of the lower extremity under isometric loading conditions using three dimensional, shaded polygonal-based graphics. The system is actually used in clinical situations and allows behaviour parameters to be altered via a graphical user-interace, enables hip osteotomies and tendon transfer work to be simulated and the effects of the procedures upon model behaviour to be quantified Papaioannou et al. [1997], Papaioannou [1997]. Chen [1993] presented an implementation where Zajac's model of skeletal muscle to construct a finite element isoparametric representation of the frog gastrocnemius muscle that both mathematically and visually approximates correct behaviour. In another study by Chao et al. [1993], a general three dimentional modelling system that allows calculation and display of motion and forces of joints, muscles and tendons: A two dimensional version was applied to knee and hip osteotomy preoperative planning, total joint replacement prosthesis design and dimentional selection, and ostechondral allograft sizing and reconstruction using radiographic data. The advances in new computer technology as reviewed above have certainly advanced experimental biomechanics but had no direct impact in the clinical field to date. Vast improvements in

sheer numerical processing power need to be added to enhanced graphics display capabilities of the new computer technology. The graphics technology in particular has been benefited enormously from the explosion of interest in the technology of immersive virtual environment systems. Although all the above approaches can be criticized to an extend for their several assumptions there is a growing need to combine biomechanical mathematical models, computer processing power and the computer graphics technologies to produce interactive, computer-based graphical simulations of the musculoskeletal system. Solutions providing robust algorithms, simultaneous visualization and user friendly environment will have an impact in the clinical environment and are possible with the existing technology.

3.3 ANATOMICAL MODELS

Two different approaches to modelling categorisation exist in the experimental literature. According to the first the catergorising of the models depends upon the type of motion reproduced by the mathematics. This categorisation gives the three major areas of kinematics, statics and dynamics, the latter two being collectively known as kinetics. In kinematic models only the position, velocity and acceleration of the joint are considered. There is no regard for component masses, nor external and internal forces giving rise to the motion. Static models consider only positions of equilibrium in which both the internal and the external forces acting on the joint balance out and quasi-static models are employed to approximate the effects of motion. Dynamic models incorporate the kinematic and static treatments to consider both the forces giving rise to joint motion, and the motion itself. The second approach categorises models according to their structural basis. There is a vast number of studies attempting to model specific component structure and behaviour which will be evaluated in order to identify the optimum method for the modelling of each specific component.

3.4 REVIEW OF TIBIAL-FEMORAL JOINT STUDIES BY TYPE OF MOTION

3.4.1 Coordinate systems

All the knee characteristics of motion could be represented by any of three possible methods to relate and orient the bones of the joint: projected angles, Euler angles or Cardan and Bryant angles.

The projected angles approach is adopted by Sutherland et al. [1981] in clinical gait analysis. Body segment local coordinate axes are projected on to the XY, YZ, and ZX planes of a global fixed reference coordinate system giving the angles of each segment with respect to the reference frame. Joint angles are obtained as the difference between corresponding distal and proximal segments. This approach is simple and easy to implement but is kinematically unreliable for segment angles, incorrect for joint angles greater than 5 degrees and is insufficient for more complex representations.

The rotational motion about three independent axes in space is parameterised by the use of Euler, and Cardan and Bryant angles. With three orthogonal axes, i,j, and k, Euler angles are defined by rotation about the axis sequence kjk , while Cardan/Bryant axes are defined by the cyclic rotation sequence ijk , Ensberg et al. [1988], Moeinzadeh et al. [1983]. Some clasic studies using euler angles can be found in the work of Levens et al. [1948] , Kettlekamp et al. [1970], Lewis et al. [1977], Suntay et al. [1978], Chao [1980], Wismans et al. [1980], Grood et al. [1983] , Blankevoort et al. [1984], Kadaba et al. [1990], Blankevoort et al. [1988],
Selvik [1989], Kaufmann et al. [1988], Garg et al. [1990], Yeadon [1990],
Davis et al. [1991], Ramakrishnan et al. [1991]. The results from either parameterisation are sequence dependent but this effect is small if only one component (not that about j) is large. The main disadvantage of this approach is the occurence of a singularity close to which small variations in the rotation matrix correspond with large variations in the angular sums or differences of the component rotations. This is known as gimbal lock, and occurs when rotation about j is $\pm\pi/2$. The non-singular case results in two solutions and is known as Codman's Paradox Miyazaki et al. [1991].

3.4.2 Representation of displacement axes

Techniques employed in robotics have been used towards a simplified representation in which the axes of translation are assumed to be collinear with a set of orthogonal, intersecting rotation axes Lafortune [1984], ($Faro^{TM}$, Faro et al. [1986]). Such systems are termed three-cylindric open chains. Pennock et al. [1990] put the axes system of Grood et al. [1983] in this group but in fact their system employs non-orthogonal axes. These three representations are slightly different in the methods of axes construction, more details can be found in Pennock et al. [1990] who provide a review of each method.

The Joint Coordinate System (JCS) proposed by Grood et al. [1983] and shown in figure 4.1 consists of an axis, e_1 fixed in the proximal segment and acting as a medial-lateral axis, an axis, e_2, fixed in the distal segment and acting as an inferior-superior axis and a floating axis, e_3. The JCS has been adopted by many other research workers with two slight variations depending on which axis, i.e. flexion-extension, varus-valgus, etc., is fixed in which segment. The original JCS is employed by Cappozzo [1984], Soutas-Little et al. [1987], Ensberg et al. [1988], Kaufmann et al. [1988], Areblad et al. [1990], Kadaba et al. [1990], Davis et al. [1991], Ramakrishnan et al. [1991] and Hefzy et al. [1993]. The alternative configuration employs the e_3 axis as an anterio-posterior axis in the distal segment , Wismans et al. [1980], Blankevoort et al. [1984],Blankevoort et al. [1988], Selvik [1989]. Cole et al. [1993] quantify the differences between the two different JCS's encountered in biomechanics and propose a standardisation where e_1 is the flexion-extension axis fixed in the proximal segment, valgus-varus motion occurs about the floating axis, e_2, and e_3 is the medial-lateral axis fixed in the tibia. A closer look reveals this to be the original configuration adopted by Grood et al. [1983](FIGURE 3.1 on page 30.

In three dimensions the instantaneous centre of rotation (ICR) can be extended to an instant axis of rotation or a screw axis. As Kinzel et al. [1983] relate, the screw axis approach was employed by Thompson [1972] and Pottoff [1968]. They define the relative motion between two bodies by successive displacements rather than by instantaneous positions and each relative displacement is represented by a different screw axis. Other workers to employ the instant axis method are Delange et al. [1982], Duke et al. [1977], Lewis et al. [1978], McLeod et al. [1974], Murray [1974] and VanDijk et al. [1979].

Several researchers represent joint surface profiles by polynomials and the kinematics of the joint are determined analytically. Crowninshield et al. [1976] assume axial rotation of the tibia varies as a fifth root of the angle of flexion about an axis centred on the medial condyle, while Garg et al. [1990] employ femoral-tibial kinematic motion parameters that are fifth order functions of the flexion angle and calculate the femoral-patellar angle as a quadratic function of the angle of flexion. The above review aims in presenting the variety of solutions and the lack of a global view in settling some of the most characteristic issues of knee modelling. All of the studies described above, justify several assumptions with varying degrees of uncertainty.

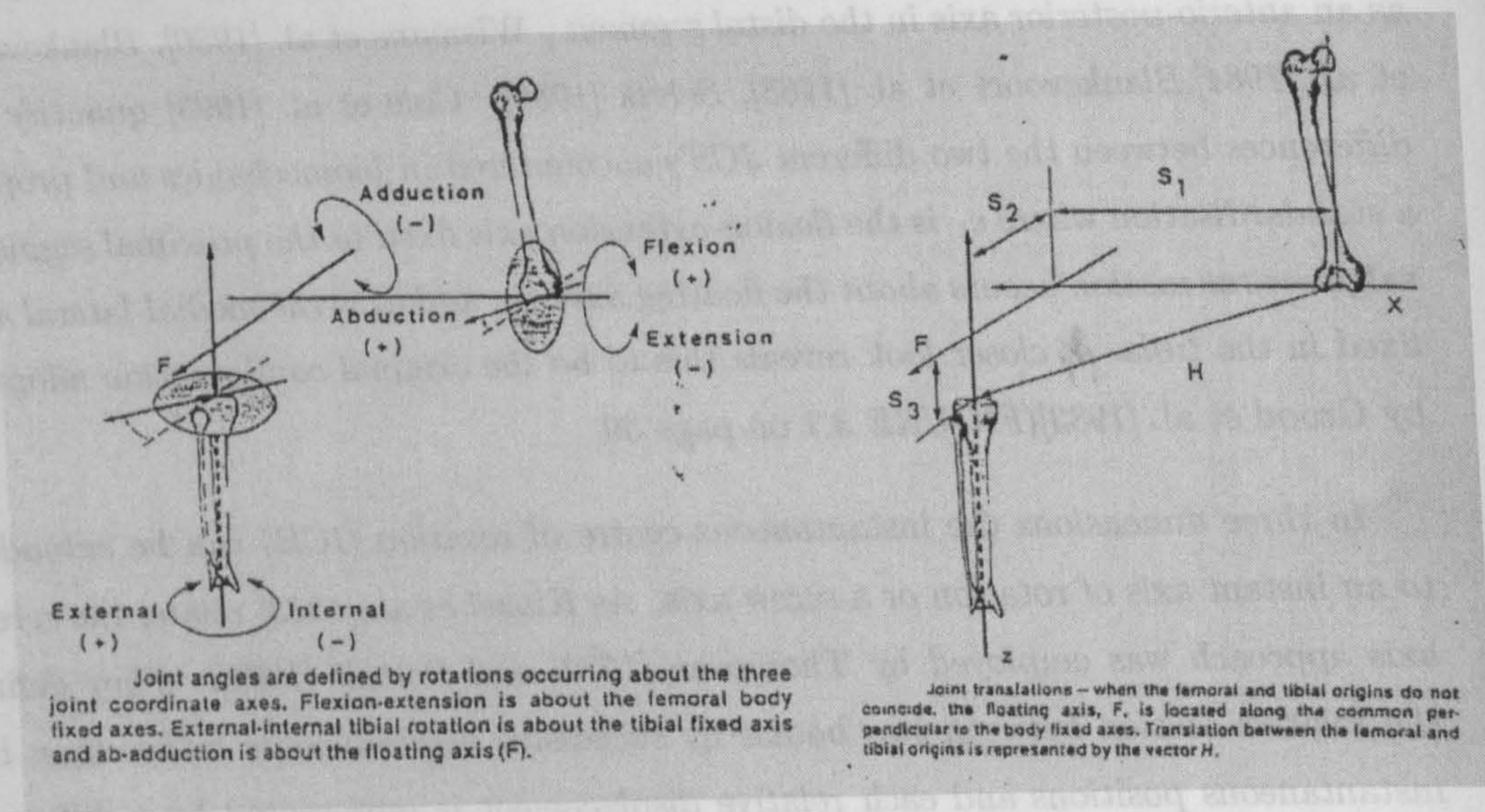

Figure 3.1: The joint coordinate system (Adopted from Hefzy and Grood, Hefzy et al. [1983]

3.5 STATIC MODELS

The use of kinematic models is limited in the amount of information that can be obtained about the behaviour of the joint. This insufficiency can be attributed to the failure to consider the action of external and/or internal forces acting on the joint. Bone contact at the articular surfaces results in contact forces. The distribution and direction of the latter are determined by the bone geometry, and their magnitude, location and direction are also affected by the sum of the forces developed by the supporting ligamentous and muscular structures. In an attempt to describe the behaviour of the knee more accurately many researchers have modelled the forces occurring within the joint under equilibrium conditions, the majority limiting the structure described to the passive knee joint. These so called static models comprise the largest group of computer-based models to date. The behaviour of the joint in motion is approximated by quasi- static models in which the forces acting on the joint are considered at many different equilibriums occurring at points along the trajectory of the joint. Hefzy et al. [1988] classify the static/quasi-static models into four main groups, Type I, those "used to determine the distribution of forces in the muscles and the ligaments during different types of joint loading conditions", Type II those "where forces in each of the ligaments are determined as a function of joint position", Type III, those "used primarily to determine the contact forces and stresses between the femur and tibia", and Type IV, those "more complex models that include both ligamentous structures and the geometric constraints on motion which result from the geometry of the bones". The above classification ought to be approached with care since it refers mainly to methodological differences and not to validity and accuracy of the model prediction.

3.5.1 Type I- Models of Load Sharing

3.5.1.1 The Reduction Method

The reduction method reduces the number of unknown forces to correspond with the number of equations governing the distribution problem (or increases the number of equations to agree with the number of unknowns, e.g. the deformation-force relations for the unknown forces). For the general three-dimensional distribution problem, this implies that the number of unknown scalar forces (M+L+3C) must be reduced to six

to allow for a unique solution. Previous investigators have reduced the number of unknowns by (a) grouping muscles and ligaments with apparently similar functional roles, (b) grouping multiply-connected bony contact force regions, (c) assuming a direction for the unknown bony contact force, (d) using EMG data to determine when a muscle is active, (e) ignoring ligament forces except near the limits of the range of motion, and (f) ignoring antagonistic muscular activity.

Paul [1965],Paul [1966] predicted muscle forces and the bony contact force at the hip during locomotion. In these studies, the indeterminate distribution problem at the hip was made determinate through several simplifying assumptions. The hip muscles were combined into six functional groups (long flexors, short flexors, long extensors, short extensors, abductors and adductors), and ligament function at the hip was assumed to be negligible. The forces transmitted by these six muscle groups, combined with the three components of bony contact force, comprised nine unknown scalar quantities. Only two of the three components of the resultant hip moment were considered; analysis of the component tending to internally or externally rotate the femur relative to the pelvis was rejected as inaccurate. Previous reports of EMG activity were to demonstrate that there is little antagonistic muscle action, and only muscle agonists were considered. Despite these simplifications, the possibility of activity in both the long and short flexors and extensors still made the problem indeterminate. A solution was obtained, however, by assuming activity in only one flexor (either long or short, but not both) and one extensor.

Such models have been proposed for experimental studies by Harrington [1976], Morrison [1968], Morrison [1969] and Morrison [1970], Nissan [1980], Reilly et al. [1972], Seedholm et al. [1976], and Tooth [1976]. Reilly et al. [1972] presented a 2 dimensional model for the leg-raise exercise where only four forces were accounted for: the patellar tendon force, the tibio-femoral reaction force, the weight of the limb, and the weight of an exercise boot. Moments were summed about the point of application of the tibio-femoral reaction force to determine the patellar tendon force without solving for the contact force. Their analysis simplified the load sharing by assuming that the location of the joint contact force was constant throughout flexion, although it is known to move posterior on the tibial plateau as the knee is flexed.

One of the most studied models of the knee is the 3- dimensional model developed by Morrison [1968], Morrison [1969], Morrison [1970] at the University of Strathclyde. The model predicted the way the external load transmitted across the knee joint was

shared by the internal joint structures. The model was also employed and extended by other researchers Paul [1976] Harrington [1976], Nissan [1980] , Tooth [1976]. Morrison adopted the experimental approach by Bresler et al. [1950] which employs a force plate to measure the ground-to-foot reaction force during walking. Three- dimensional limb segment displacements were obtained from cine records of the motion of markers placed on the skin of subjects at selected landmarks. Activity of selected muscles was also recorded using a multichannel electromyograph.

In the first part of his analysis he combined the force- plate measurements with the motion data obtained from film analysis and used the six equations of motion of the leg segment to determine the complete external force system acting on the knee joint. A nine-point double differentiation procedure was used to obtain the acceleration of each limb segment from the displacement-time graphs for each marker (Lanczos [1957]). In the second part of his analysis, Morrison assumed the functionally equivalent muscle and ligament system acting at the knee joint to consist of three muscle groups, hamstrings, gastrocnemius, and quadriceps femoris, and four ligaments, the two cruciates and the two collateral ligaments. Equilibrium was obtained by contact force, and by the ligamentous and muscle forces. The mechanical system to describe the knee joint is then simplified using the "REDUCTION METHOD" that is reduced to six equilibrium equations where the number of unknowns is more than the number of equations. To reduce the number of unknowns, Morrison introduced assumptions based on his experimental data of subjects performing normal level walking. To determine the forces in the three muscle groups, Morrison assumed that they functioned at different times during the motion, and never together. The selection of which muscle was active was based upon the electromyographic data. The forces in the cruciate ligaments were determined by assuming that a tension in one cruciate ligament implies no force action in the other. An anterior displacement of the tibia thus caused the tensioning of the anterior cruciate, while a posterior displacement caused the tensioning of the posterior cruciate.

The remaining of the unknowns were determined by introducing different assumptions by considering different conditions of loading separately. The collateral ligaments were unloaded whenever the compressive stresses existed on both condyles. As the pressure on one condyle tended to zero, equilibrium was achieved by the force action in the appropriate collateral ligament. When there was no force transmitted by the condyles, both collateral ligaments became tense. Forces acting in the lateral collateral

ligament were four times larger than those in the medial collateral, and forces in the posterior cruciate were twice as large as those in the anterior cruciate. The average values of the maximum force developed in the quadriceps femoris muscle group were 0.6 percent of those in the hamstrings and 0.7 percent of those in the gastrocnemius muscle group.

A total of fourteen experiments was performed using nine male and three female subjects in the age group eighteen to thirty-eight. The author's data for all subjects (normal level walking)presented three main periods of peak loading in the joint force cycle and that the maximum joint force at the knee was 4 times body weight -normal subjects- attributing the above three peaks to the activity of hamstrings, quadriceps femoris, and gastrocnemius respectively. The author concluded that the maximum joint force calculated at the knee during walking was in the range of 2-4 times body weight, the average value of 12 subjects being 3.03 times body weight Morrison [1970]. When the joint was highly loaded, the greater portion of the load was transmitted by the medial condyles. Forces acting on the joint in the mediolateral direction were generally small. Their mean maximum value was calculated to be 0.26 times body weight.

In the ?], Poulson [1973] and Morrison [1970] studies, solutions were found to indeterminate problems by anatomical or functional simplifications. The degree of redundancy of the remaining structures was not large, thus permitting, at most, only a few possible determinate solutions. The general method of finding multiple determinate solutions was formulated and applied to larger scale problems by Chao et al. [1976]. They described a permutation-combination method of determining all possible determinate solutions to a complex indeterminate problem. In the case of the finger, they identified 126 possible determinate solutions. The solution set, however, contained some inadmissible solutions. The inadmissibility of a solution was defined by constraints restricting tendon forces to tension and bony contact forces to compression, and by somewhat arbitrary constraints on tendon and pinch or grasp force magnitudes. These authors speculated that the physiological solution of the finger distribution problem fell within the region in solution space bounded by all the possible admissible determinate solutions.

3.5.1.2 THE OPTIMIZATION METHOD

The previous discussion indicates that the distribution problem at a joint is typically an indeterminate problem, since the number of muscles, ligaments and bony contact regions available to transmit forces across a joint in many cases exceeds the minimum number required to generate a determinate solution to the joint equilibrium equations. Determinate solutions are obtainable only with significant simplification of joint function or anatomy. In contrast, the optimization method of solving the general joint distribution problem does not require such simplification. Rather, it retains many of the anatomical complexities incorporated in defining the problem, and seeks an optimum solution (i.e. a solution that maximizes some process or action).

Optimization techniques may be divided into linear and nonlinear methods. Simultaneous use of linear cost and constraint functions in the model formulation constitutes the so-called linear optimization method. In contrast, if the cost function and/or one or more of the constraint functions is nonlinear, solution of the problem requires the use of nonlinear optimization methods. Both of these optimization methods have been made practical with high speed computers, since the techniques require many iterations of equation-solving to find an optimum solution.

Neuromuscular function is complex and poorly understood at the conceptual, if not detailed level. However, it is generally assumed that physiological functions are optimized in some way. In 1836, the Weber brothers commented that we walk and run in "the way that affords us the least energy expenditure for the longest time and with the best results". Experimental evidence suggests that oxygen consumption (and presumably energy expenditure) is minimal at freely-selected walking speeds, supporting the assumptions of optimal physiological neuromuscular function Ralston [1958].

The optimization criteria that the neuromuscular control system "chooses", either consciously or unconsciously, to select muscle action may vary considerably with the nature of the physical activity to be performed and the physical capabilities of the individual. For example, muscle control in sprint running may serve to maximize velocity, while in walking the control process may serve to maximize endurance. In a painful pathological situation such as degenerative joint disease, muscular control may serve to minimize pain. If this pain occurs due to the joint surface pressure, the appropriate optimization criterion may be to minimize to bony contact force. Muscular control

may also serve to minimize the forces transmitted by passive joint structures such as ligaments. These examples indicate that there are possible optimization criteria to choose from, and the choice of a criterion to solve a particular distribution problem may not be obvious.

Given that gait presents a relatively unambiguous performance criterion, one can claim that it fits into the framework of optimum control theory. Additionally, gait presents a characteristic bilateral symmetry which leads to relatively simple representation of the dynamical system. Activity in the stance phase of gait is described by equality constraints on the "states", knowing that each gait stage involves dynamic constraints that reflect the particular nature of the phasic activity. However, our motivation in the use of optimum control for the study of movement relies upon the belief that it is currently the most sophisticated methodology available in the solution of extremely synthetical problems. Optimal control theory requires not only that the system dynamics are precisely determined and formulated but also that an appropriate performance criterion is chosen. Therefore, deficiencies in the modelling that are present in either the system dynamics or the performance criterion are indicated by differences between model and experiment.

Hatze [1980] reported extensively on the application of Optimum Control Theory in the investigation of Human Movement and Human Biomechanics (Hatze [1978] Hatze [1981c] Hatze [1981d] Hatze [1981a] Hatze et al. [1981] Hatze [1981b] Hatze [1976] Hatze [1983] Hatze [1979] Hatze [1988] Hatze [1995]). In his work of "complete optimization of a Human Motion" Hatze simulated the right leg of a human subject with a mathematical model which contains two control paramenters for each of the five muscle groups involved. A time-optimal problem in which the right-hand end point of the state trajectory is variable was formulated and an optimization was performed. The computational procedure was based on an algorithm of differential dynamic programming. The optimal model solution was then compared with the performance of the living system.It is found that any motion of the biosystem which deviates from the predicted optimal one takes longer time to complete and therefore is not optimal. Also the trajectories and control functions of near-optimal motions as measured on the living system were found to be very close to the theoretical optimal process thus again confirming the optimality of the model solution. In addition the model predicts biologically highly significant phenomena such as the occurrence of a stretch reflex, the incompatibility of speed and accuracy in a genetically non-determined biomotion,

etc.

Barbenel [1972] reported an analysis of the force distribution problem at the temporomandibular joint. His model included four muscles (masseter, temporalis, internal pterygoid and external pterygoid), an occlusal load and the temporomandibular bony contact force. The results were estimated by minimizing a linear objective (cost) function of the bony contact force and the muscle forces to determine the bony contact force as a function of occlusal load.

Penrod et al. [1972] reported a linear optimization method to solve the wrist distribution problem using two models, one having four and the other having seven potentially active muscles. Ligaments were ignored and the bony contact force was assumed to pass through the joint centre and not to enter into the flexion-extension moment equilibrium equation. The linear objective (cost) function used in this study required the minimization of the sum of the muscle force magnitudes. They concluded that the optimal response principle and the corresponding mathematical analysis result in a unique solution for the redundant statics problem at a load supporting joint. Although the assumptions in the analysis create sources for discrepancies between calculated and observed results the procedure provides a systematic technique for determining the ideal force distribution in terms of effort.

Seireg and Arvikar (1975) presented a linear optimization method to solve the distribution problem at the three joints of the lower extremity during both walking and squatting. They reported a number of cost functions: (a) minimization of the forces in the muscles, (b) minimization of the work done by the muscle to attain the given posture (i.e. minimize the product of the muscular tension and muscle elongation or contraction), (c) minimization of the vertical bony contact forces at the three joints, and (d) minimization of the moments carried by the ligaments at the three joints (Seireg et al. [1973], Seireg et al. [1975]).

Chow et al. [1971] referred to the principle of optimality that characterises normal walking and suggested that " the performance criterion is meaningful in that it is shown to be proportional to the mechanical work done during normal walking". Optimum control allowed for decomposition of the locomotion behavior into pertinent submodes or configurations. Information on the feasible initial and terminal conditions, temporal patterns, step length, and speed parameters forms a gross characterization. From this, one can generate the kinematic behavior of the gait, that is, displacement, velocity, and acceleration trajectories for the various angles.

Crowninshield [1978] simultaneously solved the distribution problem at the hip, knee and ankle with 30 potentially active muscle elements in the lower extremity. The optimization criteria minimized the sum of the muscle stresses; that is, the sum of the quotients of the individual muscle forces divided by the corresponding physiological cross-sectional areas. This cost function preferentially predicted forces in muscles with large products of moment arm and physiological cross-sectional area.

Audu et al. [1988] compared optimal control algorithms for complex bioengineering studies. Two optimal control problems were solved using five dynamic optimization algorithms carefully selected from among the most widely recognised gradient-based algorithms. They found that the best algorithms for solving some of the small-sized optimal control problems are the gradient-restoration algorithm (GR), the Variance algorithm (VA), and the method of parallel tangents(PT) in that order. Even though some of these algorithms retain their superiority for the larger complex problems considered in the above study, it is at the expense of either extra long computation time (PT) or very large computer storage requirements and further increases in computation time (GR). The VA algorithm seemed to be "the golden rule" example particularly when a medium-sized mainframe computer is the operating platform. Computation of constrained optimal controls using parameterisation techniques finds also another successful scenario in the work of Sirisena et al. [1974]. The authors presented an algorithm for computing optimal controls by approximating the control profiles by piecewise polynomials. The algorithm was extended to treat optimal control problems with saturation-type control constraints and boundary constraints on the state variables. The method appears to be very applicable to the class of problems associated with partially free initial state and/or free final time.

All the foregoing linear optimization methods proved to be of limited applicability because the number of active muscles could be no greater than the number of constraint equations Pedersen et al. [1987].

Pedotti et al. [1978] employed an optimization procedure to predict lower extremity muscle forces during gait using both linear and nonlinear cost functions. Their optimization criteria included the sum of the muscle force magnitudes and the sum of the squares of the muscle forces. Additional cost functions were also investigated, including the sum of the quotients formed by dividing each muscle force by the maximum possible force exerted by the muscles. Since the maximum possible force in a muscle was based on the muscle's physiological cross-sectional area (PCSA), this

criterion produced results that were identical to those produced by the minimization of the sum of the muscle stresses.

Crowninshield et al. [1981] later reported nonlinear optimization procedures minimizing a function of the unknown muscle, ligament and bony contact forces. The cost function U(F) was of the form

$$U(F) = Wm \sum_i (Cm_i Fm_i)^{nm} + Wl \sum_j (Cl_j Fl_j)^{nl} + Wc \sum_k (Cc_k Fc_k)^{nc} \qquad (3.1)$$

were F defines a vector of design variables, Fm_i, Fl_j and Fc_k denote the forces (design variables) transmitted by the ith muscle, jth ligament and kth bony contact region, Cm_i, Cl_j and Cc_k are constants associated with the ith muscle, jth ligament and kth bony contact region, nm, nl, and nc represent muscle, ligament and bony contact region exponents, and Wm, Wl, and Wc are muscle, ligament and bony contact region weighting factors.

Pandy et al. [1992] suggested a parameter optimization approach for the optimal control of large-scale, non-linear musculoskeletal dynamic systems with the special application to jumping activities. The authors found that there are computational difficulties surrounding the use of parameter optimization algorithms, particularly as system dimension becomes very large. For example, when simulating human movement using a three-dimensional musculoskeletal model with many muscles, computation of the first derivatives of the performance intex and the contstraints with respect to the unknown variables (controls) becomes prohibitive. Since each iteration of the parameter optimization algorithm requires forward intergrating the system differential equations at least as many times as there are number of control nodes, performing these integrations consecutively (or serially) is computationally exhaustive, and may prove unmanageable for very high-dimension systems. An attractive alternative, and one made possible by the emergence of powerful processors (R10000) or massively parallel machines, involves modifying the structure of the algorithm so that the computation can be performed in parallel.

Pandy et al. [1990] applied the optimization algorithms in the study of maximum-height jumping because this activity presents a relatively unambiguous performance criterion and fits well into the framework of optimal control theory (Pandy et al. [1991] Pandy et al. [1992]). The mechanical behaviour of muscle is described by a Hill-type

contractile element, including both series and parallel elasticity. Driving the musculotendon model is a first-order representation of excitation-contraction (activation) dynamics. The optimal control problem is to maximize the height reached by the center of mass of the body subject to body-segmental, musculotendon, and activation dynamics, a zero vertical ground reaction force at lift-off, and constraints which limit the magnitude of the incoming neural control signals to lie between zero (no excitation) and on (full excitation). A computational solution to this problem was found on the basis of a MaynePolak dynamic optimization algorithm. Qualitative comparisons between the predictions of the model and previously reported experimental findings indicate that the model reproduces the major features of a maximum-height squat jump (i.e. limb-segmental angular displacements, vertical and horizontal ground reaction forces, sequence of muscular activity, overall jump height, and final lift-off time).

Nagurka et al. [1990] developed a Fourier-based method for generating near optimal trajectories of dynamic systems represented by deterministic, lumped -parameter models. The method is conceptually simple, computationally robust, and applicable to a broad class of physical problems. Simulation studies demonstrate the effectiveness of the proposed approach for handling linear, unconstrained problems, while sidestepping many of the numerical difficulties typically encountered in implementing optimal control theory. The results show that for all problems, except bang-bang control problems, the near optimal trajectories achive optimality accurately and with high speed of convergence.

Davy et al. [1987] used a dynamic optimization algorithm (Fletcher-Reeeves conjugate gradient algorithm) to solve the muscle force sharing problem for the swing phase of gait and compared it to a typical static optimization algorithm solution (Gradient-restoration algorithm). The objective function for the dynamic optimization algorithm was a combination of the tracking error and the metabolic energy consumption. The latter was taken to be the sum of the total work done by the muscles and the enthalpy change during the contraction. The objective function in the respective static optimization was the sum of the cubes of the muscle stresses. To solve the problem using the static approach, the inverse solution was firstly obtained to determine the resultant joint moments required to generate the given hip, knee and ankle trajectories. The results showed that the dynamic methodology presents several advantages but any conclusions about discrepancies must be tentative. Discontinuous information and "previous state" related problems are the main weaknesses of the static approach.

It was also noted that the main source of error in the inverse dynamics problem is the numerical differentiation process in accordance with previous findings Hardt [1978].

Chao et al. [1973] developed a method based on the principles of optimization to obtain the approximate joint moments during gait directly from a set of measured displacement history. The suggested method requires no numerical differentiation of experimental data and therefore the possibility of magnifying inherent experimental errors is minimized. The method of steepest descent often utilised for the solution of continuous problems in optimization is used as the basic tool in solving the above problem. The problem "becomes a mathematical programming problem which is very similar to the optimal control problems discussed by Luenberg (1969) and Strauss (1966)" Chao et al. [1973]. If the objective function is driven to zero based on a systematic and successive variation of the design variables then one will obtain a set of applied moments which will produce a displacement pattern for the system closely matching the experimentally measured values.

Goh et al. [1988] reported on a unified computational technique based on control parameterization that supports certain convergence properties and solves fixed terminal time optimal control problems subject to general constrains. Their aim was to produce a user-friently algorithm alternative to the existing -difficult to implement- algorithms in the literature. The great efficiency of this solution method is partially contributed to the fast-converging mathematical programming algorithm used, which serves to absorb a large portion of the complex computation done. The protocol was used with unspecified terminal time, minimax and problems with free or interrelated boundary conditions.

Patriarco et al. [1981] evaluated the significance of various factors which contribute to the formation of a muscle force optimization solution and introduced appropriate improvements which provide more accurate determination of the temporal patterns and quantitative levels of the muscle forces during gait. The study showed that the resolution of the problem of muscle redundancy is not responsive to the minimal criterion of any optimization model. The imposition of additional physiologically-based constrains are essential to distinguishing the role of individual muscles. It is noted that the addition of constraints among functionally similar muscles was found to be more successful in producing a synergistic distribution of force load than was the application of stress limits on the individual muscles.

Other studies using optimization techniques Yeo [1976] revealed that the "principle

of minimal total muscular force" ought to be applied with caution and only when accurate biomechanical modelling is implemented. Yeo et. al. applied minimal total muscle force (Elbow joint load distribution problem) as the optimization criterion and found that the theoretical results contradicted the exprerimental results of Basmajian and Latif.

Recently optimum control has become a necessary tool in the study of sports and high performance movement Behncke [1987]. Maronsky [1996] reported on optimization of running and swimming indexes for competitive athletes and Hatze H. (1981,1994) investigated complex movement patterns in gymnastics (i.e. skip on the horizontal bar) and athletics (i.e. optimization problem of the long jump). Studies also include work in force/energy optimization for wheelchair athletics Cooper [1990] and optimization of energy expenditure and muscular activity in handrim wheelchair propulsion Vanlandewijck et al. [1994] Spaepen et al. [1996]. Other energy efficiency related optimization studies refer to gait patterns when stepping over obstacles Chen et al. [1991], Patla et al. [1993], Chou et al. [1997] and the optimum trajectory of the swinging leg Chou et al. [1995]. Most of the above numerical solutions are based on extensive algorithms and are performed on very advanced computer engineering platforms. The computation time required for calculations involving movement and its study with optimization is generally very extensive. In addition the learning curve for optimum control problem formulation and its involvement with post processing for better understanding of the results decrease the clinical applicability of such formulations. We aim in our work to combine firstly the visualization tools that enhance lower limb 3D model development in terms of reduction of time and ease of model manipulation with clinical relevance with secondly the advanced engineering algorithms that will be provided in a user friendly environment (X-windows based). A new user friendly environment ought to allow faster and easier creation of models and model libraries, robust optimum control algorithms that do not require extensive learning curves, no additional post-processing of the optimization data and easy to comprehend results for the possible clinical applications. We used Design of Experiments techniques (DOE) to get the maximum amount of information out of the simulation runs while minimizing the number of runs. The theory of DOE concerns cost-effective experimentation. While traditionally one control parameter (factor) is changed at a time, from one experiment(run) to the next, a DOE approach changes all control parameters at the same time.

Although this way of experimenting seems awkward, because the insights from the data obtained this way are not immediately apparent to normal thought, it has been proven that it contains much more information than the traditional approach. Some post-processing is required in order to get access to this information. The post-processing is done by creating approximate, analytical, models of each Design Output as a function of all Design Inputs. These approximate models are called Response Surface Models (RSM). We aimed in generating user friendly interfaces that include this post-processed information resulting in a dramatic rise in the comprehension of optimum control data while the time for trial and error laborious computing drops also dramatically. The DOE and RSM techniques reduce drastically the number of simulation runs, allow quantification of how the Design Inputs influence the Design Outputs, detect correlated Design Outputs and predict Design Output values for untried Design Input values.

3.5.2 Type II - Models of Ligament Length

Early models were developed by Edwards et al. [1970] and Crowninshield et al. [1976]. Edwards et al. [1970] studied the kinematics of the knee joint to determine the length of the cruciate and collateral ligaments. The tibia was considered to be fixed and the motion of the femur about the tibia was limited to three degrees of freedom; tibial rotation in the transverse plane, flexion in the sagittal plane and compression-distraction in the proximal-distal direction. The work of Edwards et al. [1970] who presented one of the first analytical models of the knee, permits prediction of the response of the joint to either external forces or displacements. Crowninshield et al. [1976] extend the work of Edwards et al. [1970] by adding two further degrees of freedom to the joint motion, allowing valgus-varus rotation in the coronal plane and anterior-posterior drawer.

The joint stiffness was calculated using the inverse method, also used by Wismans et al. [1980], in which the joint is displaced, the new insertion points and hence the new length of the ligaments are calculated so allowing the tensile force in the ligaments to be determined. The changes in joint force divided by the associated joint displacement result in a value for joint stiffness. The predictions of the model were compared with experimentally obtained data, and as also reported by Hefzy et al. [1988], reasonable agreement was found between the two for valgus-varus and tibial-torsional stiffness,

but not so for anterior-posterior stiffness.

In the first of two papers Grood et al. [1982] also evaluated the contribution of the ligaments to the stiffness characteristics of the knee by using matrix structural analysis.

3.5.3 Type III. Models of Femoro-tibial Contact Stress

These models were developed primarily to evaluate how proximal tibial osteotomy changes the contact force distribution in the knee. Various models have been developed by Maquet et al. [1977], Denham et al. [1978], Kettlekamp et al. [1972], Engin et al. [1974], Minns [1981] and Chand et al. [1976]. For more information the reader should refer to the review paper by Hefzy et al. [1988].

3.5.4 Type IV - Models Including both Ligamentous Structures and Geometric Constrains

To date the models of Wismans et al. [1980], Andriacchi et al. [1983] and Blankevoort et al. [1991b] are the only three models that fall into this group.

Wismans et al. [1980] report a three dimensional quasi- static model of the tibio-femoral joint. Articular contact is achieved by satisfying three contact conditions. Geometric compatibility gives the coincidence of a femoral contact point with a tibial contact point. Collinearity of the normals at each of the corresponding contact points provides the second and third conditions. The first condition yields six equations while the other two result in two equations each, giving 10 in total for the contact conditions, i.e. five for each contact point. The force and moment equilibrium considerations result in three equations each. The problem thus reduces to 16 non-linear equations with 16 unknowns - the position vector of the femur with respect to the tibia (3), component rotation angles in the orientation matrix used to orientate the femur with respect to the tibia (2), contact point variables (8), contact forces (2) and magnitude of moment (1). The numerical solution was achieved using a Newton-Raphson iteration after the set of unknowns was reduced.

Andriacchi et al. [1983] created a three dimensional model in which they represented the femur and tibia as rigid bodies and modelled the ligaments, the menisci and cartilage using a FEM approach. Each rigid body had its own local body coordinate system located at a point termed a primary node. Varus-valgus rotation, internal rota-

tion and posterior-anterior stability as predicted by the model were compared quantitatively with experimental data for mid-range stiffness reported by Markolf et al. [1976]. Andriacchi et al. [1983] found that: a)the imposition of motion constraints shifts the axis of rotation sufficiently to alter the knee's response and, therefore, concluded that b)the capability to simulate a moving axis of rotation in a model of the knee is very important. They also proposed that c)experiments which fix the axes of rotation may be artificially imposing motion not normally encountered.

Blankevoort et al. [1991a] employ a quasi-static model that takes account of deformable articular contact to describe the quasi-static behaviour of the knee under moderate loading conditions (Blankevoort [1991] Blankevoort et al. [1991b]) . The description of the three dimensional geometry is based on the studies of Wismans et al. [1980] and the mathematical description of the deformable contact follows the work of Essinger et al. [1989] and An et al. [1990]. Treatment of the force and moment balances results in six equations, each comprising terms due to external forces/moments respectively, ligament loads, constraint loads employed to maintain the applied kinematic constrains, and contact forces. For rigid contact, the contact conditions that were employed were similar to those used by Wismans et al. [1980], giving 5n equations for n contact points. The total equation count is therefore equal to 6+5n. In contrast, the description of deformable contact is accounted for within the equations of force and moment equations -giving six equations in total. The equations are solved using a Newton-Raphson iterative method. The results led to the general conclusion that for higher loading conditions the use of non-linear contact and the inclusion of the menisci into the model should be considered.

3.6 DYNAMIC MODELS

If the ultimate goal is the accurate biomechanical modelling of a joint and simulation of its behaviour under a wide variety of conditions then the in-vivo response of the joint must be represented accurately. Static and quasi-static models place artificial restrictions on joint behaviour and are thus not sufficient for achieving this goal. The representations achieved in these models must be extended to allow the study of the response of the joint to dynamically applied loads. Only six models incorporating the dynamics into the tibial-femoral joint have been identified. Kaufmann et al. [1988] and Moeinzadeh et al. [1983] are the only researchers to construct three dimensional models

while two dimensional dynamic representations have been investigated by Tumer et al. [1993], Abdel-Rahman et al. [1993], Wongchalsuwat et al. [1984] and Moeinzadeh et al. [1983] who implemented a simplified version of their three dimensional model.

Abdel-Rahman et al. [1993] model the knee joint as two rigid bodies connected by five ligaments. For 20 to 90 degrees of flexion it was concluded that the anterior fibres of the posterior cruciate ligament and medial collateral ligament are the primary restraints against a posteriorly directed force, in agreement with much of the experimental literature.

It will be evident from the above review of the dynamic models that a large number of equations is required to describe the joint behaviour relatively accurately. Many different mathematical tools exist for the numerical solution of systems of differential and algebraic equations. However, if real-time or near real-time response is required from the simulation then the choice of method is very important one. It should be noted that these models have very limited clinical applicability, and luck robustness and ease of implementation.

3.7 REVIEW OF TIBIOFEMORAL STUDIES BY STRUCTURE

3.7.1 Bone Geometry

In three dimentions Kurosawa et al. [1985] and Garg et al. [1990] modelled the geometry of the posterior femoral condyles as spherical surfaces of radii 20mm with a medial-lateral spacing of 46mm. In contrast, other researchers have fitted surfaces to experimentally obtained data points representing the articular surfaces in three-dimensions using either interpolation methods or approximation techniques. Wismans et al. [1980] were the first to employ 4th degree polynomials of the form $y=f(x,z)$ to approximate the data points. This approach forms the basis of more recent work by Blankevoort et al. [1991a] and Essinger et al. [1989]. Blankevoort [1991] employ high degree polynomials of order six and seven to describe the medial and lateral femoral condyles respectively, in spherical coordinates. A similar range of techniques is employed to model the tibial surface. Wismans et al. [1980] interpolate third degree polynomials to represent the geometry of the tibial plateaux, while Blankevoort et al. [1991b] employ an approximation fit using both high and low-degree polynomials in conjunction with

a 'least-squares fitting' procedure. For a high degree polynomial representation a sixth order polynomial is used for the medial tibial plateau and a seventh-order polynomial for the lateral plateau, while fourth-order polynomials are used to represent the low degree geometry of both plateaux.

3.7.2 Ligamentous structures

To date the ligamentous structure models incorporated into biomechanical models are all phenomenologically based on spring line segments. There are three main criteria by which these existing representations can be further categorised. The first defines the assumed behaviour of the ligaments under loading unloading conditions to be either linearly elastic or nonlinearly elastic. The second criterion specifies the geometry of the ligaments in terms of the linearity/nonlinearity of the origin-to-insertion path, with the latter taking account of ligament-bone and ligament- ligament interaction while the former can result in the ligament representations penetrating the bone geometry. The third criterion specifies the geometry of the ligament in terms of the number of fibre bundles used to define the body of the ligament.

3.7.2.1 Linearly elastic, Linearly Geometric, multiple fibre bundle ligament models

In reality ligaments are constructed from many fibre bundles with different bundles brought into action at different positions of the knee motion (Evans [1986], Brantigan et al. [1941], Girgis et al. [1975], Fu et al. [1993], Race et al. [1996] Race et al. [1991] rather than from a single fibre. To take account of this behaviour a number of researchers model ligaments as nonlinearly elastic multiple elements with linear geometry from origin to insertion (Crowninshield et al. [1976], Wismans et al. [1980], Andriacchi et al. [1983], Essinger et al. [1989], Garg et al. [1990], Abdel-Rahman et al. [1993]).

To date Abdel-Rahman et al. [1993] are the only workers to have constructed a dynamic knee model that incorporates multiple bundle representations for the ligaments. A quadratic force-strain relation is used to model the anterior and posterior portions of the ACL and PCL, the anterior, posterior, deep and oblique portions of the MCL, and the LCL and posterior capsule. Stiffness values are obtained from Moeinzadeh

et al. [1983] and insertion data from Crowninshield et al. [1976].

While these recent approaches are more advanced than their predecessors the majority of them employ data from the same sources as the earlier models. More up-to-date experimental techniques take into account the multiple fibre bundle construction of the ligaments but as Race et al. [1991] point out previous lack of attention to this has resulted in inaccurate data. The studies of Trent et al. [1976], Kennedy et al. [1976], Marinozzii et al. [1983] and Prietto et al. [1988] result in data that is inferior to those obtained by Butler et al. [1986] who accounts for the multiple bundles.

3.7.2.2 Nonlinearly elastic, nonlinearly geometric, multiple fibre bundle ligament models

Multiple bundle ligaments capable of interacting with bone are currently only modelled by Blankevoort et al. [1991a] and Garg et al. [1990] employ interaction as an extension of their ligament modelling work detailed earlier. Blankevoort et al. [1991a] present a model for the wrapping of the MCL around bone, based on the treatment proposed by Grood et al. [1983], and incorporate it into a three dimensional mathematical model of the knee joint. The literature suggests that this is the first implementation of the treatment as it appears that Grood et al. [1983] did not implement it themselves.

Although the phenomenological models provide various different representations of ligament behaviour they do not relate this physiology to the biological structure of the ligament. 'Stand alone' constitutive models of ligament behaviour based on the known/assumed behaviour of the constituent parts of the tissue and which involve modelling its microstructure have been constructed. These so-called structural models are more suited to studying the connection between structure and mechanical properties than are phenomenological models (Woo [1993]). A good review of work in this field is provided by Woo [1993], Mow et al. [1993], and Lai et al. [1993]. Johnson et al. [1992] use a continuum model known as Single Integral Finite Strain (SIFS) viscoelastic theory for modelling ligaments and tendons in three-space. This approach employs different constitutive equations for different levels of strain and patches them together mathematically but so far they have only considered uni-axial tension.

3.8 Parameters influencing the model

3.8.1 Footwear effects on walking

Although foot biomechanics is a well investigated area of research, gait studies with footwear as the variable parameter are rare in the literature. Moreover the interaction of footwear and speed of walking has not been studied in the past. An attempt to estimate the magnitude of the footwear effect on the intersegment load distribution during walking was carried out in the present study. The biomechanical interest in shoe-design and evaluation started with the running-mania of 1970s. It was when the " citizen" started to realize the amount of hours that were spent sitting in a chair on a daily basis and decided to introduce running as an alternative, more natural part of the way of living. Today a vast array of sophisticated equipment is available and being used to study all types of shoes and their performance. Several reports on methodological aspects of shoe analysis (lateral stability, shock absorption characteristics, foot and shoe pressure, effects on ground reaction forces and gait, skeletal transients), testing and evaluation of shoes, were conducted in the past Ariel [1976], Stacoff et al. [1985], Cavanagh [1985], Snel et al. [1985], Johnson [1986], Valiant et al. [1987], Light et al. [1980], Jorgensen [1990].

The shoes and clothing influence our movements and loadings, as does our physiological or psychological state: someone on an adrenaline high often induces higher active loads due to more intense locomotor activity. Cushioning in shoes is desirable to a point. The shock wave of a footstrike on its way towards the skull is attenuated first by the shoes and then by the musculoskeletal system. The long term medical consequences of the impact wave can include arthritis of the knees or hips. Cavanagh's group tested the heel pad by striking it with a 1.9 kg pendulum at accelerations up to 20 g.: the heel effectively dissipated 85 % of the impact energy, behaving like a spring with stiffness as a function of deformation. A high speed film showed that displacement peaked at 3 ms about 1.5 ms after impact (Baer et al. [1986]). Maclellan conducted impact tests along the leg. Rather than use a force plate, which does not reveal localized damping effects, he placed three sets of accelerometers on the body. High-speed filming of the tests showed a rippling from the heel, indicating horizontal transmission of shock from bone to soft tissue before transferring shock to it. Maclellan believes that in the long run the shearing phase of this process could damage the blood supply to the tendon. Further tests by Nigg's team revealed that

all the thicker material samples, including those made of firmer material, dispersed shock more readily, with the best result coming during the increase from 10 to 20 mm. Stacoff et al. [1985], measured the influence of shoe height on lateral stability of sport shoes in sideways movements. Three shoes of different height were used: (a) low height, which is usually found in running shoes, (b) medium height, which is known in basketball shoes, and (c) high cut, which is found in boxing shoes. The average range of total supination for one subject was found to be 20 degrees over all shoes. The range of all shoes, however, was found to be 43 degrees. Therefore, in sideways movement the variability of all subjects equalled about twice the variability of one subject. Therefore, under the given test conditions, there was greater lateral stability with the medium-height and the high-cut shoes than with the low-height shoes. Designing of athletic shoes should take into account the shoe's weight. It has been well documented that added weight carried on the feet causes an increase in oxygen uptake during distance running Cavanagh [1985]. Therefore, the running pattern of the same individual might change from that aspect of shoe design in the long and some times in the short run. Rear foot stability is defined as the amount and rate of pronation after foot-strike. Bates reported that the degree of foot pronation during running is increased McPoil [1988]. This increase in foot pronation, forced manufacturers to use several techniques to enhance rear foot stability, like extending the shoe counter medially, reinforcing the counter with an additional plastic stabilizer place between the midsole and counter, reinforcing the counter with leather foxing, or extending the sides of the midsole superiorly to reinforce the inferior aspect of the counter. Several authors have reported that the peak acceleration values obtained from an impact tester increase from the softest to the harder materials. The same tendency appeared by the impact force values measured under the barefoot condition (Luethi et al. [1987] Baer et al. [1986]). Snel et al. [1985], reported that the major differences between the various shoes under test appear to be mainly restricted to differences in rise time and force to time ratio and not to differences in the magnitude of the impact peak. The author's results confirmed the results of Snel et al. [1985] for a larger variety of footwear, showing a striking absence of differences in the magnitude of impact forces between running with different types of shoes and barefoot. The effects of running shoes on three components of the ground reaction forces and their relationship to selected aspects of lower extremity function were studied by Bates et al. [1981]. He concluded that the barefoot was not an extreme condition. Several authors have in-

vestigated the effect of footwear on shock absorption. In the early 1980s the effect of walking barefoot, with conventional and with shock-absorbing footwear on the accelerations observed in a normal subject was studied by Light et al. [1980]. The shape of the tibial transient was characteristic of the heel construction -the hard leather heel giving a short transient of very abrupt onset and the two compliant heels showing smoother and lower deceleration waves. The shock absorbent construction resulted in less reverberation after the initial transient than the crepe rubber. Nigg's data showed that initial angular velocity of the Achilles tendon increased with both running speed and sole hardness. The data conflicted with the accepted theory that compression of softer midsoles exaggerates pronation. Nigg hypothesizes that a firm midsole rotates faster, the way a firm lever bent over a fulcrum will snap-to quicker than a soft one.

Jorgensen et al. [1988] reported that the most important shock absorber in the shoe-heel complex is the heel pad and added that running shoes provide significantly high shock absorption whereas high muscle activity due to increased musculoskeletal transients at heel strike when the shock absorbency is low was also observed (Jorgensen et al. [1989], Jorgensen [1990],Jorgensen [1990]).

Chapter 4

Methods and Procedures

In an attempt towards the betterment of our understanding of the normal and the abnormal joint function both classical and modern bioengineering approaches provide quantitative evaluation of the forces in and the forces transmitted between hard and soft tissues of the body. In classical mechanics structural analysis involves measurement and prediction of internal structural loads and stresses. Kinematic information such as position, velocity and acceleration of the structure and its parts can also be subject to measurement and prediction. In the following chapter the methodology of investigating the above is explained and analyzed. It should be pointed out that the human body is viewed as a mechanism with rigid supporting structures complete with bearing interfaces allowing movement and passive movements and active soft tissues providing stability and force generation.

The approach towards a 3 dimensional model of the knee joint used in the present study can be divided into two main parts; In the first part, synchronous accurate information of the kinetic and kinematic behaviour of the relevant structures (followed by detailed analysis -APPENDIX A) allows the employment of the standard technique termed "inverse dynamics". The latter follows the principles of rigid body mechanics Winter [1987], , by applying Newton's second law of motion. Therefore, the output of the first part is related to the net effect of external forces (i.e. the action of other bodies on the rigid body of interest), such as knee, hip and ankle moment patterns during the activities in question.

The second part of the methods refers to the biomechanical model of the knee, the elements, properties and input data. A new iterative solution algorithm for the joint distribution problem is also explained as part of the three dimensional analysis.

The approach is based on the notion of parallel solution algorithms for the non-linear problems utilising high performance computer architectures.

4.1 Kinetic and kinematic measurements

4.1.1 PROTOCOL

The average duration of each data collection procedure was about one and a half hours (whereas another one hour was required for the camera setting and calibration). Initially the subject was introduced to the laboratory environment and a brief explanation of the procedure, the aims, and the important aspects of the subject's point of view was given. The subject was asked to put on the clothing that was going to be used in the test which was emphasized to be kept as light as possible (usually comprising a swimsuit or a pair of shorts and a T-shirt). At this stage the markers were attached at the subjects' skin for the static trial, that is the ones used for the calculation of the hip and joint centres. Before that, all the anthropometric measurements were carried out as described in the end of section 5.1.1. Then the subject was asked to stand still in the calibrated area on the origins of the force plates for the capture of the data. After a short period of familiarization with the markers the subject was asked to practice gait along the walk-path, starting to walk approximately 5 m before the force plate and stopping about 4 m after the force plate. Practice was necessary in order to minimize psychological pressure caused by the subject's feeling that she/he was the centre of what was happening in the laboratory. During the practice runs the locations on the floor at which the test subject started to walk at each different speed were noted so that both right and left feet would hit the force plates, with foot contact area enclosed by the force plates boundaries. It should be noted that the subjects were not told about the existence of the force plate. It was found however that in most cases the subjects became aware of the existence of the force plate during the test since its boundaries were noticeable and also because the investigators were not successful always in concealing their interest in what was happening in the particular area where the force plate was located.

In the first category of tests each subject ought to follow a three stage procedure. First the subject was asked to walk barefooted in a natural and relaxed manner and to try to look straight forward while walking. Whenever it was decided to record a

test-run, the subject was notified about it. The subject was then instructed to start walking. The operation of the system was started from the control unit, when the subject was approximately 2.5 m before the force plate and stopped 2.5 m after the force plate; then the subject was instructed to repeat the task walking slowly this time. The last part of this stage requires the subject to walk at fast walking speed. The next three stages are a repetition of the previous procedure but with three different types of footwear, namely athletic shoes, boots, and oxford shoes.

The second category of tests involved trials of turning during walking. Trials required the subject to walk towards the force plates and at prearranged timing to turn on the right leg. The indication for turning involved either an object that the subject had to avoid or a characteristic sound to initiate the turn. All different directions of turn were tried and the data and laboratory configuration suggested that the most reproducible were turning on the left leg at 45 and 90 degrees in the direction of progression when the subject turned left. Therefore in the present study the participants were chosen to be right leg dominant. During normal level walking one axis of the plate, the X, refers to the direction of progression, another, the Y, to the vertical direction, and the final one, the Z, orthogonal to the right.

According to this configuration the X-axis corresponds to the anterio-posterior braking and accelerating forces the Z-axis, to mediolaterally directed forces, and the Y-axis to the vertically directed force.

The notation adopted with regards to the axes depends on the set up of the laboratory and should be considered when comparing data from different laboratories.

The positions of the gait laboratory equipment used in the present study are shown in FIGURE 4.1 on page 56.

The two forceplates are installed so that data from two sequential steps can be obtained. Temporal parameters of one gait cycle can therefore be assessed and analyzed.

Although forceplates are considered one of the most essential tools in biomechanics there exists a major drawback of kinetic analysis based on forceplate data; the data is only recorded for one gait cycle per trial. A large number of loadcells connected in a walkpath has been suggested (Whittle [1991]) but has not been experimentally successful.

ANTHROPOMETRIC MEASUREMENTS: The measurements of specific distances in the lower limbs of every subject taking part in the tests involved: Pelvic depth and width, the distance between the two epicondyles (m-l), the distances S1, S2, S3, S4 (see APPENDIXES), foot length and width and body height. The mass of the subject was also measured.

4.2 KINEMATIC METHODS AND ANALYSIS

Kinematic analysis refers to the movements, both angular and linear, of the structures in question. The body subjected to measurement is assumed to consist of a number of rigid segments interlinked by joints. In the present study the rigid segments of particular importance are the foot, shank, thigh and pelvis Bresler et al. [1950].

Absolute measurement of the segmental motion requires relation of all segmental movements to a single reference point in space. The vectorial movements relate the moving system to the defined orthogonal axis in space.

At least two cameras are required (we used six in the present study) for three dimensional analysis so that there exist two views of the subject -each from a different perspective. The calibration object enables each camera field of view to be calibrated in the three dimensions.

4.2.1 The Vicon system (Oxford Metrics Ltd)

The Vicon system (Oxford Metrics Ltd) based on six cameras is used in the present study. Reflective markers are fixed to the subject's limbs, to identify their orientation. The type of marker used here was a "raised marker". Each marker was prepared using a plastic sphere. Each sphere was covered with "Scotchlite" paper, that is, proper material which causes the markers to show up a very bright spots for the six cameras

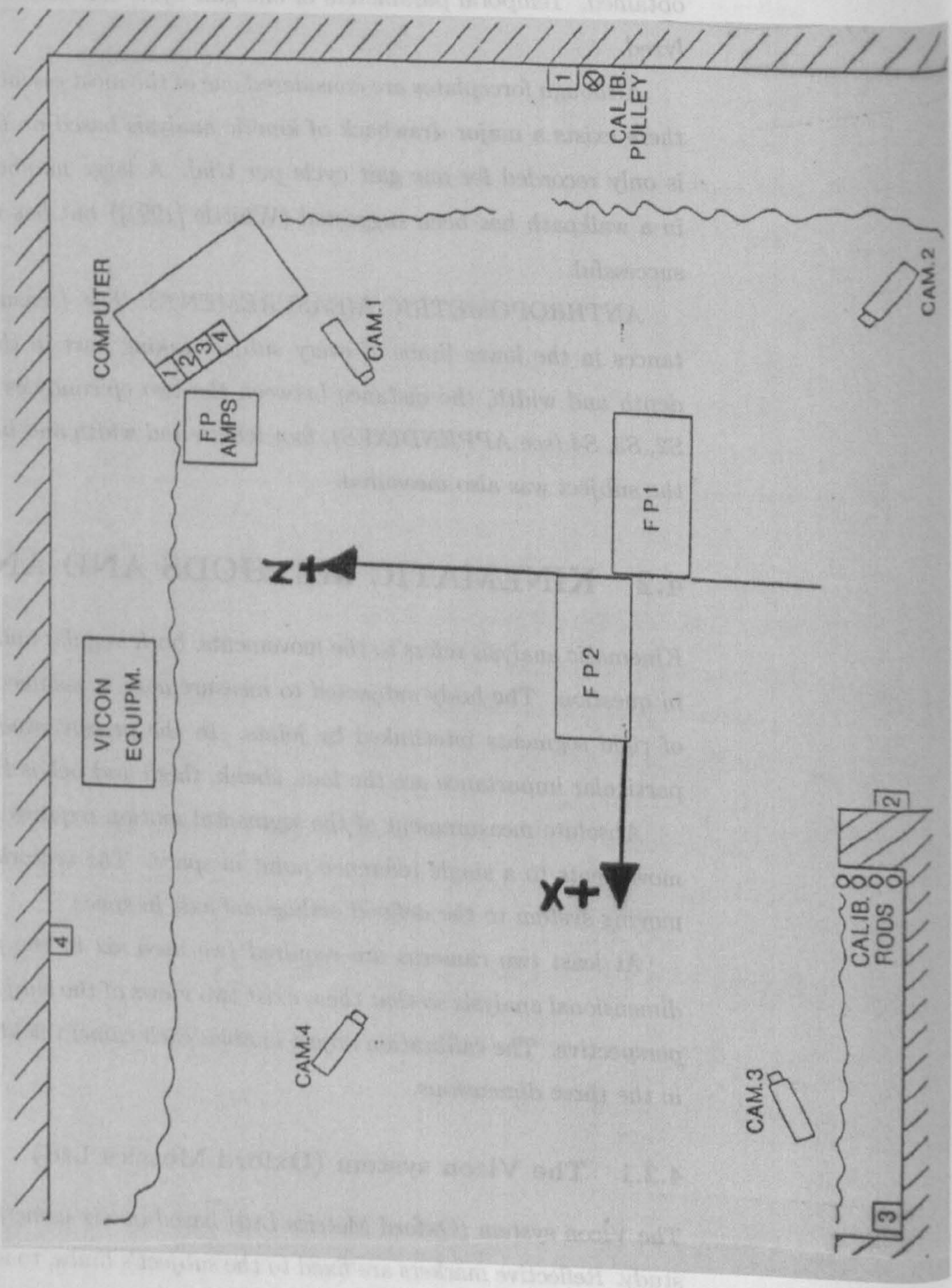

Figure 4.1: The Strathclyde Gait analysis laboratory

to view. Then a plastic pin was pinned into the body of the marker. These pins had a characteristic flat exagonal ending that enabled a peace of two sided adhesive tape to be attached. The diameter of the sphere is 0.03 m whereas the height from the base of the pin to the centre of the markers is kept consistent for all the markers at a value of 0.023 m. Close to the lens of each television camera is a light source, which causes the markers to show up as very bright spots. To avoid the "smearing" which occurs if the marker is moving, a short exposure time is used. If two or more cameras are used, they are synchronized together. The interface is capable of handling seven cameras simultaneously, but the present study is concerned with six. For normal purposes, a conventional television frame rate of 50 Hz (the case here) or 60 Hz is used, but specialised systems running at higher speeds (typically 200 Hz) are also available. As a general rule, the extra speed is accompanied by a reduction in measurement accuracy. The cameras point towards each other in pairs, but interference is eliminated by mounting them about 2m above floor level, angled slightly down, so that the opposing strobe is out of the field of view. Reflections from the polished floor are eliminated by covering it with brown paper. When used for combined Kinetic/Kinematic studies data are also taken into the computer from two Kistler forceplates, by means of an analog to digital converter. Thus the simultaneous positions of the markers and the ground reaction force are provided.

Three types of information are obtained from the Vicon and force plate data: (a) Knee angles when standing, in sagittal, transverse and coronal planes. (b) General gait parameters (cadence, stride length, and velocity). (c) Knee angles and external moments when walking, in sagittal, transverse and coronal planes. The most serious limitation of this measurement technique at present is the lack of information on knee rotation in the transverse plane. While good information can be obtained on the movements of the tibia, the orientation of the femur in this plane is difficult or impossible to determine accurately using skin markers. The other disadvantage of the technique is the relatively high capital cost of the equipment.

Two force plates were used so that kinetic information for both feet was available. The force plates were Kistler, type 9281B11 and 9261A (multicomponent measuring platform for biomechanics and industry). These platforms consist of piezoelectric transducers for measuring the following variables: (a) the 3 components Fx, Fy, and Fz of a force acting on the platform and (b) the 3 components Mx, My and Mz of the resulting moment vector M related to the origin of the coordinate system. The

technical data of this type of platform are: Ranges of Fx,Fy in kN=-10...10, Fz in kN=- 10...20, threshold: < 10 in mN, Natural freqency:approximately 800 Hz, Operating temperature range:-20...70(C^o), dimensions 600mm×400mm×100mm, mass:40 kg. The second force plate's technical data were: Calibrated ranges: Fx,Fy=0...5 in kN, Fz 0...10 in kN, threshold: Fx,Fy,Fz: < 50 in mN, Operating temperature range:0...50(C^o), natural frequency: 200 Hz, mass:26kg. The better characteristics of the first force platform allowed increased accuracy and although no great differences were observed between the two legs the left lower limb's data are presented for the sake of demonstration (since this limb corresponds to the first force plate).

If no tensile stresses are able to act on the top plate in the z direction, it is possible to determine in addition: the 2 coordinates ax and ay of the position of the resultant force on the platform surface, and the moment Mz about an axis normal to the platform surface. The electrical charges yielded by the measuring platform are strictly proportional to the measurands. They are converted by charge amplifiers into analog dc voltages, and can then be recorded, displayed or otherwise processed at will. In the present study the VICON gait analysis system's normal sampling frequency was 50 Hz, limited essentially by the kinematic sampling frequency. In summary, simultaneous acquisition of both kinematic and kinetic data is possible with the VICON system. The kinematic sampling frequency limits the normal sampling frequency of the system to as low as 50Hz. This is fully justified due to the very low frequency content of walking (about 20Hz) Paul [1970]. Activities with a higher frequency component such as running and jumping (which have frequency components greater than 25Hz) require the use of greater than 50Hz sampling frequency based on the Nyquist sampling theorem.

The data refer to the consecutive positions of the external markers and not to the actual body segments. In the suggested methodology by Cappozzo et al. [1988] three major points ought to be considered with respect to marker placement: (a) minimal soft tissue movement relative to the underlying bone due to soft tissue deformation, (b) large distance between markers, (c) sufficient image coordinates of the marker should be available at all times of testing. Care must be taken with the selection of landmarks and arrays of markers on the segments so that gross motions and joint centres about which the motions occur can be deduced. Finally, a three dimensional model of the moving body can be obtained. A model may consist of a number of segments each with their own local (ANATOMICAL) axis system. The anatomical

axis system is related to the ground axis system by 3×3 direction cosine matrices as will be explained later in this section and may be different to those produced by just the external (TECHNICAL AXIS) markers arrays Cappozzo [1984]. There is a great variety of models starting from simple applications i.e. Hardt [1978] used a five segments (2 shanks, 2 thighs and a torso), to more complicated ones i.e. Hatze [1976] Hatze [1980] employs a seventeen segment model. The complexity of the model depends on its application which means that there is no real standard model in the research environment. In the pathological application the models tend to be more specific and standardisation is preferable (i.e. the Newington Hospital model is the current standard model in Cerebral Palsy gait analysis) (Gage et al. [1991]).

In three dimensional space a body segment has six degrees of freedom and kinematic analysis requires information on both its position and orientation. Therefore, three position and three orientation pieces of information are the 3D descriptive requirements. The position and orientation of the moving segment is continuously compared to a stationary or global (GROUND) reference system. As pointed out earlier, absolute joint kinematics refer to the comparison of a cartesian coordinate system defined within the segment to an inertial coordinate system based outside the segment. However, segment kinematics refer also to comparing position and orientation of the distal segment with respect to a coordinate system in the proximal segment, the moving and stationary coordinate systems respectively. The relationship between moving and stationary coordinate system is explained in detail in APPENDIX A.

4.2.2 JOINT ANGLES

The joint angles represent the relative motions of the segments and have been described in terms of flexion- extension, abduction-adduction and internal-external rotations. However, the terms flexion-extension, abduction- adduction etc. are subjective since all relative movements occur synchronously -the joint motion being three dimensional and not only planar or biplanar (Grood et al. [1983], Kadaba et al. [1990], Winter [1987]. It ought to be pointed out here that the knee joint has translations associated with the rotations Blankevoort et al. [1988]. These translations continuously change the centre of rotation of the joint.

There are four major techniques for the description of the behaviour of joint angles: the projected angles, the Euler angles, the floating axis (used here) and the helical

screw axis. According to Andrews [1982] the choice of analytical method is based on individual experience and taste rather than on any objective criteria. However, not all the techniques give the same answers, which suggests that one ought to place additional attention when selecting the technique to describe the joint motion.

4.2.3 THE FLOATING AXIS TECHNIQUE

The floating axis technique was used in the present analysis. The floating axis technique as suggested by Grood et al. [1983], refers to three nonorthogonal unit vectors, e_1, e_2, e_3 as rotation axes.(FIGURE 4.2 on page 61)

The e_1, e_3 axes are the body fixed axes embedded in the two coordinate systems or segments whose relative motion is to be analyzed. The third axis, e_2, is termed the floating axis and is defined as normal to the plane of e_1 and e_3. The direction cosine matrix determines the orientation of the these axes using:

$$e_1 = \{0, 0, 1\} \tag{4.1}$$

$$e_3 = \{B_{1,1}, B_{1,2}, B_{1,3}\} \tag{4.2}$$

$$e_2 = e_3 * e_1 \tag{4.3}$$

For example, e_1 axis describes the joint's flexion-extension , e_2 the abduction-adduction i.e. the floating axis and e_3 the internal-external rotation. The three rotation angles which describe the relative orientation of the two coordinate systems or segments can be calculated as follows:

FLEXION-EXTENSION,

$$\alpha = \sin^{-1}(-e_2 * I) \tag{4.4}$$

when $-\pi/2 \leq \alpha \leq \pi/2$

ABDUCTION-ADDUCTION,

$$\beta = \sin^{-1}(K * i) \tag{4.5}$$

when $-\pi/2 \leq \beta \leq \pi/2$

INTERNAL-EXTERNAL ROTATION,

$$\gamma = \sin^{-1}(-e_2 * k) \tag{4.6}$$

when $-\pi/2 \leq \gamma \leq \pi/2$

Where X,Y,Z (unit vectors I,J,K) denote the stationary coordinate system, x,y,z (unit vectors i,j,k) the moving coordinate system and the rotation axes are the same as those used for the Euler angle analysis technique.

The major advantage of the floating axis technique refers to rotation angles which are order independent. This is a result of the fact that the rotation axes are explicitly

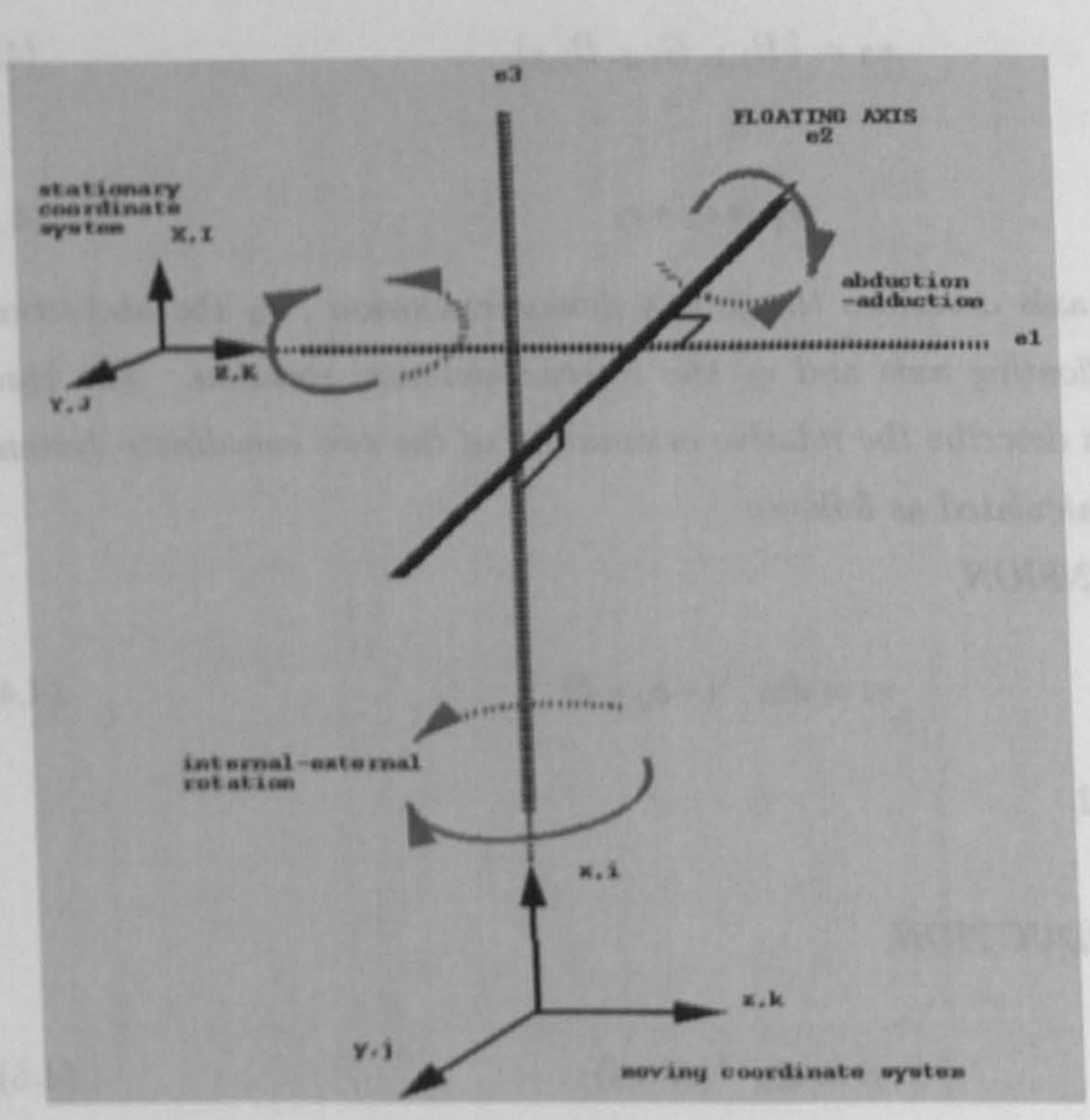

Figure 4.2: The floating axis technique refers to three nonorthogonal unit vectors, e_1, e_2, e_3, as rotation axes. e_3 is defined as perpendicular to both e_1 and e_2.

defined by the format of the analysis technique thus eliminating confusion which arises when interpreting Euler angle technique kinematic data.

4.3 JOINT LOADING-FORCES AND MOMENT CALCULATIONS

Bresler and Frankel (1950) have used the 'inverse dynamics' technique to determine the loading behaviour of the joints. The method follows the principles of rigid body mechanics and therefore by assuming that the segments of the body are rigid they are assumed not to deform under load. Moments as measured about an axis, represent the measurement of the tendency of the force to impart to the body a motion of rotation (Andriacchi et al. [1984]). Forces and moments are balanced by equal and opposite forces to achieve equilibrium. These forces are generated mainly by muscle contraction, articular reaction forces and passive soft tissue stretch. The technique is also employed for two dimensional analysis which, although simpler, is more prone to error (due to its assumptions of planar motion) than the three dimensional one. All body segments are defined to move relative to fixed joint centres. Stepwise analysis is performed distal to proximal while each joint is considered in turn using free body diagrams. During the stance phase, for example, the forces and moments applied to the foot are referred to the ankle joint. The kinematic data provide the moment arms about which the ground forces act resulting in moments acting on the ankle joint. The result is added to the existing moments to give the moments acting on the joint (Bresler et al. [1950]). The analysis includes also the mass of the segment so that gravitational and inertial forces due to the mass can be evaluated. Gravitational loading is experienced by any object that possesses mass and exists in our environment. The gravitational force effect on a body segment is a function of segment mass, acceleration due to gravity and location of the centre of segment mass. Using body segment parameter information from an anthropometric study by Drillis and Contini (1966) or others, external segment loading due to gravity can be calculated. The direction of this is vertically down and its point of application is through the segment centre of mass.

The accelerating segment is subjected to inertial loading. The magnitude of inertial forces about the principal axis of inertia depends on the segment mass, segment mass distribution and segment kinematics and can be calculated for a segment according

to:

$$Fi = Ms * a \tag{4.7}$$

where Fi is the inertial force, Ms is relevant segment mass and a is the linear acceleration of the centre of mass. Fi acts through the segment centre of mass and its direction is opposite to that of the acceleration. Similarly inertial moments can be obtained with:

$$Ti = Is * \alpha \tag{4.8}$$

where

$$Is = Ms * K^2 \tag{4.9}$$

with Ti being the moment applied to the segment, Is the segment principal axis mass moment of inertia, K the segment radius of gyration and α the angular acceleration of segment orientation. Ti is directly opposite to the angular acceleration. The above quantities as well as many of the parameters required for determining external segment and joint loading are difficult to measure experimentally. Anthropometric studies provide the solution with data on body segment parameters that have been determined for a sample population. Drillis et al. [1966] (FIGURE 4.3 on page 64) measured body segment parameters for 20 male subjects between the age of 20 and 40. They determined segment length as a ratio of overall body height and segment masses as a percentage of total body weight, a procedure followed also in the present study.

All the above calculations produce a three dimensional system of three net forces and three net moments acting on the joint. These are used as input to the next step of the segment analysis. In the swing phase, when no external forces act (air resistance is considered negligible) on the segment, only the gravitational and inertial effects of the mass are considered to act on the most distal segment of the lower limb. The above phenomenon characterizes the upper limb segments in the equivalent analysis Opila et al. [1987]. Ignoring the mass effects in such analysis causes underestimations of the force actions of the joint which are, however, of small magnitude.

Any frame of reference can be used to express the above net forces and moments but for useful interpretation the general convention is to express them in the distal local frame of reference of the segment. (Ishai [1975]). Problems exist according to the way moment plots are presented in terms of which side of the joint is being considered. The notion that equal and opposite forces and moments occur in either side of the joint can be misleading. The convention followed here considers forces and moments as those applied by the distal segment on the proximal joint.

4.4 Measurement errors

Paul [1966] suggested that errors involved in the inverse dynamic approach indicated that it was possible to conceive errors up to 42% if the errors in measurement and philosophy were considered to be additive. He concluded though that this was not the case and that the worst error involved was of the order of 15-20% (Paul [1970]). The classic work of Paul was followed by modern improved technology that reduced the error margin more. However, errors still exist, a fact to be considered in the interpretation of the data. One of the major sources of error is that of the skin and soft tissue movement relative to the underlying bone structure (Cappozzo et al. [1988]). The result of that is inaccuracies of the prediction of the assumed joint centre locations. Another source of error is that the polycentric nature of certain joints, such as the knee (Blankevoort et al. [1988]), is ignored by the assumptions of the models.

4.5 GAIT ANALYSIS-MODELS

The methodology used in the present study required a mathematical model allowing gait evaluation of the subjects participating in tests. This model referred to as Gait-1

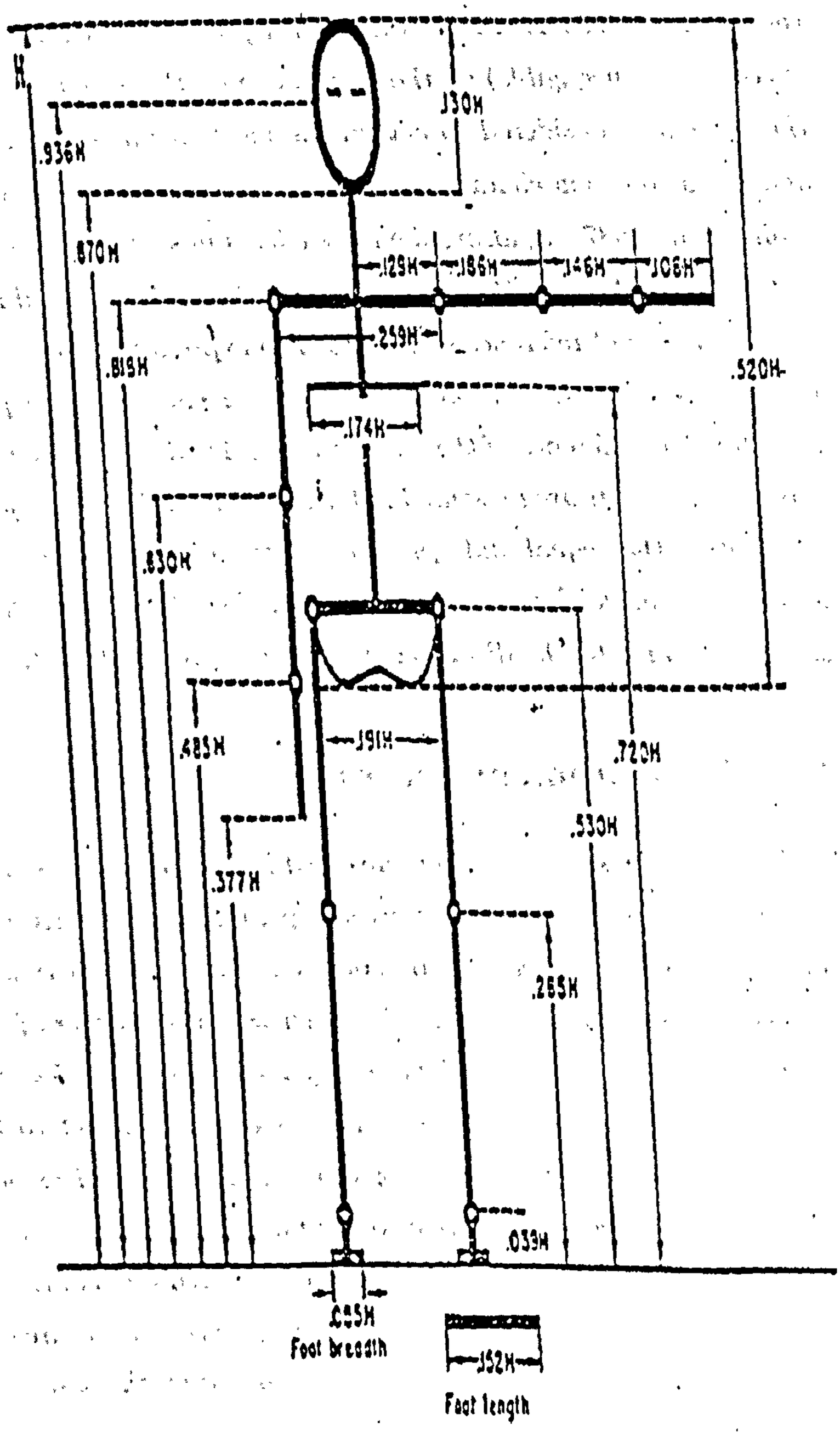

Figure 4.3: Segment length as a ratio of overall body height (Drillis et al. [1966]

uses the marker positions presented and analytically explained in APPENDIX A. This model was mainly used in the evaluation of normal gait, as well as in the footwear studies and turning studies. Using this model, within and between subject variability of the intersegment load behaviour for different activities can be assessed. The number and position of markers allows fast data aquisition, processing and analysis. It should be pointed out here that keeping the number of markers to less than 20 improved the recording and interpretation of the kinematic history of each marker. It seems that the history of the pathway that each marker follows in space is much faster and better evaluated using the current software when markers are kept at considerable distance from each other which is possible only when a certain number is used at the lower limbs.

The second model Gait-2 was used to provide the external loads to the three dimensional model of the knee described later in this chapter. The model differs from Gait-1 in the sense that the coordinate systems and knee joint centre estimations ought to match those of the remaining input data adopted by the model (see APPENDIX A for the marker's positions for Gait-2 and Gait-1 models). The latter coordinate systems refer to the muscle and ligament origin and insertion coordinate systems of the source studies (Brand [1992], Brand et al. [1982]).

4.6 Shortcomings of the Methods

The reduction and optimization methods for solving the distribution problem have a number of associated shortcomings and assumptions.

4.6.1 Modelling Assumptions

Regardless of the solution methodology used, the equilibrium equations are the equality constraints that must be satisfied in the distributed process. In expressing these equilibrium equations, biomechanists characteristically make a number of standard modelling assumptions. The first of these is that only the muscles, ligaments and bony contact regions transmit significant forces in the neighbourhood of the joint. Strong support for this assumption may be inferred from the growing body of experimental evidence describing the stress-strain/strain rate/strain history characteristics of the various anatomical structures in the joint neighbourhood. Thus the forces transmitted by the skin, blood vessels, nerves, etc., are regarded as negligible compared to

those forces transmitted by the muscles, ligaments and bony contact regions Andrews [1982].

The second standard modelling assumption is that all joint geometry, or all geometrical information contained in the equilibrium equations, is determinable or known. This implies that, in addition to modelling the joint as an axis, the lines of action of all muscle and ligament forces have been established (e.g., the straight line model as discussed by Jansen et al. [1975] or the data from the SIMM approach by Delp et al. [1996b]. Hence, the directions and moment arms of all muscle and ligament forces, and the points of application of all bony contact forces, are regarded as known.

The third standard modelling assumption is closely associated with the second and is incorporated by neglecting the resultant "local" moment effect when replacing the distributed force system present in any joint structure (e.g. muscle, ligament or bony contact region) by a single resultant force at a particular point in the joint neighbourhood Andrews [1982]. This assumption can always be satisfied, even for large joint structures, by simply sub-dividing these structures into a number of smaller components that each transmits its own resultant force and has no local resultant moment effect about the point of force application.

A fourth modelling assumption concerns the moment contributions of the ligament and bony contact forces to the resultant joint moment. These moment contributions vary from one joint to another and as the joint configuration and motion change. In addition, these moments are generally three-dimensional and have components parallel to all three joint axes (i.e., the flexion/ extension, abduction/adduction, and internal/external rotation axes). The standard assumption is that the moment contributions of the muscles to the resultant joint moment may by identified and separated from those due to the ligaments and bony contact regions, provided the relative motion at the joint in question takes place sufficiently far removed from the limits of the range of motion. Furthermore, this separability can be achieved either because the moment contributions of the ligaments and bony contact areas are regarded as negligible, or when they are appreciable they can be estimated. For some joints, it is reasonable to assume that ligament function is negligible during many activities and that there is only one region and one point of bony contact force application. If the joint centre is chosen to fall on the line of application of the bony contact force, this bony contact will not contribute to the intersegmental resultant moment.

The hip is a good example of such a simplified joint. At the hip, ligament function

is often ignored based on the clinical observation that motion at many body joints is restrained by ligamentous activity only near the extremes of the functional (i.e, physiological) range of joint motion. This assumption is further supported by the demonstration of small moments created by passive (i.e., non-contractile) elements with a physiological range of motion Vrahas et al. [1987]. If the bony contact force is then assumed to always act along a radial line through the common centre of the almost spherical acetabulum and the femoral head, and if that centre is defined as the joint centre, then the moment contributions of the muscles will be the only contributions to the resultant joint moment. Generally speaking, if joint motion is near the limits of the range of motion, both the ligaments and the bony contact forces can contribute significantly to the resultant joint moment. These contributions usually can not be separated from the moment contributions of the muscles.

4.6.2 Errors in Solution of Inverse Dynamics Problem

A number of different sources lead to errors in solving the inverse dynamics problem for the intersegmental resultants at the joint(s) in question. Errors of various magnitude and significance may be introduced in determining the location history of the body joints, in smoothing or filtering these data, and in differentiating the processed data to obtain velocity and acceleration quantities. In addition, errors of major significance may or may not be introduced in estimating the body segment inertia properties (i.e, segment masses, mass centre locations, and moments and products of inertia), and in experimentally measuring the applied external forces which influence the motion of the body segments.

4.6.3 Simplification of the Reduction Process

Nearly all joints of the body are crossed by a large number of musculotendinous units and ligamentous structures. In many instances, the situation is further complicated by relatively large and sometimes changing regions of articular contact rather than single points. In the reduction process, muscles and ligaments are often neglected or grouped together using anatomical or functional arguments to achieve a determinate distribution problem. In addition, antagonistic muscle activity, if present, is mostly ignored, and EMG data, based on arbitrarily-chosen levels of signal intensity, are often used to determine when muscles are active. These simplifications, taken together,

may lead to substantial errors in determining the actual forces transmitted by the anatomical structures present in the joint neighbourhood Nissan [1980].

4.6.3.1 Assumptions in Optimization Procedure

The optimization procedures seek a solution (i.e., a set of muscle, ligament, and bony contact forces), subject to the equality constraints of the equilibrium equations, such that some function of these unknown quantities is minimized. In addition, inequality constraints are often imposed to the unknown scalar muscle, ligament and bony contact forces. These constraints include the requirement that muscle and ligament forces be tensile, and the requirement that bony contact forces be compressive. In addition, each of these forces may also have a maximum permissible value. However, the most important factor in employing the optimization method is that a physiologically reasonable cost function is not known apriori, and one must be chosen and subsequently validated. Previous researchers have used a variety of linear and nonlinear cost functions that depended on muscle forces or muscle stresses.

Pedotti et al. [1978] and Crowninshield et al. [1981] have suggested that nonlinear criteria based on muscle stresses may give more realistic predictions in many cases, particularly in those instances when endurance is clearly an important factor in muscle selection.

Grosse-Lordeman et al. [1937] first proposed a nonlinear quantitative relationship between a muscle's contractile force and the maximum time for which the contraction could be held. This muscle force-endurance relationship was proposed to be of the form

$$lnT = -n * lnf + C \tag{4.10}$$

where T is the maximum time of contraction, f is the contractile force, and n and C are experimentally determined constants. More recently, several experimental studies reported values for these constants in the proposed muscle force-endurance relationship (Gunnar [1963], Kaijser [1970], Hermiston et al. [1975], Dons et al. [1979]). These experiments involved a variety of human muscular activities in both static and dynamic situations. The estimates of the constant n resulting from these studies vary from 1.4 to 5.1, with an average of about 3.0. Dons et al. [1979] showed that this muscle force-endurance relationship can be normalized to an individual's force

exertion capability. Fick [1911] and others have reported that the individual muscle force exertion capability can, at least in an approximate manner, be related to muscle cross-sectional area through a constant of proportionality with units of stress. Based on these reports, Crowninshield et al. [1981] assumed that in an approximate manner, the muscle force-endurance relationship is a basic property of the muscle tissue. Using these data along with information on muscle cross-sectional area, Crowninshield et al. [1981] suggested that minimizing muscle stresses to the third power will result in predicted muscle action that maximizes activity endurance.

In a lower extremity model of gait, Pedersen et al. [1987] used an optimization procedure with a cost function equal to the sum of the cubes of the muscle stresses to quantitatively determine lower extremity muscular activity in 47 muscle elements. They predicted muscle activity that generally agreed with EMG data on a temporal basis. However, they emphasized that while the criterion of maximum endurance might be reasonable for an activity such as level walking at a comfortable pace (in which endurance is clearly a factor in muscle selection), it might not be reasonable for other activities such as climbing stairs, sprinting, or pathological gait. In such other cases, the body may instead select muscles through a very different criterion.

The other important parameter in cost functions that involves muscle stresses is the physiological cross-sectional area (PCSA). The PCSA is generally taken to be the muscle's volume divided by gross muscle length (an average cross-sectional area). It must be noted, however, that relatively little data on muscle PCSA can be found in the literature. Gross et al. [1976] have published one of the few reports of method and data related to the determination of PCSA. A similar report on the analysis of leg musculature was presented by Ripperger et al. [1980]. These investigators found that the particular values obtained for the muscle's PCSA were significantly dependent on the method of measurement.

Crownshield et al. [1978] showed that imposing an upper limit constraint on muscle stress compared with no muscle stress upper limit led to physiologically more reasonable forces in all muscles and to an increase in synergistic muscle action. They assumed that a muscle stress had an upper limit value a and the smallest value of a for which a solution to the problem existed was denoted ac. If the determination of muscle activity was to be made with a equal to ac then the predicted forces in the muscles would be proportional to their physiologic cross-sectional area.

The extent to which a was larger than ac determined the extent to which a pre-

dicted muscle force may vary from this proportionality. Small values of a encouraged the prediction of activity in synergist muscles while the use of large value of a may result in the predicted force as a single agonist. Furthermore, the muscle force predictions were sensitive to PCSA within the known ranges of variability of PCSA defined by volume over muscle fibre length Brand et al. [1986].

4.6.4 Validation of Results:EMG

Most previous researchers who used optimization methods have attempted to validate the cost function by comparing the predicted muscle activity patterns to the activity patterns inferred from EMG data. Such data clearly have a role to play in the prediction of muscle forces, and it may be incorporated in three different ways: (1) by using processed EMG signals to directly estimate muscle forces directly; (2) by using EMG signals above some arbitrarily selected level of intensity as a temporal constraint on the presence of muscle activity; and (3) by using EMG signals to temporally validate mathematically estimated muscle activity.

The use of processed EMG signals to estimate individual muscle force during contraction is based on the assumption that a quantitative relationship between the EMG signal intensity and the muscle force magnitude is known or exists and can be determined. However, at the present time such a relationship has been shown to exist only for isometric contraction, and no reliable results are yet available or have yet been established for more complex situations Olney et al. [1985].

The second use of EMG data is as a temporal constraint on the existence of muscle activity. In this case, a threshold level of EMG signal intensity is selected to determine when a muscle is active or inactive. Only those solutions to the distribution problem that predict muscle forces when the muscles are shown to be active by this EMG criterion are allowed. The technique may therefore eliminate many mathematically feasible solutions to the indeterminate distribution problem, but it ensures a solution that is physiologically more realistic than those produced without the use of such constraints. Morrison [1970] and Chao et al. [1976] have both discussed such a technique. Several limitations exist, however. First, a threshold of activity must be established to avoid the problem produced by the presence of minor signals that do not reflect physiologically significant contractions. Second, the mathematical solution may be physiologically unreasonable since no consideration is given to the intensity of

the EMG activity. Third, the kinematic and kinetic data which are used as the basis for the muscle force predictions, as well as the EMG data, should be obtained simultaneously. This is due to the fact that EMG data can vary considerably from trial to trial, even for a given activity for a given person. Failure to make all measurements simultaneously can therefore lead to results that are open to question.

The third use of EMG data in solving the distribution problem using optimization techniques is as a validation tool alone. Muscle forces are first estimated mathematically without the use of EMG data, and the resulting muscle activity patterns are then simply compared to EMG activity patterns on a temporal basis. The mathematical solutions are then considered to be temporally validated (but not quantitatively validated) if there is good subjective agreement between the predicted and measured activity patterns. Such validation is subject to limitations similar to those described for the use of EMG signals as a constraint Pedersen et al. [1987]. Estimating the forces present in the anatomical structures at a joint is an important task for a variety of reasons, and it typically involves the solution of an indeterminate distribution problem. Using the reduction method to solve the indeterminate distribution problem requires many simplifying assumptions and has many corresponding limitations. Simplified models with unrealistic anatomical and physiological assumptions may produce invalid results and offer no assurance of accuracy. The use of optimization methods to solve the indeterminate distribution problem is also fraught with difficulties. The results are sensitive to the choice of cost function, and validation of this function is difficult. However, the use of optimization techniques seems preferred when an appropriately validated cost function can be identified.

Hof [1991] studied the EMG to force processing (Hof et al. [1987], Hof et al. [1981b], Hof et al. [1983], Hof et al. [1981d], Hof et al. [1981c] Hof et al. [1981a]). The force of a muscle or the corresponding muscle Hof et al. [1981b] moment with respect to the joint is determined from EMG and muscle length by means of a model of the muscle's contractile and elastic properties. In kinetic analysis the joint moment is calculated from the ground reaction force and the positions and accelerations of the body segments by means of Newtonian equations, based on a rigid body segment model. These two fundamentally different methods have been compared by determining simultaneously the calf muscle moment and the total ankle moment in walking at slow, moderate and fast speed and in stepping up and down a low bench. As long as there is no activity of other muscles, the moments obtained by either method should be identical. The

analysis was restricted to such periods, as assessed from the EMG of tibialis anterior. In each experimental condition three steps were analyzed in five subjects of 21-22 yr. In comparison with the results of kinetic analysis, EMG processing shows differences between 7 and 54 Nm r.m.s., with an average of 22 Nm r.m.s. Normalized with respect to the r.m.s. value of the moment itself, the differences amount to 0.13-0.51, with an average of 0.22. In the majority of cases there was no systematic deviation between EMG processing and kinetic analysis and the r.m.s. difference was of the same order of magnitude as determined previously in ergometer experiments. Elsewhere, Hof et al. [1983] investigated the calf muscle moment, work and efficiency in level walking and the role of series elasticity. He reported that, the moment and work of the human calf muscles in level walking were determined by means of an EMG to force processor, based on a muscle analogue (Hof et al. [1981b]). Nine subjects (four women, five men) walked on a level treadmill at speeds between 0.5 and 2.5 ms^{-1}, in their self-chosen pace and at forced pace with steplengths between 0.3 and 1.1 m. The calf muscles are normally only active in the stance phase. The moment increases, with a variable course, to a peak just before push-off. This peak moment increases with the walking speed, from the reference moment (the value in standing on the toes with one leg) at zero speed, to 1.5-2.1 times this value at a speed of 2 ms^{-1}, and decreases at still greater speeds. During the roll-over phase work is done on the calf muscles ('negative work'), followed by positive work in push-off. The negative work is constant, 0.20-0.36 Jkg^{-1}, depending on the subject. The positive work increases linearly with steplength–not with speed–from zero at ca. 0.35 m to 0.50 Jkg^{-1} at a steplength of 1.1 m. The interaction between the contractile and the series elastic component in the muscle could be studied by means of the analogue. A great part of the work done on the muscle and of the positive work done by the contractile component are stored in the series elastic component. The stored energy is released at a high rate in push-off. This mechanism ideally requires a concerted contraction, i.e. a contraction in which the activation is matched to the load to the effect that the length of the contractile component remains constant. The muscle then behaves like a spring. Consequences are (a) only little of the negative work gets lost, (b) the length of the contractile component remains close to the optimum of the force-length relation, (c) the shortening speed of the contractile component is now in the range were the muscle works at a high efficiency, and (d) high power peaks can be delivered due to the 'catapult action'. During the experiment, electromyographic (EMG) signals where recorded for six to

eight muscle groups. For the EMG measurements performed at the the Laboratory of Ergonomics K.U. Leuven three types of EMG measurement systems are used:

TEMPS: computer controlled 8 channel EMG system, often used in combination with ergodyn. SPIER: computer controlled 8 channel telemetry EMG system. Commands are sent to SPIER via an infrared optical link. Measurements are transmitted to the computer via FM radio waves. SPIER is portable and used for gait analysis and testing where the test subject is required to make free movements. ME3000P: stand alone 4 channel EMG system. Data can be sent to a computer for analysis via a glass fibre link. (FOR DETAILS see APENDIX E:the use of EMG in Biomechanical analysis ERGONOMICS Laboratory K.U.L.). In FIGURE 4.4 on page 71 the Calculation of Force based on EMG measurements and the resulted activity levels of a series of muscles during a Gait cycle is presented.

This EMG-data is used to validate the results of the optimisation in the following way: for every-muscle group whose recorded EMG signals exist, we look for the occurrence of activity in the recorded data and in the computated (OPTIMISED) force and therefore validate the model and the cost function used for optimisation. Firstly, the points in time where both muscle force and EMG data show an activity in the muscle are recorded. This is called active concurrence. In the opposite case, where neither muscle force, nor muscle EMG shows any activity at the same point in time, we refer to non-active concurrence. In a form of equation it is:

$$activeConcurrence = 100 * (timeEMG_ON - and - force_ON)/(timeEMG_ON) \tag{4.11}$$

$$inactiveConcurrence = 100 * (timeEMG_OFF - and - force_OFF)/(timeEMG_OFF) \tag{4.12}$$

From the point of view of muscle force, a muscle is considered active if the muscle force reaches more then 5% of the maximal muscle force. From the EMG point of view active means that the activity reaches more then 20% of its maximum value.

Relation between activation and EMG is calculated by the differentiated EMG:

$$A(t_{n+1}) = p * A(t_n) + \sqrt{|E(t_{n+1}) - E(t_n)|}$$

where A(t) is the activity of the muscle
E(t) is the Raw EMG signal
p is constant = 0.9875 for 500 Hz EMG sampling
q is a constant to convert mechanical electrical units to mechanical

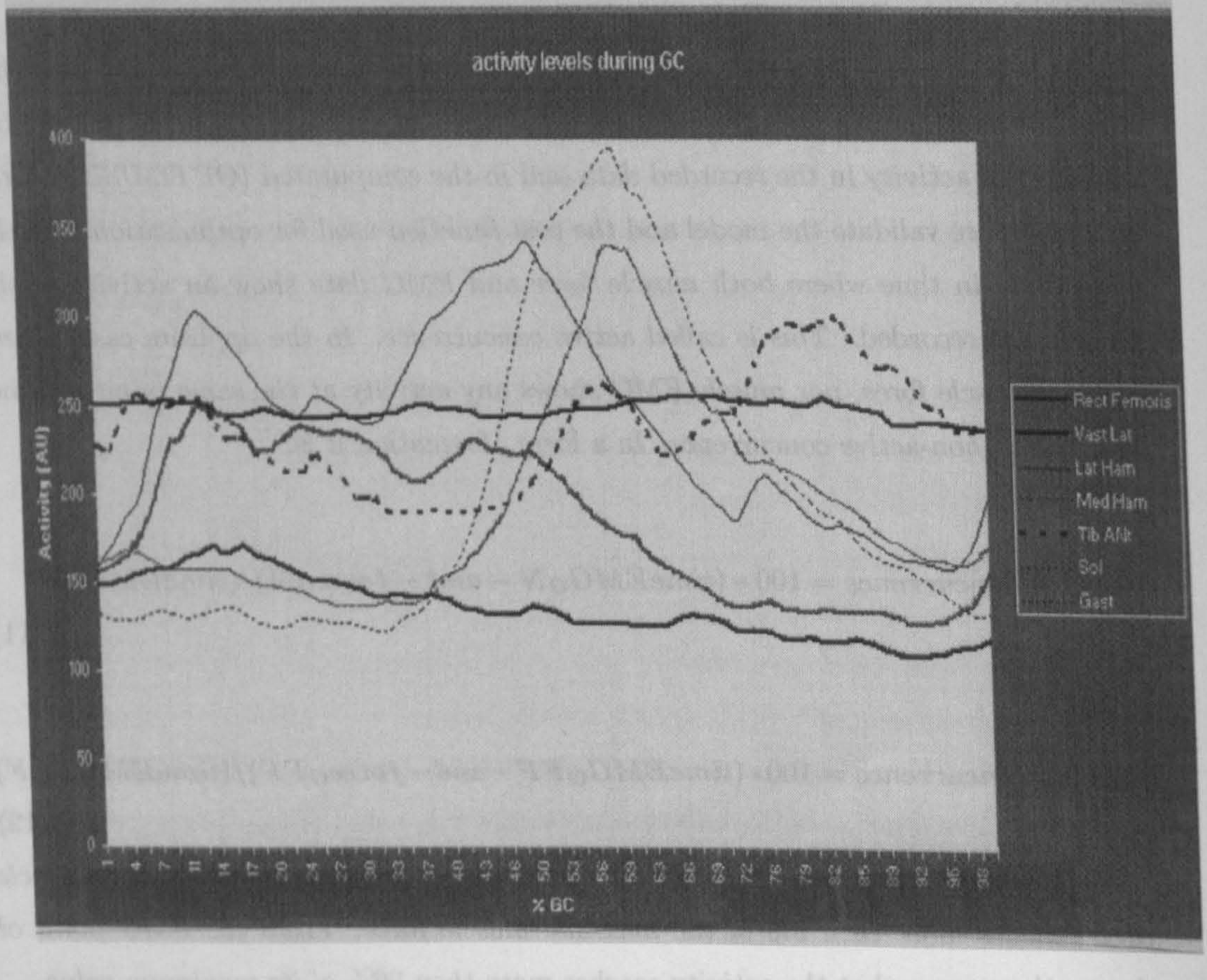

Figure 4.4: Calculation of Force based on EMG measurements and the resulted activity levels of a series of muscles during a Gait cycle:See APPENDIX E

Blank Page

Chapter 5

Biomechanical model of the knee joint

This chapter describes the mechanical model of the human knee used in the present study to solve the knee distribution problem. Six scalar joint equilibrium equations, with 13 unknown muscle force magnitudes, 13 unknown ligament force magnitudes, and two unknown bony contact force vectors, are formulated as an indeterminate system of equations that govern the distribution process. If the muscle and ligament forces are known, these six equations appear to determine the two bony contact forces uniquely, each with three scalar components. However it is shown that this system of equations is linearly dependent and no solution for the two bony contact forces exists. Therefore, to solve the problem, certain assumptions along with existing geometrical and anatomical data are used in a novel solution procedure. This procedure involves three distinct models, an optimization technique and an iterative solution process. The use of this procedure is demonstrated by solving for the bony contact forces. Several optimization criteria are investigated. The new iterative algorithm combining optimization techniques with other models is described and its significance is explained. The results obtained with the new procedure are compared with those in the literature. Finally, a discussion of assumptions and limitations of the model algorithm are discussed.

The following section contains a description of the mechanical model for the knee. A reference coordinate system based on a report by Brand et al. [1982] is described. Pedersen et al. [1987] used a simpler knee model and optimization procedures to

calculate the bony contact forces at the knee throughout the walking cycle. They found the maximum bony contact force to occur at 17% of the gait cycle (about 10° of knee flexion).

The anatomical and material data of the structures surrounding the knee are studied for 10° of knee flexion to predict the maximum bony contact force.

Section 7.2.6 contains the joint equilibrium equations and constraints for the model. If the muscle and ligament forces are regarded as known, the equilibrium equations form a system of six scalar equations with six unknowns (the two bony contact forces with three components each). As noted previously, no unique solution for the two bony contact forces can be obtained from these six equations. To obtain a solution, further assumptions to reduce the number of unknown bony contact force components are described. Also, use of these assumptions and their significance is explained.

Chapter 8 describes the new iterative algorithm for solution of the joint distribution problem. Various steps in the algorithm are explained and justified. Use of the joint equilibrium equations is delineated and assumptions made in the procedure are explained.

Section 8.2 describes the cost function used in the optimization models of the new iterative algorithm. The cost function is selected after solving the distribution problem with several candidate cost functions and comparing the final results.

In chapter 9 implementation of the new procedures is described. A few results using the new procedure are being compared with those in the literature.

Finally, in chapter 10, a discussion on the assumptions and limitations of the new model algorithm is attempted.

5.1 The Knee Distribution Problem

Knowledge of the forces transmitted across the knee is of importance in understanding knee pathomechanics, further development of reconstructive joint surgery, the design of mechanical components for partial or total joint replacement, and the understanding of joint lubrication. The knee is a primary weight-bearing joint, and there are various serious and commonly-occurring musculoskeletal problems that involve the knee and the anatomical structures that surround the joint.

As mentioned previously, there are six independent scalar equilibrium equations

that govern the three-dimensional distribution problem at any joint. At the knee, there are two separate and changing regions of tibiofemoral bony contact, and therefore two compartmental bony contact forces, each with three unknown components. The knee distribution problem is therefore indeterminate.

A lot of the studies of the knee distribution problem described in the present literature review share the limitations that are associated with the solution of the general distribution problem. One particular limitation is that those which identify only a single bony contact force or two bony contact forces without muscle force predictions provide no information about how the two bony contact forces actually share the load with muscle forces included in the model. In summary, it is clear that a relatively complete mathematical model which can be used to estimate the two bony contact forces and the forces present in the muscles and ligaments that traverse the knee is still not available. Such a model is needed to improve the understanding of how the bones, muscles and ligaments share the load at the knee during any activity of interest. The model ought to be enhanced by visualization methodologies, robust algorithms and user friendly environments to allow non-engineers to use it with a drastically reduced learning curve.

5.2 The Knee Model: Properties and Input Data

5.2.1 General Description of the Knee

Any realistic mechanical model of the musculoskeletal system in the neighbourhood of the human knee includes a representation of the proximal portion of the tibia, the distal portion of the femur, and those load-carrying structures that connect the femur to the tibia (ligaments, joint capsules and muscles).

The major functions of the ligaments (including the joint capsule) are to stabilize the joint, control joint motion, and prevent excessive motion. During gait, the knee permits a wide range of motion while acting in a weight-bearing capacity. Unlike the hip which relies largely on the shape of the articular surfaces to maintain the stability of the joint, the knee is dependent on a number of muscles and/or stabilizing ligaments which hold the adjacent bones together. The principal ligaments crossing the knee are the medial and lateral collateral and the anterior and posterior cruciate ligaments. Muscles, like ligaments, help fulfill the body's competing needs for mobility

and stability. Muscles serve a mobility function by generating tensile forces that produce the motion of one bony segment relative to the other. They serve a stability function by helping maintain proper contact between the joint surfaces throughout the range of motion. Neither the muscles nor the bony segments acting alone are capable of fulfilling all of the body's competing mobility and stability needs.

The menisci distribute the bony contact forces across the knee over a large area, and they offer some resistance to shear. Neglecting a meniscus in a knee model can be justified provided that the points of force application are chosen realistically, that localized stress distributions are not sought, and that all three components of the bony contact force acting at each point of application are somehow included in the model.

The patella is a sesamoid bone that transmits the forces in the quadriceps muscles to the tibia and femur. In determining those knee structures that transmit significant loads (and therefore contribute to the knee resultant force and moment) one may formulate the problem so that only those structures that are exposed and/or transected by a fictitious surface passing through the joint space and separating the femur from the tibia are considered. Such a surface transects the patellar ligament below the patella, and therefore reflects the presence of the patella only to the extent that forces transmitted by the quadriceps through this ligament must be included in the knee model. The effect of the patella pressing against the anterior surface of the femoral condyles is an external force on the femur that is already accounted for in solving the inverse dynamics problem.

5.2.2 The Mechanical Model of the Knee

The Mechanical Model used in this study to represent the musculoskeletal system in the neighbourhood of the human knee includes thirteen major muscles, thirteen ligaments and two bony contact forces (FIGURE 5.1 on page 80). The intersegmental resultant force (Fr) and moment (Mr) are determined by solving the inverse dynamics problem applied to a moving subject, and are considered to be acting on the tibia at the "knee centre" (see section 7.2.3). FcL and FcM represent the bony contact forces acting on the lateral and medial compartments of the tibial plateau respectively. Flj and Fmi represent the tensile forces present in the jth ligament and ith muscle, respectively. The vectors from the knee centre (origin of the knee reference frame) to the points of application of the two bony contact and the resultants of 13 ligament

and 13 muscle forces, are RcL, RcM, Rlj, Rmi, respectively.

The thirteen muscles included in this model are:

MUSCLE	**ABREVIATION**
Biceps femoris	*BF*
Gracilis	*GRA*
Rectus femoris	*RF*
Sartorius	*SART*
Semimembranosus	*SEMIM*
Semitendinosus	*SEMIT*
Tensor fasciae latae	*TFL*
Gastrocnemius medial head	*GASM*
Gastrocnemius lateral head	*GASL*
Biceps femoris short head	*BFS*
Vastus intermedius	*VI*
Vastus interalis	*VL*
Vastus medialis	*VM*

The thirteen ligament elements included in this model are:

LIGAMENT	**ABREVIATION**
anterior medial collateral ligament	*AMC*
deep medial collateral ligament	*DMC*
posterior medial collateral ligament	*PMC*
oblique medial capsular ligament	*OMC*
medial posterior capsular ligament	*MPC*
lateral posterior capsular ligament	*LPC*
oblique lateral capsular ligament	*OLC*
lateral collateral ligament	*LC*
deep lateral collateral ligament	*DLC*
anterior anterior cruciate ligament	*AAC*
posterior anterior cruciate ligament	*PAC*
anterior posterior cruciate ligament	*APC*
posterior posterior cruciate ligament	*PPC*

The lines of action of the muscles and the ligaments are considered to be straight lines directed between the respective origins and insertions.

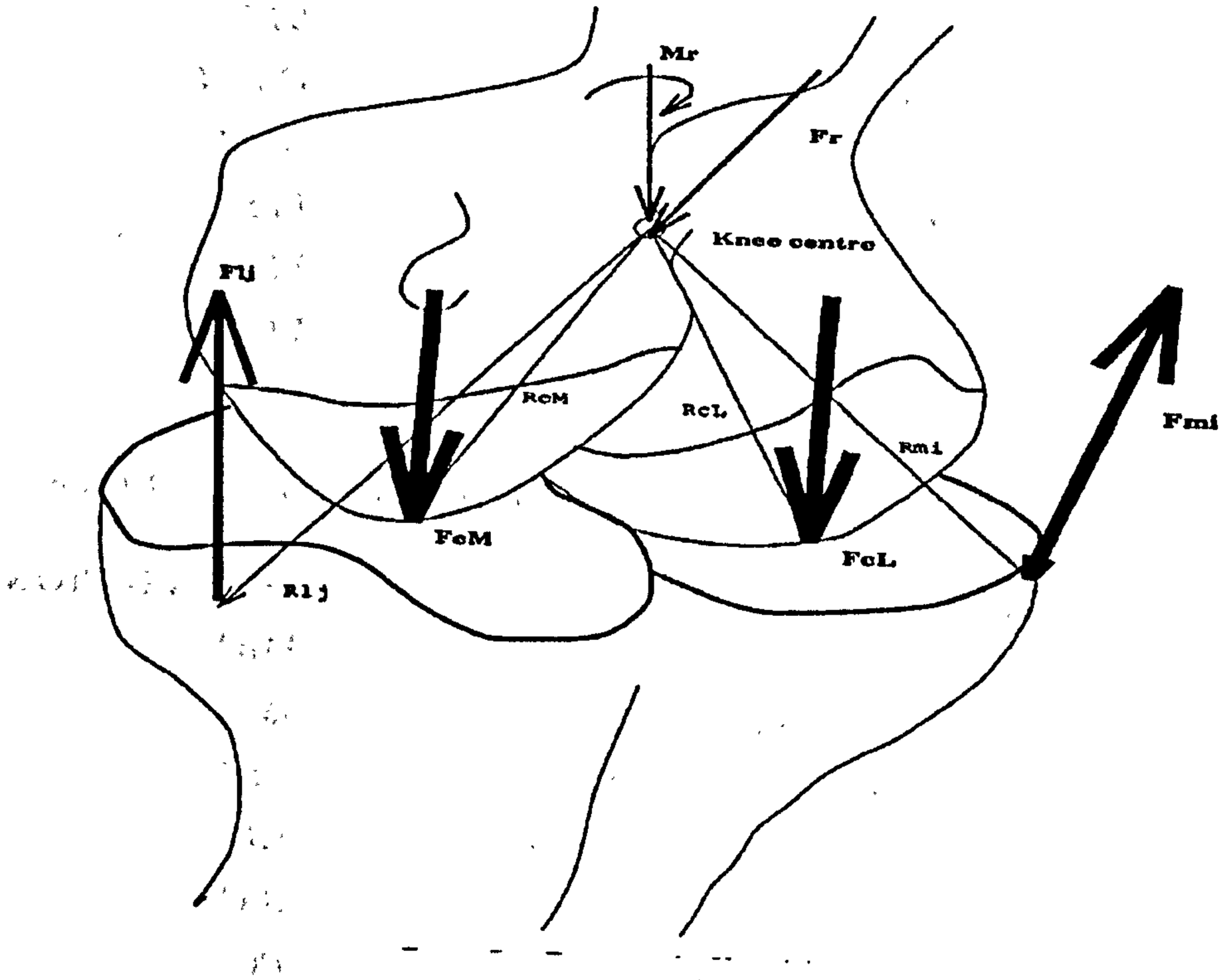

Figure 5.1: Forces at the Knee joint

5.2.3 Reference Coordinate System

Brand et al. [1982] reported a femur- based, rectangular Cartesian reference frame which will be adopted here. This reference frame has its origin at the midpoint between the medial and lateral femoral epicondyles, with X, Y, and Z axis directions defined as

$$\bar{Y} = \bar{P}_3 - \bar{P}_2 \tag{5.1}$$

$$\bar{X} = \bar{Y} x \bar{P}_1 - \bar{P}_2 \tag{5.2}$$

$$\bar{Z} = \bar{X} x \bar{Y} \tag{5.3}$$

where x denotes the vector cross product, X, Y, and Z are vectors in the three positive coordinate directions, P1 the vector locating the lateral epicondyle, P2 the vector locating the midpoint of the line joining the medial and lateral epicondyles (the origin of the reference frame), and P3 the vector locating the femoral head centre (Figure 5.2 on page 78). The moment for each of the force elements in the model is calculated with respect to the origin of the knee reference frame (K.C.).

5.2.4 External Loads

The input loads on this mechanical knee model are the intersegmental resultant force and moment values that were calculated using the Gait models described in sections6.1 to 6.7. Body segment inertial properties, segment accelerations and foot- floor reactions were used as input into a Newtonian formulation of the equations of motion, to solve the associated inverse dynamic problem for the variable intersegmental resultant force and moment vectors at the knee.

5.2.5 Mechanical Properties of the Model

The geometric and material data used in this model are based on other investigations as described below.

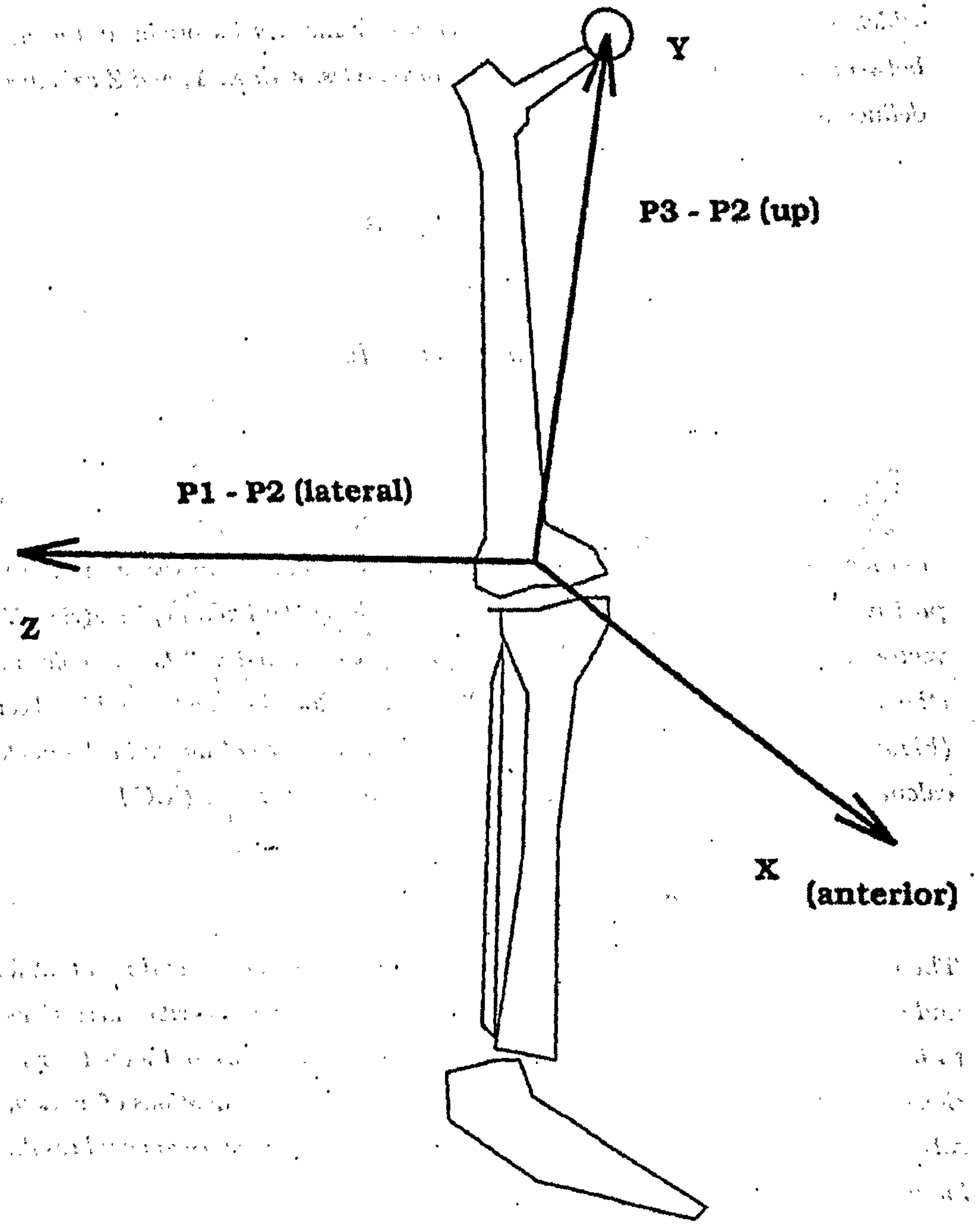

Figure 5.2: Reference Coordinate system

5.2.5.1 Location of Bony Contact Points

The bony contact area and pressure distribution of the tibiofemoral joint, as well as the assumed contact "points" are dependent on the angle of flexion-extension, on the applied loading condition, and on the involvement of menisci.

The points of application of the two bony contact forces on the tibial plateau are calculated from data given by Ahmed et al. [1983]. In the present mechanical model, which aims to solve the distribution problem with special attention to the two bony contact forces, accurate determination of these points is important since their location will affect critical moment values. Several investigators have used the pressure distribution to determine the bony contact area, including Ahmed and Burke. Harrington [1983] assumed that the centre of pressure was the effective contact point; its limiting location from the midpoint of the epicondyle axis was W/4, where W is the bicondylar width.

Walker et al. [1972] showed the dependence of the location and size of contact areas on flexion angle in cadaver knee joints for a load of 1500 N applied for 5 s along the long axis of the tibia. Results were obtained from four knees, considering flexion angles from 0 to 120 degrees. Measurements were made directly from castings of the joint cavity. Average contact areas were calculated from measurements of radii of curvature and joint configuration. Average contact areas for lateral and medial condyles were 1.4 cm^2 and 1.8 cm^2 , respectively. Both condylar contact areas diminished as flexion angle increased.

Fukubayashi et al. [1980] studied seven knees to determine the contact area and pressure distribution of the tibiofemoral joint under various loads, but only at 0 degrees of flexion, using a casting method and special sensor sheets. At a load of 1000 N the contact area of the knee was 11.5 cm^2 with menisci and 5.2 cm^2 without menisci. The menisci occupied 70 per cent of the total contact area. Peak pressure at 1000 N load was 3 MPa with the menisci and 6 MPa without them. High pressure areas were located on the lateral meniscus as well as the uncovered part of the articular cartilage in the medial compartment. After removal of the menisci the contact area decreased to below one half that of the intact knee and the contact pressure increased considerably. These data prove that the menisci have important load bearing and load spreading functions.

Brown et al. [1984] reported contact stress distributions measured across the

tibiofemoral joints of 11 fresh-frozen normal cadaver specimens. Local stress magnitudes were sensed by arrays of miniature piezoresistive transducers inset superficially in the cartilage of the femoral condyles. Knee joints were tested at 0, 10 , 20 and 30 degrees of flexion and later retested at 0 degrees following medial and dual meniscectomies. For the intact joint, both the spatial mean and peak local contact stresses rose approximately linearly with the joint force resultant, reaching levels of 2.6 and 0.8 MPa, respectively, at 3 kN of applied load. Flexion angle variations in the range studied failed to cause significant changes in the major contact parameters.

Therefore, from the above studies, the bony contact area and pressure distribution of the tibiofemoral joint, as well as bony contact points are dependent on the angle of flexion-extension, on the applied loading condition, and on the involvement of menisci.

In the present study, experimental data from Ahmed et al. [1983] with menisci included are used to determine the bony contact points for different loads and flexion angles, using a grid interpolation technique to obtain the approximate pressure distribution. The method used to estimate the bony contact points required five steps.

1. Enlarge Ahmed and Burke's right knee figures (Figure 5.3 on page 84) to the scale used in this knee model.

2. Estimate the pressure at the centre of each cell in a superimposed rectangular (31x21) grid (Figure 5.4 on page 85).

3. Compute the respective compartmental pressure centres. The compartmental pressure centres are derived by averaging, respectively, the pressure distribution in the medial and lateral compartments of the tibial plateau.

4. Check the reliability of the interpolation technique (several different grid orientations and positions were tried in order to count the pressure points and integrate the pressure distribution with the corresponding areas).

5. Construct tables of pressure centres for the different contact load and extension-flexion angles by using a linear interpolation technique.

The transformed pressure centres at different contact loads and flexion-extension angles are listed in table 5.1 on page 86. The main assumption made in this part was to consider the centre-of-pressure coordinate in the Y-direction as a constant during

different loads and flexion-extension angles.

The possibilities for errors come from several sources: (1) inaccurate magnification by the use of a copying machine, (2) approximation of data points by linear interpolation, (3) finite mesh cell area (according to the mesh, the mesh cell area must be 0.000009 square metres; however, scaling errors could cause the mesh cell area to differ slightly from this figure), (4) computer round-off error (in this study, double precision was used in the program; the rounding error, therefore, will be very small in comparison with the above sources of error).

After integrating the pressure distributions over the corresponding areas, the differences between the intergrated loads and given loads by Ahmed et al. [1983] are in the range of 15%-30%. Since Ahmed and Burke did not report checking their distribution accuracy by intergration, it can not be assumed that this 15%-30% error is due solely to imprecisions in the present grid-interpolation technique.

The locations of the computed pressure centres have a maximum difference of 0.63 cm in the X-direction and 0.35 cm in the Z-direction for different load magnitudes. This means that different loads have greater influence on contact location in the anterior X-direction than in the lateral Z-direction. This also happens at the different flexion-extension angles. For the different flexion-extension angles, there is a 1.67 cm maximum difference in the X-direction and a 0.57 cm maximum difference in the Z-direction (Table 5.1 on page 86).

5.2.5.2 Muscle Locations and Relative Physiological Cross-Sectional Areas

An accurate model of a system requires identification of the system first. A useful model of a muscle requires some identification of its different properties and the parameters that scale these properties. Different authors have tried to find out how muscles function and how the force generating properties are influenced in the dynamic muscle systems.

The main architectural features that influence muscle properties, as stated by Wickiewicz et al. [1983], are: 1. The physiological cross-sectional area (PCSA), i.e. the number of sarcomeres in parallel. This is directly related to the total amount of tension that the muscle can produce. 2. The fibre length, or the number of fibres in series. This length does not differ significantly within one muscle. The maximum

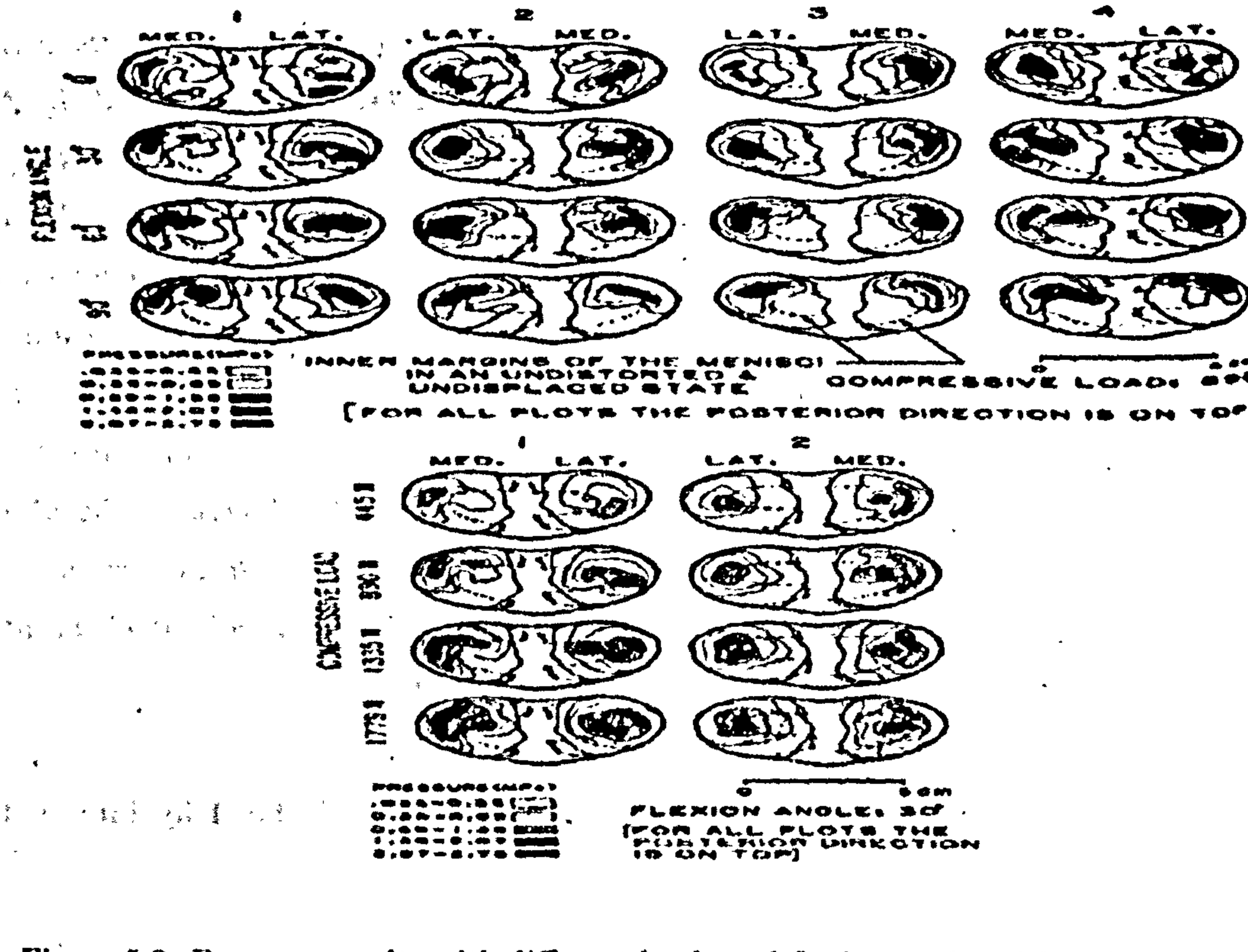

Figure 5.3: Pressure results with different loads and flexion angles, After Ahmed et al. [1983]

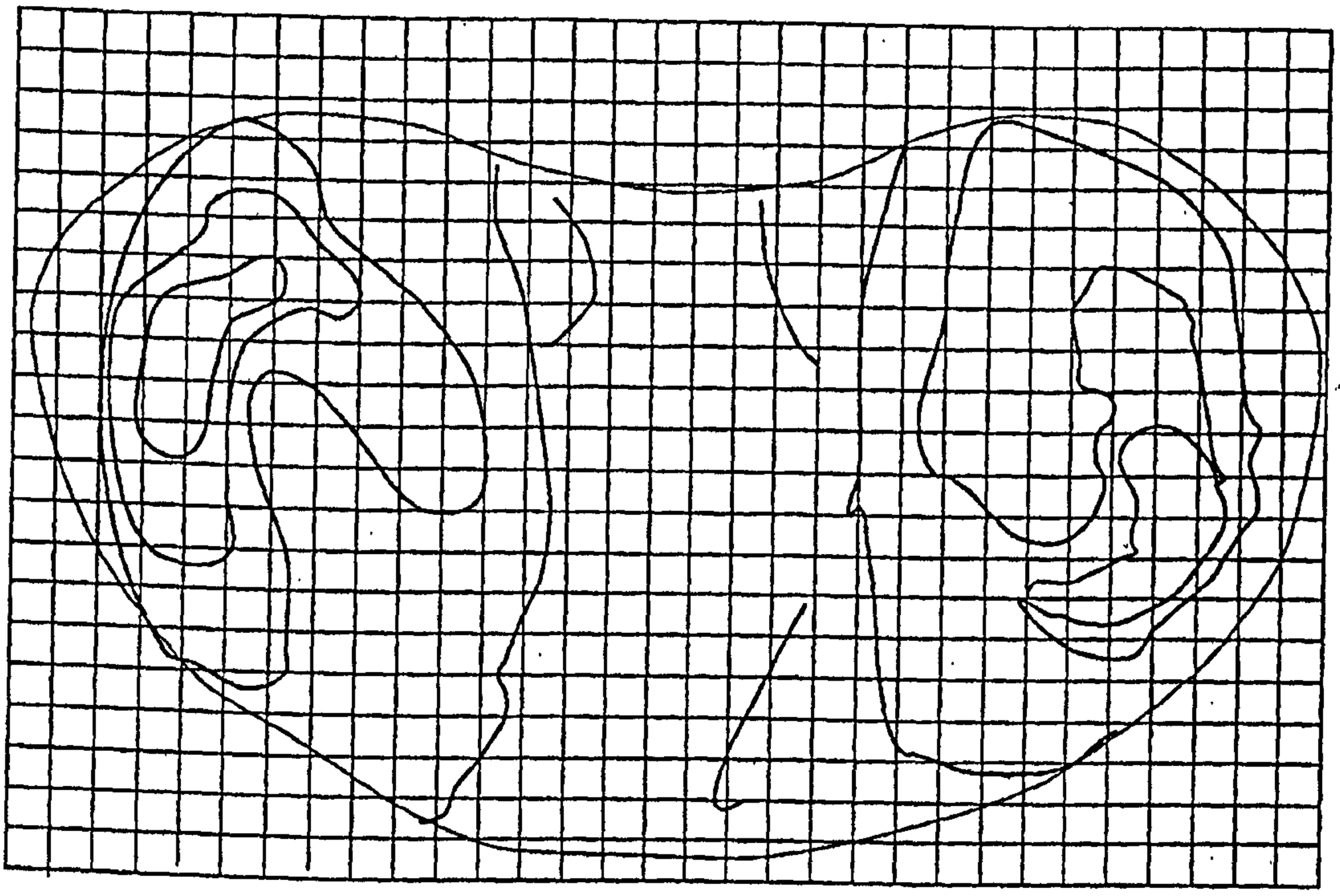

Figure 5.4: Mesh for interpolation

Degree	Load (N)	X-lat	Y-lat	Z-lat	X-med	Y-med	Z-med
0	445	-.2227	0.55	-.1720	-.2220	0.55	-.2132
0	890	-.2240	0.55	-.1705	-.2253	0.55	-.2130
0	1335	-.2229	0.55	-.1706	-.2219	0.55	-.2137
0	1779	-.2275	0.55	-.1704	-.2282	0.55	-.2103
10	445	-.2236	0.55	-.1722	-.2232	0.55	-.2135
10	890	-.2248	0.55	-.1707	-.2265	0.55	-.2133
10	1335	-.2237	0.55	-.1707	-.2232	0.55	-.2140
10	1779	-.2283	0.55	-.1706	-.2295	0.55	-.2105
20	445	-.2244	0.55	-.1723	-.2245	0.55	-.2137
20	890	-.2256	0.55	-.1709	-.2278	0.55	-.2136
20	1335	-.2245	0.55	-.1709	-.2244	0.55	-.2143
20	1779	-.2291	0.55	-.1708	-.2307	0.55	-.2108
30	445	-.2252	0.55	-.1725	-.2258	0.55	-.2140
30	890	-.2264	0.55	-.1711	-.2291	0.55	-.2138
30	1335	-.2253	0.55	-.1711	-.2257	0.55	-.2145
30	1779	-.2299	0.55	-.1710	-.2320	0.55	-.2110
40	445	-.2293	0.55	-.1737	-.2266	0.55	-.2137
40	890	-.2305	0.55	-.1723	-.2299	0.55	-.2136
40	1335	-.2394	0.55	-.1723	-.2265	0.55	-.2143
40	1779	-.2340	0.55	-.1722	-.2328	0.55	-.2108
50	445	-.2303	0.55	-.1741	-.2268	0.55	-.2137
50	890	-.2316	0.55	-.1726	-.2301	0.55	-.2135
50	1335	-.2304	0.55	-.1726	-.2268	0.55	-.2142
50	1779	-.2350	0.55	-.1725	-.2330	0.55	-.2107
60	445	-.2313	0.55	-.1744	-.2270	0.55	-.2136
60	890	-.2326	0.55	-.1729	-.2303	0.55	-.2134
60	1335	-.2315	0.55	-.1729	-.2270	0.55	-.2140
60	1779	-.2361	0.55	-.1728	-.2332	0.55	-.2106
70	445	-.2313	0.55	-.1710	-.2311	0.55	-.2130
70	890	-.2326	0.55	-.1695	-.2343	0.55	-.2129
70	1335	-.2315	0.55	-.1695	-.2310	0.55	-.2136
70	1779	-.2361	0.55	-.1694	-.2373	0.55	-.2101
80	445	-.2318	0.55	-.1706	-.2317	0.55	-.2129
80	890	-.2330	0.55	-.1692	-.2350	0.55	-.2128
80	1335	-.2319	0.55	-.1692	-.2317	0.55	-.2135
80	1779	-.2365	0.55	-.1691	-.2379	0.55	-.2100
90	445	-.2322	0.55	-.1703	-.2324	0.55	-.2128
90	890	-.2335	0.55	-.1688	-.2357	0.55	-.2127
90	1335	-.2323	0.55	-.1688	-.2323	0.55	-.2133
90	1779	-.2369	0.55	-.1687	-.2386	0.55	-.2099
max. difference		.0142	.00	.0037	.0167	.00	.0046

Table 5.1: Coordinates of Bony Contact Points during Different Contact Loads and F-E Angles(calculated from Ahmed et al. [1983])

shortening velocity is determined by this fibre length. 3. The angle of pennation of the muscle fibre with respect to the line of its tendon of insertion. The previous mentioned properties (1 and 2) are affected by this angle q (multiplication with cos q and sin q respectively). These properties were measured on the 27 muscles of the lower limbs of three human cadavers. The authors found that some muscles are better suited for tension production (i.e. muscles with high ratio of PCSA to muscle weight) and others are better suited for displacement or shortening velocity (i.e. muscles with high ratio of average normalised fibre length to PCSA). According to Edgerton et al. [1987], the PCSA, fibre length and muscle mass are the primary determinants for maximal force, velocity and power respectively. They results show that the pennation angle usually has less influence on these parameters. Alexander et al. [1975] investigated the major knee and ankle dimensions of a cadaver, with special attention to the pennation patterns. These values are then used to calculate the in vivo forces after measurements of the ground contact forces during running, walking, jumping and landing after jumping. The authors notice that there might be an important error in the calculated values due to differences between the cadaver and the living subjects.

Friederich et al. [1990] presented a technical note that gives an overview of the sarcomere lengths of the muscles of the lower limbs of two cadavers. These values are important in estimations the force generating capabilities of a muscle based on the PCSA. The note mainly consists of tables with values of sarcomere lengths, muscle lengths, fibre lengths, standard deviations on those values, averages and PCSA's.

Orientation and moment arms of the muscles about a joint are also important parameters in the accuracy of muscle and joint force calculations. The report by An et al. [1984b], therefore compares currently available techniques, based on the authors' experience.

The reviewed techniques are divided into three main groups. Each of these examined techniques has its merits and its disadvantages. Each method is well suited for some muscles and less for others. (1) Geometric Measurement: This technique is best suited for those muscles crossing the joint with a well defined pulley constraint and known joint centre of rotation. This method provides not only the moment arms, but also the orientations of the lines of muscles action. (2) Tendon and Joint Displacement Method: This method allows the determination of only the moment arm in the plane of rotation. So, the moment arm can be accurately measured without knowledge of the axis of the centre of rotation. (3) Direct Load Measurement Method: This method

should, theoretically, provide the most accurate force and moment coefficients, simply because it deals with the load directly. However, from an experimental viewpoint, the direct load method is more demanding.

The anatomical data needed to calculate the directions of muscle forces (i.e., muscle insertions and origins) are taken from cadaver studies by Brand [1992]. The relative muscle cross-sectional areas (muscle volume/muscle fibre length) are taken from the study of Pedersen et al. [1987]. These relative muscle cross-sectional areas are used with muscle forces to calculate the muscle stresses. The insertions, origins and relative cross-sectional areas (X-areas) are listed in table 5.2 on page 93. The centerlines of the muscle elements (straight line assumption) are shown in FIGURES 5.5 on page 89 5.6 on page 90 . Note: The results from the straight line approach are compared with the results from the data of Delp et al. [1996b]. In this second approach the moment arms from SIMM (Software for Interactive Musculotendon Modelling) were used as input in the present study. A small review of the technique for the calculation of the moment arms used in SIMM is presented in APPENDIX D). In FIGURES 7.19, 7.20, the various muscles' moment arms as calculated by SIMM are presented.

The musculoskeletal geometry was obtained according to the following proccedure. To acquire the bone surface data, the bone surfaces are firstly marked with a mesh of polygons, and then the coordinates of the vertices are determined with a Polhemus three-dimensional digitizer. These coordinates were used to display the pelvis, thigh, shank, and foot bones on the computer graphics system (Silicon Graphics INDIGO2 MAXIMUM IMPACT, IRIX 6.4) as either wireframe objects or Gouraud shaded surfaces. Scaling and manipulation of the meshes is possible on this high performance workstation. Based on the anatomical landmarks of the bone surface models, the paths (i.e., the lines of action) of 43 musculotendon actuators were defined. Each musculotendon path is represented as a series of line segments. Origin and insertion are necessary landmarks and, in some cases, are sufficient for describing the muscle path (e.g., soleus is represented by a single line segment). In other cases, where the muscle wraps over bone or is constrained by retinacula, intermediate points were introduced to represent the muscle path more accurately (e.g., peroneus longus is represented by a series of six line segments). The number of muscle via points can depend on the body position. For, example, the quadriceps tendon wraps over the distal femur when the knee is flexed beyond some angle, but not when the knee is extended. Thus, additional points, called wrapping points are introduced for knee flexion angles greater

than 90 degrees that the quadriceps tendon wraps over the bone, rather than passes through the bone, in that range of knee motion.

On the computer graphics system, muscle paths were visually compared with paths defined by a commonly used set of muscle coordinates Brand et al. [1982]. In the anatomical position, the paths are similar. However, interactively changing the skeletal configuration revealed that several muscle paths reported by Brand (e.g., iliacus, gluteus maximus, and sartorius) passed through the bones or deeper muscles. This occurred because each muscle path reported by Brand is defined by only two points that were measured on cadavers in the anatomical position. Displaying the muscle paths along with the bone surface models is helpful because it clearly showed where muscle points and wrapping points were needed to properly constrain the musculotendon paths. The moment arms calculated were also compared to the measurements coming from cadavers reported in the literature Yamaguchi et al. [1989],Nemeth et al. [1983], Dul et al. [1985]. These comparisons showed that the muscle paths are anatomically correct, and generate moment arms that are consistent with previous investigations. Moment arms and musculotendon lengths are calculated with the following method. First, all muscle coordinates are transformed to a common reference frame. Moment arms (ma) and musculotendon lengths (lMT) are computed as shown in FIGURE 2APB in APPENDIX D). Equation (1) (see caption for FIGURE 2APB in APPENDIX B) provides a computationally consistent, mechanically correct method to determine moment arms for all types of joints. Equation (1) is equivalent to computing moment arms with a vector cross product for ball-and-socket and revolute joints. Hoy et al. [1990]. Tables 5.16 on page 109, 5.17 on page 109 present the Musculotendon Parameters For Lower Limb Muscles from Friederich and Brand (1990) Brand et al. (1986) Wickiewicz et al. (1983) used in the models.

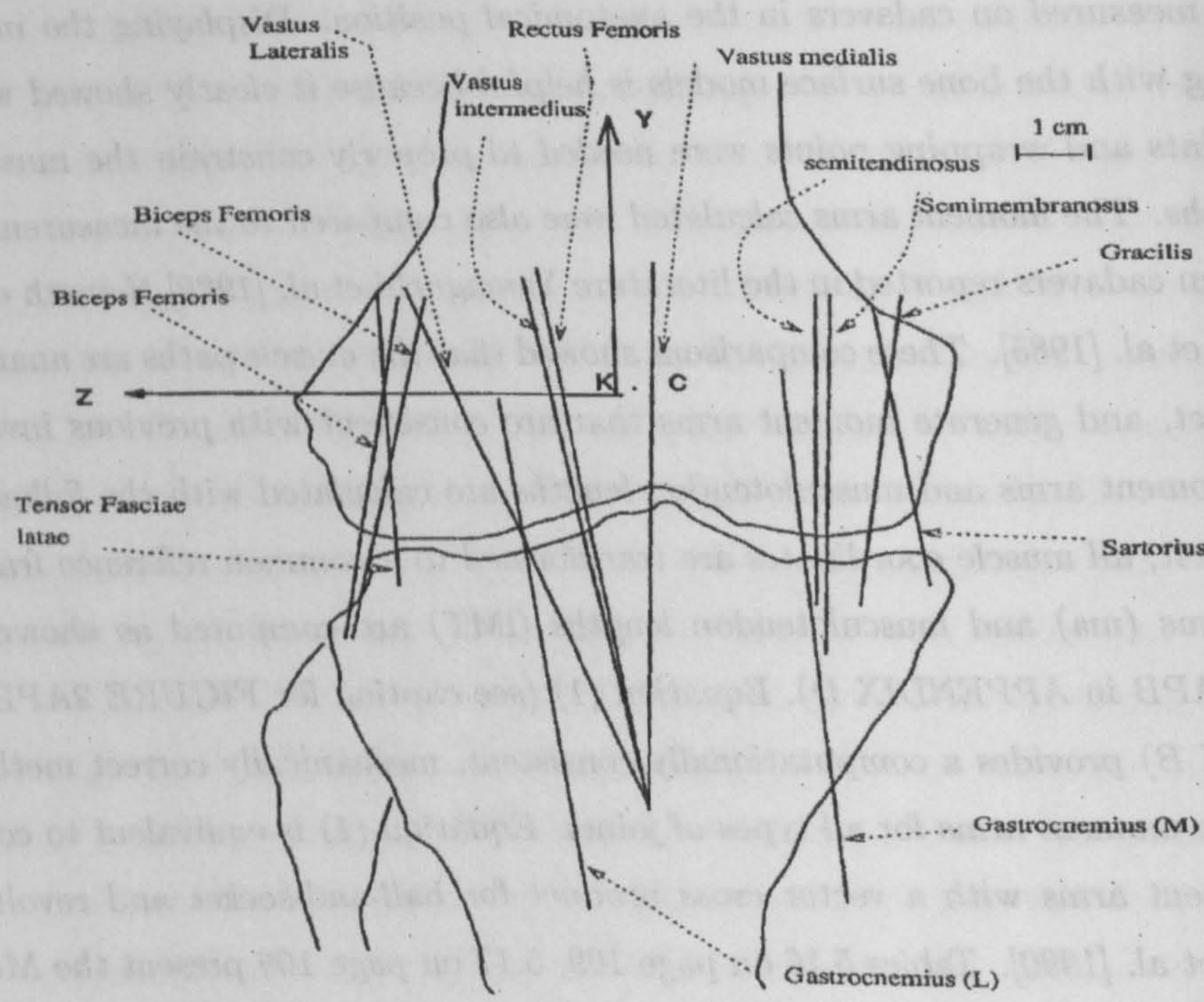

Figure 5.5: Anterior-posterior view of the muscle elements-Right lower limb

5.2.5.3 Ligament Locations and Lengths

The anatomical data needed to calculate the directions of ligament forces (i.e., ligament insertions and origins) are derived from regression coefficients reported by Wilson [1978]. However, some ligament locations calculated from his regression coefficients were not appropriate (e.g. they were far away from the bony segments). To ensure that data on the ligament insertions and origins corresponded to the muscle insertions and origins for the same specimen, the ligament origin and insertion data were scaled as in the study of Brand et al. [1982], and were superimposed on the computer generated straight line muscle model to insure reasonable locations. Since Wilson used a different coordinate system from Brand et al. [1982], it was necessary to use a transformation matrix to ensure that the ligaments coordinates coincided with the muscle coordinate system. The results are shown in Figures 5.7 on page 91, 5.8 on page 91, 5.9 on page 92 5.10 on page 92. After slight modification (maximum change of 1 cm in either direction) based on anatomical experience and comparisons with textbooks, the results are shown in Table 5.3 on page 93.

The ligament forces are estimated using a nonlinear spring model. The ligament properties (ligament length, unstrained length, spring constant, force and cross-sectional area) needed in the calculation procedures are discussed in the following paragraphs.

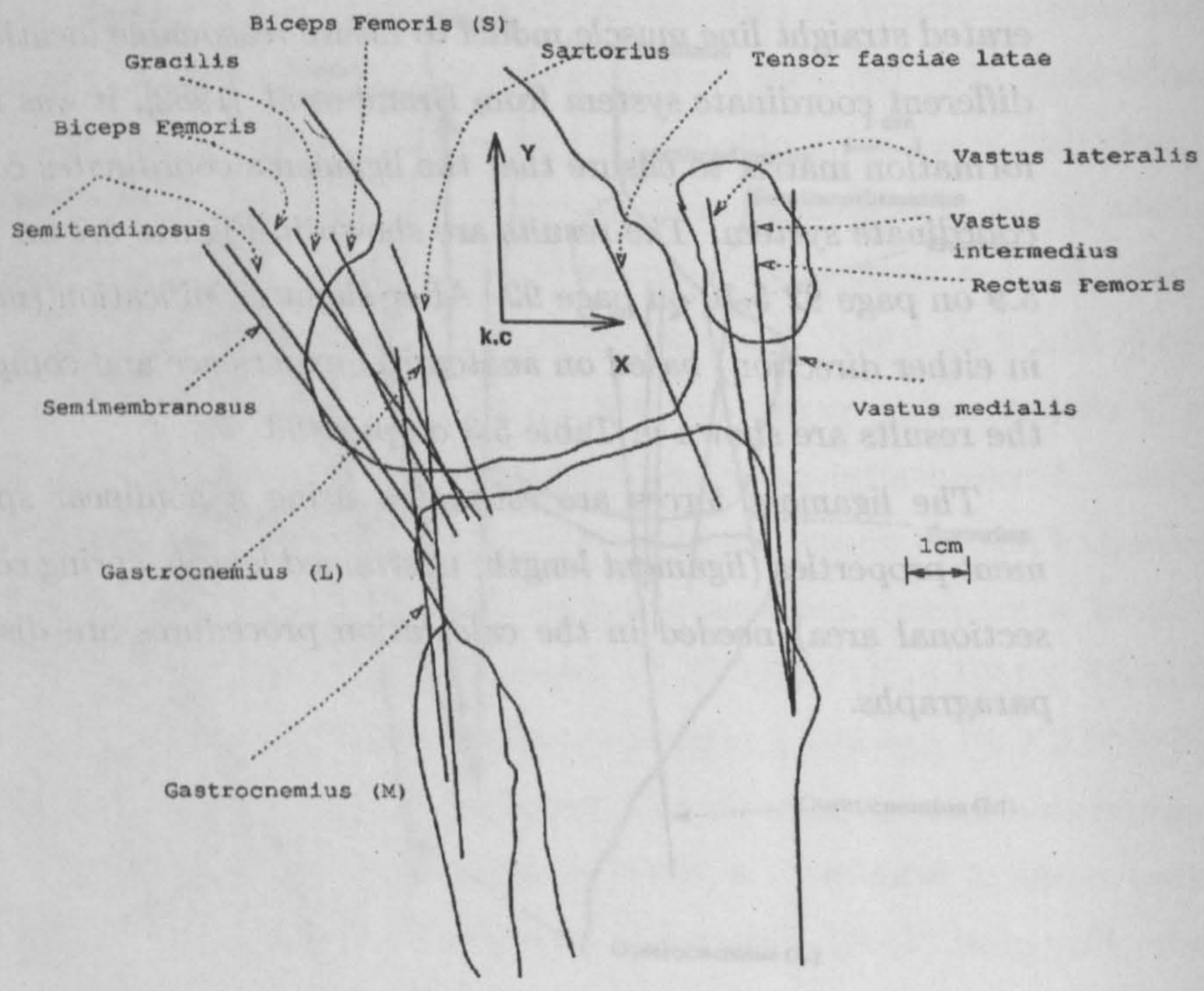

Figure 5.6: Medio-lateral view of the muscle elements-Right lower limb

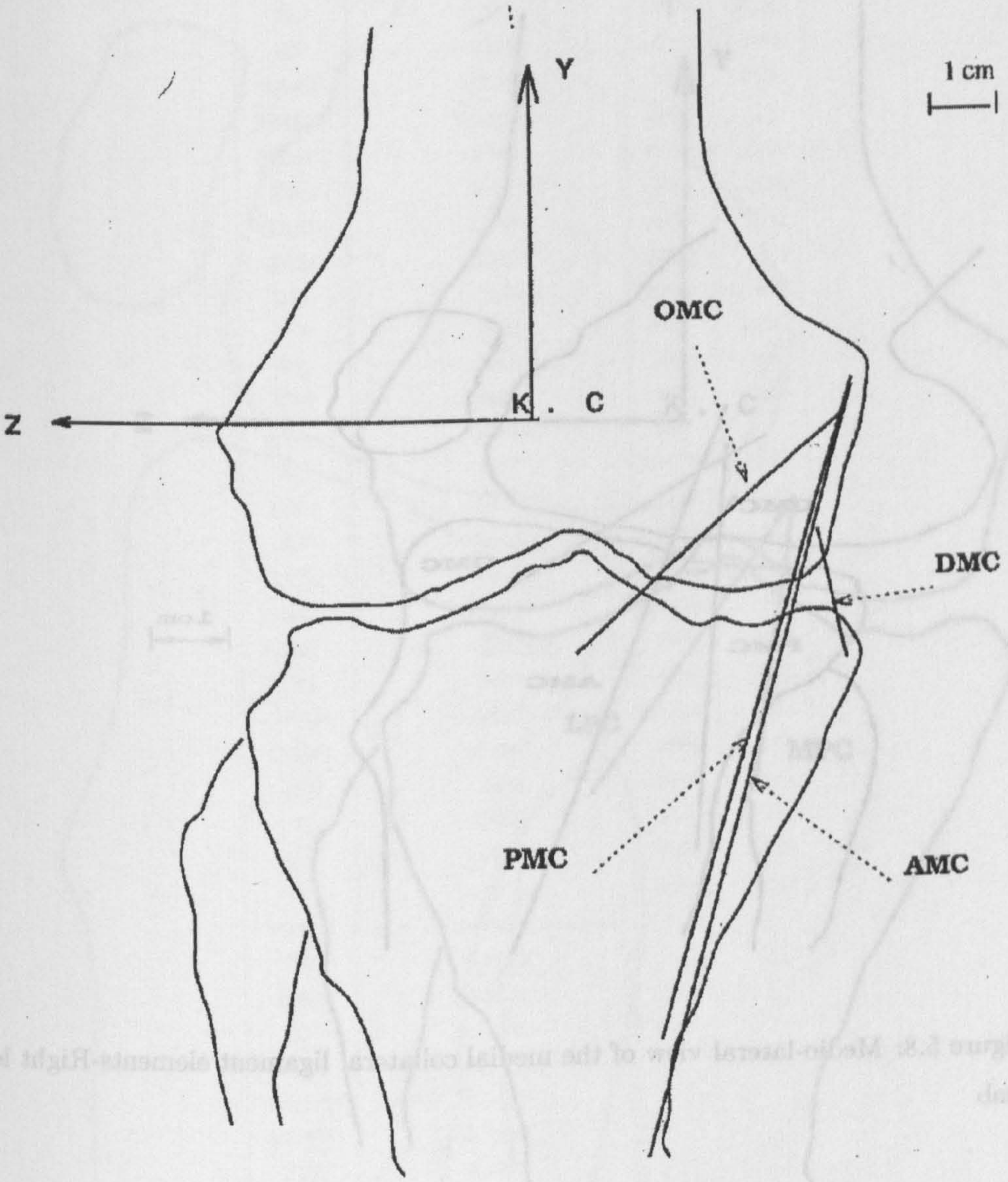

Figure 5.7: Anterior-posterior view of the medial collateral ligament elements-Right lower limb

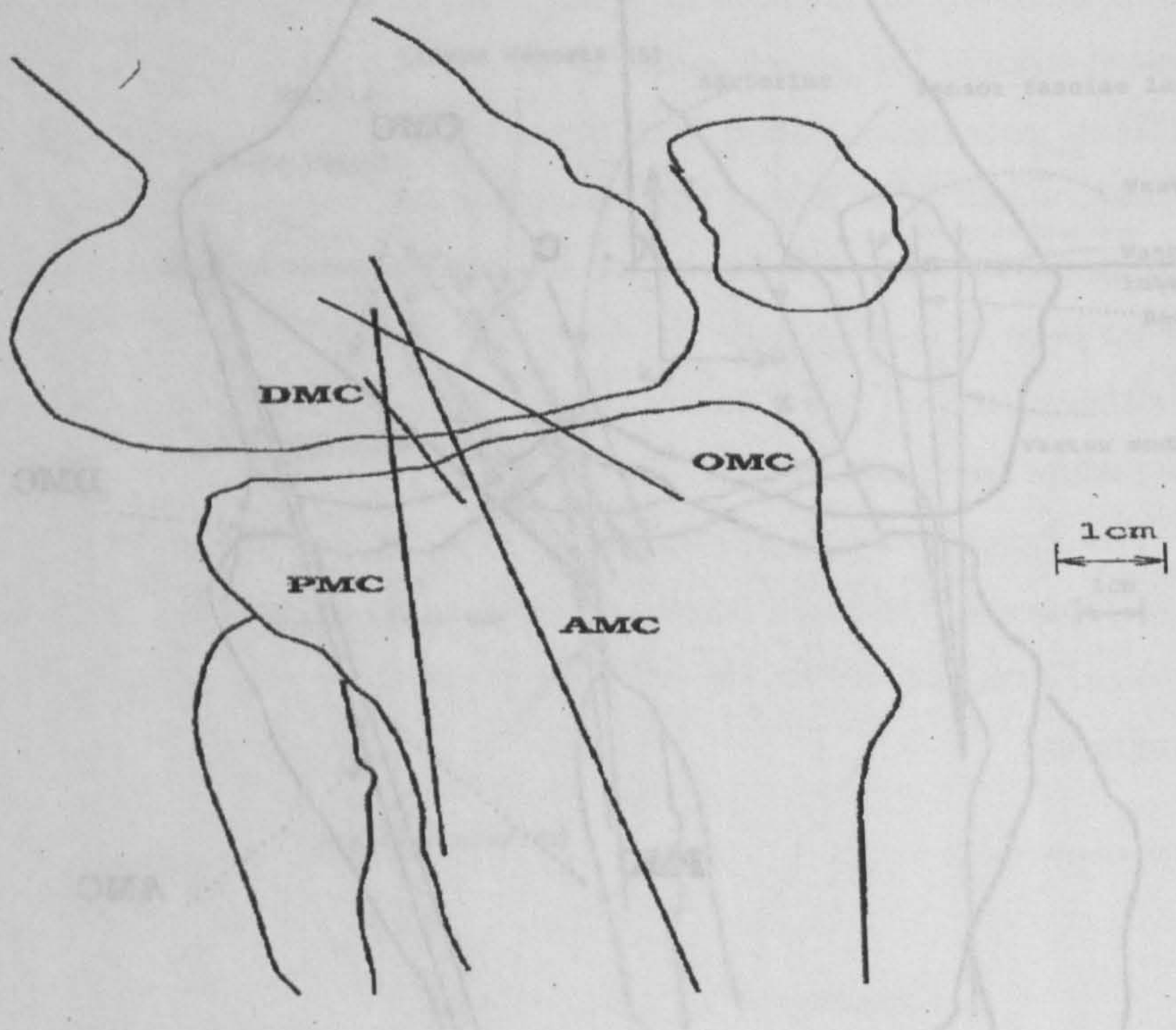

Figure 5.8: Medio-lateral view of the medial collateral ligament elements-Right lower limb

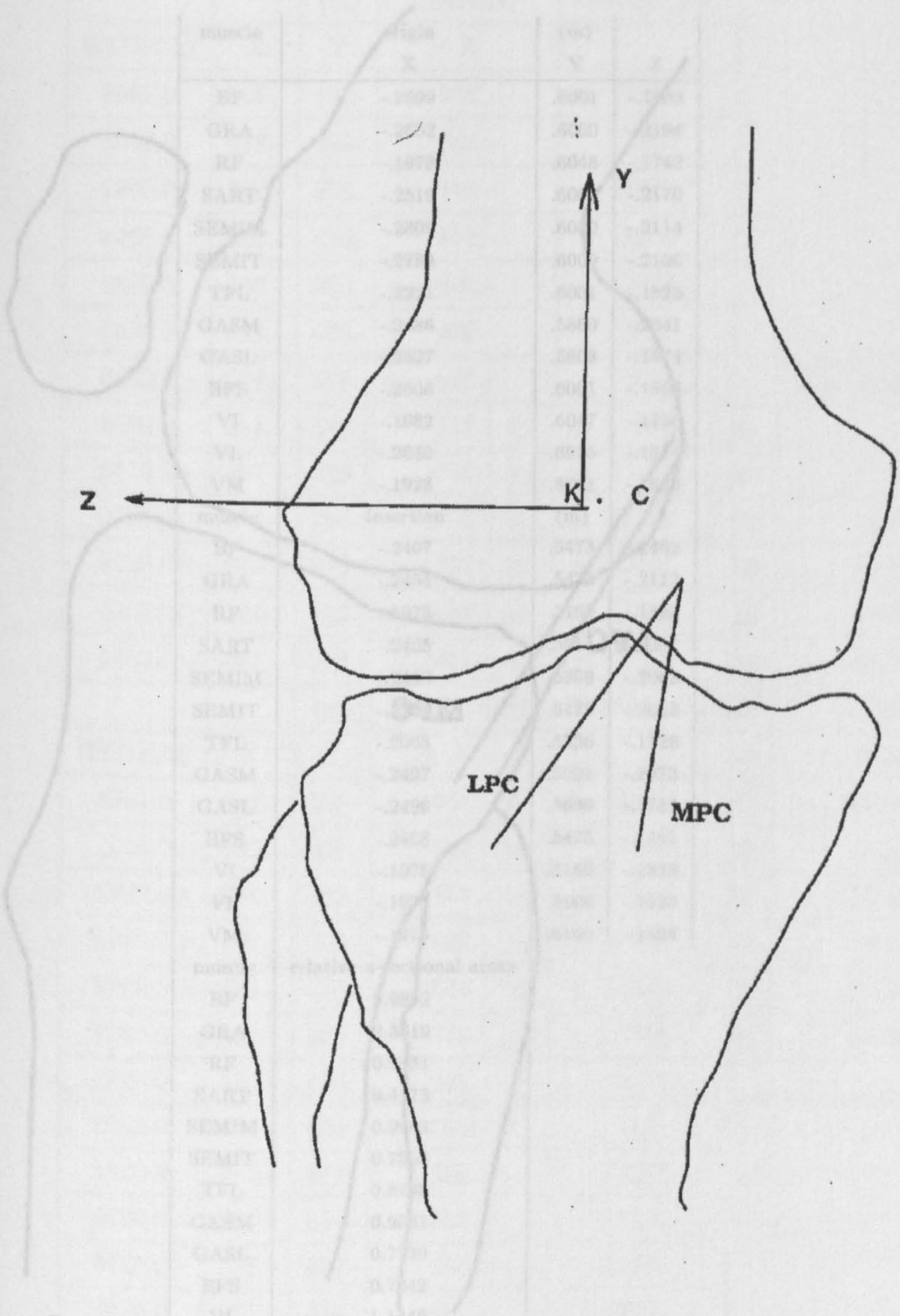

Figure 5.9: Anterior-posterior view of the posterior Capsule elements-Right lower limb

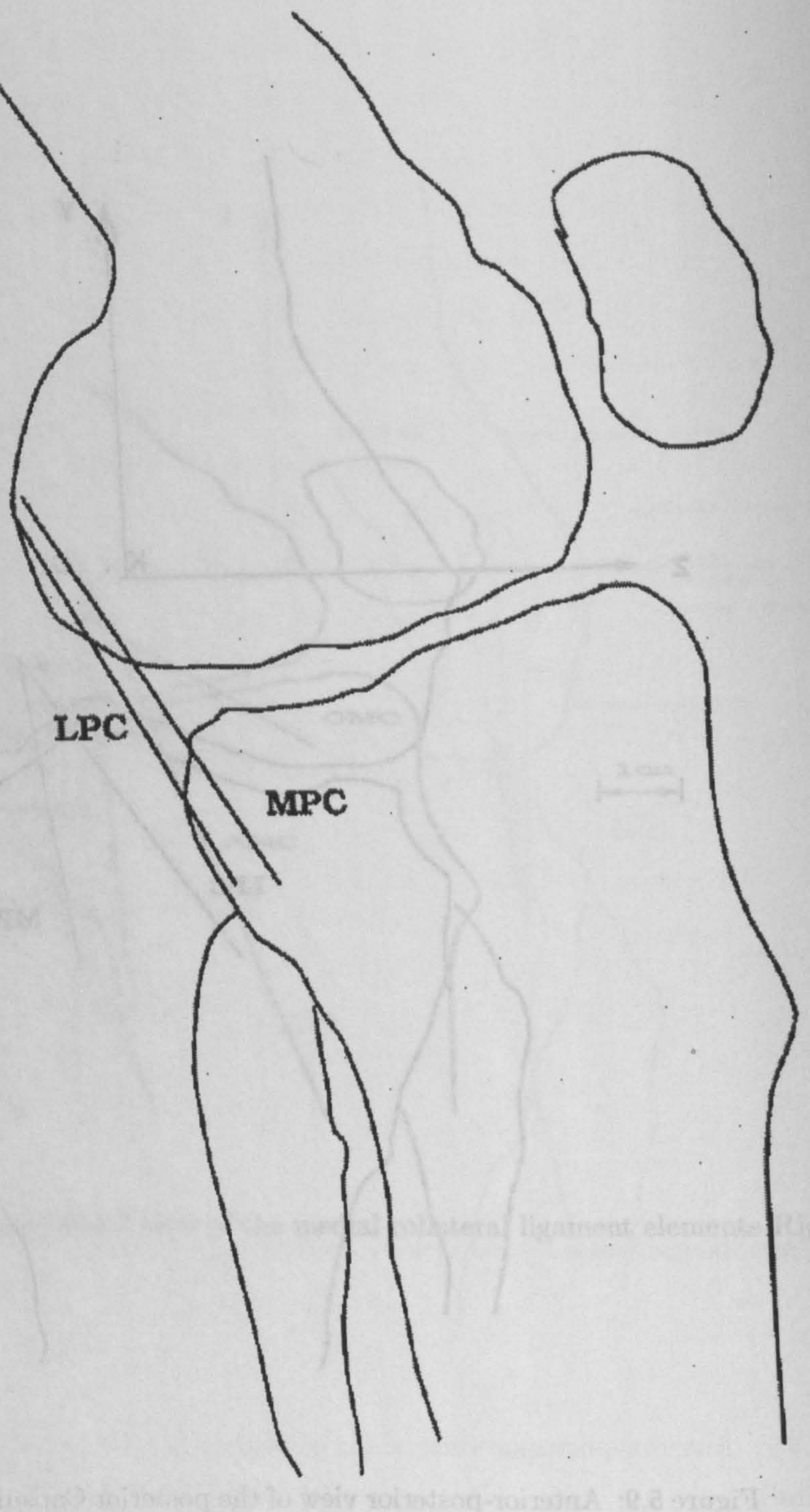

Figure 5.10: Medio-lateral view of the posterior Capsule elements-Right lower l

muscle	origin (m)		
	X	Y	Z
BF	-.2699	.6001	-.1593
GRA	-.2652	.6000	-.2194
RF	-.1978	.6048	-.1742
SART	-.2519	.6000	-.2170
SEMIM	-.2809	.6000	-.2114
SEMIT	-.2780	.6000	-.2106
TFL	-.2221	.6001	-.1526
GASM	-.2486	.5860	-.2041
GASL	-.2527	.5808	-.1674
BFS	-.2606	.6001	-.1569
VI	-.1982	.6047	-.1730
VL	-.2640	.6035	-.1571
VM	-.1928	.6061	-.1886
muscle	insertion	(m)	
BF	-.2407	.5473	-.1462
GRA	-.2454	.5473	-.2112
RF	-.1975	.5160	-.1828
SART	-.2405	.5514	-.2207
SEMIM	-.2489	.5369	-.2062
SEMIT	-.2521	.5472	-.2062
TFL	-.2065	.5526	-.1528
GASM	-.2497	.5001	-.2073
GASL	-.2496	.5000	-.1744
BFS	-.2408	.5475	-.1461
VI	-.1975	.5160	-.1828
VL	-.1975	.5160	-.1828
VM	-.1975	.5160	-.1828
muscle	relative x-sectional areas		
BF	0.9892		
GRA	0.5019		
RF	0.9031		
SART	0.4173		
SEMIM	0.9963		
SEMIT	0.7993		
TFL	0.8238		
GASM	0.9881		
GASL	0.7739		
BFS	0.7242		
VI	1.1446		
VL	1.7761		
VM	1.4044		

Table 5.2: Coordinates of Muscle Locations and Relative Cross-sectional Areas

LIGAMENT	ORIGIN	(m)		
	X	Y	Z	LENGTH
AMC	-.236	.581	-.224	0.1066
DMC	-.238	.575	-.219	0.0251
PMC	-.241	.579	-.222	0.0892
OMC	-.244	.575	-.223	0.0368
MPC	-.266	.580	-.206	0.0389
LPC	-.266	.580	-.182	0.0362
OLC	-.250	.575	-.150	0.0350
LC	-.244	.585	-.145	0.0350
DLC	-.243	.575	-.146	0.0174
AAC	-.250	.582	-.177	0.0370
PAC	-.248	.578	-.175	0.0276
APC	-.242	.579	-.192	0.0361
PPC	-.245	.582	-.196	0.0354
LIGAMENT	INSERTION	(m)		
	X	Y	Z	LENGTH
AMC	-.234	.475	-.213	0.1066
DMC	-.237	.550	-.221	0.0251
PMC	-.238	.490	-.217	0.0892
OMC	-.260	.551	-.200	0.0368
MPC	-.253	.545	-.195	0.0389
LPC	-.257	.545	-.183	0.0362
OLC	-.265	.545	-.160	0.0350
LC	-.243	.550	-.144	0.0350
DLC	-.245	.558	-.149	0.0174
AAC	-.225	.558	-.190	0.0370
PAC	-.232	.559	-.187	0.0276
APC	-.260	.555	-.172	0.0361
PPC	-.256	.555	-.176	0.0354

Table 5.3: Coordinates of Ligament Insertions and Origins (unit: m). Origin of axis system as in Brand et al. [1982]

LIGAMENT		Femoral			Tibial		LENGTH (mm)
	Xf	Yf	Zf	Xt	Yt	Zt	
AMC	-35	-7	30	-20	-7	-40	71.59
DMC	-35	0	27	35	0	-10	79.18
PMC	-35	8	30	-20	8	-50	81.39
OMC	-35	3	30	-35	30	-10	48.26
MPC	-25	25	30	-25	25	-30	60.00
LPC	25	25	30	25	25	-30	60.00
OLC	25	25	30	-25	25	-30	78.10
LC	35	10	25	45	25	-35	62.65
DLC	-25	25	30	25	25	-30	78.10
AAC	7	8	25	-7	-5	0	31.46
PAC	5	4	25	0	-2	0	26.19
APC	-5	-3	20	-5	25	-5	37.54
PPC	-5	17	20	5	25	-5	28.09

Table 5.4: Coord. of ligament Attachment sites at 0° of flexion Crowninshield et al. [1976]

Ligament length is defined as the distance from the origin point to the insertion point at any given time. The coordinates of the insertions and the origins of the ligaments at "zero flexion " reported by Crowninshield et al. [1976] are shown in Table 5.4 on page 94. These coordinates were determined by examination of anatomical specimens, and represent an average of the measurements obtained from seven subjects. Measurements were made on males in the mass range of 65-80 kg. The variability of the measurements was approximately 10%. They also provided the relative ligament lengths as predicted by an analytical model for different knee flexion angles (Figure 5.11 on page 96). These ligament lengths were given relative to the length of the deep medial collateral ligament. The deep medial collateral ligament length was assumed to remain constant for all flexion angles. From these data, the ligament lengths at 10 degrees of flexion (corresponding to the condition at 17% of the gait cycle chosen for the present model) are estimated and shown in Table 5.5 on page 96.

Wang et al. [1973] also reported lengths of lateral collateral, medial collateral, anterior cruciate and posterior cruciate ligaments. The ligament length patterns were determined for twelve specimens at flexion angles of 0, 30, 60, 90 and 120 degrees, and in neutral, internal rotation and external rotation at each angle. The lengths of the collateral ligaments steadily diminished by about 20 per cent from 0 to 120 degrees of flexion, rotation having little effect. The anterior cruciate length gradually increased 10 per cent from 0 to 120 degrees of flexion, and the posterior cruciate was 10 per cent longer at 0 degrees of flexion than at all other angles, for which the length was constant. Rotation had a significant effect on cruciate lengths, affecting the anterior cruciate more than the posterior cruciate. Interpolated results for the ligament length at 10 degrees of flexion in neutral rotation are given in Table 5.6 on page 101.

Trent et al. [1976] reported the lengths of the cruciate ligaments (anterior and posterior) in terms of three different fibres, for different degrees of flexion and neutral rotation. Ligament length changes during flexion were found to be small in the absence of rotary torque and anteroposterior forces. The average internal rotation occurring during flexion was 37°, half of which took place during the first 15° of flexion. The results are shown in FIGURES 5.12 on page 97, 5.13 on page 98, 5.14 on page 98. Interpolating from the figures, the lengths at 10° of flexion for the cruciate ligaments in the present model are shown in Table 5.7 on page 102.

Wilson [1978] used multiple regression analyses to construct regression equations Cohen et al. [1975] for prediction of ligament element attachment sites. The indepen-

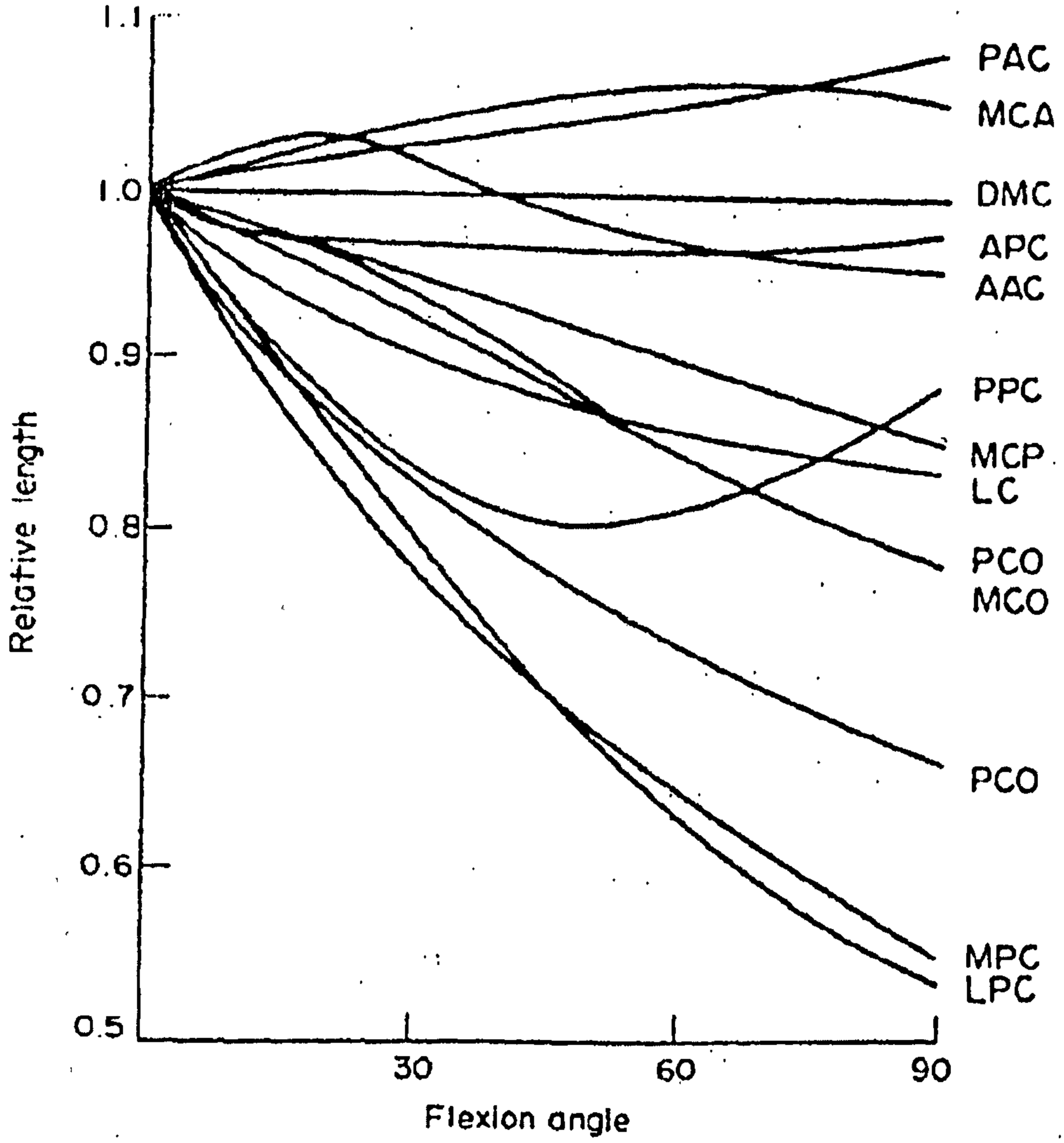

Figure 5.11: Ligament lengths relative to the lengths of the deep medial collateral ligaments Crowninshield et al. [1976]

LIGAMENT	LENGTH (m)
AMC	0.0723
DMC	0.0792
PMC	0.0802
OMC	0.0473
MPC	0.0558
LPC	0.0564
OLC	0.0726
LC	0.0596
DLC	0.0711
AAC	0.0323
PAC	0.0265
APC	0.0368
PPC	0.0259

Table 5.5: Ligament Lengths in 10° Flexion Crowninshield et al. [1976]

dent predictor variables used were : leg length (cm), tibial width (cm), femoral width (cm), subject height (cm), projected tibial width (cm), projected femoral breadth (cm), projected tibial breadth (cm), projected femoral breadth (cm). He reported the minimum and maximum ligament lengths during one gait cycle. The results are shown in Tables 5.8 on page 102 to 5.10 on page 103.

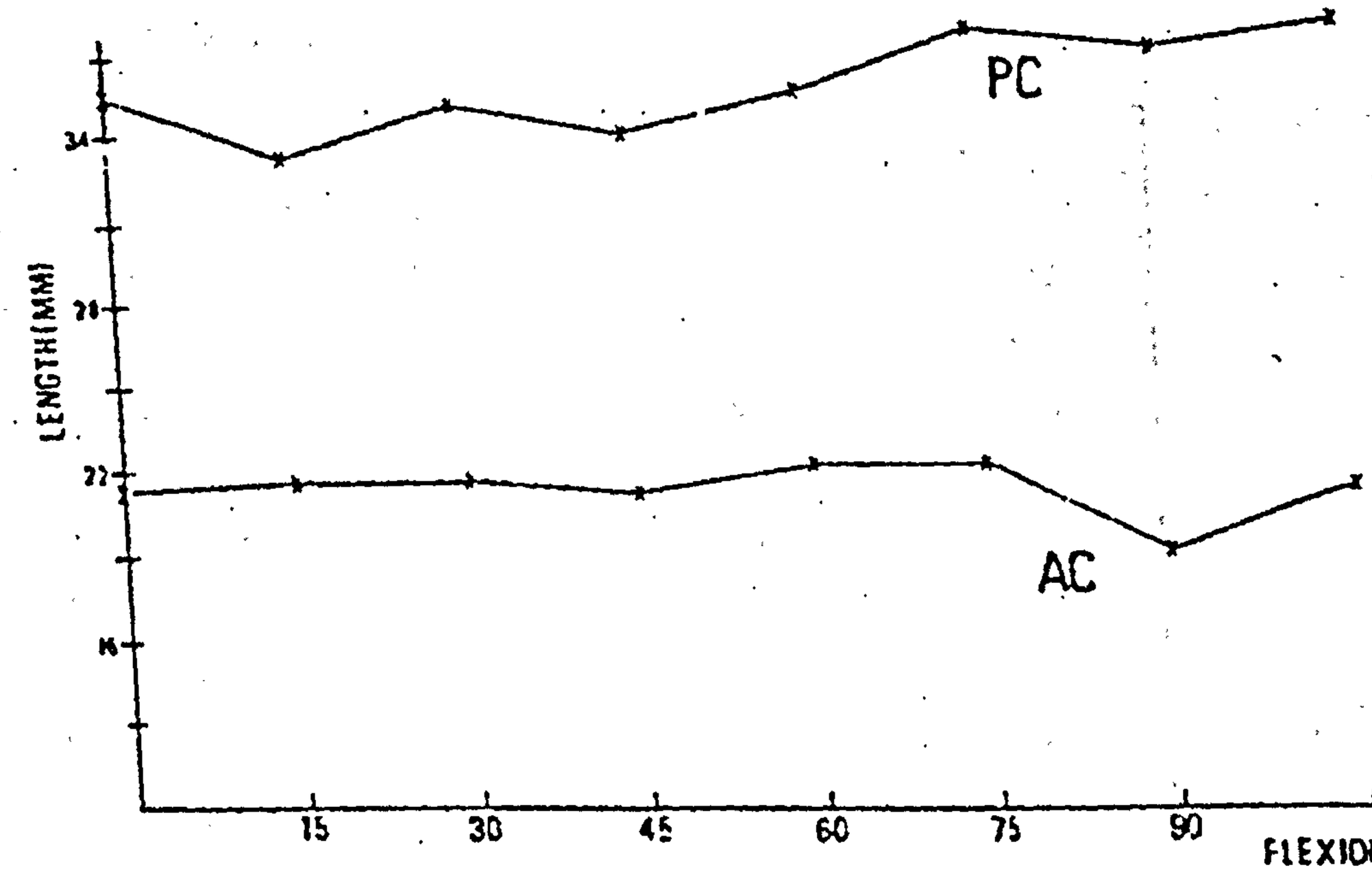

Figure 5.12: Ligament lengths of the cruciates in flexion: Posterior fibres, Neutral rotation, after Trent et al. [1976]

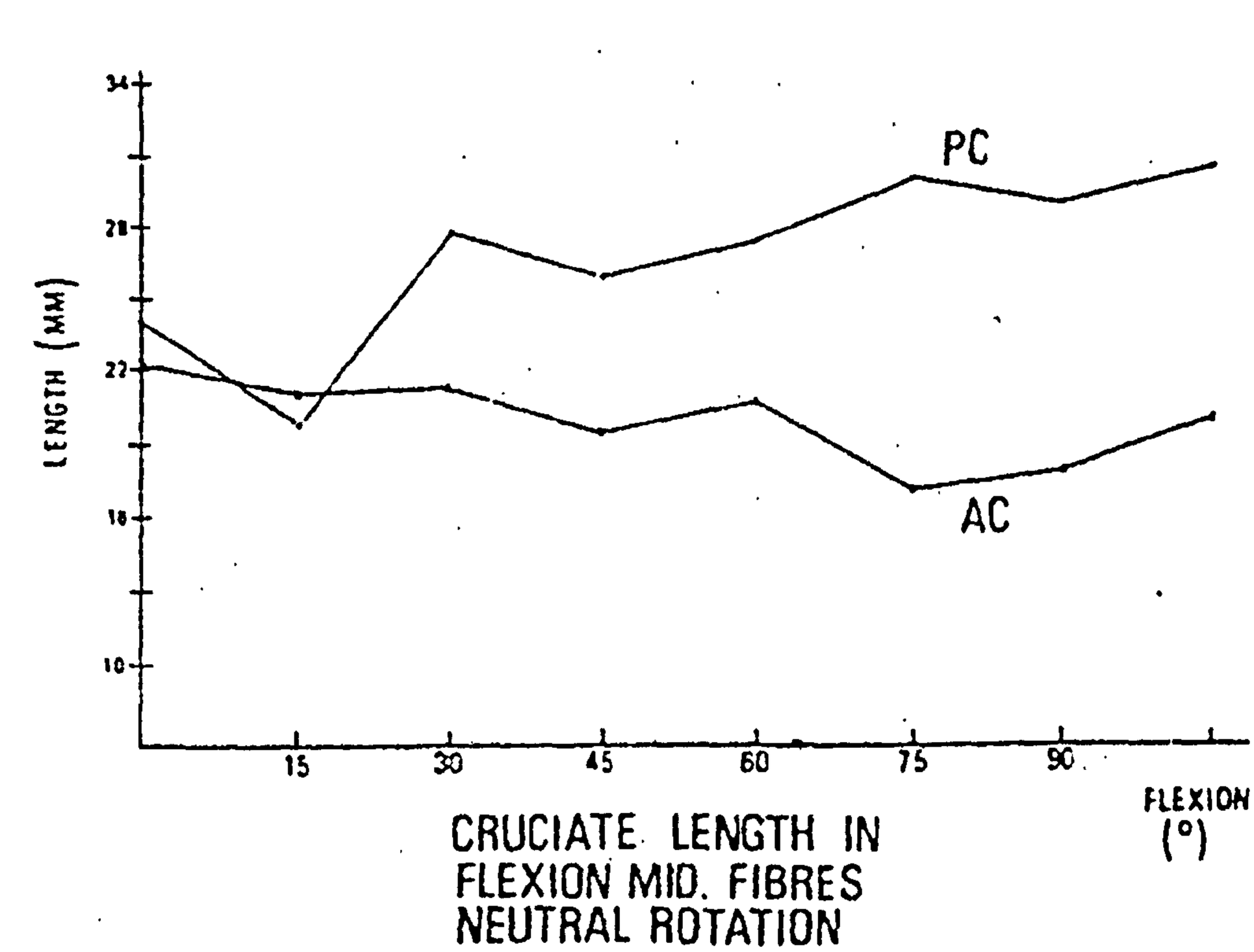

Figure 5.13: Ligament lengths of the cruciates in flexion: Middle fibres, Neutral rotation, after Trent et al. [1976]

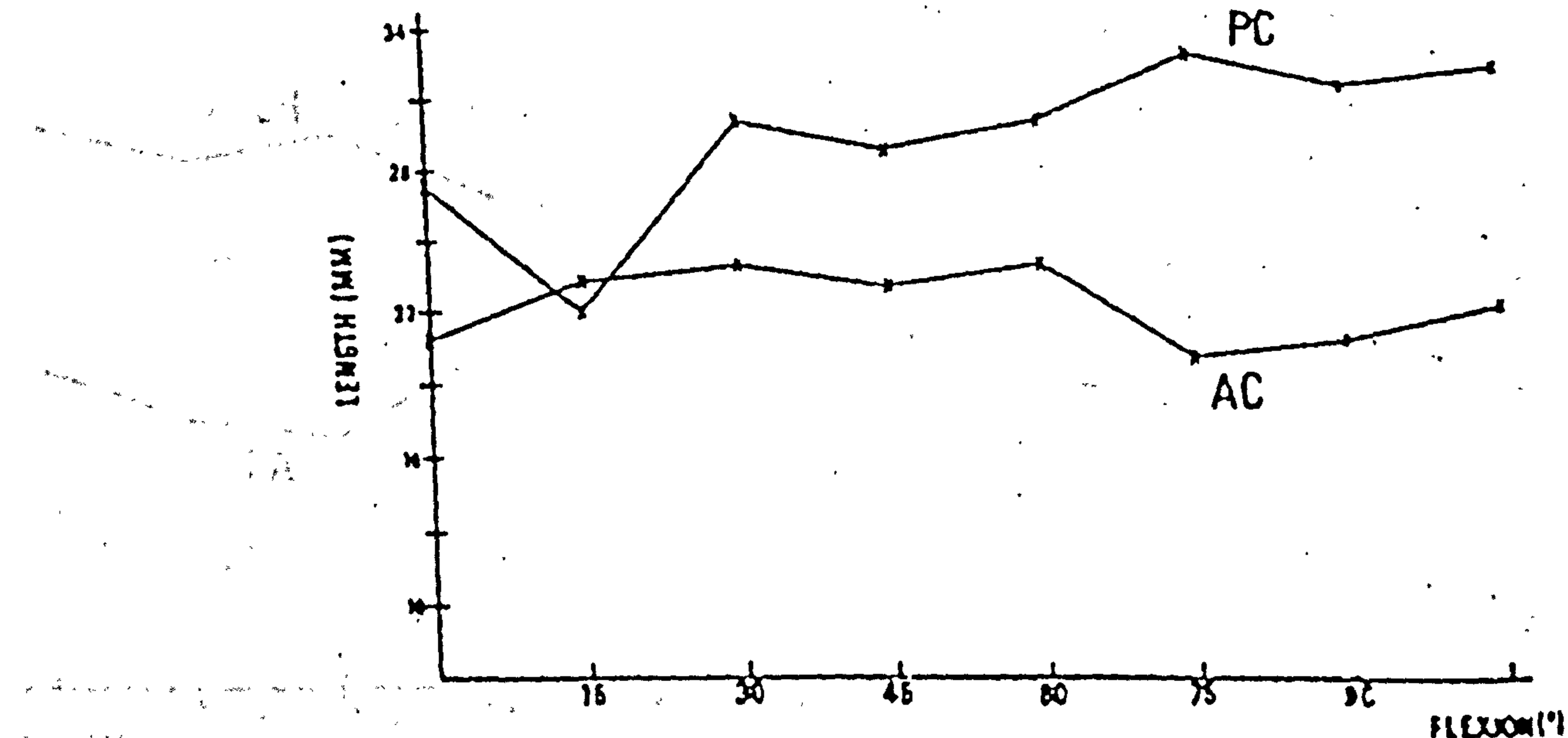

Figure 5.14: Ligament lengths of the cruciates in flexion: Anterior fibres, Neutral rotation, after Trent et al. [1976]

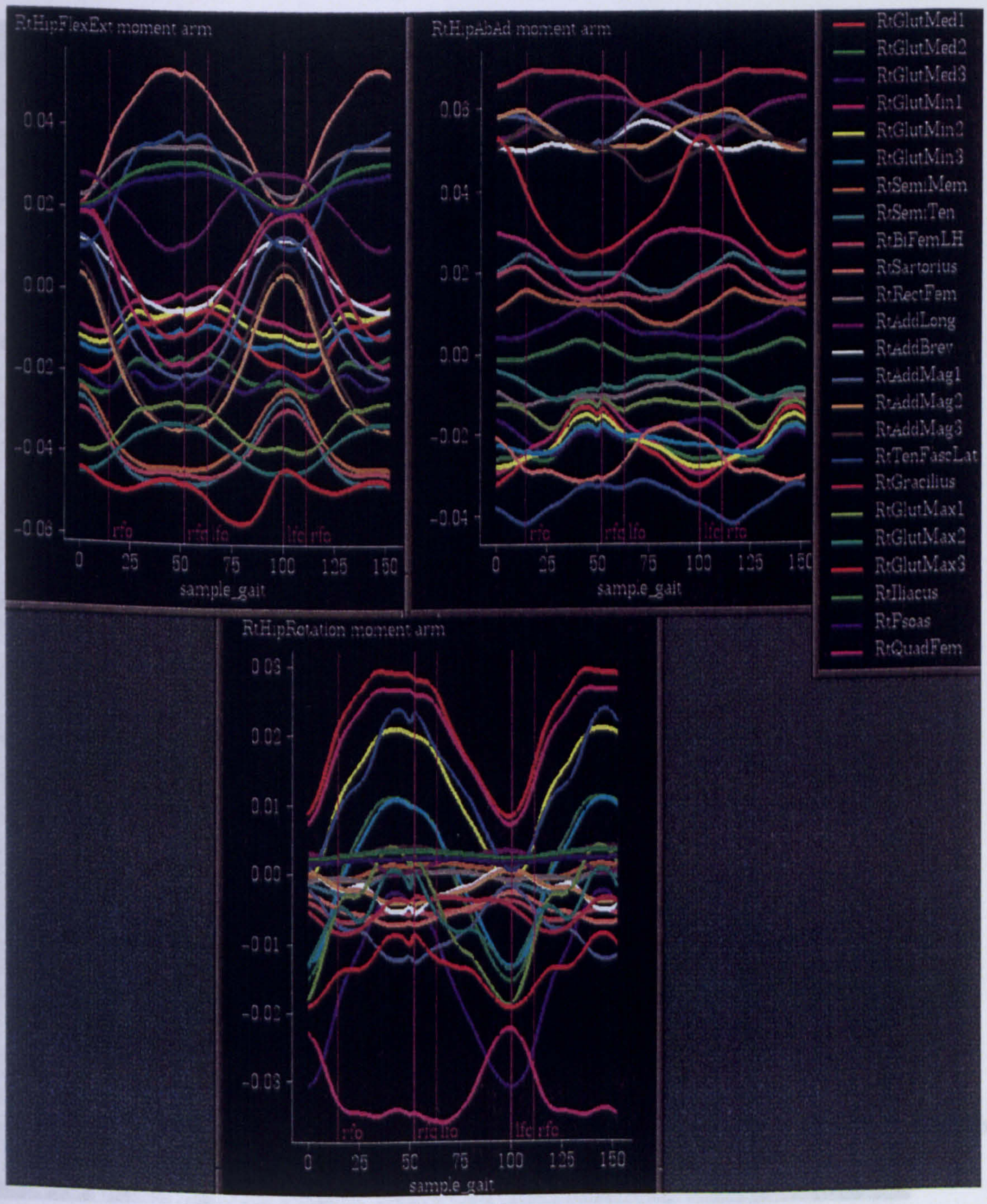

Figure 5.15: 1 MUSCLE MOMENT ARMS SIMM after Delp et al. [1996b]

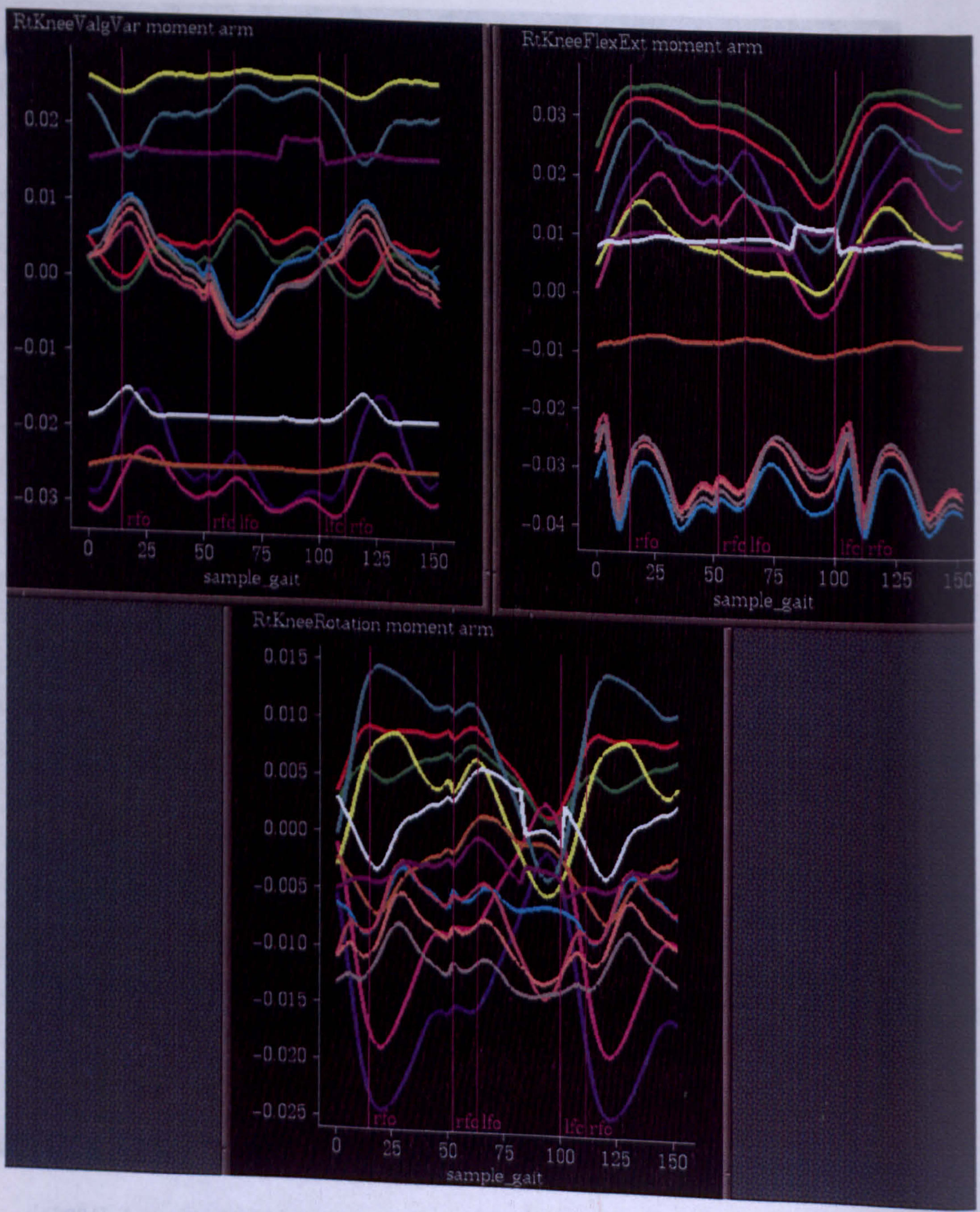

Figure 5.16: 2 MUSCLE MOMENT ARMS SIMM after Delp et al. [1996b]

LIGAMENT	LENGTH (m)
LC	0.0537
MC	0.0656
ACL	0.0292
PCL	0.0353

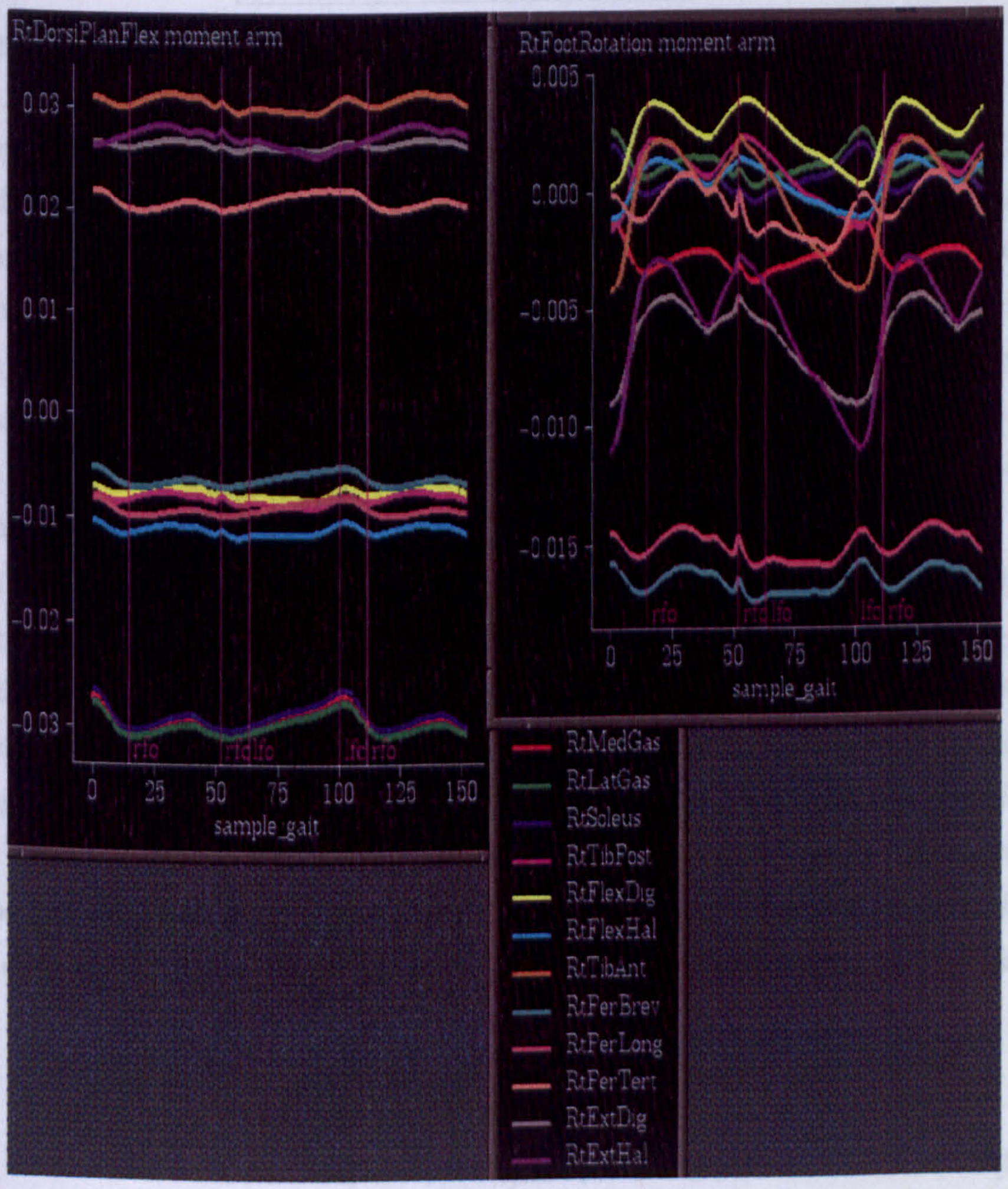

Figure 5.17: 3 MUSCLE MOMENT ARMS SIMM after Delp et al. [1996b]

LIGAMENT	LENGTH (m)
LC	0.0537
MC	0.0656
ACL	0.0292
PCL	0.0353

Table 5.6: Average Ligament Lengths in 10^o of Flexion Wang et al. [1973]

Discrepancies obviously exist between the results presented in these studies. Different techniques used to separate a group of ligaments and to choose the insertions and origins are the major reasons for most of these discrepancies. However, these studies do agree that posterior cruciate ligaments are longer than anterior cruciate ligaments, and that medial collateral ligaments are longer than lateral collateral ligaments. Importantly, reported ligament lengths generally fall in the range between the minimum and maximum ligament lengths during one gait cycle reported by Wilson [1978] (Table 5.11 on page 104).

Direct data are not available on the strain of the soft tissue structures of the knee as a function of the flexion-extension angle. Only a rough indication of these strains can be inferred from the literature (e.g. Brantigan et al. [1941]. Wismans et al. [1980] made assumptions based on this data, for the strain in knee ligaments with the joint in zero degrees of flexion. This strain was called the "initial strain" and was described as Erj for spring j. Since Wismans et al. [1980] specified Erj values for their spring model, one can use their data to calculate the corresponding unstrained length, Lo_j, from the defining equation. That is, where L_J is the ligament length at 0^o of knee flexion.

$$Er_j = (L_J - Lo_j)/Lo_j$$
$$Lo_j = L_J/(Er_j + 1) \tag{5.4}$$

LIGAMENT	LENGTH (m)
AAC	0.0220
PAC	0.0220
APC	0.0240
PPC	0.0340

Table 5.7: Ligament Lenghts in 10^o Flexion Estimated from Trent et al. [1976]

ONE	GAIT	CYCLE		STANCE	PHASE	SWING	PHASE
LIG.	MIN	MAX	error bound	MIN	MAX	MIN	MAX
AAC	0.073	0.111	0.013	0.073	0.111	0.085	0.105
AAC	0.025	0.049	0.012	0.025	0.049	0.028	0.040
AAC	0.087	0.125	0.012	0.087	0.125	0.092	0.117
AAC	0.026	O.043	0.013	0.026	0.039	0.033	0.043
AAC	0.016	0.027	0.016	0.016	0.026	0.018	0.027

Table 5.8: Collateral Lig. Lengths during Stance and Swing Phase Wilson [1978]

Ligament Length (m)							
	One Gait Cycle			Stance Phase		Swing Phase	
Ligament	Min	Max	Error Bound	Min	Max	Min	Max
AAC	.027	.046	.012	.027	.046	.020	.0436
PAC	.016	.040	.012	.017	.040	.016	.0396
APC	.019	.030	.012	.024	.030	.019	.026
PPC	.015	.030	.012	.021	.030	.015	.027

Table 5.9: Cruciate Ligament Lengths during Stance and Swing Phase

Ligament Length (m)					
	One Gait Cycle			Stance Phase	Swing Phase
Ligament	Min	Max	Error Bound	Min Max	Min Max
OMC	.023	.057	.011	.026 .057	.023 .052
MPC	.031	.050	.010	.032 .050	.031 .046
LPC	.026	.036	.011	.026 .035	.027 .036
OLC	.033	.057	.013	.033 .056	.035 .057

Table 5.10: Capsule Ligament Lengths during Stance and Swing Phase

LIGAMENT	Wilson 1978 GAIT CYCLE		Crowninshield etal 1976	Trent etal 1976	Wang etal 1973	Present Study
	Min	Max				
AMC	.073	.111	.0723		.0656	.1066
DMC	.025	.049	.0792		.0656	.0251
PMC	.087	.125	.0802		.0656	.0892
OMC	.023	.057	.0473		.0369	
MPC	.031	.050	.0558			.0389
LPC	.026	.036	.0564			.0362
OLC	.033	.057				.0350
LC	.026	.043	.0596		.0537	.0350
DLC	.016	.027		.0532	.0174	
AAC	.027	.246	.0323	.0220	.0292	.0370
PAC	.016	.040	.0265	.0220	.0292	.0276
APC	.019	.030	.0368	.0240	.0353	.0361
PPC	.015	.030	.0259	.0340	.0353	.0354

Table 5.11: Comparison of Different Investigations of Ligament Lengths

In the present study, the unstrained ligament lengths are calculated by using the estimated ligament lengths at 10° of knee flexion (given earlier), the "relative" ligament lengths of the thirteen ligament elements as the knee moved in normal flexion (FIGURE 5.11 on page 96) reported by Crowninshield et al. [1976], and the estimated initial strains (Table 5.12 on page 104) reported by Wismans et al. [1980]. The reason to use the relative ligament lengths of Crowninshield et al. [1976] is that they reported all 13 relative ligament lengths with different flexion angles. With the relative ligament lengths and the 13 ligament absolute lengths at 10° knee flexion estimated earlier, 13 ligament lengths at 10° of knee flexion can be interpolated and calculated. Thus, unstrained ligaments lengths can be calculated using Equation 7.4.

5.2.5.4 Ligament Spring Constants

Wismans et al. [1980] also reported nonlinear spring constants, Kj, for the knee ligaments. The numerical values are based on the experimental work of Trent et al. [1976], and are provided in Table 5.14 on page 106.

1	2	3
LIGAMENT	Er_J(%)	UNSTRAINED LENGTHS (m)
AMC	-3	0.1088
DMC	0	0.0251
PMC	5	0.0863
OMC	0	0.0369
MPC	5	0.0398
LPC	5	0.0367
OLC	0	0.0376
LC	5	0.0351
DLC	0	0.0191
AAC	5	0.0344
PAC	5	0.0260
APC	-1	0.0372
PPC	-1	0.0389

Table 5.12: Initial Strain Er_j and Unstrained Ligament Lengths Wismans et al. [19

1	2	3
LIGAMENT	REL. X-SECTIONAL	APPROX. X-SECTIONAL
	AREA (Crowninshield	AREA (cm^2)(PRESENT STUDY)
AMC	1.0	0.6452
DMC	0.5	0.3226
PMC	0.5	0.3226
OMC	0.5	0.3226
MPC	0.4	0.2581
LPC	0.4	0.2581
OLC	0.1	0.0645
LC	0.5	0.3226
DLC	0.2	0.1290
AAC	0.5	0.3226
PAC	0.5	0.3226
APC	0.8	0.5162
PPC	O.8	0.5162

Table 5.13: Ligament Approximate Cross-sectional areas, Crowninshield et al. [1976] and present study

5.2.5.5 Ligament Forces

The ligament forces at 10 degrees of flexion in the present spring model can be calculated using the quadratic force-elongation equations of Wismans ,
Wismans et al. [1980]:

$$Fl_j = K_j(LlO_j - Lo_j)^2$$

if $LlO_j > Lo_j$
and

$$Fl_j = 0 \quad if \quad LlO_j \leq Lo_j \tag{5.5}$$

where Fl_j *is the jth spring ligament force,* LlO_j *is the length of the jth ligament with the knee in 10 degrees of flexion, and* Lo_j *is the unstrained length calculated as explained earlier.*

5.2.5.6 Ligament Stresses and Cross-Sectional Areas

Once the ligament forces are calculated, the ligament stresses can be estimated by dividing forces by the corresponding ligament cross-sectional areas.

Trent et al. [1976] found considerable variability of ligament cross-sectional areas between specimens. However, trends within a particular specimen were clearly discernible. The lateral collateral ligament had the smallest area, averaging 0.1 in^2 (0.654 cm^2); the anterior and posterior cruciates had average areas of 0.2 in^2 (1.290 cm^2) and 0.17 in^2 (1.10 cm^2) respectively; and the wide but thin medial collateral had an area of 0.2 in^2 (1.29 cm^2). Crowninshield et al. [1976] reported ligament cross-sectional areas relative to the area of the anterior fibres of the medial collateral. The above two sets of data were combined to get approximate ligament cross-sectional areas (Table 5.15 on page 107).

5.2.6 Joint Equipollence Equations

There are six scalar equilibrium equations in the knee distribution problem: three moment and three force equations. To calculate the two bony contact force vectors (three components in each), six equations are needed. Therefore, it appears that if muscle and ligament forces are known, the six unknown bony contact force components can be determined using the six scalar joint equilibrium equations. However, it is

LIGAMENT	LIGAMENT SPRING CONSTANTS
	K;(N/m m^2)
AMC	15
DMC	15
PMC	15
OMC	15
MPC	10
LPC	10
OLC	15
LC	15
DLC	15
AAC	30
PAC	30
APC	35
PPC	35

Table 5.14: Ligament Spring Constants NOTE: Initial Strain Er_j and Spring Const
K were taken from Wismans et al. [1980]

shown in this section that no unique solution for the bony contact force components can be obtained using the joint equilibrium equations. Further assumptions to reduce the number of unknown bony contact force components are needed. Alternatively, one can use optimization techniques to develop a procedure for calculating the unknown forces. A procedure combining these two alternatives is proposed and evaluated in chapter 8.

1	2	3
LIGAMENT	REL. X-SECTIONAL	APPROX. X-SECTIONAL
	AREA (Crowninshield	AREA (cm^2)(PRESENT STUDY)
AMC	1.0	0.6452
DMC	0.5	0.3226
PMC	0.5	0.3226
OMC	0.5	0.3226
MPC	0.4	0.2581
LPC	0.4	0.2581
OLC	0.1	0.0645
LC	0.5	0.3226
DLC	0.2	0.1290
AAC	0.5	0.3226
PAC	0.5	0.3226
APC	0.8	0.5162
PPC	O.8	0.5162

Table 5.15: Ligament Approximate Cross-sectional areas, Crowninshield et al. [1976] and present study

As stated previously, the mechanical model of the musculoskeletal system in the neighbourhood of the human knee includes thirteen muscles, thirteen ligaments, and two bony contact forces. The two bony contact forces have six unknown scalar components in three directions: therefore, the total system has 32 unknown scalar forces. Since there are only six scalar equilibrium equations, this system of equations is indeterminate and a procedure is needed to calculate the forces. The six equilibrium equations can be written as

$$Fr_1 = \sum_{i=1}^{13} Fm_{i1} + \sum_{j=1}^{13} Fl_{j1} + \sum_{k=1}^{2} Fc_{k1} \tag{5.6}$$

$$Fr_2 = \sum_{i=1}^{13} Fm_{i2} + \sum_{j=1}^{13} Fl_{j2} + \sum_{k=1}^{2} Fc_{k2} \tag{5.7}$$

$$Fr_3 = \sum_{i=1}^{13} Fm_{i3} + \sum_{j=1}^{13} Fl_{j3} + \sum_{k=1}^{2} Fc_{k3} \tag{5.8}$$

$$Mr_1 = \sum_{i=1}^{13}(Fm_{i3}Rm_{i2} - Fm_{i2}Rm_{i3}) + \sum_{j=1}^{13}(Fl_{j3}Rl_{j2} - Fl_{j2}Rl_{j3}) + \sum_{k=1}^{2}(Fc_{k3}Rc_{k2} - Fc_{k2}Rc_{k3}) \tag{5.9}$$

$$Mr_2 = \sum_{i=1}^{13}(Fm_{i1}Rm_{i3} - Fm_{i3}Rm_{i1}) + \sum_{j=1}^{13}(Fl_{j1}Rl_{j3} - Fl_{j3}Rl_{j1}) \tag{5.10}$$

$$Mr_3 = \sum_{i=1}^{13}(Fm_{i2}Rm_{i1} - Fm_{i1}Rm_{i2}) + \sum_{j=1}^{13}(Fl_{j2}Rl_{j1} - Fl_{j1}Rl_{j2}) + \sum_{k=1}^{2}(Fc_{k2}Rc_{k1} - Fc_{k1}Rc_{k2}) \tag{5.11}$$

In the equilibrium expressions, Frn and Mrn are the nth components ($n = 1, 2, 3$) of the known resultant force and moment due to external loads, Fmin and Rmin are the nth components of the muscle force and corresponding moment arm of the ith muscle, Fljn and Rljn are the nth components of the ligament force and corresponding moment arm of the jth ligament, and Fckn and Rckn are the nth components of the kth bony contact force and its corresponding moment arm.

	peak muscle force (N)	optimal fiber length (cm)	pennation angle (degrees)	tendon slack length (cm)
hip muscles				
gluteus medius1 o	550	5.4	8	7.8
gluteus medius2 o	380	8.4	0	5.3
gluteus medius3 o	435	6.5	19	5.3
gluteus minimus1 o	180	6.8	10	1.6
gluteus minimus2 o	190	5.6	0	2.6
gluteus minimus3 o	215	3.8	1	5.1
gluteus maximus1 o	380	14.2	5	12.5
gluteus maximus2 o	550	14.7	0	12.7
gluteus maximus3 o	370	14.4	5	14.5
adductor magnus1 o	345	8.7	5	6.0
adductor magnus2 o	310	12.1	3	13.0
adductor magnus3 o	445	13.1	5	26.0
adductor longus o	420	13.8	6	11.0
adductor brevis o	285	13.3	0	2.0
pectineus o	175	13.3	0	0.1
iliacus o	430	10.0	7	9.0
psoas o	370	10.4	8	13.0
quadratus femoris o	255	5.4	0	2.4
gemelli o	110	2.4	0	3.9
piriformis o	295	2.6	10	11.5
hip and knee muscles				
rectus femoris *	780	8.4	5	34.6
semimembranosus *	1030	8.0	15	35.9
semitendinosus *	330	20.1	5	26.2
biceps femoris (lh)*	720	10.9	0	34.1
gracilis *	110	35.2	3	14.0
sartorius *	105	57.9	0	4.0
tensor fasciae latae *	155	9.5	3	42.5

Table 5.16: Musculotendon Parameters For Lower Limb Muscles. CONTINUED IN TABLE 7.16

	peak muscle force (N)	optimal fiber length (cm)	pennation angle (degrees)	tendon slack length (cm)
knee muscles				
vastus medialus *	1295	8.9	5	12.6
vastus intermedius*	1235	8.7	3	13.6
vastus lateralis *	1870	8.4	5	15.7
biceps femoris(sh) *	400	17.3	23	10.0
knee and ankle muscles				
medial gastrocnemius ⊕	1115	4.5	17	40.8
lateral gastrocnemius ⊕	490	6.4	8	38.5
ankle muscles				
soleus •	2830	3.0	25	26.8
tibialis posterior*	1270	3.1	12	31.0
fl. digitorum longus *	310	3.4	7	40.0
fl. hallucis longus *	320	4.3	10	38.0
peroneus brevis *	350	5.0	5	16.1
peroneus longus *	755	4.9	10	34.5
tibialis anterior*	600	9.8	5	22.3
peroneus tertius ∘	90	7.9	13	10.0
ext. digitorum longus*	340	10.2	8	34.5
ext. hallucis longus *	110	11.1	6	30.5

Table 5.17: continued from table 7.15 Musculotendon Parameters For Lower Limb Muscles, Peak force derived from Brand et al. (1986) fiber length and pennation from Friederich and Brand (1990).Coding: * Peak force, fiber length, and pennation angle drived from Wickiewicz et al. (1983). ⊕ Peak force derived from Brand et al. (1986) fiber length and pennation derived from Wickiewicz et al. (1983). • Peak force derived from Wickiewicz el al.(1983) multiplied by 0.8 fiber length from Friederich and Brand (1990)

It is interesting to note that even if muscle and ligament forces are assumed to be known, the six scalar equilibrium equations still cannot be solved for the six scalar components of the bony contact forces. In order to demonstrate this observation, assume the muscle and ligament forces are known. The six scalar equilibrium equations in Equations (7.6) to (7.11) can be rewritten as :

$$Fc_{11} + Fc_{21} = Fr_1 - \sum_{i=1}^{13} Fm_{i1} - \sum_{j=1}^{13} Fl_{j1} = Fr_1^{'} \tag{5.12}$$

$$Fc_{12} + Fc_{22} = Fr_2 - \sum_{i=1}^{13} Fm_{i2} - \sum_{j=1}^{13} Fl_{j2} = Fr_2^{'} \tag{5.13}$$

$$FC_{13} + Fc_{23} = Fr_3 - \sum_{i=1}^{13} Fm_{i3} - \sum_{j=1}^{13} Fl_{j3} = Fr_3^{'} \tag{5.14}$$

$$FC_{13}Rc_{12} - Fc_{12}Rc_{13} + Fc_{23}Rc_{22} - Fc_{22}Rc_{23} =$$
$$Mr_1 - \sum_{i=1}^{13}(Fm_{i3}Rm_{i2} - Fm_{i2}Rm_{i3}) - \sum_{j=1}^{13}(Fl_{j3}Rl_{j2} - Fl_{j2}Rl_{j3}) = Mr_1^{'} \tag{5.15}$$

$$FC_{11}Rc_{13} - Fc_{13}Rc_{11} + Fc_{21}Rc_{23} - Fc_{23}Rc_{21} =$$
$$Mr_2 - \sum_{i=1}^{13}(Fm_{i1}Rm_{i3} - Fm_{i3}Rm_{i1}) - \sum_{j=1}^{13}(Fl_{j1}Rl_{j3} - Fl_{j3}Rl_{j1}) = Mr_2^{'} \tag{5.16}$$

$$FC_{12}Rc_{11} - Fc_{11}Rc_{12} + Fc_{22}Rc_{21} - Fc_{21}Rc_{22} =$$
$$Mr_3 - \sum_{i=1}^{13}(Fm_{i2}Rm_{i1} - Fm_{i1}Rm_{i2}) - \sum_{j=1}^{13}(Fl_{j2}Rl_{j1} - Fl_{j1}Rl_{j2}) = Mr_3^{'} \tag{5.17}$$

where Rcij is the moment arm of the ith component of the jth bony contact force measured from the knee centre (the origin of the knee reference frame) to the bony contact points. These six equations can be written in the matrix form as [R]F = fr, where

$$[R] = \begin{bmatrix} 1 & 0 & 0 & 1 & 0 & 0 \\ 0 & 1 & 0 & 0 & 1 & 0 \\ 0 & 0 & 1 & 0 & 0 & 1 \\ 0 & -Rc_{13} & Rc_{12} & 0 & -Rc_{23} & Rc_{22} \\ Rc_{13} & 0 & -Rc_{11} & Rc_{23} & 0 & -Rc_{21} \\ -Rc_{12} & Rc_{11} & 0 & -Rc_{22} & Rc_{21} & 0 \end{bmatrix}$$

$$(F) = \begin{bmatrix} Fc_{11} \\ Fc_{12} \\ Fc_{13} \\ Fc_{21} \\ Fc_{22} \\ Fc_{23} \end{bmatrix}$$

$$(Fr) = \begin{bmatrix} Fr_1^* \\ Fr_2^* \\ Fr_3^* \\ Fr_1^* \\ Fr_2^* \\ Fr_{3^*} \end{bmatrix} \qquad (5.18)$$

The determinant of the coefficient matrix [R] is

$$\begin{bmatrix} 1 & 0 & 0 & 1 & 0 & 0 \\ 0 & 1 & 0 & 0 & 1 & 0 \\ 0 & 0 & 1 & 0 & 0 & 1 \\ 0 & -Rc_{13} & Rc_{12} & 0 & -Rc_{23} & Rc_{22} \\ Rc_{13} & 0 & -Rc_{11} & Rc_{23} & 0 & -Rc_{21} \\ -Rc_{12} & Rc_{11} & 0 & -Rc_{22} & Rc_{21} & 0 \end{bmatrix}$$

$$= \begin{bmatrix} 1 & 0 & 0 & 1 & 0 \\ 0 & 1 & 0 & 0 & 1 \\ -Rc_{13} & Rc_{12} & 0 & -Rc_{23} & Rc_{22} \\ 0 & -Rc_{11} & Rc_{23} & 0 & -Rc_{21} \\ Rc_{11} & 0 & -Rc_{22} & Rc_{21} & 0 \end{bmatrix}$$

$$-\begin{bmatrix} 0 & 1 & 0 & 1 & 0 \\ 0 & 0 & 1 & 0 & 1 \\ 0 & -Rc_{13} & Rc_{12} & -Rc_{23} & Rc_{22} \\ Rc_{13} & 0 & -Rc_{11} & 0 & -Rc_{21} \\ -Rc_{12} & Rc_{11} & 0 & Rc_{21} & 0 \end{bmatrix} = 0 \tag{5.19}$$

Because of the zero determinant of the matrix [R], the system of equations $[R]\{F\} = \{fr\}$ *has either an infinite number of solutions or no solution. A check of the ranks of the coefficient and the augmented matrices is necessary to distinguish between these two possibilities. The Gaussian elimination method is used in APPENDIX F to show that the rank of the 6x6 matrix [R] is equal to the rank of the 6x7 augmented matrix [R—Fr], which is five. This means that the system of equations is consistent and has an infinite number of solutions Kreyszig [1972]. Since [R] has five linearly independent rows, the intersegmental resultant force and moment cannot be uniquely distributed between the two bony contact forces (six scalar bony contact force components).*

An assumption that either reduces the number of unknowns or increases the number of independent equations therefore needs to be made. In this study, it is assumed that, at the instant during the support phase of gait when the joint resultants were to be distributed, the bony contact forces act perpendicular to the assumed plane of the tibial plateau (i.e they are oriented in the Y-direction, perpendicular to the X-Z plane). The justification for this assumption is low friction on the essentially flat tibial plateau and high meniscal compliance. Using such an assumption, there are only two unknown bony contact force components (one per condyle). Therefore, the idealized bony contact forces make no contribution in three of the six equilibrium equations; the X and Z components of the resultant joint force, and the Y component of the resultant joint moment. Furthermore, just two of the three remaining equilibrium equations (Y component of the force, and Y and Z components of the moment) can be used to determine the two unknown bony contact force components, once the ligament and muscle forces are known. Thus, one of the three remaining equilibrium equations needs to be neglected. The Z moment of the moment equation is discarded because moment arms causing the unbalanced moments about the medial-lateral Z-axis are relatively small compared to those about the anterior-posterior X-axis. In addition, deformity of degenerative genu varus and valgus occurs in the Y-Z plane. This deformity is at least consistent with the notion that the X component of the resultant joint moment has a greater influence on the distribution of the bony contact forces than the Z component. Therefore, retention of the moment equation about the X axis is justified. The two retained equations (Y force; X moment) are later identified as the determinate model (SECOND).

The six equilibrium equations of the model now have 28 unknowns (two Y-component bony contact forces, 13 muscle forces and 13 ligament forces). While the number of unknowns has thus been reduced, the problem still remains indeterminate. Although a solution to this equation system could be obtained solely by optimization techniques, the limitations of such an approach can be reduced if the solution also incorporates additional relevant information not dependent upon the choice of the specific optimization criterion. A new iterative algorithm to solve this indeterminate knee problem is described in Chapter 8 that utilizes only two of the six equilibrium equations, together with an optimization formulation.

MUSCLE NAME	JOINTS CROSSED
gluteus medius1	H
gluteus medius2	H
gluteus medius3	H
gluteus minimus1	H
gluteus minimus2	H
gluteus minimus3	H
gluteus maximus1	H
gluteus maximus2	H K
gluteus maximus3	H K
adductor magnus1	H
adductor magnus2	H
adductor magnus3	H
adductor longus	H
adductor brevis	H
pectineus	H
iliacus	H
psoas	H
quadratus femoris	H
gemelli	H
piriformis	H
rectus femoris	H K
semimembranosus	H K
semitendinosus	H K
biceps femoris (lh)	H K
gracilis	H K
sartorius	H K
tensor fasciae latae	H K
vastus medialus	K
vastus intermedius	K
vastus lateralis	K
biceps femoris(sh)	K
medial gastrocnemius	K A
lateral gastrocnemius	K A
soleus	A
tibialis posterior	A
fl. digitorum longus	A
fl. hallucis longus	A
peroneus brevis	A
peroneus longus	A
tibialis anterior	A
peroneus tertius	A
ext. digitorum longus	A
ext. hallucis longus	A

Table 5.18: Muscle mapping according to one and two joint muscles at the Hip (H), Knee (K) and Ankle (A)

Chapter 6

New Iterative Algorithm

6.1 General Description of the Algorithm

The algorithm for the solution of the joint dustribution problem includes three parts. The first part, an initial optimization model (KNEE1), uses a cost function having 28 design variables (13 ligament, 13 muscle and 2 bony contact forces) and the six equilibrium equations as constraints. The muscle force solutions alone are then used as input to the second part, a determinate model (SECOND), along with values for ligament forces estimated by the nonlinear spring ligament model given in Equation (7.5). Solution of the second part provides a pair of initial bony contact forces. These bony contact forces are then used as input to the third part of the algorithm, a second optimization model (KNEE2), which uses a cost function having 26 design variables (13 ligament and 13 muscle forces) and six equilibrium equations as constraints. The muscle forces from the third part are then used as input to the determinate model (SECOND), so that new bony contact forces are generated. The initial and second set of the two Y-component bony contact forces are then compared. If the change between these two sets of bony contact forces is less than a specified convergence criterion (e.g., 0.005 N in FiIGURE 6.1 on page 116), then the second set of forces is taken as the solution for the bony contact forces. If not, the second set of bony contact forces is again used as input to the third part (KNEE2) to obtain a new set of muscle forces, which are in turn used as input to the second part (SECOND) to get another set of bony contact forces. The process continues until the difference between the new bony contact forces generated and previous bony contact forces is less than the convergence parameter. That is, the iterative process is continued until the bony contact forces

consistent with the muscle and ligament forces appropriate for the determinate model become essentially equal to the bony contact forces computed by the optimization procedure. The flow chart of the proposed algorithm is presented in FIGURE 6.1 on page 116. From the flow chart, it can be seen that this algorithm includes an input module, two optimization models and a determinate model. These models will be further described in the following sections.

6.1.1 Definition of Optimization Problem

The general optimization problem is defined as follows: Find an n-vector F of design variables (forces in the present problem) that minimizes a cost function U(F) subject to :

(1) p equality constraints: $H_i(F) = 0$, $i=1,2,...,p$

(2) m inequality constraints: $G_i(F) \leq 0$, $i=1,2,...,m$

(3) n explicit bounds on design variables: $F_{il} \leq F_i \leq F_{iu}$, $i=1,2,...,n$

where Fi1 is the smallest value (lower bound), Fiu the largest value (upper bound), and Fi the value of the ith design variable. The optimum solution depends on the cost function U(F) used in the problem formulation. Several cost functions are studied in a later section.

6.1.2 Explanation of Input Module

The input module uses all the data necessary for the prediction of forces transmitted across the joint. These data include the location of the knee centre (the coordinate system origin of the model), the insertions and origins of ligament and muscle elements, the locations of the bony contact forces, the intersegmental resultant force and moment, and a preselected convergence parameter for the bony contact forces. The computer program used in the optimization models to solve the distribution problem is IDESIGN, which requires some user selected parameters and user subroutines (Arora et al. [1984]).

6.1.3 Explanation of First Optimization Model KNEE1

KNEE1 is an optimization model having 28 design variables, which is used in the first part of the algorithm to get initial values for muscle forces for use in the SECOND model. KNEE1 uses a cost function minimizing the sum of the cubed muscle stresses,

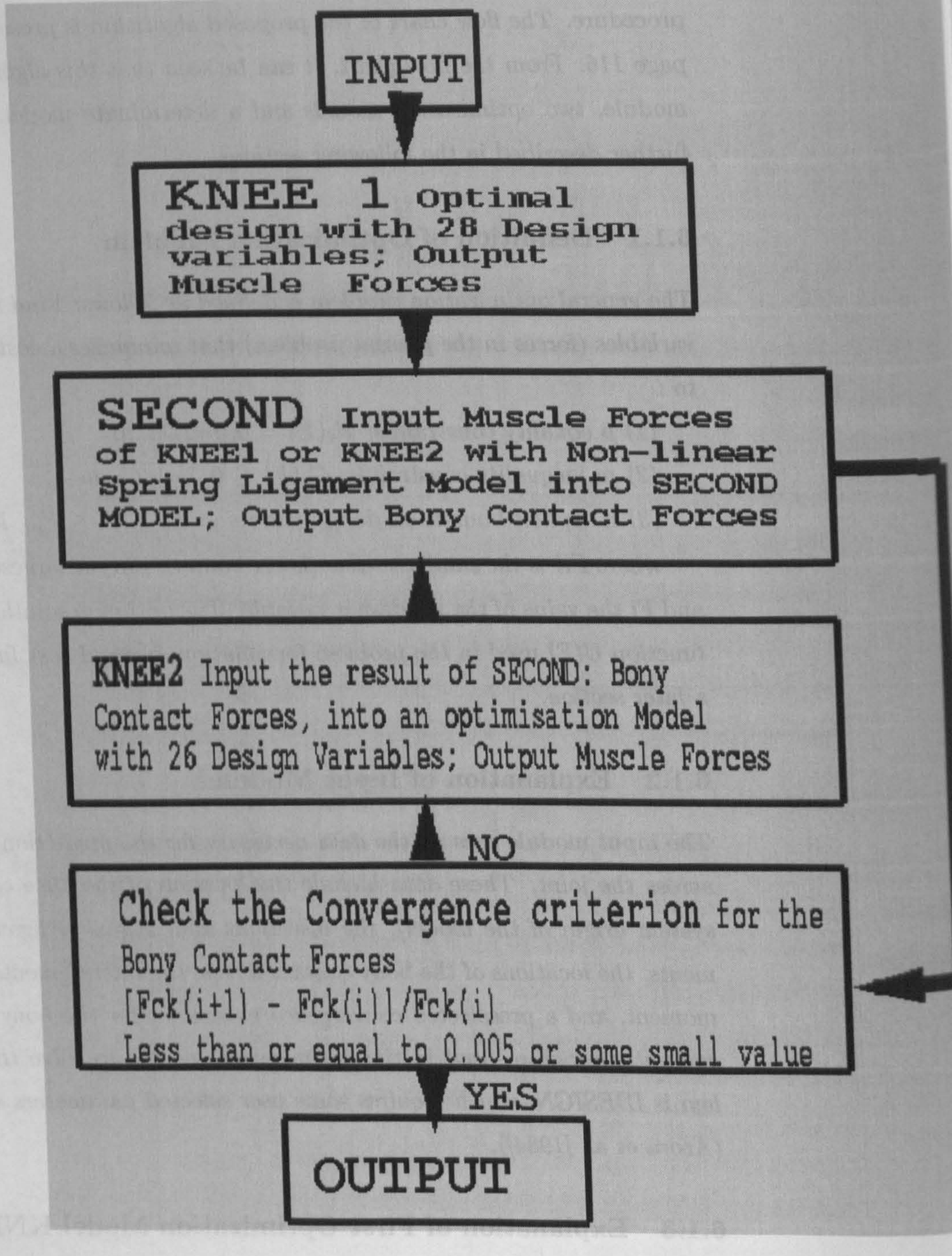

Figure 6.1: The flow chart of the proposed algorithm

the cubed ligament stresses, and the cubed bony contact forces. The constraints are the six equilibrium equations and explicit bounds on the design variables:

Design Variables: Fm_i, Fl_j, Fc_k, i=1,...13, j=1,...13, and k=1,2

Cost Function:

$$\sum_{i=1}^{13} fm_i^{e1} + \sum_{j=1}^{13} fl_j^{e2} + \sum_{k=1}^{2} fc_k^{e3}$$

where fm_i are muscle stresses, $fm_i = Fm_i/Am_i$. Am_i are muscle relative PCSA (physiological cross-sectional area). fl_j are ligament stresses, $fl_j = Fl_j/Al_j$. Al_j are ligament cross-sectional areas. Fc_k are resultant bony contact forces, $Fc_k = |Fc_{k2}|$. Fc_{k2} are Y-component of the kth bony contact forces. e1 is the exponent of muscle stresses. e2 is the exponent of ligament stresses. e3 is the exponent of bony contact forces.

Equality Constraints: (six equilibrium equations)

$$Fr_1 = \sum_{i=1}^{13} Fm_{i1} + \sum_{j=1}^{13} Fl_{j1} \tag{6.1}$$

$$Fr_2 = \sum_{i=1}^{13} Fm_{i2} + \sum_{j=1}^{13} Fl_{j2} + \sum_{k=1}^{2} Fc_{k2} \tag{6.2}$$

$$Fr_3 = \sum_{i=1}^{13} Fm_{i3} + \sum_{j=1}^{13} Fl_{j3} \tag{6.3}$$

$$MR_1 = \sum_{i=1}^{13}(Fm_{i3}Rm_{i2} - Fm_{i2}Rm_{i3}) + \sum_{j=1}^{13}(Fl_{j3}Rl_{j2} - Fl_{j2}Rl_{j3}) + \sum_{k=1}^{2}(-Fc_{k2}Rc_{k3}) \tag{6.4}$$

$$Mr_2 = \sum_{i=1}^{13}(Fm_{i1}Rm_{i3} - Fm_{i3}Rm_{i1}) + \sum_{j=1}^{13}(Fl_{j1}Rl_{j3} - Fl_{j3}Rl_{j1}) \tag{6.5}$$

$$Mr_3 = \sum_{i=1}^{13}(Fm_{i2}Rm_{i1} - Fm_{i1}Rm_{i2}) + \sum_{j=1}^{13}(Fl_{j2}Rl_{j1} - Fl_{j1}Rl_{j2}) + \sum_{k=1}^{2}(Fc_{k2}Rc_{k1}) \tag{6.6}$$

Fr_1, Fr_2 and Fr_3 are the intersegmental resultant force components in the X, Y and Z directions, respectively. Mr_1, Mr_2 and Mr_3 are the intersegmental resultant moment components in the X, Y and Z directions, respectively. Fmi_1, Fmi_2 and Fmi_3 are the muscle force components for the ith muscle in the X, Y and Z directions, respectively. Fl_{j1},Fl_{j2} and Fl_{j3} are the ligament force components for the jth ligament in the X, Y and Z directions, respectively. Fc_{k2} is the Y-component of the kth bony contact force. Rm_{i1}, Rm_{i2}, Rm_{i3}, Rl_{j1}, Rl_{j2}, Rl_{j3}, Rc_{k1} and Rc_{k3} are corresponding

moment arms. The X and Z components of the bony contact forces are not used in KNEE1.

Inequality Constraints: None in this formulation.

Explicit Bound on Design Variables:

$0 \leq Fm_i \leq Fm_u$, $0 \leq Fl_j \leq Fl_u$, $0 \leq Fc_k \leq Fc_u$

where $Fm_u$is the upper bound for muscle forces, Fl_u is the upper bound for ligament forces and Fc_u is the upper bound for bony contact forces (In the present study, $Fm_u$and Fl_u are 1000 N and Fc_u is 10000 N). Although these upper bound constraints are large values, they serve primarily to provide the assurance that the solution does not reach unreasonable values. Normal walking will never introduce forces in one muscle or one ligament higher that one time body weight. Similarly the condyle contact forces never reach the value of ten times body weight during normal walking of a healthy individual of average mass (75-80 Kg).

6.1.4 Explanation of the Determinate Model SECOND

The determinate model (SECOND) used in the second part of the algorithm uses two equilibrium equations to solve for the two unknown bony contact forces. As previously discussed, the two equilibrium equations are the resultant joint force in the Y-direction and the resultant joint moment in the X-direction. The assumption of the bony contact forces being perpendicular to the tibial plateau and acting at known locations leads to only two unknown bony contact forces in the equilibrium equations. In these two equilibrium equations, the known ligament forces calculated from nonlinear spring equations, and the known muscle forces predicted from the optimization models (KNEE1 or KNEE2) are substituted to uniquely determine the two bony contact forces.

6.1.5 Explanation of 2nd Optimization Model

KNEE2 is the second optimization model having 26 design variables, which is used in the third part of the algorithm to re-calculate the muscle and ligament forces. Although KNEE1 and KNEE2 have different numbers of design variables and different cost functions, the constraints on the design variables are the same. In the KNEE2 model, the design variables are muscle and ligament forces, since the bony contact forces are "known" from SECOND. The optimization problem is formulated as follows:

Design Variables : Fm_i, Fl_j *and* i,j = 1,2...,13

Cost Function:

$$\sum_{i=1}^{13} fm_i^{e1} + \sum_{j=1}^{13} fl_j^{e2} \tag{6.7}$$

Equality Constraints: (six equilibrium equations)

$$Fr_1^* = \sum_{i=1}^{13} Fm_{i1} + \sum_{j=1}^{13} Fl_{j1} \tag{6.8}$$

$$Fr_2^* = \sum_{i=1}^{13} Fm_{i2} + \sum_{j=1}^{13} Fl_{j2} \tag{6.9}$$

$$Fr_3^* = \sum_{i=1}^{13} Fm_{i3} + \sum_{j=1}^{13} Fl_{j3} \tag{6.10}$$

$$Mr_1^* = \sum_{i=1}^{13}(Fm_{i3}Rm_{i2} - Fm_{i2}Rm_{i3}) + \sum_{j=1}^{13}(Fl_{j3}Rl_{j2} - Fl_{j2}Rl_{j3}) \tag{6.11}$$

$$Mr_2^* = \sum_{i=1}^{13}(Fm_{i1}Rm_{i3} - Fm_{i3}Rm_{i1}) + \sum_{j=1}^{13}(Fl_{j1}Rl_{j3} - Fl_{j3}Rl_{j1}) \tag{6.12}$$

$$Mr_3^* = \sum_{i=1}^{13}(Fm_{i2}Rm_{i1} - Fm_{i1}Rm_{i2}) + \sum_{j=1}^{13}(Fl_{j2}Rl_{j1} - Fl_{j1}Rl_{j2}) \tag{6.13}$$

where $Fr_1^* = Fr_1$

$$Fr_2^* = Fr_2 - Fc_{12} - Fc_{22} \tag{6.14}$$

$$Fr_3^* = Fr_3 \tag{6.15}$$

$$Mr_1^* = Mr_1 - \sum_{k=1}^{2}(-Fc_{k2}Rc_{k3}) \tag{6.16}$$

$$Mr_2^* = Mr_2 \tag{6.17}$$

$$Mr_3^* = Mr_3 - \sum_{k=1}^{2}(-Fc_{k2}Rc_{k1}) \tag{6.18}$$

Explicit Bounds on Design Variables:

$0 \leq Fm_i \leq Fm_u$, $0 \leq Fl_j \leq Fl_u$

6.1.6 Rationale for the Algorithm

In the present knee model, there are 28 unknowns in the six scalar equilibrium equations. A solution to these equations can be obtained solely by an optimization technique (e.g., KNEE1). However, such a solution would not be unique, since it would depend on the cost function used. The degree of uncertainty in the final solution can be reduced by incorporating additional conditions in the solution process which are not dependent upon the choice of a cost function. This is the fundamental motivation for proposing and developing the new iterative algorithm that combines optimization techniques (KNEE1 and KNEE2) with a determinate model (SECOND).

A novel iterative algorithm, with its convergence criterion based on the bony contact forces, is proposed to reduce the uncertainties of SECOND and KNEE2. Since six equilibrium equations can not be solved uniquely for two bony contact forces (with three components each), a determinate model (SECOND) is developed consisting of two of the six equilibrium equations and with known ligament and muscle forces. The ligament forces are calculated from a nonlinear spring model. The muscle forces used in SECOND are predicted from KNEE2. The iterative process in the model algorithm can then reduce the uncertainties of SECOND (two of six equilibrium equations used and uncertain spring ligament properties) by using all six equations and unknown (and variable) ligament forces in KNEE2 to predict muscle forces. However, different convergence criteria used for the bony contact forces in the entire new algorithm can lead to slightly different convergent solutions. The convergence criterion in the algorithm serves only to produce a mathematically unique solution, but not necessarily one with biological or physiological meaning.

In the present study, a change in each bony contact force of less than 0.005 N from one iteration to the next is used as the convergence criterion because this criterion causes the solution of the bony contact forces to converge to the second decimal accuracy of the body weight. In addition, the bony contact forces calculated by SECOND are used as known input into KNEE2. This reduces the uncertainty of

using the bony contact forces as variables in the cost function. Also, this reduces the degree of redundancy in the formulation of KNEE2 from 28 to 26 variables. However, the formulation in KNEE2 is still indeterminate. Therefore, an optimization technique is used in KNEE2 to mathematically solve this indeterminate problem.

The reason for using the initial optimization model (KNEE1) as the first part of the new algorithm is simply to find a reasonable set of initial muscle forces for the overall solution algorithm. Initial muscle forces along with nonlinear spring ligament forces are then used as input in the determinate model to calculate the bony contact forces.

The reason for using the determinate model (SECOND) as the second part of the new algorithm is to uniquely solve for the two bony contact force components. To accomplish this, two major assumptions are made. One is that the two bony contact forces are perpendicular to the tibial plateau. The second is that the Y force and X moment scalar equilibrium equations are the appropriate equations to use to determine these bony contact forces. Ligament forces calculated by the nonlinear spring model are used in SECOND to provide additional information that is not dependent upon the choice of a specific optimization criterion.

The reason for using the second optimization model (KNEE2) as the third part of the new algorithm is to calculate an updated set of muscle forces for the determinate model. To reduce the number of unknowns and to avoid the assumption that the cost function really determines the bony contact forces, the two bony contact forces calculated from SECOND are used as known values. Twenty-six unknowns (thirteen muscle and thirteen ligament forces) are estimated in this second optimization model. In general, the ligament forces calculated from KNEE1 are not consistent with those calculated by the nonlinear spring model (Equation (7.5)). Also, the lack of accurate information regarding the ligament material properties used in the nonlinear spring equation makes KNEE2 important for recalculation of the muscle and ligament forces with "known" bony contact forces. The lack of accurate information on the ligament properties is also a reason to include the ligament forces in this second optimization model. The ligament forces calculated by the optimization models depend on the upper and lower bound constraints imposed, and thus may be different from the ligament forces calculated from the nonlinear spring model (Equation (7.5)). During the iterative procedure, KNEE2 provides muscle forces which are used as input into SECOND with calculated known spring ligament forces to estimate the two bony

contact forces. Since the convergence criterion of this model algorithm includes only bony contact forces, convergence of the muscle forces is not guaranteed in the final solution.

The reason for using a nonlinear cost function in the optimization models of the new algorithm is that the linear optimization methods are of limited applicability because the number of active muscles can be no greater than the number of constrained equations Pedersen et al. [1987]. The cost function used in this new iterative algorithm is described further in the next section.

Mathematically, the nonlinear cost functions used in this algorithm depend on the muscle stresses cubed and bony contact forces cubed, and the ligament stresses with different exponents. Since the design variables (i.e., muscle forces, ligament forces and bony contact forces) are all non-negative, the matrix of second derivatives of the cost function is positive semidefinite. In other words, the cost function is convex. Furthermore, the constraint functions are linear and convex. This means these optimization problems are convex, and that a local minimum is the global minimum. However, the global minimum need not lead to a unique solution set of muscle, ligament and bony contact forces Arora [1989].

Since there is no a priori basis for choosing the cost function, the cost function used in the optimization models is empirically chosen based on comparisons between predicted solutions and results reported in the literature. Use of different cost functions will change the results. A better basis for choosing a cost function for the optimization model may improve the proposed algorithm.

This new iterative algorithm includes additional information (i.e., an iterative process with its convergence criterion dependent on bony contact forces, plus a determinate model) that is not dependent upon the choice of a specific optimization criterion. It therefore improves the procedure by predicting activity in more muscles than the pure optimization model (KNEE1), and by predicting bony contact forces that are consistent with the results of previous investigations.

6.2 Cost Function of the Optimization Models

In this section, the cost function to be used in the optimization models of the new algorithm will be determined by comparing solutions (obtained using different cost functions) with results published in the literature. As mentioned in the last section,

linear optimization methods prove to be of limited applicability because the number of active muscles can be no greater than the number of constrained equations. Therefore, several nonlinear cost functions are evaluated in this section.

As shown in section 8.1.3, the nonlinear cost function includes the sum of the muscle stresses with exponent e1, the sum of the ligament stresses with exponent e2, and the sum of the two Y-component bony contact forces with exponent e3. Various cost functions are evaluated by varying the exponents e1, e2 and e3.

The use of a cubic exponent for the muscle stresses in the cost function is based on the relationship of muscle force to contraction endurance Pedersen et al. [1987]. Therefore, e1 is fixed at 3 for both KNEE1 and KNEE2 for the normal walking calculations.

Since no bony contact forces are included in the cost function of KNEE2, a cubic exponent of bony contact forces in the cost function is used only in KNEE1 for the data refering to normal walking. This choice is based on comparing the solutions obtained by changing only the exponent of bony contact forces and fixing the exponents of muscle and ligament stresses. In the first part of the new iterative algorithm (KNEE1), changing only the exponent of bony contact forces (e3) from 1 to 3 and fixing the exponents of muscle and ligament stresses (e1 and e2) in the cost function changes the solution of the total bony contact force (FcT) obtained from KNEE1 itself, but does not change the results of the entire new algorithm (Table 6.1 on page 124). In Table 6.1 on page 124, the exponent of muscle stresses is fixed at 3 and the exponents of ligament stresses and bony contact forces are varied from 1 to 3. In the first three columns of Table 6.1 on page 124, the exponent of ligament stresses is fixed at 1 and the exponent of bony contact forces is varied from 1 to 3. The total bony contact force varies from 2037 N to 2250 N. In the fourth to sixth columns of the Table 6.1 on page 124, the exponent of ligament stresses is fixed at 2 and the exponent of bony contact forces is varied from 1 to 3. The total bony contact force varies from 2051 N to 2302 N. In the last three columns of the Table 6.1 on page 124, the exponent of ligament stresses is fixed at 3 and the exponent of bony contact forces is again varied from 1 to 3. The total bony contact force of these three columns varies from 2087 N to 2172 N. However, the final converged results from the overall model algorithm for the total bony contact force are the same (2199 N) with different exponents for the bony contact force, as seen in Table 6.2 on page 126. In the first three columns of Table 6.2 on page 126, the total bony contact force is 2199 N with e3 as 1, 2 or 3 and e2 =

1. *In the fourth to sixth columns, the values for the total bony contact force are very close, varying from 2176 N to 2188 N with e3 = 1, 2 or 3 and e2 = 2. In the last three columns, the values of the total bony contact force are again reasonably close, varying from 2930 N to 2978 N with e3 = 1, 2 or 3 and e2 = 3. Therefore, one can conclude that the different exponents for the bony contact forces do change the solution from KNEE1, but not the final converged results of the overall algorithm. This behaviour is due to the fact that KNEE1 is only the initial model of the overall model algorithm, and the overall model algorithm uniquely modifies the solution obtained from KNEE1 due to iterations with the determinate model. The cubic exponent of bony contact forces is used for KNEE1 of the present model algorithm.*

Different cost function exponents for ligament stresses in the optimization models (KNEE1 and KNEE2) of the new model algorithm do greatly change the final results. For example, the sixth column of Table 6.2 on page 126 shows that using a ligament stress exponent of 2 and a bony contact force exponent of 3, leads to a muscle force distribution with just six muscles active. However, the ninth column of Table 6.2 on page 126 shows that by using a ligament stress exponent of 3, ten muscles are predicted to be active. The total bony contact force is also changed significantly from 2188 N to 2978 N. To demonstrate this, five different integer exponents for ligament stresses, together with a cubic exponent for the muscle stresses and the bony contact forces, are used in the cost function of the optimization models (KNEE1 and KNEE2) to estimate the bony contact forces and muscle force distributions. The solutions from the new algorithm with different exponents for ligament stresses used in the initial and second optimization models, are shown in Table 6.3 on page 127. Note the difference in the bony contact forces and muscle force distributions as the ligament stress exponent (e2) varies from one to five.

	1	2	3	4	5	6	7	8	9
	e1=3 e2=1 e3=1	e1=3 e2=1 e3=2	e1=3 e2=1 e3=3	e1=3 e2=2 e3=1	e1=3 e2=2 e3=2	e1=3 e2=2 e3=3	e1=3 e2=3 e3=1	e1=3 e2=3 e3=2	e1=3 e2=3 e3=3
BF	0	0	0	0	0	0	0	0	0
GRA	0	0	0	0	0	0	0	0	0
RF	158	158	146	158	158	155	160	160	177
SART	12	12	0	12	12	0	32	29	0
SEMIM	0	0	0	0	0	0	0	0	0
SEMIT	0	0	0	0	0	0	0	0	0
TFL	73	73	366	73	73	443	65	65	167
GASM	0	0	0	0	0	0	0	0	0
GASL	0	0	0	0	0	0	0	0	0
BFS	0	0	0	0	0	0	0	0	0
VI	219	219	203	219	219	215	222	222	249
VL	204	204	145	204	204	119	231	230	148
VM	392	392	410	392	392	392	389	390	441
AMC	0	0	0	0	0	0	0	0	0
DMC	0	0	0	0	0	0	0	0	0
PMC	0	0	0	0	0	0	0	0	0
OMC	0	0	0	0	0	0	0	0	0
MPC	0	0	0	0	0	0	0	0	0
LPC	0	0	0	0	0	0	0	0	0
OLC	6	6	114	6	6	150	0	1	27
LC	0	0	0	0	0	0	0	0	113
DLC	0	0	35	0	0	23	0	0	50
AAC	63	63	15	63	63	2	26	29	5
PAC	0	0	0	0	0	0	19	17	53
APC	0	0	0	0	0	0	0	0	0
PPC	0	0	0	0	0	0	0	0	0
Fc_M	1834	1834	1692	1834	1834	1655	1852	1850	1809
Fc_L	203	217	558	217	217	647	238	237	363
Fc_T	2037	2051	2250	2051	2051	2302	2090	2087	2172

Table 6.1: Results from 1st Optimization Model KNEE1: where e1: the exponent of mus
stresses in the KNEE1 and KNEE2 cost functions, e2:the exponent of ligaments stresses in t
KNEE1 and KNEE2 cost functions, e3: the exponent of bony contact forces in the KNE
and KNEE2 cost functions:Subj:1; 17% of GC

Increasing the exponent of the ligament stresses gives them more weight in the cost function. Therefore, minimizing the cost function after increasing the exponents of the ligament stresses results in decreased ligament forces. Note, however, that the bony contact forces and muscle forces increase when the exponent of ligament stresses is increased (Table 6.3 on page 127). This can be explained by the three force equilibrium equations (2.4.4 to 2.4.6). No X and Z components of the bony contact forces are considered in this knee model. Only the Y component of the bony contact forces is considered in the force equilibrium equations. Since the intersegmental resultant force is known and constant, decreasing the X and Z components of the ligament forces will increase the X and Z components of the muscle forces. The increased muscle forces affect the Y component of the force equilibrium Equation (2.4.5). The combination of the increased muscle forces and the decreased ligament forces is accompanied by an alteration of the bony contact forces. This also explains the difference in solutions with differing exponents of ligament stress. The cost function values are much increased when the exponent of ligament stress, e2, is 3. This increase comes from the muscle stresses and bony contact forces, since they are considerably increased when the exponent of ligament stresses is raised to 3. Physically, the ligament forces become smaller as the ligament stresses exponent increases. As mentioned above, the precise ligament properties for the spring ligament model are not presently known. The relative insignificance of the ligament forces in the optimization models further supports the chosen cost function of the new iterative algorithm.

	1	2	3	4	5	6	7	8	9
	e1=3 e2=1 e3=1	e1=3 e2=1 e3=2	e1=3 e2=1 e3=3	e1=3 e2=2 e3=1	e1=3 e2=2 e3=2	e1=3 e2=2 e3=3	e1=3 e2=3 e3=1	e1=3 e2=3 e3=2	e1=3 e2=3 e3=3
BF	0	0	0	0	0	0	0	0	0
GRA	0	0	0	0	0	0	0	0	0
RF	169	169	169	169	168	169	242	253	256
SART	12	12	12	14	14	17	57	66	64
SEMIM	0	0	0	0	0	0	49	35	57
SEMIT	5	5	5	0	1	0	45	33	53
TFL	123	124	124	111	108	115	52	66	26
GASM	0	0	0	0	0	0	139	106	109
GASL	0	0	0	0	0	0	185	204	188
BFS	0	0	0	0	0	0	0	0	0
VI	236	236	236	236	237	235	333	333	344
VL	258	258	258	248	258	255	329	303	351
VM	409	409	409	410	410	410	562	555	557
AMC	151	151	151	154	145	155	67	89	60
DMC	0	0	0	0	0	0	28	29	33
PMC	0	0	0	0	0	0	18	11	24
OMC	0	0	0	0	0	0	0	0	0
MPC	0	0	0	0	0	0	0	0	0
LPC	0	0	0	0	0	0	12	23	20
OLC	43	43	43	30	30	34	8	10	9
LC	48	47	48	42	43	43	55	66	60
DLC	20	20	20	24	33	31	19	20	20
AAC	36	36	36	44	38	40	0	0	0
PAC	0	0	0	0	0	0	0	0	0
APC	0	0	0	0	0	0	56	50	62
PPC	0	0	0	0	0	0	0	0	10
Fc_M	1807	1807	1806	1814	1813	1813	2109	2065	2114
Fc_L	392	392	393	362	370	375	857	865	864
Fc_T	2199	2199	2199	2176	2183	2188	2966	2930	2978

Table 6.2: Final Converged Results with Different Cost Functions e1: the expon ent of muscle stresses in the KNEE1 and KNEE2 cost functions, e2:the exponent of liga ments stresses in the KNEE1 and KNEE2 cost functions, e3: the exponent of bony contac t forces in the KNEE1 and KNEE2 cost functions,:Subj:1; 17% of GC

	e1=3 e2=1 e3=3	e1=3 e2=2 e3=3	e1=3 e2=3 e3=3	e1=3 e2=4 e3=3	e1=3 e2=5 e3=3
BF	0	0	0	0	0
GRA	0	0	0	0	0
RF	169	169	256	560	664
SART	12	17	64	131	0
SEMIM	0	0	57	68	0
SEMIT	5	0	53	49	0
TFL	124	115	26	7	0
GASM	0	0	109	995	1180
GASL	0	0	188	1060	2080
BFS	0	0	0	154	332
VI	236	235	344	711	709
VL	258	255	351	155	0
VM	409	410	557	1361	2136
AMC	151	155	60	41	24
DMC	0	0	33	23	0
PMC	0	0	24	22	8
OMC	0	0	0	7	20
MPC	0	0	0	0	8
LPC	0	0	20	26	0
OLC	43	36	9	8	2
LC	48	43	60	46	15
DLC	20	31	20	12	5
AAC	36	40	0	0	0
PAC	0	0	0	0	0
APC	0	0	62	81	39
PPC	0	0	10	68	37
Fc_M	1806	1813	2114	3105	3147
Fc_L	393	375	864	3062	4909
Fc_T	2199	2188	2978	6167	8056

Table 6.3: Predicted Force Distributions with Different Exponents of Ligament Stresses in the Cost Functions of KNEE1 and KNEE2: e1: the exponent of muscle stresses in the KNEE1 and KNEE2 cost functions, e2:the exponent of ligaments stresses in the KNEE1 and KNEE2 cost functions, e3: the exponent of bony contact forces in the KNEE1 and KNEE2 cost functions, :Subj:1; 17% of GC

6.3 Evaluation of the Model

In the present study, ligament stresses cubed are used in the cost function. Solving the force distribution problem by using ligament stresses that are raised to the third power leads to more physiologically reasonable bony contact force solutions that are obtained otherwise. The term physiologically reasonable refers to the notion of muscle convergence and increased predictability of muscle activity in agreement with EMG records (active concurrence). Also, this produces more reasonable muscle force distributions. Comparing the bony contact forces calculated with this new algorithm with data in the literature shows that using ligament stresses raised to the third power is most appropriate. Two sorts of bony contact force values can be found in the literature: the total bony contact force, and the ratio of the lateral and medial bony contact

forces. Morrison [1970] suggested that the maximum bony contact force calculated at the knee during walking was in the range of 2-4 times body weight, and when the joint was highly loaded the greater portion of the load was transmitted through the medial condyle. Harrington [1983] estimated that the average maximum knee bony contact force was 3.5 times body weight for normal subjects during walking. Using ligament stresses raised to the fifth power with the new algorithm leads to a resultant bony contact force of approximately 12 times body weight. Likewise, using ligament stresses raised to the fourth power leads to a resultant bony contact force of 8.94 times body weight (fourth column of the Table 6.3 on page 127), while using ligament stresses raised to powers less than 4 leads to resultant bony contact force in a more credible range (3.17 to 4.31 times body weight). Therefore, it seems reasonable to use ligament stress exponents that are less than 4.

Andriacchi et al. [1983] calculated the distribution of forces at the knee during various phases of the walking cycle. At 20% of the walking cycle, the medial plateau had a bony contact force of 1040 N, while the lateral plateau had a bony contact force of 250 N. The proportion of lateral bony contact force to medial bony contact force was therefore approximately 1:4. Using a normal 60 kg subject with a less-than-average tibiofemoral angle, Kettlekamp et al. [1973] reported the ratio of compressive forces on the lateral to medial plateau during standing to be 1:10. Using ligament stresses raised to the first power, the ratio of bony contact forces between the lateral and medial plateaux is 1:4.6 with the new algorithm. Using ligament stresses raised to the 2nd power, the ratio of resultant bony contact forces is 1:4.8. On the other hand, using ligament stresses raised to the third power, the resultant bony contact force ratio is 1:2.5, which appears more reasonable, given an almost anatomically symmetric tibia. The present algorithm therefore uses the cubic exponent of ligament stresses in the cost function.

Further justification for using the sum of the cubes of the ligament stresses in this model can be made by comparing its muscle force distribution predictions to muscle activity patterns based on existing EMG data.

Andriacchi et al. [1984] reported EMG records for the knee muscles at 10 degrees of flexion (i.e., at about 17% of the gait cycle). Their data showed the highest activity in eight muscles at this point. (SART, GASL SEMIT, TFL, VL, VI, VM and RF). Using ligament stresses squared or raised to the first power, the present algorithm predicts activity in only six of the eight muscles. On the other hand, using ligament stresses

to the third power predicts activity in ten muscles, including all eight of the muscles shown to be active by EMG data (Table 6.4 on page 129). Collection of EMG data was also performed within our data acquisition scheme described in APPENDIX E as part of the CAMARN European Project and in collaboration with the Kinesiology Department of K.U. Leuven.

Also, the ligament forces predicted by using the sum of the cubes of the ligament stresses are much less than their ultimate strength values and have large safety factors (3.4 to 8.5). Trent et al. [1976] reported that the ultimate strengths of MCL (medial collateral ligament) ICL (lateral collateral ligament), ACL (anterior cruciate ligament), and PCL (posterior cruciate ligament) were 0.74 BW, 0.54 BW, 0.90 BW and 0.85 BW, respectively. In the present study, the ligament forces (ninth column of Table 6.2 on page 126) predicted by the model algorithm are 0.17 BW (117 N), 0.16 BW (109 N), 0.0 BW, and 0.1 BW (72 N) for the MCL, LCL, ACL and PCL, respectively. Therefore, the safety factors (ultimate strength divided by predicted ligament force) vary from 3.4 to 8.5. These small ligament force solutions are further supported by Lewis et al. [1981]. They concluded from data measured using buckle transducers that in level walking there was, at most, minimal ligament force. These results further support the use of the present cost function.

6.4 Discussion

As stated previously, the mechanical model used in this study to represent the musculoskeletal system in the neighbourhood of the human knee includes thirteen major muscles, thirteen ligaments and two bony contact forces. All the force elements (muscle, ligament and bony contact forces), properties and numerical data needed in the model calculations are depicted and discussed in chapters 7 and 8.

6.4.1 Assumptions Made in Development of the Model Algorithm

The main assumptions made in the knee model are summarized as follows:

1. Anatomical Data: Since anthropometric data of muscle and ligament insertions/origins and bony contact point locations could not be found for the same specimen, the anatomical data (geometric data) used in the present study are based on different studies presented in the literature. The tibial plateau is considered to lie in

	1	2	3	4
	e1=3	e1=3	e1=3	Andriacchi 1984)EMG
	e2=1	e2=2	e2=3	RECORDINGS
MUSCLE	e3=3	e3=3	e3=3	AT HIGHEST ACTIVITY
BF	0	0	0	
GRA	0	0	0	
RF	169	169	256	ACTIVE
SART	12	17	64	ACTIVE
SEMIM	0	0	57	
SEMIT	0	0	53	ACTIVE
TFL	124	115	26	ACTIVE
GASM	0	0	109	
GASL	0	0	188	ACTIVE
BFS	0	0	0	
VI	236	235	344	ACTIVE
VL	258	255	351	ACTIVE
VM	409	410	557	ACTIVE

Table 6.4: Comparison of Predicted Muscle Force Activity with EMG data e1: the exponent of muscle stresses in the KNEE1 and KNEE2 cost functions, e2:the exponent of ligaments stresses in the KNEE1 and KNEE2 cost functions, e3: the exponent of bony contact forces in the KNEE1 and KNEE2 cost functions

a plane perpendicular to the global Y-axis. The points of application of the bony contact forces are estimated from data presented in Ahmed et al. [1983]. The anatomical information needed to calculate the direction of muscle forces (i.e, muscle insertions and origins) are taken from cadaver studies reported by Brand et al. [1982]. The anatomical data needed to calculate the direction of ligament forces are calculated from regression coefficients reported by Wilson [1978] and modified with textbook drawings Anderson [1983]. Further analysis was advanced from recent data by Delp et al. [1996b].

2. Structural Characteristics of Knee: Although many investigators have concluded that a major portion of the compressive load is transmitted through the menisci, in the present study the menisci are used only to estimate the locations of the points of application of the bony contact forces Ahmed et al. [1983]. Since the objective of the study is to predict the maximum bony contact forces, neglecting the menisci does not decrease the load transmitted to the tibial plateau, even though menisci can significantly affect the load distribution. Friction between femoral and tibial joint surfaces is ignored since the coefficient of friction between cartilage surfaces is very low Radin et al. [1973]. Deformations of the bones and of the cartilage layer of the condyles are ignored as these are relatively small compared to the displacements in the joint Walker et al. [1972]. Therefore, the knee is assumed to be composed of two rigid bodies, without friction. The only structural elements considered are 13 ligaments, 13 muscles, and 2 bony contact forces.

3. A new algorithm combining optimization models with a determinate model was developed to solve the knee distribution problem, In order to uniquely solve for the two bony contact forces, two major assumptions are made. The two bony contact forces are assumed to act perpendicular to the tibial plateau, and only the Y force and X moment equilibrium equations are used in the determinate model to determine these two bony contact forces. In the optimization models, a cost function constrained with all six equilibrium equations and upper and lower bounds on the forces is used. The different number of equilibrium equations that are used in the determinate model and the optimization models (KNEE1 and KNEE2) generates a solution set that violates the joint equilibrium equations. The converged bony contact forces and spring ligament forces calculated from SECOND, along with the corresponding muscle forces

estimated from KNEE2 of the overall algorithm, are substituted into the other four equilibrium equations that SECOND does not use (Equations 8.1, 8.3, 8.5 and 8.6). A maximum relative error of 25% in the X-component of the intersegmental resultant force with respect to the original X component of the intersegmental resultant force is found. However, these errors of the X and Z components, compared with the total bony contact force (Y-component), are very small, i.e., only 0.6 % and 0.2 % of X and Z components, respectively. These results are depicted in Table 6.5 on page 131. The first column of Table 6.5 on page 131 shows the calculated four intersegmental resultant forces and moments. The third column is the error between the first (calculated values) and the second (original values) columns. The fourth column shows the relative error between the calculated and original values of these intersegmental resultant forces and moments (the error divided by the original value and multiplied by one hundred to get percentage values). The fifth column shows the relative error compared to the total bony contact force predicted (the third column divided by the total bony contact force shown in the ninth column of the Table 6.3 on page 127). The results imply that a better understanding or modification of the determinate model needs to be made in the future, because different assumptions regarding the vectors of bony contact forces used in SECOND will generate different solutions. Furthermore, the ligament properties for the spring ligament model used in SECOND have considerable uncertainties.

4. The optimization models used the sum of the cubed muscle stresses, cubed ligament stresses and cubed bony contact forces (the last one is used only in KNEE1) as cost functions. The use of a cubic exponent for muscle stresses is based on the relationship of muscle force to contraction endurance. It is found that the use of different exponents for bony contact forces in the cost functions of KNEE1 and KNEE2 changes the solutions obtained from KNEE1 in the initial calculation, but not the final results of the overall algorithm. Therefore, in this study a cubic exponent of bony contact forces is used. Also, different exponents for the ligament stresses in the cost function are studied. After comparing the results with those in the literature, the cubic exponent for the ligament stresses is used. However, different cost function exponents for ligament stresses in the optimization models (KNEE1 and KNEE2) do greatly affect the final results. The choice of ligament stress exponent plays an important role in the new algorithm.

1	2	3	4	5
	CALCUL.VAL.	ORIG.VAL.	ERROR	REL. ER.(%)	REL. ER. TO Fc_T
Fr_1	78.278 N	62.5 N	15.778 N	25.2(%)	0.6%
Fr_3	102.229 N	96.3 N	5.929 N	6.2%	0.2%
Mr_2	-2.780 Nm	-2.5 Nm	-0.280 Nm	7.6 %	—
Mr_3	26.053 Nm	25.1 Nm	0.953 Nm	3.8%	—

Table 6.5: Errors in other four equilibrium equations of the SECOND model NOTE: Fr_1 and Fr_3 are the X and Z components of the intersegmental resultant force Mr_2 and Mr_3 are the Y and Z components of the intersegmental resultant force (CALCUL:CALCULATED, ORIG: ORIGINAL, REL: RELATIVE, ER: ERROR, VAL: VALUES

6.4.2 Limitations of the Model Algorithm

The limitations of the model are:

1. Anatomical information necessary for this mathematical model cannot be obtained easily from living subjects. Lack of complete anatomical data limits the model's practical applications. 2. In this model, only normal specimen behaviour is considered. The behaviour of an abnormal knee with pathological elements (e.g., ligaments) can be predicted only with modified data. 3. The results depend on the accuracy of the intersegmental resultant forces and moments derived from the inverse dynamics problem. Different subjects, equipment, and methods lead to different results for these parameters. 4. The results obtained by using the new algorithm depend on the determinate model. There are two main factors which affect the accuracy of solutions in the determinate model. One is the limited accuracy of the spring model (spring properties of the ligaments). The other is the assumption that the joint bony contact forces are perpendicular to the tibial plateau (reduced set of equilibrium equations). The lack of further information regarding the spring ligament model and the direction of joint bony contact forces leads to the introduction of errors in this knee model. 5. The cost function used in the optimization model is based on the comparisons between the predicted solutions and results reported in the literature. Different cost functions do change the results. A better cost function for the optimization models may further improve the proposed algorithm. 6. This new model algorithm leads to a solution that has an appropriate number of active muscles and predicts bony contact forces that are consistent with solutions presented by previous investigators. However, to make this model algorithm applicable to research arising from clinical observations (e.g., to determine quantitative values for comparing the same knee or for comparing different knees pre- and post-operatively), there are three more limitations in using the model algorithm software that need to be addressed. First, approximately one and a half hour on a VAX 11/730 is required for each run (case). The above action resulted in the need to change all the programs (Fortran mainly, the graph possibilities of idesign, the connection to Fortran and C++ subroutines etc) to the new adopted platform and operating system. Therefore everything is now compatible with Unix (and Irix 6.4 silicon graphics) platforms. The above change however, helped descrease the computation time and provided new ideas in a very diverse and powerful operating system made for heavy duty applications. Overall the following

software was used at different stages of the thesis: Operating Systems:IRIX 6.4 (SILICON GRAPHICS -INDIGO2 MAXIMUM IMPACT R10000) -UNIX, MS-DOS, VMS; Platforms:SGI, SUN (OS/Solaris), VAX, microVAX, IBM-PC, PDP-11;SOFTWARE: SILICON GRAPHICS VARSITY SOFTWARE PACKAGE, OpenGL, Open Inventor, RAPIDUP, INPERSON, IRIS ANNOTATOR, COSMO-3D, Acrobat READER 2.1, I3DM, DEVELOPER MAGIC (CVD), IRIS PERFORMER, AVS/EXPRESS, GSHARP, IRIS SHOWCASE, MODELMASTER, WEBFORCE, Latex, Uniras,X-WINDOWS, XEMACS,WEBFORCE SGI, WEBMAGIC,WEBSPACE,SGI DIGITAL MEDIA TOOLS, IMAGEVISION, Gnuplot, PC tools,Windows 95, Microsoft Office, Minitab, Macintosh,Genguide, Toolkit, Lotus, Quatro, Excel, Matlab, Plotlib, Imaker, MacWord Second, the user interactive computer program as originally developed is not user friendly. HOWEVER, RapidUP APPLICATIONS AND THE SGI IRIX 6.4 ENVIRONMENT AND DESKTOP ARE CURRENTLY SUCCESSFULLY COMBINING THE DIFFERENT PARTS OF THE SOFTWARE. Third, a great deal of data (muscle origins and insertions, ligament origins and insertions, bony contact points, muscle cross-sectional areas, ligament cross-sectional areas, spring ligament forces, and intersegmental resultant forces and moments) must be obtained and entered before running the program.

Blank Page

Chapter 7

RESULTS AND SENSITIVITY ANALYSIS

7.1 Results from the laboratory experiments

The following chapter presents graphs and tables from the laboratory experiments. (SEE PROTOCOL section 5.1.1 and FIGURE 7.1 on page 137). Several subjects (57 subjects see Table 7.1 on page 136) were tested in a group of protocol tests. The subjects were the basketball players of the Strathclyde University First and second team for three consecutive years(12 Females and 45 males, average height: 1.799122807 m (SD:0.0874), average body mass: 78.12280702 kg (SD:9.571), average age: 22.96491228 years (SD: 2.859601073)).

SUBJECT	HEIGHT (m)	BODY MASS (kg)	AGE (years)	SUBJECT	HEIGIIT	BODY MASS	AGE
1	1.75	75	23	30	1.70	69	23
2	1.78	82	22	31	1.95	88	22
3	1.84	76	23	32	1.86	80	24
4	1.79	70	22	33	1.78	74	19
5	1.91	85	21	34	1.79	80	24
6	1.76	73	21	35	1.669	60	25
7	1.65	59	22	36	1.7	86	24
8	1.89	82	24	37	1.68	62	24
9	1.78	72	24	38	1.89	81	23
10	1.74	67	23	39	1.90	97	23
11	1.79	69	23	40	1.56	60	21
12	1.85	76	23	41	1.83	86	22
13	1.70	71	22	42	1.75	78	22
14	1.95	98	21	43	1.89	95	21
15	1.86	90	20	44	1.96	89	21
16	1.78	84	25	45	1.73	78	23
17	1.79	72	27	46	1.78	85	22
18	1.76	75	32	47	1.85	81	31
19	1.76	72	21	48	1.97	99	23
20	1.84	86	23	49	1.78	71	22
21	1.79	80	33	50	1.92	78	21
22	1.91	81	21	51	1.86	75	22
23	1.76	65	23	52	1.69	72	21
24	1.65	69	21	53	1.85	79	21
25	1.89	89	21	54	1.79	89	32
26	1.78	82	21	55	1.65	60	22
27	1.74	77	21	56	1.78	81	23
28	1.79	74	22	57	1.84	83	21
29	1.85	86	22	58	0	0	0

Table 7.1: Subjects participanting in the study: Subject's height, body mass, and age are presented here

The effect of: a)speed , b)footwear, and c)turning in the direction of progression (see Harrison et al. [1990] for comparisons), on the intersegmental loads was studied by means of integrated gait analysis using the protocol and models developed in the present thesis. When the variability between the several parameters was taken into consideration a set of data from a radom normal subject was chosen for demonstration and further analysis (SUBJ. 1). This was the case in the footwear variation and speed variation analysis. Inrtersubject variation plots are attempted and graphical envelopes describing the gait parameters for different subjects are presented.

The average velocities were measured with the help of two photocell switches

placed at the beginning and at the end of the walking pathway. The following ranges for the three different speeds were recorded for all subjects: normal speed:1.7-1.088, slow speed: 0.825-1.442, fast speed: 2.36-1.537 (all values in m/s). The corresponding values for subject one were: 1.199, 0.978, 1.737 m/s . The different footwear -in addition to barefooted trials- used was OXFORD SHOES, ATHLETIC SHOES (running shoes) and above the ankle BOOTS. During walking, the resultant force acting through the hip can be resolved into three forces acting along three axes, X, Y and Z . Computation of data, obtained from force plate readings and limb displacement, allowed several diagrams to be drawn (as explained in methods, the hip joint forces are presented as orthogonal components relative to the thigh axis, whereas the knee and ankle joints in the shank axis. The time base has been normalised both for the stance and the swing phase to make the results more comparable.

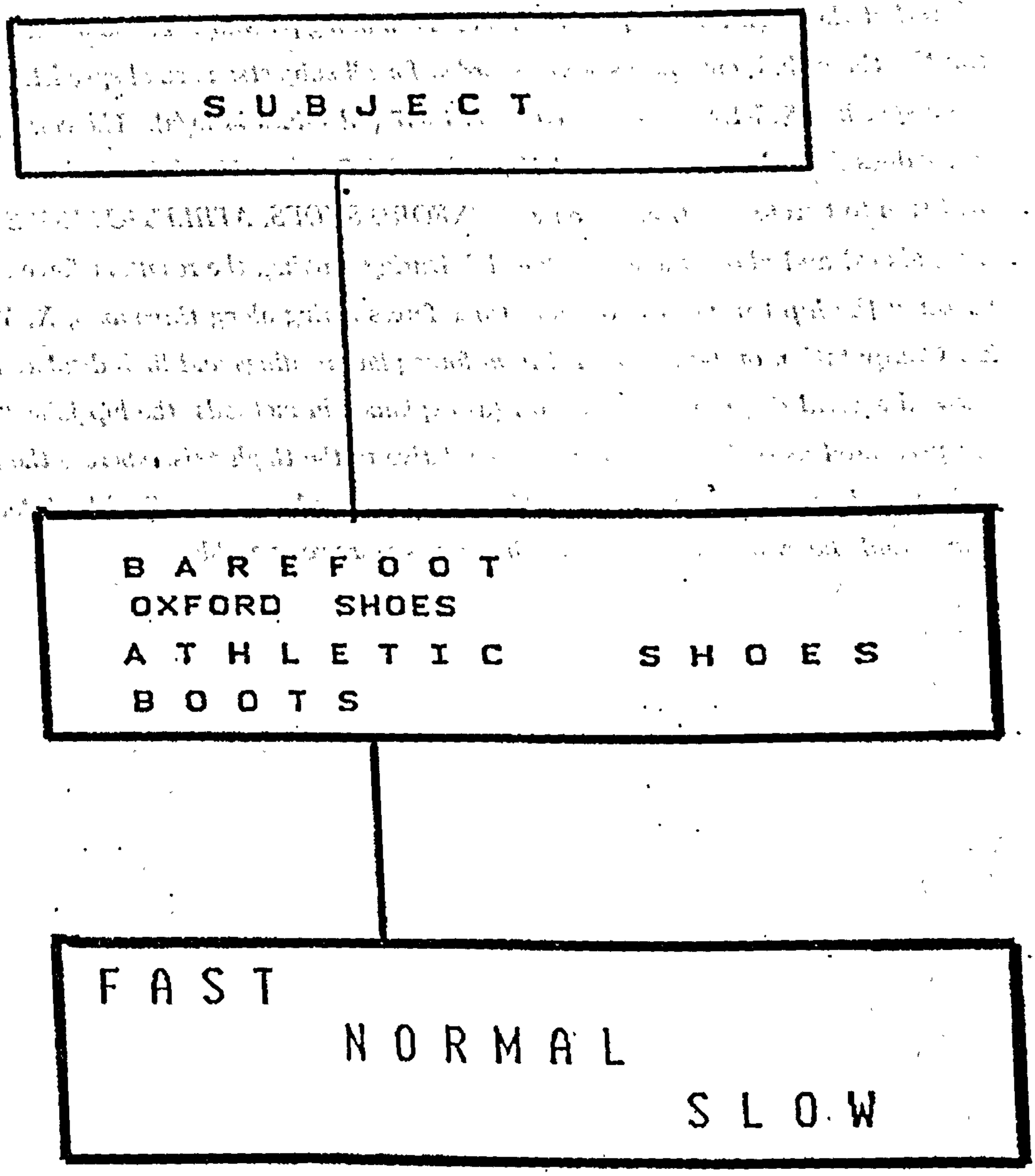

Figure 7.1: Schematic representation of the TEST PROTOCOL

7.1.1 Knee moments

The effect of speed on MZ component of the knee moment (FIGURE 7.4 on page 139) appeared as a rapid change in its sign (just after heel contactat about 8% and up to 30% of walk cycle). The fast trial MZ component was considerably higher than that of the rest of the trials (approximately 70 Nm), followed by the normal trial(approximately 50 Nm), whereas the slow component appeared to have the lowest magnitude of approximately 10 Nm. The moment switch after mid stance was more abrupt for the fast and normal trials but it revealed no differences amongst the three speeds for the rest of the stance period. The highest value reached at this stage was approximately 30 Nm at about 45% of walk cycle. The MY component of the knee moments was consistent with the classic curve presented in the past. Winter [1987]. MY moment components (FIGURE 7.3 on page 139) for all three speeds showed that the shape of the motor patterns remains essentially the same. The slow speed MY component appears slightly smaller at about 50% of walk cycle where the magnitude envelope was almost 20 Nm. The MX component revealed considerably greater variation with speed. (FIGURE 7.2 on page 139). The slow trial MX component had the higher magnitude throughout the stance phase, reaching values of about 50 Nm at 20% of the stance decreasing to approximately 30 Nm before toe off (55% of walk cycle).

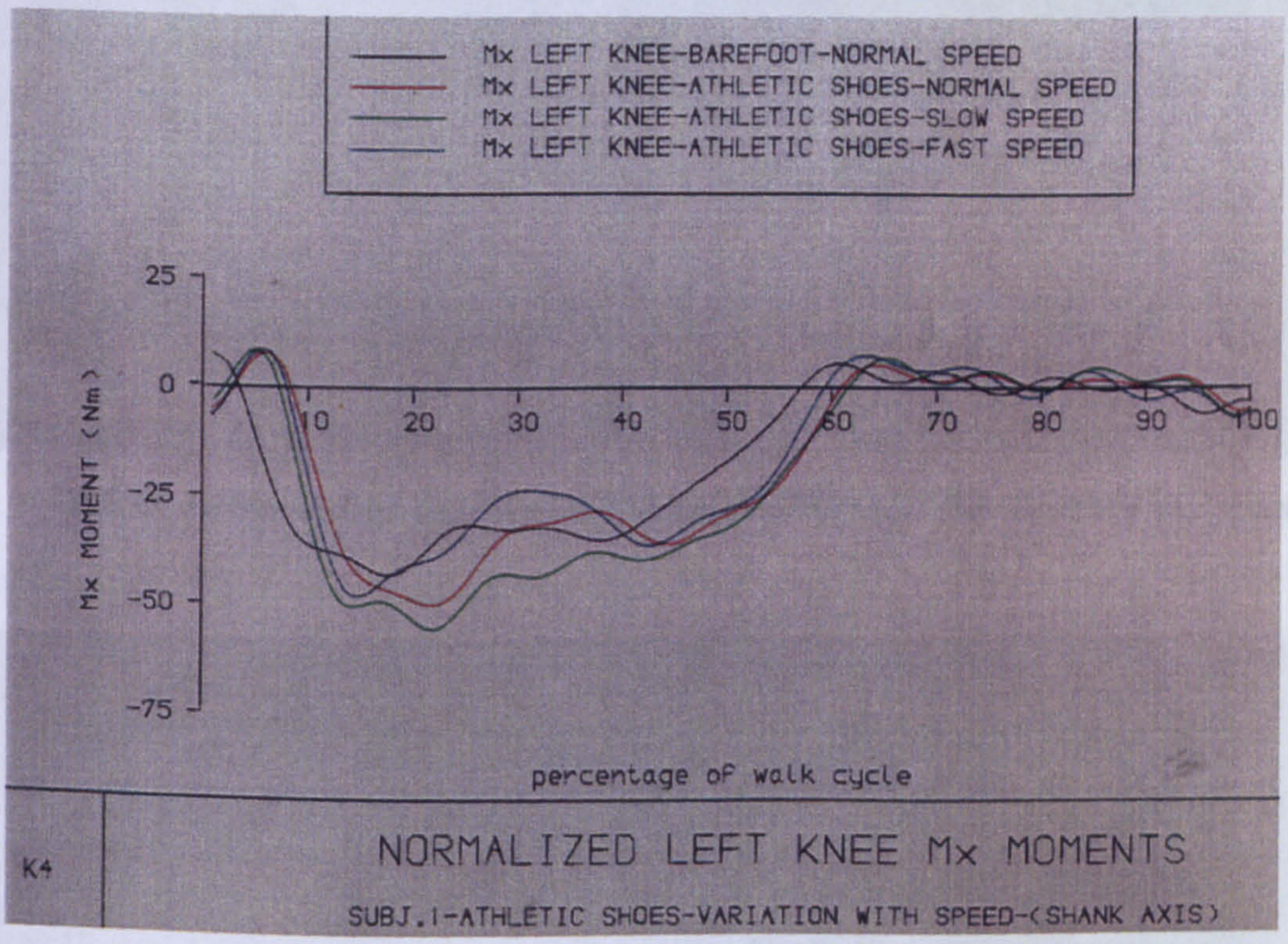

Figure 7.2: LEFT KNEE MOMENT -Mx history:variation with SPEED

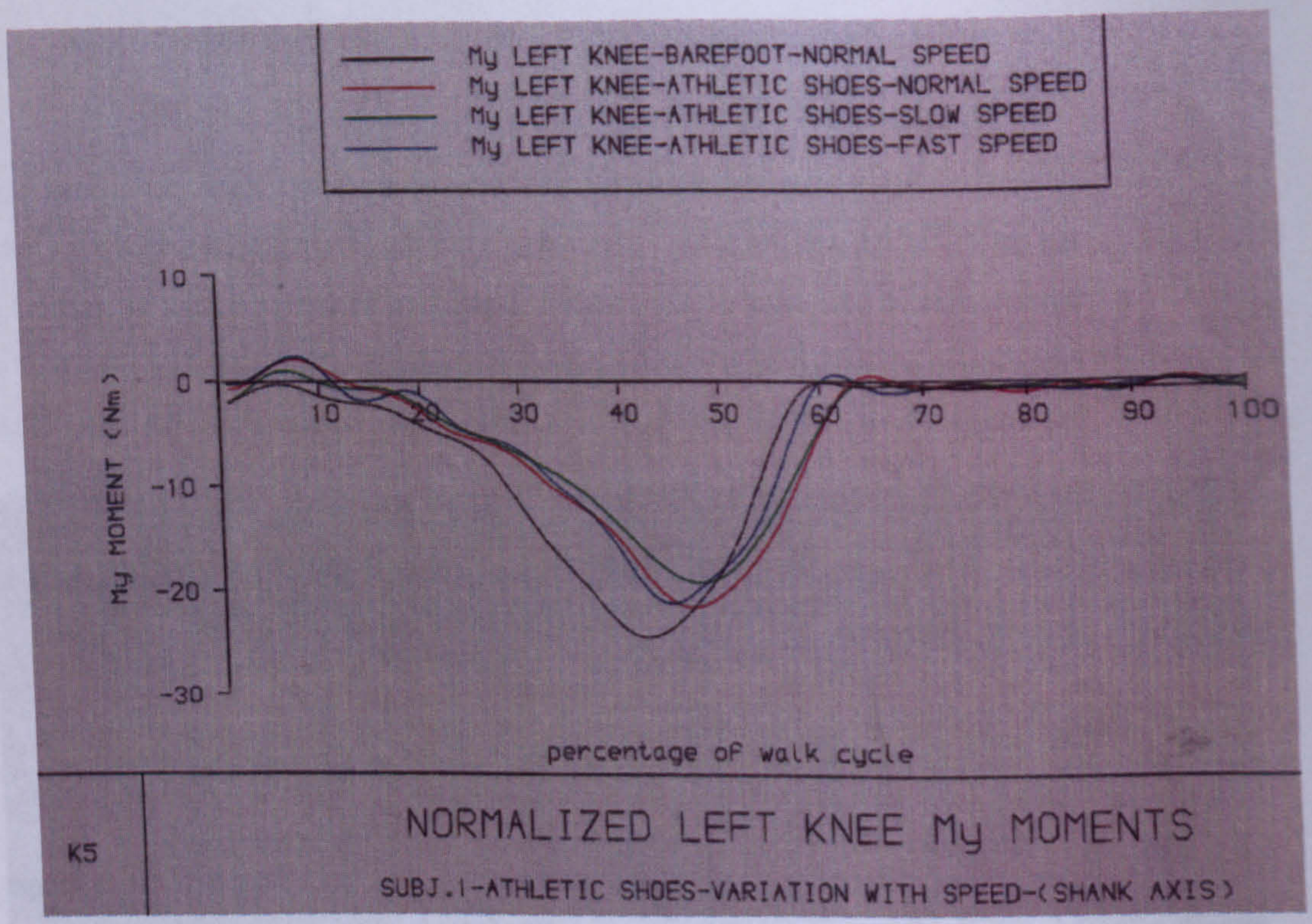

Figure 7.3: LEFT KNEE MOMENT -My history:variation with SPEED

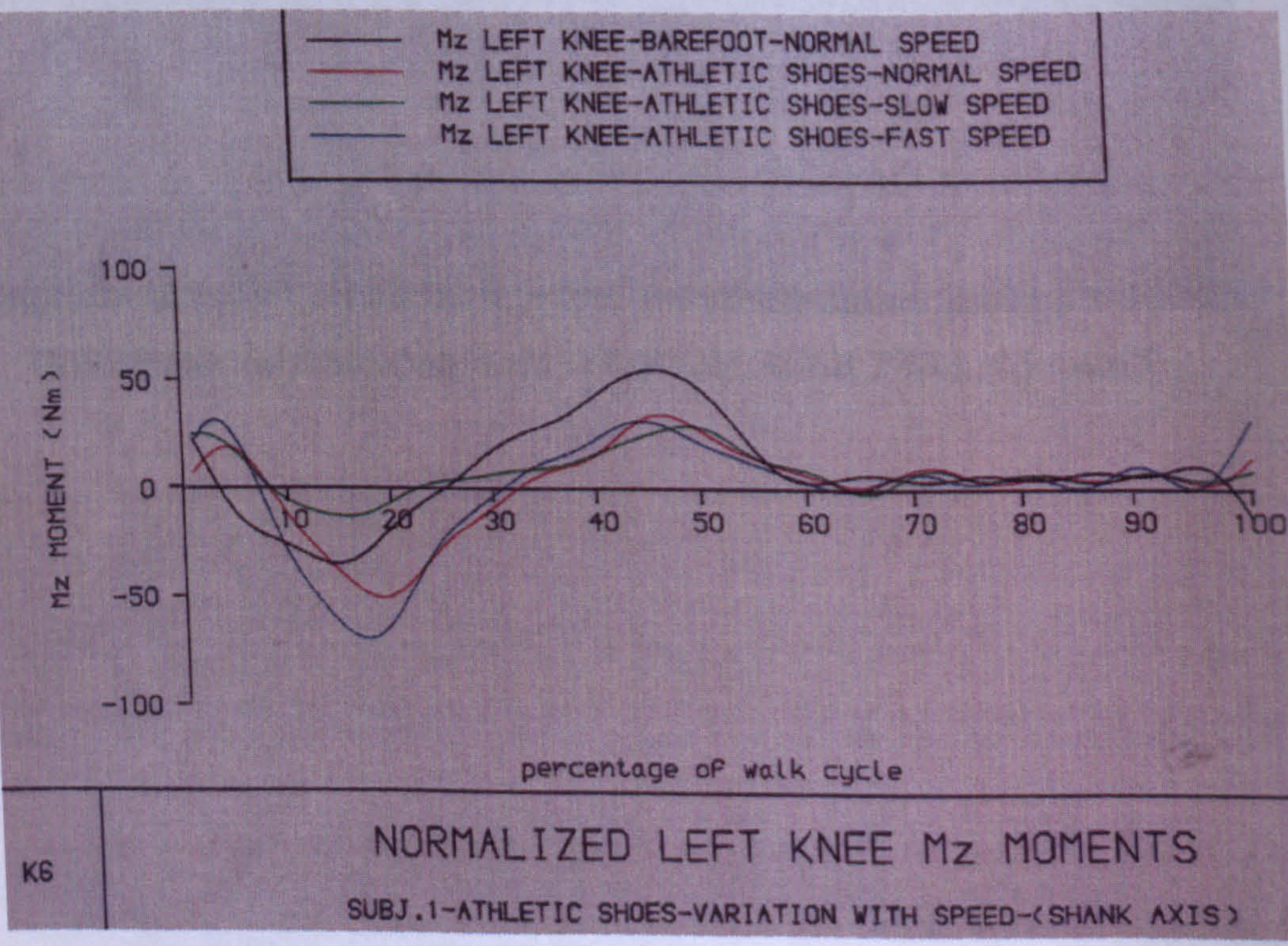

Figure 7.4: LEFT KNEE MOMENT -Mz history:variation with SPEED

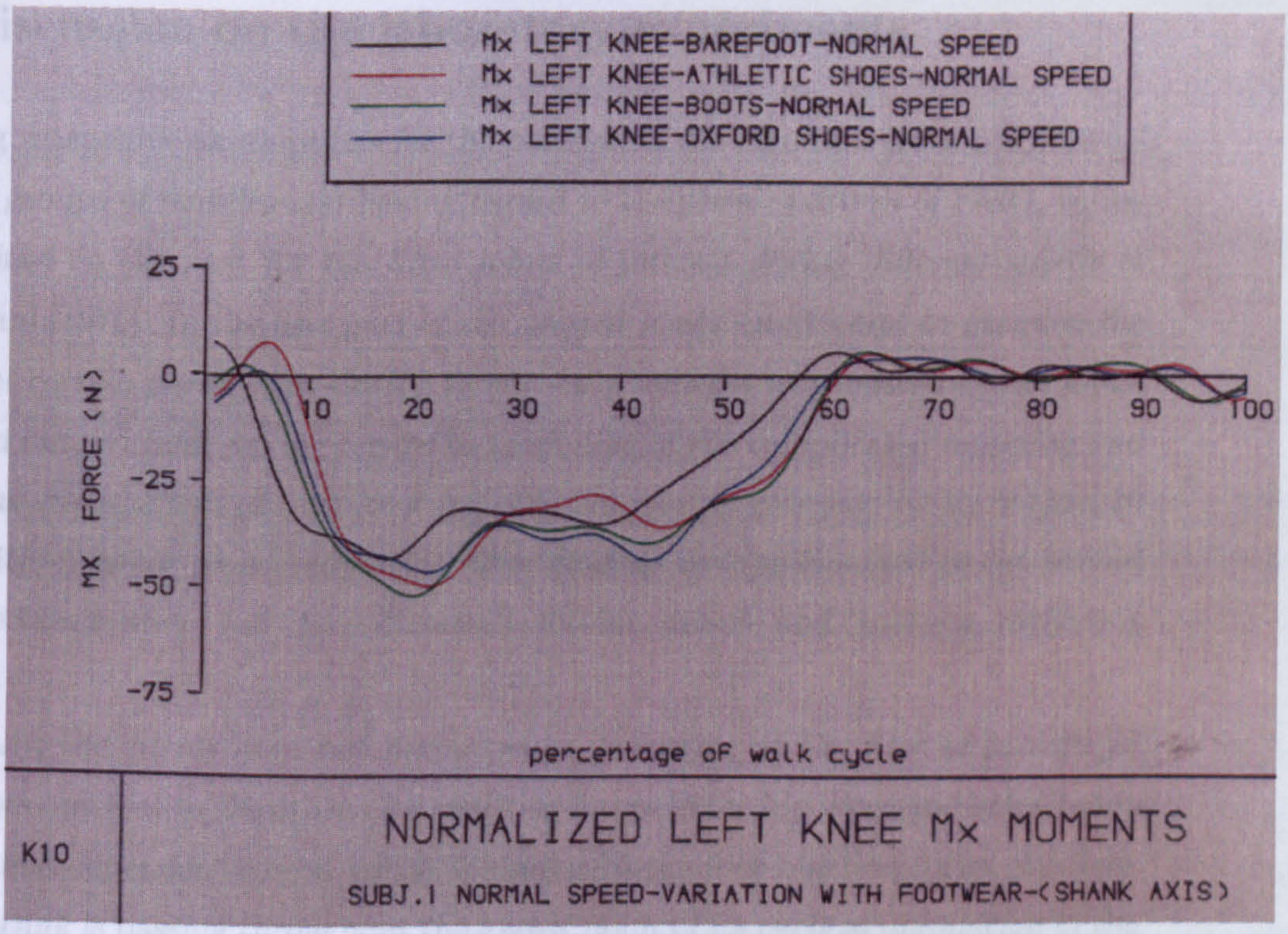

Figure 7.5: LEFT KNEE MOMENT -Mx history:variation with Footwear

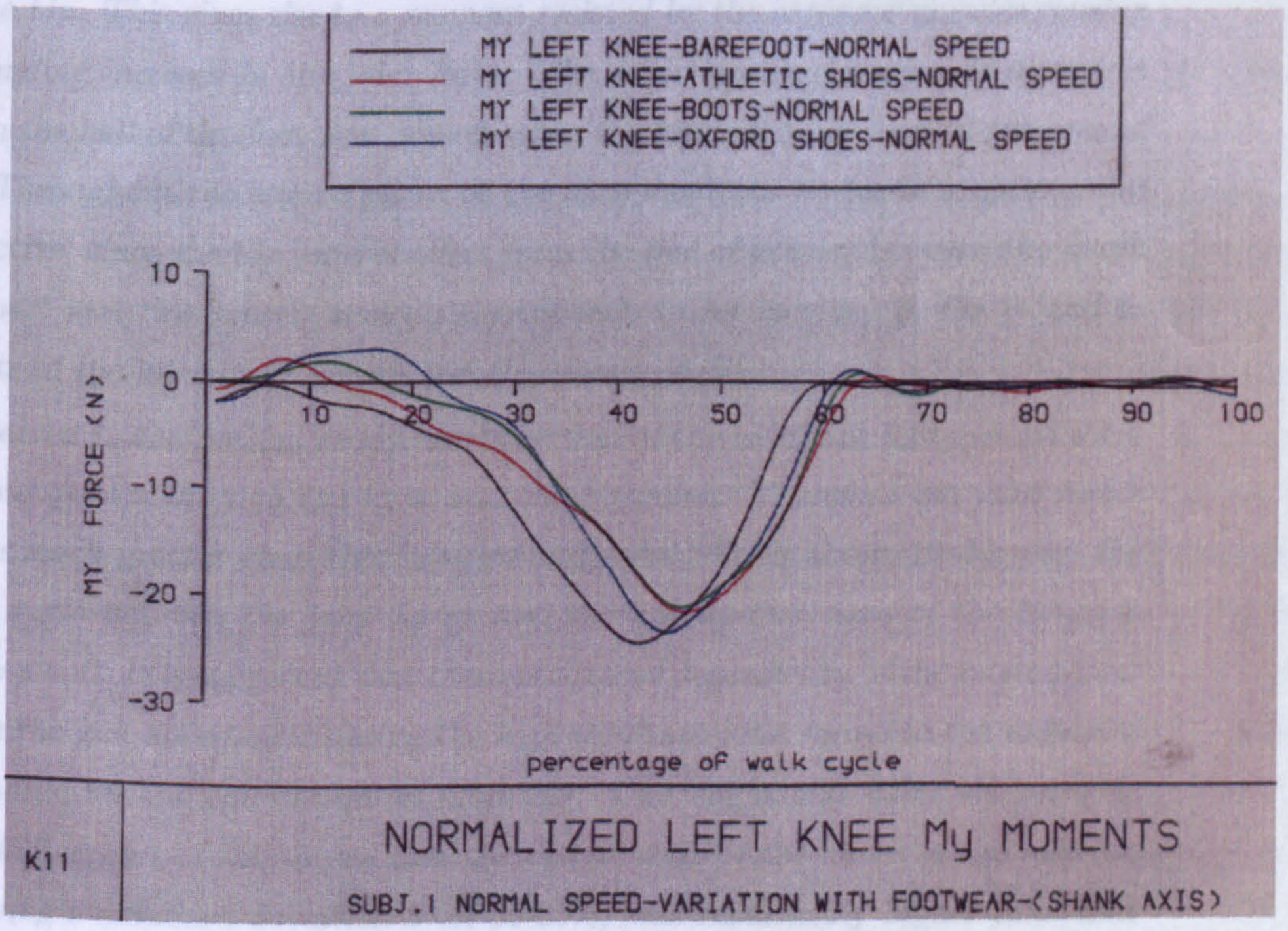

Figure 7.6: LEFT KNEE MOMENT -My history:variation with Footwear

7.2 Discussion on the laboratory experiments

By making reasonable assumptions for the position of the resultant force transmitted by certain groups of muscles and having regard to the phasic pattern of EMG, values were obtained in the past for the three joints of interest during different speeds of walking Paul [1976]. In the first part of the present study an attempt to examine the influence of certain parameters on the forces and moments transmitted at the joints was carried out, without paying regard to modelling of the complicated muscular and ligamentous environment of each joint (eg. the hip joint is governed by more than 20 muscles with different phasic activity). This analysis is supplemented in the second part of the thesis where full three dimensional joint, muscle and ligament analysis is attempted.

Generally, the curves have two major peaks, occurring at the time of transfer of support from one foot to the other. All resulting forces in the hip, knee and ankle joints display a time dependent course which is similar to the foot-reaction force. At these times the trunk is passing throughout the lowest point of its cyclical undulation in the vertical direction, and there will be a downward inertia force present. Just after heel strike, body weight is taken increasingly on a foot which is situated some distance in front of the hip. This gives rise to a moment resisted by the extensor muscles causing a corresponding increase in the joint force. The second peak corresponds to weight support on the ball of the foot near toe-off when the hip will be in front of the area of support. Throughout the stance phase of the movement the abductor muscle group must be active, since the hip joint is offset from the line of gravity between the trunk and the foot, and this muscle tension corresponds to an increase in the y- and z-components of the joint force throughout the stance phase.

As observed in the present study, the direction of the resultant foot-ground force by no means passes through the knee and the hip joint. Therefore the joint forces have to be much greater than the foot- ground force. With about 10 degrees, the maximum angle between the joint forces and the longitudinal axes of the bones is remarkably small. It is suggested that there is a linear dependency of the related joint forces with the gait speed, attributing the high resultant joint forces to the muscular action required for the equilibrium of moments. One might add -after the analysis in the modelling part of the thesis- that the distribution of the forces in the relevant joint (showing a standard deviation S ,of 20-25%) was remarkably higher than that

of the ground reaction forces, the latter being insufficient to interpret the joint forces. Paul et al (1975), investigated the effect of speed on hip joint forces and concluded that in rapid walking, the mean values of joint force are significantly higher.

The above is supported in the literature by the work of Morrison [1970], Poulson [1973]
Harrington [1976], Perry et al. [1986], Seireg et al. [1975], Stauffer et al. [1977] whose data envelopes include the data of the present study.

The several distributions, either of forces or moments, in the three joints have been attributed to individual gait characteristics, simplifications in the calculation model with respect to the inertial forces and the geometry of the joints (or of the muscles if involved in the model-see chapters 7, 8).

In an overall estimation, the hip moment patterns for the three speed groups are somewhat similar in shape over the stride but do show some timing differences, especially for the fast cadence trials. Initially the hip extensors are active to assist in absorbing energy at initial contact (IC) by controlling hip flexion (and, ultimately, control knee collapse) and also the forward rotation of the pelvis and thereby stabilize the trunk. At fast cadences, this event is over by 10% of the walk cycle while at slow cadences, it lasts until 25% of the stride period. Then, during the remainder of the walk cycle, the hip flexors become active Winter [1987]. During mid- stance (15%-50%), these hip flexors serve to control the backward rotating thigh and thus arrest its backward rotation. Finally, at 50% of cycle, it reverses and the hip flexors now contract concentrically to start a "pull-off" of the lower limb. This continues into mid- swing. Pull-off cannot have much effect until the contralateral limb is on the ground; it is during the double support phase that the new base of support can be used to advantage and allow the hip flexors to pull the swinging limb upward and forwards. Many gait related pathologies use this pull-off to advantage to compensate for a weak or non-existent push-off. Paul [1971] investigated the force and moment patterns at the hip for a normal subject walking at fast speed. His suggestions apply in the present study, particularly when the case is the moment patterns. At 4% of cycle time it is apparent that the biceps muscle group is unbalanced since it would require to transmit 1023 N at the knee and 2224 N at the hip. The alternatives are to keep the 2224 N value and maintain knee equilibrium by tensing the vasti, thus further loading the knee joint.

7.2.1 FORCES AND MOMENTS AT THE KNEE-SHANK AXIS

Morrison [1970], studied the mechanics of the knee joint of 12 normal subjects. In his "joint model" joint force and moment evolution during walking were discussed. The author suggested that immediately prior to heel strike, force action in the hamstrings decelerates the forwards motion of the leg. At heel strike, the foot is positioned well in front of the knee and hip and hence vertical force acting on the foot causes a moment, -Mz, to act at both joints. In the present study, the Mz component was fount to increase with speed, a fact mainly observed early in the stance. In most experiments this moment was increased by the action of an anteriorly directed force on the foot at heel strike (as seen in the pedotti diagrams also). This moment action is resisted by force action in the hamstrings which, having biarticular function, influence the moment patterns of both the knee joint and the hip joint (assisted by the gluteal muscles-see chapter 8). The advantage of the biarticular muscle in these circumstances can be illustrated. Following heel strike the knee is subject to a moment, +Mzs, (i.e. a tendency to flex the joint), and force action in the quadriceps femoris resists this moment and controls the position of the knee. In the second half of the stance phase, force action in the calf muscles causes plantar flexion of the ankle and hence produces forwards acceleration of the body and a corresponding anteriorly directed force acting at the foot(as illustrated in the Pedotti plots). Moment.-Mzs, acting at the knee tends to extend the joint and is resisted by the action of gastrocnemius. Being a biarticular muscle the gastrocnemius both develops the flexing moment at the knee and produces plantar flexion of the ankle (assisted by soleus). At toe-off force action in the quadriceps femoris imparts a forwards acceleration to the leg. It should be noted that in Morrison's study in the calculation of the force values acting in the hamstrings it was assumed that there was no assistance of this muscle group from the gracilis or sartorius muscles. Gracilis is mainly an adductor of the hip and its line of action affords it little leverage at the knee in comparison to the hamstring muscles. Sartorius, has less leverage and smaller cross-sectional area than hamstrings, and therefore it is a relatively weak muscle. It is reasonable to assume therefore that the components of moment,-Mzs, transmitted by these two muscles are of a minor nature. Similar justification was given to the assumption of the quadriceps femoris as the sole extensor of the knee. The increasing inward torque, -Mys, acting at the knee during the stance phase of walking is described as a moment action Mys, about the

long axis of the tibia which must be mainly balanced by force actions in the ligaments. Furthermore, tests on male and female subjects revealed no obvious differences in the magnitude or cyclic variation of joint force between the sexes Morrison [1970].

Variations in peak values of joint force and their phasing in the walking cycle shown by different subjects are considered to be due partly to anthropometric differences between subjects and partly to different characteristics in the gait of the subjects. Paul [1970], reported that in normal subjects the knee joint force is generally smaller than that of the hip joint during walking.

For the knee extensors, Inman et al. [1981], reported large variations in increases of knee extensor moments with increased knee flexion in three subjects. The changes were linear from the most shortened position of the knee extensors to the angle of maximum moments, which itself varied from about 40 to nearly 70 degrees. Percentage changes per degree, calculated from plots, were between about 1.5% and nearly 5% per degree of angular change, depending upon the subject. Thorstensson et al. [1976], reporting mean values from 25 subjects, found percentage increases in maximum moments produced per degree increases in knee flexion angle at zero velocity to be between 1.2% and 3.3% for angles between 0 and 60 degrees of flexion. Changes at higher constant velocities were consistently larger, ranging from 0.71% to 5.2% per degree increase in knee flexion. Olney et al. [1985] and Hof et al. [1981b] , pointed out that the effect of joint angle change on moment output for a given level of EMG has not been reported to be linear one for the full range of movement though the smaller the range of movement over which the effects are predicted, the more likely this is to be a good approximation of the real function. Because the large moments occur during stance, and because angular changes are relatively small during this period, a linear constant is reasonably accurate. Arguments to be considered when analyzing moments could be the variation of the perpendicular distance from the line of action of the muscle to the instantaneous centre of rotation which affects the moment. In the present study the different shank and thigh lengths among the five subjects resulted in different lever lengths and configurations of the kinetics revealing considerable intersubject variability. Differences in muscle origins and insertions also produce intersubject variability. For example, the gastrocnemii as ankle plantarflexors would be affected by changes in knee angle in addition to alterations in ankle angle. In figure 7.8 on page 148 it can be seen that at slow speed the flexion- extension angles in the knee joint were significantly smaller in the early part of the stance corresponding to

smaller Mz moments (FIGURE 7.4 on page 139) which might be partially attributed to the above explanation with regards to angle-moment relationship. Perry et al. [1986], studied the arc of knee flexion used in spontaneous slow gait by persons without limb disability but with energy limitations due to respiratory impairment. They found that maximum knee flexion during swing in these slow walking patients (mean=56.4 degrees) was significantly different from maximum knee motion during swing of normal velocity gait subjects. Therefore, knee flexion during swing could not be correlated with subject's gait velocity or stride length. Shiavi et al. [1981] reported electromyographic patterns for level surface walking through a range of self-selected speeds of normal subjects. The authors suggested that the foot contact patterns demonstrate a bilateral symmetry and no change in the sequencing of foot events with respect to speed. The relative timing for most of the foot events is fairly consistent as indicated by the small standard deviations of the same study. Only two foot events, toe-contact and heel-off, had a large range of times. In the present study in several subjects the toe did not contact the walking surface until the middle of stance phase. As walking speed increases, the stance and double- limb support phases decrease in relative and actual time. The swing phase duration increases in relative time though it, too, decreases somewhat in actual time. The reduction in stance phase duration is about five times greater than that of swing phase. On the average, some of the events on opposite feet occur concurrently. During very slow speed walking, heel-off on one foot occurs at heel-on of the contralateral foot. During free speed walking the ipsilateral first metatarsal head ground contact instant and the contralateral first metatarsal head off-ground instant are concurrent. Whereas, at fast speed, a person will make contact of the fifth metatarsal concurrently with the offset of the opposite first metatarsal. Therefore, the foot-fall pattern of the majority of normal individuals is a stereotyped pattern.

Shiavi et al. [1981] found that EMG patterns at various speeds might help for a better interpretation of the moments about the joints of interest at the three different speeds. Tibialis anterior exhibits activity during the whole cycle at all speeds. As walking speed increases, the percentage of subjects exhibiting swing- to-stance peroneus longus activity increases from 14% at very slow speed, to 26% at normal speed, to 68% at fast speed. Those subjects incorporating late-swing stage activity to one speed also utilized it at a faster speed. The EMG of the gastrocnemius muscle during very slow speed walking is consistent with the classical descriptions. However, as a

person walks faster there is a trend for the gastrocnemius to become active earlier in stance and even during late swing. The soleus muscle is active within the stance phase except at fast walking speeds. As speed increases, the soleus commences activity earlier in the gait cycle. At fast speed, late swing stage activity is exhibited. For the hamstring muscle group Paul [1966] found no activity at the stance-to-swing transitional stage. Shiavi et al. [1981] found that the activity of the hamstrings during the late stance becomes less prevalent as walking speed decreases. No speed trends were found for the rectus femoris. The main trend of vastus lateralis exhibited was that the subjects exhibiting biphasic pattern at free speed tended to exhibit the longer duration monophasic pattern at fast speed. Finally, gluteus medius was found to be active from late-swing stage through midstance. The author concluded that there is an intersubject variability in the electromyographic gait patterns of eight muscles and that the pattern types change with the speed of progression. Miyashita (1971) reported also that electrical activity increases according to the rate of speed in walking. This finding has been a useful evidence for the interpretation of moments in the past and has given a partial explanation of the speed effect on gait parameters. Cavanagh et al. [1975], studied the knee joint moment at the swing phase of subjects walking barefoot on a treadmill. They suggested that a moment tending to extend the knee during early swing develops at greater than 2 m/h (0.894 m/s) speeds replacing a moment that tended to flex the knee at slower speeds. The peak of that moment increases in magnitude steadily as the speed of walking increases. There was a considerable intersubject variability in the peak moments at any speed. The author pointed out that the qualitative similarity of the changes in the intergraded electromyograms and net moment-time curves was striking feature of the results in all subjects. Obvious were also the changes in the power characteristics as the speed increased. While being a relatively passive component at lower speeds of walking, the function of the knee joint at higher speeds becomes increasingly that of dissipation of power. The considerable amounts of power dissipated at the knee during the swing phase at higher speeds indicates that possibilities for energy storage exist during this phase of the cycle. However, it must be emphasized that both dissipation and output of power at the knee joint are greater during the stance phase than during the swing (Bresler and Berry, 1951). Therefore, speed of walking should be a major variable in locomotion. In summary, the knee moment patterns as seen in the present study show that the shape of the motor patterns remains essentially the same at all cadences, except that

"gain" is higher as the speed increases. (FIGURES 7.2 on page 139, 7.3 on page 139, 7.4 on page 139). At Heel contact, the knee has a flexor moment but very rapidly -within 4% of stride- the knee extensors begin a major burst of activity, initially to absorb energy and control the amount of knee flexion (until 15% of stride), and then to assist in extending the knee and adding potential energy to the body (which, in later stance, is converted to kinetic energy). Between 30% and 50% of stance, the knee moment becomes slightly flexor and this is mainly due to the action of the gastrocnemius muscles whose forces become quite high at this point in time (start of push off). However, knee moment rapidly shifts to extensor during late stance through to mid swing. The function of these extensors is two fold. During the powerful ankle push-off, the knee is starting to flex , thus, the degree of flex is being controlled by these eccentrically contracting quadriceps whose contribution increases with speed. Winter [1983], reported that the more we flex our knees during weight bearing, the greater the energy cost. As knee flexion increases during stance, the extensor muscles of the knee, hip, and ankle must contract to limit knee flexion and, to cause the knee to extend again during midstance. Such muscle activity further increases the metabolic cost of walking and also results in a drastic increase in the bone-on-bone forces at the knee and hip. Then, in early swing, these same muscles create an extensor moment to decelerate the backward swinging leg. However, they provide negligible energy to actually accelerate the leg forward. During the later half of the swing, a very distinct knee flexor moment is seen and this results from the hamstring muscles decelerating the swinging leg. It will be noted that a similarly shaped extensor moment curve, is seen at the hip, confirming the synergistic role of the hamstring muscles at these two joints. The above considerations are supported by the tendencies observed in the Pedotti diagrams (FIGURES. 7.15 on page 154, 7.19 on page 156, 7.20 on page 156) where it can be seen that as the speed increases the very first force vector becomes more vertical, and the force reaches greater magnitude. As an additional comment to all the above, step length changes with speed must be given priority when speed is the central question. It was observed that increasing speed results in an increased step length , a fact which affects the lever arms of the several moments increasing the latter's magnitude. It has been reported in the past that a linear relationship exists between cadence and step length/height Lamoreaux [1971].

7.2.2 KNEE JOINT FORCES

Knee joint forces have been the subject of study of several authors with regards to normal or pathological gait. Johnson et al. [1979] revealed joint force peaks at 5 times body weight in accord with prediction whereas the centre of force was located slightly medial of the midline of the joint during the majority of the stance phase.. Morrison [1969], reported the subject who recorded the greatest joint force value, adopted a speed of gait of 5.5 ft/s (1.67 m/s), comparable to that of level walking and therefore considerably faster than the other two subjects whose speeds of progression were 4.2 (1.28m/s) and 3.9 ft/s (1.18 m/s) respectively.

Harrington [1976], described a three peak knee force, with the second peak between 20%-40% of stance being the one with greatest magnitude (peak a and c appear before 20% and after 80% of the stance respectively). The average values of the three peaks at his study with normals were 1.7, 3.5, and 2.4 BW respectively. Morrison [1968], reported that the maximum joint force at the knee was 4 times body weight (normal subjects) and attributed the above three peaks to the activity of hamstrings, quadriceps femoris, and gastrocnemius respectively. Paul [1966] presented results indicating that the average of the greatest peak values of the ratio of knee joint force to body weight was 3.39 with maximum value of 4.46. It was observed that high values of force at the knee are carried in two of the four positions of zero relative velocity. The author concluded that forces of 3.4 times body weight may be exerted at periods of low relative velocity.

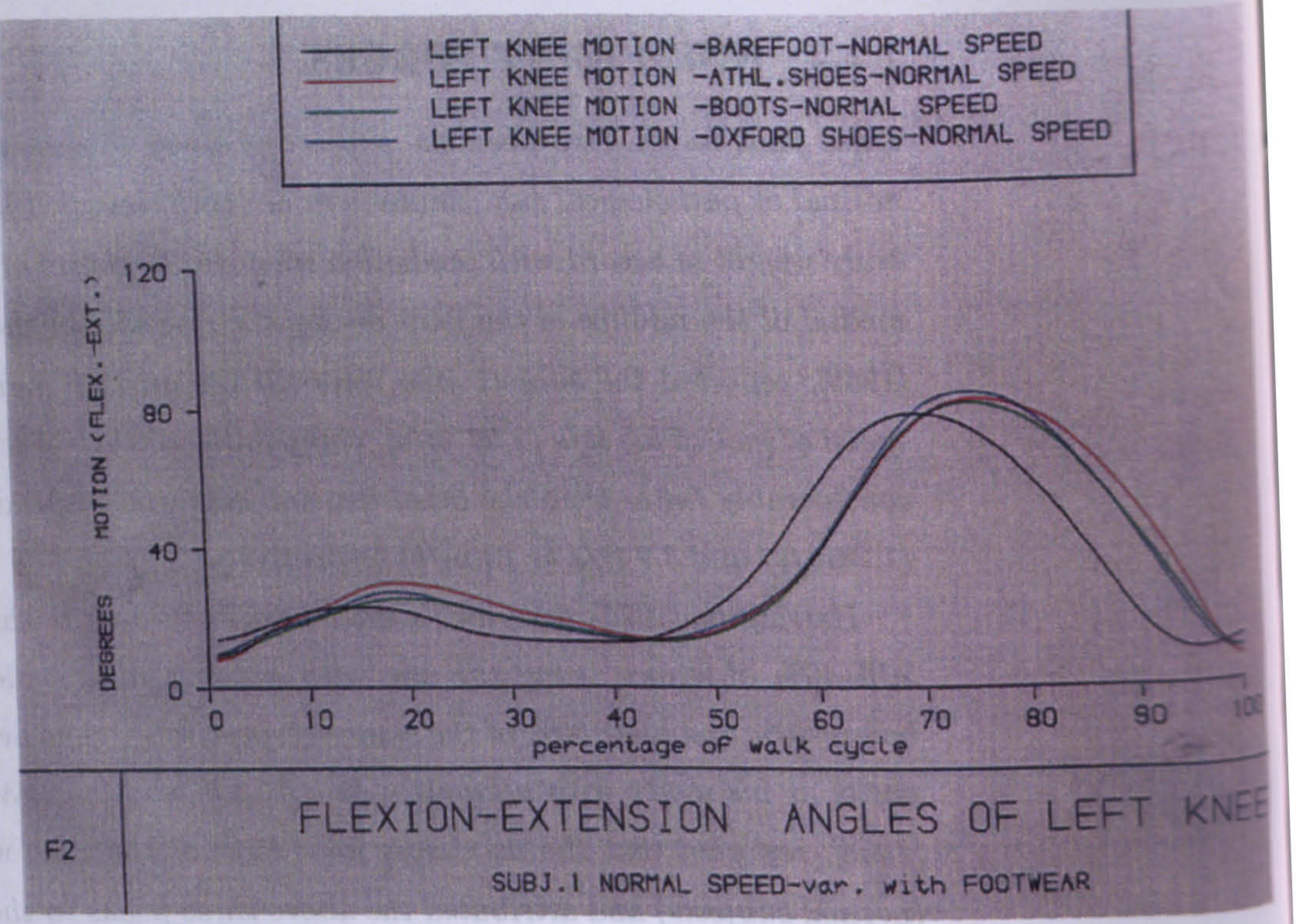

Figure 7.7: LEFT KNEE FLEXION-EXTENSION ANGLES:variation with footwear

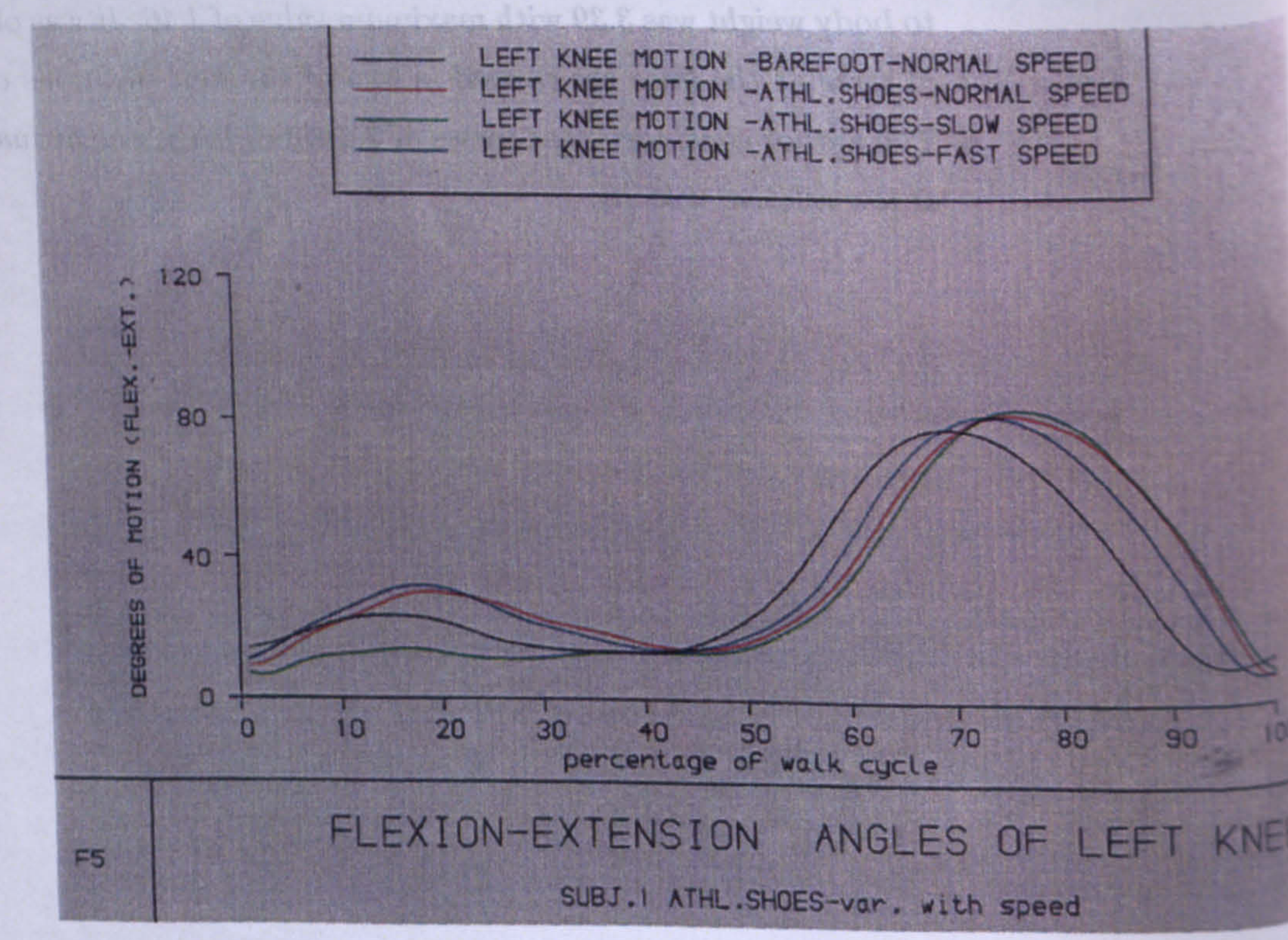

Figure 7.8: LEFT KNEE FLEXION-EXTENSION ANGLES:variation with SPEE

7.2.3 ANGLES

In the study reported here, the ankle, knee and hip angles from the three different cadences have been documented. Figures 7.12 on page 150, 7.8 on page 148, 7.13 on page 150, present the ankle, knee, and hip motion during walk cycle for subject 1. It is evident from these joint angle plots that there is very little difference between the cadence groups. The only minor difference shows up in the knee flexion during early stance and even in the ankle flexion in the early stance. At 15% of stance, the knee reaches maximum flexion and this increases from approximately less than 10 degrees for the slow trial to 30 degrees for the fast cadence trial. The ankle plot shows differences of 10 degrees magnitude at this time. Thus, with respect to the stride period, the joint angle histories are essentially the same. These findings are in accordance with Winter [1987] data. It should be noted that correlations between groups of subjects walking at different speeds which were recorded along with the R.M.S difference over the stride period. For the ankle, knee, and hip, the slow/natural values of the correlations were 2.1, 3.1, and 4.1 degrees respectively, whereas the fast/natural values were 2.8, 3.3, 2.3 degrees respectively. It must be stressed that the joint angle histories for repeat trials on the same subject done days apart presented a very low variability as measured by the coefficient of variance (CV). The average variability over the stride is less than 2 degrees at all joints. In similar manner, repeat trials done minutes apart resulted in a very low variability. However, it could be seen that the patterns for the five subjects of the present study were somewhat different from each other and are probably the reason why one can often recognize an individual from his/her characteristic gait pattern. More information can be drawn from the statistical analysis that follows in a later section .

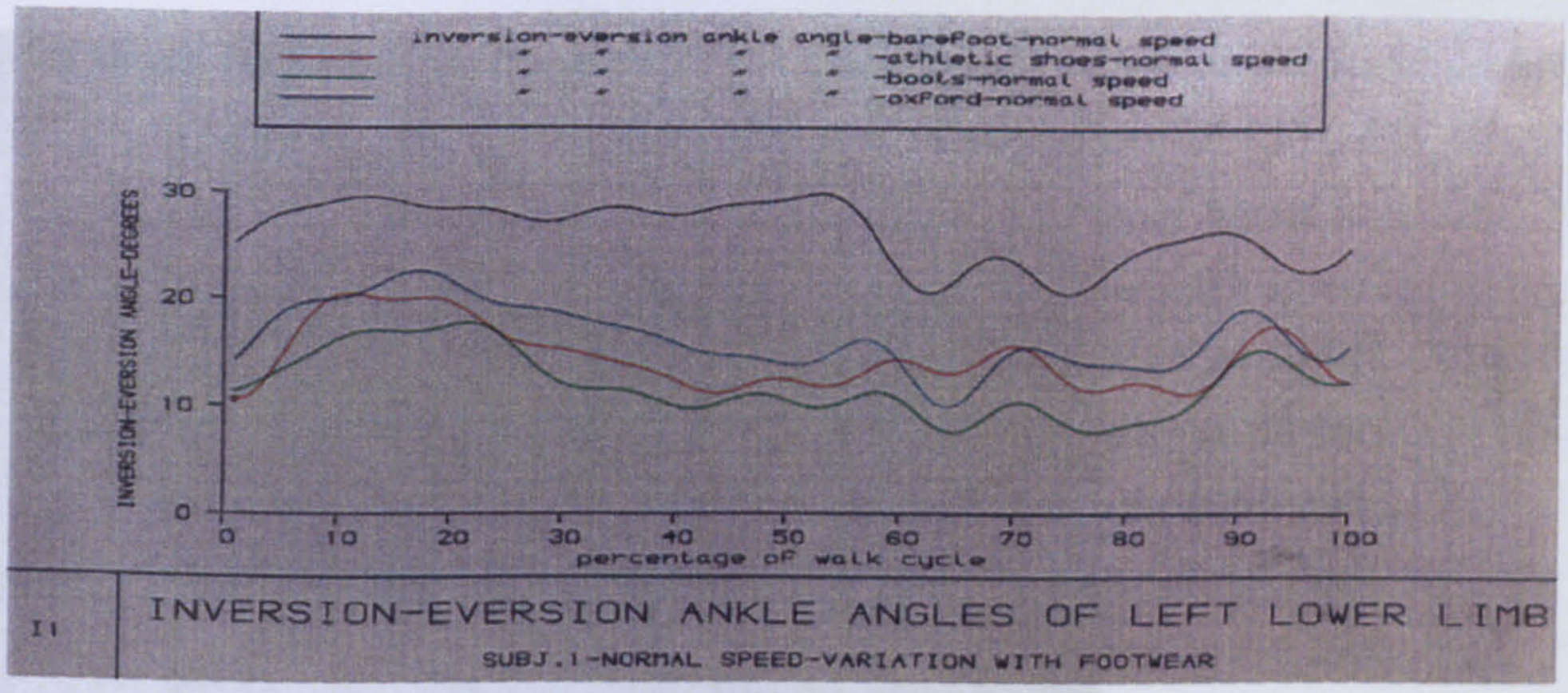

Figure 7.9: LEFT ANKLE INVERSION-EVERSION ANGLES:variation with footwear

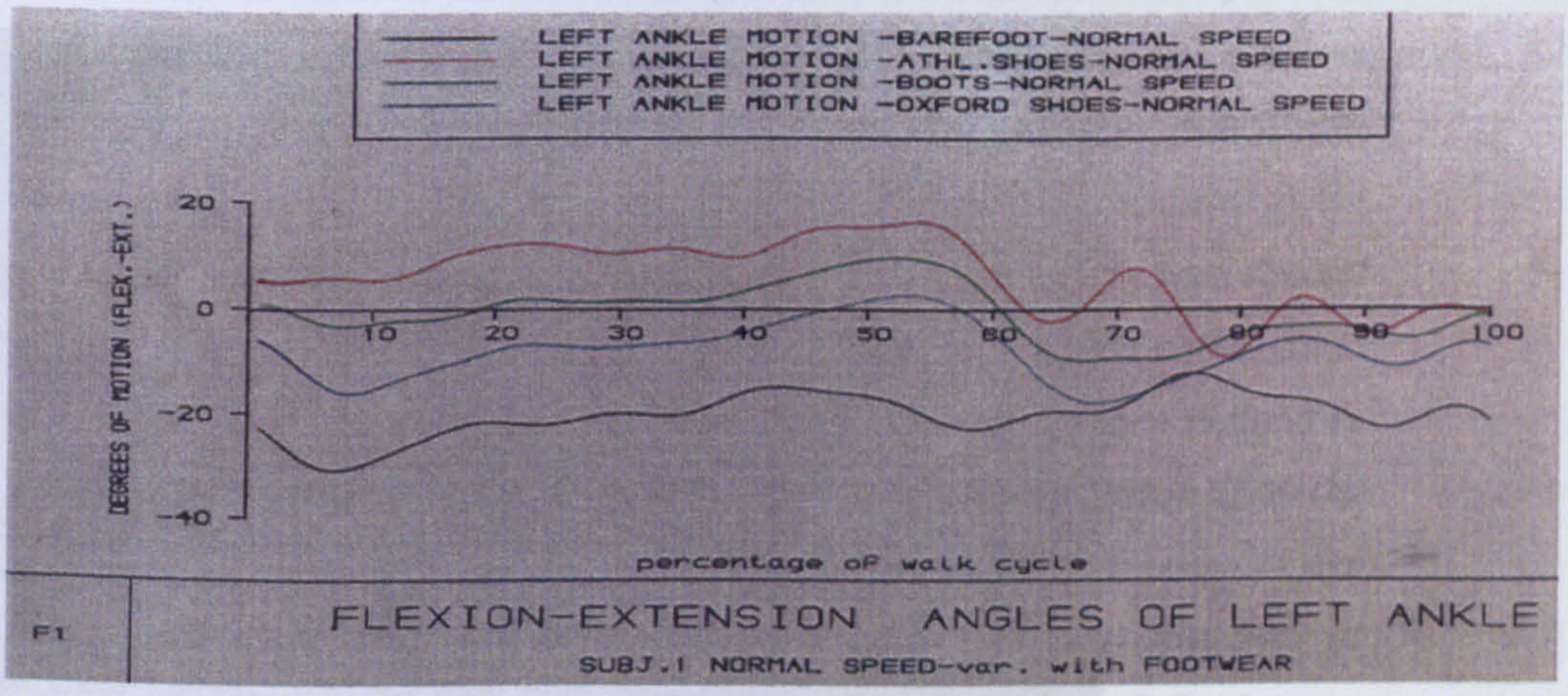

Figure 7.10: LEFT ANKLE FLEXION-EXTENSION ANGLES:variation with footwear

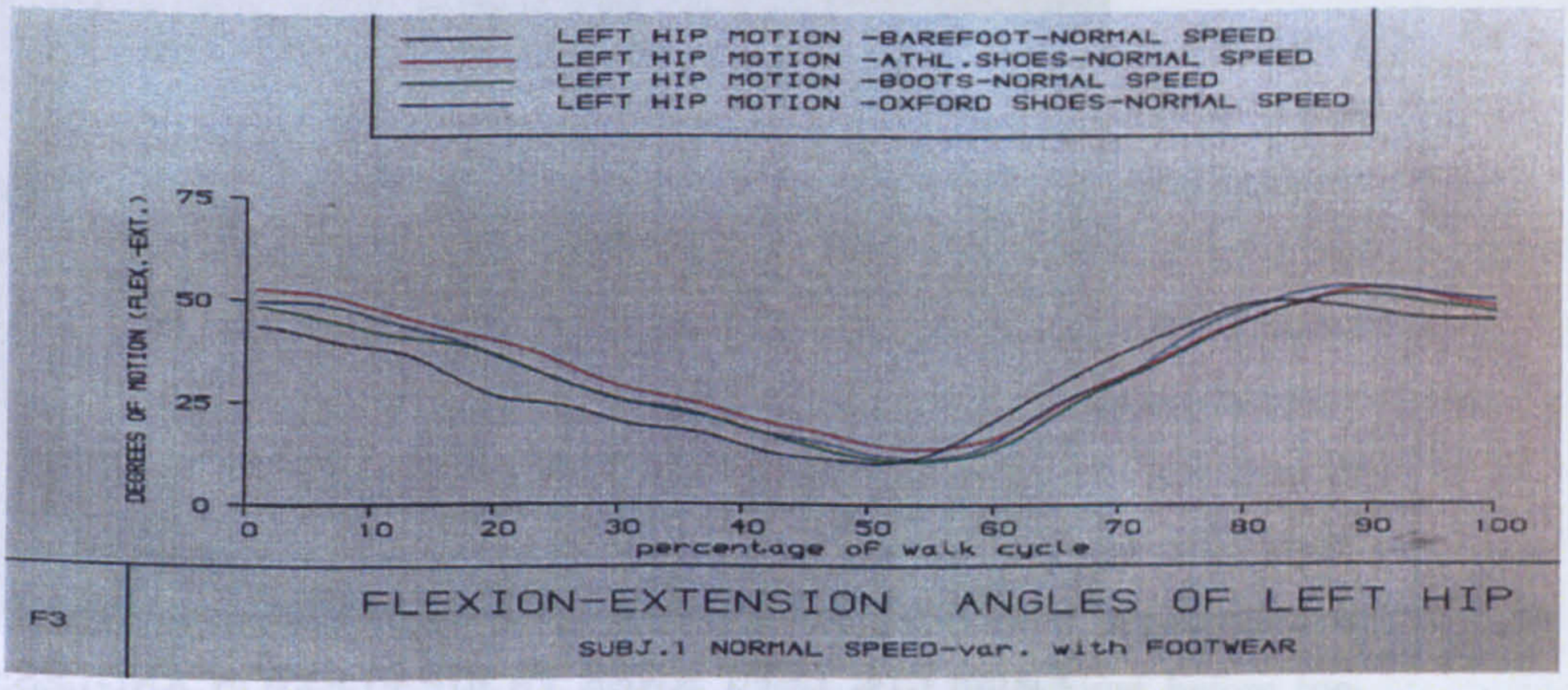

Figure 7.11: LEFT HIP FLEXION-EXTENSION ANGLES:variation with footwear

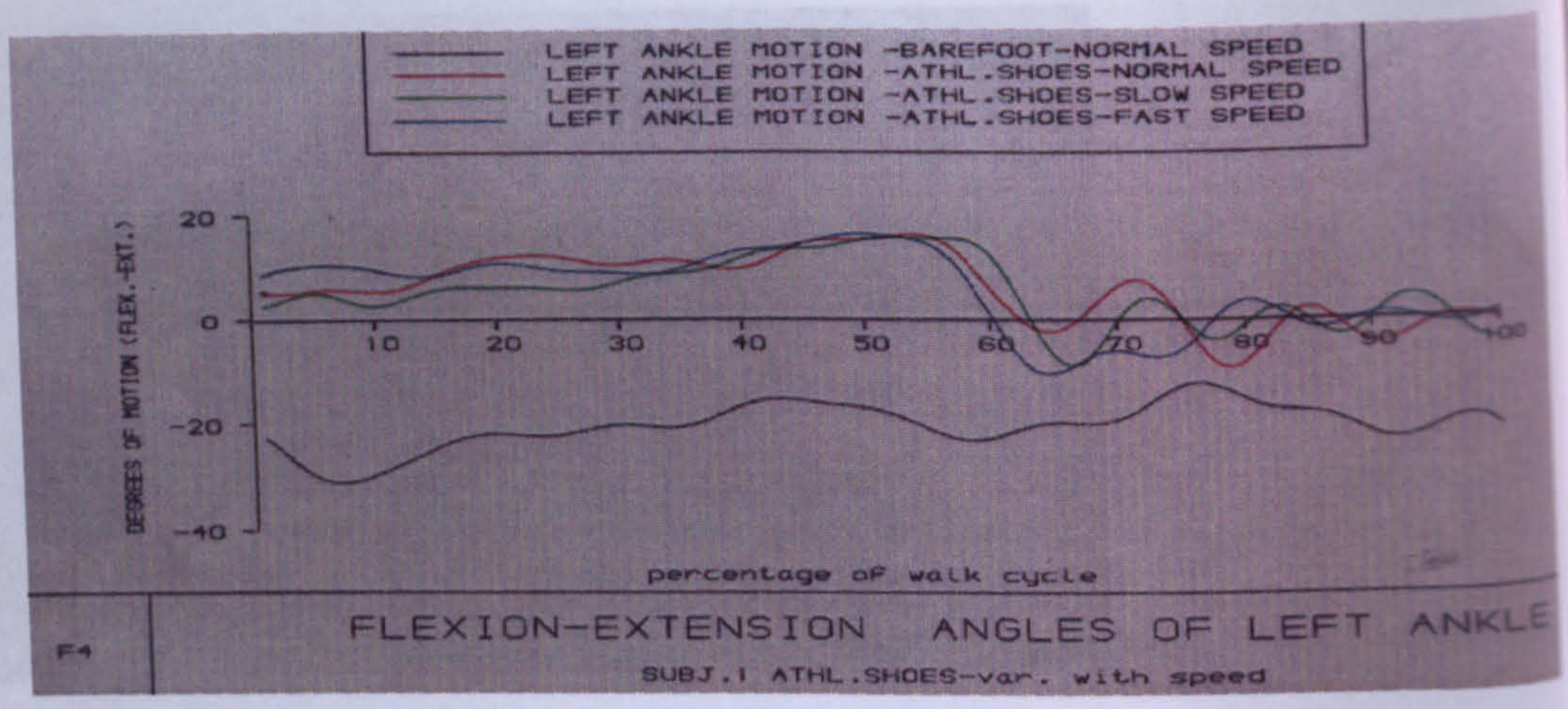

Figure 7.12: LEFT ANKLE FLEXION-EXTENSION ANGLES:variation with SPEED

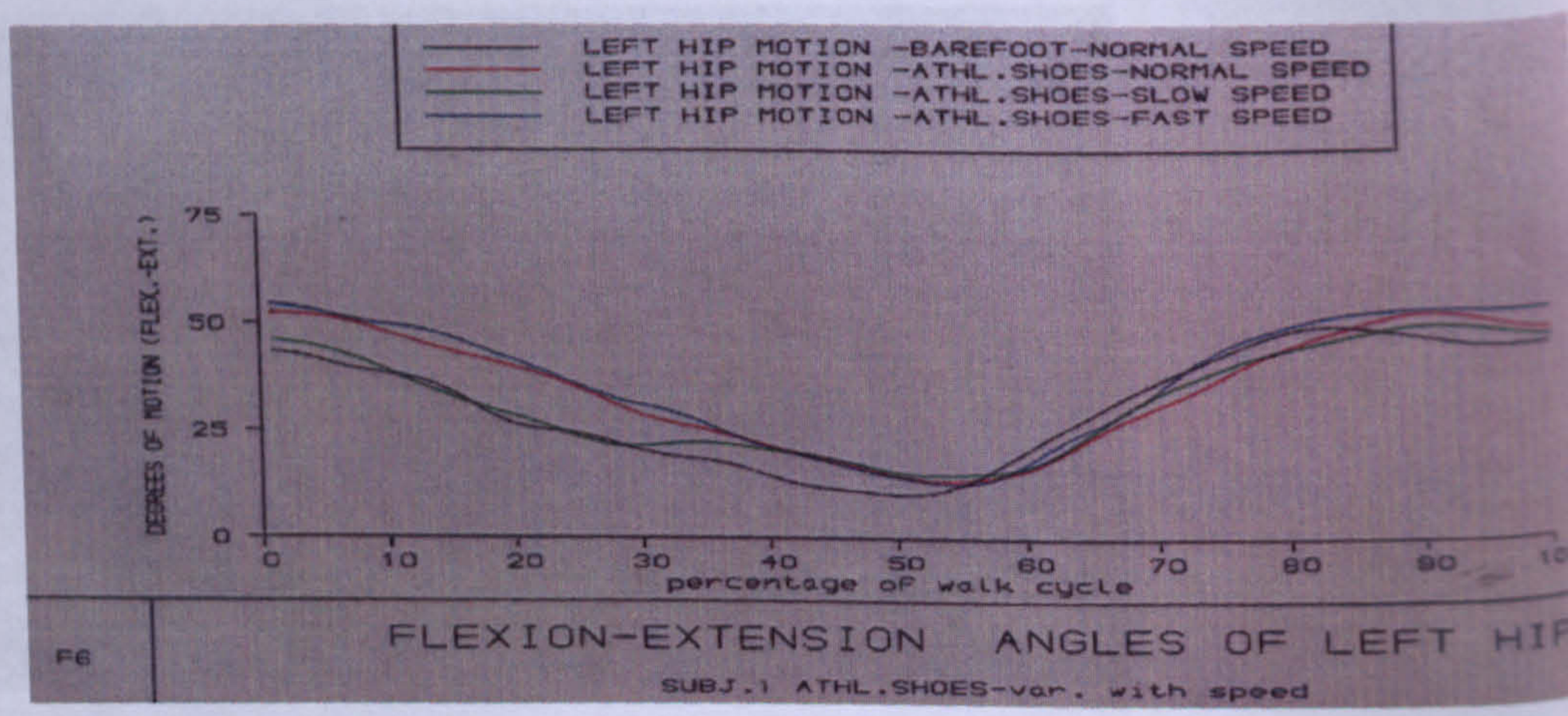

Figure 7.13: LEFT HIP FLEXION-EXTENSION ANGLES:variation with SPEED

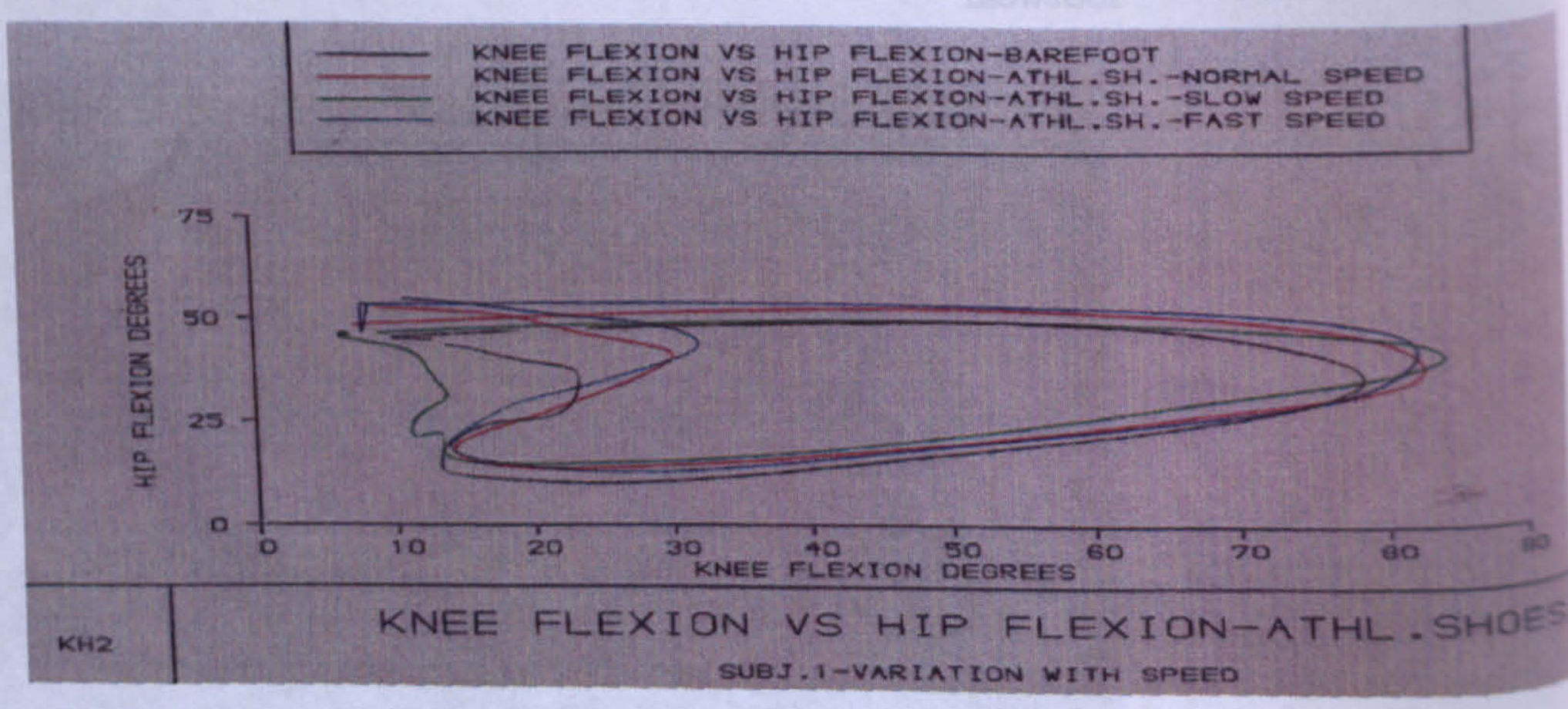

Figure 7.14: LEFT KNEE VS HIP FLEXION ANGLES:variation with SPEED

7.2.4 FOOTWEAR

It was not until the early 1970s that biomechanical or functional testing began to have a considerable impact on shoe design and evaluation. The use of high speed cinematography (100 to 500 pictures per second) was probably the first truly scientific attempt on the part of researchers in conjunction with shoe manufacturers to design more functional shoes. Today a vast array of sophisticated equipment is available and being used to study all types of shoes and their performance. A series of machine tests was designed to simulate the various shoe components considered to be the most important based upon runner surveys, clinical experience, and biomechanical research on runners. Although, these tests were all mechanical in nature, they are based upon biomechanical criteria and were changed and modified over the years as more information became available. The primary components evaluated are rearfoot and forefoot shock absorption and rearfoot control. These functions are considered by many to relate to the two most important functions of the shoe: (a) to protect the foot and body from excessive force, and (b) to provide adequate stability and control in the mediolateral (sideways) direction. All shoes must be designed and constructed to provide rear-foot stability and shock attenuation. Rear foot stability is defined as the amount and rate of pronation after foot-strike. Bates et al have shown that the degree of foot pronation during running is increased McPoil [1988]. Because of the increase in foot pronation, manufacturers have used several techniques to enhance rear foot stability, including extending the shoe the shoe counter medially, reinforcing the counter with an additional plastic stabilizer placed between the midsole and counter, reinforcing the counter with leather foxing, or extending the sides of the midsole superiorly to reinforce the inferior aspect of the counter. With regard to the lateral stability, in the present study, an obvious variability with footwear was observed in the Mx component of the left ankle which corresponded to a parallel variability in the inversion-eversion ankle angles (FIGURE 7.9 on page 150). The barefoot trial had the greatest Mx ankle moment throughout the stance phase revealing a peak of about 50 Nm at 45% of the walk cycle-just before toe-off. The next greater value belongs to the oxford shoes -approximately 35 Nm- followed by the athletic shoes (less than 25 Nm) and finally the boots (25 Nm), the peaks having very small timing differences. The trial with the highest eversion , is the barefoot (which revealed approximately 30 degrees eversion throughout the stance with a decrease observed just before toe-

off of almost 10 degrees towards inversion), had the largest Mx moment. The same relationship holds for the rest of the trials the order being, oxford, athletic, boots. It was observed in the past that medium-height shoes or high-cut shoes contribute to the reduction of supination in sideways movements Stacoff et al. [1985]. The author measured the influence of shoe height on lateral stability of sport shoes in sideways movements. Three different in terms of height shoes were used: (a) low height, which is usually found in running shoes, (b) medium height, which is known in basketball shoes, and (c) high cut, which is found in boxing shoes. The average range of total supination for one subject was found to be 20 degrees over all shoes. The range of all shoes, however, was found to be 43 degrees. Therefore, in sideways movement the variability of all subjects equalled about twice the variability of one subject. Hence, under the given test conditions, there was greater lateral stability with the medium-height and the high-cut shoes than with the low-height shoes. In comparing the results with or without borders, no significant differences in supination were found, thus indicating that the presence of borders had no effect on the lateral stability. Therefore, in the present study the previously described eversion relationships might be attributed to the fact that the higher the height of the shoe, the greater the amount of eversion expected (in this case the order of heights were boots, athletic, shoes). Furthermore, the corresponding increase in the Mx that follows the eversion angle increase is attributed to the fact that when the lateral stability decreases as seen with the reduction of shoe height, the moment about the ankle in the x-axis increases to compensate for that instability. It should be noted that boots revealed the best lateral stability with the smallest Mx moment about the ankle, the barefoot trial being the other extreme. In addition to the previously described enhancing of the rear-foot stability referred to as reinforcing the counter, another method to improve stability as used in the Anatomical Last is to modify the midsole to permit the individual's calcaneus to sit in the midsole rather than on top, as in most cement- or board-lasted shoes (the latter with reference to the athletic shoes in particular) McPoil [1988]. Shoe manufacturers have also varied the density of the material in the midsole to enhance stability. Shoes designed to control pronation, for example, would have higher density material on the medial half of the mid-sole compared with the lateral half. Nike filmed runners on a treadmill for the first 150 ms of a 3.3 and 4.5-m/s gait. Two reference points for each leg denoted its angle relative to the calcaneus. These were used to record touch-down and maximum pronation angles,

time period after the footstrike until maximum pronation, and pronation velocity. The tests confirmed that shoes move the heel and increase pronation over the natural motion barefoot (cited in Baer,1986). In parallelism with this finding one could claim that in the present study pronation was enhanced in the barefoot trial rather than in the trials with footwear on. However, direct comparisons can not be attempted since the results refer to running. Nigg et al. [1979] reported data that contradicted Nike's suggestion about pronation Baer et al. [1986]. Luethi et al. [1987], reported that the peak acceleration values obtained from an impact tester increase from the softest to the harder materials. The same tendency was demonstrated by the impact force values measured under the barefoot condition. The average peak force values increase by 5% from soft to medium and by 24% from medium to hard. A slight increase in peak force value from the soft shoe to the medium shoe could be observed. The hardest shoe, however, demonstrates an average peak force that is lower by 9% than the value for the medium shoe. The kinematic analysis shows considerable differences in the foot behaviour during impact. The maximum rate of pronation, was different between running barefoot and running in shoes. The influence of the material on the maximum rate of pronation between the shoe conditions is considerably greater. No difference in touch-down velocity was registered between shoes and between barefoot conditions. The author concluded that the results demonstrated the relationship between angular motion of the joints at the hindfoot and the magnitude of the impact forces. Harder shoe soles produce greater moments around the joint axes, which in turn results in increased joint motion. As a side effect, the impact forces do not increase as expected. The results show that in running barefoot the muscles of the foot are able to stabilize the foot during impact. The internal structures that are mainly loaded in this case are the soft tissue beneath the heel, the joints, and the bones. Running in shoes, however, changes the situation drastically. The same muscles can not equalize the greater moments produced especially by harder shoe soles. The effect is increased initial joint motion during early stance. This change in foot behaviour changes the internal load conditions. The occurrence of fast initial pronation, for example, means that the everting muscles, which are under a certain pretension immediately before impact, are loaded eccentrically at a fast rate. With regards to the above, the results of the present study confirm the effect of the material on joint motion and moments. From FIGURES 7.9 on page 150, 7.10 on page 150, it is obvious that the joint (ankle) motion increases with increased hardness of the shoe (the order from harder to softer for the shoes is:

oxford, boots, athletic). However, the only ankle moment component clearly affected appears to be the Mx moment, with oxford shoes revealing the highest peak of all types of footwear. The My component shows slight differences whereas no differences appear in the Mz component. The barefoot trial's Mz, however, is almost 30 Nm greater than that of the footwear confirming the above findings. With regards to the HIP moments and their variation with the footwear an interesting finding of the present study refers to the Mz component of the barefoot trial. Although all trials with footwear showed no significant differences in the curve shape, the barefoot trial appeared to have a considerable timing difference with the rest of the trials. For example, at about 5% of the walk cycle all footwear trials reveal a value of approximately 60 Nm whereas the corresponding value for the barefoot trial was about 25 Nm. Similar magnitude relationships appeared at the time just before toe-off where the barefoot trial had the greatest value of all, nearly 70 Nm, the rest having a value of a approximately 40 Nm showing a considerable time difference by appearing almost 10% of the walk cycle later. This timing difference may be attributed to the fact that during the barefoot trial different temporal characteristics might cause a different configuration of the forces and lever arms that produce the particular moments resulting in a completely different dynamic response of the muscular and skeleton system. In our study it was of interest to compare the direction and magnitude of the initial force value as seen in the Pedotti diagrams (FIGURES 7.15 on page 154, 7.16 on page 154, 7.17 on page 154, 7.18 on page 154, 7.19 on page 156, 7.20 on page 156). In the barefoot trial a more vertical initial force was observed when compared to the rest of the trials with footwear on, the latter revealing smaller initial peak values.

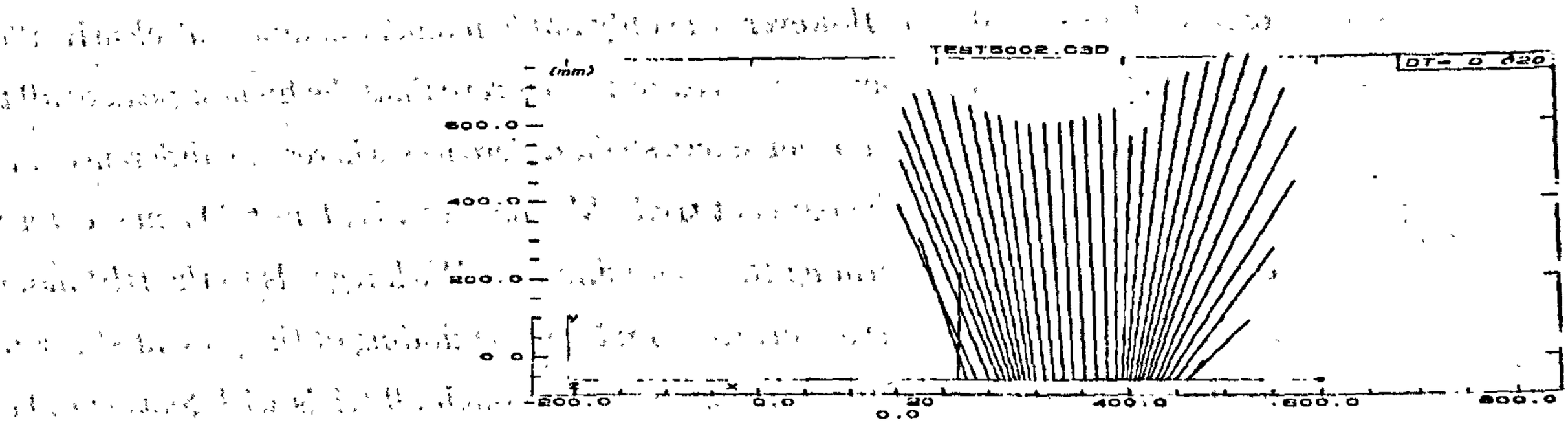

Figure 7.15: PEDOTTI Diagram of SUBJ. 1: Barefoot-NORMAL SPEED

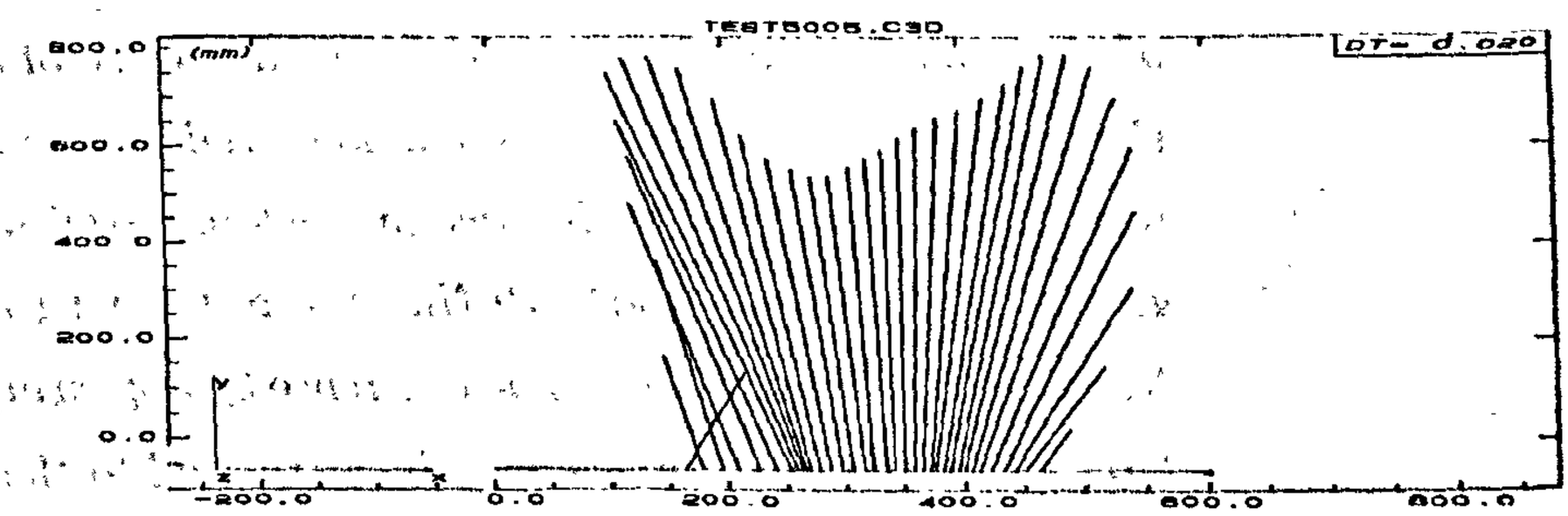

Figure 7.16: PEDOTTI Diagram of SUBJ. 1: Athletic sh.-NORMAL SPEED

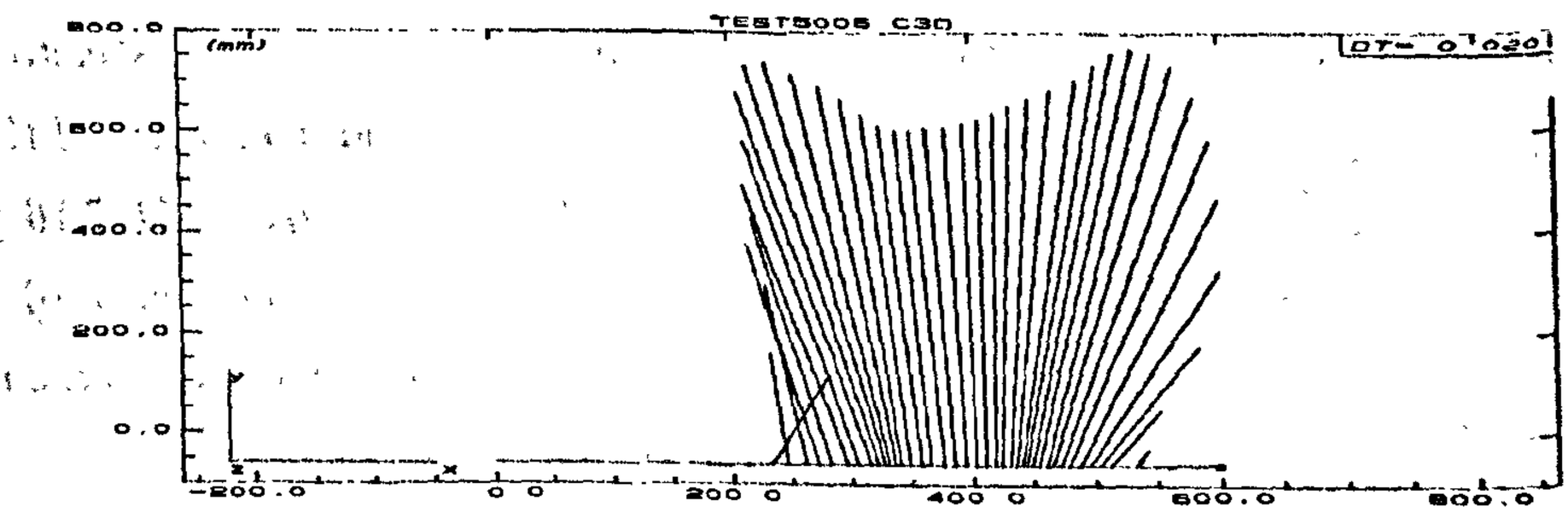

Figure 7.17: PEDOTTI Diagram of SUBJ. 1: Athletic sh.-SLOW SPEED

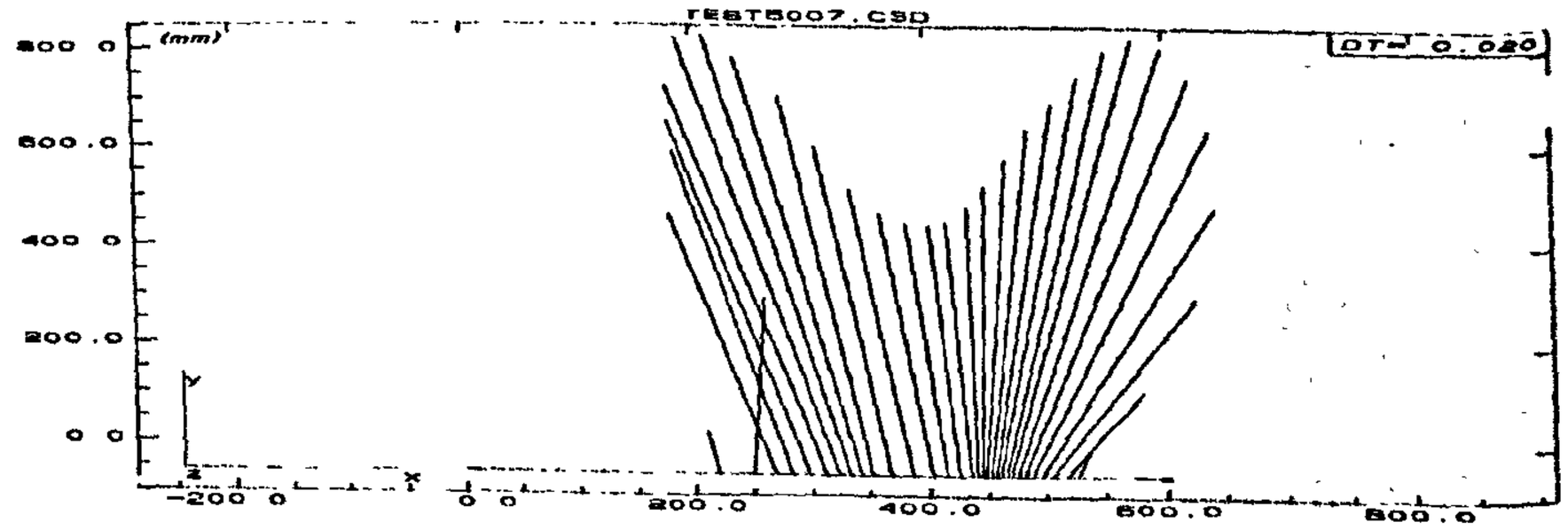

Figure 7.18: PEDOTTI Diagram of SUBJ. 1: Athletic sh.-FAST SPEED

Snel et al. [1985], in their studies of running reported that the major differences between the various shoes under test appear to be mainly restricted to differences in rise time and not to differences in the magnitude of the impact peak. The author suggested that, (for a larger variety of footwear), there was a striking absence of differences in the magnitude of impact forces between running with different types of shoes and barefoot.

The results of the present study show similar patterns suggesting that this phenomenon can not only be explained by the passive shock-absorbing characteristics of the shoes. It seems that another explanation could apply in both running and walking studies when this phenomenon is in question. It is more likely that the walking subject and moreover the runner anticipates the expected impact force, in such a way that stiffness of the sole can influence the neuromuscular control system.
Therefore, it could be inferred that walking barefooted and its effect in temporal characteristics (different pronation angles, lateral stability, step length, pressure distribution under the foot, flexion-extension angles, angular and linear accelerations, etc), is related to an automatic neuromuscular response which finally affects the moments about the joints.

With regards to the My hip component the comparatively smaller My component for the barefoot trial at about 15% of walk cycle reveals that hip extensors which are responsible for assisting in absorbing energy at IC by controlling hip flexion (and, ultimately, control knee collapse) at that stage, produce a smaller My moment for the controlling of the forward rotation of the pelvis and thereby the stabilization of the trunk. With footwear on this stabilization task of the hip extensors becomes more demanding. All the above apply when the knee is taken into consideration, since the same magnitude relationships hold, that is, the curves of all the footwear trials follow a certain magnitude envelope (FIGURE 7.6 on page 140), whereas the barefoot trial reveals time and magnitude differences. Plantar flexion at the ankle occurred immediately after heel strike. This can be explained by the large ground reaction forces acting on the heel part of the sole, which result in a plantar- flexing moment. This moment could overload the anterior tibial muscle in greater speeds e.g. running. One can conclude that it is questionable whether a shoe with good absorption properties is also a good shoe from an energetical point of view. The absence in differences in the magnitude of the impact forces between all shoes and the barefoot condition

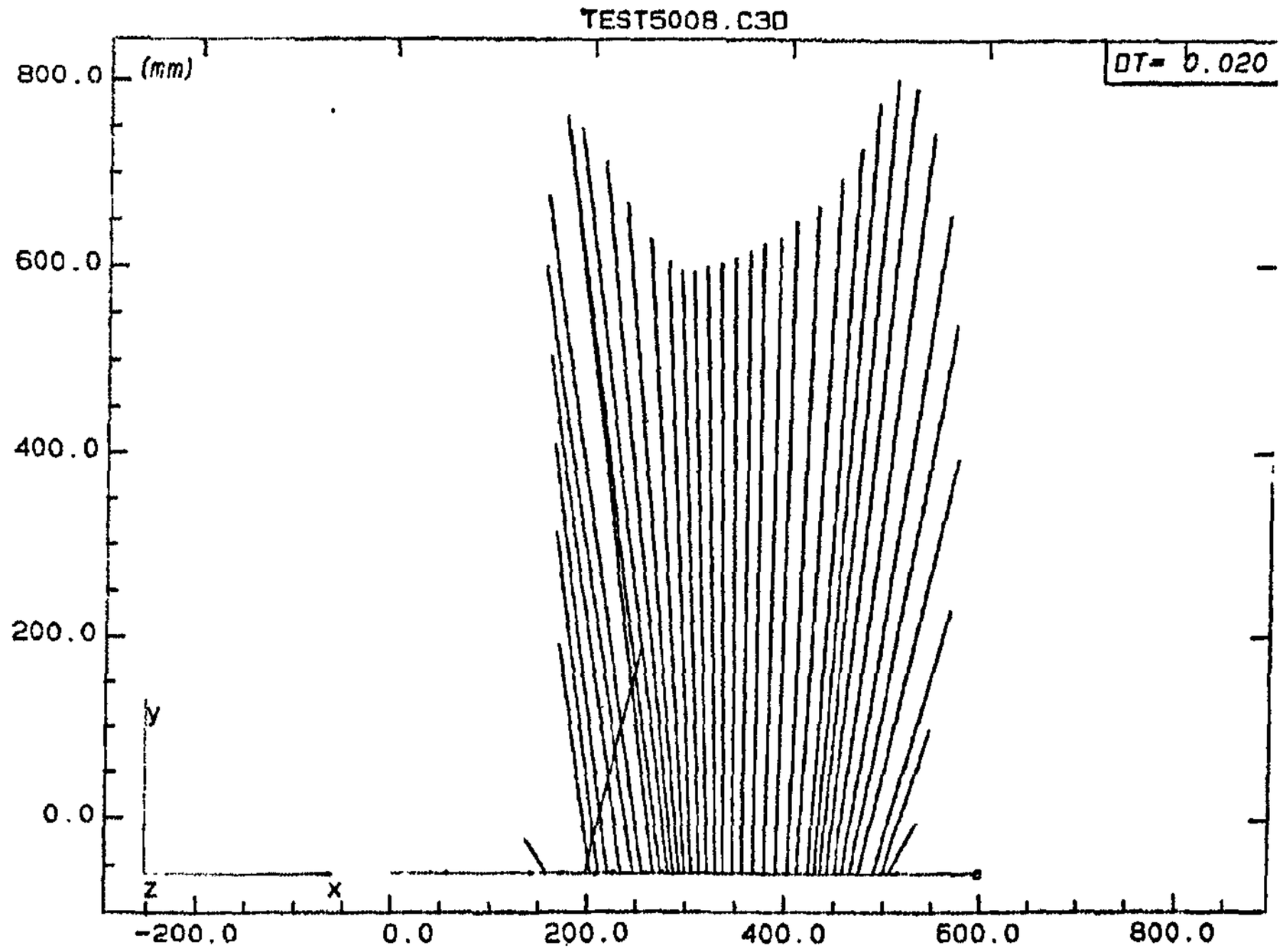

Figure 7.19: PEDOTTI Diagram of SUBJ. 1: Boots-NORMAL SPEED

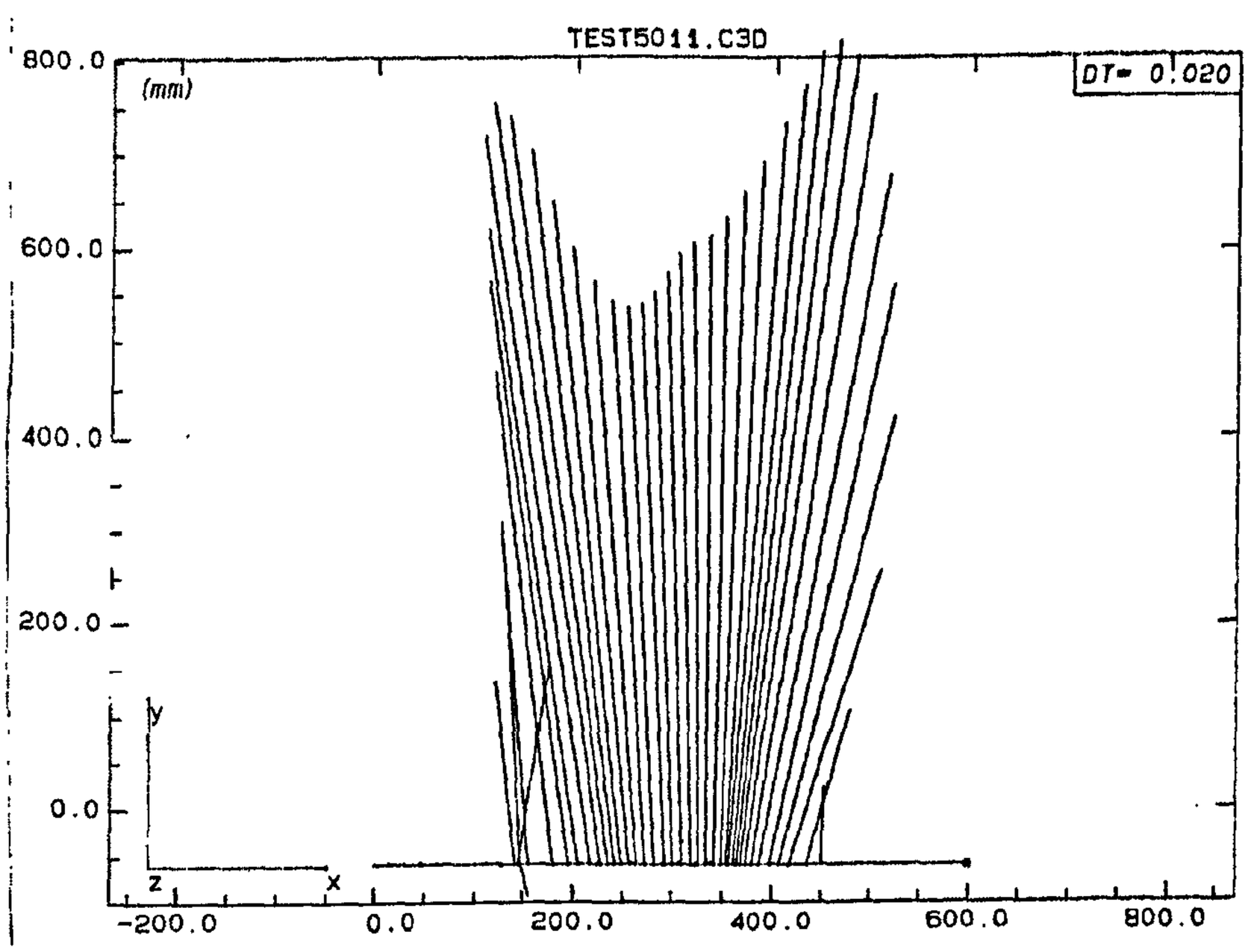

Figure 7.20: PEDOTTI Diagram of SUBJ. 1: Oxford sh.-NORMAL SPEED

during actual running and the absence of a relation between measured parameters in other studies (Snel et al. [1985]) and the results of the material test lead to the conclusion that the material test is not a good method of comparing running shoes. The complete statistical analysis of interactive effects between walking speed and different footwear presented later in this chapter reveals other areas of discussion and supports the above statement. An aspect of the design of athletic shoes that usually contributes to the variability is the shoe's weight. It has been well documented that added weight carried on the feet causes an increase in oxygen uptake during distance running (Cavanagh [1985]). Although this may not apply directly in the present study the fact that the boots are much heavier than the oxford and athletic shoes could be a reason of excess effort of the walker since walking is a task much slower than running, with active stages being more than the passive ones. Bates et al. [1981], investigated the effects of running shoes on three components of the ground reaction forces and their relationship to selected aspects of lower extremity function. He concluded that barefoot was not an extreme condition. Possibly the mind senses a potential danger and modifies performance technique. He suggested an inverse relationship between initial impact force and average pronation. The same tendency appeared between average pronation and the percent of total impulse of the X-component.

In the present study a greater Fy ground reaction force in terms of magnitude for the barefoot trial was observed and a corresponding greater eversion ankle angle for the barefoot trial was also very clear (FIGURE 7.9 on page 150). However, it should be pointed out, that since individuals are anatomically and functionally different, future studies must evaluate more subjects and conditions in order to gain a better understanding of the effects of shoes on lower extremity function. Light et al. [1980], investigated the effect of walking barefoot, with conventional and with shock-absorbing footwear on the accelerations observed in a normal subject. The shape of the tibial transient was characteristic of the heel construction -the hard leather heel giving a short transient of very abrupt onset and the two compliant heels showing smoother and lower deceleration waves. The shock absorbent construction resulted in less reverberation after the initial transient than the crepe rubber. It should be noted that the above transients are not obvious in force plates' recordings due to their limited frequency response. Data by Nigg et al. [1979] showed that initial angular velocity of the Achilles tendon increased with both running speed and sole hardness. The data conflicted with the accepted theory that compression of softer midsoles exaggerates

pronation. Nigg hypothesizes that a firm midsole rotates faster, the way a firm lever bent over a fulcrum will snap quicker than a soft one. Johnson [1986], investigated the shock absorption characteristics, of four different types of footwear. He reported a transient acceleration at heel strike of 4.7 G. Large acceleration was recorded for athletic shoes as well. Presumably heel strike occurs because the foot has finite absolute velocity at the instant of ground contact. There is therefore, kinetic energy which must be destroyed before the stance phase of gait can proceed. It is suggested that the shoe-foot combination should be considered as a single degree of freedom system in which the force at heelstrike and its rate of application must be related directly to the overall stiffness of the spring and dashpot system. In order to reduce impact it is necessary to reduce stiffness as much as possible but it must be remembered that the reduction of load will be accompanied by an increased deflection which may modify the gait pattern (possibly in an undesirable fashion). The fourth type of shoe in that study was a pair of lace up leather shoes, with thick rubber soles and heel which is similar to the present study's oxford shoes. The author revealed that this pair showed the smallest shock reduction. This could suggest that a greater amount of kinetic energy must be absorbed before the stance phase of gait proceed. This could imply a different muscular and motion response for the energy to be absorbed. In FIGURE 9.24 the increased ankle motion for the oxford shoes and the concomitant increase in the Mx and My, confirm the above statement. By contrast the shoes with the better shock absorption, (athletic shoes and boots) revealed decreased ankle motion and decreased My and Mx moments (although to a small extend). Leeuwen [1988], reported that shock absorption may take place through storage of energy in the heel cushion, ligaments, and muscles. Estimates of transfer functions with the aid of a linear system theory give no satisfactory results because the characteristics of the tissue involved are fundamentally nonlinear. An interesting finding in this study was that the reduction of the acceleration proved to be more effective in the axial than in the anteroposterior direction which supports the explanation of the observed increase in ankle motion and moments at these axes, given in the present study. In the study of Jorgensen [1990], the best shock absorption was obtained at the speed of normal walking a finding that might support the idea of a study based on the speed-footwear interaction for greater number of subjects in the future.

The same author revealed elsewhere, (Jorgensen et al. [1988]), Jorgensen et al. [1989], that the most important shock absorber in the shoe-heel

complex is the heel pad and added that running shoes provide a significantly high shock absorption. High muscle activity due to increased musculoskeletal transients at heel strike when the shock absorption is low was also reported (Jorgensen [1990]). However, Bates et al. [1981], Bates et al. [1987], Bates [1985], demonstrated an inverse relationship between stability and shock attenuation. Some shoe models that provide good shock attenuation, therefore, may not provide foot stability.

7.2.5 The effect of anthropometric differences on the kinetic and kinematic parameters

It can be seen in FIGURES 7.21 on page 160 to 2.2 on page 14 that there exists a variability between subjects, although any valuable discussion should be based on statistical significance of the data. The observed tendencies in the shapes of the curves will be shortly discussed here. Knee Moment graphs from all the participating subjects (FIGURES 7.36 on page 163, 7.37 on page 163, 7.38 on page 163, 7.39 on page 164, 7.40 on page 164, 7.41 on page 164) show the width of the graphs for a considerable large amount of subjects (58) with age range of 20 to 36 years. Large variety of weights and heights as well as walking styles were recorded. One of the tallest subjects (subject three) revealed the greater Mz whereas a considerable shorter subject which was of the same mass revealed almost similar values. This was the case in the My moment as well, a fact supporting the variability due to intersubject anthropometric differences (mainly weight and height) and differences in walking style as they are related to segment lengths (all three speeds were used in the comparisons). The shortest and lightest subject revealed the lowest Mz and My moment values. However, almost the reverse was observed in the ankle Mx moments (FIGURE 7.33 on page 163) with the differences being not significant. It seems that as the centre of gravity gets higher due to the longer lower limbs ankle mediolateral moments contribute less to the moment patterns of this joint. It was of interest the fact that as speed increases the magnitude relationships remain as described above when Mz and My are considered, this not being the case in the Mx moment where a considerable increase occurs in the shortest subject's value. It must be stressed here that a decrease in the magnitude of the moment values was observed in subject 4 which happens to be the subject involved in almost no exercise at all. On the contrary, subject 2 revealed high values a fact possibly related to its increase level of fitness and well-trained legs (basket-ball

player)(FIGURES 7.30 on page 162 to 7.35 on page 163).

The same could be observed for the magnitude relationships of the knee joint between the five subjects with My revealing the smaller variability and Mz and Mx the greater. Again the shorter and lighter subject as well as the less fit revealed the same reversed to the rest subjects and comparably smaller moment values.

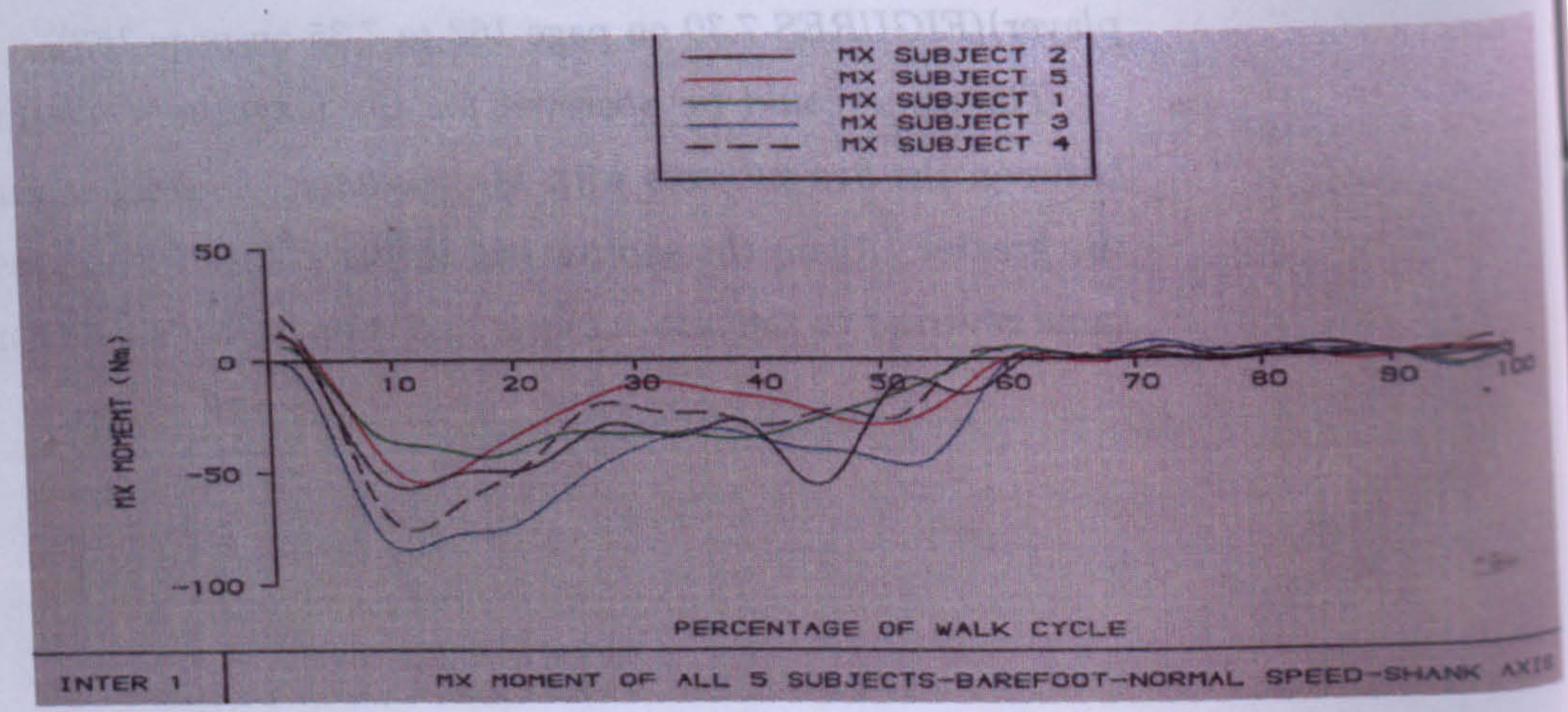

Figure 7.21: Mx KNEE MOMENT-5 subj-Barefoot-NORMAL SPEED

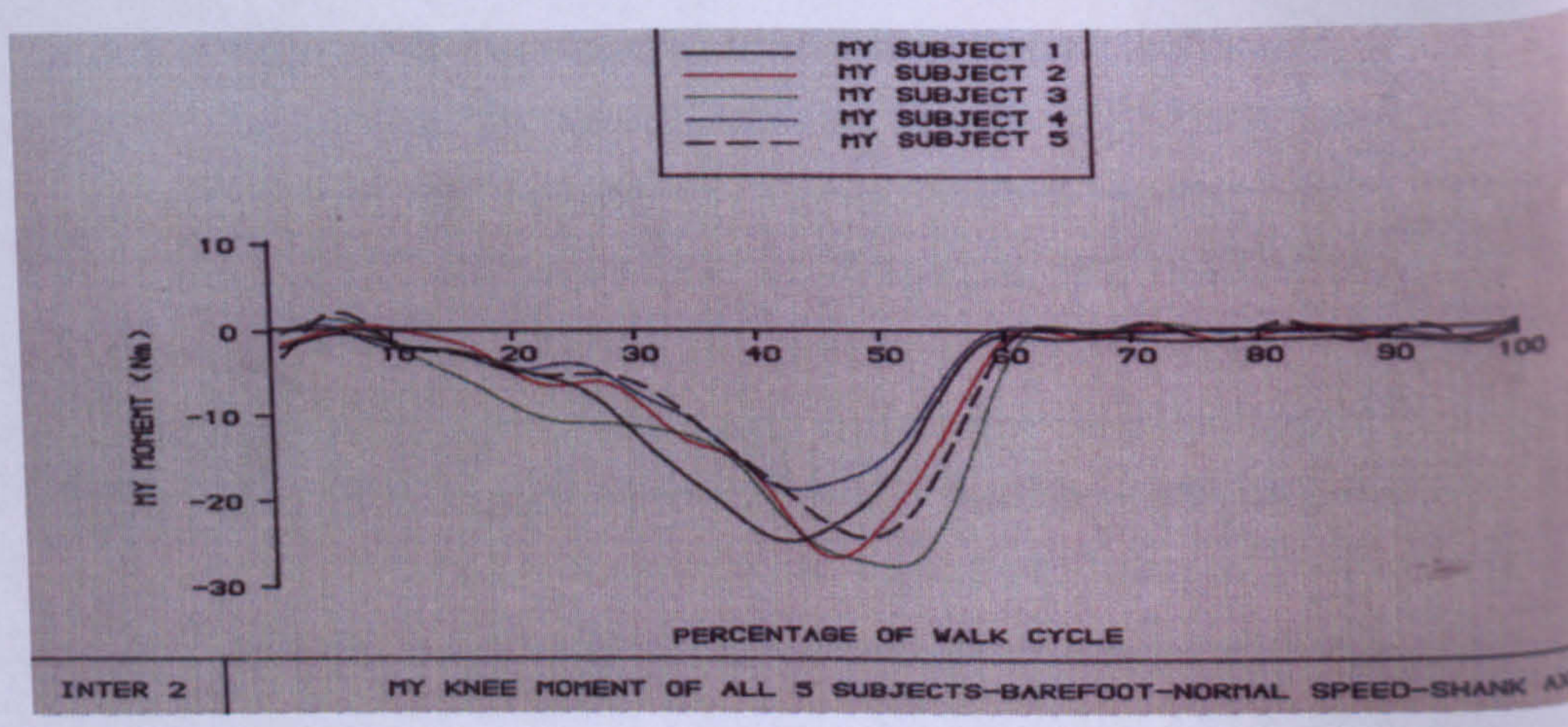

Figure 7.22: My KNEE MOMENT-5 subj-Barefoot-NORMAL SPEED

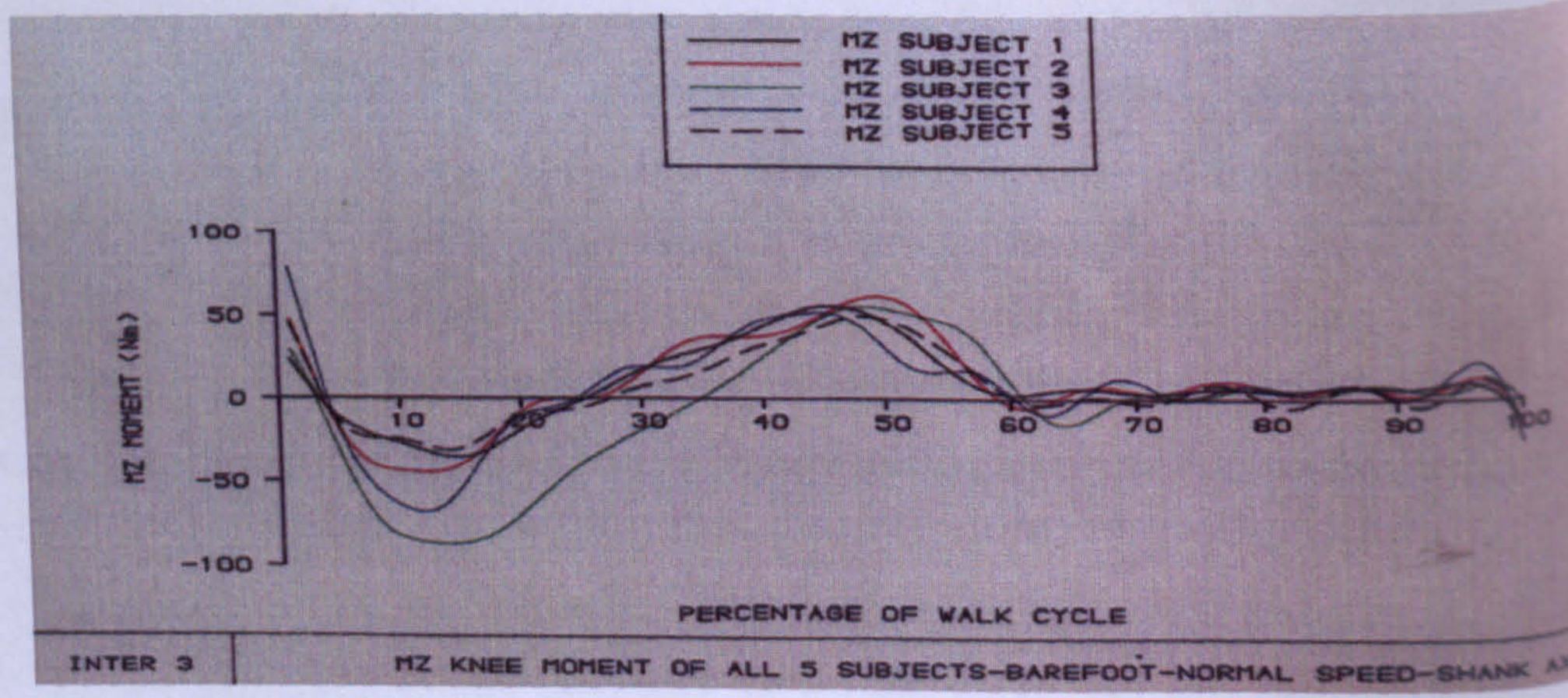

Figure 7.23: Mz KNEE MOMENT-5 subj-Barefoot-NORMAL SPEED

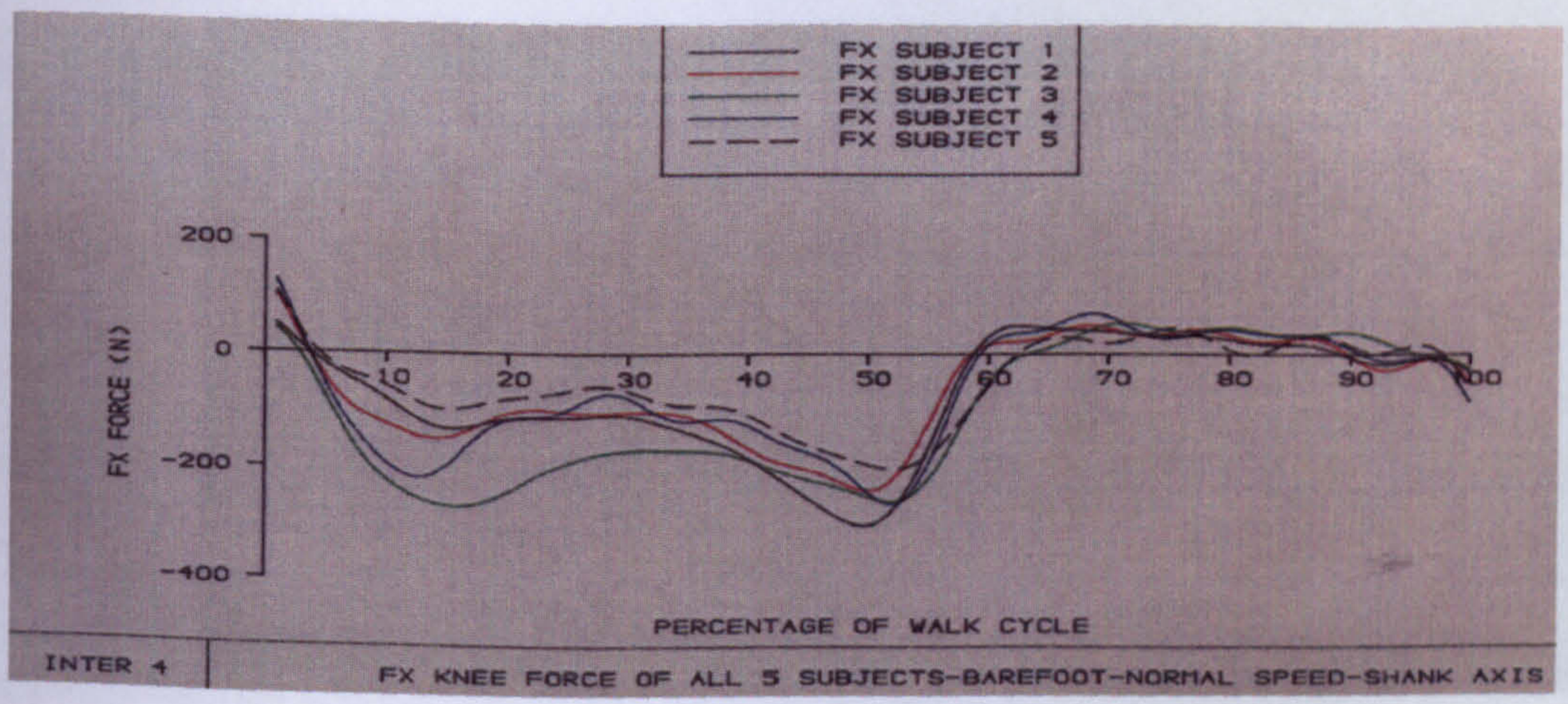

Figure 7.24: Fx KNEE FORCE-5 subj-Barefoot-NORMAL SPEED

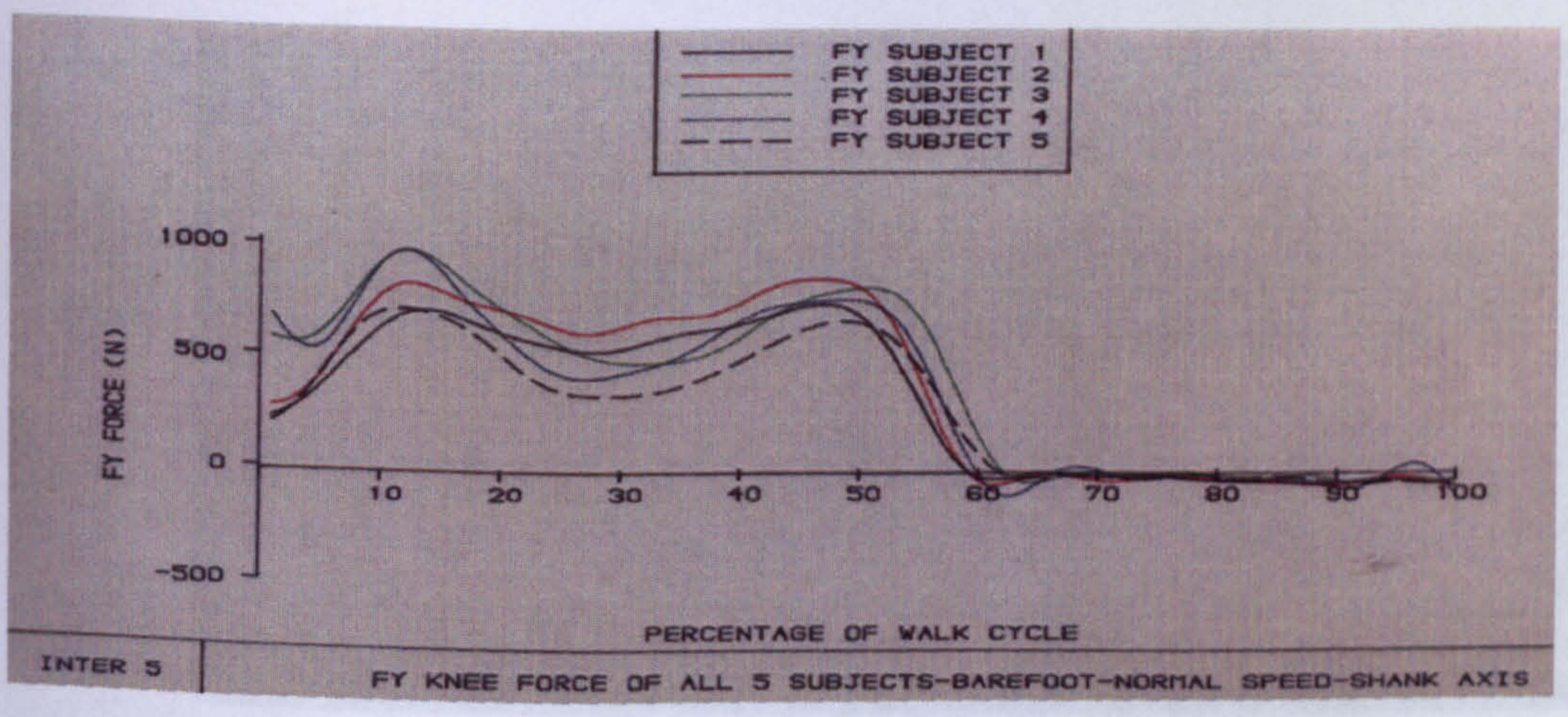

Figure 7.25: Fy KNEE FORCE-5 subj-Barefoot-NORMAL SPEED

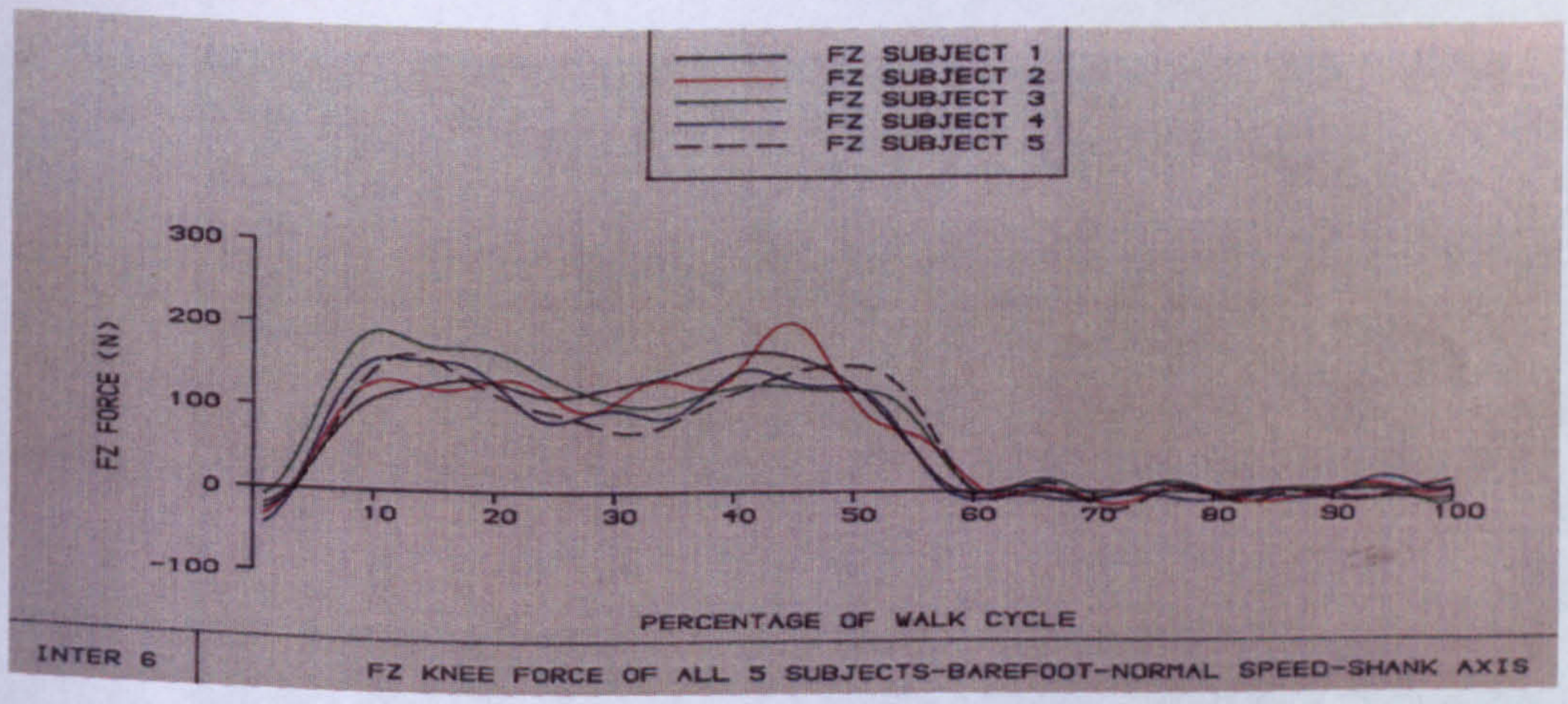

Figure 7.26: Fz KNEE FORCE-5 subj-Barefoot-NORMAL SPEED

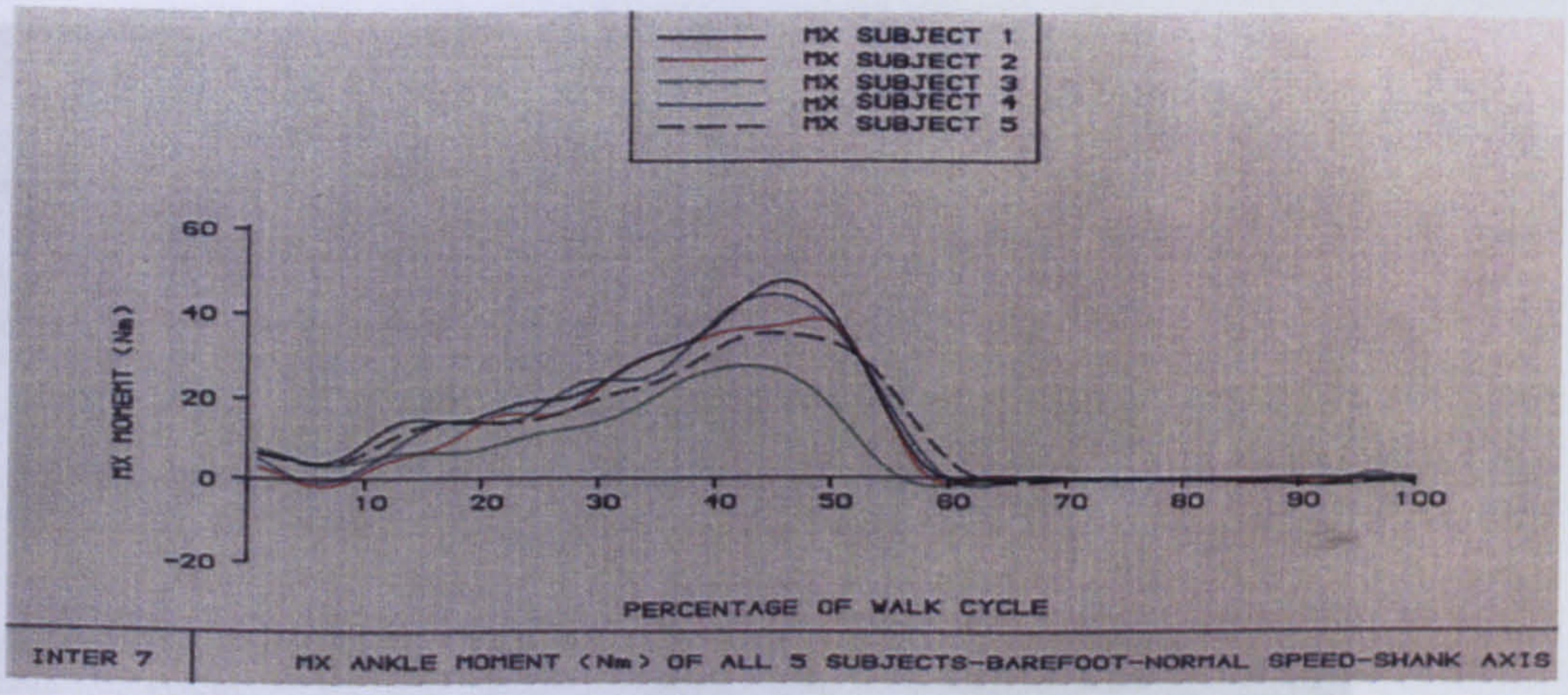

Figure 7.27: Mx ANKLE MOMENT-5 subj-Barefoot-NORMAL SPEED

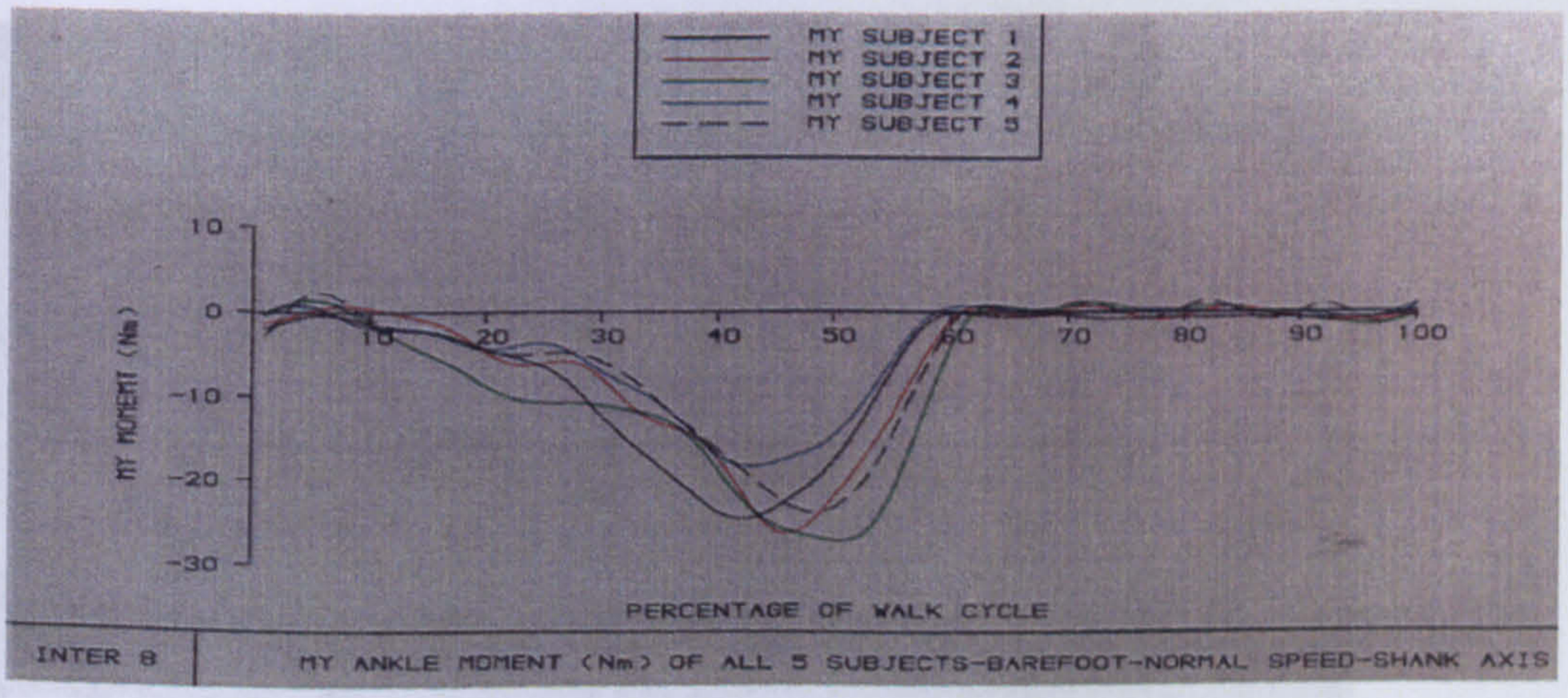

Figure 7.28: My ANKLE MOMENT-5 subj-Barefoot-NORMAL SPEED

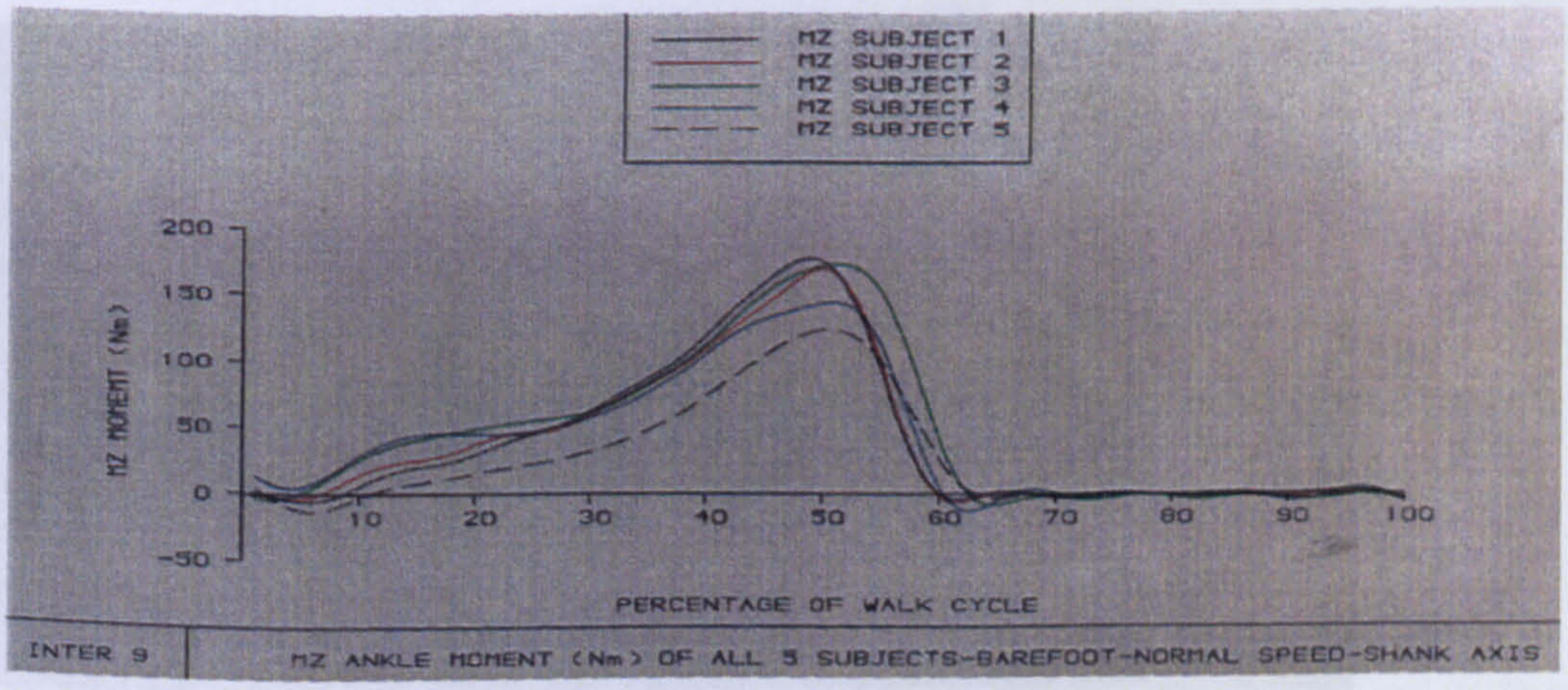

Figure 7.29: Mz ANKLE MOMENT-5 subj-Barefoot-NORMAL SPEED

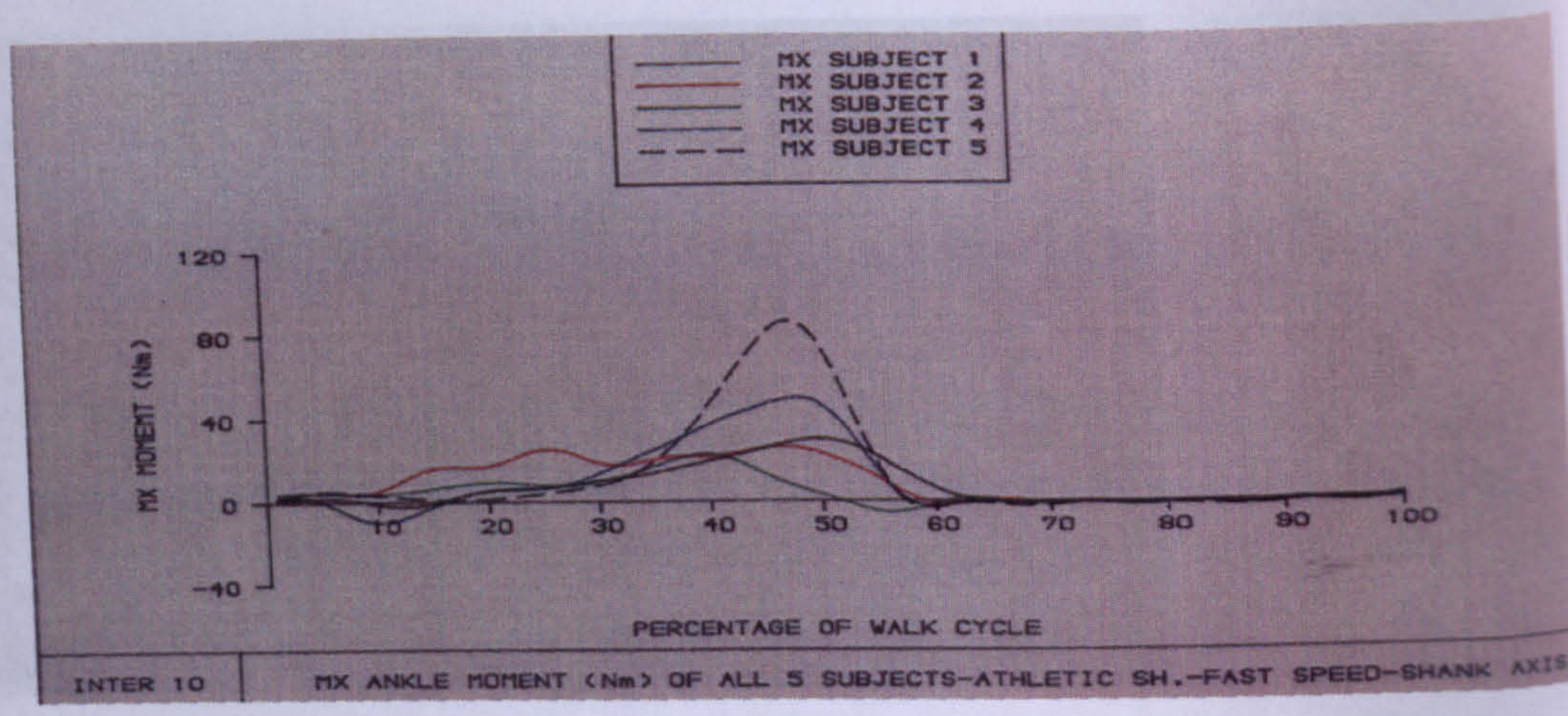

Figure 7.30: Mx ANKLE MOMENT-5 subj-Athletic sh.-FAST SPEED

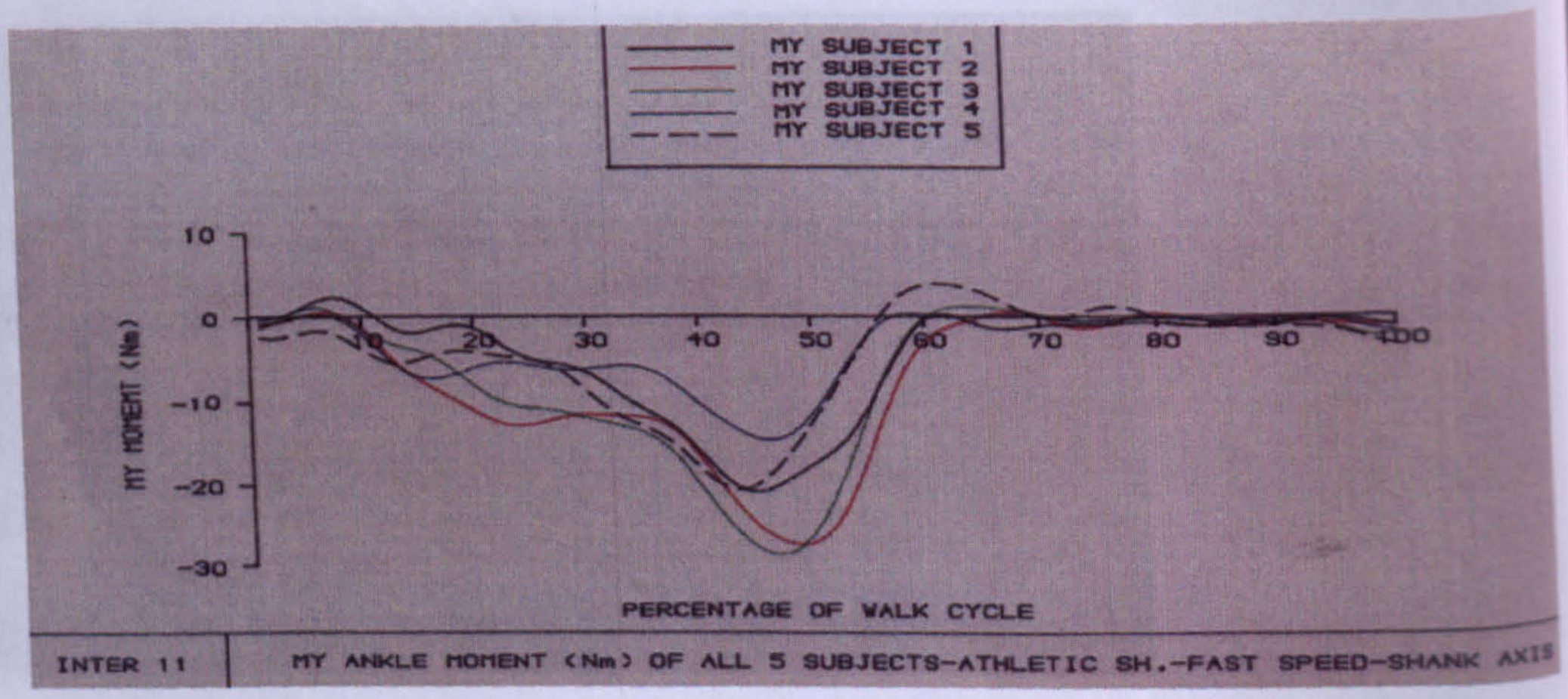

Figure 7.31: My ANKLE MOMENT-5 subj-Athletic sh.-FAST SPEED

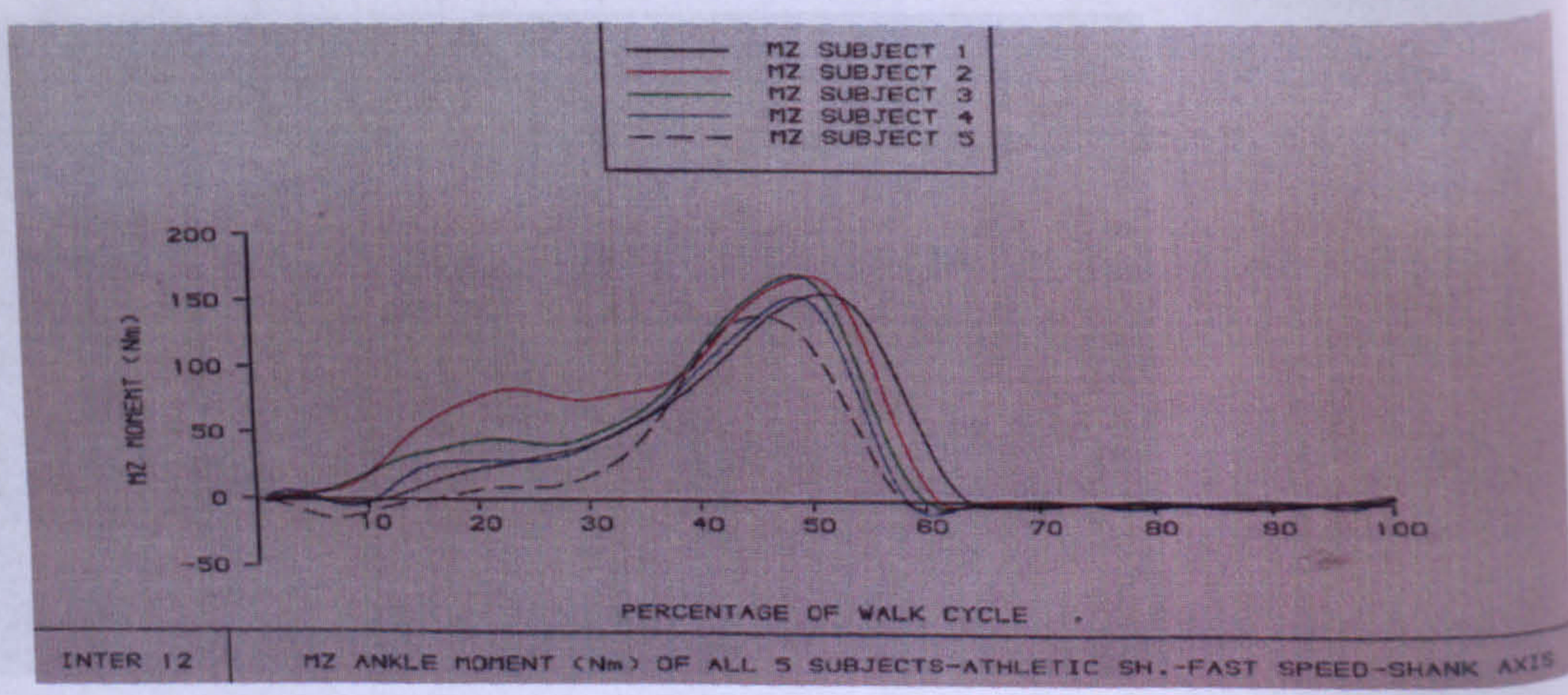

Figure 7.32: Mz ANKLE MOMENT-5 subj-Athletic sh.-FAST SPEED

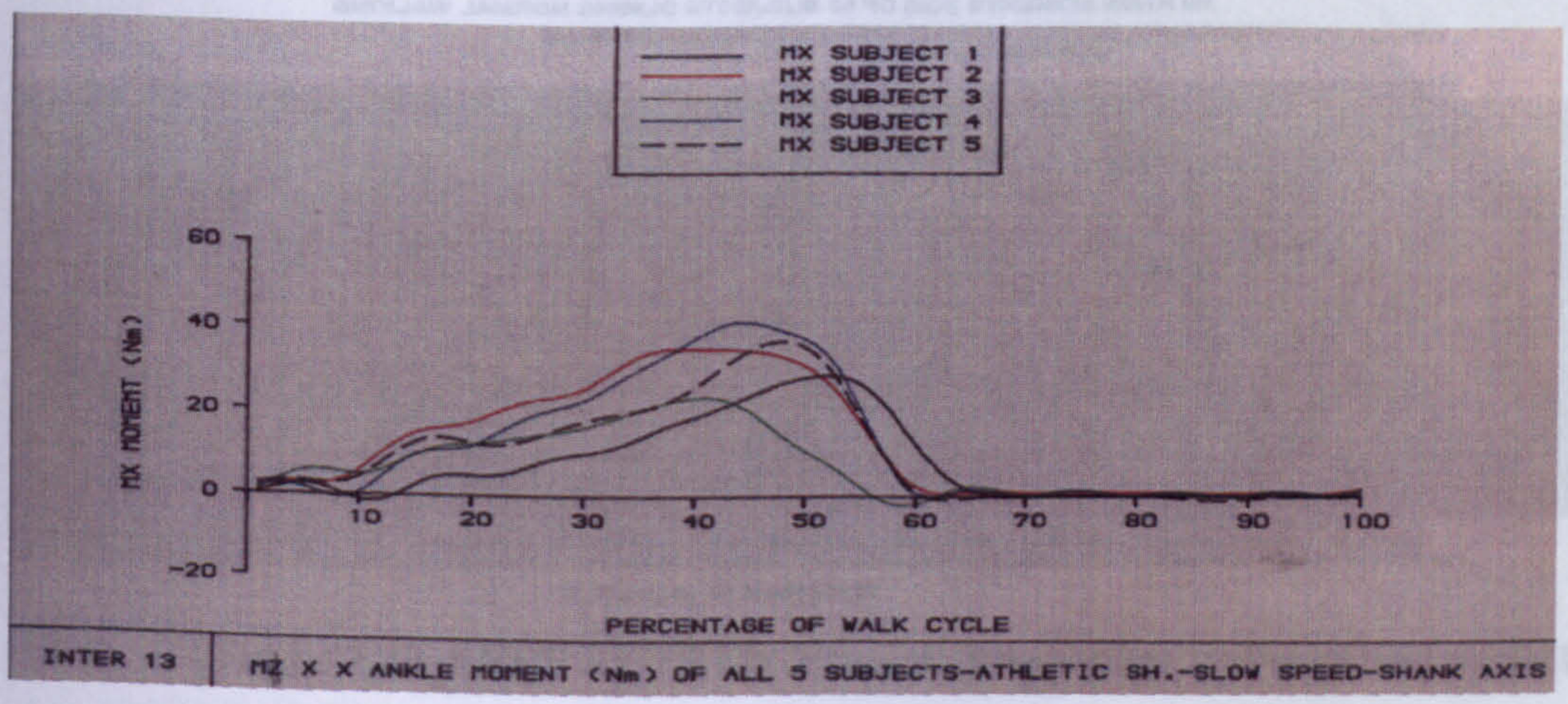

Figure 7.33: Mx ANKLE MOMENT-5 subj-Athletic sh.-SLOW SPEED

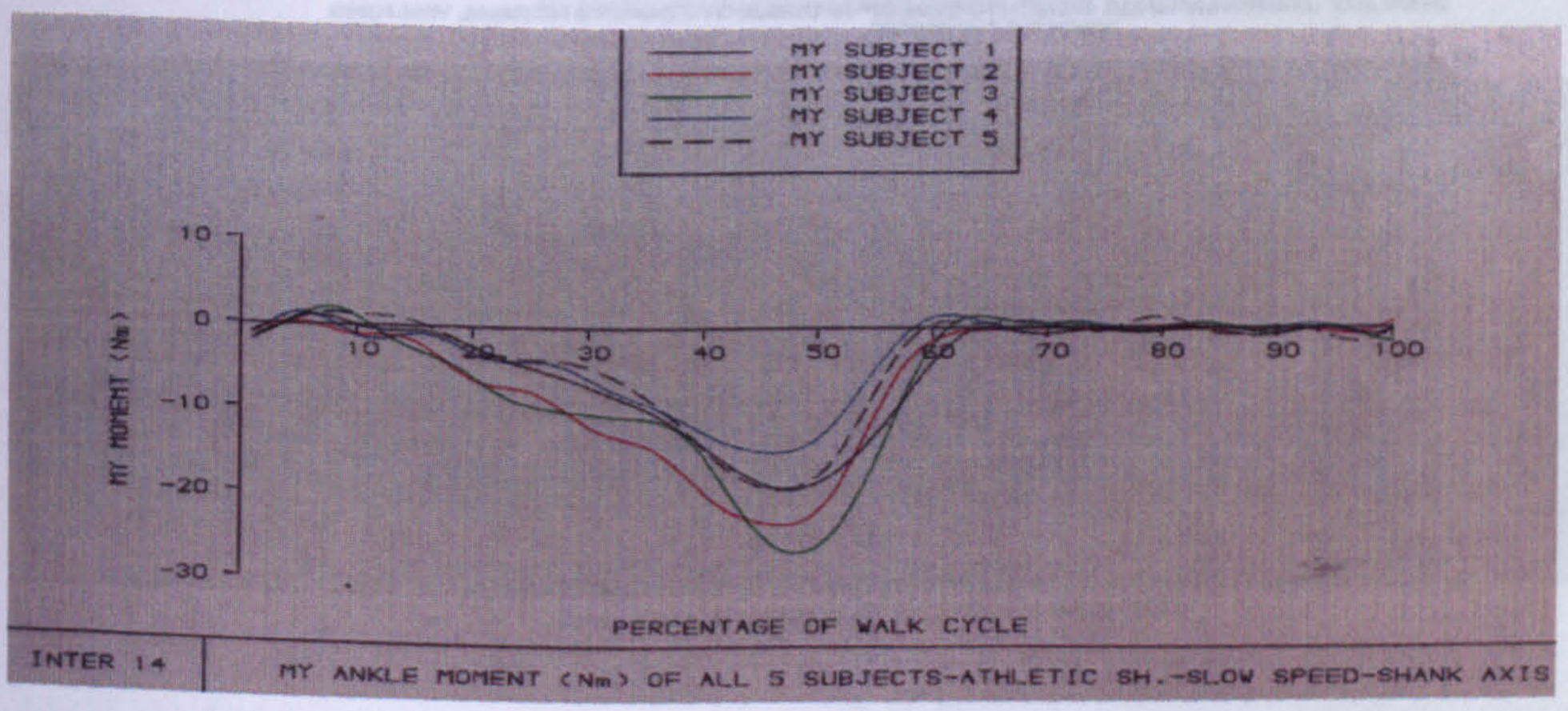

Figure 7.34: My ANKLE MOMENT-5 subj-Athletic sh.-SLOW SPEED

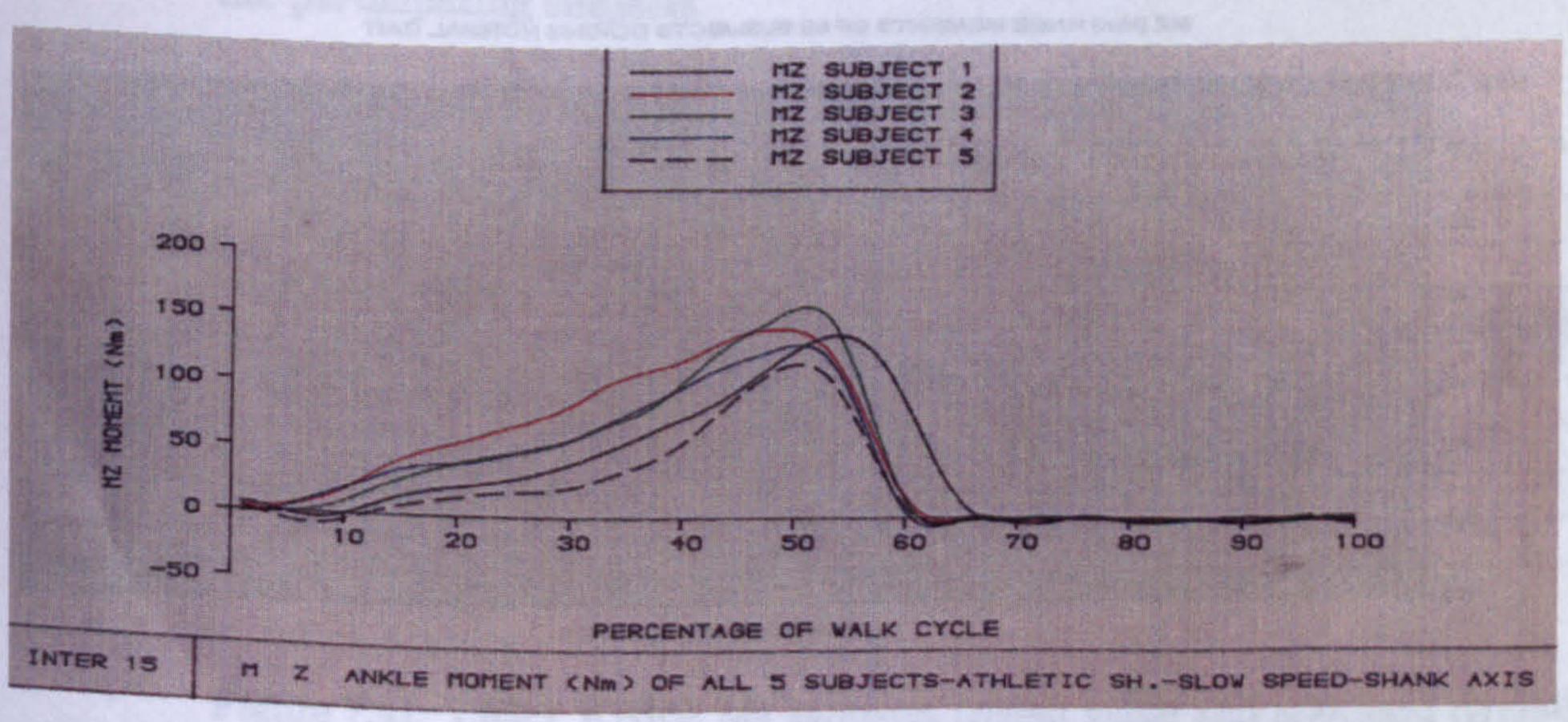

Figure 7.35: Mz ANKLE MOMENT-5 subj-Athletic sh.-SLOW SPEED

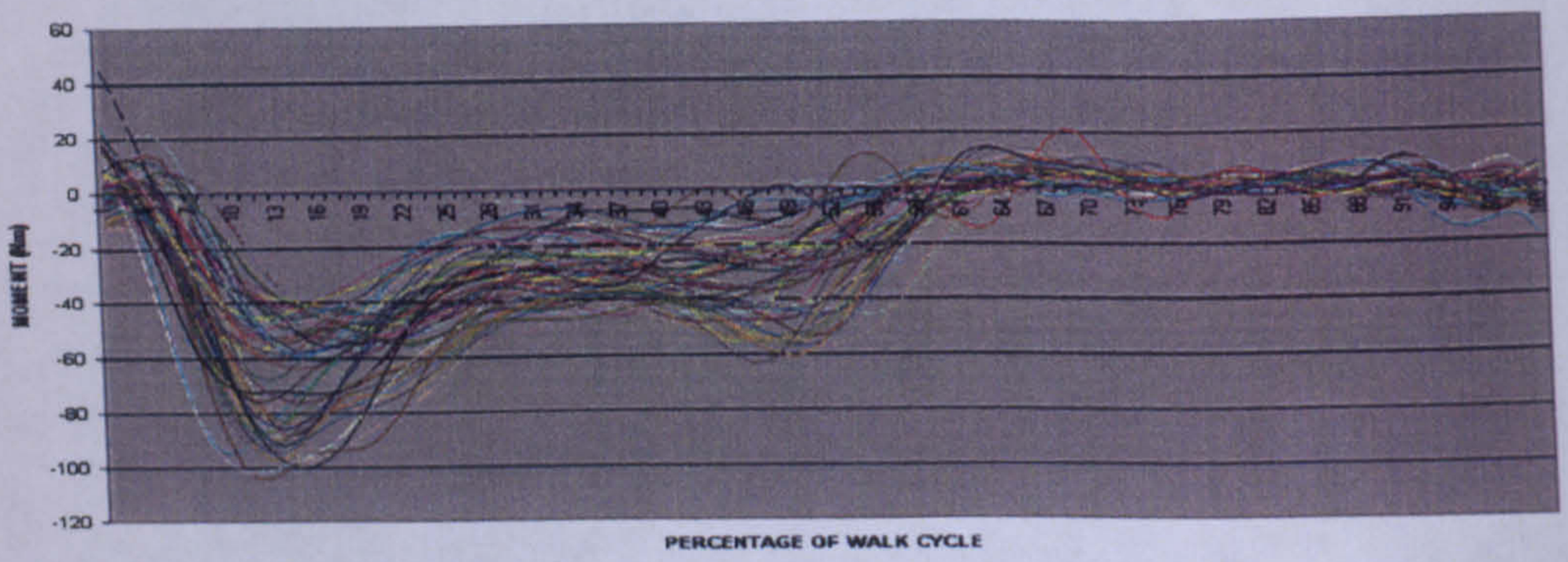

Figure 7.36: LEFT KNEE Mx Moment graphs from all the participating subjects

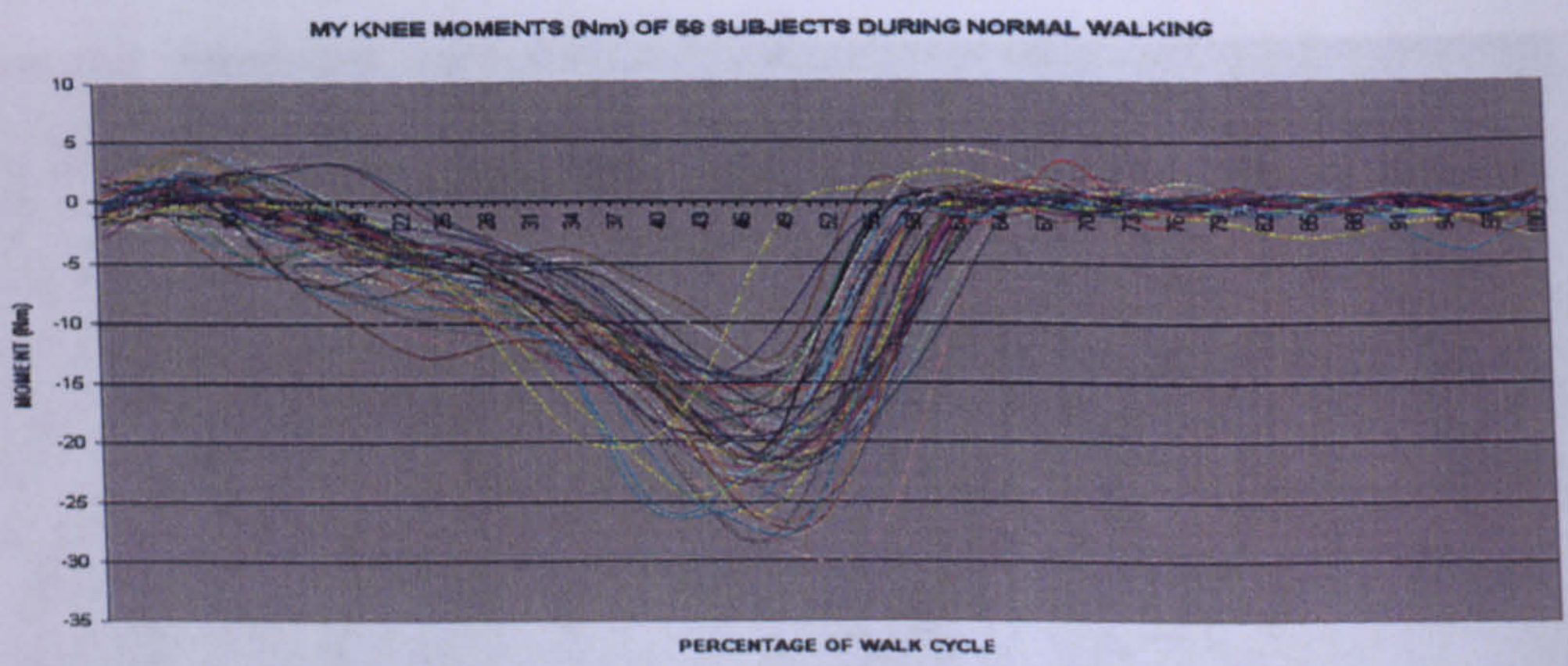

Figure 7.37: LEFT KNEE My Moment graphs from all the participating subjects

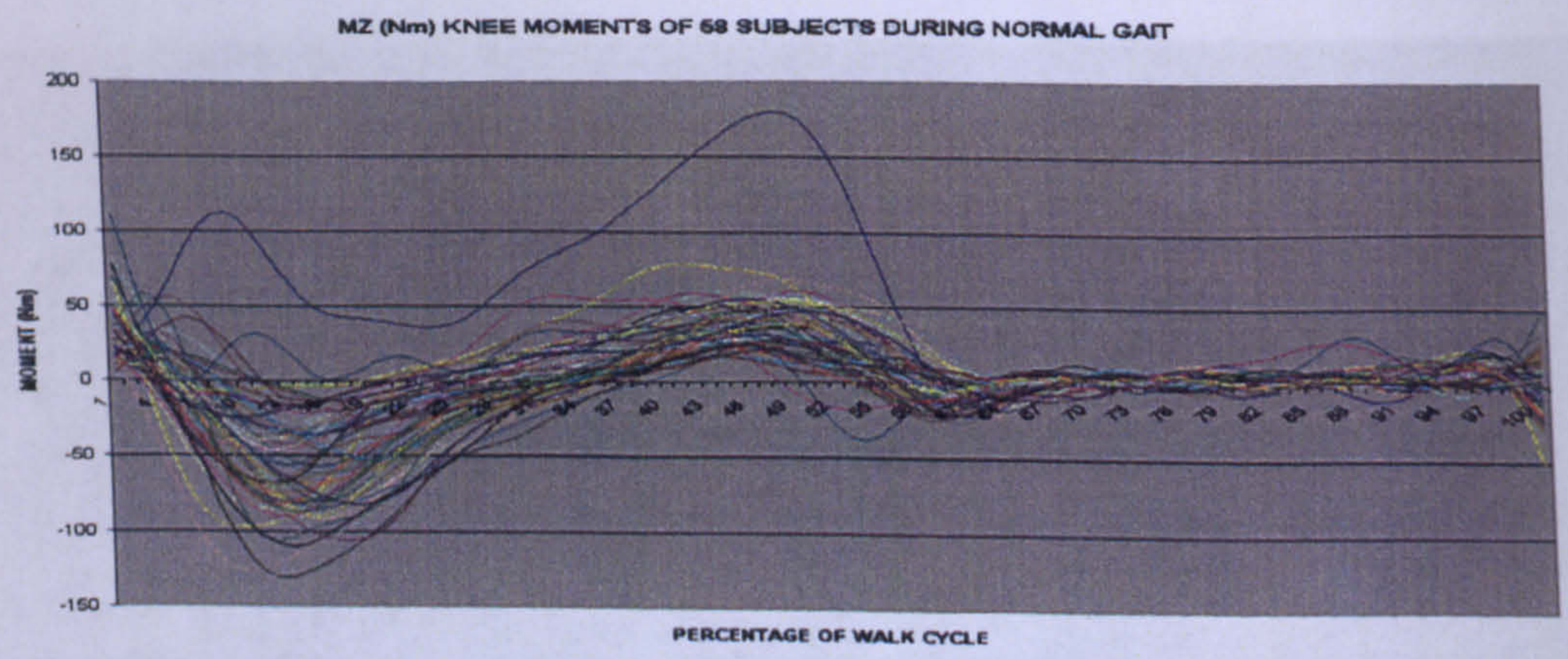

Figure 7.38: LEFT KNEE Mz Moment graphs from all the participating subjects

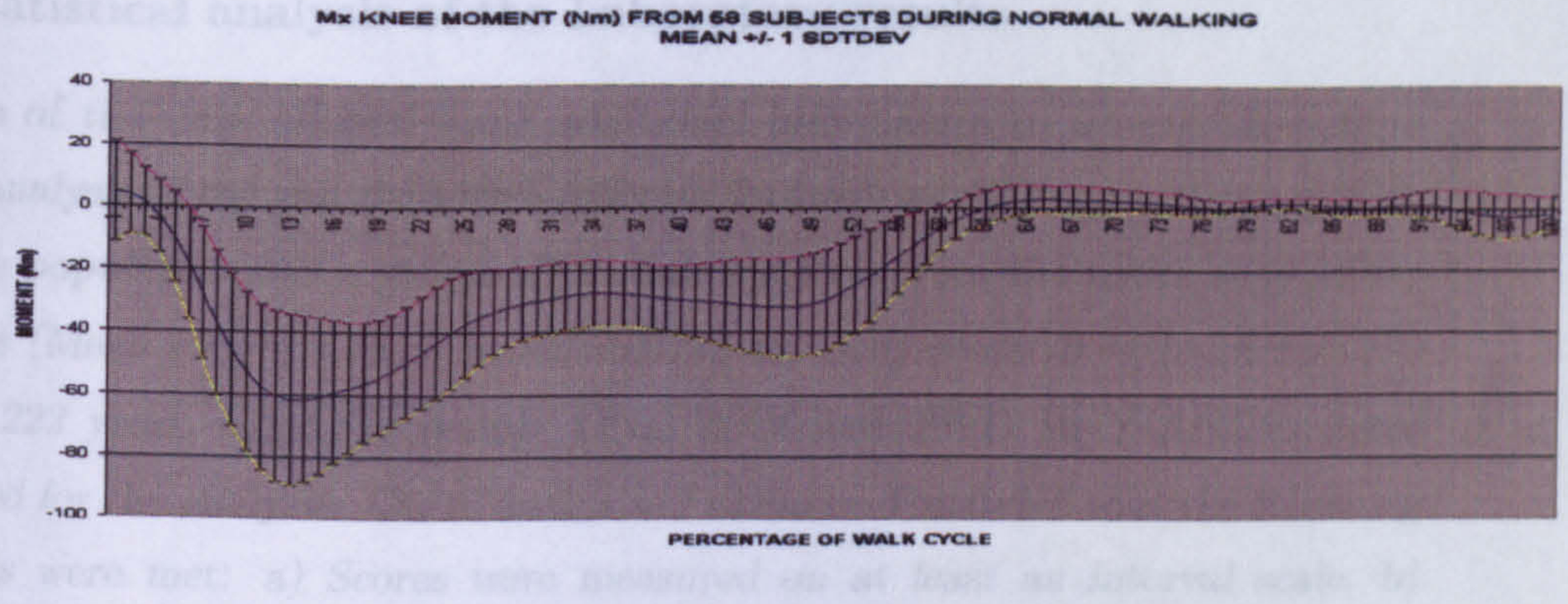

Figure 7.39: LEFT KNEE Mz Moment (mean value and standard deviation) from all the participating subjects

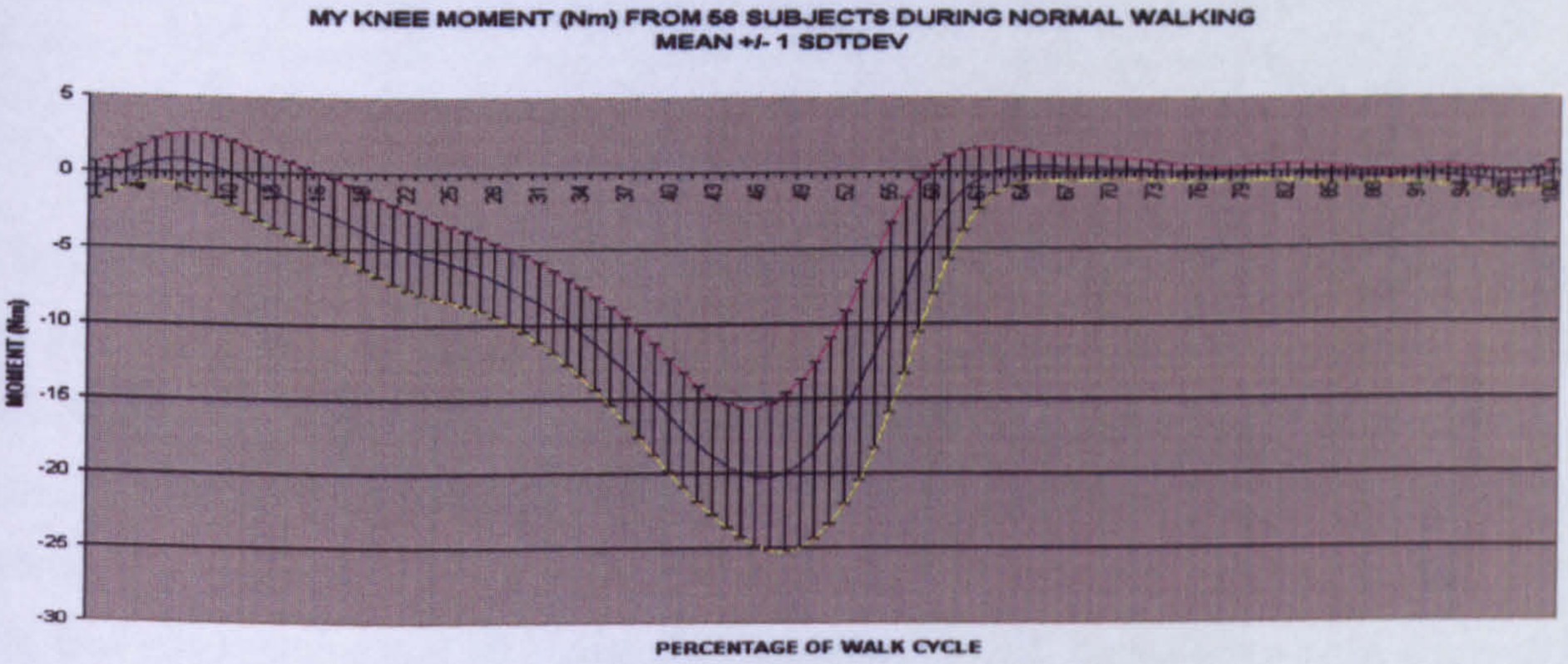

Figure 7.40: LEFT KNEE Mz Moment (mean value and standard deviation) from all the participating subjects

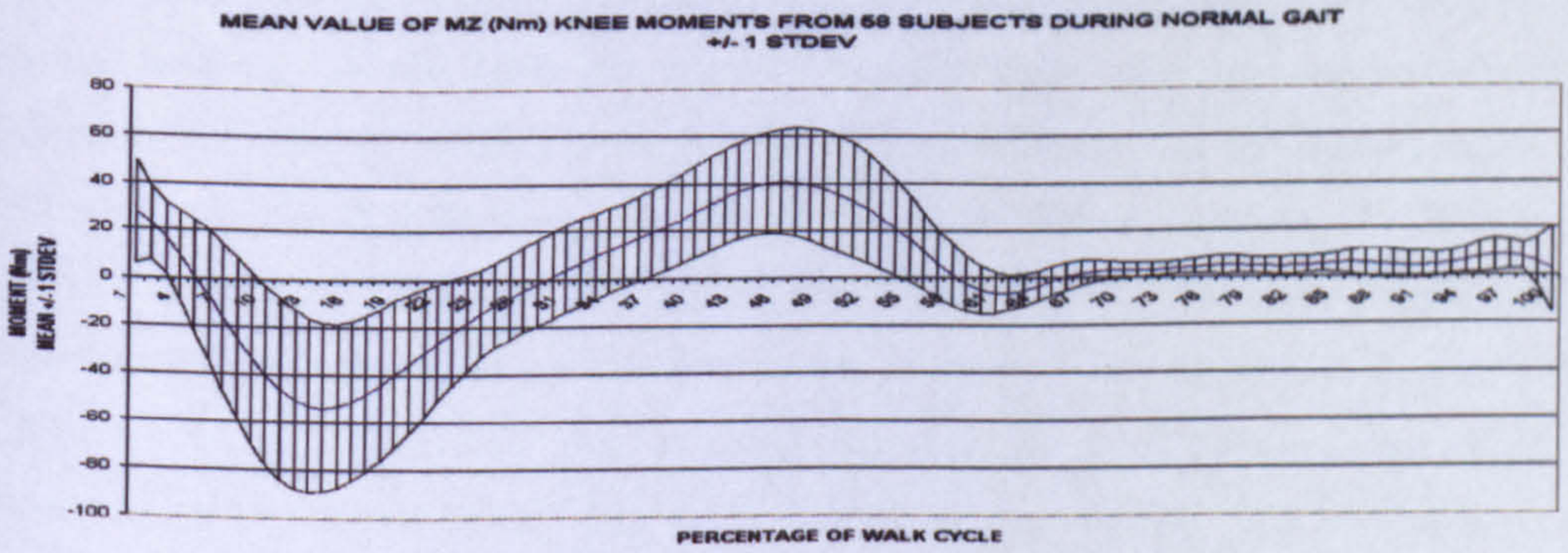

Figure 7.41: LEFT KNEE Mz Moment (mean value and standard deviation) from all the participating subjects

7.2.6 Statistical analysis of the Laboratory results

The nature of the data allowed some additional information to be extracted from statistical analysis of the gait data with different footwear at different walking speeds. The sample population was a group of 18 male subjects from the main body of the participants (Mean Height:1.7945 m, SD=0.0742 m, Body mass:76.44 kg, SD:9.1279 kg, Age:23.222 years, SD:2.734 years). ONE WAY and TWO WAY ANOVA were implemented for the analysis. Use of analysis of variance demanded that the following assumptions were met: a) Scores were measured on at least an interval scale, b) Samples were taken in random, c) Samples were taken from normally distributed populations, d) The variances of the same populations were equal.

SPEED	Fx	Fy	Fz	Mx	My	Mz	JOINT	LIMB
FAST	A*3	B*	A	A	A	A*3C	HIP	LEFT
NORMAL	A*3	A	A	A	A	B*2C	HIP	
SLOW	B	A	A	A	A	C	HIP	
FAST	A	B*	A*	A	B*	A*2B	KNEE	
NORMAL	A	A	B	A	A	B	KNEE	
SLOW	A	A	B A	A	A	B	KNEE	
FAST	A	B*	A*	A	B*	A	ANKLE	
NORMAL	B	A	B	B	A	A	ANKLE	
SLOW	B*	A	B A	A	A	A	ANKLE	
FAST	B*2	B*	A	A	A*	B	HIP	RIGHT
NORMAL	A	A	A	B	B	A*2B	HIP	
SLOW	B*2	A	A	A*	A	B	HIP	
FAST	A	B*	B A	B	B	A*2B	KNEE	
NORMAL	A	A	A	C	B	B	KNEE	
SLOW	A	A	B*	A*	A*	A	KNEE	
FAST	A	B*	B A	B	B	A	ANKLE	
NORMAL	A	A	A	C	B	A	ANKLE	
SLOW	A	A	B*	A*2C	A	A	ANKLE	

Figure 7.42: One way analysis of variance showing the effect of SPEED of walking on the forces and moments of the left and right lower limbs during normal walking. (Coding of the table: when trials appear with different letters their means are significantly different (at level of 0.0001). The trial with the highest mean (from the three trials: fast, normal, slow) is indicated with the star (*). The indication that follows some of the letters e.g. *2B shows that the present trial is twice the magnitude of the trial labeled with the letter B

*Table 7.42 on page 166 presents the One way ANOVA study to evaluate the effect of SPEED of walking on the forces and moments of the left and right lower limbs during normal walking. In the table the equality signs indicate that there is no significant difference (at level of 0.0001) between the respective trials and the non-equality sign indicates significant difference. In general the three different speeds (Coding of the trials: F= walking trial with fast speed, N= normal speed, S= slow speed) had an significantly different effect on the forces and moments of all three major joints(HIP, KNEE, ANKLE). From the total of thirty six variable combinations (three force + three moments * three joints* two lower limbs) we can observe 72% in which all the three speeds are significantly different from each other. An indication of asymmetry is the fact that in nine combinations of the left leg and in eleven of the right we observe the speed influence. It is important to stress (see Table 7.43 on page 167) that the KNEE fx, fy, and fz forces show significant variation with the fast speed having always the higher magnitude value for all subjects with Fy force appearing to be more affected that the other components. Very small differences are seen at the KNEE Fx and Fz components. The KNEE moment plots (see Table 7.44 on page 167)are show a tendency of all three moment components Mx, My, Mz to increase in magnitude.*

It can be also seen that the slow speed differs from the normal and fast trials for the force and moments components of the right limb to a greater extend (in 77% of the cases where the three speeds were different) than that of the left limb (in 66% of the cases where the three speeds were different). Speed has no influence on the Fx components of knee force whereas the fz component is differently affected between the two limbs. In all subjects the knee moment components are more affected than the knee force components (only in Mx of left leg speed showed no influence). There is a left-right leg asymmetry for all subjects' knee Fz, Mx, My, Mz, and there is a more or less left-right symmetry in the way Fx is affected by speed for all joints. These symmetries seem to not be reproduced in the other variables. It is obvious that the ankle is in a slightly plantar flexed attitude at heel strike. The amount of plantar flexion at heel strike is dependent upon the height of the shoe heel. Further plantar flexion occurs until foot flat. The pattern rapidly reverses to dorsiflexion during mid-stance as the body passes over the supporting foot, then plantar flexion occurs again after heel-off in the terminal portion of stance phase. The effect of increasing walking speed on the magnitude and pattern of ankle motion showed that while the general biphasic motion pattern remained unchanged, the magnitude of ankle motion decreased with increasing cadence. Dorsiflexion remained essentially unchanged, but the magnitude of plantar flexion occurring early after heel strike was decreased. This was an unexpected finding in that the magnitudes of both hip and knee joint motion have been found to increase directly with increasing cadence. The study revealed that the "aft" shear force in normal subjects consistently reached significant levels. Marsh et al. [1981],reported dorsiflexion moments of 25 subjects at various levels of stimulated contraction at angles ranging from 20 degrees dorsiflexion to 30 degrees plantarflexion. Between 20 degrees dorsiflexion and 10 degrees plantarflexion, the moment increased linearly with angular changes, the slope being steeper for higher levels of contraction. In some contrast to this were the results of Inman et al. [1981], reporting on maximum ankle dorsiflexion moments in six subjects. In all but one case, the ankle dorsiflexion moment increased linearly between the position at which no moment was generated to near the position of maximum moment, but the position of zero moment varied between 40 and 10 degrees dorsiflexion and the position of maximum moment ranged between 15 degrees of dorsiflexion and 25 degrees of plantarflexion. We could conclude that for the increased Mz required at higher speeds the human body switches to a certain configuration of plantarflexing or dorsiflexing (which seems to be equal to

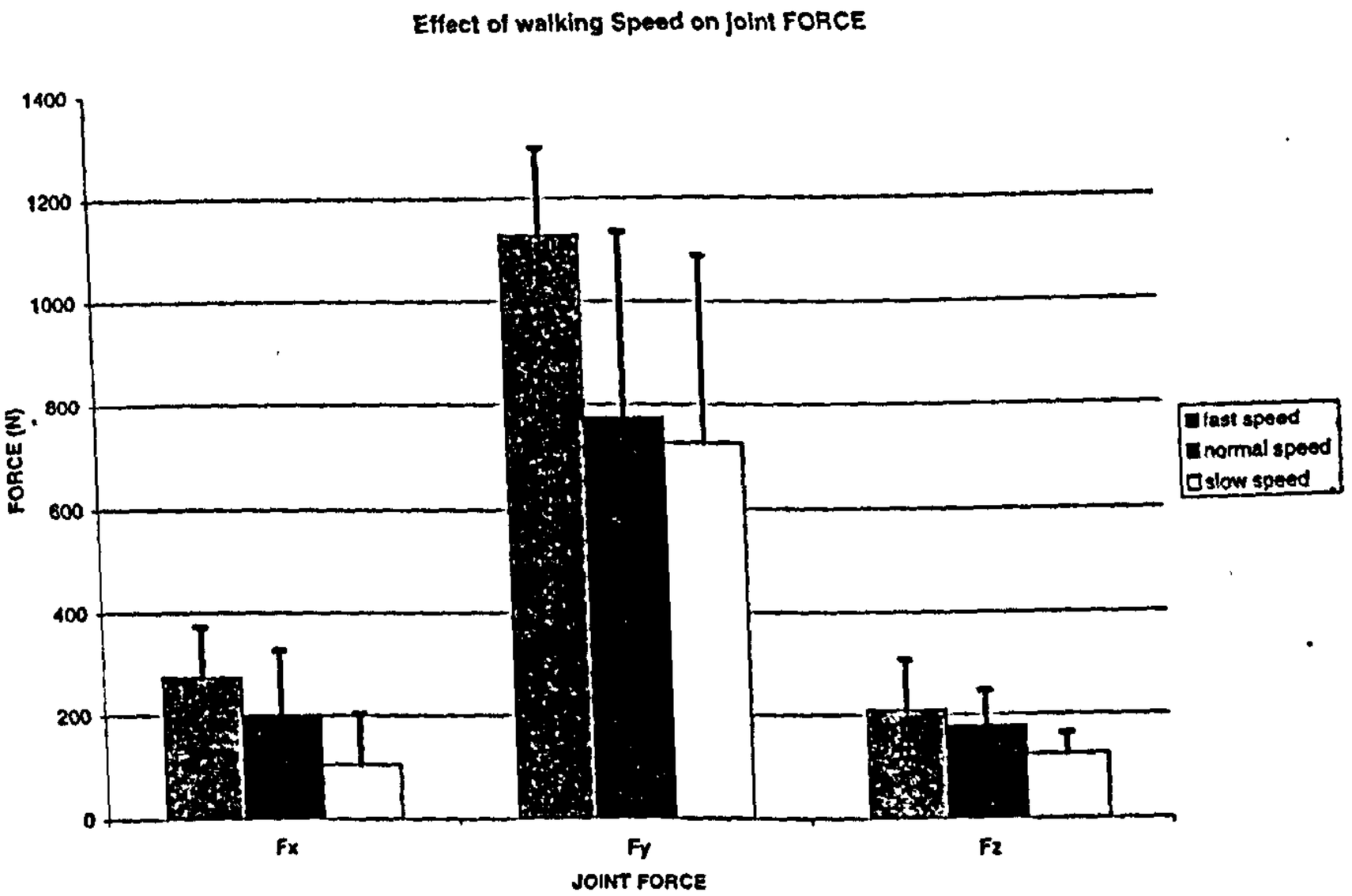

Figure 7.43: The effect of speed on knee forces of 18 male subjects

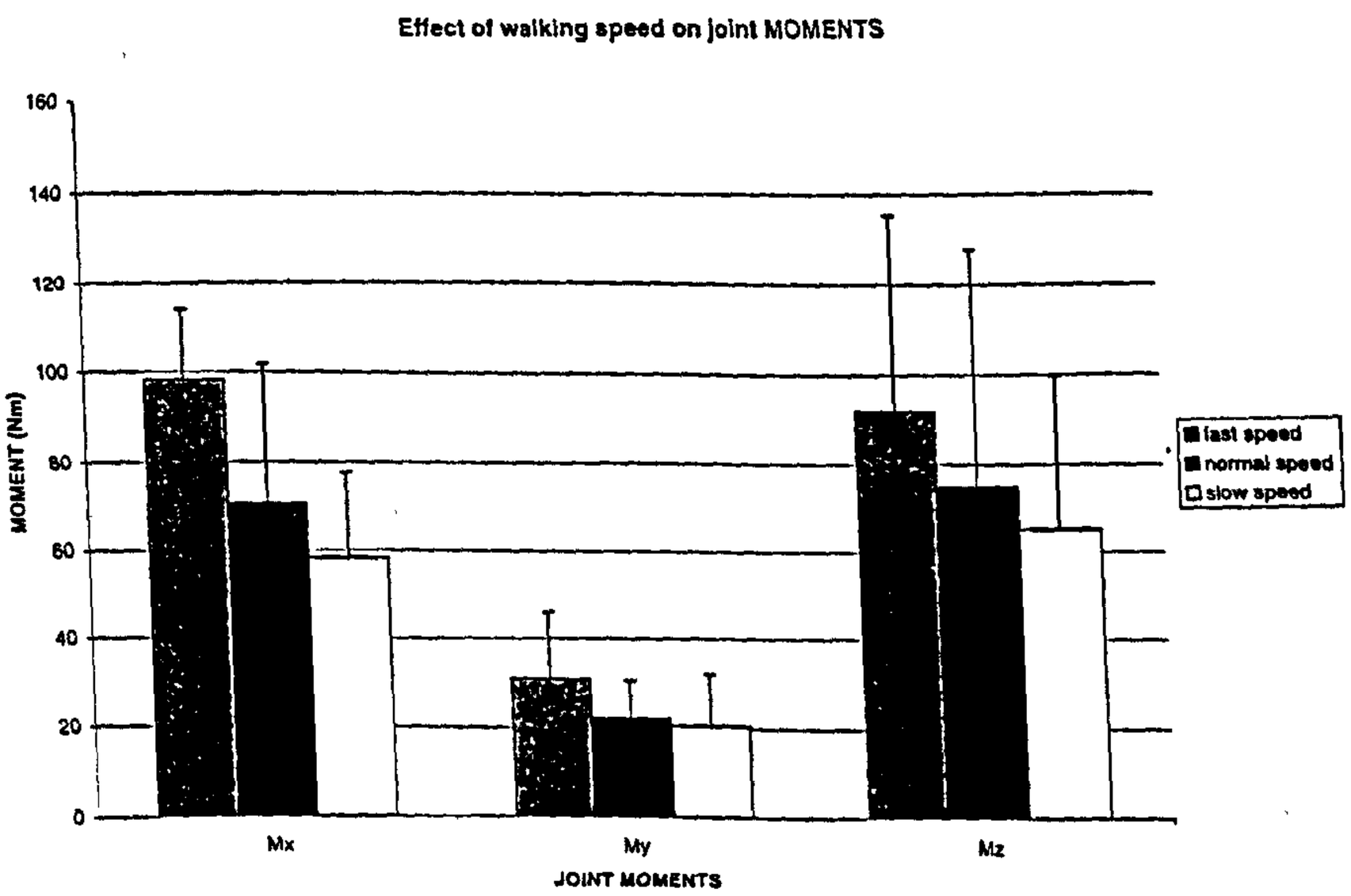

Figure 7.44: The effect of speed on knee moments of 18 male subjects

reduction in ankle motion, particularly at heel contact) that allows the high magnitude moments to develop. Although this "configuration" is highly individually determined, in the present study the subjects showed clearly a reduced ankle motion with increased speed which corresponted to an increased Mz moment. Morrison [1969] reported on the function of the knee joint in various activities suggesting that in level walking, the use of high heeled shoes caused only minor differences from the joint force pattern calculated for the same subject when wearing flat shoes. The only consistent variation detected by these experiments was an increase in joint force at heel strike of the order of 12 to 24 % when wearing high heeled shoes.

The effect of FOOTWEAR on the forces and moments of the left and right lower limbs during normal walking is shown in Table 7.45 on page 169. The use a force plate does not reveal localized damping effects of the footwear but from this study asymmetries and the effects on forces and moments as well on kinematics of all three lower limb joints can be evaluated. Twenty nine variables (80% of forces and moments of different joints of both lower limbs) have been influenced by footwear. The effect on the forces (88% of all the forces has been influenced) is more evident than that on the moments (72% has been influenced).

There is also a very small asymmetry in the influence of the FOOTWEAR on the left (83% influence) and right (77% influence) leg respectively. Although it is not easy to describe the tendencies that result from the influence of the different footwear on the above parameters, table 7.45 on page 169 reveals that: a) in 16% of the cases the Barefoot trial was not significantly different from the oxford shoes trial, b) the trial with boots is different from all other trials only at the 16% of the cases whereas it has a significant effect on the Fz forces. c)the athletic shoes trial is only significantly different from all the other cases for 0.08%, d) the Barefoot trial differs form all the other trials for a very small 0.05%, e) the Oxfort shoes trial is not significantly different from the trial with boots for the 11% of the cases. It can also be seen that in the left knee the influence of FOOTWEAR is somewhat less obvious when compared to the right knee for all subjects. The major differences between the various shoes under test appear to be mainly restricted to differences in rise time and not only (and also to smaller extend) to differences in the magnitude of the impact peak. Snel et al. [1985] also reported that there was a striking absence of differences in the magnitude of impact forces between running with different types of shoes and barefoot. This phenomenon can not only be explained by the passive shock-absorbing characteristics of the shoes. It seems that another explanation could apply in both running and fast walking studies when this phenomenon is in question. It is more likely that the walking subject and moreover the runner anticipates the expected impact force, in such a way that stiffness of the sole can influence the neuromuscular control system.

Therefore, it could be inferred that walking barefooted and its effect in temporal characteristics (different pronation angles, lateral stability, step length, pressure distribution under the foot, flexion-extension angles, angular and linear accelerations, etc), is related to an automatic neuromuscular response which finally affects the moments about the joints. Baer et al. [1986], suggested that loads in physical activity

footwear	Fx	Fy	Fz	Mx	My	Mz	JOINT	LIMB
oxford	A1*2at	B1	B4	A4	A	A1	HIP	L
boots	B3	A	B A2	B A2	A	C B3		E
athletic	B4	A	BA3	B A3	A	C4		F
barefoot	B A2	A	A1	B1	A	B2		T
oxford	B A3	B1	A1	A	B3	A	KNEE	
boots	A4	A	B4	A	A4	A		
athletic	C1	A	A3	A	B2	A		
barefoot	B C2	A	A2	A	B1	A		
oxford	A3	B1	A1	A2*2bo	B3	B3	ANKLE	
boots	A4	A	B4	B4	A4	B4		
athletic	B2	A	A3	A3*2bo	B2	A2		
barefoot	B1	A	A2	A1*2bo	B1	A1		
oxford	A	B1	A	A2	A	A	HIP	R
boots	A	A	A	B3	A	A		I
athletic	A	A	A	B4	A	A		G
barefoot	A	A	A	A1	A	A		H
oxford	B1	B1	B1	A1	B A2	B3	KNEE	
boots	A3	A	A4	B3	C4	B1		T
athletic	B A2	A	B2	B4	B C3	A2		
barefoot	A4	A	B3	A2	A1	B4		
oxford	B1	B1	C1	A3	B A2	A1	ANKLE	
boots	B A3	A	A4	A2	C4	B3		
athletic	B A2	A	C B2	B4	B C3	A2		
barefoot	A4	A	B3	A1*2at	A1	B4		

Figure 7.45: One way ANOVA showing the effect of different FOOTWARE on the forces and moments of the left and right lower limbs during normal walking. (Coding of the table: when trials appear with different letters their means are significantly different. The highest to lowest mean (related to the four trials: oxford, boots, athletic, barefoot) is indicated with numbers 1 to 4 respectively. The indication that follows some of the letters e.g. *2bo shows that the present trial is twice the magnitude of the trial with boots on (Coding of the trials: BA= walking trial BAREFOOTED , OX= walking with OXFORD shoes, AT= walking with ATHLETIC shoes , BO= walking with BOOTS)

are often classified by source. Passive loads are induced by external forces, and active loads are by-products of the body's locomotor response to passive loads. The body strives to balance the two types (one in a response to the other), but at times in various activities one can predominate. Passive loads predominate in foot impact, while active loads take over during the rest of the gait, especially toe-off. Nigg and his colleague Denoth have proposed that active forces tend to predominate in slower movements Baer et al. [1986]. Active loads are shaped by the point and direction at which a passive load is being applied. A wide range of dynamic factors and boundary conditions influence the active loading of the locomotive systems. For instance, the type of movement is critical, e.g. in running, rearfoot strikers place more active loading on their ankle and knee joints, but toe-strikers exert greater tensile load up front. When walking on harder surfaces like the one of the Strathclyde laboratory where our experiments were carried out, the loading of the lower limb can be considerably different from the corresponding load distrubution on a softer ground.

Johnson [1986], investigated the shock absorption characteristics, of four different types of footwear. Large acceleration was recorded for athletic shoes. Presumably heel strike occurs because the foot has finite absolute velocity at the instant of ground contact. There is therefore, kinetic energy which must be absorbed before the stance phase of gait can proceed. In order to reduce impact it is necessary to reduce stiffness as much as possible but it must be remembered that the reduction of load will be accompanied by an increased deflection which may modify the gait pattern (possibly in an undesirable fashion). The fourth type of shoe in that study was a pair of lace up leather shoes, with thick soles which showed the smallest shock reduction. This could suggest that a greater amount of kinetic energy must be destroyed before the stance phase of gait proceed. However it should be noted that shock absorption may take place through storage of energy in the heel cushion, ligaments, and muscles. This is an individual characteristic which introduces difficulties in the interpretation of shock absorption data and the kinetic and kinematic paramenters of the present study.

The effects of SPEED on the joint angles of the different joints of both lower limbs are presented on table 7.46 on page 171. The 72% of all the cases (angles of adduction-abduction, flexion-extension and iversion-eversion for foot or rotation of the three major joints-HIP, KNEE, ANKLE of both lower limbs) one of the fast, normal and slow trials was significantly different from the others (in 22% of the case all three of them were significantly different from each other). In the left lower limb 66% of the cases differ significantly comparing to a the higher percentage (88.8%) occurring at the right lower limb. Left hip and right ankle and hip seem to be the cases were the angles are always affected by speed. There is a 27% chance that the fast trial will be significantly different from both normal and slow trials whereas the two latter will give no indication of significant differences. Similarly, for a 27% of the chances the normal trial will be significantly different from the fast and slow trial with the latter one being almost the same.

The effects of FOOTWEAR on the angles of the different joints of both lower limbs are presented on table 7.47 on page 172. The effect of footwear on joint angle is more evident here (88.8% of the cases)for both lower limbs. All trials differ significantly from each other in the 27% of the cases. The barefoot trial is significantly different from all the rest at the 33.3% of the cases and equal to the oxford shoes trial at the 22.2% of the cases. The oxford trial seem to be different from all the other trials at the 16.6% of the cases. The Athletic shoes trial shows similar results to the trial with boots for the 16.6% of the cases.

speed	LEFT ANKLE	LEFT KNEE	LEFT HIP	RIGHT ANKLE	RIGHT KNEE	RIGHT HIP	
FAST	A	B3	A3	C3	A	A2	Abdu-
NORMAL	A	A1	B1	A1	A	A3	-addu-
SLOW	A	A2	A2	B2	A	B1	
FAST	A	B3	B2	A3	B3	B2	Flexio-
NORMAL	A	A1	A1	B2	A1	A1	extensi
SLOW	A	B2	C3	B1	B2	C3	
FAST	A1	A	C1	B3	B3	A1	Inversi
NORMAL	B3	A	B2	A1	A1	B2	eversi
SLOW	B2	A	A3	B2	B2	B3	

Figure 7.46: ONE WAY ANOVA showing the effect of speed on abduction-adduction, flexion-extension, Inversion-eversion of left and right lower limb during normal gait. (Coding of the table: when trials appear with different letters their means are significantly different. The highest to lowest mean (related to the three trials: fast, normal, slow) is indicated with numbers 1 to 3 respectively.

A two factorial ANOVA is performed to test whether there is an interaction between the two variables, speed and footwear and whether this interaction is evident between the different force, moment and angle components. The interaction between speed and footwear is therefore included in the model. Performing the analysis of variance for balanced designs, we find for the usual F-test some significant interaction effect between speed and variable with p values presented in detail in tables 7.48 on page 173 and 7.49 on page 174 . Because the interaction is present, the speed related variable "means" for each footwear are compared separately. With regard to the forces and moments interaction (p¡0.05) between speed and footwear is present for the 41.6% of the cases whereas the corresponding percentage for interaction with regard to the different joint angles is 77.

footwear	LEFT ANKLE	LEFT KNEE	LEFT HIP	RIGHT ANKLE	RIGHT KNEE	RIGHT HIP	ANGLE
oxford	B4	B1*2at	A1	B2*2at	C1	A	Abduction-adduction
boots	D2*10ox	A2	B2	D3	A4	A	
athletic	C3	A4	B3	C4	B2	A	
barefoot	A1*10at	A3	B1	A1*2.5at	A3	A	
oxford	C4	A	A2	C2*5bo	B3	B2	Flexion-extension
boots	A2*3at*6ox	A	A1	A4	A1	A1	
athletic	B3	A	B4	B3	B2	C4	
barefoot	D1*8ox	A	A3	D1*10bo *2bo	B4	B3	
oxford	B2	B1*3at	C1*2ba	C3	C4	A1	Inversion-eversion
boots	C3	A3	B2	D4	B2	B4	
athletic	C4	A4	A4	B2	B3	B3	
barefoot	A1	A2	A3	A1*2bo	A1*2ox	A2	

Figure 7.47: ONE WAY ANOVA showing the effect of footwear on abduction-adduction, flexion-extension, Inversion-eversion of left and right lower limb during normal gait. (Coding of the table: when trials appear with different letters their means are significantly different. The highest to lowest mean (related to the four trials: oxford, boots, athletic, barefoot) is indicated with numbers 1 to 4 respectively. The indication that follows some of the letters e.g. *2bo shows that the present trial is twice the magnitude of the trial with boots on (Coding of the trials: BA= walking trial BAREFOOTED , OX= walking with OXFORD shoes, AT= walking with ATHLETIC shoes , BO= walking with BOOTS)

Fx	Fy	Fz	Mx	My	Mz	JOINT	LIMB
0.0001*	0.9999	0.0856	0.0122*	0.0803	0.0001*	HIP	LEFT
0.0011*	0.4393	0.4946	0.0453*	0.0401*	0.0001*	KNEE	LEFT
0.0001*	0.4008	0.3701	0.3142	0.0400*	0.4009	ANKLE	LEFT
0.7713	0.5022	0.5945	0.0001*	0.3769	0.4378	HIP	RIGHT
0.3939	0.4805	0.6666	0.0001*	0.0001*	0.0001*	KNEE	RIGHT
0.4362	0.4743	0.5499	0.0001*	0.0001*	F=N=S	ANKLE	RIGHT

Figure 7.48: Two way ANOVA to indicate the interaction effects between SPEED and FOOTWEAR with respect to joint forces and moments. The star (*) indicates interaction (p¡0.05)

Table 7.50 on page 175 shows the complete interaction analysis with respect to joint angles. It can be seen that in 83.3 percent of the interactions between speed and footwear reveled in the ANOVA there is significant difference between at least one variable (force, moment, angle of joint) and the other variables (type of footwear). Only in 16.6% of the cases all four variables (footwear types) differ significantly with each other with left ankle having the most occurrences meaning that all different trials differ with each other. The barefoot trial differs from all the rest in a total of 22.2% and the athletic shoes in a total of 27.7%. The boot trial differs also from all the rest in a 27.7% of the cases and the oxford trial also with a 24 percent. Looking vertically at the columns of the table 7.50 on page 175 it can be seen that the interaction is not so evident for the left knee where the individual ANOVAS showed that the tendencies at the slow, normal and fast trial are reproduced for all angles in a similar fashion. This is not reproduced in the left ankle and moreover in the left ankle. No interaction is observed at all for most of the right lower limb combinations.

Tables 7.51 on page 176, 7.52 on page 177, 7.53 on page 178, 7.54 on page 179, show the complete interaction analysis with respect to its effects on joint forces and moments. From table 7.51 on page 176, it can be seen that there is no interaction whatsoever between the speed and footwear for the right lower limb with respect to force Fx. For the left lower limb 66 percent of the cases present some interaction with most of the variables showing significant differences with each other. The least affected joint seems to be the left HIP joint for which only at the fast speed the oxford shoes trial differs from all the rest. The force Fx at the left knee during walking with slow speed for all subjects seemed to give the same results for all different types of footwear. For the normal speed left knee Fx however the boots trial was significantly different from all the rest which was also observed for the ankle Fx. The most affected knee Fx combination refers to the fast speed where all parameters differ significantly with each other.

LEFT ANKLE	LEFT KNEE	LEFT HIP	RIGHT ANKLE	RIGHT KNEE	RIGHT HIP	
0.0001*	0.0001*	0.0001*	0.0001*	0.3678	0.4257	Abduction -adduction
0.0001*	0.0001*	0.0001*	0.0001*	0.0004*	0.0001*	Flexion-extension
0.0001*	0.0001*	0.0001*	0.4399	0.0804	0.0025*	Inversion-eversion

Figure 7.49: Two way ANOVA to indicate the interaction effects between SPEED and FOOTWEAR with respect to joint angles. The star * indicates interaction (p¡0.05)

footwear	LEFT ANKLE	LEFT KNEE	LEFT HIP	RIGHT ANKLE	RIGHT KNEE	RIGHT HIP	speed	angle
Oxford	B4	B1*6ba	A4	B3			FAST	Abduction adduction
Boots	D2*10ox	A2	B1	D2				
Athletic	C3	A4	B2	C4				
Barefoot	A1*5at	A3	B3*2ox	A1*3at				
Oxford	B3	A	A	B2			NORMAL	
Boots	D2*10ox	A	A	D3				
Athletic	C4	A	A	C4				
Barefoot	A1*14at	A	A	A1*2.5at				
Oxford	B3	A	A	A2*2bo			SLOW	
Boots	D1*10ox	A	A	C3				
Athletic	C4	A	A	B4				
Barefoot	A2*8at	A	A	A1*3at				
Oxford	A3	A	A1	B2*5bo	A	A1	FAST	Flexion extension
Boots	A2	A	A2	A4	A	A2		
Athletic	A4	A	B4	B3	A	B4		
Barefoot	B1*4at	A	A3	C1*10bo *2ox	A	A3		
Oxford	C4	A	A1	C2*6bo	B4	A2	NORMAL	
Boots	A2*7ox	A	A2	A4	A1	A1		
Athletic	B3	A	A3	B3	B2	B4		
Barefoot	D1*8at	A	B4	D1*10bo	B3	A3		
Oxford	C4	A	B3	C2*3bo	B3	B4	SLOW	
Boots	A1*4at	A	B2	A4	B2	B2		
Athletic	B3	A	A1	B3	A1	A1		
Barefoot	D2*6ox	A	B4	D1*5bo	B4	B3		
Oxford	A1*2at	B1*3ba	C1*3ba* 5at			A1	FAST	Inversion Eversion
Boots	B3	A3	B2			B4		
Athletic	B4	A4	A4			A3		
Barefoot	A2	A2	B3			A2		
Oxford	B3	A	A2			A1*2bo	NORMAL	
Boots	C4	A	B1			B4		
Athletic	B2	A	A3			B3		
Barefoot	A1	A	A4			A2		
Oxford	C3	A	A3			A1	SLOW	
Boots	B2	A	B1*2ox			B4		
Athletic	C4	A	A4			B3		
Barefoot	A1	A	A2			A2		

Figure 7.50: The complete two way ANOVA of the interaction of speed and footwear with respect to joint angles

From table 7.52 on page 177, it can be seen that there is interaction between the speed and footwear for the left and right lower limb with respect to moment Mx, a fact not confirmed for forces Fy, Fz for certain combinations of the moments as it will be described below. In the above table there is a 66.6 percent chance that the interaction will indicate significant differences due to speed and footwear. In a 16.6 percent of the Mx moment cases the trial with boots differs significantly from all the rest trials and it is in all these cases refer to the left ankle with speed having no effect on the trends. The right barefoot trial for fast walking is always different from the other trials for all joints. For the same analysis the oxford trial was always different from the rest for a percentage of 16.6.

From table 7.53 on page 178, it can be seen that there is interaction between the speed and footwear for the left and right lower limb with respect to moment My, but only for the knee and ankle joints. In the above table there is a 83.3 percent chance that the interaction will indicate significant differences due to speed and footwear. There is a characteristic mirroring between knee and ankle joints, with the effects seen in the knee to be reproduced exactly for the ankle joint. In 66.6 percent of the cases the trial with boots is significantly different from the rest of the trials.

Fx FORCE					
speed	FOOTWEAR	HIP	KNEE	ANKLE	L
S	OXFORD	A	A	B A	E
L	BOOTS	A	A	A	F
O	ATHLETIC	A	A	B	T
W	BAREFOOT	A	A	B A	
N	OXFORD	A	B	B	L
O	BOOTS	A	A	A	O
R	ATHLETIC	A	B	B	W
M	BAREFOOT	A	B	B	E
A L	OXFORD	A	A	A	R
F	BOOTS	B	B A	B	
A	ATHLETIC	B	C	C	L
S	BAREFOOT	B	B C	C B	I
T					M
					B

Figure 7.51: The complete two way ANOVA to indicate the interaction of speed and footwear with respect to Fx forces

MxMOMENT SPEED	FOOTWEAR	HIP	KNEE	ANKLE
SLOW	OXFORD	A	A	A
	BOOTS	A	A	B
	ATHLETIC	A	A	A
	BAREFOOT	A	A	A
NORMAL	OXFORD	A	A	A
	BOOTS	A	A	B
	ATHLETIC	A	A	A
	BAREFOOT	A	A	A
FAST	OXFORD	A	A	A
	BOOTS	B	B	B
	ATHLETIC	B	B	A
	BAREFOOT	B	B	A
SLOW	OXFORD	A	A	B A
	BOOTS	A	A	A
	ATHLETIC	A	A	B
	BAREFOOT	A	A	B A
NORMAL	OXFORD	A	A	A
	BOOTS	C	C	B
	ATHLETIC	C B	B	B
	BAREFOOT	B	B	B
FAST	OXFORD	B	C B	B
	BOOTS	B A	B	A
	ATHLETIC	B	C	C
	BAREFOOT	A	A	A

LEFT RIGHT

Figure 7.52: The complete two way ANOVA to indicate the interaction of speed and footwear with respect to Mx Moments

Different results can be seen in the corresponding analysis of interaction for the Mz moment (table 7.54 on page 179). The analysis showed only the left hip joint and both left and right knee to be influenced. In 77.7 percent of the cases there is a chance that there will be variability between the different types of footwear. For the slow and fast cases for hip and knee respectively the effects seem to mirror giving the same results.

My MOMENT				
SPEED	FOOTWEAR	KNEE	ANKLE	
SLOW	OXFORD	B A	B A	LEFT
	BOOTS	A	A	
	ATHLETIC	B A	BA	
	BAREFOOT	B	B	
NORMAL FAST	OXFORD	B A	B A	
	BOOTS	A	A	
	ATHLETIC	B	B	
	BAREFOOT	B	B	
	OXFORD	B	B	
	BOOTS	A	A	
	ATHLETIC	B A	B A	
	BAREFOOT	B	B	
SLOW	OXFORD	A	A	RIGHT
	BOOTS	A	A	
	ATHLETIC	A	A	
	BAREFOOT	A	A	
NORMAL	OXFORD	A	A	
	BOOTS	C	C	
	ATHLETIC	B	B	
	BAREFOOT	B A	B A	
FAST	OXFORD	B	B	
	BOOTS	B A	B A	
	ATHLETIC	B	B	
	BAREFOOT	A	A	

Figure 7.53: The complete two way ANOVA to indicate the interaction of speed a footwear with respect to My Moments

Mz MOMENT				
SPEED	FOOTWEAR	HIP	KNEE	
SLOW	OXFORD	B	B	LEFT
	BOOTS	B A	B	
	ATHLETIC	B	B	
	BAREFOOT	A	A	
NORMAL	OXFORD	A	B	
	BOOTS	A	A	
	ATHLETIC	A	B A	
	BAREFOOT	A	B A	
FAST	OXFORD	A	A	
	BOOTS	B	B	
	ATHLETIC	B	B	
	BAREFOOT	B	B A	
SLOW	OXFORD		A	RIGHT
	BOOTS		A	
	ATHLETIC		A	
	BAREFOOT		A	
NORMAL	OXFORD		B A	
	BOOTS		C	
	ATHLETIC		A	
	BAREFOOT		B C	
FAST	OXFORD		B	
	BOOTS		B	
	ATHLETIC		A	
	BAREFOOT		B A	

Figure 7.54: The complete two way ANOVA to indicate the interaction of speed and footwear with respect to Mz Moments

7.2.7 The effects on the magnitude of the different parameters

Table 7.42 on page 166 indicates that from all the combinations of different forces and moments for all the three joints for both lower limbs only a 27% shows magnitude increases due to fast walking. It is surprising to observed that at a high percentage (22 %) the slow walking trials seem to increase the magnitude of the above parameters indicating more effect on the right lower limb whereas the fast trial seems to have more affect on the left lower limb. Wherever the fast trial is dominant in magnitude the difference is at least two-fold (a lot of the times three-fold) which is not the case with the dominance in magnitude by the slow trials. The fast speed seems to have more effect on parameters like Fx force and My and Mz moment. In table 7.45 on page 169

in can be observed that subjects walking with the oxford shoes on, had an increase in the magnitude in 27% of their lower limb forces and moments. The most characteristic increase occurred at the magnitude of force Fx (two-fold). The same can be inferred for the barefoot trial with a percentage of 30. The moment Mx is the most affected by the barefoot trial. The trial with boots on had the lowest influence on the magnitude of forces and moments.In the Mx component of the left ankle the oxford, athletic and barefoot trial had twice as much magnitude when compared to the boots trial. In the right ankle the Mx barefoot trial was twice the magnitude of the athletic trial. The oxford trial increased mostly the Fz component of force whereas the barefoot trial influenced the magnitude of mainly the Mx and My components of moments. The lower limb motion was more increased in magnitude during the normal walking trial (50%) (table 7.46 on page 171) and less during the fast and slow trials. Normal walking increases abduction-adduction and flexion-extension angles of all joints when compared with fast walking which seems to affect more the inversion-eversion angles. The barefoot trial increased the 45% of the different joint angles of both legs with oxford increasing a 33% and boots only a 18% of the total motion parameters.

The oxford shoes increased more the motion of the lower left knee and left hip and the adduction-abduction angles of almost all joints (table 7.47 on page 172) . The flexion-extension angle seem to be more increased in magnitude by walking with boots whereas the barefoot trial increases more the left and right ankle angles and most of the adduction-abduction and inversion-eversion angles of all joints.

The interaction effects table 7.50 on page 175 with respect to joint angles, suggests that the barefoot trial increases the magnitude of the joint motion considerably (three to ten-fold increase) when combined with fast speed. The barefoot trial presents increased joint motion for 22.5% of the cases of which a 30% refers to the fast speed walking. It is also noticeable that the inversion-eversion angles are mostly augmented in magnitude with oxford shoes during fast speed walking (three-fold). Twenty percent of the cases with the interaction of speed and footwear suggests that the oxford shoes increase joint motion and from that percent 60% refers to fast speed. The oxford trial increases the inversion-eversion angles whereas the barefoot affects mainly the adduction-abduction and flexion-extension angles of all joints. It is also important to note that the trials with boots and athletic shoes on increase mainly the flexion-extension angles of all joints. It should be noted that in the different tables discussed above occasionally an extensive increase in magnitude is shown as a multiple of the

magnitude of another parameter. In the cases where this is note shown the reader should assume that the numbering one to four gives the magnitude variation of the parameters indicating differences between 10 to 30%.

7.2.8 Turning during walking

Some subjects were asked to perform several tasks for better understanding of the effect of the different parameters -such as INTERSEGMENTAL LOAD- on the models. One of their tasks were to turn at 90 and 45 degrees in the direction of progression respectively. In all cases the PIVOTING leg was the right leg while the subject turned to the left side. Therefore we made sure that all subjects participating in this study were right leg dominant. The indication for turn was a characteristic sound and a few practice trials were performed before each measurement. FIGURES 7.55 on page 182 to 7.66 on page 185 present characteristic KNEE FORCES and MOMENTS during walking and turning. It is revealed from the kinematics (also observed during the trials) that the hip and knee joints begin to move out of the sagittal plane at the push off phase of turning during walking. In normal level walking one expects the MZ moment at the knee to produce a flexion at the knee when negative and an extension when positive. It the turning cases, however, at the last phase of push off (as the subject's limb continues in the forward direction), there is a moving of the plane of motion to the position between the positive directions of the X and Z laboratory reference frame. The above mentioned flexion-extension moment is now responsible for a rather different result, tending to adbuct/adduct (FIGURES 7.58 on page 183 7.64 on page 184). One can not guarantee intersubject variability analysis since the amount of twisting at push off varies greately between individuals. GAIT-2 model with the orientation triangle produced by three markers improves the compensation problems from the cameras views thus allowing for the segment's directional cosine matrix to be calculated properly. The three markers are: tibia tuberosity, lateral malleolous and the marker placed at the midpoint of the tibia's length. This last marker is also somewhat longer than the others to improve the calculation of the rotations at the Y direction It is also obvious that the shape of the force and moment grapus differ between the trials of 45 and 90 degrees turning in the direction of progression but not with a very characteristic magnitude difference. More subject trials and a full parametric study are required for covering questions like that. Kinetic

data for the pivoting and the following leg are also provided for comparisons. In the present study the following leg was the left leg and the subject turned to the left side by pivoting at the right leg. After the turn the left leg becomes again the support leg. The results of this analysis are comperable to the findings of Harrison and Nicol (Harrison et al. [1990]).

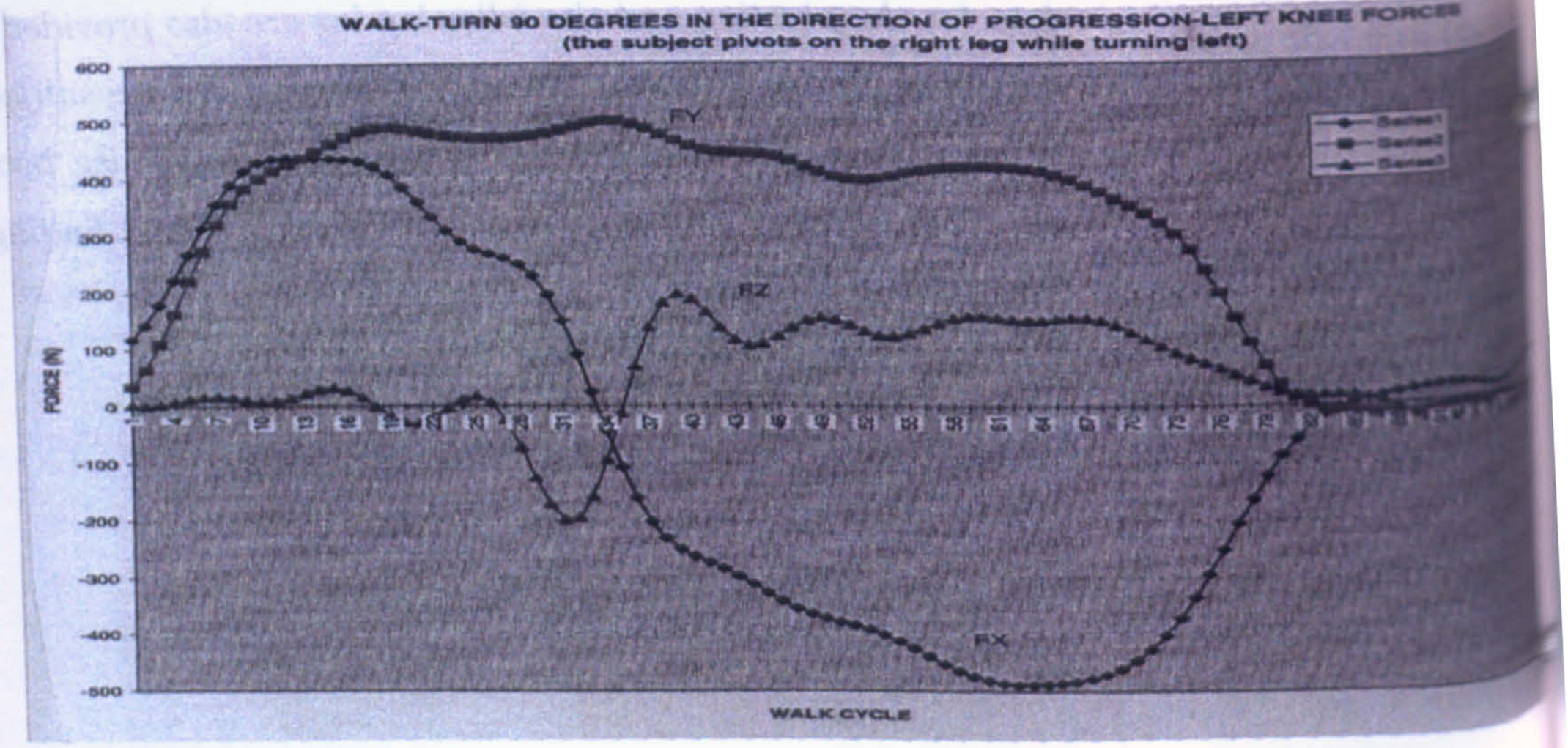

Figure 7.55: Walking and turning at 90 degrees in the direction of progression: LEFT KNEE FORCES (N)-subject 1 pivots on the right leg while turning left- the first leg (left) lands on the first force plate and the pivoting leg (right) lands in the second force plate

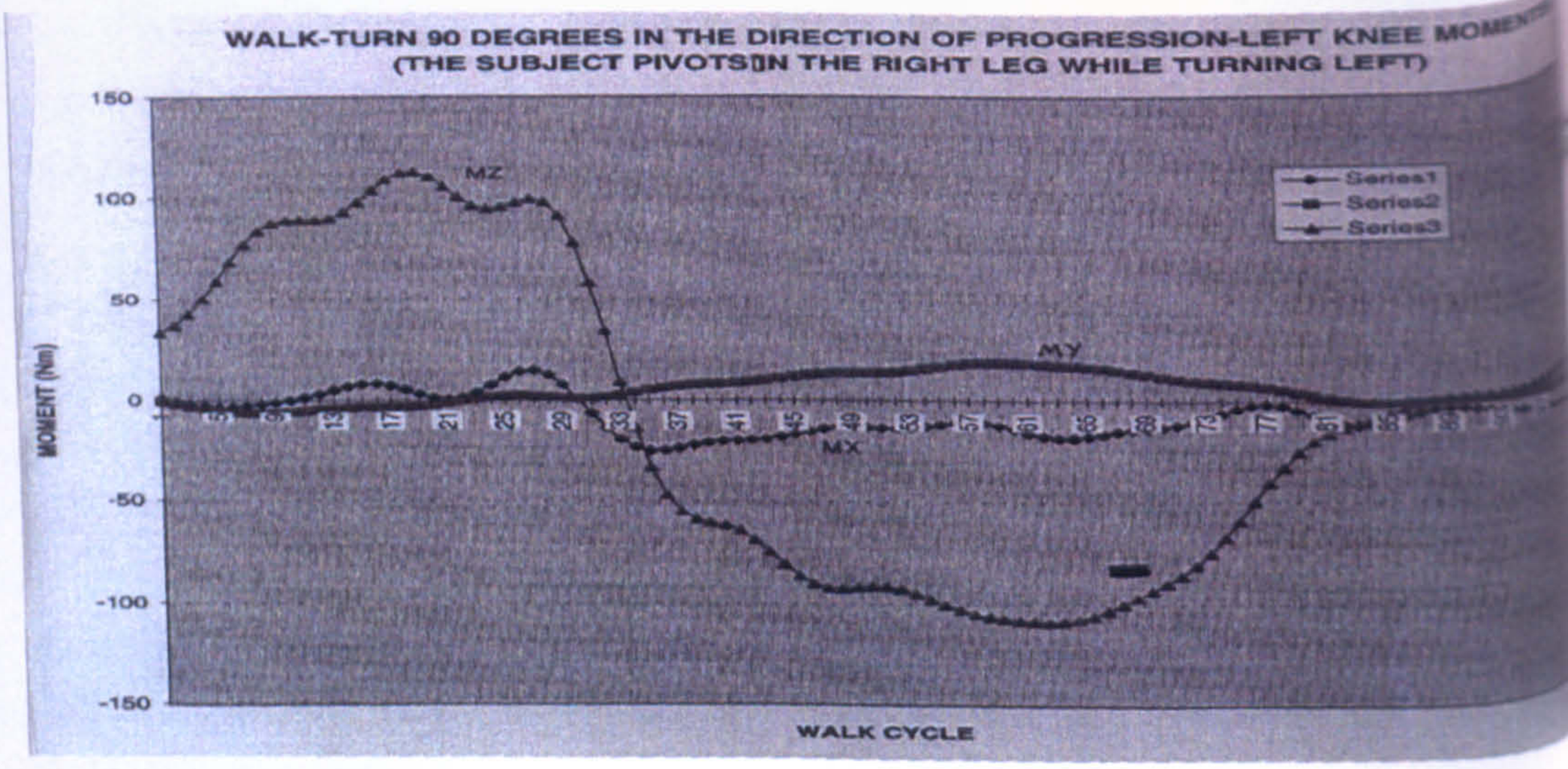

Figure 7.56: Walking and turning at 90 degrees in the direction of progression: LEFT KNEE MOMENTS (N)-the subject 1 pivots on the right leg while turning left- the first leg (left) lands on the first force plate and the pivoting leg (right) lands in the second force plate

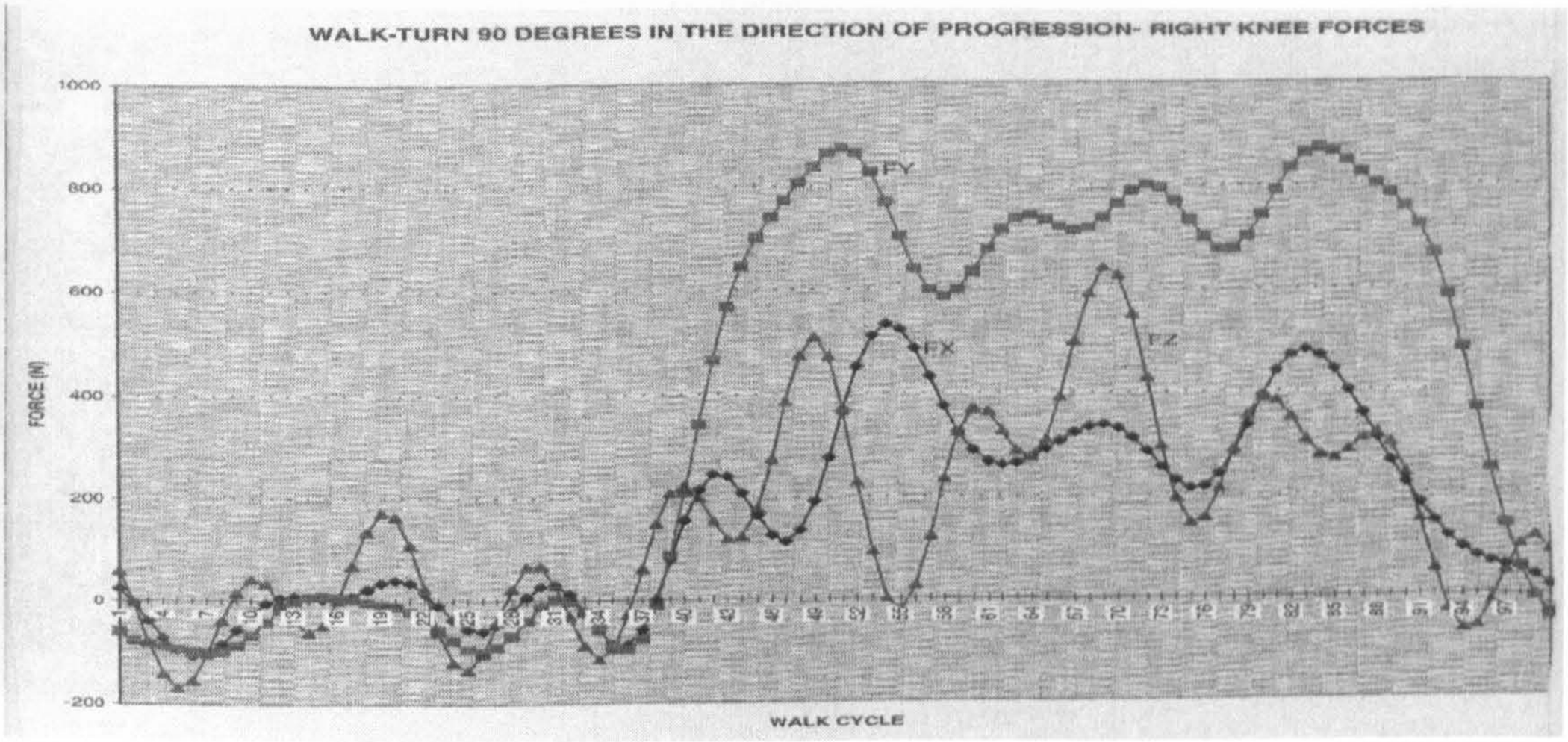

Figure 7.57: Walking and turning at 90 degrees in the direction of progression: RIGHT KNEE FORCES (N)-subject 1 pivots on the right leg while turning left- the first leg (left) lands on the first force plate and the pivoting leg (right) lands in the second force plate

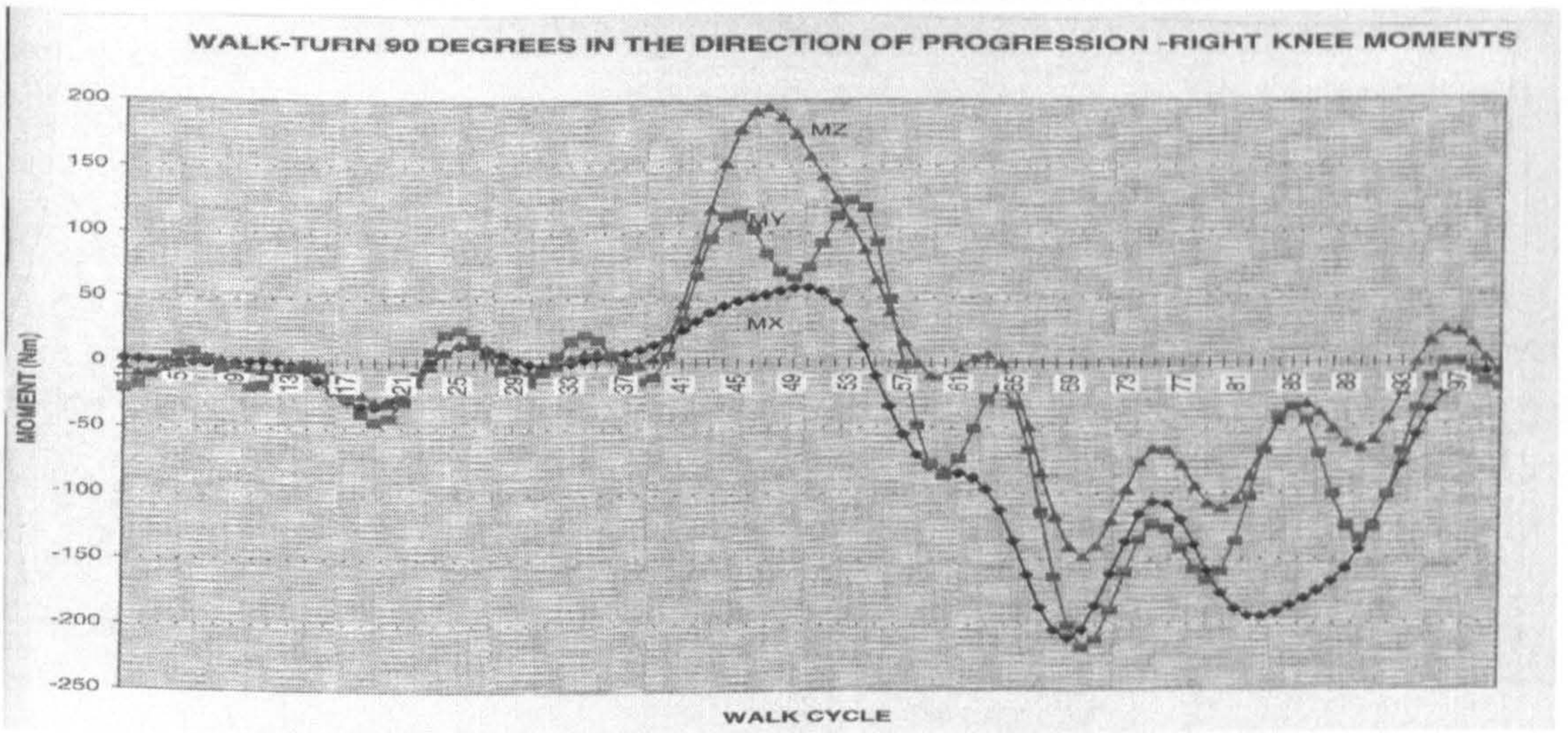

Figure 7.58: Walking and turning at 90 degrees in the direction of progression: RIGHT KNEE MOMENTS (N)-subject 1 pivots on the right leg while turning left- the first leg (left) lands on the first force plate and the pivoting leg (right) lands in the second force plate

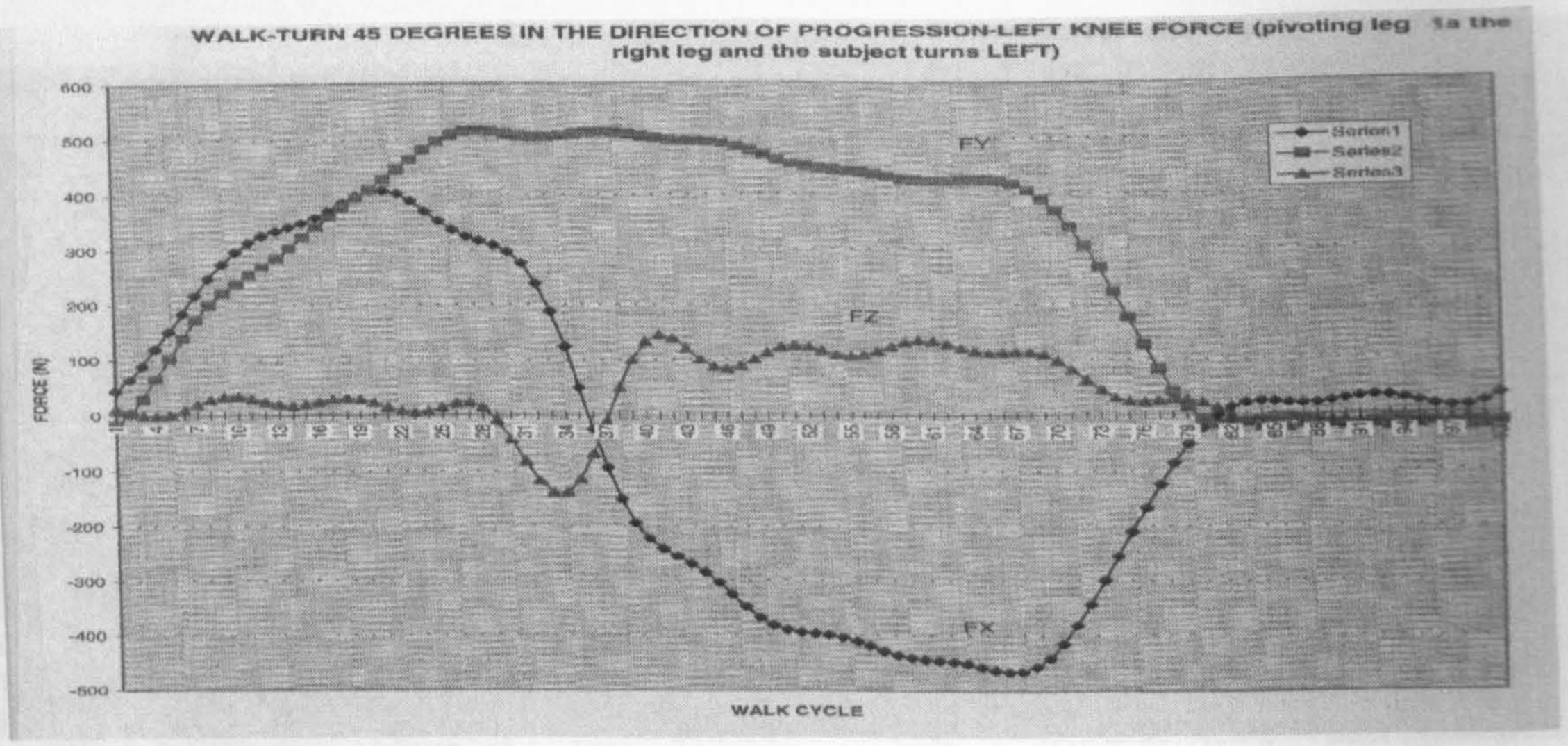

Figure 7.59: Walking and turning at 45 degrees in the direction of progression: LEFT KNEE FORCES (N)-subject 1 pivots on the right leg while turning left- the first leg (left) lands on the first force plate and the pivoting leg (right) lands in the second force plate

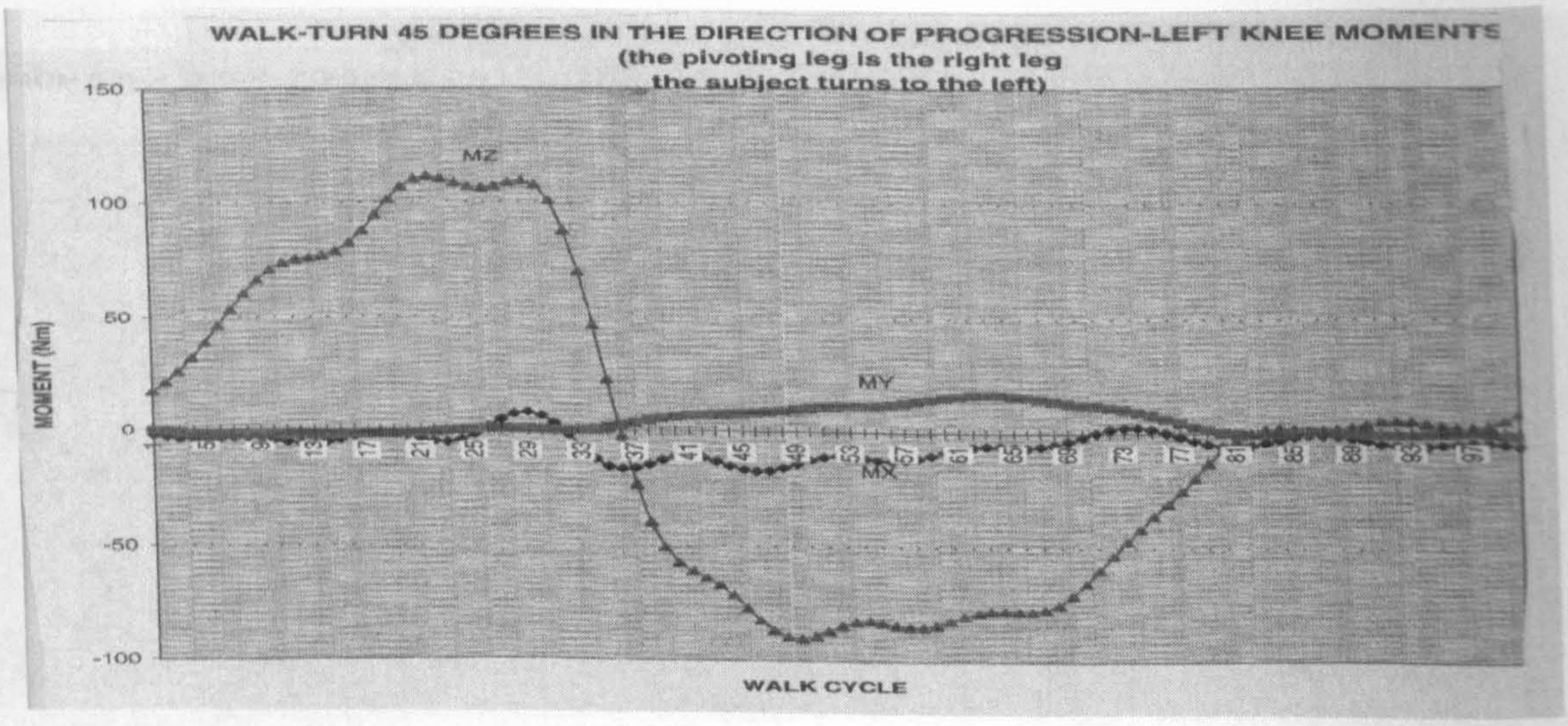

Figure 7.60: Walking and turning at 45 degrees in the direction of progression: LEFT KNEE MOMENTS (N)-subject 1 pivots on the right leg while turning left- the first leg (left) lands on the first force plate and the pivoting leg (right) lands in the second force plate

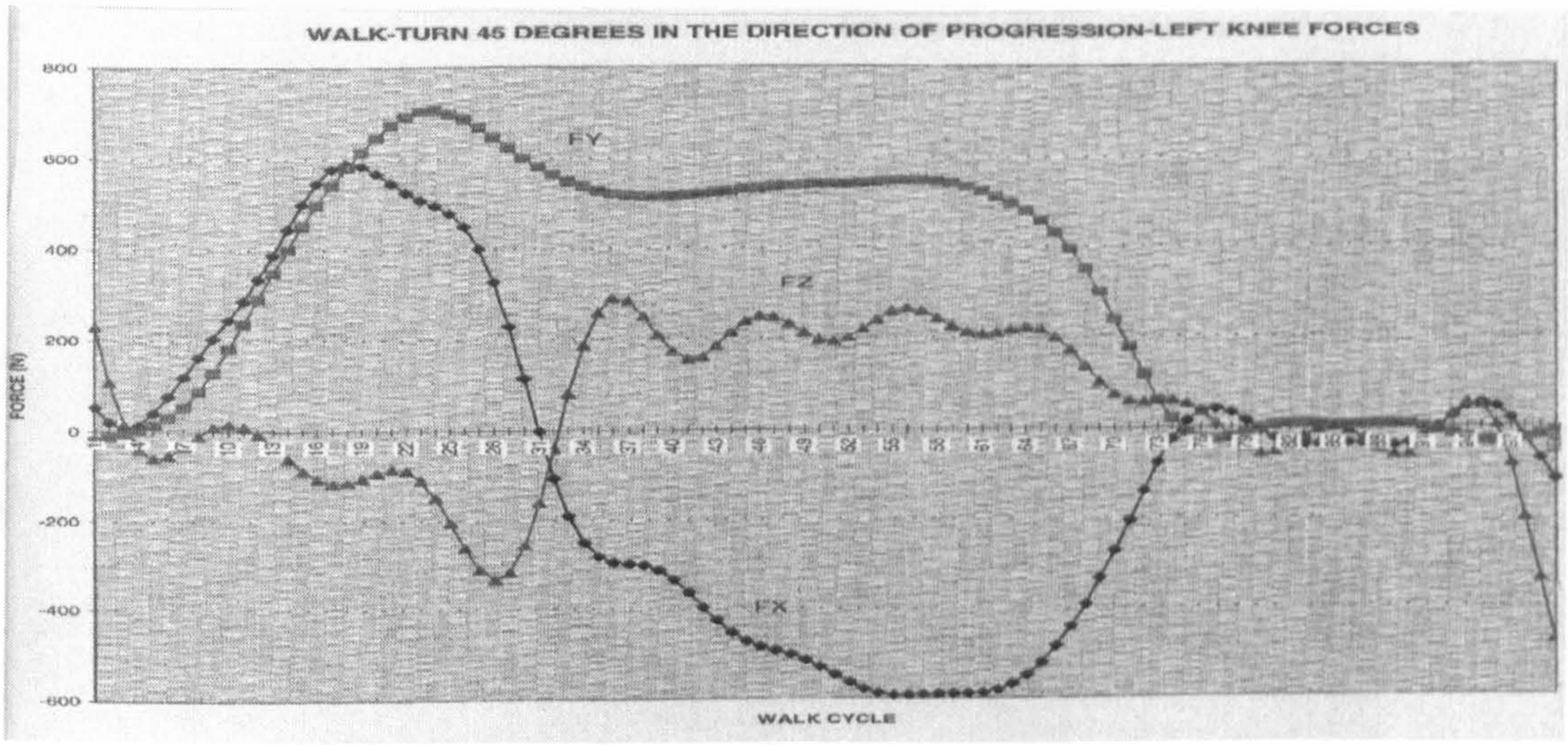

Figure 7.61: Walking and turning at 45 degrees in the direction of progression: LEFT KNEE FORCES (N)-subject 2 pivots on the right leg while turning left- the first leg (left) lands on the first force plate and the pivoting leg (right) lands in the second force plate

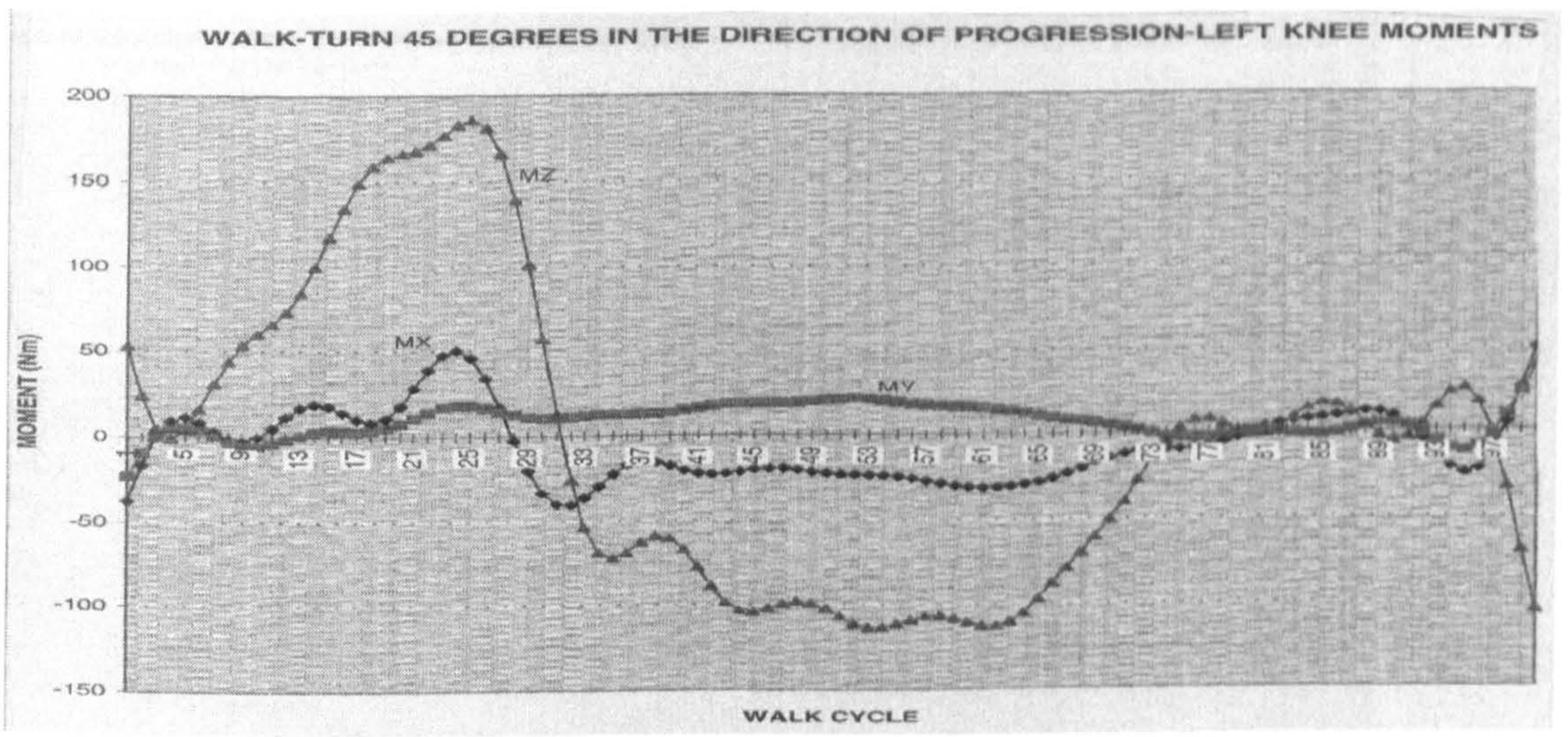

Figure 7.62: Walking and turning at 45 degrees in the direction of progression: LEFT KNEE MOMENTS (N)-subject 2 pivots on the right leg while turning left- the first leg (left) lands on the first force plate and the pivoting leg (right) lands in the second force plate

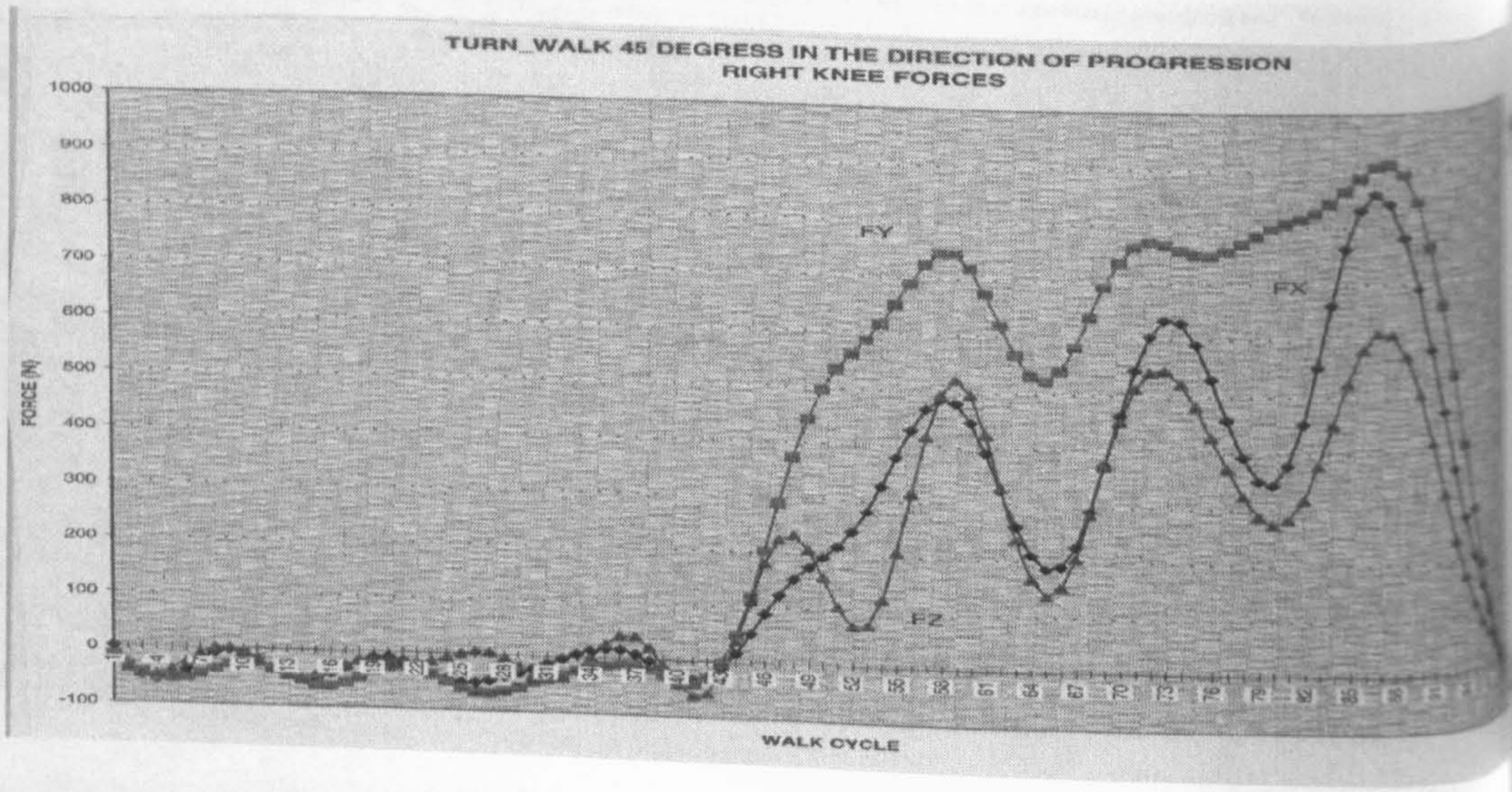

Figure 7.63: Walking and turning at 45 degrees in the direction of progression: RIGHT KNEE FORCES (N)-subject 2 pivots on the right leg while turning left- the first leg (left) lands on the first force plate and the pivoting leg (right) lands in the second force plate

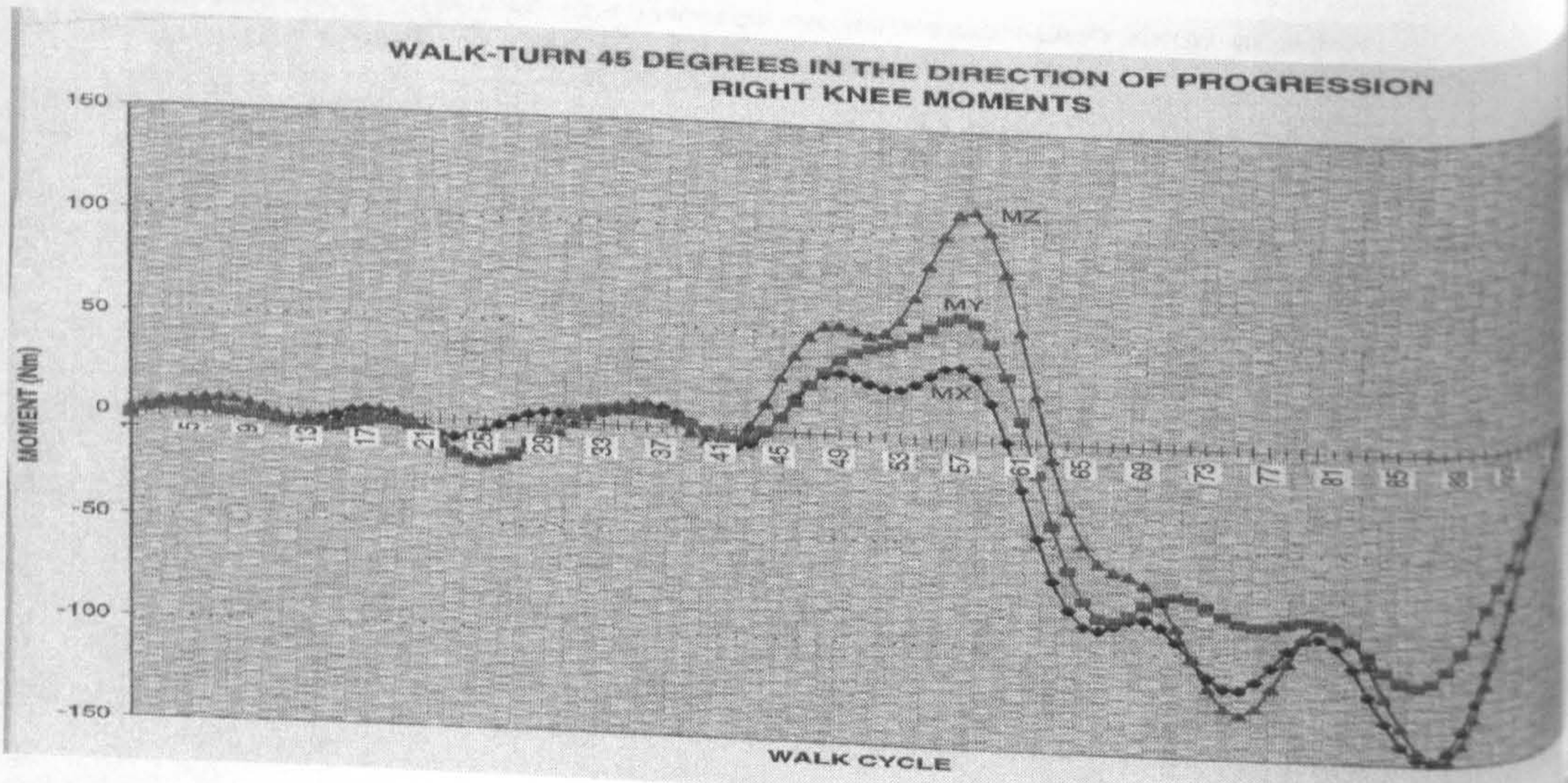

Figure 7.64: Walking and turning at 45 degrees in the direction of progression: RIGHT KNEE MOMENTS (N)-subject 2 pivots on the right leg while turning left- the first leg (left) lands on the first force plate and the pivoting leg (right) lands in the second force plate

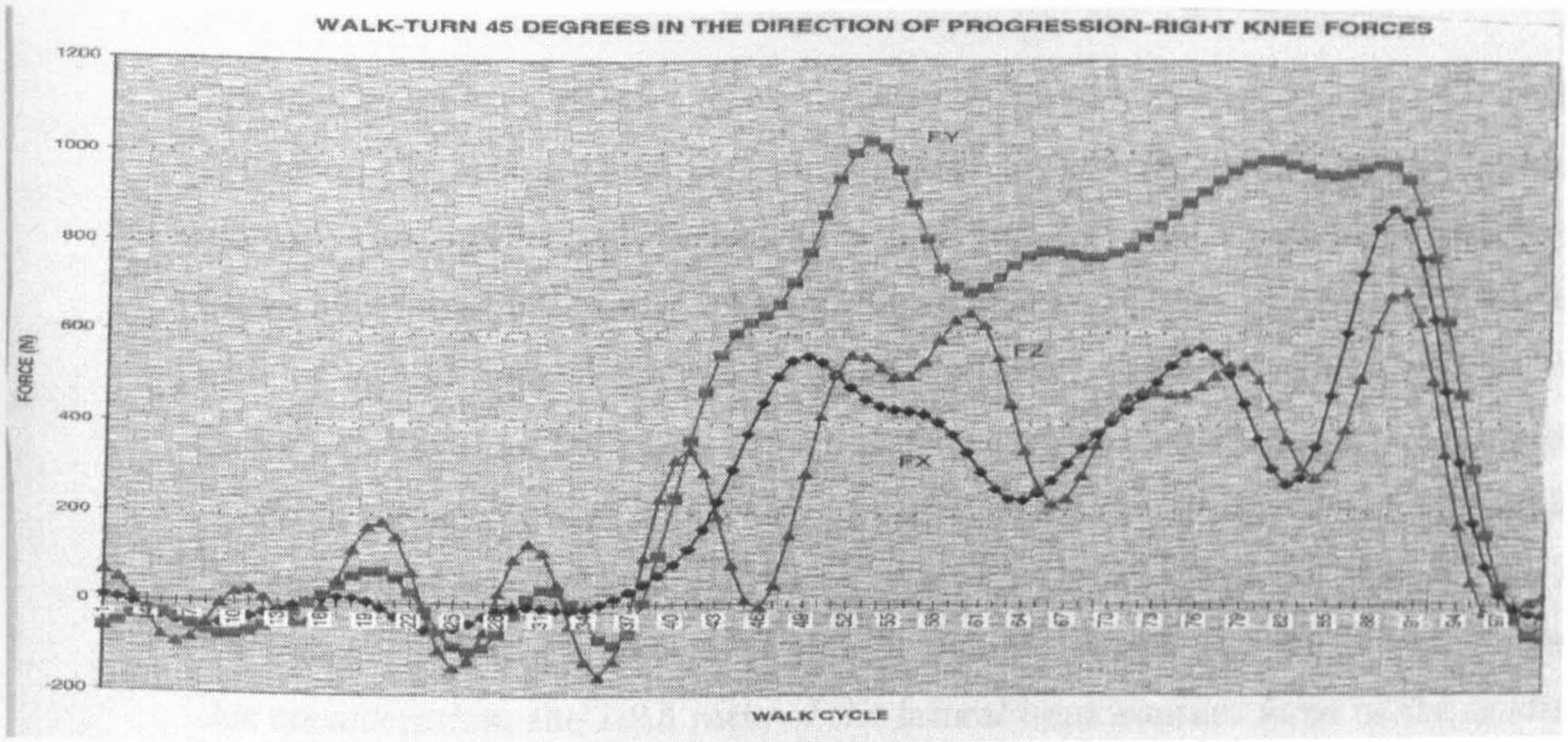

Figure 7.65: Walking and turning at 45 degrees in the direction of progression: RIGHT KNEE FORCES (N)-subject 2-trial 2 pivots on the right leg while turning left- the first leg (left) lands on the first force plate and the pivoting leg (right) lands in the second force plate

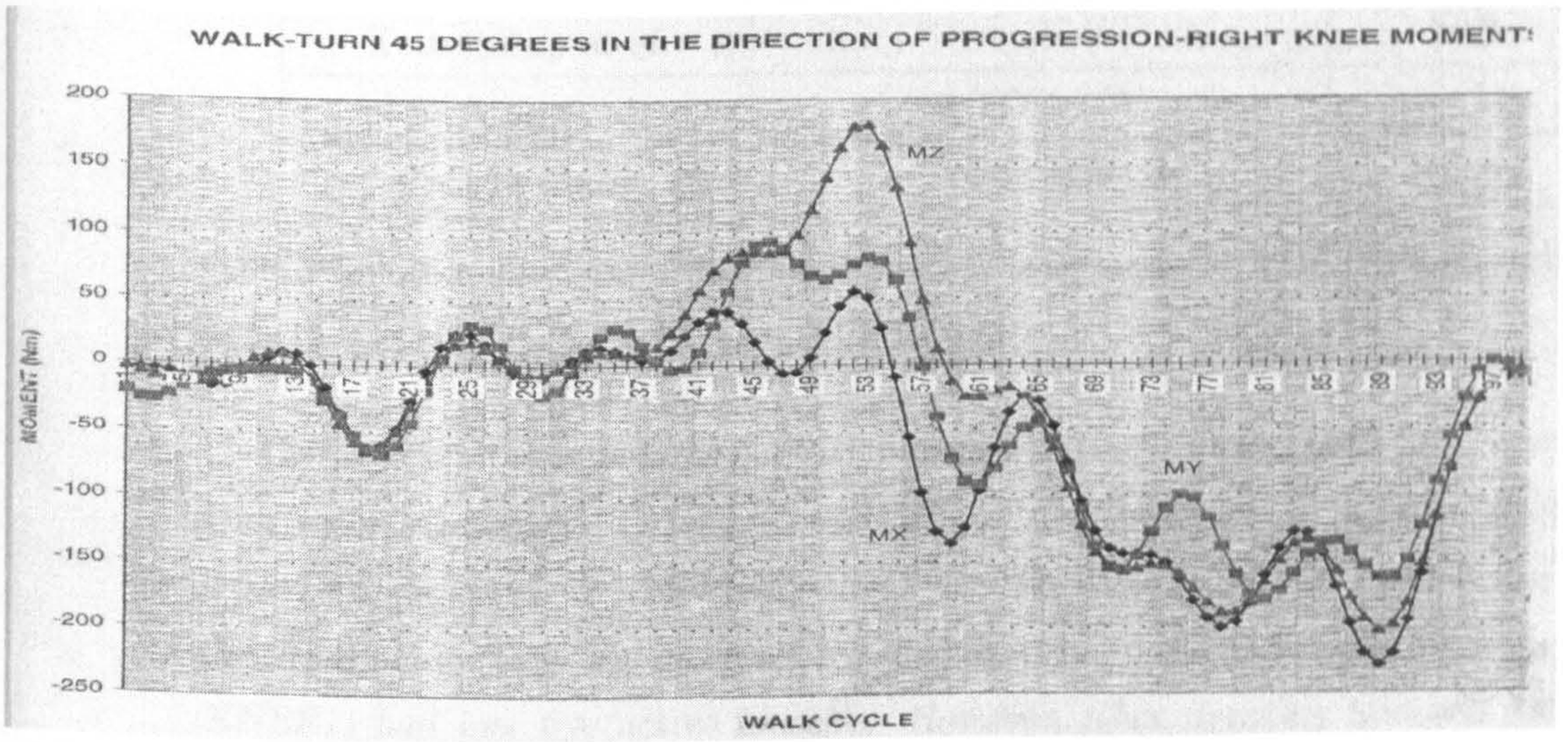

Figure 7.66: Walking and turning at 45 degrees in the direction of progression: RIGHT KNEE MOMENTS (N)-subject 2-trial 2 pivots on the right leg while turning left- the first leg (left) lands on the first force plate and the pivoting leg (right) lands in the second force plate

7.3 Results from the 3D Knee models

The maximum bony contact forces estimated during human gait were 1.25 times body weight on the lateral tibial plateau and 3.06 times body weight on the medial tibial plateau. The total bony contact force was therefore 4.31 times body weight. These values agree reasonably well with values predicted by other researchers. The resultant ratio of lateral bony contact force to medial bony contact force was 1:2.5, which is somewhat less than the ratios reported by other researchers (Table 7.2 on page 186).

From the anatomical point of view, the tibial plateau is almost symmetric although the contact area of the medial plateau is slightly greater than that of the lateral. Therefore, a slightly greater medial bony contact force might be expected. Based on this consideration, the 1:2.5 ratio of the lateral bony contact force to the medial bony contact force seems reasonable.

1	2	3
INVESTIGATORS	MAX BONY C.FORCE (BW)	RATIO L/M
Andriacchi et al. (1984)	—	1:4
Harrington et al. (1983)	3.5 BW (AVERAGE)	L<M
Kettelkamp et al.	—	1:10
Morrison et al.	2 TO 4 BW	L<M
Present study	4.31 BW	1:2.5

Table 7.2: table 9.1 Comparison of Predicted bony contact force solutions with previous investigations, L:LATERAL, M:MEDIAL

The predicted muscle force activity patterns were compared with EMG records by Andriacchi, Andersson, Ortengren and Mikosz Andriacchi et al. [1984] and Spaepen A. and Papaioannou G. (see APPENDIX E). The history of iterations in the model algorithm shows that the muscle force distribution in the initial optimization model (KNEE1) had just five active muscles. However, after iterating between SECOND and KNEE2, the number of active muscles increased to ten.

Andriacchi Andriacchi et al. [1984] reported EMG records of twelve muscles (BF, GRA, RF, SART, SEMIM, SEMIT, TFL, GASM, GASL, VI, VL and VM) at various angles of knee flexion and extension. Comparing to the thirteen muscles in the present model, the only muscle they did not study is BFS. In their study, muscle activity was measured in response to unidirectional loads tending to flex and extend the knee, and

to combined loads of flexion-adduction, flexion-abduction, extension-adduction, and extension-abduction. Results indicated that the individual muscle responses were dependent upon the direction, magnitude, and combination of external moments, as well as on the flexion angle of the knee. Although their experimental study only considered knee flexion/extension and abduction/adduction with a static loading condition, from their findings eight muscles (SART, GASL, SEMIT, TFL, VL, VI, VM and RF) were highly active when the knee was at 10 degree of flexion. This is very close to the posture at 17% of the gait cycle. The present study predicts activity in ten muscles, including all eight of the muscles shown to be active by their EMG data (see Table 7.3 on page 188 and particularly 7.67 on page 188 shows the timing agreement -active concurrence- for the muscles with the most reproducable results).

1	2	3	4	5	6	7	8	9	10	11	12	13
ANDRIA.	ACTIVE	EMG	REC. (X)									
		X	X	0	X	X	0	X	0	X	X	X
ITER 1												
0	0	177	0	0	0	167	0	0	0	249	148	441
ITER 2												
0	0	180	35	29	27	62	0	66	0	253	293	429
ITER 3												
0	0	198	40	37	34	47	27	85	0	277	308	429
ITER 4												
0	0	205	45	43	39	46	54	107	0	286	323	477
ITER 5												
0	0	213	47	48	44	44	76	126	0	298	331	498
ITER 6												
0	0	221	49	52	47	40	92	142	0	308	338	516
ITER 7												
0	0	233	54	53	49	33	93	153	0	321	342	526
ITER 8												
0	0	232	52	58	52	34	112	163	0	323	349	541
ITER 9												
0	0	236	53	62	54	31	124	170	0	329	354	551
ITER 10												
0	0	248	59	59	53	26	115	180	0	338	353	552
ITER 11												
0	0	248	58	61	55	27	120	187	0	340	354	558
ITER 12												
0	0	256	64	57	53	26	109	188	0	344	351	557

Table 7.3: table 9.2 Comparison of muscle force activity EMG records of Andriacchi (ANDR.) Andriacchi et al. [1984] Muscle 1 to 13 are: BF, GRA, RF, SART, SEMIM, SEMIT, TFL, GASM, GASL, BFS, VI, VL, VM, see section 7.2.2

The corresponding ligament forces predicted by KNEE2 are much less than their ultimate strength and have large safety factors (3.4 to 8.5). Trent et al. [1976] reported that ultimate strength of MCL (medial collateral ligament), LCL (lateral collateral ligament), ACL (anterior cruciate ligament), and PCL (posterior cruciate ligament) were 0.74 BW, 0.54 BW, 0.90 BW and 0.85 BW, respectively. In the present solution, the ligament forces predicted by KNEE2 were 0.17 BW (117 N), 0.16 BW (109 N), 0.0 BW, and 0.1 BW (72 N) for MCL, LCL, ACL and PCL, respectively. Therefore, the safety factors (ultimate strength divided by predicted ligament force) ranged from 3.4 to 8.5. The ligament forces estimated from the nonlinear spring model of SECOND were 0.18 BW (126 N), 0.0 BW, 0.40 BW (280 N) and 0.0 BW for MCL, LCL, ACL and PCL, respectively, with two ligaments inactive. Although these forces depend on the uncertain ligament properties (initial strains, spring constants, etc.), the safety factors are still from 2.25 to 4.1. These small ligament force solutions are further supported by Lewis et al. [1981]. They concluded from their data (measured by buckle transducers) that in level walking there was, at most, minimal ligament force.

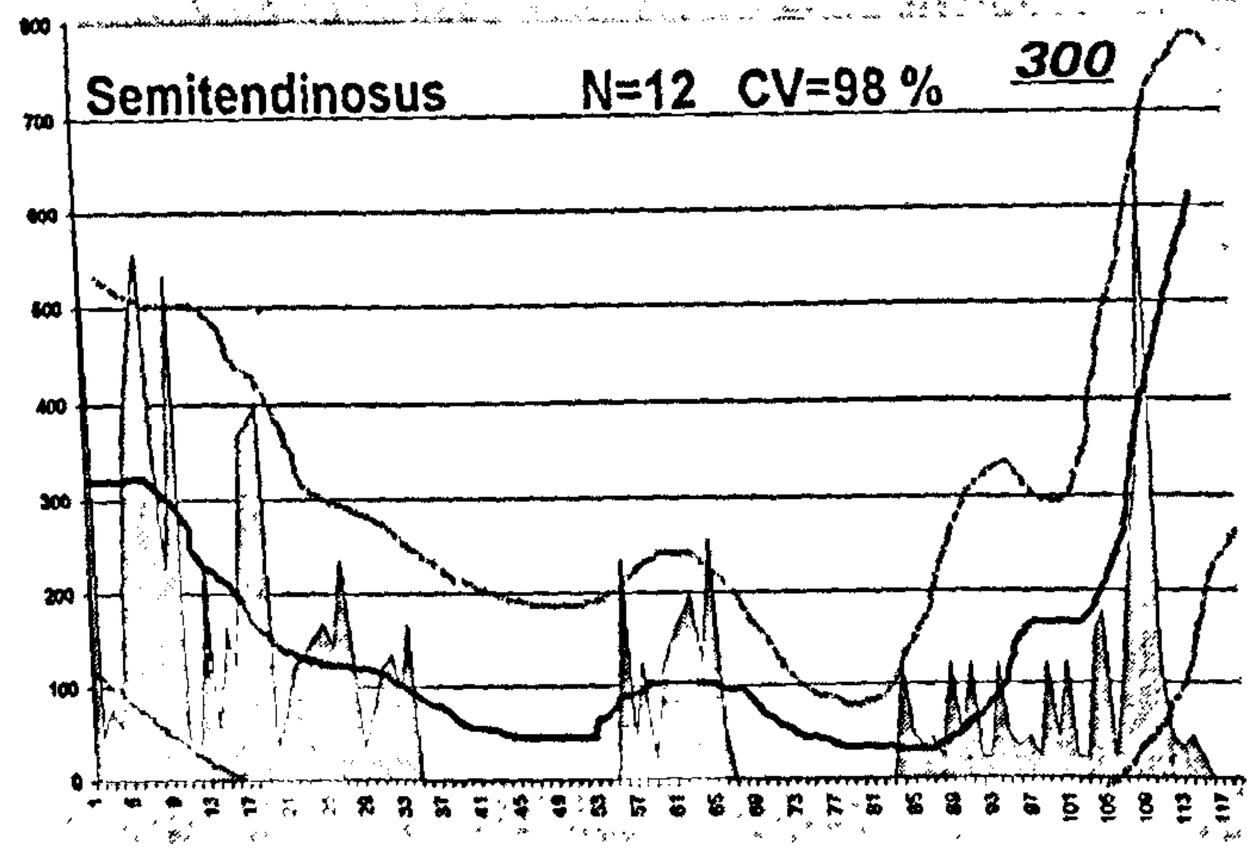

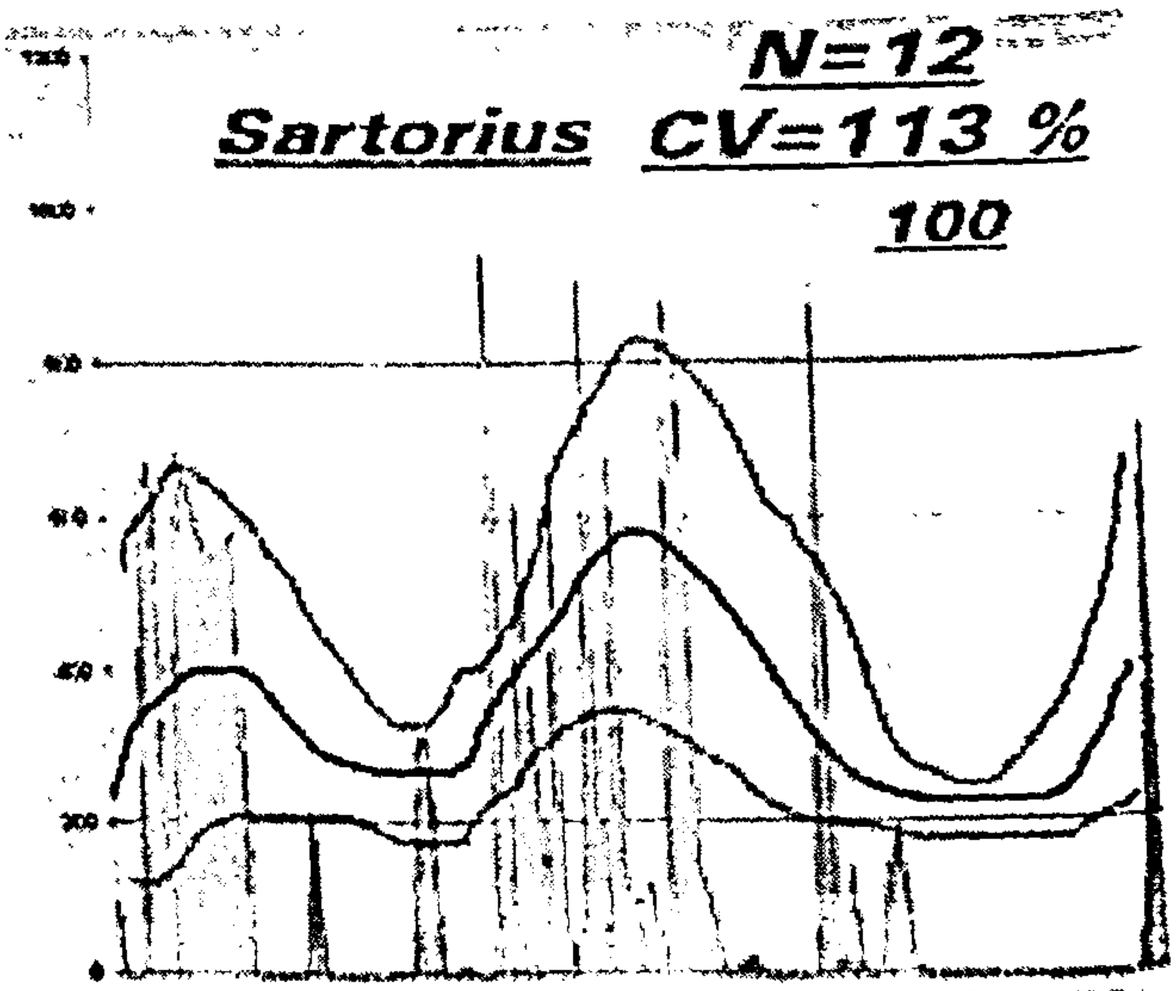

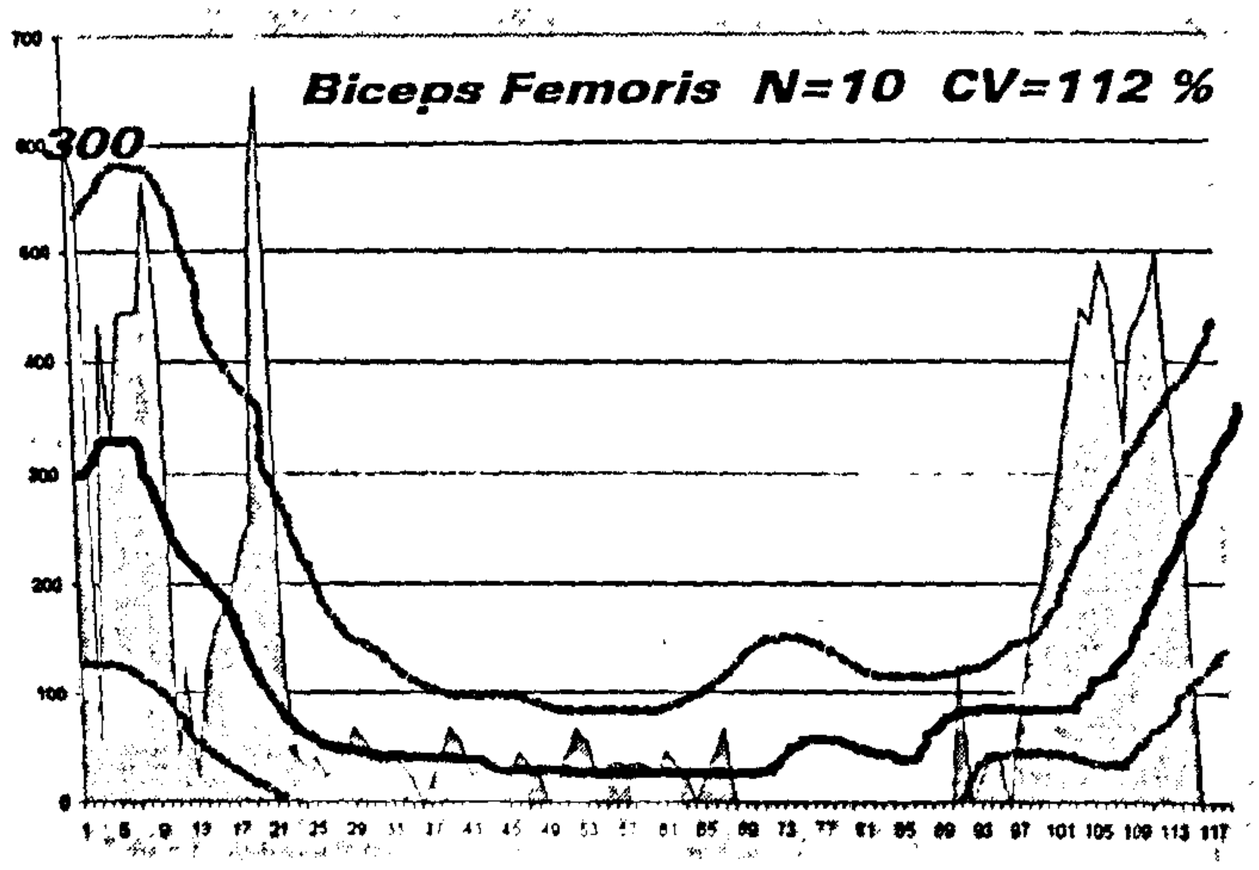

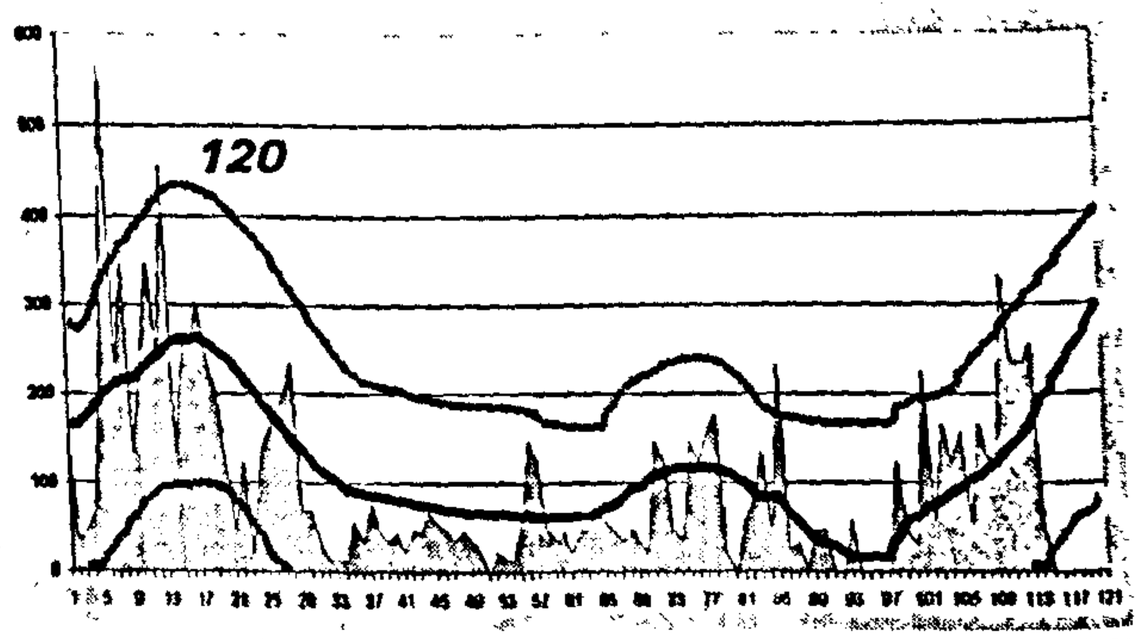

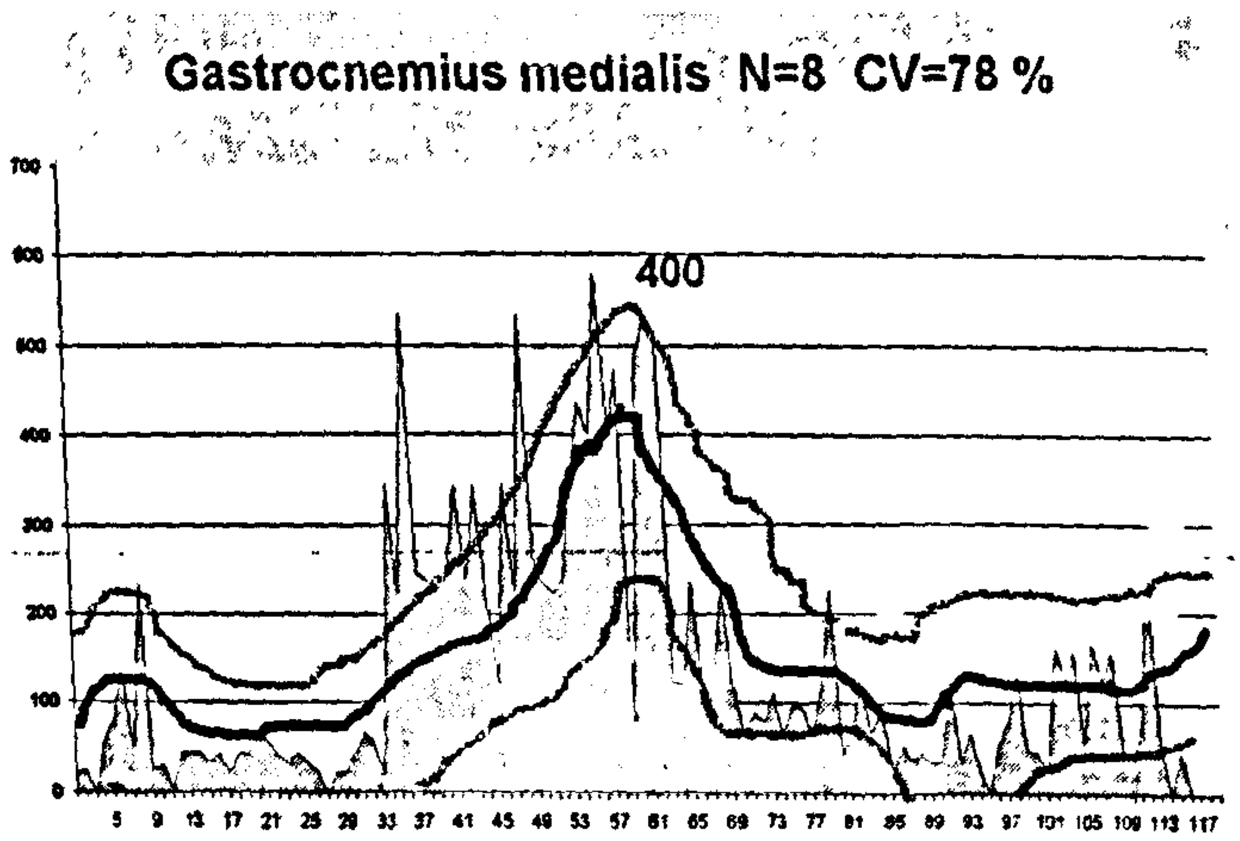

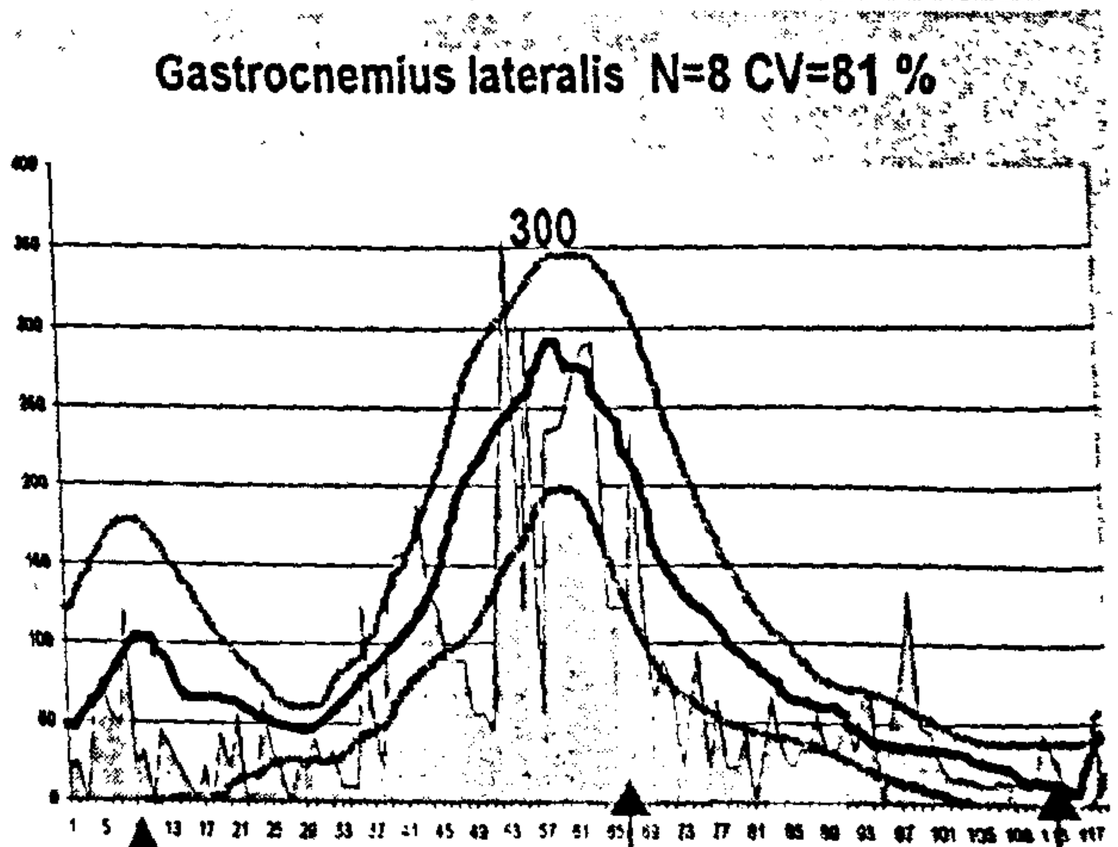

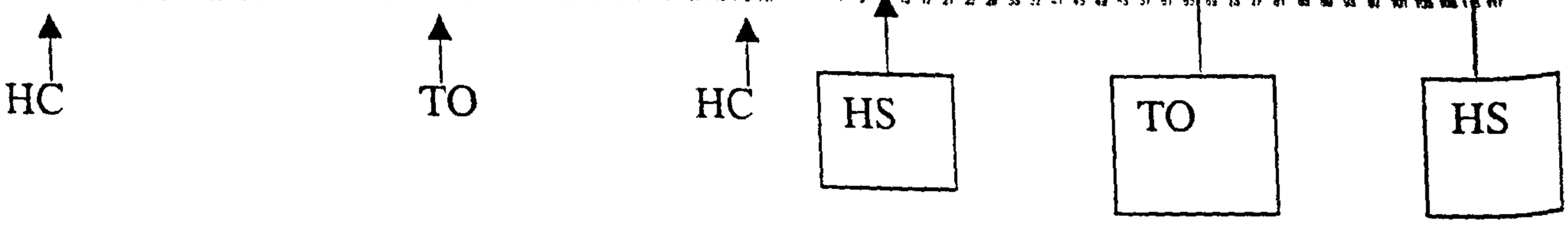

Figure 7.67: Active concurrence of several muscles of several subjects; The grey filled curves represent the force predictio of the corresponding muscle which is in timing agreement with the EMG activity. The solid lines represent the average valu of EMG of the muscles in μV. The dotted lines represent the standard deviation (SD) from 15 circles. The number of subj is indicated with N. The variation coefficient CV is related to the SD. Every muscle is registered at the right side, with surface electrodes while the subject is walking at natural cadence.

7.4 Intra- and inter-subject validation of the model

To further the sensitivity analysis and study the behaviour of the model with a varying input data we performed some additional calculations on the same subject's data (intra-subject validation) and with data collected from four other different subjects. The model was not changed for the intrasubject calculations. Data from eight different normal gait sessions were used with the model, which means that the information for the inverse analysis solving for the three main lower limb joints was calculated each time and was the input to the model.

In the case of the inter-subject study the model was scaled to much some of the geometric variability between the different subjects. It should be noted that we did not perform the full collection of the several geometry parameters as described in the methodology. We rather scaled the model according to several parameters that were available from all the four different subjects. These parameters were: subject height and body mass, the distances S1,S2,S3,S4, that are described in the methodology (section 6.2.1) and correspond to the distance between lateral and medial condyle of tibia, the distance between medial condyle of tibia and the head of fibula, the distance between medial to lateral malleolus and the distance between the tibial tuberosity to the tibiofibular articulation respectively. The scaling was also assisted by data taken from the static calculation performed before all gait trials which served initially for the calculation of the hip joint centers. We used the static (anatomical position, the subject is standing in the erect position very still) data, that is the distances from the trochander marker to the marker of fibula head, and the distance of fibula head to the lateral malleolus. The above information was adequate to scale the mesh describing the bones in the visualization protocol which then scales the muscle data and their wrapping characteristics. All the information about the knee geometry (knee pressure maps, history of joint force application point, ligament characteristics etc.) followed in the lines of the subject's morphology whose analysis is fully described in several chapters. The scalling parameters described above for the four subjects and the reference subject analysed here in detailed are presented in table 7.4 on page 190.

The maximum bony contact forces estimated during human gait from these five subjects were on average 1.48 (SD:0.22 BW) times body weight on the lateral tibial plateau and 3.91 (SD: 0.62 BW) times body weight on the medial tibial plateau. The total average of five subjects bony contact force was 5.4 times body weight with a standard deviation of 0.82 BW. Analytically, subject 3 presented the highest maximum bony contact force with 1.75 times body weight on the lateral tibial plateau and 4.46 times body weight on the medial tibial plateau (ratio lateral to medial: 1:2.5, total bony contact force 6.21 BW). Subject 1 had the lowest maximum bony contact force with 1.25 times body weight on the lateral tibial plateau and 3.06 times body weight on the medial tibial plateau (ratio lateral to medial: 1:2.5, total bony contact force 4.31 BW). Subject 2 had a maximum bony contact force of 1.3 times body weight on the lateral tibial plateau and 3.95 times body weight on the medial tibial plateau (ratio lateral to medial: 1:3, total bony contact force 5.25 BW). Subject 4 had a maximum bony contact force of 1.68 times body weight on the lateral tibial plateau and 4.56 times body weight on the medial tibial plateau (the highest) (ratio lateral to medial: 1:2.7, total bony contact force 6.24 BW). Subject 5 had a maximum bony contact force of 1.45 times body weight on the lateral tibial plateau and 3.54 times body weight on the medial tibial plateau (ratio lateral to medial: 1:2.5, total bony contact force 4.99 BW).

These values agree reasonably well with values predicted by other researchers. The resultant ratio of lateral bony contact force to medial bony contact force from all subjects was on average 1:2.5, which is somewhat less than the ratios reported by other researchers (Table 7.2 on page 186).

Kettlekamp et al. [1973] reported a method of planar analysis for determining compression forces (bony contact forces) on the tibial plateau during standing. Their purely static model included two bony contact regions and two collateral ligaments, but no muscles. The normal knee and the pathological cases of degenerative genu varus and valgus were studied. In a normal 60 kg subject, the calculated bony contact force on the medial condyle was 25.5 kg (240.1 N), and that on the lateral condyle was 2.5 kg (24.5 N). Hence, the ratio of the bony contact forces on the lateral to medial condyles was approximately 1:10. Harrington [1983] modified Morrison's model to simplify the analysis. The point of bony contact force application was restricted to lie within one-quarter of the bicondylar width from the midpoint of the medio-lateral reference line through the joint centre. He estimated that the average maximum bony contact force

subject	height(m)	body mass)(kg)	S1	S2	S3	S4	Lower limb
1	1.75	68	9.99	9.19	6.9	5.48	left
			9.99	9.35	6.56	5.27	right
2	1.77	85	9.89	9.05	6.8	5.50	left
			9.82	9.26	6.75	5.38	right
3	1.835	84.75	10.96	9.89	7.28	5.13	left
			10.87	9.83	7.35	5.13	right
4	1.845	83.65	9.61	9.01	6.73	4.65	left
			9.36	9.06	6.28	4.65	right
5	1.79	77	9.3	10.20	7.18	3.5	left
			9.17	10.00	7.00	3.3	right

Table 7.4: The model scalling parameters for the four subjects and the reference subject are presented here:S1,S2,S3,S4, that are described in the methodology (section 6.2.1) correspond to the distance between lateral and medial condyle of tibia the distance between medial condyle of tibia and the head of fibula, the distance between medial to lateral malleolus and the distance between the tibial tuberosity to the tibiofibular articulation respectively

was 3.5 times body weight (BW) for normal subjects during level walking. The centre of pressure for normal subjects was localized to the medial compartment throughout most of the stance phase, and particularly during maximum load transmission. He also noted that the magnitude of the bony contact force for normal subjects depended on body weight and walking speed and was directly proportional to the net intersegmental forces and moments at the joint. This may partly explain the variation in the value of the maximum bony contact force reported by different investigators.

Andriacchi et al. [1983] reported an indeterminate three-dimensional model of the knee that included a representation of the interconnecting ligaments, joint capsule, joint surfaces and menisci. The bony portions of the femur and tibia were idealized as rigid bodies, while the ligaments, menisci and joint capsule were represented as disc-like shear beams. The joint surfaces were represented by a series of hydrostatic elements which allowed rolling and sliding contact. The computational scheme employed the direct stiffness method of structural mechanics with incremental linearization to deal with both geometric and material nonlinearities. Using this model, they calculated force distribution at the knee during various phases of the walking cycle. At 20% of the level walking cycle (i.e., from the instant of heel strike), the medial condyle had a bony contact force of 1040 N, while the lateral condyle had a contact force of 250 N. Hence, the ratio of lateral to medial condyle bony contact force was approximately 1:4.

The eight different model calculations (intrasubject sensitivity) with subject's 1 input data while changing every time the external forces and moments calculated from the inverse analysis revealed a variation similar to that predicted from the sensitivity analysis. The lateral bony contact force reached values of 1.25, 1.28, 1.26, 1.34, 1.23, 1.24, 1.25, 1.24 BW (average 1.26 BW, SD: 0.035BW) and the medial bony contact force reached values of 3.06, 3.3, 3.21, 3.21, 3.09, 3.24, 3.0, 3.02, 3.12 BW (average 3.13 BW, SD: 0.108 BW) for the eight separate runs respectively. The different intrasubject runs affected neither the rate of convergence nor the active concurrence, that is the agreement of the EMG profiles with the magnitude of the predicted muscle force, in other words the muscle convergence.

Trent et al. [1976] reported that ultimate strength of MCL (medial collateral ligament), LCL (lateral collateral ligament), ACL (anterior cruciate ligament), and PCL (posterior cruciate ligament) were 0.74 BW, 0.54 BW, 0.90 BW and 0.85 BW, respectively. In the present solution for all the five subjects , the ligament forces predicted

by KNEE2 were in the range of 0.17 BW (117 N)(subject one) to 0.22 BW (183 N)(subject 4), 0.16 BW (109 N subject one) to 0.27 BW (225 N subject 4), 0.0 BW (subject one) to 0.1 BW (83 N -subject 4) , and 0.1 BW (72 N- subject one) to 0.18 BW (150 N -subject 4) for MCL, LCL, ACL and PCL, respectively. Therefore, the safety factors (ultimate strength divided by predicted ligament force) are still large numbers ranging from 2 to 8.5.

The rate of convergence both for bony contact forces and muscle prediction was enhanced in the intersubject variability study. Design of experiments (DOE) and Response Surface Models (RSM) allowed a reduction of the computation time of about 400 % once we run the intrasubject variability study and earned some experience in interpretation of DOE and RSM. Tables 7.6 on page 192 and 7.5 on page 192indicate that solution (optimum) was reached with an extreme reduction in the iteration time and the iterations and with a better muscle force prediction in terms of magnitude and EMG active concurrence as seen from the average and standard deviations of the convergence calculations from the five subjects.

NONLINEAR	FORCE	STRESS	SOLUTIONS
MUSCLE	FORCE	FORCE CUBED	STRESS CUBED
biceps femoris (lh)	12.0:3.0	12.0:3.0	35.0:8.0
gracilis	0.0	0.0	0.0
rectus femoris	32.0:5.0	19.0:4.0	32.0:9.0
sartorius	70.0:6.0	100.0:10.0	0.0
semimembranosus	28.0:5.0	28.0:4.0	38.0:7.0
semitendinosus	0.0	0.0	0.0
tensor fasciae latae	80.0:7.0	80.0:9.0	80.0:6.0
medial gastrocnemius	65.0:10.0	65.0:9.0	45.0:4.0
lateral gastrocnemius	95.0:5.0	95.0:4.0	80.0:9.0
biceps femoris(sh)	20.0:2.0	20.0:2.0	20.0:2.0
vastus intermedius	0.0	20.0:5.0	10.0:4.0
vastus lateralus	0.0	5.0:2.0	0.0
vastus medialus	65.0:6.0	70.0:6.0	85.0:10.9

Table 7.5: Active concurrence of EMG and muscle force predictions (in %):NONLINEAR SOLUTIONS: 5 subjects. Mean +/-SD

7.5 Sensitivity Analysis

The force distributions are a function of the input module's geometrical data (muscle insertions and origins, ligament insertions and origins, bony contact points, and the

1	2	3	4	5	6	7	8	9	10	11	12	13
	ACTIVE	EMG	REC. (X)									
		X	X	0	X	X	0	X	0	X	X	X
ITER 1												
0	0	169	0	0	0	146	0	0	0	260	153	456
ITER 2												
0	0	171	40	30	28	70	0	59	0	265	285	445
ITER 3												
0	0	185	51	32	39	61	0	71	0	268	319	436
ITER 4												
0	0	230	57	39	42	60	0	99	0	290	334	457
ITER 5												
0	0	245	58	45	54	59	70	130	0	301	339	506
ITER 6												
0	0	262	59	57	56	55	71	157	0	305	349	542
ITER 7												
0	0	265	60	54	60	52	78	158	0	332	356	558
ITER 8												
0	0	278	62	55	64	56	81	162	0	356	372	569

Table 7.6: table 9.2 Comparison of muscle force activity EMG records Muscle 1 to 13 are: BF, GRA, RF, SART, SEMIM, SEMIT, TFL, GASM, GASL, BFS, VI, VL, VM. see section 7.2.2. The rate of convergence for muscle prediction was enhanced in the intersubject variability study (subject 3 is shown). Design of experiments (DOE) and Response Surface Models (RSM) allowed a reduction of the computation time of about 400 % once we run the intrasubject variability study and earned some experience in interpretation of DOE and RSM.

cross-sectional areas of muscles and ligaments), spring ligament forces generated by ligament spring constants and ligament strains, and the intersegmental resultant force and moment at the joint. A sensitivity analysis was therefore undertaken to evaluate the model response due to variations in these model parameters, and also to gain a better understanding of the functional behavior of model parameters.

In this section, twelve sensitivity analyses of the model are considered. Solution sensitivity was studied relative to specified changes in twelve group parameters (muscle insertions and origins, ligament insertions and origins, bony contact points, muscle cross-sectional areas, ligament cross-sectional areas, spring ligament forces and the six intersegmental resultant force and moment components). Although perturbing a group of variables simultaneously (e.g., all ligament insertions and origins), may lead to over-optimistic assessments of model sensitivity (i.e., some "cancelling-out" of individual solution changes), such an approach at least provides some appreciation of the solution's relative sensitivity to each category of physically-derived input.

The perturbation units were chosen to be +1 cm in each direction (i.e., a vectorial deviation of (1,1,1) cm from the origin point) for bony contact forces, muscle insertions and origins, and ligament insertions and origins. Although this perturbation magnitude was chosen somewhat arbitrarily, preliminary trials using a 1 mm perturbation resulted in very small solution changes (0.1 BW, 0.01 BW, 0.02 BW), which could not reliably be distinguished from those attributable to other computation "variables" such as round-off or marginal satisfaction of convergence criteria. For the remaining system parameters (relative muscle cross-sectional area, ligament cross-sectional area, spring ligament forces, and the six intersegmental resultant force and moment components), the perturbation units were taken as +10% for the default values.

The physical variables to which the computed bony contact force was most sensitive were the locations of the bony contact points (27.6% change), the spring ligament forces (22% change), and the locations of the muscle insertions and origins (14% change). Variables to which the computed bony contact force was least sensitive were the locations of the ligament insertions and origins (3% change), the relative muscle cross-sectional areas (3.2% change), the ligament cross-sectional areas (1.9% change), and the intersegmental resultant force and moment components (4.2% to 7.4% change). The total bony contact force was described as "sensitive" to any factor if the total bony contact force was changed by more than 10% after that factor was perturbed by the predetermined amount. A complete and detailed explanation of the

sensitivity analysis follows.

The muscle insertions and origins used in this model were taken from the data of Brand [1992] and Brand et al. [1982] based upon the marking of insertions and origins in three cadavers. Since a straight line assumption is used for the muscle force line-of-action, errors in identifying and marking the insertions and origins can affect the direction and moment arm of the muscle forces. To get a brief understanding of this parameter, variations in all three locations of +1 cm in each direction were made simultaneously. Comparing the results with the original values, the muscle force distributions were almost the same but with slightly smaller magnitude. The total bony contact force had a reduction of about 14% (0.6 BW) (Table 7.7 on page 197). From the equilibrium equations, the smaller muscle forces should result in smaller bony contact forces as well. Such errors (+1 cm in each direction) of measuring the muscle insertions and origins did not affect which muscles were active, but did affect the magnitude of the muscle and bony contact forces in this model (e.g., maximum change of muscle force occurred in the vastus medialis muscle which was changed from 557 N to 391 N, and in the total bony contact force which was changed from 2987 N to 2559 N). Recall from section 7.2.5.3 that Wilson's regression analysis (modified by anatomical experience and compared with anatomy textbooks), were used to obtain the ligament insertions and origins for this model. Comparing the present ligament lengths with those of previous investigations, it is clear that discrepancies exist. The maximum discrepancy (5.41 cm) occurred for the deep medial collateral ligament, and the minimum discrepancy of 0.72 cm occurred for the posterior anterior cruciate ligament (Table 5.11 on page 104). Since the ligaments are simulated by nonlinear springs in the determinate model, these discrepant ligament lengths will result in different ligament forces. To have a general understanding of the sensitivity of the model to ligament length values, all ligament insertions and origins were altered simultaneously by +1 cm in each direction. Comparing the results with the original values, the total bony contact force exhibited a difference of only about 3% (0.13 BW) with the same muscles active (Table 7.8 on page 198).

The bony contact points were estimated from the static pressure distributions measured by Ahmed et al. [1983]. These points were used to calculate the moment arms of the bony contact forces at different flexion-extension angles. For different load magnitudes, the estimated bony contact points have a maximum difference range of 0.63 cm in the anterior X-direction and 0.35 cm in the lateral Z-direction. For

the different flexion-extension angles, there is a 1.67 cm maximum difference in the X-direction and a 0.57 cm maximum difference in the Z-direction. Therefore different loads and different flexion-extension angles can produce a nominal change of about 1 cm in the X and Z-coordinates of the contact points. In this mathematical model, the bony contact point locations were found to be very sensitive to the change of +1 in each direction, since this change affected critical moment arm values. The muscle force distributions were much different from, and the magnitudes were generally larger than the original values (Table 7.9 on page 198). Even more remarkable than the 27.6% change in the total bony contact force was the fact that the ratio of the lateral bony contact force to the medial bony contact force changed from 1:2.5 to 1:6. Clearly, this model is very sensitive to these variations of bony contact force locations.

The relative muscle cross-sectional areas used in this study were based on the report of Pedersen et al. [1987]. The maximum relative cross-sectional area is 1.78 in the vastus lateralis and the minimum is 0.42 in the sartorius. To explore the sensitivity of the model to these muscle cross-sectional areas, all the relative cross-sectional areas were simultaneously changed by +10%. Comparing these latter results with the original values, the active muscle force distributions were similar but with slightly reduced force magnitudes (Table 7.10 on page 199). The variation of the total bony contact force was a relatively insensitive 3.2%.

Trent et al. [1976] found considerable variability of ligament cross-sectional area between specimens; however, trends within any one specimen were clearly discernible. The lateral collateral ligament had the smallest area, averaging 0.100 in^2 (0.645 cm^2), and the anterior and posterior cruciates had average areas of 0.200 in^2 (1.29 cm^2). Crowninshield et al. [1976] provided the areas relative to that of the anterior fibers of the medial collateral ligament. In the present model, the above two sets of data were combined to approximate ligament areas (Table 5.15 on page 107). The maximum ligament cross-sectional area is about 0.645 cm2 for the AMC. To test the sensitivity of this model to these ligament cross-sectional areas, an analysis was made by changing all the ligament areas +10% at the same time. Changing the cross-sectional areas by +10% changed the force distribution insignificantly (Table 7.11 on page 199). The variation of the total bony contact force was only about 1.9%.

Next, the sensitivity of the model to spring ligament forces was studied. Recall from Chapter 2 that the ligament forces were modeled by a quadratic force-elongation function, which depends on the spring constant and ligament elongation. Since the

exact state of the initial strain is not available, the unstrained length will vary for different estimation methods. Wismans et al. [1980] made assumptions based on the Brantigan et al. [1941] data for the strain in spring in elongation. Those assumptions were also used in this study. The spring constants were based on experimental work by Trent et al. [1976]. Wismans et al. [1980] conducted a sensitivity analysis of the spring constant, initial strain and ligament insertions. The effect of doubling the spring constant on the anterior-posterior laxity was rather small, while the effect of a relatively small variation in the initial strains was found to be very important. To test the sensitivity of the present model to these parameters (spring constant, initial strain and ligament insertions), an analysis is made by changing all the spring ligament forces +10%. Changing all the spring ligament forces +10% does substantially affect the muscle forces (Table 7.12 on page 200). The variation in the total bony contact force is 22%.

Some degree of imprecision in calculating the intersegmental resultant force and moment, such as from computer round-off or from other sources, cannot be avoided. The sensitivity of the model to the intersegmental resultant force and moment was studied by changing the force and moment by +10%, one component at a time. The maximum corresponding variation of the total bony contact force, 7.4%, occurred by changing the Y-component of the resultant joint force by +10%. The resulting changes in the force distribution do vary slightly from one directional component to the next, but the range of the variations of the total bony contact force was only 4.2% to 7.4%, which is less than 10% (Tables 7.13 on page 200 to 7.18 on page 207).

In the sensitivity analysis discussed above, the largest variation in the total bony contact force was 27.6%, resulting from a change in the bony contact points by +1 cm in each direction. Since a +1 cm in each direction (i.e., about one eighth of the tibial width) is by no means a small change, the solution sensitivity can only be qualitatively addressed. A change of the location of bony contact points alters critical moment arm values, and thus can substantially change the distributions between the medial and lateral bony contact forces. There was a 22% change of the total bony contact force due to changing all spring ligament forces of SECOND simultaneously by +10%. One can therefore conclude that changes in the spring ligament forces of SECOND can significantly affect the force distributions in this mathematical model. After changing all locations of muscle insertions and origins simultaneously by +1 cm in each direction, there was a 14% change in the total bony contact force. This

factor can therefore also be considered crucial to the force distribution computed by the model algorithm.

However, the solution was relatively insensitive to the other input perturbations considered. These included the locations of ligament insertions and origins (a 3% contact force change for uniform 1 cm perturbations), the relative muscle cross-sectional areas (a 3.2% contact force change for uniform 10% area changes), the ligament cross-sectional areas (a 1.9% contact force change for uniform 10% area changes), and the intersegmental resultants (between 4.2% and 7.4% contact force change for 10% changes in the resultant force and moment).

MUSCLE	change in all directions by +1cm	orig.values (N)
BF	0	0
GRA	0	0
RF	163	256
SART	57	64
SEMIM	39	57
SEMIT	31	53
TFL	0	26
GASM	230	109
GASL	193	188
BFS	0	0
VI	226	344
VL	245	351
VM	391	577
Fc_M	1753(2.54 BW)	2114 (3.06 BW)
Fc_L	806(1.17 BW)	846 (1.25 BW)
TOTAL Fc_T	BONY CONTACT FORCE 2559 (3.71 BW)	2978 (4.31 BW)

Table 7.7: Sensitivity Solution of changing muscle Insertions and Origins in all three directions by +1 cm

MUSCLE	change in all directions by +1 cm	orig.values (N)
BF	0	0
GRA	0	0
RF	214	256
SART	56	64
SEMIM	70	57
SEMIT	59	53
TFL	34	26
GASM	120	109
GASL	152	188
BFS	0	0
VI	303	344
VL	424	351
VM	485	577
Fc_M	2023(2.93 BW)	2114 (3.06 BW)
Fc_L	861(1.25 BW)	846 (1.25 BW)
TOTAL Fc_T	BONY CONTACT FORCE 2884 (4.18 BW)	2978 (4.31 BW)

Table 7.8: Sensitivity Solution of changing Ligament Insertions and Origins in all three directions by +1 cm

MUSCLE	change in all directions by +1cm	orig.values (N)
BF	0	0
GRA	0	0
RF	433	256
SART	86	64
SEMIM	30	57
SEMIT	54	53
TFL	85	26
GASM	0	109
GASL	118	188
BFS	0	0
VI	597	344
VL	311	351
VM	1111	577
Fc_M	3257(4.72 BW)	2114 (3.06 BW)
Fc_L	537(0.78 BW)	846 (1.25 BW)
TOTAL Fc_T	BONY CONTACT FORCE 3794 (5.50 BW)	2978 (4.31 BW)

Table 7.9: Sensitivity Solution of changing Bony Contact points in all three directions by +1 cm

MUSCLE	change all x-areas by +10 percent	orig.values (N)
BF	0	0
GRA	0	0
RF	251	256
SART	77	64
SEMIM	30	57
SEMIT	33	53
TFL	65	26
GASM	102	109
GASL	170	188
BFS	0	0
VI	327	344
VL	305	351
VM	536	577
Fc_M	2068(3.00 BW)	2114 (3.06 BW)
Fc_L	806(1.17 BW)	846 (1.25 BW)
TOTAL Fc_T	BONY CONTACT FORCE 2874 (4.17 BW)	2978 (4.31 BW)

Table 7.10: Sensitivity Solution of changing Relative Muscle Cross-sectional Areas by +10 percent

MUSCLE	change all x-areas by +10 percent	orig.values (N)
BF	0	0
GRA	0	0
RF	246	256
SART	61	64
SEMIM	39	57
SEMIT	42	53
TFL	58	26
GASM	118	109
GASL	175	188
BFS	0	0
VI	331	344
VL	319	351
VM	549	577
Fc_M	2082(3.02 BW)	2114 (3.06 BW)
Fc_L	832(1.21 BW)	846 (1.25 BW)
TOTAL Fc_T	BONY CONTACT FORCE 2914 (4.23 BW)	2978 (4.31 BW)

Table 7.11: Sensitivity Solution of changing Relative Ligament Cross-sectional Areas by +10 percent

MUSCLE	change all spring lig.forces by +10 percent	orig.values (N)
BF	0	0
GRA	0	0
RF	299	256
SART	78	64
SEMIM	79	57
SEMIT	72	53
TFL	18	26
GASM	250	109
GASL	281	188
BFS	0	0
VI	408	344
VL	388	351
VM	682	577
Fc_M	2365(3.43 BW)	2114 (3.06 BW)
Fc_L	1266(1.83 BW)	846 (1.25 BW)
TOTAL Fc_T	BONY CONTACT FORCE 3631 (5.26 BW)	2978 (4.31 BW)

Table 7.12: Sensitivity Solution of changing Spring Ligament Forces by +10 percent

MUSCLE	change moment Mr_1 by +10 percent	orig.values (N)
BF	0	0
GRA	0	0
RF	249	256
SART	58	64
SEMIM	73	57
SEMIT	61	53
TFL	25	26
GASM	179	109
GASL	196	188
BFS	0	0
VI	347	344
VL	373	351
VM	597	577
Fc_M	2319(3.36 BW)	2114 (3.06 BW)
Fc_L	806(1.17 BW)	846 (1.25 BW)
TOTAL Fc_T	BONY CONTACT FORCE 3125 (4.53 BW)	2978 (4.31 BW)

Table 7.13: Sensitivity Solution of changing intersegmental Resultant Moment in X-component by +10 percent

MUSCLE	change moment Mr_2 by +10 percent	orig.values (N)
BF	0	0
GRA	0	0
RF	251	256
SART	60	64
SEMIM	59	57
SEMIT	54	53
TFL	49	26
GASM	171	109
GASL	197	188
BFS	0	0
VI	346	344
VL	364	351
VM	581	577
Fc_M	2155(3.12 BW)	2114 (3.06 BW)
Fc_L	948(1.37 BW)	846 (1.25 BW)
TOTAL Fc_T	BONY CONTACT FORCE 3103 (4.53 BW)	2978 (4.31 BW)

Table 7.14: Sensitivity Solution of changing intersegmental Resultant Moment in Y-component by +10 percent

MUSCLE	change moment Mr_3 by +10 percent	orig.values (N)
BF	0	0
GRA	0	0
RF	270	256
SART	67	64
SEMIM	61	57
SEMIT	57	53
TFL	43	26
GASM	161	109
GASL	196	188
BFS	0	0
VI	364	344
VL	353	351
VM	625	577
Fc_M	2184(3.17 BW)	2114 (3.06 BW)
Fc_L	983(1.42 BW)	846 (1.25 BW)
TOTAL Fc_T	BONY CONTACT FORCE 3167 (4.59 BW)	2978 (4.31 BW)

Table 7.15: Sensitivity Solution of changing intersegmental Resultant Moment in Z-component by +10 percent

MUSCLE	change force Fr_1 by +10 percent	orig.values (N)
BF	0	0
GRA	0	0
RF	254	256
SART	61	64
SEMIM	67	57
SEMIT	61	53
TFL	40	26
GASM	171	109
GASL	199	188
BFS	0	0
VI	350	344
VL	358	351
VM	598	577
Fc_M	2181(3.16 BW)	2114 (3.06 BW)
Fc_L	946(1.37 BW)	846 (1.25 BW)
TOTAL Fc_T	BONY CONTACT FORCE 3127 (4.53 BW)	2978 (4.31 BW)

Table 7.16: Sensitivity Solution of changing intersegmental Resultant Force in X-component by +10 percent

MUSCLE	change force Fr_2 by +10 percent	orig.values (N)
BF	0	0
GRA	0	0
RF	257	256
SART	62	64
SEMIM	62	57
SEMIT	57	53
TFL	37	26
GASM	171	109
GASL	199	188
BFS	0	0
VI	353	344
VL	357	351
VM	603	577
Fc_M	2209(3.20 BW)	2114 (3.06 BW)
Fc_L	988(1.43 BW)	846 (1.25 BW)
TOTAL Fc_T	BONY CONTACT FORCE 3197 (4.63 BW)	2978 (4.31 BW)

Table 7.17: Sensitivity Solution of changing intersegmental Resultant Force in Y component by +10 percent

7.6 Linear and Nonlinear Programming

An undetermined joint-muscle force distribution problem with many possible solutions requires implementation of mathematical optimization which in turn incorporates additional assumptions about the system to resolve this indeterminacy and uniquely distribute segment resultant forces to the anatomic structures. Linear optimization algorithms encouraged initial linear formulation and solution of the distribution problem (Chao et al. [1978], Chao et al. [1978], Crowninshield [1978],Crownshield et al. [1978], Hardt [1978], Patriarco et al. [1981],Rohrle et al. [1984]). In Hardt's paper it is suggested that certain assumptions necessary to conform muscle energetics to the linear programming format, but also pointed out that linear methods imposed the limitation that the number of non-zero muscle forces could be no greater than the number of equations available for resolution, often creating an unphysiological solution: electromyography related studies strongly suggest many more active muscles during level gait than predicted by linear optimization techniques (Shiavi [1985]).

Reduction methods along with linear optimization can take the solution to convergence paying sometimes a high price due to the simplifying assumptions. Reducing the number of unknown variables, or increasing the number of equations, that involve them and therefore increasing the number of predicted active muscles are possible remedies. Combination principles (Chao et al. [1976], Pierrynowski [1982]) suggest implementation of additional inequality constraints, limiting each muscle to a common upper bound of muscle stress. A critical muscle stress defined the minimum muscle strength that would permit that activity to occur. Minimising the sum of individual muscle stresses with the help of linear programming Crowninshield [1978] showed that unrestrained procedures predicted more independent muscle action. Lowering also the upper bound toward the critical minimum muscle stress was used to "tune" the tailoring of the predicted muscle synergism. The term "synergism" is a state in which two or more active muscles help satisfy a given component of the intersegmental resultant moment, while "antagonism" is the state in which one or more active muscles counteract opposing those muscles satisfying that moment component. Patriarco et al. [1981], grouped functionally similar muscles and constrained them separetely. The synergy in the system was reached by assuming equal stresses within each group and was controlled by limiting the increase in the sum of all muscle forces and by "relaxation" of the requirement to satisfy the moment constraints. Synergy

was obtained in the analysis of An et al. [1984a] by imposing a common upper limit on individual muscle stresses to determine the minimum common stress which permitted a solution predicting a more even distribution of muscle stress among synergistic muscles. Considering the lack of physiological bases for linear criterion selection and/or inherent linear method limitations, nonlinear techniques have been proposed by several researchers. Pedotti et al. [1978] pointed out the dependence of a solution on choise of optimization criteria and suggested two nonlinear criteria which produced predicted patterns of muscle forces more consistent with EMG than did their two linear criteria. Additionally, Crownshield et al. [1981] revealed that muscle contraction endurance time relates inversely to contraction force raised to a power, and developed a numerical criterion for maximum endurance of musculoskeletal function. Similarly, Dul et al. [1984a], Dul et al. [1984b] proposed a nonlinear muscle fatique criterion, involving muscle fiber type as well as muscle size and moment arm. All the above approached differ and therefore produce different results. They differ because in just about every aspect of modelling from gait input data to optimization criteria they use different philosophies. The above introduces us to the problem of direct comparisons of model based analysis due to the inherent inflexibility of the modelling procedure and the programming algorithms. This however in less evident in our approach since IDESIGN allows greater flexibility in problem formulation and also provides unified solution methods, thereby allowing direct evaluations of some of the effects of optimisation criteria and constraints, without entering the realm of optimization technique comparisons.

7.6.1 Linear versus nonlinear predictability

A different procedural design is required for evaluating predictability of different formulations. That is, formulations based on the advantage of IDESIGN platform flexibility. The formulation here is very similar to KNEE1 and SECOND models described earlier. One must point out that non-negativity was established, therefore muscles can actively contract but they can not extend. Two-joint muscles must always contribute the same force at their attachments across either joint. optimization techniques must satisfy these explicitly stated constraints, while minimising a cost function. The choise of cost function coefficients suggests a unique solution as in the example of the reciprocals of relative muscle physiological cross-sectional areas being weight contributions.

The three moments at each joint (Hip, Knee and Ankle) calculated in the inverse computations are expressed in the Ground (Laboratory) reference frame. The current formulation requires the muscles to satisfy all moment components of flexion extension and varus-valgus at the knee -in the femoral reference frame. A further design where all the information for the three joints and most of the muscles will be implemented requires the muscles to satisfy all moment components at the hip (in a pelvic reference frame), flexion-extension and varus-valgus moments at the knee (in a femoral reference frame), and only the flexion extension moment at the ankle (in a tibial reference frame). This follows the assumption for the above formulation that ligaments and/or bony geometry satisfy axial moment components at the knee in level gait, and axial and valus-valgus moment components at the ankle; that is, the muscles do not contribute to these components.

The above assumption is one based on empirical observations, and need not necessarily be made for problem formulation (i.e. hip, knee and ankle joints could be considered as ball and soccet joints). Patriarco et al. [1981], reported on a similar assumption, constraint tolerance. A very limited constraint tolerance is the numerical equivalent of requiring muscles to satisfy the absolute Newtonian intersegmental resultant moment. Since constraint tolerance bounds the acceptable muscle force's moment, one can determine how much tolerances varying from 0.001 percent to 1.0 percent affected the solutions. FIGURES 7.73 on page 208, 7.78 on page 213, 7.79 on page 213, 7.76 on page 210, 7.77 on page 210, show the different IDESIGN formulations using six linear and nonlinear problem formulations. Also FIGURES 7.70 on page 207, 7.71 on page 207, 7.68 on page 206, 7.69 on page 206, 7.74 on page 208, 7.75 on page 208 present analytically the different muscle predictions from the final successful optimization output. IDESIGN combines linear and nonlinear optimization techniques into a single program. Comparison between the different formulations is thus very straightforward. To validate the various muscle force solutions, one can use the ensemble-averaged and time-normalised rectified integrated EMG signals from eight muscles in sixteen normal subjects during free walking speed. For the procedure for EMG validation the reader should refer to Chapter 5.

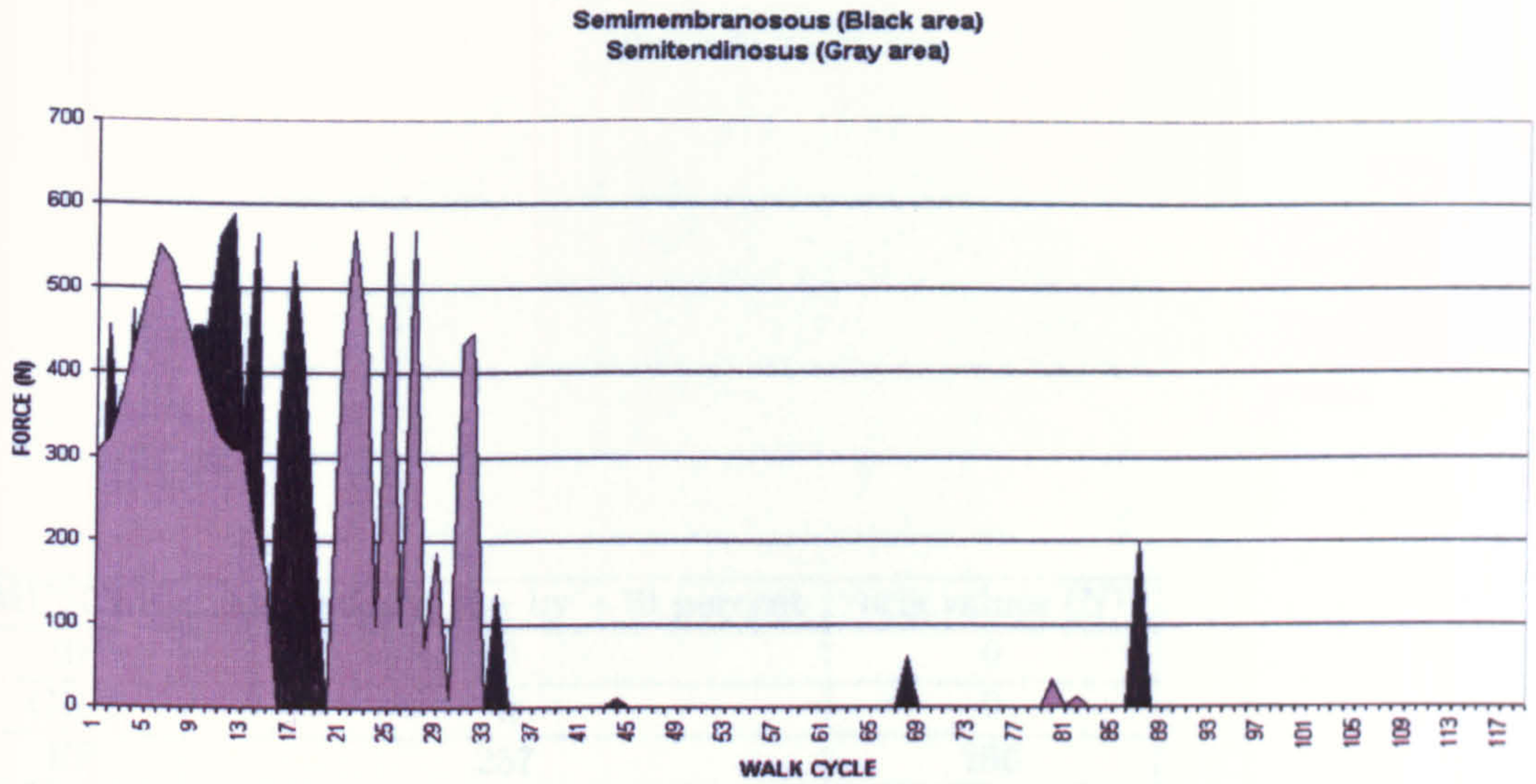

Figure 7.68: Muscle force predictions using IDESIGN'S nonlinear minimisation of the sum of muscle stresses cubed; Semimembranosus and Semitendinosus are shown here; the x axis shows the duration of the walking cycle from heel contact to toe-off.

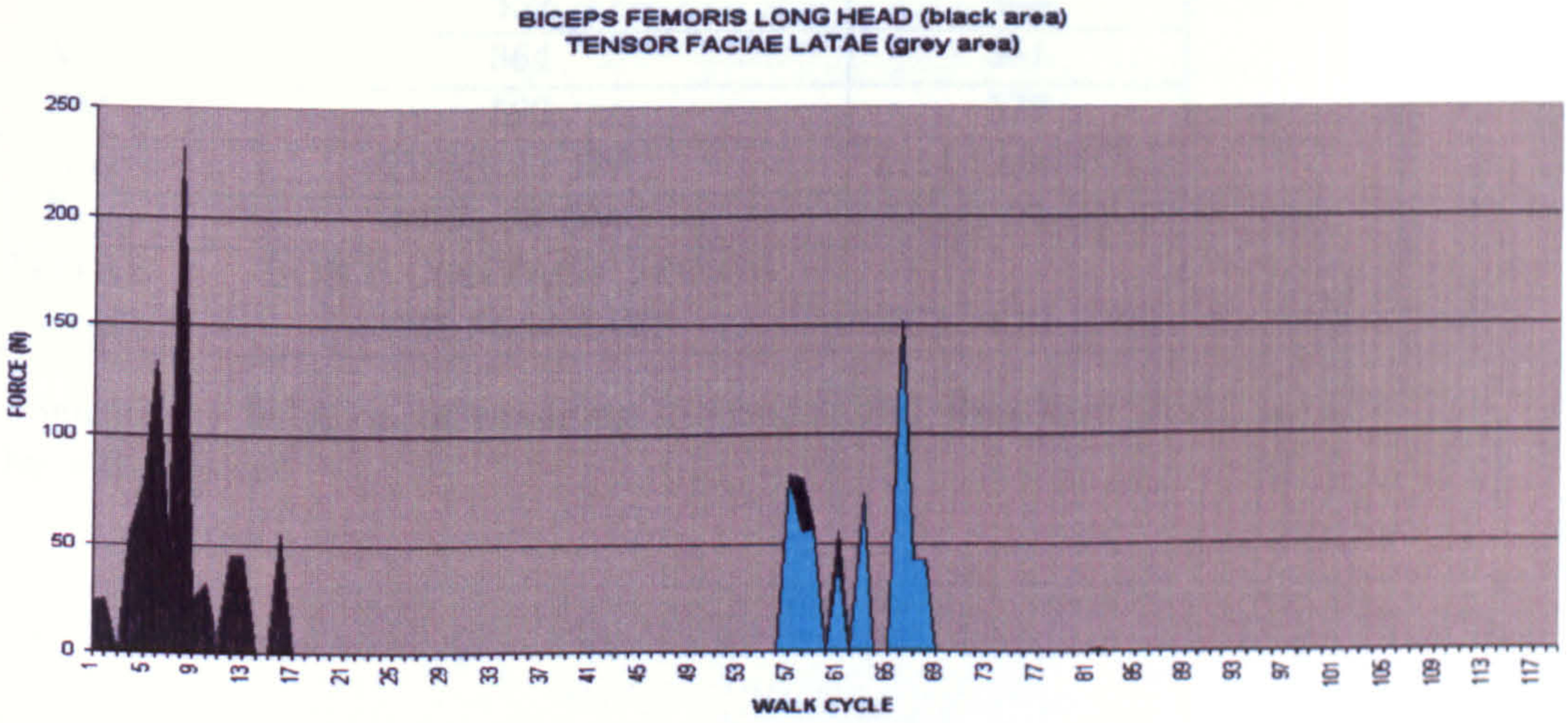

Figure 7.69: Muscle force predictions using IDESIGN'S nonlinear minimisation of the sum of muscle stresses cubed; Biceps femoris (long head) and Tensor fasciae latae are shown here; the x axis shows the duration of the walking cycle from heel contact to toe-off.

MUSCLE	change force Fr_3 by +10 percent	orig.values (N)
BF	0	0
GRA	0	0
RF	257	256
SART	68	64
SEMIM	58	57
SEMIT	3	53
TFL	28	26
GASM	181	109
GASL	206	188
BFS	0	0
VI	352	344
VL	364	351
VM	592	577
Fc_M	2185(3.17 BW)	2114 (3.06 BW)
Fc_L	946(1.37 BW)	846 (1.25 BW)
TOTAL Fc_T	BONY CONTACT FORCE 3131 (4.54 BW)	2978 (4.31 BW)

Table 7.18: Sensitivity Solution of changing intersegmental Resultant Force in Z-component by +10 percent

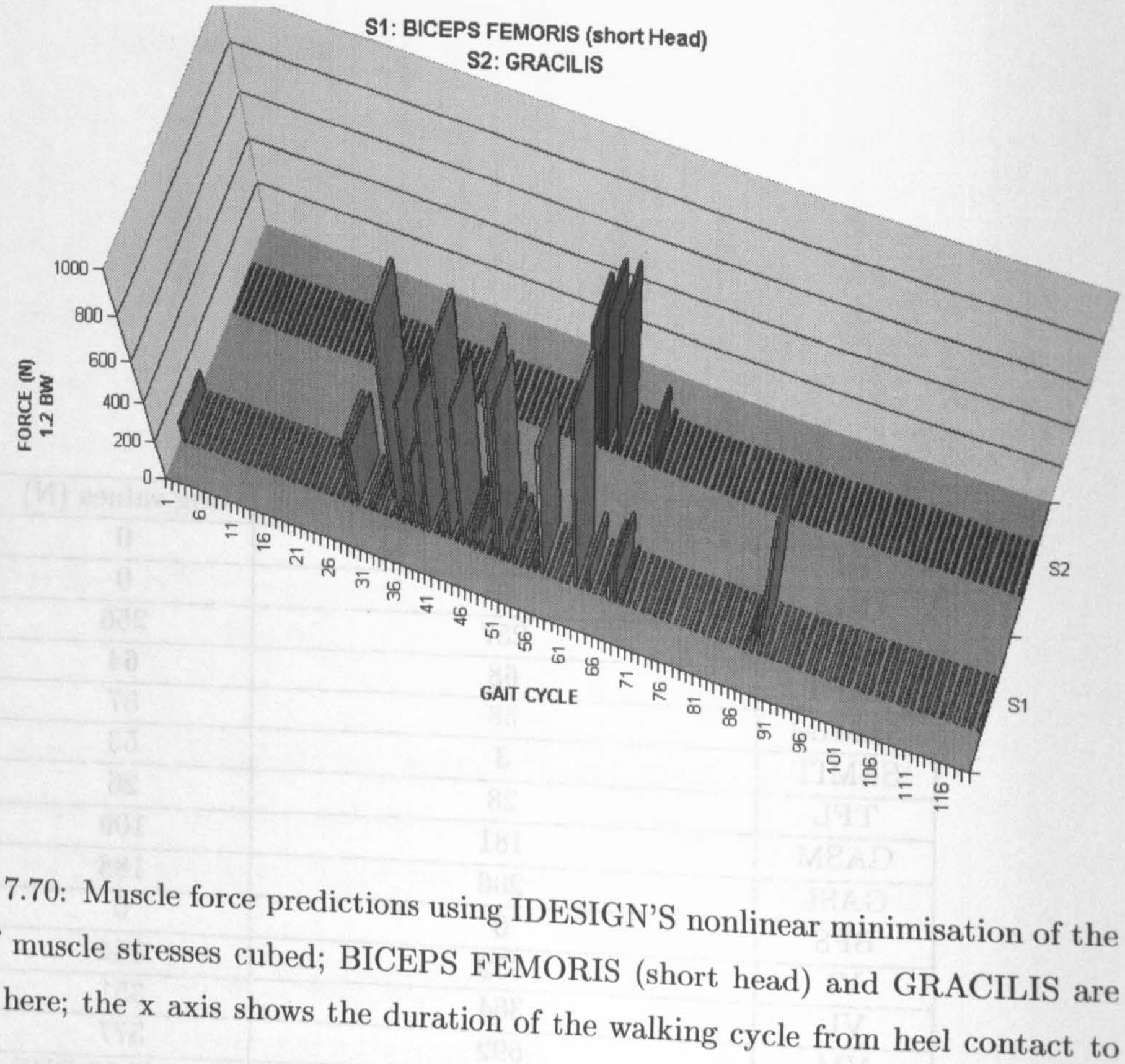

Figure 7.70: Muscle force predictions using IDESIGN'S nonlinear minimisation of the sum of muscle stresses cubed; BICEPS FEMORIS (short head) and GRACILIS are shown here; the x axis shows the duration of the walking cycle from heel contact to toe-off.

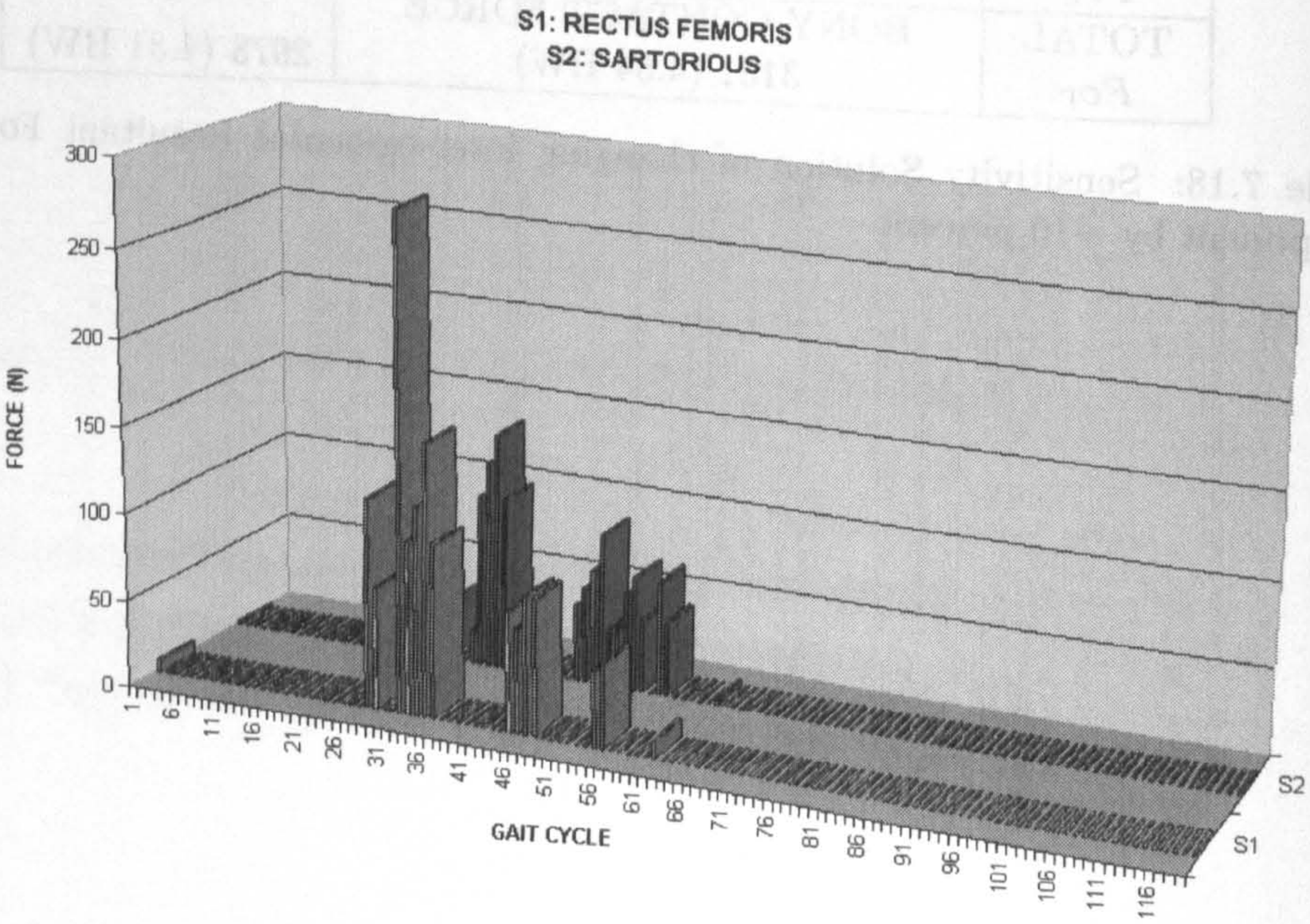

Figure 7.71: Muscle force predictions using IDESIGN'S nonlinear minimisation of the sum of muscle stresses cubed; RECTUS FEMORIS and SARTORIOUS are shown here; the x axis shows the duration of the walking cycle from heel contact to toe-off.

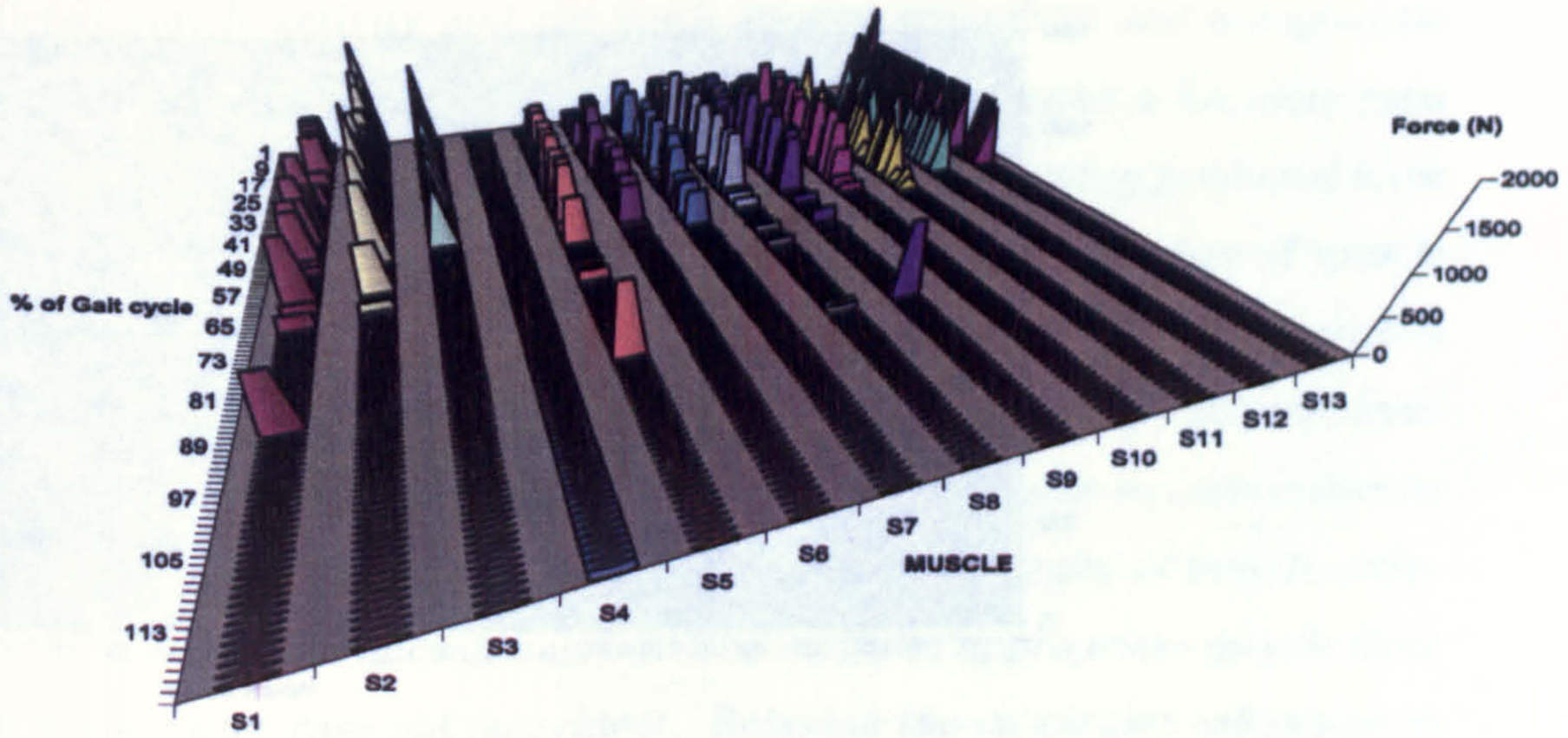

Figure 7.72: Muscle force predictions using IDESIGN'S linear minimisation of the sum of muscle stresses; from left to right x axis shows the 13 divisions corresponding to the 13 muscles described as knee muscles in chapter 7.2.2; the z axis shows the duration of the walking cycle from heel contact to toe-off.

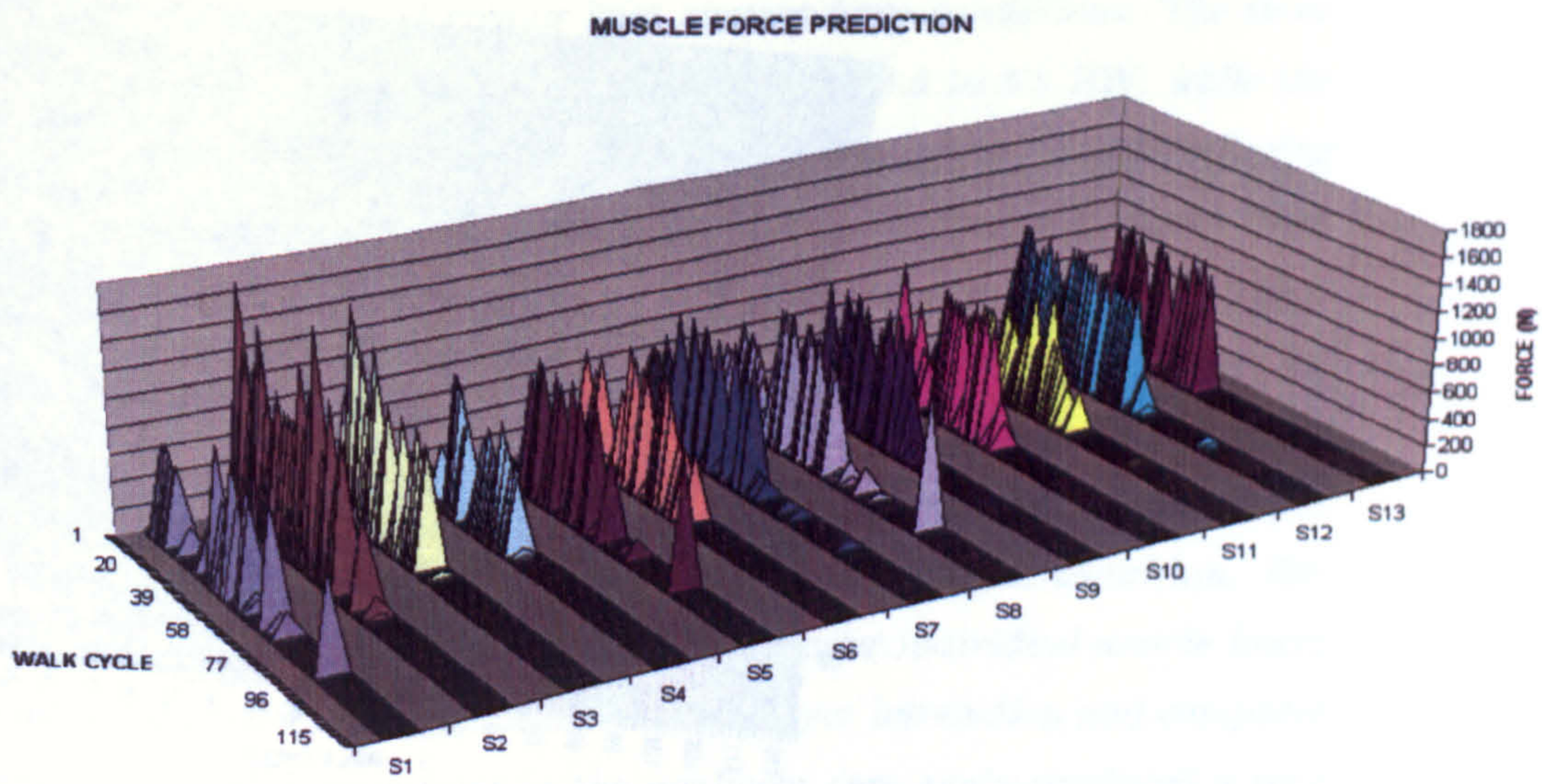

Figure 7.73: Muscle force predictions using IDESIGN'S linear minimisation of the sum of muscle forces with relaxed equality constraints; from left to right x axis shows the 13 divisions corresponding to the 13 muscles described as knee muscles in chapter 7.2.2; the z axis shows the duration of the walking cycle from heel contact to toe-off.

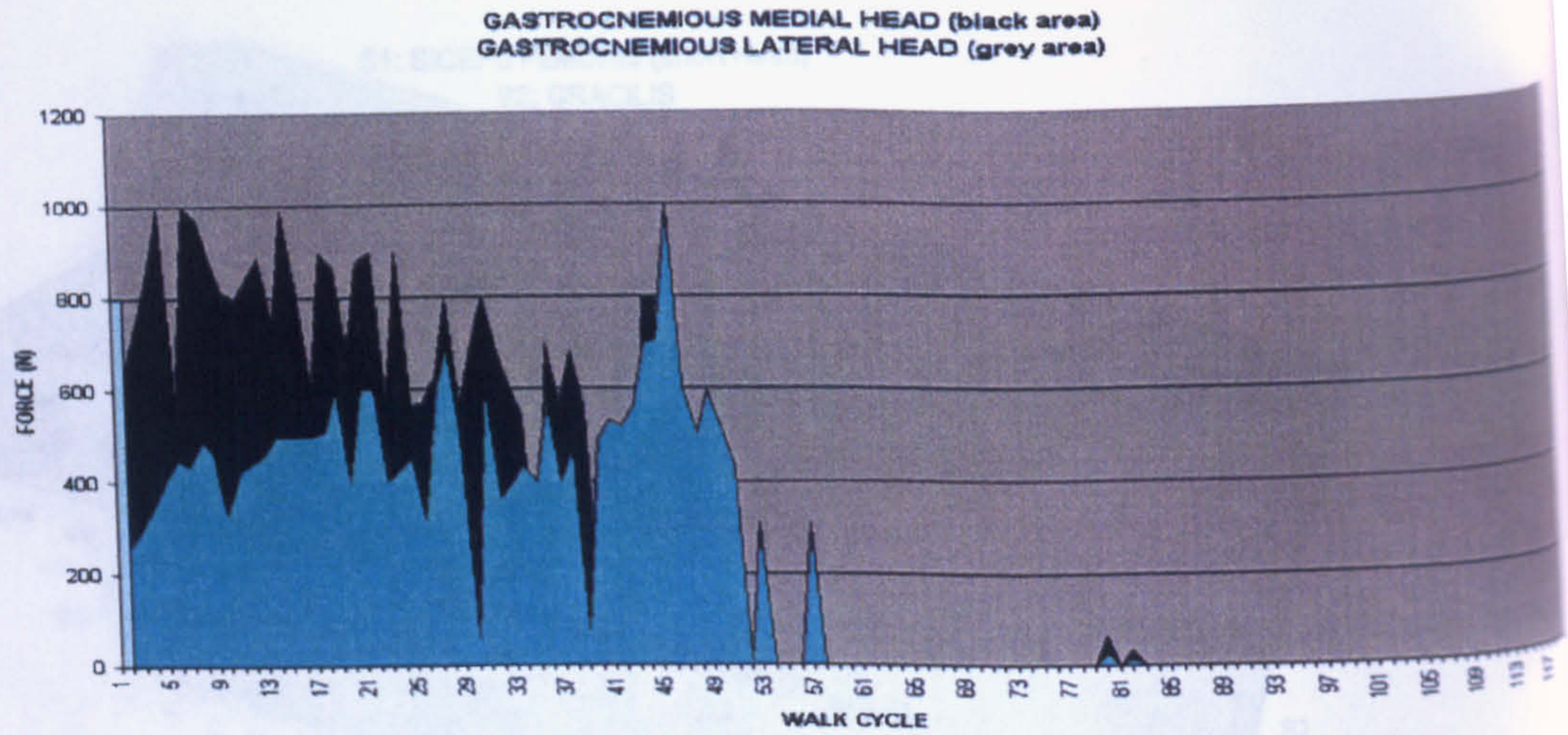

Figure 7.74: Muscle force predictions using IDESIGN'S nonlinear minimisation of the sum of muscle stresses cubed; Gastrocnemius medial head and Gastrocnemius lateral head are shown here; the x axis shows the duration of the walking cycle from heel contact to toe-off.

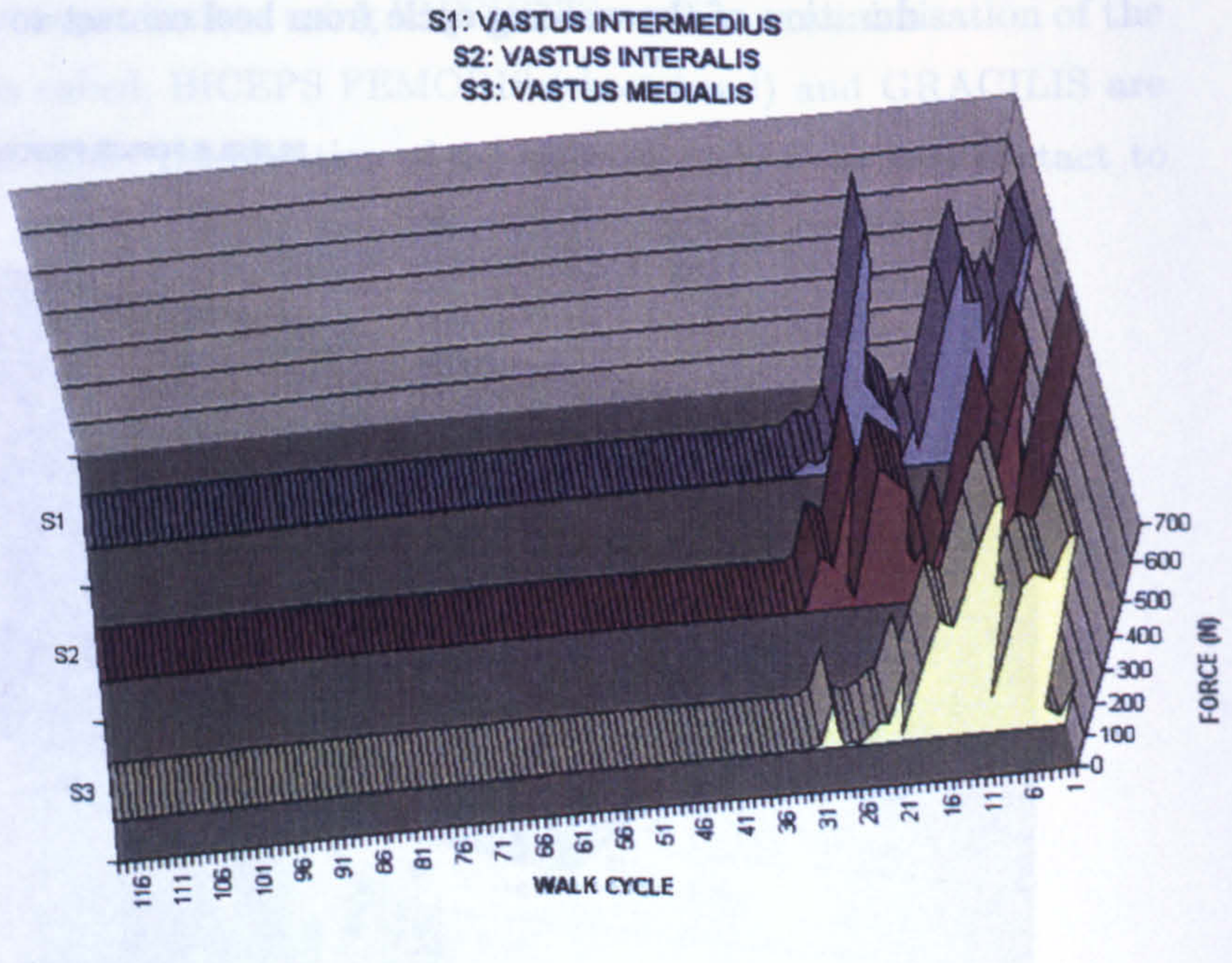

Figure 7.75: Muscle force predictions using IDESIGN'S nonlinear minimisation of the sum of muscle stresses cubed; Vastus intermedius, Vastus interalis and Vastus medialis are shown here; the x axis shows the duration of the walking cycle from heel contact to toe-off.

The most important though somewhat expected finding was the sparseness of linearly predicted muscle activity and the much greater synergistic and antagonistic activity predicted with nonlinear techniques. In the linear examples a lot more gaps appear in the discrete time with as much as only three muscles having predicted force of appropriate magnitude. The nonlinear method solution of summation of muscle forces (a linear otimisation criterion) (FIGURE 7.78 on page 213) grossly mimicked the linear method solution (FIGURE 7.72 on page 208). It allowed but did not force more active muscles into the solution. Comparing the sum of muscle stresses cubed to the sum of muscle stresses shows that there is an improved continuity of muscle activity. The phenomenon of rapid fluctuations between zero and appropriate muscle force predictions is in the latter case not so evident. Relaxing the constraint tolerances in the muscle stresses cubed case predicted smoother transitions through levels of muscular activity and eased predicted antagonistic behaviour. Qualitatively, the nonlinear schemes produced better correlation between EMG and predicted muscle force than did the linear schemes. The nonlinear schemes produced not only more muscle activity, but also greater active concurrence of EMG activity. Active concurrence averaged 32, 36 and 42 percent for the three linear cases while the nonlinear techniques averaged 32, 60 and 55 percent. Correlating with increased muscle activity predictions, the nonlinear techniques produced greater joint contact force predictions. The three linear techniques produced peak joint force predictions of 3.5 to 3.8 BW, while the three nonlinear criteria resulted in predictions ranging from 4.9 to 5.4 BW. Altering the constraint tolerance slightly affected both the muscle and the joint contact force solution. The requirement of muscles to satisfy 99.999 percent of the intersegmetal resultant moment components in the first case where one can use the cost summation of forces with Constraint tolerance 0.001 percent and linear algorithm to an acceptable range of 99 to 101 percent in the second case where we used the cost summation of forces with a constraint tolerance of 1.0 percent and again a linear algorithm. Expanding the constraint limits produced a set of very similar individual muscle forces with the beneficial side-effect of significantly reducing user interaction and computer time. Relaxing the equality constraint in the nonlinear case again produced a very similar muscle force solution but modestly reduced the predicted knee joint force.

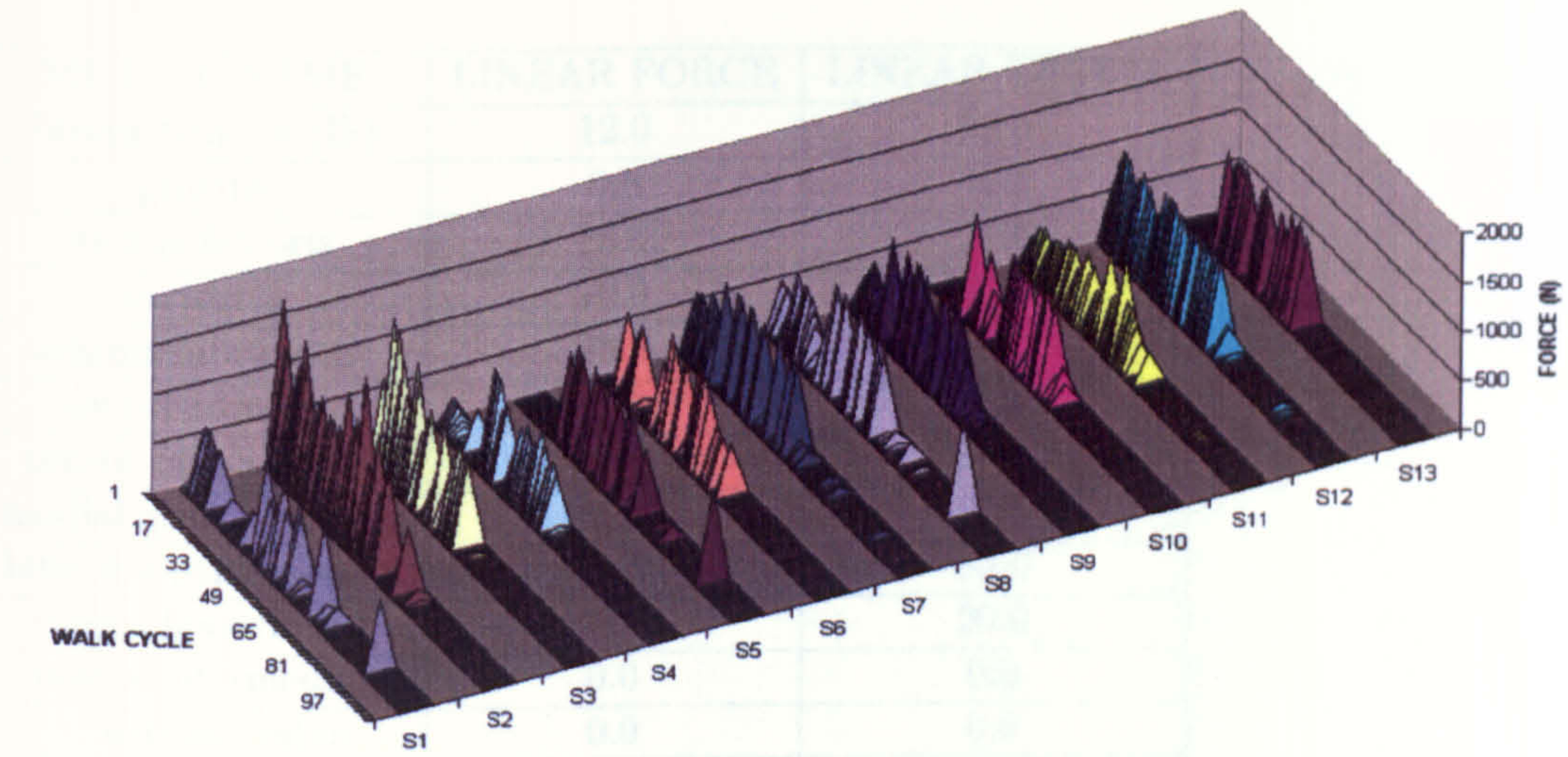

Figure 7.76: Muscle force predictions using IDESIGN'S nonlinear minimisation of the sum of muscle stresses cubed; from left to right x axis shows the 13 divisions corresponding to the 13 muscles described as knee muscles in chapter 7.2.2; the z axis shows the duration of the walking cycle from heel contact to toe-off.

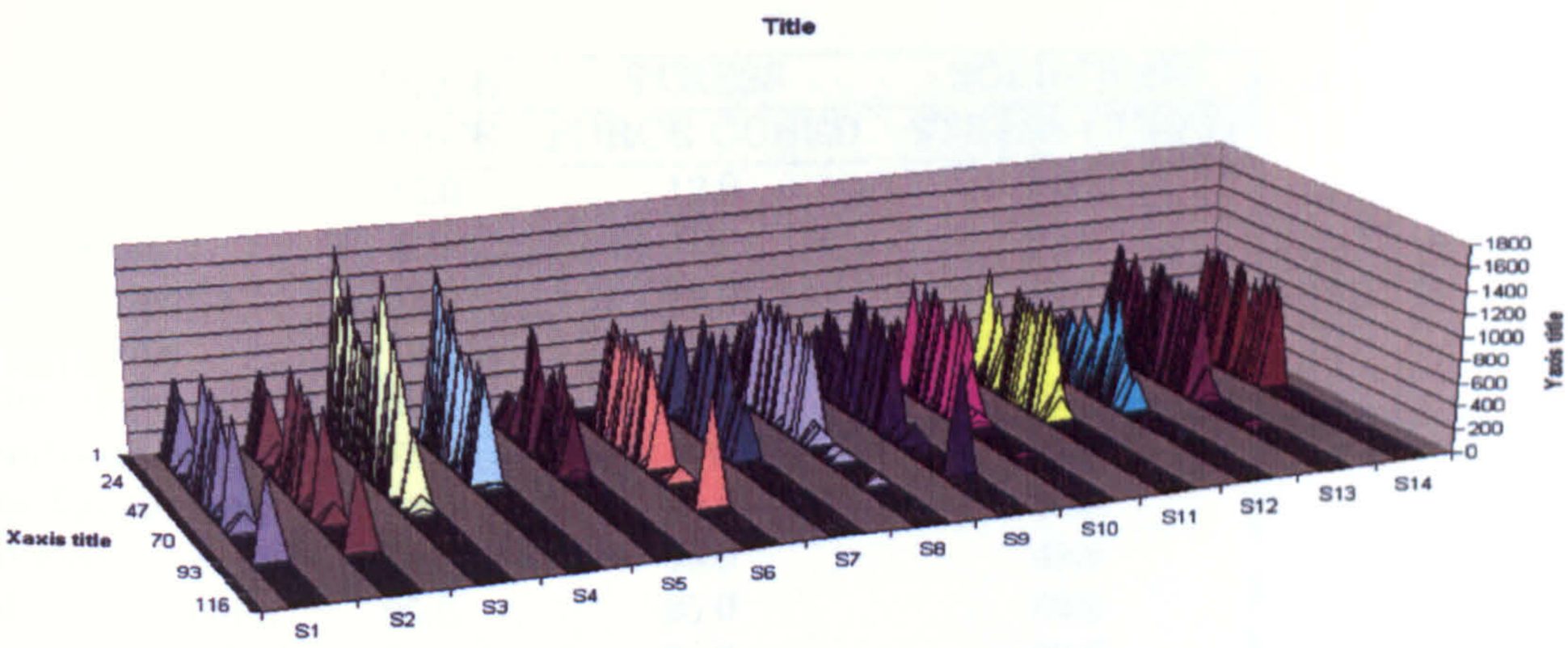

Figure 7.77: Muscle force predictions using IDESIGN'S nonlinear minimisation of the sum of muscle stresses cubed with relaxed equality constraints; from left to right x axis shows the 13 divisions corresponding to the 13 muscles described as knee muscles in chapter 7.2.2; the z axis shows the duration of the walking cycle from heel contact to toe-off.

MUSCLE NAME	LINEAR FORCE	LINEAR STRESS
biceps femoris (lh)	12.0	12.0
gracilis	0.0	0.0
rectus femoris	25.0	22.0
sartorius	70.0	0.0
semimembranosus	28.0	36.0
semitendinosus	0.0	0.0
tensor fasciae latae	80.0	80.0
medial gastrocnemius	65.0	62.0
lateral gastrocnemius	95.0	95.0
biceps femoris(sh)	20.0	20.0
vastus intermedius	0.0	0.0
vastus lateralus	0.0	0.0
vastus medialus	65.0	65.0

Table 7.19: Active concurrence of EMG and muscle force predictions:LINEAR SOLUTIONS

NONLINEAR	FORCE	STRESS	SOLUTIONS
MUSCLE	FORCE	FORCE CUBED	STRESS CUBED
biceps femoris (lh)	12.0	12.0	35.0
gracilis	0.0	0.0	0.0
rectus femoris	32.0	19.0	32.0
sartorius	70.0	100.0	0.0
semimembranosus	28.0	28.0	38.0
semitendinosus	0.0	0.0	0.0
tensor fasciae latae	80.0	80.0	80.0
medial gastrocnemius	65.0	65.0	45.0
lateral gastrocnemius	95.0	95.0	80.0
biceps femoris(sh)	20.0	20.0	20.0
vastus intermedius	0.0	20.0	10.0
vastus lateralus	0.0	5.0	0.0
vastus medialus	65.0	70.0	85.0

Table 7.20: Active concurrence of EMG and muscle force predictions:NONLINEAR SOLUTIONS

MUSCLE NAME	LINEAR FORCE	STRESS CUBED
biceps femoris (lh)	12.0	30.0
gracilis	0.0	0.0
rectus femoris	25.0	32.0
sartorius	70.0	0.0
semimembranosus	28.0	40.0
semitendinosus	0.0	0.0
tensor fasciae latae	80.0	80.0
medial gastrocnemius	65.0	32.0
lateral gastrocnemius	95.0	85.0
biceps femoris(sh)	20.0	20.0
vastus intermedius	0.0	10.0
vastus lateralus	0.0	0.0
vastus medialus	65.0	65.0

Table 7.21: Active concurrence of EMG and muscle force predictions:RELAXED CONSTRAINTS SOLUTIONS

MUSCLE NAME	LINEAR FORCE	LINEAR STRESS
biceps femoris (lh)	77.0	63.0
gracilis	100.0	100.0
rectus femoris	100.0	94.0
sartorius	83.0	100.0
semimembranosus	71.0	60.0
semitendinosus	100.0	100.0
tensor fasciae latae	60.0	49.0
medial gastrocnemius	100.0	100.0
lateral gastrocnemius	94.0	94.0
biceps femoris(sh)	31.0	55.0
vastus intermedius	100.0	100.0
vastus lateralus	100.0	100.0
vastus medialus	80.0	77.0

Table 7.22: Inactive concurrence of EMG and muscle force predictions:LINEAR SOLUTIONS

NONLINEAR	FORCE	STRESS	SOLUTIONS
MUSCLE	FORCE	FORCE CUBED	STRESS CUBED
biceps femoris (lh)	80.0	54.0	36.0
gracilis	100.0	100.0	100.0
rectus femoris	95.0	68.0	53.0
sartorius	87.0	67.0	82.0
semimembranosus	71.0	65.0	40.0
semitendinosus	100.0	63.0	92.0
tensor fasciae latae	60.0	58.0	66.0
medial gastrocnemius	91.0	86.0	89.0
lateral gastrocnemius	92.0	78.0	94.0
biceps femoris(sh)	28.0	8.0	31.0
vastus intermedius	100.0	92.0	100.0
vastus lateralus	93.0	84.0	92.0
vastus medialus	86.0	61.0	69.0

Table 7.23: Inactive concurrence of EMG and muscle force predictions:NONLINEAR SOLUTIONS

MUSCLE NAME	LINEAR FORCE	STRESS CUBED
biceps femoris (lh)	76.0	30.0
gracilis	100.0	100.0
rectus femoris	100.0	52.0
sartorius	82.0	90.0
semimembranosus	71.0	46.0
semitendinosus	100.0	87.
tensor fasciae latae	60.0	66.0
medial gastrocnemius	100.0	89.0
lateral gastrocnemius	94.0	96.0
biceps femoris(sh)	31.0	31.0
vastus intermedius	100.0	100.0
vastus lateralus	100.0	87.0
vastus medialus	80.0	69.0

Table 7.24: Inactive concurrence of EMG and muscle force predictions:RELAXED CONSTRAINTS SOLUTIONS

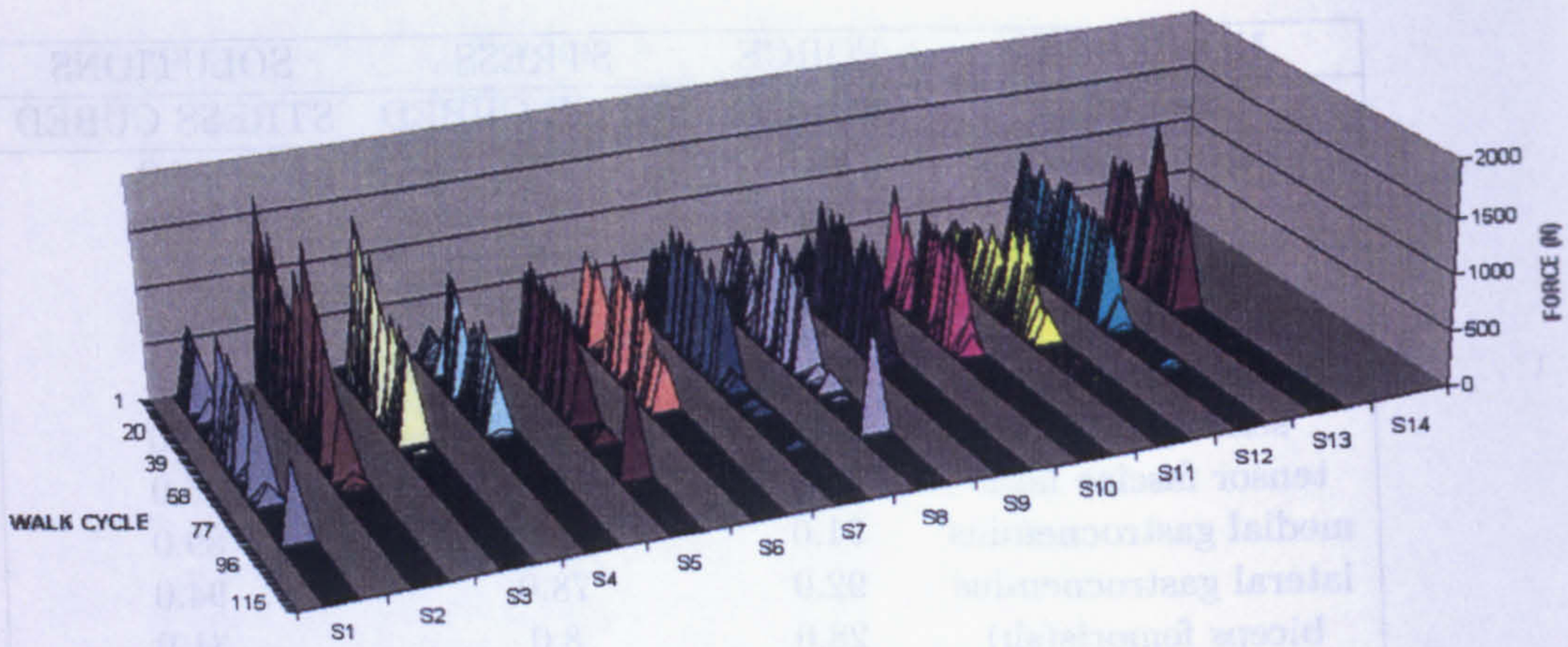

Figure 7.78: Muscle force predictions using IDESIGN'S nonlinear minimisation of the sum of muscle forces;from left to right x axis shows the 13 divisions corresponding to the 13 muscles described as knee muscles in chapter 7.2.2; the z axis shows the duration of the walking cycle from heel contact to toe-off.

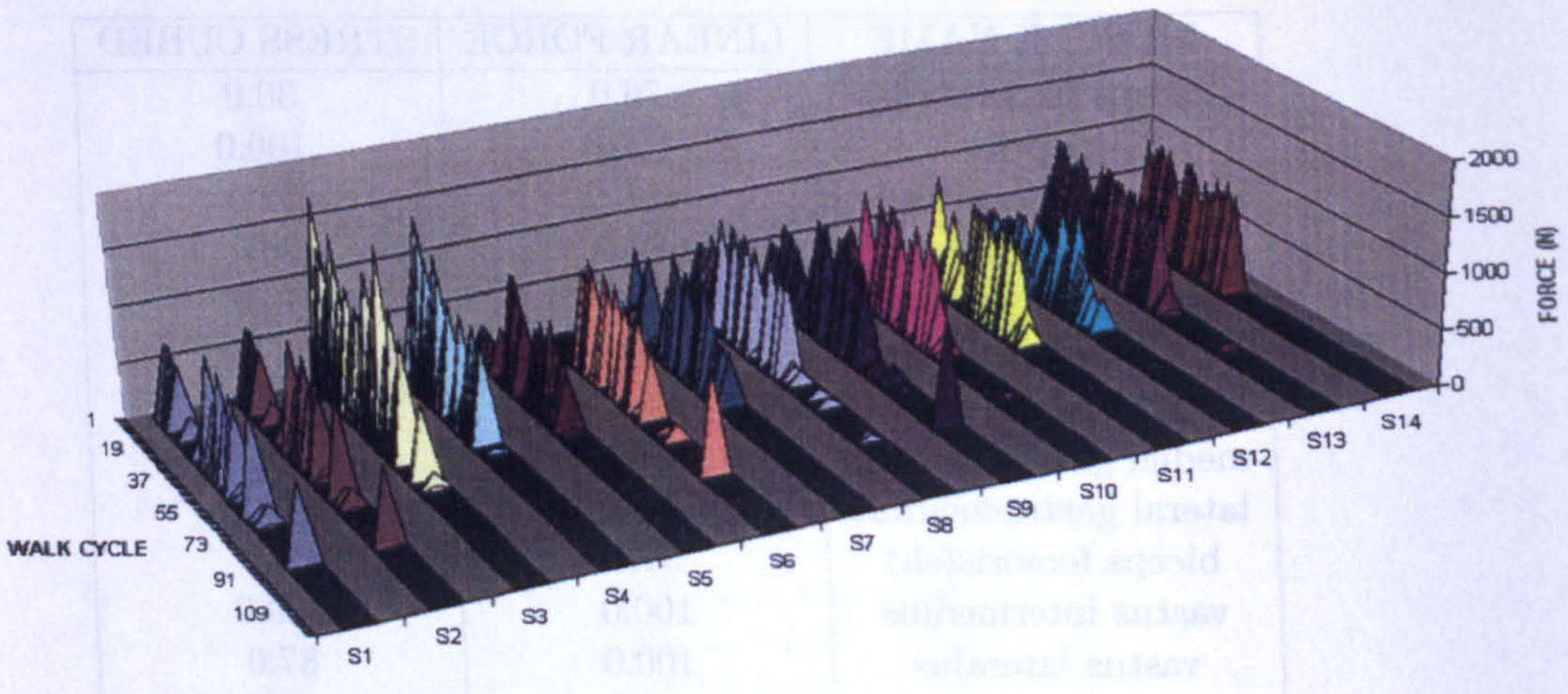

Figure 7.79: Muscle force predictions using IDESIGN'S nonlinear minimisation of the sum of muscle forces cubed; from left to right x axis shows the 13 divisions corresponding to the 13 muscles described as knee muscles in chapter 7.2.2; the z axis shows the duration of the walking cycle from heel contact to toe-off.

Blank Page

Chapter 8

DISCUSSION AND CONCLUSION

8.1 CONCLUSIONS ON THE EXPERIMENTAL DATA

An estimation of the variability within and between subjects (N=18) according to the effect of variables like speed, footwear on the kinetic and kinematic patterns of walking requires detailed project design and control of many parameters. In the present study it was obvious that the patterns and the magnitude of forces and particularly of moments in the three joints (Hip, Knee, Ankle) vary with speed. Another type of differences was observed when the variable became the type of footwear and variability was particularly obvious in the temporal gait characteristics. In general the three different speeds (fast speed, N= normal speed, S= slow speed-in (72%) of the different parameter combinations) had a significantly different effect (at level of 0.0001) on the forces and moments of all three major joints (HIP, KNEE, ANKLE). In all cases the barefoot trial presents a more vertical initial force when compared to the rest of the trials with footwear on (Pedotti diagrams), the latter revealing smaller initial peak values. One in three variables (the variables being the three different joint paramenters-forces, moments, angles- for both lower limbs) is affected (increased in magnitude up to three fold) by fast speed alone. One third is also affected by slow speed (only significantly different with the other trials-no characteristic increase in magnitude).

Subjects walking with the oxford shoes on, had an increase in the magnitude in

27% of their different lower limb forces and moments.

Oxford shoes increase Fx force and walking barefooted increases Mx moment of all subjects. The lower limb motion was more increased in magnitude during normal walking (50%) and less during the fast and slow trials. Normal walking increases extensively abduction-adduction and flexion-extension angles of all joints when compared with fast walking which seems to affect more the inversion-eversion angles. The barefoot trial increased the 45% of the different joint angles of both legs with oxford increasing a 33% and boots only a 18% of the total motion parameters. The oxford trial increases the inversion-eversion angles whereas the barefoot affects mainly the adduction-abduction and flexion-extension angles of all joints. It is also important to note that the trials with boots and athletic shoes on increase mainly the flexion-extension angles of all joints.

It is important to stress the the Fy forces show significant variation with speed (fast speed always increases magnitude) for all joints and all subjects whereas there is a left to right lower limb asymmetry in the nature of that influence. As seen in the results the slow speed differs from the normal and fast trials for the force and moments components of the right limb to a greater extend (in 77% of the cases where the three speeds were different) than that of the left limb (in 66% of the cases where the three speeds were different). It is obvious from the subjects that were analyzed in detail for their data input to the 3D models that left to right asymmetries in lower limb anatomy occur frequently. In all subjects the knee moment components are more affected than the knee force components. The Fx force component is affected by speed for all joints, a fact that is not reproduced for all the rest force and moment components.

Eighty percent of the forces and moments of different joints of both lower limbs have been affected by footwear. Also with footwear the forces are more affected than the moments but there is no asymmetry in the influence of the FOOTWEAR on the left and right leg respectively. The Oxfort shoes trial is significantly different from the trial with boots for the 89% of the cases,and 62% different from the barefoot trial whereas the barefoot trial itself and the athletic shoes trial do not significantly differ from the rest of the shoes in a very small amount of the cases.

The effect of footwear on joint angle is more evident (88.8% of the cases) for both lower limbs. The barefoot trial is significantly different from all the rest at the 33.3% of the cases and equal to the oxford shoes trial at the 22.2% of the cases. The rest of

trials affected the parameters in question to a smaller extend.
The complete interaction analysis with respect to joint angles showed that for the 83.3 percent of the interactions between speed and footwear reveled in the ANOVA there is significant difference between at least one variable (force, moment, angle of joint) and the other variables (type of footwear). Variability is met for percentages ranging between 15% and 30% of the cases for all the types of footwear. It can be seen that the interaction is not so evident for the left knee where the individual ANOVAS showed that the tendencies at the slow, normal and fast trial are reproduced for all angles in a similar fashion. No interaction is observed at all for most of the right lower limb combinations. For the left lower limb 66 percent of the cases present some interaction with most of the variables showing significant differences with each other. Knee and ankle Fx seem to have shown the greatest variability. The right barefoot trial for fast walking is always significantly different from the other trials for all joints. It can be concluded that the interaction effects of footwear and speed on joint forces, moments and joint angles differ according to joint and leg.

8.2 Discussion of Model Algorithm

The modelling approach presented here is an effort to strengthen the traditional modelling techniques with new aspects of problem formulation, numerical solutions and state of the art optimization and visualization tools. Our main effort to determine two bony contact forces at the knee joint was assisted by: a) The advanced three dimensional visualization protocols adopted for the present application (OpenGL, SIMM, AVS, ShowCase). These applications enhanced the efficiency of the accumulation and processing of the model input data. A three dimensional digitiser scaled the three dimensional mesh of polygons that produced the bone surfaces of the subjects-participants. The muscle and ligament insertion and origins as well as their wrapping constrains were therefore efficiently corrected with the help of the above visualization tools. The computer platforms that supported the work were designed to enhance user friendly interfaces. The interface allows all the different parts of the model's geometry to be implemented and checked for errors (e.g. muscle wrapping) by even a novice user of computer interfacing thus producing a bridging with the educational importance of modelling for students and the clinical environment. In addition the approach allows for efficiency in working time when one considers the complexity of

the data input that can make the clinical evaluation and clinical use of the model very laborious.

b) The combination of two state of the art Optimization Algorithms (IDESIGN and OPTIMUS). Enhancement of the optimization related work with additional implementation of file managing subroutines, user-friendly interfaces with drug and drop applications that allows novice users of optimization to learn quickly and efficiently the process of problem formulation in Optimum control. The present formulation takes care of the tedious work of file preparation, submission of simulation runs, extracting data from output files and file book-keeping. The user defines the Design Inputs used for the simulations and the set of values for all Design Inputs for each simulation. Furthermore, the user defines which Design Outputs to extract from the simulation output files.The algorithm will then automatically prepare all the simulator input files, launch all the simulation runs, extract all the Design Outputs, and so do all the file house-keeping by tagging all the input and output files with a run number, also cleaning-up files which are not needed.

c) The increased information content of the simulation runs. We used Design of Experiments techniques (DOE) to get the maximum amount of information out of the simulation runs while minimizing the number of runs. The theory of DOE is well-developed and its concerns are being used in many fields of engineering, interested with cost-effective experimentation. The same concepts apply to simulation runs as well. While traditionally one control parameter (factor) is changed at a time, from one experiment (run) to the next, a DOE approach changes all control parameters at the same time.

Although this way of experimenting seems awkward, because the insights from the data obtained this way are not immediately apparent to normal thought, it has been proven that it contains much more information than the traditional approach.

d) The data needed to be post-processed in order to get access to the above information. The post-processing is done by creating approximate, analytical, models of each Design Output as a function of all Design Inputs. These approximate models are called Response Surface Models (RSM). The DOE and RSM techniques reduce drastically the number of simulation runs, allow quantification of how the Design Inputs influence the Design Outputs, detect correlated Design Outputs and predict Design Output values for untried Design Input values.

e) Non-Linear programming (NLP) techniques to optimize a process control. The

user defines the objective function to be minimized or maximized. This objective function can be a Design Output, but can also be a function consisting of many Design Outputs and Design Inputs. Furthermore, the user defines the constrains on Design Inputs and Design Outputs. The design outputs are either the direct result of a simulation run, or are predicted using a Response Surface Model. Using NLP techniques in combination with response surface models provides a powerful and rapid way to explore several approximating optimal solutions, which then gives an ideal starting point for doing optimization using the more expensive but more accurate methods often included in simulation tools. Mathematically, the nonlinear cost functions used in our formulation depend on the muscle stresses cubed and bony contact forces cubed, and the ligament stresses with different exponents. Since the design variables (i.e., muscle forces, ligament forces and bony contact forces) are all non-negative, the matrix of second derivatives of the cost function is positive semidefinite. In other words, the cost function is convex. Furthermore, the constraint functions are linear and convex. This means these optimization problems are convex, and that a local minimum is the global minimum. However, the global minimum need not lead to a unique solution set of muscle, ligament and bony contact forces (Arora [1989]). A large number of studies using optimization neglects the above very laborious but very crucial pre-calculation of the mathematical definition of Optimum control producing solutions related to local instead of global minima.

In the knee distribution problem, the bony contact forces are difficult to determine with confidence due to the indeterminacy. The necessary assumptions associated either with the reduction or optimization methods, while different, make the results obtained by either method questionable. The new approach presented here combines the optimization method and a determinate model with an iterative procedure to estimate the two bony contact forces and the forces present in the knee muscles and ligaments during human gait. The ligament forces computed from the determinate model strongly depend on the ligament spring constants and strains. Unfortunately, the literature contains limited experimental data on these spring constants and strains as a function of the flexion-extension angle. Approximations of these data, based on the results of Brantigan et al. [1941] and of Trent et al. [1976] were therefore used. The spring ligament forces were generated from this rough data. As mentioned in

Chapter 9, predicted muscle and bony contact force distributions are very sensitive to changes in the forces determined using this spring ligament model. The ligament forces obtained using optimization models depend on geometric considerations (force components and moment arms), on the optimization criterion selected and on the external loads. In contrast, the ligament forces obtained using the spring model depend on the spring constants chosen and on the strains in the ligaments as well as again on the external loads. These differences are the reasons for the distinct ligament force distributions obtained from KNEE2 and SECOND.

Another limitation of SECOND is that the six scalar equilibrium equations do not uniquely determine the two vector bony contact forces (with 3 scalar components each). This unanticipated result led to the assumption that the bony contact forces act normal to the tibial plateau. As a result, there were only two unknown bony contact force components (i.e., no force components exist in the x and z-directions). Thus only two of the six equilibrium equations were used in SECOND as discussed earlier. This algorithm using optimization models combined with a determinate model is then dependent on the formulation of the determinate model. Since different simplifying assumptions for the bony contact forces in abbreviated versions of the determinate model will involve certain errors from "neglected" equilibrium conditions, further development of the determinate model is warranted.

Additionally, one ought to be sceptical with regard to the practice of using EMG patterns to qualitatively validate muscle force predictions Spaepen et al. [1997]. Since the relationship between muscle force and EMG is unknown during dynamic conditions, EMG cannot currently be used as a quantitative validation tool, but it is of some value to validate muscle force predictions (i.e., is the muscle active or is it inactive during a given period of time?). However, even determining when the EMG signal is active or inactive can not be straightforward and a compromise of some more or less arbitrary criterion must be established to distinguish noise from "true" signal. Several authors establish a threshold -in the present study 20 percent of the peak- for the muscle in question for a range of activities. Note though that different thresholds would predict different concurrence. EMG is also sensitive to walking speed, but ensembled-averaged signals will to some extent "average out" these differences when a single activity is considered. Yang and Winter, showed that "the method of normalisation affects the apparent intersubject variability and that normilisation by the "peak of the within-subject ensemble average" of Dynamic EMG (i.e., not the maximum vol-

untary contraction) resulted in the lowest variability (Yang et al. [1984]). Predictions are more appropriate for a limited number of muscles, usually the large muscles that produce good surface EMG. Up to eight (possibly ten) EMG channels is the norm in gait studies. Comparing EMG activity and force predictions on a limited number of large, superficial muscles, seems to be in good agreement with linear predictions, since those mathematical techniques preferentially predict activity in precisely those muscles. For prediction of deeper and smaller muscles linear methodologies become less valid. A high inactive concurrence is probably of less importance in evaluating the relative merits of several optimization schemes than a high active concurrence. Evaluating active concurrence suggests a critical way to evaluate various schemes which qualitatively appear to be reasonable. This is due to the fact that optimization must not only predict force for EMG on periods but also predict no activity for the EMG-off periods. The latter case (EMG-off) is true for most of the muscles for the whole duration of gait cycle. Inactive concurrence is more likely to validate any scheme that predicts no activity (due to the optimization design or some physiological rationale or both). Antagonistic activity is certainly maximized with nonlinear programming techniques. Since muscle activity generates most of the joint force in a weight bearing joint, linear programming techniques will create a lower bound solution. That suggests that irrelevantly of whether the solution is physiologically reasonable or not linear approaches will predict low joint force solutions consistent with the moment constrains. The latter is not the case with nonlinear techniques which allow not only synergistic activity but also antagonistic muscle activity (without however any explicit rationale used by the neuromuscular system which is unknown). In the present study the model with the implementation of muscle wrapping information and the fully three dimensional approach demonstrates that muscles have not only a primary function (e.g., an extensor) but may also have secondary functions (e.g., adductor, internal rotator). A primary muscle function is always sidelined by some muscle antagonistic activity which is required to balance any secondary function. The more muscle activity as in the above "antagonistic" formulation the less chance of bringing the joint force solution to a lower bound solution. Higher joint force solutions and solution continuity with the use of nonlinear approach illustrate it clearly in the present work. It is not assumed here that antagonistic activity occurs only because of the requirement to satisfy a moment, as suggested with the present model formulation. Instead, one can suggest that nonlinear programming allows for such activity when such rationale

becomes clear.

Relaxation of constraint tolerance has an effect on the muscle force solutions Patriarco et al. [1981]. We did not manage to support this in the present analysis since the above changes had a small effect on the force solutions. This might be due to the particular formulation, since there was no effect on the joint force prediction in the linear case.

The problem of convergence has been tackled by the use of new tools from the theory of optimization on the one hand and by the use of new problem formulation to shape the optimization inquire by criteria chosen independently from the optimization criteria themselves (e.g. Ligament non-linear spring models). Similarly whole muscle models (Hill type active and passive actuators) can also be used in a formulation like the present alongside the ligament models for similar purposes. In this case convergence will be assisted by a combination of forward and inverse analyses with the user being able to check the progress of the calculation at different parts of the gait cycle changing and manipulating the different parameters during the pathway to optimum.

8.3 Recommendations for future study

As previously mentioned, the ligament and muscle properties (insertions, origins and cross-sectional areas), and the bony contact locations were from different studies in the literature. Also, the assumption of the bony contact forces being perpendicular to the tibial plateau reduces the number of the equilibrium conditions used in the determinate model from six to two. Furthermore, the ligament spring properties can significantly affect the determinate model, as shown by the final solutions reported in Chapter 9. Therefore, to improve this model, the muscle and ligament insertions/origins, bony contact force locations/directions, and material properties of the ligaments (spring properties) all need to be determined carefully from the same specimens. Once systematically obtained geometric and material data are available, the model algorithm can be improved by changing the determinate model to include five equilibrium equations, or adding one equation (assumption) to the determinate model (e.g., $Fc11 = Fc21$). In addition, an appropriate validation procedure needs to be correspondingly developed to verify the solutions. The present work tried to blend software coming from different platforms and was used before at various in-

compatible applications. A heavily versatile Library of OPTIMIZATION algorithms (IDESIGN) is combining data coming out of inverse analysis algorithms implemented on VAX environments (now rewritten to be used with UNIX systems) and everything is analysed on an IRIX 6.2 operating system (a UNIX offspring) and visualized with the help of OPENGL and INVENTOR MENTOR based applications. The attempt is finally functional but required an endless debugging procedure. The high end IRIX 6.2 operating system on a R10000 processor reduced drastically the "waiting" between the runs.

The model and algorithm could be applied to several problems:

(a) The modeling of deformities and their correction. Proximal tibial osteotomy is a relatively common method of redistributing compressive forces in degenerative genu varus and valgus. Although most investigators recommend correction of the deformity so that the weight-bearing line passes through the centre or slightly to the unaffected side of the articulation, they do not relate the amount of correction to the magnitude of force change. Because the purpose of tibial osteotomy is to alter the distribution of compressive force on the tibial plateau, it is reasonable to base the amount of correction on force redistribution.

(b) Computations of force distributions during running and other activities. The human knee is composed of bone, cartilage, muscle and other soft tissue structures. These structures function as elements in a dynamic system, and will respond to external demands. Their role depends upon a number of mechanical and physiological factors including muscle activity and tonus, joint flexion angle, tonic reflex contributions and weight distribution. It is of interest to study the dynamic response of the force distribution at the knee, with emphasis on the relationship between leg dynamics and injuries.

(c) Evaluating the effect of inaccurate positioning of condylar prostheses. The reasons for prosthesis loosening are not completely understood at the present time. This model, given more realistic geometry and material property input, can predict the effects of inaccurate positioning of the condylar prosthesis on the contact force experienced by the prosthesis. Information of this nature may help to delineate the role of contact pressures on prosthesis loosening.

(d) Computations of bony contact stresses during recreational and occupational activities (e.g., running). As mentioned in (b), the structures at the knee function as elements in a dynamic system, and thus respond to external demands. This model, if

combined with finite element techniques and using an appropriate cost function (e.g., minimizing the sum of the potential energy and kinetic energy), could be used to estimate the bony contact stresses during during such activities.

8.4 Conclusions

This study reported a new algorithm combining optimization models with a determinate model to uniquely predict the two compartmental bony contact forces and the muscle forces at the knee during human gait. One should not imply that one or more of the formulations presented here are ideal. In the complexity of a system like the human knee one ought to search for the possible, not the ideal. One must emphasize that a unified approach offers the potential to explore a greater variety of optimisation formulations and the potential for a more reasonably validated solution, given the reality of many active muscles.

The knee distribution problem is a highly indeterminate problem. Optimization techniques using various optimization criteria will generate different solutions. Although the present model algorithm has certain and definite limitations, the solutions of the algorithm provides additional information dependent not simply upon the choice of a specific optimization criterion. This provides a new method to solve indeterminate distribution problems. The advances in new computer technology have certainly advanced experimental biomechanics but had no direct impact in the clinical field to date. Vast improvements in sheer numerical processing power were to be added in our attempt to model the lower limb based on enhanced graphics display capabilities of the new computer technology. The graphics technology in particular has been benefited enormously from the explosion of interest in the technology of immersive virtual environment systems. We combined biomechanical mathematical models, computer processing power and the computer graphics technologies to produce interactive, computer-based graphical simulations of the musculoskeletal system. The clinician can use very robust, fast (some times 800% faster than in the past) and user friendly (X-windows based) algorithms to run advanced optimization problems with high degree of convergence. The algorithms have internal intelligent formulations to provide the user with suggestions for avoiding designs that will not converge, therefore enhancing the optimum control design procedure. At the end of the calculation the visualization tools allow the user to visualize the results with state of the art

computer-based graphical simulations.

The following conclusions appear warranted.

1. This study predicts maximum bony contact forces at the knee during human gait from subject 1 (whose full detailed geometry input was available) that are 1.25 times body weight on the lateral tibial plateau and 3.06 times body weight on the medial tibial plateau. The total bony contact force is then 4.31 times body weight. Scaling of the full 3d model of subject 1 allowed repeat the calculation for four more subjects. The maximum bony contact forces estimated during human gait from all the above subjects (five including subject 1) were on average 1.48 (SD:0.22 BW) times body weight on the lateral tibial plateau and 3.91 (SD: 0.62 BW) times body weight on the medial tibial plateau. The total average of five subjects bony contact force was 5.4 times body weight with a standard deviation of 0.82 BW. This is consistent with the values predicted by other researchers. Morrison [1968] reported a maximum bony contact force during level walking in the range of two to three times body weight (BW). The average maximum value of the bony contact force for 12 subjects was 3.03 BW, with the greater portion of this force being transmitted by the medial condyle. The forces acting on the joint in the medio-lateral direction were generally small (e.g., 0.26 BW).

2. The different intrasubject runs (eight runs with different external input data-different gait sessions) affected neither the rate of convergence nor the active concurrence, that is the agreement of the EMG profiles with the magnitude of the predicted muscle force, in other words the muscle convergence.

3. The resultant ratio of the lateral bony contact force to the medial bony contact force is 1:2.5. Anatomically, the tibia plateau is almost symmetric, with the area of the medial tibia plateau slightly greater than the area of the lateral. The plateau are each formed from two smooth concave surfaces located laterally and medially. The medial plateau is bi-concave in shape an is longer in the anterior-posterior direction than the lateral plateau. In contrast, the lateral plateau is saddle-shaped, more circular and broader than the medial plateau. In general, the medial plateau is larger than the lateral and consequently is thought to bear more. Therefore, the medial bony contact force being greater than the lateral bony contact force is not surprising.

4. The corresponding muscle force distributions showed activity in ten muscles (SART, GASM, GASL, SEMIT, SEMIM, TFL, VL, VI, VM and RF). These findings are consistent with the EMG records reported by Andriacchi et al. [1984] and Spaepen

et al. [1997].

5. Sensitivity analyses show that the mathematical model is quite sensitive to muscle insertion and origin locations, to locations of bony contact forces, and to ligament forces calculated by the nonlinear spring model of SECOND, but insensitive to cross-sectional areas of muscles and ligaments, and to the intersegmental resultant force and moment.

6. The nonlinear techniques improved continuity of predicted muscular activity, a clearly more physiological situation since whole muscle action is not simply and rapidly turned off and on (as in the case of posing multiple discrete optimisation problems at various times). Especially considering the nonlinear nature of most physiological parameters (e.g., the relationship between contraction velocity and muscle force), nonlinear optimisation allows greater flexibility in incorporating varius muscle and/or ligament models as more and more of such models become available to implement into optimisation.

The rate of convergence for muscle prediction was enhanced in the intersubject variability study. Design of experiments (DOE) and Response Surface Models (RSM) allowed a reduction of the computation time of about 400 % once we run the intra-subject variability study and earned some experience in interpretation of DOE and RSM increasing the clinical applicability of such formulations.

Despite certain assumptions in the model (i.e., regarding menisci, joint friction, geometric data, material properties, external loadings, etc.), two compartment bony contact forces may be uniquely calculated. In order to improve upon the present model these uncertainties and assumptions must be removed through more fundamental anatomical studies and through experiments dealing with joint loading.

Bibliography

Abdel-Rahman, E., and Hefzy M.S. "A 2D Dynamic Anatomic Model of the Human Knee Joint". Journal of Biomechanical Engineering, Trans. of the ASME, *115(4): 357–365, 1993.*

Ahmed, A.M., and Burke D.L. "In-Vitro Measurment of Static Pressure Distribution in Synovial Joints -Part 1:Tibial Surface of the Knee: ". Journal of Biomechanical Engineering, Transactions of the ASME, *105:216–225, 1983.*

M.H.S. Al-Turaiki. "The Human Knee ". First Published in Saudi Arabia Edition, *1986.*

Alexander, R.McN., and Vernon A. "The Dimensions of Knee and Ankle muscles and the Forces they Exert". Journal of Human Movement Sciences, *1:115–123, 1975.*

An, K.n., Himeno, S., Tsumura, H., Kawai, T., and Chao E.Y.S. "Pressure Distribution on Articular Surfaces:Application to Joint Stability Evaluation ". Journal of Biomechanics, *23(10):1013–1020, 1990.*

An, K.N., Kwak, B.M., Chao, E.Y.S., and Morrey B.F. "Determination of Muscle and Joint Forces: A New Technique to solve the Indeterminate Problem ". ASME, Journal of Biomechanical Engineering, *106:364–367, 1984a.*

An, K.N., Takahashi, K., Harrigan, T.P., and Chao E.Y.S. "Determination of Muscle Orientation and Moment Ams ". Journal of Biomechanical Engineering, *106:280–282, 1984b.*

J.E. Anderson. Grant's Atlas of Anatomy. *William Wilkins and Baltimore and Maryland, 8th edition, 1983.*

J.G. Andrews. "*On the Relationship Between Resultant Joint Torques and Muscular Activity* ". Medicine and Science in Sports and Excercise, *14:361–367, 1982.*

Andriacchi, T.P., Andersson, G.B.J., Ortengren, R., and Mikosz R.P. "*A study of Factors Influencing Muscle Activity About the Knee Joint* ". Journal of Orthopaedic Research, *1:266–275, 1984.*

Andriacchi, T.P., Mikosz, R.P., Hampton, S.J., and Galante J.O. "*Model Studies of the Stiffness Characteristics of the Human Knee Joint* ". Journal of Biomechanics, *16:23–29, 1983.*

Areblad, M., Nigg, B.M., Ekstrand, J., Olsson, K.O., and Ekstrom H. "*Three-Dimensional Measurement of Rearfoot motion During Running* ". Journal of Biomechanics, *23:933–940, 1990.*

G.B. Ariel. " *Biomechanics of athletic shoe design* ". Biomechanics V-B, *pages 361–367, 1976.*

Arora, J.S., E., Atrek, R.H., Gallagher, K.M., Ragsdell, and O.C. Zienkiewicz. "An Algorithm for Optimum Structural Design Without Line Search , Chapter 20,New Directions in Optimum Structural Design". *John Wiley and Sons Co. N.Y., 1984.*

J.S. Arora. "Introduction to Optimum Design". *John Wiley and Sons Co. N.Y., 1989.*

R.M. Aspden. "*Model for the Function and Failure of the Meniscus* ". Engineering in Medicine, *199:119–122, 1985.*

Audu, M.L., and Davy D.T. "*A Comparison of Optimal Control Algorithms for Complex Bioengineering studies*". Optimal Control Applications and Methods, *9: 101–106, 1988.*

Baer, T., and Braham R. "*Shoes and shocks* ". Soma, *April issue:39-43, 1986.*

J.C. Barbenel. "*The Biomechanics of the Temperomandibular Joint : A Theoretical Study* ". Journal of Biomechanics, *5:251–256, 1972.*

Bates, B.T., James, S.L., Osterning, L.R., and Sawhill J.A. "*The effects of running shoes on ground reaction forces* ". Biomechanics VI-B, *pages 226-233, 1981.*

Bates, B.T., Simpson, K.J., and Panzer V. P. "*The evaluation of subject, shoe and movement variability* ". Biomechanics X-B, *pages 909–912, 1987.*

B.T. Bates. "Testing and evaluation of running shoes ". Biomechanics IX-B, pages 128–132, 1985.

H. Behncke. "Otimisation Models for the Force and Energy in Competitive Sports ". Mathematical Methods in Applied Sciences, 9:298–311, 1987.

Bingham, D.N., Weinstein, A.M., Klawitter, J.J., and Cooke F.W. "Mechanical Characterisation of the Anterior Cruciate Ligament ". Orthopaedic Research Society, 8 (14), 1976.

Blankevoort, L., Huisces, R., and de Lange A. Advances in Bioengineering. R.L. Spilker ,ASME, WAM New Orleans LA,, 1984.

Blankevoort, L., Huiskes, R., de, and Lange A. "The Envelope of Passive Knee Joint Motion ". Journal of Biomechanics, 21:705–720, 1988.

Blankevoort, L., Kuiper, J.H., Huiskes, R., and Grootenboer H.J. "Articular Contact in a 3D Model of the Knee ". Journal of Biomechanics, 24(11):1019–1031, 1991a.

Blankevoort, L., and Huiskes R. " Ligament-Bond Interaction in a Three-Dimensional Model of the Knee ". Journal of Biomechanichal Engineering and Transactions of the ASME, 113:263– 269, 1991b.

L. Blankevoort. " Recruiment of Knee Joint Ligaments ". Journal of Biomechanical Engineering-Transactions of the ASME, 113:94–103, 1991.

Bonnel, F., and Michaleff J-P. "Biomechanics of the Ligament of the Human Knee and of Artificial Ligaments ". Surg and Radiol. Anat., 10:221–227, 1988.

Brand, R.A., Crowninshield, R.D., Wittstock, C.E., Pedersen, D.R., Clark, C.R., and vanKrieken F.M. "A model of lower extremity muscular anatomy". Journal of Biomechanical Engineering, 104(4):304–310, 1982.

Brand, R.A., Peterson, D.R., and Friederich. "The sensitivity of muscle force predictions to changes in physiologic cross-sectional area ". Journal of Biomechanics, 19: 589–596, 1986.

R.A. Brand. "PERSONAL COMMUNICATION ". MUSCLE INSERTION AND ORIGIN DATA, Lower limbs:15, 1992.

Brantigan, O.C., and Voshell A.F. "The Mechanisms of the Ligaments and Menisci of the Knee Joint ". Journal of Bone and Joint Surgery, *23:44-66, 1941.*

Bresler, B., and Frankel J.P. "The Forces and Moments in the Leg during Level Walking ". Trans. Am. Soc. Mech. Engrs., *72:27, 1950.*

Brown, T.D., and Shaw D.T. "In Vitro Contact Stress Distribution on the Femoral Condyles ". Journal of Orthopaedic Research, *2:190-199, 1984.*

Bullogh, P.G., Munuera, L., Murphy, J., and Weinstein A.M. "The Strength of Meniski of the Knee as it Relates to Fine Structure ". Journal of Bone and Joint Surgery, *52-B:564-570, 1970.*

Butler, D.L., Kay, M.D., and Stouffer D.C. "Comparison of Material Properties in Fascile-Bone Units from Human pattelar Tendon and Knee Ligaments ". Journal of Biomechanics, *19:425-432, 1986.*

Cappozzo, A., Gazzani, F., and Macellari V. "Skin artifacts in gait analysis ". Journal of Biomechanics, *23b(4):363, 1988.*

A. Cappozzo. "Gait Analysis Methothology ". Human Movement Science, *3:27-50, 1984.*

Cavanagh, P., and Gregor R. "The knee joint torque during the swing phase of normal treadmill walking ". Journal of Biomechanics, *8:337-344, 1975.*

P.R. Cavanagh. "Current approaches and problems and and future direction in shoe evaluation techniques ". Biomechanics IX-B, *pages 123-12, 1985.*

Chand, R., Haug, E., and Rim K. "Stresses in the Human Knee Joint ". Journal of Biomechanics, *9:417-422, 1976.*

Chao, E.Y.S., and K.N. An. "Graphical Interpretation of the Solution to the Redundant Problem in Biomechanics ". ASME, Journal of Biomechanical Engineering, *100:159-167, 1978.*

Chao, E.Y.S., Lynch, J.D., and Vanderploeg M.J. "Simulation and Animation of Musculosketal Joint System ". Journal of Biomechanical Engineering Trans. of the ASME, *115(4):562-568, 1993.*

Chao, E.Y.S., Opgrande, J.D., and Axmear F.E. "Three-Dimensional Force Analysis of Finger Joints in Selected Isometric Hand Functions ". Journal of Biomechanics, 9:387–396, 1976.

Chao, E.Y.S., and Kwan Rim. "Application of Optimisation Principles in determining the Applied Moments in Human Leg Joints During Gait". Journal of Biomechanics, 6:497–510, 1973.

E.Y.S. Chao. "Justification on Triaxial Goniometer for the Measurment of Joint Rotation ". Journal of Biomechanics, 13:989–1006, 1980.

Chen, H.C., Ashton-Miller, J.A., Alexander, N.B., and Schultz A.B. "Stepping over obstacles:gait patterns of Healthy young and old adults". Journal of Gerontology, 46(46):196–203, 1991.

D.T. Chen. "Pump it Up: Computer Animation of a Biomechanically Based Model of Muscle Using the Finite Element Method". *PhD thesis, Massachusetts Institute of Technology, 1993.*

Chou, L., Draganich, L.F., and Song S. "Minimum Energy Trajectories of the Swing Ankle when Stepping over Obstacles of Different Heights". Journal of Biomechanics, *30(2):115–120, 1997.*

Chou, L., Song, S., and Draganich L.F. "Predicting Kinematics and Kinetics of Gait based on the Optimum Trajectory of the Swing Limb". Journal of Biomechanics, *28:377–385, 1995.*

Chow, C.K., and Jacobson D.H. "Studies of Human Locomotion via Optimal Programming". Mathematical Biosciences, *10:239–306, 1971.*

Cohen, J., and Cohen P. "Applied Multiple Regression/Correlation Analysis for the Behavioral Sciences ". *John Wiley and Sons Co., New York, 1975.*

Cole, G.K., Nigg, B.M., and Ronsky J.L. "Application of the Joint Coordinate Sustem to Three Dimensional Joint Attitute and movement Representation: A Standardization Proposal ". Journal of Biomechanical Engineering, Trans. of the ASME, *115:344–349, 1993.*

R.A. Cooper. "A Force/energy optimisation model for wheelchair athletic". IEEE Trans. Systems, Man, Cybernet, *20:444–449, 1990.*

Crowninshield, R., Pope, M.H., and Johnson R.J. "An Analytical Model of the Knee ". Journal of Biomechanics, *9:397–405, 1976.*

Crowninshield, R.D., and Brand R.A. "The Prediction of Forces in Joint Structures Distribution of Intersegmental Resultants: Editor D.I. Miller ". In Excercise and Sports Sciences Reviews, The Franklin Institute Press, *9:159–181, 1981.*

R.D Crowninshield. "Use of Optimization Techniques to Predict Muscle Forces ". Journal of Biomechanical Engineering, *100:88–92, 1978.*

Crownshield, R.D., Johnston, R.C., Andrews, J.G., and Brand R.A. "A Biomechanical Investigation of the Human Hip ". Journal of Biomechanics, *11:75–85, 1978.*

Crownshield, R.D., and Brand R.A. "A Physiologically Based Criterion of Muscle Force prediction in Locomotion ". Journal of Biomechanics, *14:793–801, 1981.*

Davis, III, R.B., Ounpuu, S., Tyburski, D., and Gage J.R. "A Gait Analysis Data Collection and Reduction Technique ". Human Movement Science, *10:575–587, 1991.*

Davy, D.T., and Audu M.L. "A Dynamic Optimization technique for predicting muscle forces in the swing phase of gait". Journal of Biomechanics, *20(2):187–201, 1987.*

Delange, A., VanDijk, R., Huiskes, R., Selvik, G., and VanRens Th.J.G. "The Applications of Roentgenstereophotogrammetry for Evaluation of Knee joint Kinematics in-vitro, Editor:Huiskes, Martinus Nijhoff ". Biomechanics: Principles and Applications, The Hague, Boston. London, *1:177–184, 1982.*

Delp, S.L., Arnold, A.S., Speers, R.A., and Moore C.A. "Hamstrings and Psoas Lengths During Normal and Grouch Gait:Implications for Muscle-Tendon Surgery ". The Journal of Bone and Joint Surgery, *14:144–151, 1996a.*

Delp, S.L., Loan, and J.P. "SIMM VISUALISATION EXCHANGE DATA ". PERSONAL COMMUNICATION, *1:1–3, 1996b.*

Delp, S.L., Loan, J.P., Hoy, M.G., Zajac, F.E., Topp, E.L., and Rosen J.M. "Force and Moment-Generating Capacity of Lower-Extremity Muscles before and After Tendon Lengthening". Clinical Orthopaedics, *284:247–259, 1992.*

Delp, S.L., P.J., Loan, M.G., Hoy, F.E., Zajac, F.E., Topp, and E.L. Rosen. "An interactive graphics-based model of the lower extremity to study orthopaedic surgical procedures". IEEE Transactions on Biomedical Engineering, *37(11):757–767, 1990.*

Delp, S.L., Statler, K., and Carrol N.C. " Preserving Plantar Flexion Strength After Surgical Treatment for Contracture of the Triceps Surae:A Computer Simulation Study". The Journal of Bone and Joint Surgery, *13:96–104, 1994.*

Delp, S.L., and Maloney W. "Effects of Hip Center Location on the Moment Generating Capacity of the Muscles". Journal of Biomechanics, *26:485–499, 1993.*

Denham, R.A., and Bishop R.E.D. "Mechanics of the Knee and Problems in Reconstractive Surgery ". Journal of Bone and Joint Surgery, *60-B(3):345–352, 1978.*

L.C. Detenbeck. "Function of the Cruciate Ligaments in the Knee Stability ". Journal of Sports Medicine, *2:4, 1974.*

Dons, B., Bollerup, K., Bonde-Petersen, F., and Hancke S. "The Effect of Weight-Lifting Exercise Related to Muscle Fiber Composition and Muscle Cross-Sectional Area in Humans ". European Journal of Applied Physiology, *40:95–106, 1979.*

Drillis, R., and Contini R. " Body segment parameters. Technical report No.116603 ". New York University and School of Engineering and Science, University Heights, New York N.Y. 10453, *1966.*

Duke, R.P., Somerset, J.H., Blacharski, P., and Murray D.G. "Some Investigations of the Accuracy of Knee Joint Kinematics ". Journal of Biomechanics, *10:659-673, 1977.*

Dul, J., Johnson, G.E., Shiavi, R., and Townsend M.A. "Muscular Synergism-I. A criteria for Load Sharing between Synergestic muscles". Journal of Biomechanics, *17:675–684, 1984a.*

Dul, J., Shiavi, R., and Green N.E. "Simulation of Tendon Transfer Surgery ". Engineering Mechanics, *14:31–38, 1985.*

Dul, J.and Townsend, M.A., Shiavi, R., and Johnson G.E. "Muscular Synergism-II. A Fatique Criterion for Load Sharing between Synergestic muscles". Journal of Biomechanics, *17:675–684, 1984b.*

Edgerton, V.R., Roy, R.R., Gregor, R.J., and Rugg S. "Morphological Basis of Skeletal Muscle Power Output ". IN HUMAN MUSCLE POWER, JONES, N. L., MCCARTHNEY, N., MC COMAS, A. J., EDS. HUMAN KINETICS PUBLISHERS INC., ILLINOIS, *4:43–64, 1987.*

Edwards, R.G., Lafferty, J.F, and Lange K.O. "Ligament Strain in the Human Knee Joint ". Journal of Basic Engineering, *92:131–136, 1970.*

Engin, A.E, and Korde M.S. "Biomechanics of Normal and Abnormal Knee Joint ". Journal of Biomechanics, *7:325–334, 1974.*

Ensberg, J.R., Grimston, S.K., and Wackwitz J.H. "Predicting Talocalcaneal Joint Attitutes from Talocalcaneal/Talocrunal Joint Attitutes ". Journal of Orthopedic Research, *6:749–757, 1988.*

Essinger, J.R., Leyvraz, P.F., Heegard, J.H., and Robertson D. "A mathematical Model foe the Evaluation of the Behavior during Flexion of Condylar-Type Knee Prosthesis ". Journal of Biomechanics, *22(11/12):1229–1241, 1989.*

P. Evans. "The Knee Joint; A Clinical Guide ". *Churchill Livingstone, 1986.*

Faro, TM, Medical, Technologies, and Inc. "Genucom Instruction Manual". Faro (TM) Medical Technologies Inc.,, *1986.*

R. Fick. Handbuch der Anatomie und Mechanik der Gelenke. *Fisher and Jena, 1911.*

Freeman, M.A.R., Swanson, S.A.V., and Manley P.T. "Stress-Lowering Function of Articular Cartilage ". Med. Biol. Eng., *13:245–251, 1975.*

Friederich, J.A., and Brand R.A. "Muscle fiber architecture in the Human lower limb ". Journal of Biomechanics, *23:91–95, 1990.*

Fu, F.H., Harner, C.D., Johnson, D.L., Miller, M.D., and Woo S.L.Y. "Biomechanics of the Knee Ligaments - Basic Concepts and Clinical Applications ". Journal of Bone and Joint Surgery - American volume, *75(11):1716–1727, 1993.*

Fukubayashi, T., and Kurosawa H. "The Contact Area and Pressure Distribution Pattern of the Knee ". Acta Orthopaedica Scandinavica, *51:871–879, 1980.*

Gage, J.R., and Ounpuu S. "Surgical intervention in the correction of primary and secontary gait abnormalities ". Patla A.E. editor: Adaptability of Human Gait ;North Holland: Elsevier Science Publishers B.V., *pages 359–385, 1991.*

Garg, A., and Walker P.S. "Prediction of Total Knee Motion Using a 3D Computer. Graphics Model ". Journal of Biornechanics, *23(1):45–58, 1990.*

Girgis, F.G, Marshall, J.L, , and Monajem A.R.S. "The Cruciate Ligaments of the Knee Joint. Anatomical and Functional and Experimental Analysis ". Clinical Orthopaedics, *106:216–220, 1975.*

Goh, C.J., and Teo K.L. "Control Parametrization: A Unified Approach to Optimal Control Problems with General Constrains". Automatica, *24(1):3–18, 1988.*

H. Gray. "Gray's Anatomy". London,EDITION: Magpie Books Limited, *pages 450–580, 1993.*

Grood, E.S., and Hefzy M.S. "An Analytical Technique for Modelling Knee Joint Stiffness - Part I: Ligamentous Forces ". ASME Journal of Biomechanical Engineering, *104:330–337, 1982.*

Grood, E.S., Noyes, F.R, Butler, D.L., and Suntay W.J. "Ligamentous and Capsular Restraints Preventing Medial and Lateral Laxity in Intact Human Cadavers Knees ". Journal of Bone and Joint Surgery, *63(8):1257–1269, 1981.*

Grood, E.S., and Suntay W.J. "A Joint Coordinate Sytem for the Clinical Description of Three Dimensional Motions: Application to the Knee ". Journal of Biomechanical Engineering, Transactions of the ASME, *105:136–144, 1983.*

Gross, R.M., and Chao E.Y. Quantitative analysis of forearm musculature. In Proceedings of the 29th Annual Conference of Engineering in Medicine and Biology, *pages 18–47, 1976.*

Grosse-Lordeman, H., and Muller E.A. "Der Einfluss der Leistung und der Arbeitsgeschwindigkeit auf das Arbeitsmaximum und der Wirkungsgrad beim radfahren ". Arbeitsphysiologie and 9:454-475., *9:454–475, 1937.*

T. Gunnar. "Assessment of Physical Capabilities ". Acta. Physiol. Scand., *58:5–102, 1963.*

Gupta, B.N., Brinker, W.O, and Subramanian K.N. "Breaking Strength of Cruciate Ligaments in the Dog ". JAMA, *155(10):1586–1588, 1969.*

D.E. Hardt. "Determining Muscle Forces in the Leg during Normal Human Walking- An application and evaluation of Optimisation methods". Transactions of the ASME, *100:72–78, 1978.*

I. J. Harrington. "A bioengineering analysis of force actions at the knee in normal and parhological knee ". Biomedical engineering, *May:167–172, 1976.*

I.J. Harrington. "Static and Dynamic Loading Patterns in Knee Joints with Deformities ". Journal of Bone and Joint Surgery, *65A:247–259, 1983.*

Harrison, D.W., and Nicol A.C. "Knee Joint Loads during running and Turning activities". Internal Report: Bioengineering Unit, University of Strathclyde, *1: 13–18, 1990.*

Hatze, H., and Venter A. "Practical Activation and Retention of Locomotion in Neuromusculoskeletal Control System Models". Journal of Biomechanics, *14(12): 873–877, 1981.*

H. Hatze. "The complete Optimization of a Human Motion ". Mathematical Biosciences, *28:99–135, 1976.*

H. Hatze. "A General Myocybernetic Control Model of Skeletal Muscle ". Biological Cybernetics, *28:143–157, 1978.*

H. Hatze. "A Teleological Explanation of Weber's Law and the Motor Unit Size Law". Bulletin of Mathematical Biology, *41:407–425, 1979.*

H. Hatze. "Neuromuscular Control Systems Modelling- A Critical Survey of Recent Developments ". IEEE Transactions on Automatic Control, *AC-25(3):375 385, 1980.*

H. Hatze. "A Comprehensive Model for human Motion Simulation and its Application to the Take-off Phase of the Long Jump". Journal of Biomechanics, *14(3):135 142, 1981a.*

H. Hatze. "Analysis of Stretch Responses of a Myocybernetic Model Muscle Fibre ". Biological Cybernetics, *39:165–170, 1981b.*

H. Hatze. "*Estimation of Myodynamic Parameter Values from Observations on Isometrically Contracting Muscle Groups* ". European Journal of Applied Physiology, *46:325–338, 1981c.*

H. Hatze. "*The use of Optimally Regularized Fourier Series for Estimating Higher-Order Derivatives of Noisy Biomechanical Data*". Journal of Biomechanics, *14: 13–18, 1981d.*

H. Hatze. "*Computerized Optimisation of Sports Motions: An overview of Possibilities, Methods and Recent Developments*". Journal of Sport Sciences, *1:3-12, 1983.*

H. Hatze. "*Comments on A DYNAMIC OPTIMIZATION TECHNIQUE FOR PREDICTING MUSCLE FORCES IN THE SWING PHASE OF GAIT by D.T. Davy and M.L. Audu, and General trends in contemporary muscle modelling*". Journal of Biomechanics, *21:888–891, 1988.*

H. Hatze. "*The Extended Transentropy Function as a useful Quantifier of Human Motion Variability*". Medicine and Science in Sports and exercise, *27(5):751–759, 1995.*

Hefzy, M.S., and Grood E.S. "*An Analytical Technique for Modelling Knee Joint Stiffness - Part II: Geometrical Non-Linearities* ". Journal of Biomechanical Engineering - Transactions of the ASME, *105:145–153, 1983.*

Hefzy, M.S., and Yang H. "*A 3D Anatomical Model of the Human Patello-Femoral Joint for the Determination of Patello-Femoral Motions and Contact Characteristics* ". Journal of Biomechanical Engineering and Trans. of the ASME, *115(4):289, 1993.*

Hefzy, M.S., and Zoghi M. "*The Meniscus: A Finite Element Model* ". Transactions of the 34th Orthopaedic Research Society, *page 149, 1988.*

Hermiston, R.T., and Bonde-Petersen F. "*The Influence of Varying Oxygen Tensions in Inspired Gas on Xenon Muscle Clearance and Fatigue Levels During Sustained and Dynamic Contractions* ". Journal of Applied Physiology, *34:291–302, 1975.*

Hof, A.L., Geelen, B.A., Vanden, and Berg J. "*Calf muscle moment, work and efficiency in level walking; role of series elasticity* ". Journal of Biomechanics, *16(7), 1983.*

Hof, A.L., Pronk, C.N., and Best J.A. "Comparison between EMG to force processing and kinetic analysis for the calf muscle moment in walking and stepping ". Journal of Biomechanics, *20(2), 1987.*

Hof, A.L., Vanden, and Berg J. "EMG to force processing I: An electrical analogue of the Hill muscle model". Journal of Biomechanics, *14(11), 1981a.*

Hof, A.L., Vanden, and Berg J. "EMG to force processing II: estimation of parameters of Hill muscle model for the human triceps surae by means of a calfergometer. ". Journal of Biomechanics, *14:747–770, 1981b.*

Hof, A.L., Vanden, and Berg J. "EMG to force processing III: Estimation of model parameters for the human triceps surae muscle and assessment of the accuracy by means of a torque plate ". Journal of Biomechanics, *14(11), 1981c.*

Hof, A.L., Vanden, and Berg J. "EMG to force processing IV: Eccentric-concentric contractions on a spring-flywheel set up ". Journal of Biomechanics, *14(11), 1981d.*

A.L. Hof. "Errors in frequency parameters of EMG power spectra ". IEEE Transactions of Biomedical Engineering, *38(11), 1991.*

Hoy, M.G., Zajac, F.E., and Gordon M.E. "A Musculoskeletal Model of the Human Lower Extremity: the effect of muscle. tendon, and moment arm on the moment-angle relationship of musculotendon actuators at the hip, knee, and ankle". Journal of Biomechanics, *203:157–159, 1990.*

Hughston, J.C., and Eilers A.F. "The Role of the Posterior Oblique Ligament in Repairs of Acute Medial (Collateral) Ligament Tear of the Knee ". Journal of Bone and Joint Surgery, *51-A:1045, 1965.*

Inman, V. T., Ralston, H.J., and Todd F. Human Walking. *Williams and Wilkins, Baltimore, 1981.*

G.A. Ishai. "Whole body gait kinetics". *PhD thesis, Bioengineering Unit, University of Strathclyde, 1975.*

Jansen, R.H., and Davy D.T. "An investigation of muscle lines of action about the hip: a centroid line approach vs the straight line approach ". Journal of Biomechanics, *8(2):103–101, 1975.*

Johnson, F., and Waugh W. "Method for routine clinical assessment of knee-joint forces ". Medical and Biological Engineering and Computing, *17:145–154, 1979.*

Johnson, G.A., Rajagopal, K.R., and Woo S.L.Y. "A Single Integral Finite Strain (SIFS) Model of Ligaments and Tendons ". Advances in Bioengineering, *22:245–248, 1992.*

G.R. Johnson. "The use of spectral analysis to assess the performance of shock absorbing footwear ". Engineering in medicine, *15(3):117–122, 1986.*

Jorgensen, U., and Bojsen-Moller F. "Shock absorbency of factors in the shoe/heel interaction- With special focus on role of heel pad ". Foot and ankle, *9(11):294–299, 1989.*

Jorgensen, U., and Ekstrand J. "Shock absorbance in shoes with or without heel support during walking and running ". Acta Orthopaedica Scandinavica, *59(1): 101–106, 1988.*

U. Jorgensen. "Implication of heel strike ". Acta Orthopaedica Scandinavica, *61(1 Supplementum):235–290, 1990.*

Kadaba, M.P., Ramakrishnan, H.K., and Wootten M.E. " Measurement of Lower Extremity Kinematics During Level Walking". Journal of Orthopaedic Research, *8: 383–392, 1990.*

L. Kaijser. "Limiting Factors for Aerobic Muscle Performance the Influence on Varying Oxygen Pressure and Temperature ". Acta Physiol. Scan., *346:5–95, 1970.*

Kaufmann, K.R., An, K.N., and Chao E.Y.S. "A Dynamic Mathematical Model of the Knee Joint Applied to Isokinetic Exercise ". Computational Methods in Bioengineering, *9, 1988.*

G.E. Kempson. The Mechanical Properties of Articular Cartilage: Editor L. Sokoloff. *Academic Press, New York, 1980.*

Kennedy, J.C., Hawkins, R.J., Willis, R.B., and Danylchuk K.D. "Tension Studies of Human Knee Ligaments ". Journal of Bone and Joint Surgery - American volume, *58:350–355, 1976.*

Kennedy, J.C., and Fowler P.F. "Medial and Anterior Instability of the Knee ". Journal of Bone and Joint Surgery, *53-A(7):1257–1270, 1971.*

Kennedy, J.C., and Gralnger R.W. "The Posterior Cruciate Ligament ". Journal of Trauma, *7(3):367–376, 1957.*

Kennedy, J.C., Weinberg, H.W., and Wilson A.S. "The Anatomy and Function of the Anterior Cruciate Ligament ". Journal of Bone and Joint Surgery, *56-A(2): 223–235, 1974.*

Kettlekamp, D.B., and Jacobs A.W. "Tibiofemoral Contact Area - Determination and Implications ". ournal of Bone and Joint Surgery, *1.54-A:349–356, 1972.*

Kettlekamp, D.B., and Chao E.Y.S. "A Method for Quantitative Analysis of Medial and Lateral Compression Forces at the Knee During Standing ". Clinical Orthopaedics Related Research, *83:202–213, 1973.*

Kettlekamp, D.B., Johnson, R.J., Smidt, G.L., Chao, E.Y.S., and Walker M. "An Electrogoniometric Study on Knee Motion in Normal Gait ". Journal of Bone and Joint Surgery, *52-A:775–790, 1970.*

Kinzel, G.L., and Gutkowski L.J. "Joint Models and Degrees of Freedom and and Anatomical Measurement ". Journal of Biomechanical Engineering, Transactions of the ASME, *105:55–62, 1983.*

F. Kreyszig. Advanced Engineering Mathematics. *John Wiley and Sons, Inc., New York, 1972.*

Kurosawa, H., Walker, P.S., Garg, A., , and Hunter T. "Geometry and Motion of the Knee for Implant and Orthotic Design ". Journal of Biomechanics, *18:487 499, 1985.*

M.A. Lafortune. "The Use of Intra-Cortical Pins to Measure the Motion of the Knee Joint During Walking". *PhD thesis, Pennsylvania State University, 1984.*

Lai, W.M., Mow, Van, C., and Zhu W. "Constitutive Modelling of Articular Cartilage and Biomacromolecular Solutions ". Journal of Biomechanical Modelling and Transactions of the ASME, *115:474–496, 1993.*

L.W. Lamoreaux. *"Kinematic Measurements in the Study of Human Walking ".* Bulletin of Prosthetics Research, *pages 3–84, 1971.*

C. Lanczos. Applied Analysis. *Pitman, 1957.*

Laros, G.S., Tipton, C.H., and Cooper R.R. *"Influence of Physical Activity on Ligament Insertions in the Knee of Dogs ".* Journal of Bone and Joint Surgery, *53-A: 275–286, 1971.*

J.L. Leeuwen. *"Shock absorption by the human foot ".* Acta Orthopaedica Scandinavica, *59(2):226–237, 1988.*

Levens, A.S., Berkeley, C.E, Inman, V.T., and Blosser J.A. *"Transverse Rotation of the Segments of the Lower Extremity in Locomotion ".* Journal of Bone and Joint Surgery, *30-A:859–872, 1948.*

Lewis, J.L., and Shybut G.T. *"In Vivo Forces in the Collateral Ligaments of Canine Knees ".* Transaction of Orthopaedic Research Society, *1981.*

Lewis, J.L., and Lew W.D. *"A Note on the Description of Articulating Joint Motion ".* Journal of Biomechanics, *10:675–678, 1977.*

Lewis, J.L., and Lew W.D. *"A Method for Locating an Optimal Fixed Axis of Rotation for the Human Knee Joint ".* Journal of Biomechanical Engineering, *100:187–193, 1978.*

Light, L.H., McLellan, G.E., and Klenerman L. *" Skeletal transients on heel strike in normal walking with different footwear ".* Journal of Biomechanics, *13:477–480, 1980.*

Luethi, S.M., Denoth, J., Kaerin, X., Stacoff, A., and Stuessi E. The influence of shoe on foot movement and shock attenuation in running. *Biomechanics X-B, 1987.*

Maquet, P.G., and Pelzer G.A. *"Evolution of the Maximum Stress in Osteoarthritis of the Knee Joint ".* Journal of Biomechanics, *10:107–117, 1977.*

Marinozzii, G., Pappalardo, S., and Steindler R. *"Human Knee Ligaments: Mechanical Tests and Ultrastructural Observations ".* J. Orthop. Traumatol., *9:231–240, 1983.*

Markolf, K.L., Mensch, J.S., and Amstutz H.C. "Effects of the Ligaments and Menisci on Knee Stiffness and Laxity. An in-vitro Sectioning Study ". Orthopaedic Research Society, *51(176), 1976.*

R. Maronsky. "Minimum-time Running and Swimming: An Optimal Control Approach". Journal of Biomechanics, *29(2):245–249, 1996.*

Marsh, E., Sale, D., McComas, A.J., and Quinlan J. " Influence of joint position on ankle dorsiflexion in humans ". Journal of Applied Physiology, *51:150–167, 1981.*

McLeod, W.D, and Cross M.J. Knee joint axis of rotation. In Proceedings of the 27th ACEMB, Philadelphia PA, *1974.*

T.G. McPoil. " Footwear ". Physical therapy, *68(12):1857–1865, 1988.*

R.J. Minns. "Forces at the Knee Joint: Anatomical Considerations ". Journal of Biomechanics, *14(9):633–643, 1981.*

Miyazaki, S., and Ishida A. "New Mathematical Definition and Calculation of Axial Rotation of Anatomic Joints ". Journal of Biomechanical Engineering and Transactions of the ASME, *113:270–275, 1991.*

Moeinzadeh, M.H., Engin, A.E., and Akkas N. "Two-Dimensional Dynamic Modelling of Human Knee Joint ". Journal of Biomechanics, *16(4):253–264, 1983.*

Moffatt, C.A., Harris, E.D., and Haslam E.T. "An Experimental and Analytic Study of the Dynamic Properties of the Human Leg ". Journal of Biomechanics, *2:373–387, 1969.*

J.B. Morrison. "Bioengineering Analysis of Force Actions Transmitted by the Knee Joint ". Biomedical Engineering, *3:164–170, 1968.*

J.B. Morrison. "Function of the knee Joint in Various Activities ". Biomedical Engineering, *4:573–580, 1969.*

J.B. Morrison. "The Mechanics of the Knee Joint in Relation to Normal Walking ". Journal of Biomechanics, *3:51–61, 1970.*

Mow, Van, C., Ateshian, G.A., and Spilker R.L. "Biomechanics of Diarthrodial Joints: A Review of Twenty Years of Progress ". Journal of Biomechanical Engineering, Transaction of the ASME, *115:460–467, 1993.*

D.G. Murray. "*Laboratory Studies of Kinematics Involving the Axes of the Normal Knee* ". Proceedings of a Workshop on Total Knee Arthroplasty, Charlottesville, *VA, 1974.*

Nagurka, M.L., and Yen V. "*Fourier-Based Optimal Control of Nonlinear Dynamic Systems* ". Journal of Dynamic Systems, Measurement and Control, *112:17–26, 1990.*

Nemeth, Ekholm, Arborelius, Ringdahl, and Schuldt. "*Influence of knee flexion on isometric hip extensor strength* ". Scand Journal of Rehabilitation, *15:97–101, 1983.*

Nigg, B.M., Eberle, G., Frey, D., Luethi, S., Segesser, B., and Weber B. Gait analysis and sport-shoe construction. Biomechanics VI-A, *Nigg B M:303–309, 1979.*

M. Nissan. "*Review of Some Basic Assumptions in Knee Biomechanics* ". Journal of Biomechanics, *13:375–381, 1980.*

Nordin, M., and Frankel V.H. Basic Biomechanics of the Musculoskeletal System. *Lea and Febiger, Philadelphia, 1989.*

Noyes, F.R., Delucas, J.L., and Torvik P.J. "*Biomechanics of Anterior Cruciate Ligament Failure : An Analysis of Strain-Rate Sensitivity and Mechanisms of failure in Primates* ". Journal of Bone and Joint surgery, *56-A:263–253, 1974.*

Noyes, F.R., and Grood E.S. "*The Strength of the Anterior Cruciate Ligament in Humans and Rhesus Monkeys and Age-Related and Species-Related Changes* ". Journal of Bone and Joint Surgery, *58(A):1074–1076, 1976.*

Olney, S.J., and Winter. "*Predictions of Knee and Ankle Moments of Force in Walking From EMG and Kinematic Data* ". Journal of Biomechanics, *18:9–20, 1985.*

Opila, K.A., Nicol, A.C., and Paul J.P. "*Upper limb loadings of gait with crutches*". Journal of Biomechanical Engineering, *109(4):285–290, 1987.*

Pandy, M.G., Anderson, F.C., and Hull D.G. "*A parameter Optimization Approach for the Optimal Control of Large-Scale Musculoskeletal Systems*". Transactions of the ASME, *114:450–460, 1992.*

Pandy, M.G., F.E., Zajac, E., Sim, and Levine W.S. "An Optimal Control Model for Maximum-Height Human Jumping". Journal of Biomechanics, *23(12):1185-1198, 1990.*

Pandy, M.G., and Zajac F.E. "Optimal Muscular Coordination Strategies for Jumping ". Journal of Biomechanics, *24(1):1-10, 1991.*

Papaioannou, G., Jonkers, I., and Spaepen A. "An interactive 3D Musculoskeletal model to study different muscle activation patterns during the swing phase of gait". Proceedings of The Third International Symposium on Computer Methods in Biomechanics and Biomedical Engineering; Barcelona 7-10 May 1997, *1:35-39, 1997.*

G. Papaioannou. "Forward Dynamics and the Human Gait: A 3D graphics based approach". Virtual Reality in Medicine; SGI Brussels Symposium, 15th April 1997;, *1:1-24, 1997.*

Patla, A.E., and S. Rietdyk. "Visual Control of Limb Trajectory over Obstacles during locomotion:effect of obstacle height and width". Gait and Posture, *1:45-60, 1993.*

Patriarco, A.G., Mann, R.W., Simon, S.R., and Mansour J.M. "An Evaluation of the Approaches of Optimization Models in the Prediction of Muscle Forces during Human Gait". Journal of Biomechanics, *14(8):513-525, 1981.*

J.P. Paul. Bioengineering Studies of the Forces Transmitted by Joint. II. *London : Pergamon Press, Biomechanics and Related Bioengineering Topics:Editor R.M. Kenedi, 1965.*

J.P. Paul. *Forces transmitted by joints in the human body.* In Proceedings of the institution of mechanical engineers, *volume 181, pages 8-15, 1966.*

J.P. Paul. *The effect of walking speed on the force actions transmitted at the hip and knee joints.* In Proceedings of the Royal Society of Medicine, *volume 63, pages 200-204, 1970.*

J.P. Paul. " *Load actions on the human femur in walking and some resultant stresses* ". Experimental Mechanics, *pages 121-125, 1971.*

J.P. Paul. "*Loading on normal hip and knee joints and on joint replacements* ". Engineering in medicine, *2:53-70, 1976.*

Pedersen, D.R., Brand, R.A., Cheng, C.K., and Arora J.S. "Muscle Force Estimations Using Nonlinear Optimization Techniques ". Journal of Biomechanical Engineering, *109:192–199, 1987.*

Pedotti, A., Krishnan, V.V., and Stark L. "Optimization of Muscle Force Sequencing in Human Locomotion ". Math. Bioscience, *38:57–76, 1978.*

Pennock, G.R., and Clark K.J. "An Anatomy-BasedCoordinate System for the Description or the Kinematic Displacements in the Human Knee ". Journal of Biomechanics, *23(12):1209–1218, 1990.*

Penrod, D.D., Davy, D.T., Singh, and D.P. "An Optimization Approach to Tendon Force Analysis". Proceedings of the 25th Annual Conference of Engineering in Medicine and Biology, *page 247, 1972.*

Perry, J., Locke, M.T., Lowe, R., Barto, P., and Gronley J. "Knee motion in spontaneous slow gait ". Physical Therapy, *66(5):802–803, 1986.*

M.R. Pierrynowski. "A Physiological Model for the Solution of Individual Muscle Forces During Normal Human Walking ". PhD Thesis: Simon Fraser University, Vancouver, British Columbia, *1:1–256, 1982.*

Piziali, R.L., Seering, W.P., and Shunnan D.J. "The Functions of the Primary Ligaments of the Knee in Anterior-Posterior and Medial-Lateral Motions ". Journal of Biomechanics, *13:777–784, 1980.*

W. Platzer. "Color Atlas and textbook of Human Anatomy". LOCOMOTOR SYSTEM, *1:170–270, 1986.*

Pope, M.H., Crowninshield, R., Miller, R., and Johnson R. "The Static and Dynamic Behaviour of the Human Knee in Vivo ". Journal of Biomechanics, *9:449-452, 1976.*

R.E. Pottoff. "An Analysis of the Biomechanics of the Human knee", 1968.

J. Poulson. " Biomechanics of the leg". *PhD thesis, University of Strathclyde, 1973.*

Prietto, M.P, Baln, J.R, Stonebrook, S.N., and Settlage R.A. "Tensile Strength of Human Posterior Cruciate Ligament (PCL) ". Transactions of 34th Annual Orthopaedic Research Society, *13:195, 1988.*

Race, A., and Amis A.A. "*The Mechanical Properties of the Two Bundles of the Human Posterior Cruciate Ligament*". Journal of Biomechanics, *27:13-24, 1991.*

Race, A., and Amis A.A. "*Loading of the Two Bundles of the Posterior Cruciate Ligament: An Analysis of Bundle Function in A-P Drawer* ". Journal of Biomechanics, *29:873–879, 1996.*

Radin, E.L., Parker, H.G., Pugh, J.W., Steinbert, R.S., Paul, I.L., and Rose R.M. "*Response of Joints to Impact Loading - III. Relationship Between Trabecular Microfracture and Cartillage Degeneration* ". Journal of Biomechanics, *6:51–57, 1973.*

H.J. Ralston. "*Energy-Speed Relation and Optimal Speed during Level Walking* ". Int. Z. Angew. Physiol. Einschl. Arbeitsphysiologie, *17:277–283(s), 1958.*

Ramakrishnan, H.K., and Kadaba M.P. "*On the Estimation of Joint Kinematics During Gait* ". Journal of Biomechanics, *24:969–977, 1991.*

J. Rastegar. "Measurement of the Nonlinear and Coupled Structural Characteristics of the Human Knee". *PhD thesis, Stanford University, USA, 1977.*

Reilly, D.T., and Martens M. "*Experimental Analysis of the Quadriceps Muscle Force and Patello-Fenoral Joint Reaction Force for Various Activities* ". Acta Orthopaedica Scandinavica, *43:126–137, 1972.*

Ripperger, R.R., Chao, E.Y., and Stauffer R.N. "*A Quantitative Analysis of Leg Musculature* ". Transactions of the 26th Annual Meeting of the Orthopaedic Research Society, *5:52, 1980.*

Robichon, J., and Romero C. "*The Functional Anatomy of the Knee Joint and With Special Reference to the Medial Collateral and Anterior Cruciate Ligaments* ". The Canadian Journal of Surgery, *2:36–40, 1968.*

Rohrle, R., Scholten, R., Sigolotto, C., and Sollbach W. "*Joint forces in the human pelvis-leg skeleton during walking* ". Journal of Biomechanics, *17(6):409-421, 1984.*

Seedholm, B.B., and Terayama K. " *Knee Forces During the Activity of Getting Out of a Chair With and Without the Aid of Arms*". Biomedical Engineering, *pages 278–282, 1976.*

Seering, W.P., Piziali, R.L., Nagel, D.A., and Schurman D.J. "The Function of the Primary Ligaments of the Knee in Varus-Valgus and Axial Rotation ". Journal of Biomechanics, *113:785–794, 1980.*

Seireg, A., and Arvikar R.J. "A Mathematical model for evaluation of forces in lower extremities of the musculo-skeletal system". Journal of Biomechanics, *6:313-326, 1973.*

Seireg, A., and Arvikar R.J. " The Prediction of Muscular Load-Sharing and Joint Forces in the Lower Extremities During Walking". Journal of Biomechanics, *8: 89–102, 1975.*

G. Selvik. "Roentgen Stereophotogrammetry - A Method for the Study of the Kinematics of the Skeletal System ". Acta Orthopaedica Scandinavica, *60 Suppl. No.32, 1989.*

Shiavi, R., Champion, S., Freeman, F., and Griffin P. "Variability of electromyographic patterns for level- surface Walking through a range of self selected speeds ". Bulletin of prosthetics Research, *l. 18(1):5–14, 1981.*

R. Shiavi. "Electromyographic Patterns in Adult Locomotion: A Comprehensive Review". Journal of Rehabilitation Research and Development, *22:85–98, 1985.*

Sirisena, H.R., and Tan K.S. "Computation of Constrained Optimal Controls Using Parameterization Techniques". IEEE Transactions on Automatic Control, *pages 431–433, 1974.*

I.S. Smillie. Injuries of the Knee Joint. *E. and S. Livingstone Ltd, Edinburgh, 1970.*

Snel, J.G., Delleman, N.J., Heerkens, Y.F., van, Ingen, and Schenau G.J. Shock absorbing characteristics of running shoes during actual running. *Biomechanics IX-B, 1985.*

Soutas-Little, R.W., Beavis, G.C., Verstraete, M.C., and Markus T.L. "Analysis of Foot Motion During Running Using a Joint Coordinate System ". Med. Sci. Sports Exercise, *19:285–293, 1987.*

Spaepen, A.J., Jonkers, and I. "The use of EMG in Biomechanical Analysis". Internal Report:Ergonomics and Occupational Biomechanics Laboratory; K.U.Leuven, *1:1-40, 1997.*

Spaepen, A.J., Vanlandewijck, Y.C., and Lysens R.J. "Relationship between Energy expenditure and Muscular activity patterns in Handrim Wheelchair Propulsion ". Industrial Ergonomics, *17:163–173, 1996.*

Stacoff, A., Stuessi, E., and Sonderegger D. 1985.

Stauffer, N.R., Chao, Y.S., and Brewster R.C. "Force and motion analysis of the normal and diseased and and prosthetic ankle joint ". Clinical Orthopaedics and related research, *127:189–196, 1977.*

Suntay, W.J., Grood, E.S, Noyes, F.R., and Butler D.L. A Coordinate System for Describing Joint Position. *Adv. Bioengineering and ASME and WAM and San Fransisco, CA, 1978.*

Sutherland, D.H., Olshen, R., and Coolper L. "The Pathomechanics of Gait in Duchenne Muscular Dystrophy ". Develop. Med. Child Neurol., *23:3-22, 1981.*

C.T. Thompson. "A System for Determining the Spatial Motions of Arbitrary Mechanisms -Demonstrated on the Human Knee". *PhD thesis, Stanford University, USA, 1972.*

Thorstensson, A., Grimby, G., and Kaarlsson J. "Force- velocity relations and fiber composition in human knee extensor muscles ". Journal of Applied Physiology, *40: 12–16, 1976.*

R. Tooth. "The Biomechanics of Arthrodesis and Arthroplasty in the Human Leg". *PhD thesis, University of Strathclyde U.K., 1976.*

Trent, P.S., Walker, P.S., and Wolf B. "Ligament Length Patterns and Strength and and Rotational Axes of the Knee Joint ". Clinical Orthopaedics and Related Research, *117:263–270, 1976.*

Tumer, S.T., and Engin A.E. "3-Body Segment Dynamic Model of the Human Knee ". Journal of Biomechanical Engineering and Trans. of the ASME, *115(4):350 356, 1993.*

Valiant, G.A., McMahon, T.A., and Frederick E.C. A new test to evaluate the cushioning properties of athletic shoes, *pages 937–941. Biomechanics X-B, 1987.*

VanDijk, R., Huishes, R., and Selvik G. "Roentgen Stereophotogrammetric Methods for the Evaluation of the Three Dimensional Kinematic Behaviour and Cruciate Ligament Length Patterns of the Human Knee Joint ". Journal of Biomechanics, *12:197, 1979.*

Vanlandewijck, Y.C., Spaepen, A.J., and Lysens R.J. "Wheelchair Propulsion Functional Ability Dependent Factors in Wheelchair Basketball Players ". Scandinavian Journal of Rehabilitation Medicine, *26:37–48, 1994.*

Viidik, A., and Ekholm R. "Light and Electron Microscopy of Collagen Fibers Under Stress ". Z. Anat. EntwGesch., *1:154, 1968.*

A. Viidik. Biomechanics and Functional Adaptation of Tendons and Joints Ligaments. Studies on the Anatomy and Function of Bones and Joints, Editor: G. Evans. *Springer Verlag, 1966.*

A. Viidik. "A Rheological Model for Calcified Parallel-Fibred Collagenous Tissue ". Journal of Biomechanics, *1:3 – 11, 1968.*

Vrahas, M.S., Brown, T.D., Andrews, J.G., Brand, R.A., and Pedersen D.R. "In Vivo Passive Moment Measurements in the Human Hip ". Trans. Orthopaedic Research Society, *12:212, 1987.*

Walker, P.S., and Hajek J.V. "The Load Bearing Area in the Knee Joint ". Journal of Biomechanics, *5:581–589, 1972.*

Wang, C., and Walker P.S. "Rotary Laxity of the Human Knee ". Journal of Bone and Joint Surgery, *65-A:161, 1974.*

Wang, C., Walker, P.S., and Wolf B. "The Effects of Hexion and Rotation on the Length Patterns of the Ligaments of the Knee ". Journal of Biomechanics, *6:587–596, 1973.*

Warren, L.F., Marshall, J.L., and Girgis F. "The Prime Static Stabiliser of the Medial Side of the Knee ". Journal of Bone and Joint Surgery, *56-A:665-674, 1974.*

Weightman, B.O., and Kempson G.E. Load Carriage,Adult Articular Cartilage, Editor:M.A.R. Freeman, *page 293. Pitman Medical and London, 1979.*

Weisman, G., Pope, M.H., and Johnson R.L. On the mechanical properties of ligaments under cyclic loading. In Proceedings of the 7th New England Bioengineering Conference, *pages 395–397, 1979.*

M.W. Whittle. Gait analysis:an introduction. *Butterworth Heinemann, London, 1991.*

Wickiewicz, T.L., Roy, R.R., Powell, P.Y.L., and Edgerton V.R. "Muscle architecture of the human lower limb ". Clinical Orthopaedics Related Research, *179:275-283, 1983.*

B.D. Wilson. " Knee Ligament Length Changes During Walking". *PhD thesis, University of Iowa and Iowa City - Iowa, 1978.*

B.D. Wilson. Knee Ligament Length Changes During Walking in:Biomechanics VII -International Series on Biomechanics. *University Park Press, Baltimore, Maryland, 1981.*

D.A. Winter. "Knee flexion during stance as a determinant of inefficient walking ". Physical Therapy, *63(3):331–333, 1983.*

D.A. Winter. "The biomechanics and motor control of human gait". Waterloo: University of Waterloo Press, *pages 161–280, 1987.*

Wismans, J., Veldpaus, F., and Janssen J. "A Three Dimensional Mathematical Model of the Knee Joint ". Journal of Biomechanics, *13:677-685, 1980.*

Wongchalsuwat, C., Hemami, H., and Buchner H.J. "Control of Sliding and Rolling at Natural Joints ". Journal of Biomechanical Engineering Transactions of the ASME, *106:368–375, 1984.*

S.L.Y. Woo. " Mathematical Modelling of Ligaments and Tendons". Journal of Biomechanical Engineering Trans. of the ASME, *115(4):468–473, 1993.*

Yamaguchi, G.T., and Zajac F.E. "A Planar Model of the Knee Joint to Characterise the Knee Extensor Mechanism ". Journal of Biomechanics, *22:1–10, 1989.*

Yang, J.F., and Winter D.A. "Electromyographic Amplitude Normalization Methods: Improving Their Sensitivity as Diagnostic Tools in Gait Analysis". Archives of Physical Medicine and Rehabilitation, *65:517–521, 1984.*

M.R. Yeadon. "The Simulation of Aerial Movement - I. The Determination of Attitude Angles from Film Data ". Journal of Biomechanics, 23:59–66, 1990.

B.P. Yeo. "Investigations concerning the Principle of Minimal Total Muscular Force". Journal of Biomechanics, 9:413–416, 1976.

APPENDIXES

Appendix A

The list below indicates the program files to be found in the diskete that accompanies the thesis. THE PROGRAMS REFER TO THE CALCULATIONS OF CHAPTERS 3, 7, 8, 9.

copstat.for;6, dcjcp.for;104, diff2.for;23 , filter1.for;1 , flaxis.for;9, lankle.for;13, lhip.for;23, lknee.for;33, lshank.for;4, lthigh.for;4, normang.for;5, normdpl.for;5, normdpr.for;3, normgrfp.for;4, normp.for;8, phipstat.for;9, presdat.for;6, rankle.for;22, rhip.for;17, rknee.for;17, rshank.for;4, rthigh.for;4, scale2.for;55, PRES for, mainNEWFOR, OPTIMISEFOR, terminNEWFOR.

0.1 SIGNAL PROCESSING

The noise associated with the signals from electrical devices results in deterioration of the information obtained. Filters are employed to cut off the unwanted frequency components of the signal. For activities such as walking the higher frequency components of the signal are the ones normally removed since the activity is characterised by its low frequency. High frequency components are known to have a greater influence on differentiated signals than low frequency ones therefore high frequency noise is propagated by differentiation. This is an important aspect in gait analysis since double differentiation for acceleration values is sometimes necessary. Both analog and digital (for real time and post event respectively) filters have been used in the past with digital filters dominating the modern biomechanical analysis. The most commonly used filters are low pass, zero phase lag filters, such as the Butterworth 4th order filter (Andrews et. al 1981), (Winter [1987]) or Fourier analysis (Cappozzo [1984]). The frequency characteristics of the activity under analysis will determine the cut-off frequency used in the filtering. Winter [1987] suggests using the sixth harmonic of the stride frequency. If for example, the cadence is 120 step/min, then the stride frequency is 1Hz, therefore the cut- off is 6Hz. Antonsson and Mann (1985) reported that 98% of walking signal power had frequencies below 10Hz and 99% below 15Hz. A cut-off frequency of 10Hz has also been used. Differentiation of displacement data allows velocities and accelerations to be obtained. According to Winter [1987] the finite difference method for smoothed data can be employed. If x is displacement, a is acceleration, v is velocity, T is sample period and i is the reference time point then:

$$v_i = (x_{i+1} - x_{i-1})/2T$$
$$a_i = (v_{i+1} - v_{i-1})/2T \quad (1)$$

Paul [1970] used a five point span for velocity calculation and a nine point one for acceleration. A quadratic is fitted to the raw data using a 'least squares' procedure and the gradient is taken at the central point.

$$V_i = (-2x_{i-2} - x_{i-1} + x_{i+1} + 2x_{i+2})/10T$$
$$a_i = (4x_{i-4} + 4x_{i-3} + x_{i-2} - 4x_{i-1}$$
$$-10x_i - 4x_{i+1} + x_{i+2} + 4x_{i+3} + 4x_{i+4})/100T^2 \quad (2)$$

This involves smoothing additional to that already implemented and loss of high Frequency (HF) information.

0.2 NORMALISATION OF THE DATA

The completion of analysis leaves the procedure with the question of the representation of the data with respect to the individual so that generalisations and comparisons based on statistical analysis can be performed. Winter [1987] summarised the normal procedure in that an individual should repeat the test run a number of times, and calculate an average curve with an associated measure of the variation and range. A method which has been used to overcome the fact that individual runs vary in their time period is the normalisation of the data to the gait cycle (the unit of the gait cycle has been adopted as the standard expression). Fourier analysis techniques have been employed for the above task. Alternatively, scaling the timings up to the maximum found in a series of runs, again with the use of Fourier analysis gives a similar starting point for comparisons. However, with both techniques the points of interest will occur as a period of the gait cycle rather than as an instant in time. For example, if an event occurs for 60ms independent of the gait period, in the shorter period gait cycles it will be skewed in the average normalised plot. Therefore if that does occur data will be lacking. Normalisation with respect to the mass of the individual allows better interpretation of between

subject variability studies. The forces generated by the individuals can be expressed as a percentage of the body weight (Winter [1987]). Other normalisation methods refer to considering distance measures such as step length as a proportion of stature or stride length. Relative velocity can also be a criterion if the unit of measure is the stature per second.

0.3 Moving and stationary coordinate systems

The moving and stationary coordinate systems can be kinematically related by a vector relating the position of the moving coordinate system origin with respect to the stationary coordinate system and the direction cosines relating the orientation between the two coordinate systems as seen in Figure 1 on page 4.

The stationary coordinate system can be defined as X,Y,Z with unit vectors I,J,K, origin O and the moving coordinate system as x,y,z with unit vectors i,j,k and origin o. The vector to relate the position of o, with respect to the stationary coordinate system would be in terms of X,Y,Z. Orientation of the moving coordinate system is therefore given with respect to the stationary system as:

$$\begin{bmatrix} i \\ j \\ k \end{bmatrix} = \begin{bmatrix} i \cdot I & i \cdot J & i \cdot K \\ j \cdot I & j \cdot J & j \cdot K \\ k \cdot I & k \cdot J & k \cdot K \end{bmatrix} \begin{bmatrix} i \\ j \\ k \end{bmatrix} = [B_{movimg-stationary}] \cdot \begin{bmatrix} I \\ J \\ K \end{bmatrix} \tag{3}$$

$$[B_{movimg-stationary}] = \begin{bmatrix} B_{1,1} & B_{1,2} & B_{1,3} \\ B_{2,1} & B_{2,2} & B_{2,3} \\ B_{3,1} & B_{3,2} & B_{3,3} \end{bmatrix} \tag{4}$$

The direction cosines are elements in matrix [B] and represent the projection of the moving coordinate system unit vectors on the stationary coordinate system unit vectors (Small et al. [1992] FIGURE 2 on page 8).

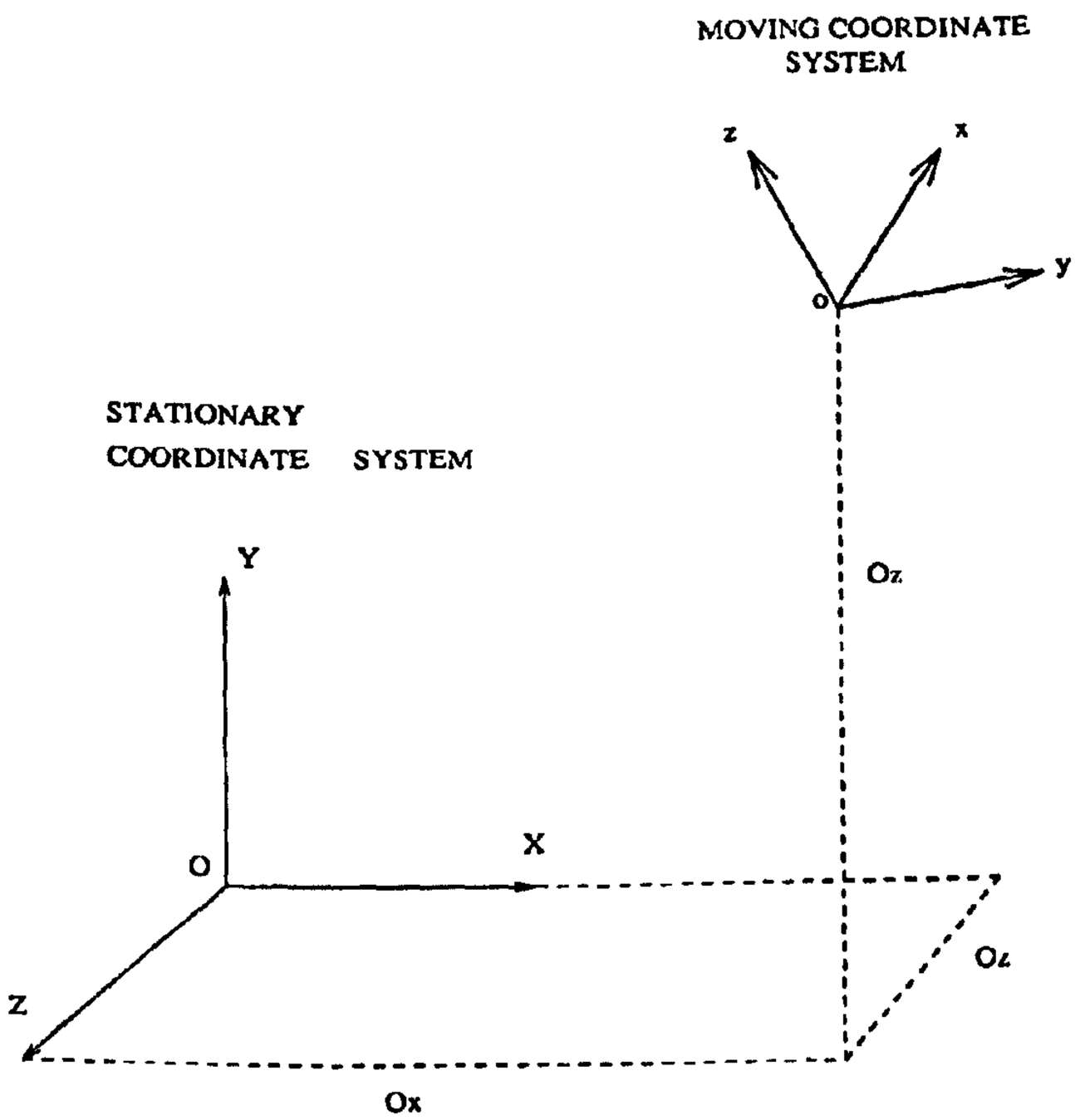

Figure 1: Stationary and moving coordinate systems. The position of the latter with respect to the former is defined by a vector, which is equivalent to the vector sum of o_x, o_y and o_z.

From the nine elements of matrix [B], only three are independent since the sums of squares for both rows and columns equal 1. These three independent elements and the three terms of the position vector comprise the six pieces of information needed to completely describe the physical location of the segment. Although the several techniques of three dimensional kinematics vary according to the method of manipulation and interpretation of the information contained within the vector and matrix, they converge in the fact that they all use a position vector and direction cosine matrix.

0.4 Models of the Lower Limb

0.4.1 GAIT-1 The segmental approach

Location coordinates of points of interest were recorded in three dimensions, in the ground frame of reference, at regular intervals of 20ms. Kinematic data in conjunction with kinetic data by considering sequential frames were recorded and analysed with the help of the following model to quantify the loading behaviour of the three major lower limb joints. The segmental approach for modelling the lower limb of the test subject involved splitting the body into seven segments: right and left foot, shank and thigh and pelvis. According to rigid body mechanics fixed joint centres and constant mass distribution properties were assumed. In most of the segments three non-linear markers were placed on anatomical landmarks and therefore, local segmental technical axes were produced. These allowed local anatomical axes to be produced where applicable. The anatomical local axes relate to the joint centres of the segment in question. Similar methods were used for calculating these axis systems for the segments and are described in the following sections. The hip joint centre position was calculated by static relations. This required additional markers to those used in the dynamic tests which allowed the relationship between the calculated joint centres and the dynamic marker array to be determined. The algorithm DCJCP.FOR was used to perform the calculations for each frame of dynamic data in turn. The static relations of the pelvis were performed by the algorithm PHIPSTAT.FOR. Appendix A contains listings of all the algorithms as well as the flow diagram of which input files were used by the algorithms and the command files that run the analysis.

In the following mathematical descriptions the terminology used was:

$$[B] = \begin{bmatrix} B11 & B12 & B13 \\ B21 & B22 & B23 \\ B31 & B32 & B33 \end{bmatrix} \tag{5}$$

where [B] is a three by three direction cosine matrix for segment B which transforms coordinates in the local axes system to the ground axes system.

$[B]^{-1}$ *is the inverse matrix which transforms from ground axis system to local axes system, where*

$$[B]^{-1} = \begin{bmatrix} B11 & B21 & B31 \\ B12 & B22 & B32 \\ B13 & B23 & B33 \end{bmatrix} \tag{6}$$

where Xn, Yn, Zn are the coordinates of marker number n and Xn_1, Yn_1, Zn_1 *are the coordinates of marker number n, expressed in the segment local axes system. The abbreviations below are used in the step by step explanations of the segmental approach that follow in the next chapters.* ϵ *is the direction qualifier indicator (+1, -1)*

ex_a *is the unit vector along the local technical x-axis*

ey_a *is the unit vector along the local technical y-axis*

ez_a *is the unit vector along the local technical z-axis*

ex *is the unit vector along the local x-axis*

ey is the unit vector along the local y-axis
ez is the unit vector along the local z-axis
R_n *is the radii vector for marker number n and* R_o *is the vector for the origin.*
The orthogonal conditions applied to the matrices used were:

$$B11^2 + B12^2 + B13^2 = 1 \tag{7}$$

$$B21^2 + B22^2 + B23^2 = 1 \tag{8}$$

$$B31^2 + B32^2 + B33^2 = 1 \tag{9}$$

$$B11 * B21 + B12 * B22 + B13 * B23 = 0 \tag{10}$$

$$B21 * B31 + B22 * B32 + B23 * B33 = 0 \tag{11}$$

$$B11 * B31 + B12 * B32 + B13 * B33 = 0 \tag{12}$$

Wherever the quadratic equation $ax^2 + bx + c = 0$ *was used the roots were calculated using (+ or - before the equation results from the sign of the included parenthesis i.e. DELTA):*

$$X = (-b \pm (b^2 - 4ac)^{1/2})/2a \tag{13}$$

0.4.2 THE SHANK SEGMENT

The definition of the shank segment in space required three technical markers situated on : the fibula head, the lateral malleolus and the tibial tuberosity. The markers were numbered 1, 2, 3, for the left shank and 4, 5, 6, for the right shank.

Ishai [1975] suggested a regression technique for predicting the knee joint centre. Four anthropometric measurements relative to these three markers were necessary (expressed in mm):

$S1$ = *the distance between the tibial condyles*
$S2$ = *medial tibial condyle to fibula head distance*
$S3$ = *medial malleolus to lateral malleolus distance*
$S4$ = *tibial tuberosity to tibial plateau distance*

As seen in FIGURE 3 on page 9 and FIGURE 4 on page 11 (the following predicted values were calculated (in mm) from the equations (Ishai [1975]:

$$K1 = 0.37 * S1 + 14.0 \tag{14}$$

$$K2 = 0.75 * S1 - 21.6 \tag{15}$$

$$K3 = 0.32 * S1 + 4.4 \tag{16}$$

$$K4 = 25.0 \tag{17}$$

$$K5 = 0.14 * S1 + 2.7 \tag{18}$$

$$D1 = S2 - K1 + H1 \tag{19}$$

$$D2 = S3 - K3 + H2 \tag{20}$$

$$D3 = K2 + H3 \tag{21}$$

$$D4 = S4 + K4 \tag{22}$$

$$D5 = D6 = 0 \tag{23}$$

Where H1, H2 and H3 are the marker heights of the markers of the shank. This assumes that the knee and the ankle joint centre lie along the longitudinal axis of the shank and that the lateral malleolus represents the ankle joint centre from the lateral view.

The shank local directional cosine matrix, $[B]_s$, which relates the moving shank frame of reference to that of the ground frame of reference (FIGURE 4 on page 11) was calculated using:

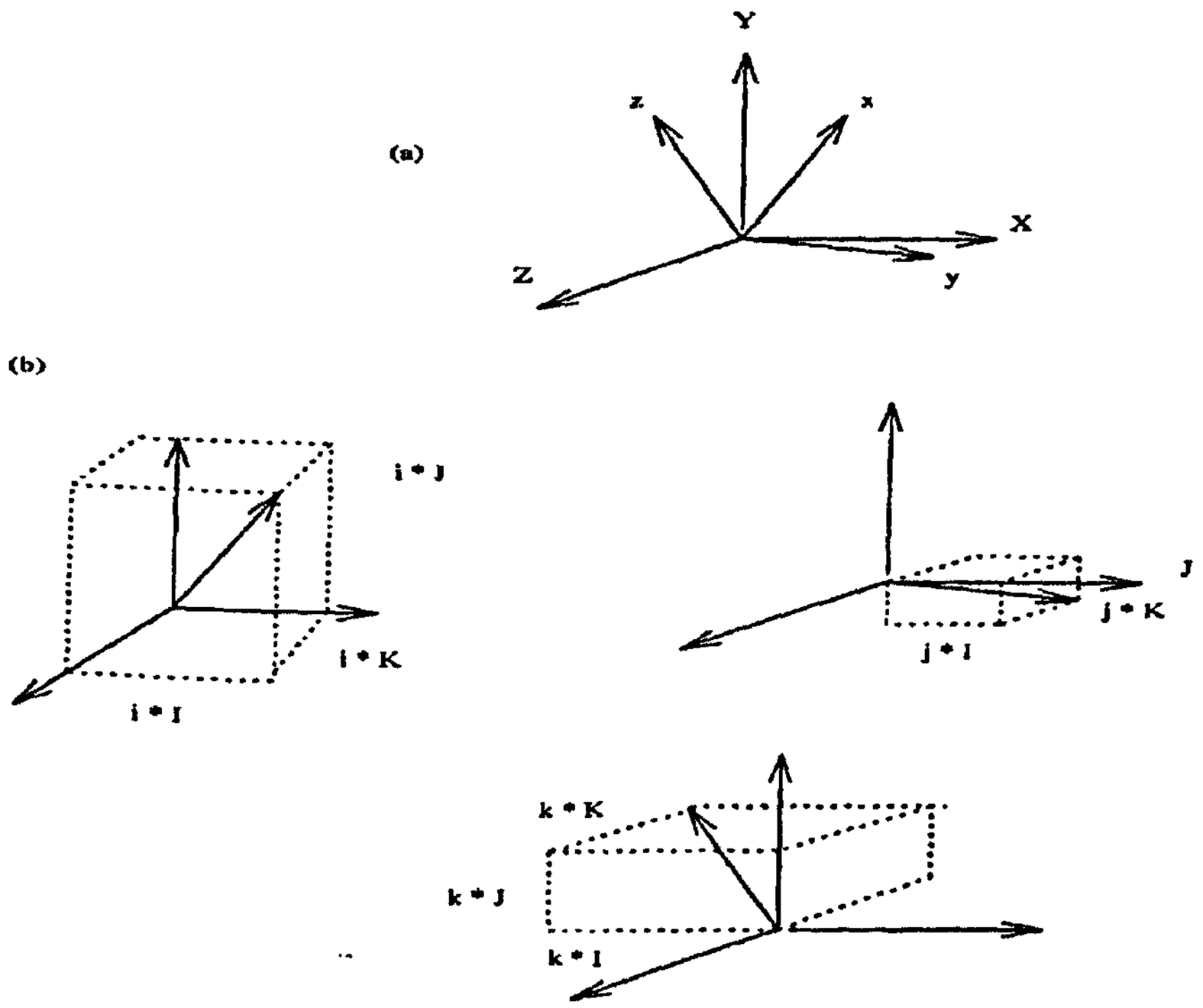

Figure 2: The nine direction cosine terms of matrix $[B_{moving-stationary}]$

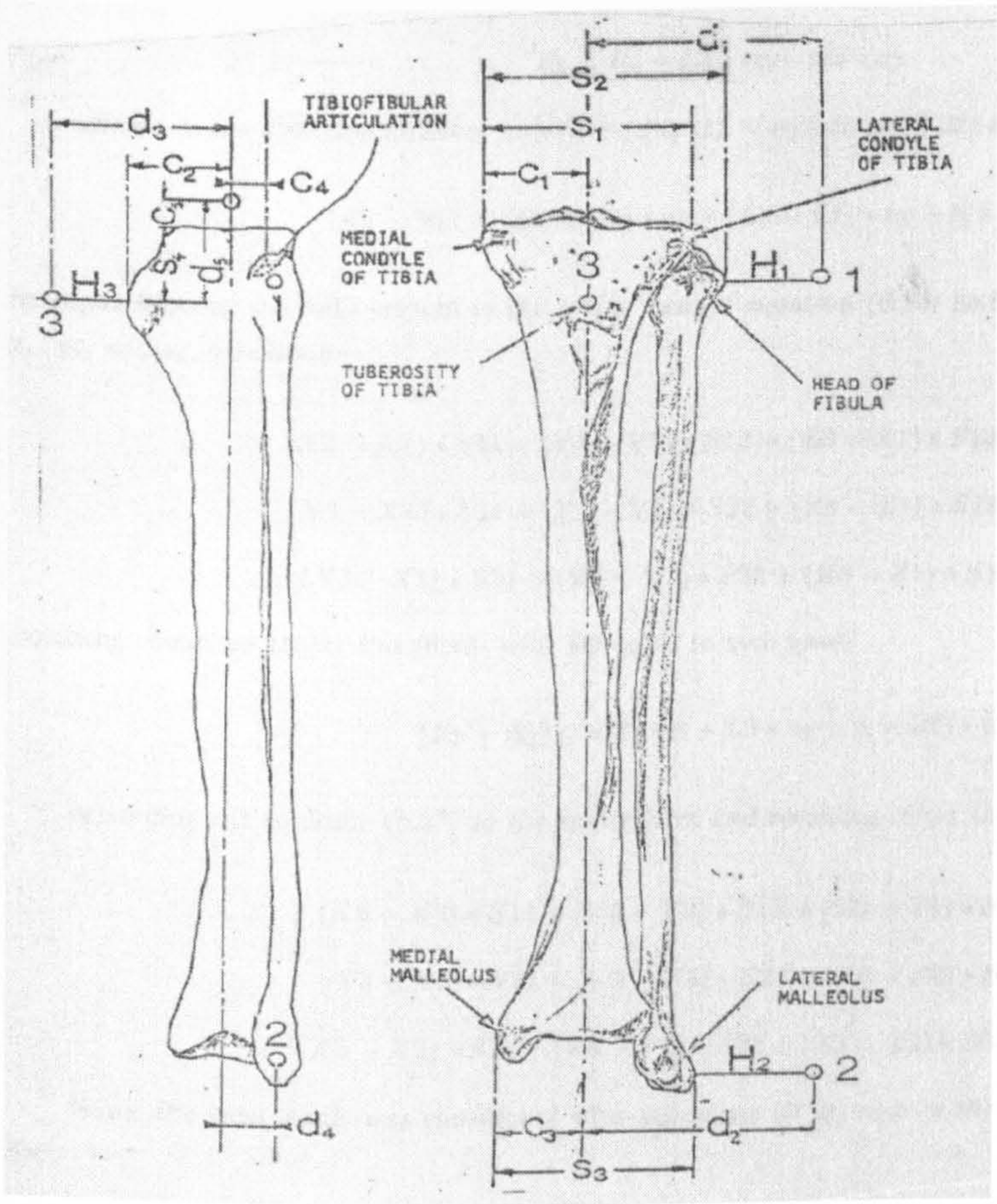

Figure 3: Left shank anthropometric values for regression analysis (Adapted from Ishai [1975]

$$R_1 = R_o - L2 * ex + L1 * ey - \epsilon * D1 * ez \tag{24}$$

$$R_2 = R_o - \epsilon * D2 * ez - D6 * ex \tag{25}$$

$$R_3 = R_o + L3 * ey + D3 * ex \tag{26}$$

where ϵ is the direction qualifier indicator (+1, -1), if equations (6.20) and (6.22) were simplified then:

$$(R_3 - R_1) = (D3 + L2) * ex + (L3 - L1) * ey + (\epsilon * D1) * ez \tag{27}$$

by expanding out the radii vectors to the scalar form of equation (6.23) and resolving along each of the local x_s, y_s, and z_s, we obtain:

$$(X3 - X1) * S11 + (Y3 - Y1) * S12 + (Z3 - Z1) * S13 = D3 + L2 \tag{28}$$

$$(X3 - X1) * S21 + (Y3 - Y1) * S22 + (Z3 - Z1) * S23 = L3 - L1 \tag{29}$$

$$(X3 - X1) * S31 + (Y3 - Y1) * S32 + (Z3 - Z1) * S33 = \epsilon * D1 \tag{30}$$

Equating equations (6.21) and (6.22) with D6 equal to zero gave:

$$(R_3 - R_2) = D3 * ex + L3 * ey + (\epsilon * D2) * ez \tag{31}$$

expanding out equation (6.27) to the scalar form and resolving along the x_s, y_s, and z_s axes we obtain:

$$(X3 - X2) * S11 + (Y3 - Y2) * S12 + (Z3 - Z2) * S13 = D3 \tag{32}$$

$$(X3 - X2) * S21 + (Y3 - Y2) * S22 + (Z3 - Z2) * S23 = L3 \tag{33}$$

$$(X3 - X2) * S31 + (Y3 - Y2) * S32 + (Z3 - Z2) * S33 = \epsilon * D2 \tag{34}$$

When the local z-axis was considered with equations (6.30) and (6.26) to give an expression in S33 for S32:

$$\begin{aligned} S32 = {} & \epsilon * D2 * (X3 - X1) - \epsilon * D1 * (X3 - X2) \\ & (Y3 - Y2) * (X3 - X1) - (Y3 - Y1) * (X3 - X2) + \\ & S33 * (Z3 - Z1) * (X3 - X2) - (Z3 - Z2) * (X3 - X1) \\ & (Y3 - Y2) * (X3 - X1) - (Y3 - Y1) * (X3 - X2) \end{aligned} \tag{35}$$

and similarly equating equations (6.30) and (6.26) forming an expression in S33 for S31 gave:

$$\begin{aligned} S31 = {} & \epsilon * D2 * (Y3 - Y1) - \epsilon * D1 * (Y3 - Y2) \\ & (X3 - X2) * (Y3 - Y1) - (X3 - X1) * (Y3 - Y2) \\ & + S33 * (Z3 - Z1) * (Y3 - Y2) - (Z3 - Z2) * (Y3 - Y1) \\ & (X3 - X2) * (Y3 - Y1) - (X3 - X1) * (Y3 - Y2) \end{aligned} \tag{36}$$

Equations (6.31) and (6.32) are of a similar form. To simplify the expressions we let:

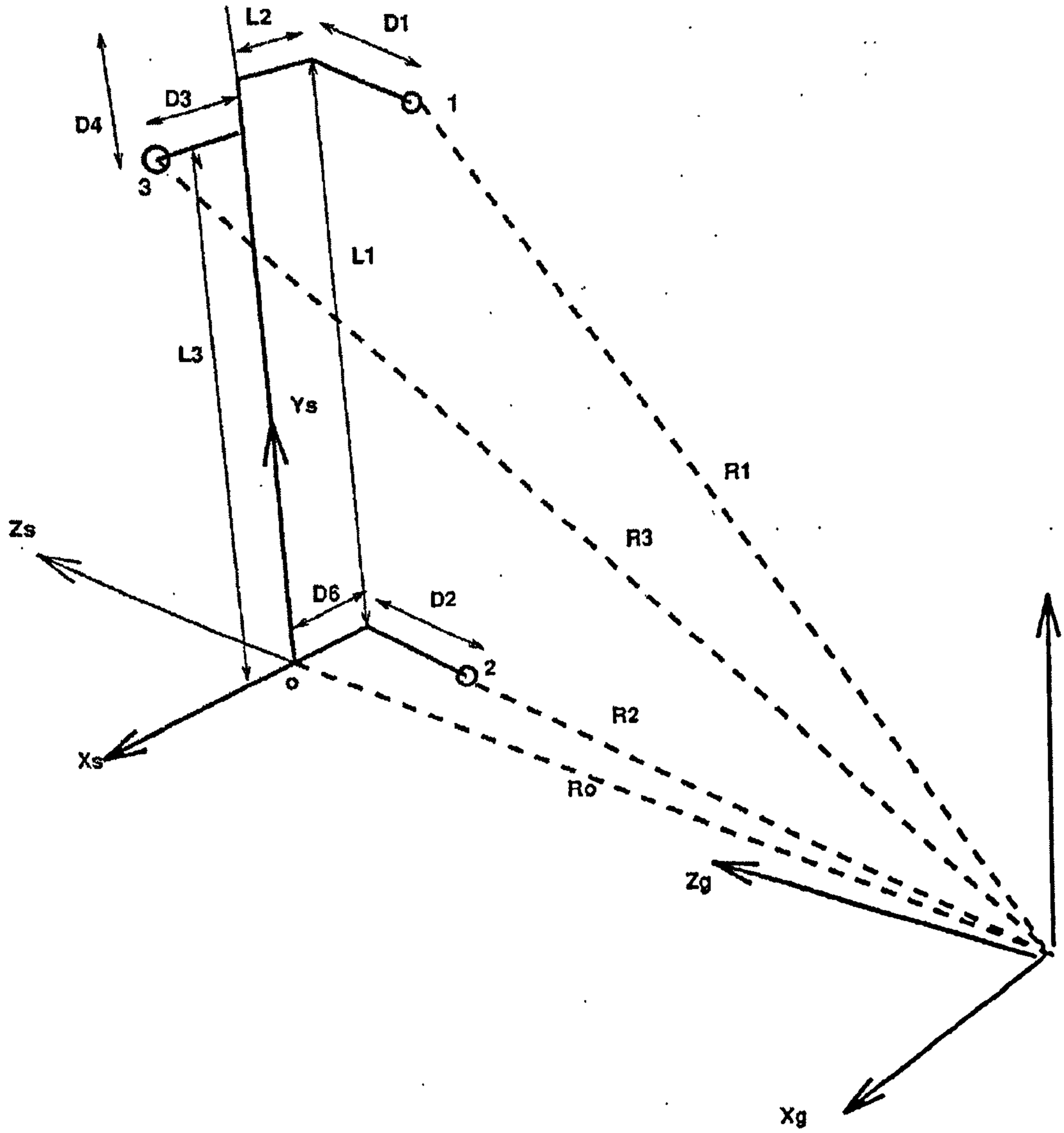

Figure 6.2: Left shank and ground axes systems and radii vectors

$$P = (Y3 - Y2) * (X3 - X1) - (X3 - X2) * (Y3 - Y1)$$
$$Gx = (\epsilon * D2 * (Y3 - Y1) - \epsilon * D1 * (Y3 - Y2)/ - P$$
$$Hx = ((Z3 - Z1) * (Y3 - Y2) - (Z3 - Z2) * (Y3 - Y1))/ - P$$
$$Gy = (\epsilon * D2 * (X3 - X1) - \epsilon * D1 * (X3 - X2))/P$$
$$Hy = ((Z3 - Z1) * (X3 - X2) - (Z3 - Z2) * (X3 - X1))/P$$

By substituting these values the equations (6.31) and (6.32) we have:

$$S32 = Gy + S33 * Hy \tag{37}$$

$$S31 = Gx + S33 * Hx \tag{38}$$

and by substituting these into the orthogonal relation (6.5) we have:
$(Gx + S33 * Hy)^2 + (Gy + S33 * Hy)^2 + S33^2 = 1$
rearranging and expanding out to form a quadratic equation terms of S33:

$$S33^2 * (1 + Hy^2 + Hx^2) + 2 * S33 * (Gx * Hx + Gy * Hy) + (Gx^2 + Gy^2 - 1) = 0 \tag{39}$$

If equation (6.9) is applied then the roots can be found. The chosen root was positive and nearest unity which gave the required cosine of the angle. S31 and S32 can be solved if we substitute the value for S33 in equations (6.31) (6.32) The unit vector ez of the local shank frame of reference is therefore determined. The local x-axis was therefore estimated and equation (6.28) and orthogonal relationship (6.8) could be rewritten as:

$$S13 = (D3 - S11 * (X3 - X2) - S12 * (Y3 - Y2))/(Z3 - Z2) \tag{40}$$

$$S13 = ((-S11 * S31) + (-S12 * S32))/S33 \tag{41}$$

When equating equations (6.31) (6.32) and with forming a new equation of available like terms in the unknown S11 and the previously calculated S31, S32 and S33:

$$\begin{aligned} S12 = &-D3 * S33 \\ &S32 * (Z3 - Z2) - S33 * (Y3 - Y2) + \\ &S11 * (S33 * (X3 - X2) - S31 * (Z3 - Z2)) \\ &S32 * (Z3 - Z2) - S33 * (Y3 - Y2) \end{aligned} \tag{42}$$

rewriting of equation (6.28) and the orthogonal relation (6.8) give:

$$S12 = (D3 - S11 * (X3 - X2) - S13 * (Z3 - Z2))/(Z3 - Z2) \tag{43}$$

$$S12 = ((-S13 * S33) + (-S11 * S31))/S32 \tag{44}$$

Equating (6.39) and (6.40) collecting like terms for a new equation in the unknown S13 and the previously calculated S31, S32 and S33 we have:

$$\begin{aligned} S13 = &-D3 * S32 \\ &S33 * (Y3 - Y2) - S32 * (Z3 - Z2) + \\ &S11 * (S32 * (X3 - X2) - S31 * (Y3 - Y2)) \\ &S33 * (Y3 - Y2) - S32 * (Z3 - Z2) \end{aligned} \tag{45}$$

Figure 4: Left shank and ground axes systems and radii vectors

Equations (6.38) and (6.41) are of a similar form. To simplify the notation of these two equations, let:

$E = S33 * (Y3 - Y2) - S32 * (Z3 - Z2)$

$Vy = (-D3 * S33)/ - E$

$Wy = (S33 * (X3 - X2) - S31 * (Z3 - Z2))/ - E$

$Vz = (-D3 * S32)/E$

$Wz = (S32 * (X3 - X2) - S31 * (Y3 - Y2))/E$

Therefore equations (6.38) and (6.41) could be rewritten as:

$$S12 = Vy + S11 * Wy \tag{46}$$

$$S13 = Vz + S11 * Wz \tag{47}$$

Therefore equations equations (6.42) and (6.43) can be substituted into orthogonal relationship (6.3) leading to: $S11^2 + (Vy + S11 * Wy)^2 + (Vz + S11 * Wz)^2$ *Again by expanding out and collecting like terms to form a quadratic in terms of S11:*

$$S11^2 * (1 + Wy^2 + Wz^2) + 2 * S11 * (Vy * Wy + Vz * Wz) + (Vy^2 + Vz^2 - 1) = 0 \tag{48}$$

Applying the same procedure as with equation (6.35) one can solve for the value of S11 from the equation (6.9). The unknowns S12 and S13 were found by substitution in equations (6.38) (6.41). The unit vector ex, along the local shank x-axis can be defined. The remaining local orthogonal axis, y, can be determined by applying the cross product:

$$S21 = S32 * S13 - S12 * S33 \tag{49}$$

$$S22 = S33 * S11 - S13 * S31 \tag{50}$$

$$S23 = S31 * S12 - S11 * S32 \tag{51}$$

Which means that the directional cosine matrix for the shank, [S], is thus defined. The coordinates of the ankle and knee joint centres can therefore be calculated. Equations (6.20), (6.21), (6.22) can be written as:

$$R_1 = R_o - L2 * ex + L1 * ey - \epsilon * D1 * ez \tag{52}$$

$$R_2 = R_o - \epsilon * D2 * ez \tag{53}$$

$$R_3 = R_o + L3 * ey + D3 * ex \tag{54}$$

Converting these into the scalar form accompanied by resolving along the local z-axis for (6.48), the y-axis for (6.49), and the z-axis for (6.49) the shank gave:

$$(X1) * S31 + (Y1) * S32 + (Z1) * S33 + EPS * D1 = (Xo) * S31 + (Yo) * S32 + (Zo) * S33 \tag{55}$$

$$(X2) * s12 + (Y2) * S22 + (Z2) * S23 = (Xo) * S21 + (Yo) * S22 + (Zo) * S23 \tag{56}$$

$$(X3) * S11 + (Y3) * S12 + (Z3) * S13 + D3 = (Xo) * S11 + (Yo) * S12 + (Zo) * S13 \tag{57}$$

The right hand sides of these three equations are equivalent to:

$$\begin{bmatrix} Xo \\ Yo \\ Zo \end{bmatrix} * [S]$$

where:

$$[S] = \begin{bmatrix} S11 & S12 & S13 \\ S21 & S22 & S23 \\ S31 & S32 & S33 \end{bmatrix} \tag{58}$$

So:

$$\begin{bmatrix} Xo \\ Yo \\ Zo \end{bmatrix} * [S] =$$

$$\begin{bmatrix} X3 * S11 + Y3 * S12 + Z3 * S13 - D3 \\ X2 * S21 + Y2 * S22 + Z2 * S23 \\ X1 * S31 + Y1 * S32 + Z1 * S33 + \epsilon * D1 \end{bmatrix} \tag{59}$$

With D5 and D6 assumed to be equal to zero, the coordinates of Ro are the same as Raj. Therefore one can calculate the ankle joint coordinates using:

$$\begin{bmatrix} Xaj \\ Yaj \\ Zaj \end{bmatrix} = [S]^{-1} *$$

$$\begin{bmatrix} X3 * S11 + Y3 * S12 + Z3 * S13 - D3 \\ X2 * S21 + Y2 * S22 + Z2 * S23 \\ X1 * S31 + Y1 * S32 + Z1 * S33 + \epsilon * D1 \end{bmatrix}$$

The knee joint was defined to lie directly along the y-axis of the shank proximal to the ankle joint by the distance L3+D4 (FIGURE 4 on page 11). Therefore:

$$Rkj = Raj + [S] * \begin{bmatrix} 0 \\ L3 + D4 \\ 0 \end{bmatrix} \tag{60}$$

which however leaves one unknown: the distance L3. Using the scalar equivalent of equation (6.23) and resolving along the shank local y-axis, the distance L3 can be calculated with:

$$(X3 - Xo) * S21 + (Y3 - Yo) * S22 + (Z3 - Zo) * S23 = L3 \tag{61}$$

Therefore the knee and ankle joint three dimensional coordinates are calculated in the ground frame of reference as well as the three by three directional cosine matrix that uniquely defines the shank in space relative to the ground frame of reference. The shank axes is defined so that the long axis passes through the ankle and the knee joint centres. X and Y axes defined the anterior-posterior plane of the shank and the Z and Y axes defined the medio-lateral plane. This allowed the force and moment calculations to be evaluated in the planes that are commonly used in the clinical environment. It ought to be pointed out that when dealing with the right shank the same methodology is used, with the directional qualifier, ϵ, equal to -1 and marker 4 replacing 1 (fibula head), 5 replacing 2 (lateral malleolus) and 6 replacing 3 (tibial tuberosity).

0.4.3 THE FOOT SEGMENT

The technical axes of the foot are formed by three markers located on the shoe and placed at mid-heel, lateral to the 5th metatarsal joint and mid-toe (FIGURE 5 on page 16). They were numbered 7, 8, 9 and 10, 11, 12 for the left and right foot respectively. The toe markers are located above the distal phalanges on the top of the shoe. This is preferable to placing them on the tip of the shoe where markers tend to fall off at the end of stance as the foot is brought forward. According to FIGURE 5 on page 16 the first approximation of the axis of the foot, ex_a was defined as lying between the heel and toe markers. Therefore,

$$ex_a = (R6 - R4)/P \tag{62}$$

Where

$$P = ((X6 - X4)^2 + (Y6 - Y4)^2 + (Z6 - Z4)^2)^{1/2} \tag{63}$$

and from the scalar form

$$F11_a = (X6 - X4)/P \tag{64}$$

$$F12_a = (Y6 - Y4)/P \tag{65}$$

$$F13_a = (Z6 - Z4)/P \tag{66}$$

the first approximation of the y-axis of the foot ey_a is defined as lying between the ankle joint and the heel marker giving:

$$ey_a = (Raj - R4)/Q \tag{67}$$

where:

$$Q = ((Xaj - X4)^2 + (Yaj - Y4)^2 + (Zaj - Z4)^2)^{1/2} \tag{68}$$

and in the scalar form:

$$F21_a = (Xaj - X4)/Q \tag{69}$$

$$F22_a = (Yaj - Y4)/Q \tag{70}$$

$$F23_a = (Zaj - Z4)/Q \tag{71}$$

The cross-product of the two above gives the z-axis. It ought to be pointed out here that both the apparent x and y axes are orthogonal to the apparent z-axis, but not necesserily to one another.

$$F31 = F12_a * F23_a - F13_a * F22_a \tag{72}$$

$$F32 = F13_a * F21_a - F11_a * F23_a \tag{73}$$

$$F33 = F11_a * F22_a - F12_a * F21_a \tag{74}$$

According to Procter et al. [1982] the foot twists characteristically about the metatarsal-phangeal (MTP) joints in stance. This fact suggested that the angle of the first approximation of the x-axis and y-axis will vary. Redefinition of the axes is needed to take account of such variations. The real action of the foot involves a rotational axis about the MTP joints which will be slightly oblique to the foot's mid-line. Therefore an assumption was required to establish that the action of the MTP takes place along the previously calculated apparent z-axis. In FIGURE 6 on page 20, M, was defined from:

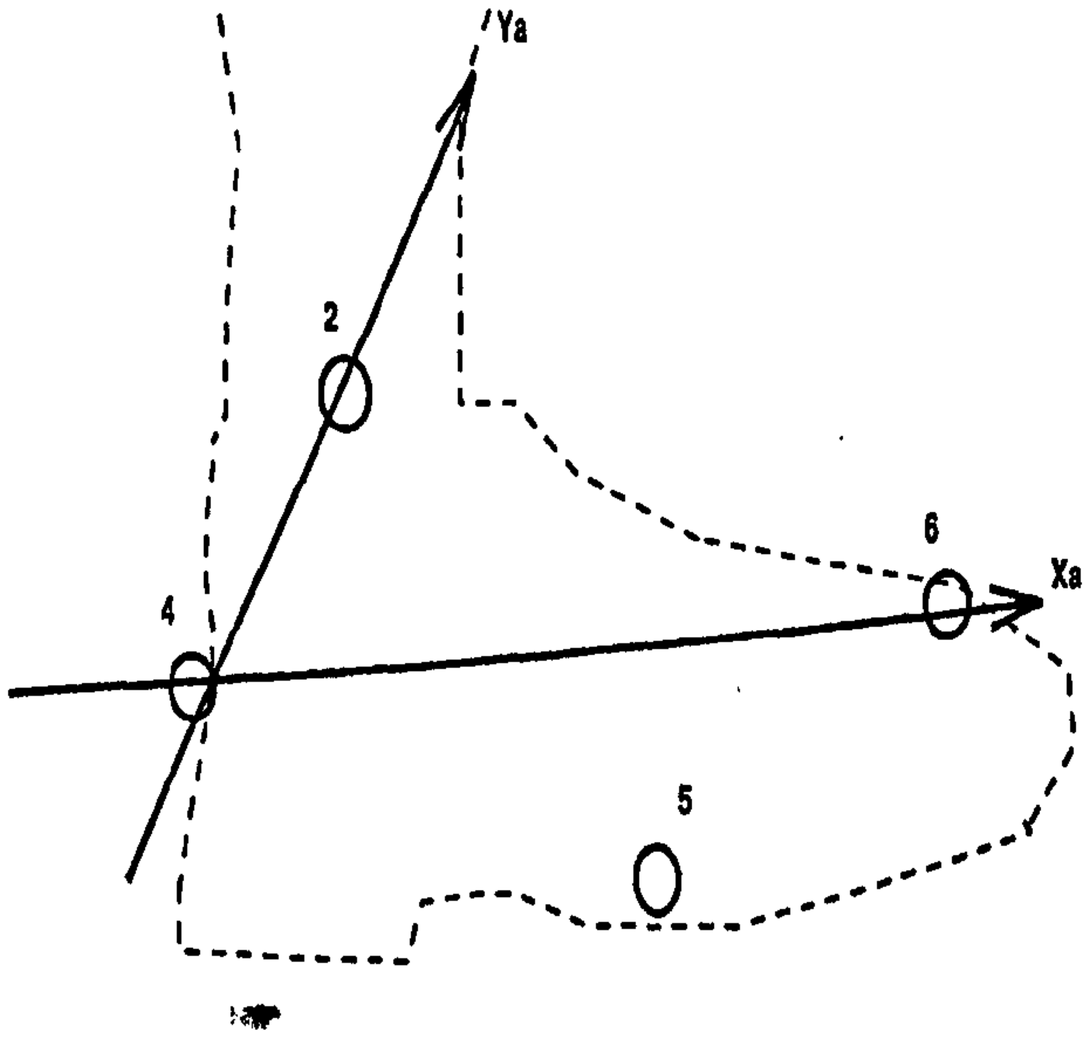

Figure 5: Right foot markers and calculation of the first approximate technical axes

$$Rm = R5 + \epsilon * S2 * ez \tag{75}$$

where $S2$ is the distance from the apparent x-axis to the 5th metatarsal marker calculated by:

$$S2 = ((X5 - X4)^2 + (Y5 - Y4)^2 + (Z5 - Z4)^2)^{1/2} \tag{76}$$

From the scalar form the coordinates of M can be calculated by

$$XM = X5 + \epsilon * S2 * F31 \tag{77}$$

$$YM = Y5 + \epsilon * S2 * F32 \tag{78}$$

$$ZM = Z5 + \epsilon * S2 * F33 \tag{79}$$

Redefinition of the x-axis is therefore possible. It is defined to lie from heel to the MTP joint which excludes twisting of the forefoot relative to the hindfoot.

$$ex = (RM - R4)/S \tag{80}$$

with

$$S = ((XM - X4)^2 + (YM - Y4)^2 + (ZM - Z4)^2)^{1/2} \tag{81}$$

In the scalar form

$$F11 = (XM - X4)/S \tag{82}$$

$$F12 = (YM - Y4)/S \tag{83}$$

$$F13 = (ZM - Z4)/S \tag{84}$$

The cross-product of x and y-axis which are defined as being orthogonal gave the redefined y-axis:

$$F21 = F32 * F13 - F33 * F12 \tag{85}$$

$$F22 = F33 * F11 - F31 * F13 \tag{86}$$

$$F23 = F31 * F12 - F32 * F11 \tag{87}$$

which concludes the orthogonal matrix for the foot [F]. The calculation of the CM of the foot is based on previous anthropometric measurements. It is known that the CM of the foot lies a certain distance from the heel relative to the footlink length. Therefore locating the heel by the heel marker coordinates the CM of the foot can be calculated using:

$$Rh = R4 + (H4 * ex) \tag{88}$$

where $H4$ is the heel marker height.

The scalar form:

$$Xh = X4 + H4 * F11 \tag{89}$$

$$Yh = Y4 + H4 * F12 \tag{90}$$

$$Zh = Z4 + H4 * F13 \tag{91}$$

The CM position (fcm) is calculated according to the $C2$ ratio of the footlink (FL):

$$Rfcm = Rh + C2 * FL * ex \tag{92}$$

The component $(C2 * FL)$ is replaced by predicted length, since in the geometric model the actual length is known, concluding therefore the directional cosine matrix and the CM location of the foot.

0.4.4 THE PELVIS

A number of methods have been employed in the past to locate the hip joint centre (HC), with prediction based on palpable landmarks being the most popular of all. Although the method is considerably less accurate than the method based on x-rays reported by Crownshield et al. [1978], is has been more applicable on the grounds of ethical considerations. Andriacchi et al. [1982] suggested that the HC ought to lie 1.5-2cm directly distal to the mid-point of a line between the pubic symphysis and the ASIS in a frontal plane projection, and directly medial to the greater trochanter in the sagittal plane. Tylkowski et al. [1982] proposed that the HC ought to lie 11 % of the distance between the ASIS medial to, 12% distal to, and 21 % posterior to the ASIS. Cappozzo [1984] suggested that the HC could be predicted by the centre of a sphere described by the three dimensional rotation of a point on the thigh.

Locating the hip centre is an important part of any gait analysis study that entails calculation of pelvi-femoral motion and hip muscle moments. Some investigators have estimated its location from their general knowledge of external landmarks (Eberhart et al. [1947], Paul [1965], Pedotti [1977] Bell et al. [1990]. Others have used radiographs to precisely locate the HC (Johnson et al. [1977]). At least two investigators developed methods to estimate HC location from certain palpable landmarks , Andriacchi et al. [1982]; Tylkowski et al. [1982]. Specifically, Andriacchi's group predicted that the HC would lie 1.5-2 cm directly distal to the midpoint of a line between the pubic symphysis and the anterior superior iliac spines in a frontal plane projection, and directly medial to the greater trochanter in the sagittal plane. Tylkowski's group predicted the HC would lie 11% of the distance between the ASIS medial to, 12% distal to, and 21% posterior to the ASIS. In the Bell et al. [1990] study the percentages in the y-z (frontal) plane from the AP radiographs of 31 normal adults, and the x (AP) direction percentage from the AP (to measure the inter- ASIS distance) and lateral radiographs of 31 normal adult skeleton pelves. The HC was located an average of 14% of the inner-ASIS distance medially, 30% distally, and 22% posteriorly to the ASIS. The difference in the X (AP) direction percentage [19% (current study) vs 22% (previous study)] is probably due to the previously mentioned difficulty in estimating the exact AP locations of the bony ASIS from the skin markers. It was also found that the x (AP) direction error was the greatest contributor to the overall error of HC prediction , larger than the errors in the other two directions, and indicates that this approach is least accurate in predicting the AP location of the HC. Once again, the authors believe that this is due to the inaccuracy of estimating the exact AP locations of the bony ASIS from the skin markers. An even more accurate method can be devised by combining the most accurate elements of Tylkowski 's and Andriacchi's approaches. Tylkowski 's approach can predict the frontal plane HC location within 0.79 cm of the true location. A marker over the greater trochanter projected onto a para-sagittal plane can predict the AP HC location within 0.73 cm, an error most gait investigators would probably consider to be acceptable.

In summary, none of the methods tested was particularly accurate. The rotational method could only predict the HC location within 3.79 cm of the true location. Andriacchi's method was slightly more accurate overall (3.61 cm), but very accurate (0.73 cm) in determining the AP location of the HC. Tylkowski et al.'s approach was significantly better than either (1.90 cm) but was least accurate in predicting the AP HC location. A more accurate method combining the approach of Tylkowski for the frontal plane and the approach of Andriacchi for the AP location predicted the HC location to within 1.07 cm and was the one that was used in the present study.

The geometry of the pelvis is defined by five markers in the static test. They are located on the two anterior superior iliac spines (ASIS), the heads of the two greater trochanters and the midpoint between the two posterior superior iliac spines (PSIS). These are numbered 13 to 17 for the right ASIS, PSIS, right trochanter and left trochanter, respectively (FIGURE 7 on page 21). Trochanter markers were found to interfere with the swinging arm during the several activities which in some cases caused the marker to be displaced. The technical axis of the pelvis was the result of an array of the two ASIS and PSIS markers. Static tests were performed for each subject that static relations could be calculated and the HC was related to the reference

marker, the right ASIS, in the pelvic technical frame of reference. When location of the two hip joint centres was established a more meaningful pelvic anatomical axes system was calculated which involved the two joint centres , thus defining a medio-lateral axis, and the PSIS marker.

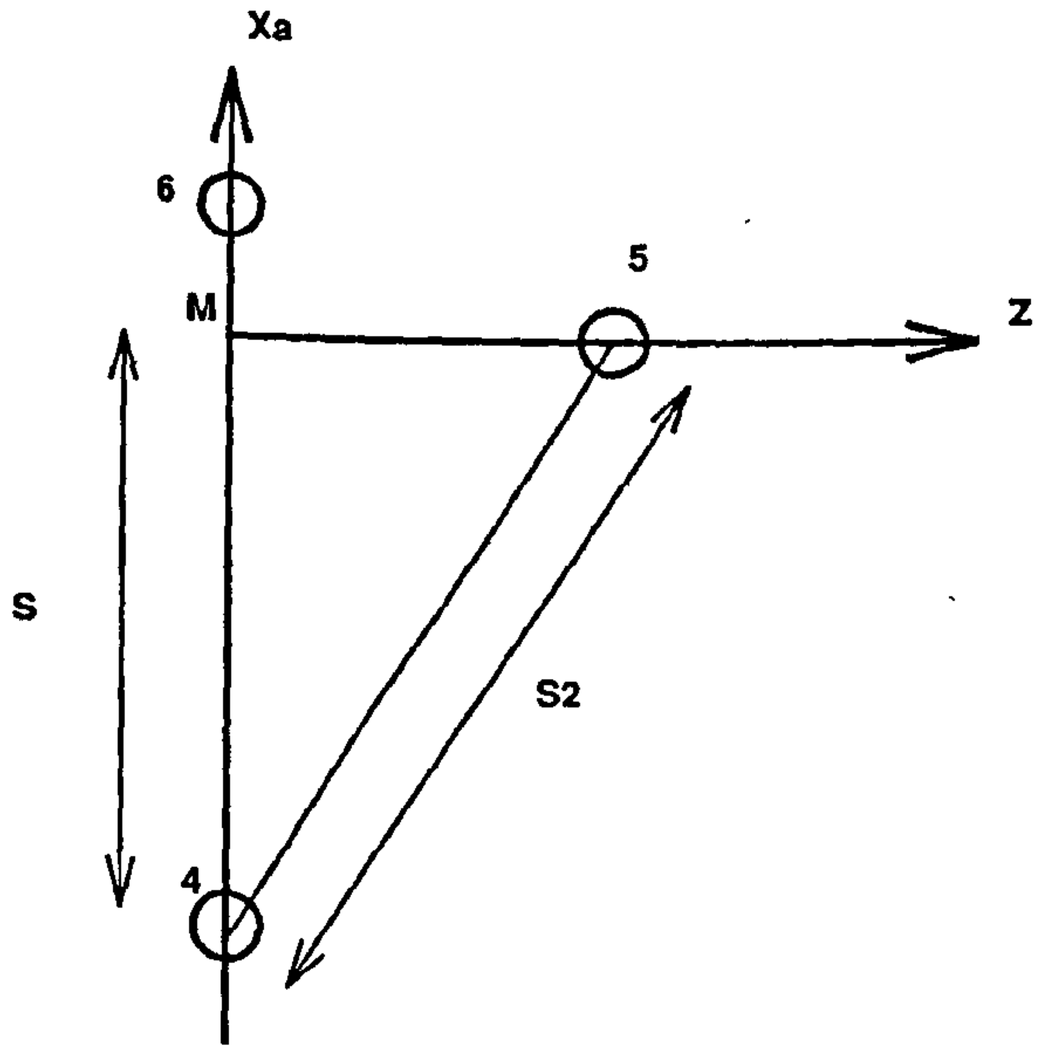

Figure 6: Calculation of the MTP joint in the right foot

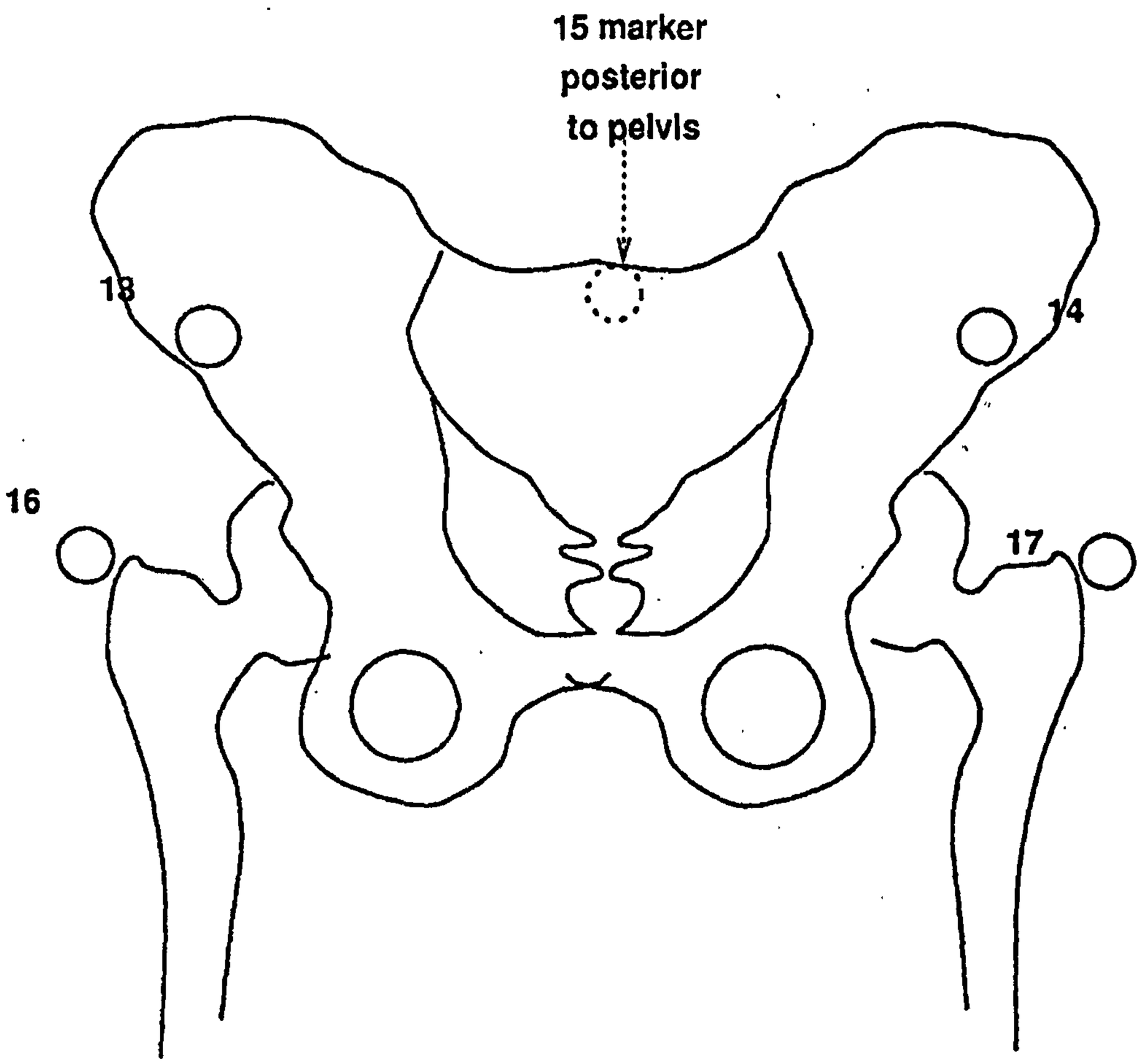

Figure 7: Positioning of the markers on the pelvis

In the static trial, the technical axes of the pelvis are defined by the PSIS and the two ASIS markers. The technical z-axis ez_a was considered to lie between the right (13) and left (14) ASIS markers. By using FIGURE 8 on page 23 and using radius vectors:

$$ez_a = (R13 - R14)/Q \tag{93}$$

where:

$$Q = ((X13 - X14)^2 + (Y13 - Y14)^2 + (Z13 - Z14)^2)^{1/2} \tag{94}$$

and in the scalar form, the three components of the z-axis were determined from:

$$P31_a = (X13 - X14)/Q \tag{95}$$

$$P32_a = (Y13 - Y14)/Q \tag{96}$$

$$P33_a = (Z13 - Z14)/Q \tag{97}$$

The technical x-axis ex_a was defined to lie on the line that joins the PSIS marker perpendicular to the previously defined technical z-axis. From FIGURE 8 on page 23 and solving along the technical z-axis we have:

$$S2 = (X13 - X15) * P31_a + (Y13 - Y15) * P32_a + (Z13 - Z15) * P33_a \tag{98}$$

The origin of the technical axes system, point A, was calculated by:

$$XA = X13 - (HA31_a * S2) \tag{99}$$

$$YA = Y13 - (HA32_a * S2) \tag{100}$$

$$ZA1 = Z13 - (HA33_a * S2) \tag{101}$$

The technical x-axis was defined to lie between the origin and the PSIS marker and by using radii vectors it is:

$$ex_a = (Ra - R15)/SX \tag{102}$$

where:

$$SX = ((XA - X15) + (YA - Y15) + (ZA1 - Z15))0.5 \tag{103}$$

in the scalar form:

$$P11_a = (XA - X15)/SX \tag{104}$$

$$P12_a = (YA - Y15)/SX \tag{105}$$

$$P13_a = (ZA1 - Z15)/SX \tag{106}$$

the third orthogonal technical axis, ey_a, can be calculated by the cross- product of the previous two:

$$P21_a = P32_a * P13_a - P33_a * P12_a \tag{107}$$

$$P22_a = P33_a * P11_a - P31_a * P13_a \tag{108}$$

$$P23_a = P31_a * P12_a - P32_a * P11_a \tag{109}$$

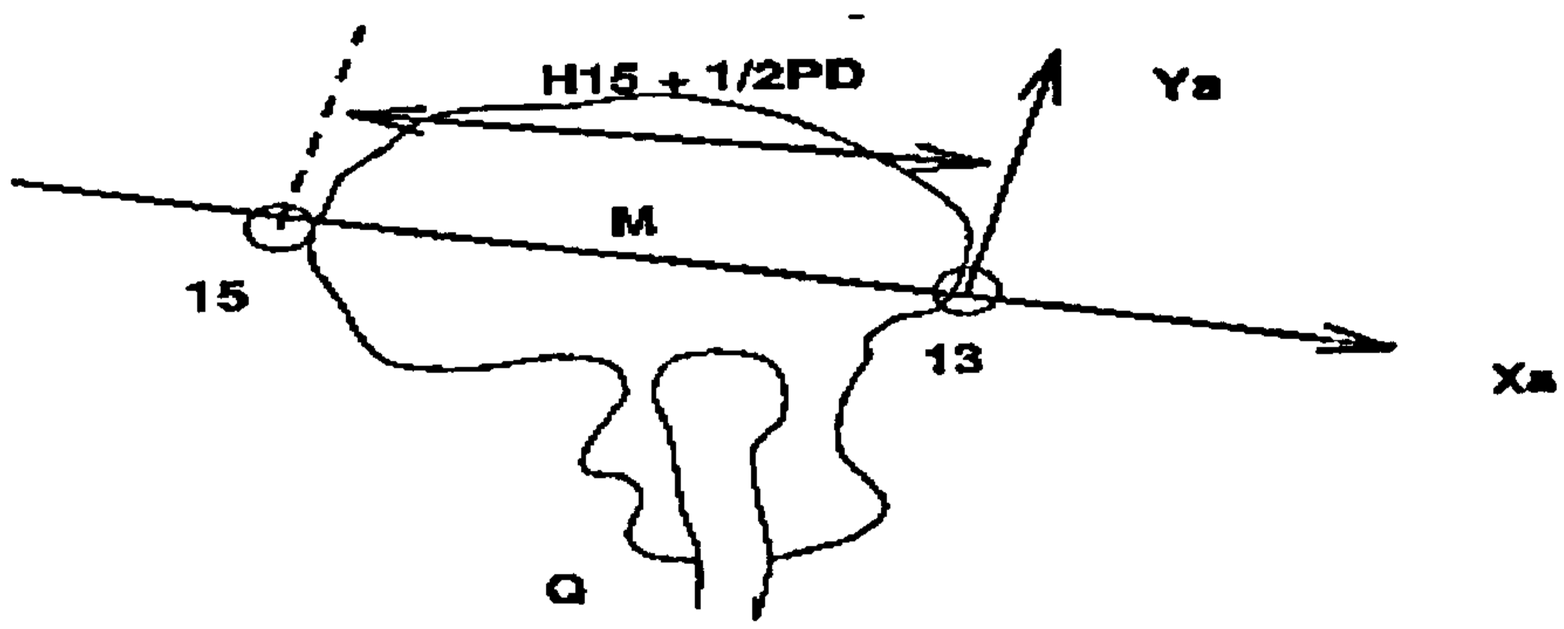
H15 + 1/2PD
Ya
M
15
13
Xa
Q

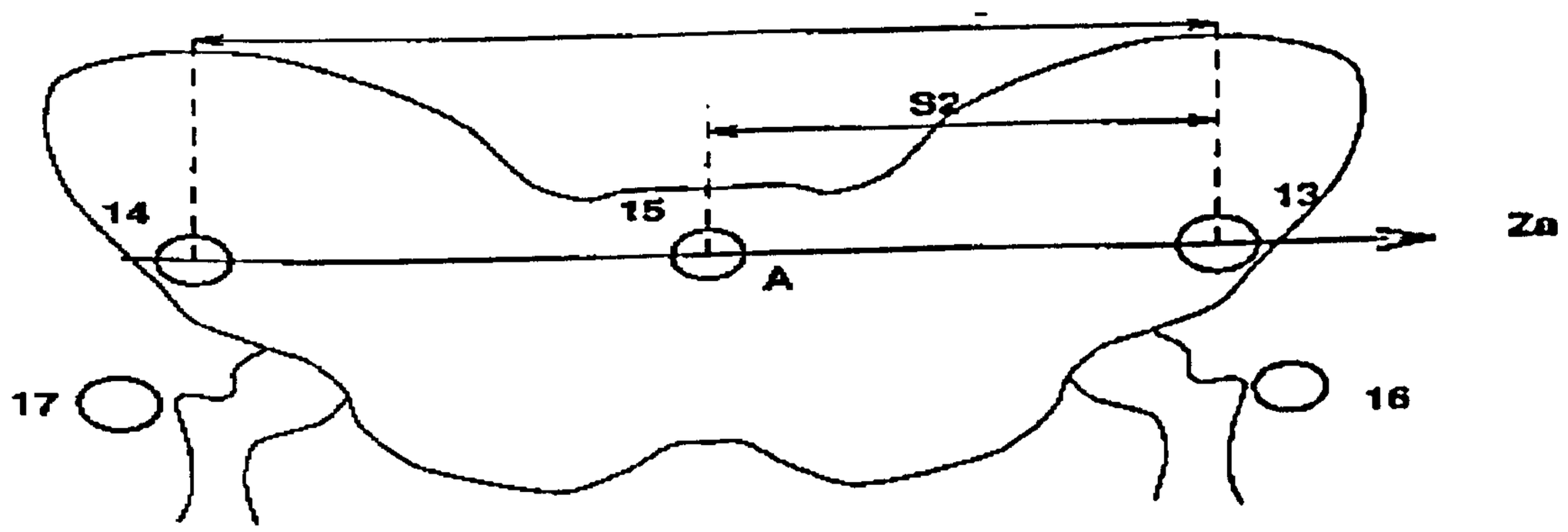
S2
14
15
13
A
Za
17
16

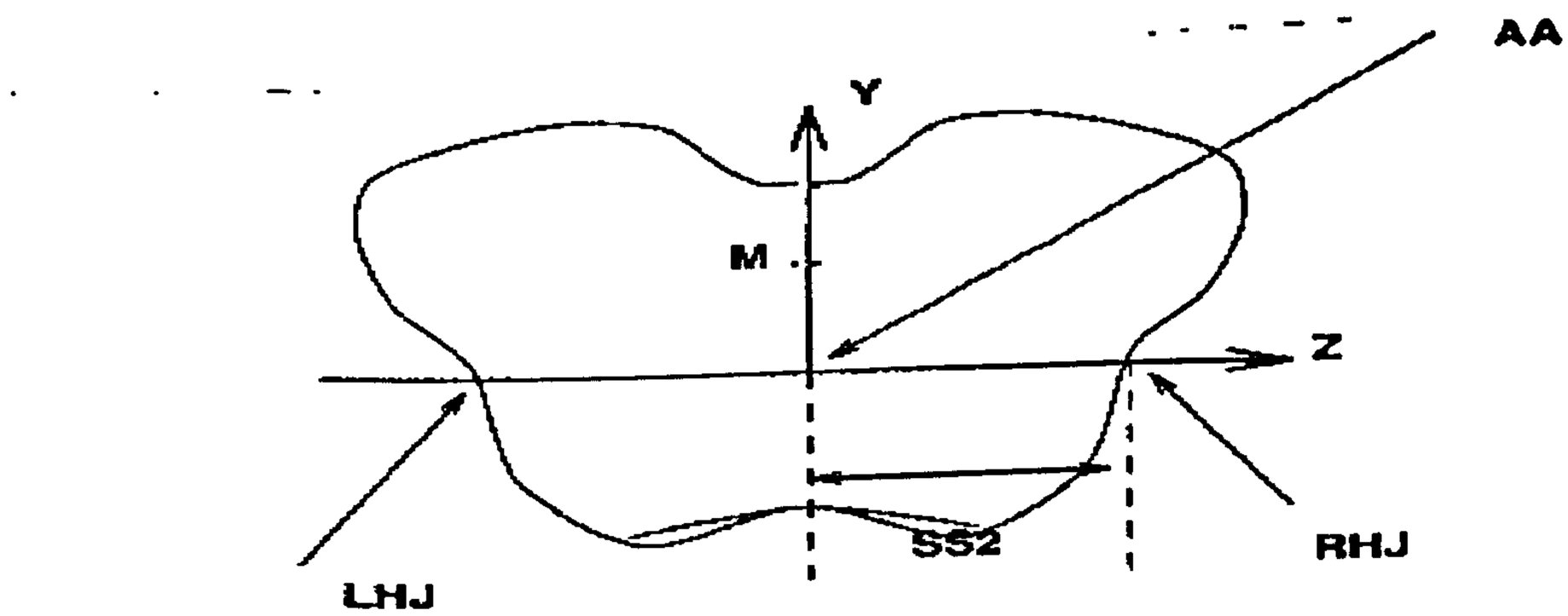
AA
Y
M
Z
SS2
RHJ
LHJ

which concludes the directional cosine matrix of the pelvis $[P_a]$.

All useful information such as the coordinates of the ASIS and the trochanter markers with the general form X_g, Y_g, Z_g *can be converted to the local pelvic technical frame of reference* (X_1, Y_1, Z_1) *using:*

$$\begin{bmatrix} X_1 \\ Y_1 \\ Z_1 \end{bmatrix} = [P_a] * \begin{bmatrix} X_g \\ Y_g \\ Z_g \end{bmatrix} \tag{110}$$

In this point the coordinates of the left (LHJ) and right (RHJ) hip joint centres were determined according to previously mentioned Bell s predictive equations keeping the local technical axes frame of reference of the pelvis the reference for the calculations:

$$XLHJ_1 = X17_1 \tag{111}$$

$$YLHJ_1 = Z14_1 - (0.3 * Q) \tag{112}$$

$$ZLHJ_1 = Z14_1 + (0.14 * Q) \tag{113}$$

$$XRHJ_1 = X16_1 \tag{114}$$

$$YRHJ_1 = Y13_1 - (0.3 * Q) \tag{115}$$

$$ZRHJ_1 = Z13_1 - (0.14 * Q) \tag{116}$$

Since ASIS is the only marker present on both the static and dynamic trials, static relations were then calculated for each ordinate relative to the right ASIS:

$$SXLHJ = X13_1 - XLHJ_1 \tag{117}$$

$$SYLHJ = Y13_1 - YLHJ_1 \tag{118}$$

$$SZLHJ = Z13_1 - ZLHJ_1 \tag{119}$$

$$SXRHJ = X13_1 - XRHJ_1 \tag{120}$$

$$SYRHJ = Y13_1 - YRHJ_1 \tag{121}$$

$$SZRHJ = Z13_1 - ZRHJ_1 \tag{122}$$

Equations (6.90) to (6.106) can be used to calculate the technical axes system $[P_a]$ *in the dynamic trials. The reference right ASIS marker can be converted to the local technical axes using equation (6.107) and the coordinates, in the local technical frame of reference, of the hip joints determined by rearranging equations (6.114 to 6.195). The coordinates of hip joint centres can then be converted to the ground frame of reference by applying the inverse matrix of the technical axes:*

$$\begin{bmatrix} X_g \\ Y_g \\ Z_g \end{bmatrix} = [P_a]^{-1} * \begin{bmatrix} X_1 \\ Y_1 \\ Z_1 \end{bmatrix} \tag{123}$$

For the calculation of the anatomical pelvic frame of reference:

The z-axis was defined as lying between the two hip joints. Using radius vectors:

$$ez = (Rrhj - Rlhj)/PZ \tag{124}$$

Figure 8: Calculation of pelvic local axis system

Where

$$PZ = ((XRHJ - XLHJ)^2 + (XLHJ - YRHJ)^2 + (ZLHJ - ZRHJ)^2)^{1/2} \quad (125)$$

In the scalar form:

$$P31 = (XRHJ - XLHJ)/PZ \quad (126)$$

$$P32 = (YRHJ - YLHJ)/PZ \quad (127)$$

$$P33 = (ZRHJ - ZLHJ)/PZ \quad (128)$$

M, the mid-point of the pelvis relative to the PSIS, was calculated based on the anthropometrical measurements of the actual depth of the pelvis (PD), the height of the PSIS marker, H15, and the previously calculated technical x- axis of the pelvis as seen in the FIGURE 8 on page 23. Using radius vectors:

$$Rm = R15 + ex_a * (H15 + (0.5 * PD)) \quad (129)$$

And from the scalar form:

$$XM = X15 + P11_a * (H15 + (0.5 * PD)) \quad (130)$$

$$YM = Y15 + P12_a * (H15 + (0.5 * PD)) \quad (131)$$

$$ZM = Z15 + P13_a * (H15 + (0.5 * PD)) \quad (132)$$

with point AA defined by:

$$SS2 = (XRHJ - XM) * P31 + (YRHJ - YM) * P32 + (ZRHJ - ZM) * P33 \quad (133)$$

$$XAA = (XRHJ - SS2 * P31) \quad (134)$$

$$YAA = (YRHJ - S22 * P32) \quad (135)$$

$$ZA1A = (ZRHJ - S22 * P33) \quad (136)$$

The axis lying between the defined points M and AA was considered the y-axis of the pelvis. Using radius vectors:

$$ey = (Rm - Raa)/SSX \quad (137)$$

Where:

$$SSX = ((XM - XAA)^2 + (YM - YAA)^2 + (ZM - ZA1A)^2)^{1/2} \quad (138)$$

And in the scalar form:

$$P21 = (XM - XAA)/SSX \quad (139)$$

$$P22 = (YM - YAA)/SSX \quad (140)$$

$$P23 = (ZM - ZA1A)/SSX \quad (141)$$

The x axis was found by applying cross-product to complete the anatomical frame of reference:

$$P11 = P22 * P33 - P23 * P32 \quad (142)$$

$$P12 = P23 * P31 - P21 * P33 \quad (143)$$

$$P13 = P21 * P32 - P22 * P31 \quad (144)$$

0.4.5 THE THIGH SEGMENT

The thigh segment imposes particular difficulties in modelling of the lower limb since markers are usually located on its extremities. The latter occurs as a consequence of a large amount of soft tissue, mainly muscle, which adds to the considerable lack of palpable landmarks. At the proximal area the only possible location of a bony landmark is the trochanter. The problem arises from the fact that if a marker is placed on the trochanter, the rotational behaviour of the thigh about the hip joint is not reproduced by the motion of the head of the trochanter, but the marker actually moves by a smaller amount, due to the underlying soft tissue. This can have a negative effect in the analysis and interpretation of the rotational thigh behaviour about the hip. The distal end provides a more suitable place for marker location i.e. the condyles of the femur. However, another problem arises because the femur condyle markers are too close to the marker on the fibular head. Identification problems in the VICON software occur as the consequence of the interference between these markers. A possible solution would be to place a cuff around the thigh and mount an array of markers on this. Movement of the cuff relative to the thigh is also inevitable. Therefore the thigh was considered to be the less satisfactory segment in terms of marker positioning. A compromise was reached in that the assumption was made that no rotation occurred at the knee, rather any rotation occurring at the shank relative to the pelvis occurred at the hip. This allowed the knee and hip joint centres to be used to define the long axes of the thigh. The z-axis of the shank was then used to predict the first approximation of the z-axis of the thigh.

As mentioned above the anatomical long axis of the thigh segment was defined as the line joining the knee and hip joint centres.

This leads to:

$$ey = (Rhj - Rkj)/P \tag{145}$$

where

$$P = ((Xhj - Xkj)^2 + (Yhj - Ykj)^2 + (ZhJ - Zkj)^2)^{1/2} \tag{146}$$

To calculate the three dimensional cosine matrix requires use of the scalar form:

$$T21 = (Xhj - Xkj)/P \tag{147}$$

$$T22 = (Yhj - Ykj)/P \tag{148}$$

$$T23 = (Zhj - Zkj)/P \tag{149}$$

and the z-axis of the shank is used as the first approximation of the z-axis and therefore by applying the cross-product of the latter and the calculated y-axis of the thigh , the x-axis (ex) can be evaluated:

$$T11 = T22 * S33 - T23 * S32 \tag{150}$$

$$T12 = T23 * S31 - T21 * S33 \tag{151}$$

$$T13 = T21 * S32 - T22 * S31 \tag{152}$$

But the above calculations of the first approximation of the z-axis of the thigh will not necessarily establish orthogonality of the z-axis to the calculated y-axis of the thigh. This is a result of the more medial location of the hip joint (FIGURE 9 on page 28) and therefore, the true z- axis of the thigh was calculated by cross-product to ensure orthogonality:

$$T31 = T12 * T23 - T13 * T22 \tag{153}$$

$$T32 = T13 * T21 - T11 * T23 \tag{154}$$

$$T33 = T11 * T22 - T12 * T21 \tag{155}$$

which concludes the directional cosine matrix of the thigh segment.

0.5 DATA FILTERING TECHNIQUES

The procedure used here was the classical approach that has been established by the biomechanics laboratory at the University of Strathclyde and has been applied to the studies of similar activities in the past.

In the first phase the output displacement data from the VICON system was filtered using a low pass filter. The filter employed was a fourth order Butterworth filter. A second filtering process was introduced by employing a polynomial based differentiator to obtain the linear velocities and accelerations of the derived joint centre coordinate data obtained from the application of marker arrays and the principles of rigid body mechanics. The two filtering procedures were not performed simultaneously because of the errors involved. A possible scenario would be to first differentiate the original coordinate data from the markers to obtain the linear velocities and accelerations of the markers used in the arrays. These would then be converted to the segmental local axes system and the velocities and accelerations of the derived joint centres and centres of mass would follow. This approach though is susceptible to errors. The most affected of all data would be the double differentiated acceleration data. Tooth [1976] described the low pass FIR digital filter that was employed here and has also been used in the past in the Strathclyde Biongineering Unit . Early studies of the filter's theoretical response to an impulse signal were performed in the Unit and provided evidence to support the use of this particular filter amongst a number of other suggestions. It was demonstrated that of a whole series of digital filters this gave the best response in the frequency range that was of interest, that is, 0 to 10 Hz, the frequency range associated with normal gait. The fourth order filter had the following properties: zero phase lag, a span of 9 points, resulting in the loss of 4 data points from the beginning and the end of data record due to end effects. This problem was solved because the record was of much greater length than that required to carry out the procedure. Appendix A provides the listing of the algorithm of the butterworth filter, referred to as FILTER.FOR. The polynomial differentiator used in the analysis was the same as that used by Paul [1966] and is described in chapter 5. Appendix A provides the listing of the algorithm as well as the position of both algorithms in the analysis.

0.6 JOINT FORCES AND MOMENT SAMPLE CALCULATIONS

The procedure of calculation of the three dimensional forces and moments at hip, knee and ankle joints involved working from the distal to the proximal end. The external reaction forces from the floor were considered to act on the foot segment and had to be combined with the inertial forces due to the mass of the foot. The first step led to a three dimensional force and moment vector applied to the ankle. This vector was the input to the shank segment and combined with the inertial effect of the shank mass, to produce the force and moment loads acting to the knee. The same procedure was followed for the thigh segment and the hip loads. The force

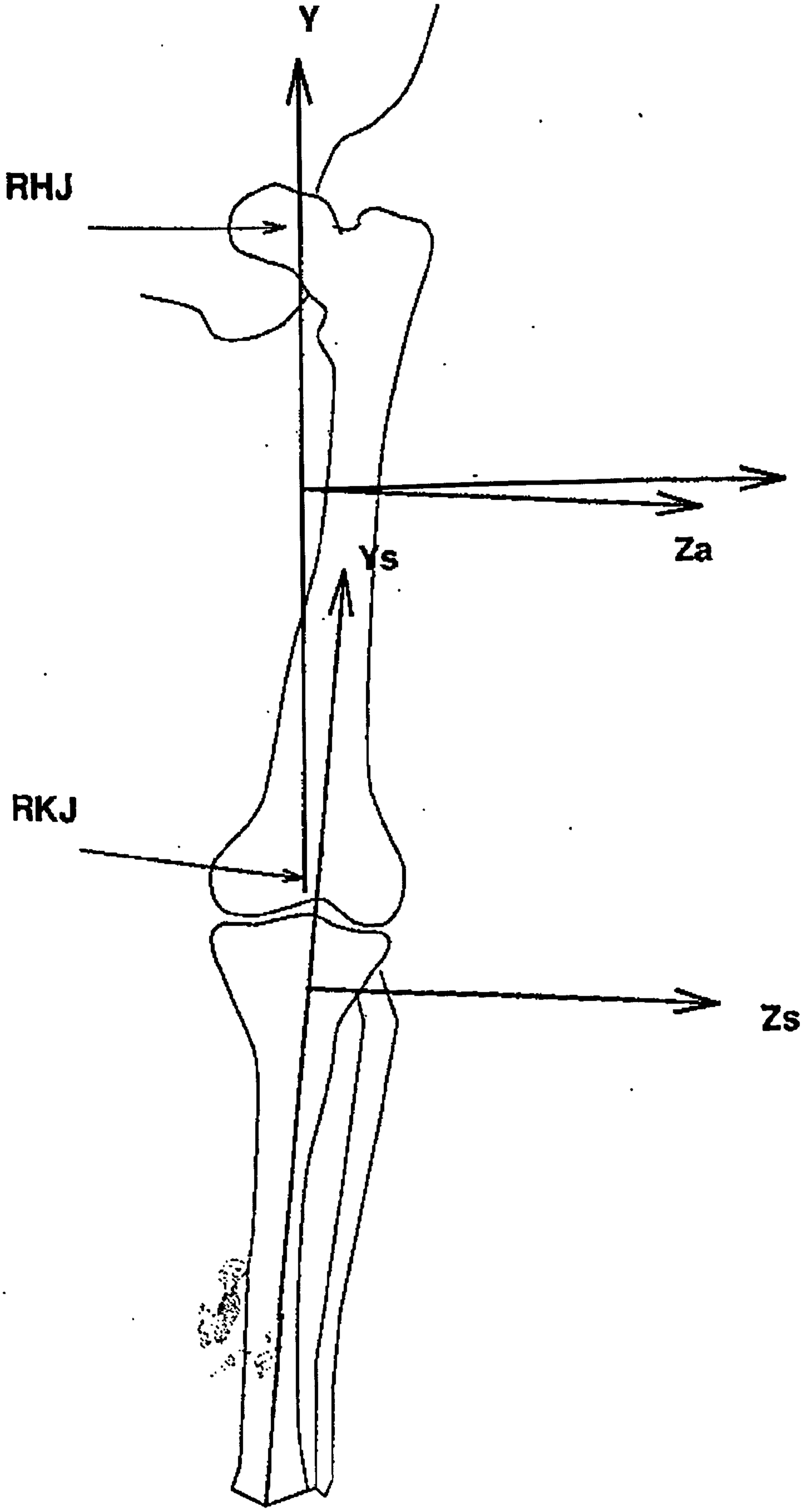
Y
RHJ
Z
Za
Ys
RKJ
Zs

and moment calculations were performed in the local axis system of the segment in question since the mass moment of inertia about the longitudinal axis of each segment was unknown. In the local frame of reference the segment length does not change and in this case the segment is behaving as a rigid body. To allow for a better interpretation of the results the net forces and moments applied to a joint were expressed in the local axes system of the segment distal to the joint. The resultant loading information is then converted to the ground frame of reference for input into the next segmental calculation.

As seen in FIGURE 10 on page 30 the calculations of the intersegmental force and moment loads applied to segment B had the following form using:

Fdj is the externally applied force to the distal end in the ground frame of reference.

Mdj is the externally applied moment to the distal end in the ground frame of reference.

[B] is the directional cosine matrix for segment B.

g is the gravitational acceleration (-9.80 ms^{-2})

Xdj, Ydj and Zdj are the distal coordinates in the ground frame of reference.

Xpj, Ypj and Zpj are the proximal joint coordinates in the ground frame of reference.

AXdj, AYdj and AZdj are the linear accelerations of the distal joint centre in the ground frame of reference.

AXpj, AYpj and AZpj are the linear accelerations of the proximal joint centre in the ground frame of reference.

The conversion of the external intersegmental forces and moments to the local frame of reference required:

$$\begin{bmatrix} Fxdj_L \\ Fydj_L \\ Fzdj_L \end{bmatrix} = [B] * \begin{bmatrix} Fxdj \\ Fydj \\ Fzdj \end{bmatrix} \tag{156}$$

and:

$$\begin{bmatrix} Mxdj_L \\ Mydj_L \\ Mzdj_L \end{bmatrix} = [B] * \begin{bmatrix} Mxdj \\ Mydj \\ Mzdj \end{bmatrix} \tag{157}$$

The conversion of the gravitational acceleration into the local frame of reference required:

$$\begin{bmatrix} gx_L \\ gy_L \\ gz_L \end{bmatrix} = [B] * \begin{bmatrix} 0 \\ g \\ 0 \end{bmatrix} \tag{158}$$

The conversion of the coordinates of the distal and proximal joint centres to the local frame of reference required:

$$\begin{bmatrix} Xdj_L \\ Ydj_L \\ Zdj_L \end{bmatrix} = [B] * \begin{bmatrix} Xdj \\ Ydj \\ Zdj \end{bmatrix} \tag{159}$$

$$\begin{bmatrix} Xpj_L \\ Ypj_L \\ Zpj_L \end{bmatrix} = [B] * \begin{bmatrix} Xpj \\ Ypj \\ Zpj \end{bmatrix} \tag{160}$$

The conversion of the linear accelerations of the joint centres to the local frame of reference required:

Figure 9: Right thigh axes system (posterior view)

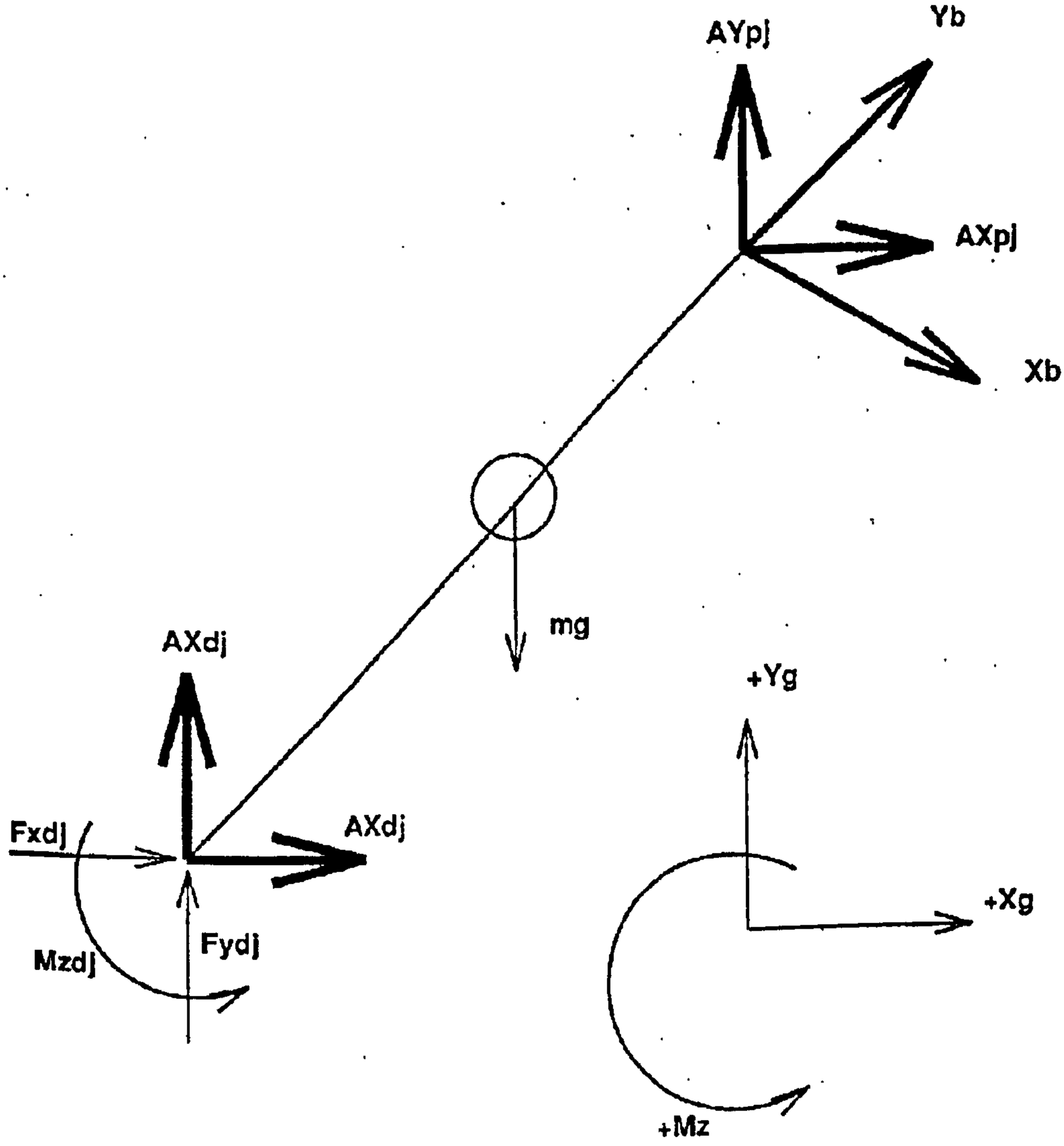
AYpj
Yb
AXpj
Xb
mg
AXdj
Fxdj
AXdj
Fydj
Mzdj
+Yg
+Xg
+Mz

$$\begin{bmatrix} AXdj_L \\ AYdj_L \\ AZdj_L \end{bmatrix} = [B] * \begin{bmatrix} AXdj \\ AYdj \\ AZdj \end{bmatrix} \tag{161}$$

$$\begin{bmatrix} AXpj_L \\ AYpj_L \\ AZpj_L \end{bmatrix} = [B] * \begin{bmatrix} AXpj \\ AYpj \\ AZpj \end{bmatrix} \tag{162}$$

The calculation of the segment length proximal to distal joint centre required:

$$Y = (Ypj_L - Ydj_L) \tag{163}$$

The calculation of the angular acceleration components of the segment (as mentioned earlier, the angular acceleration about the longitudinal y-axis is zero, according to rigid body mechanics) required:

$$AAx = (AXpj_L - AXdj_L)/Y \tag{164}$$

$$AAz = (AZpj_L - AZdj_L)/Y \tag{165}$$

The calculation of the linear accelerations of the CG of the segment in question, based on the distance C2 from the proximal joint centre required:

$$AXcg_L = (C2 * Y * AAx) \tag{166}$$

$$AZcg_L = (C2 * Y * AAz) \tag{167}$$

The calculation of the inertia forces applied to the proximal joint centre imparted by the segment mass required:

$$IFxpj_L = mass * (gx_L + AXcg_L) \tag{168}$$

$$IFypj_L = mass * gy_L \tag{169}$$

$$IFzpj_L = mass * (gz_L + AZcg_L) \tag{170}$$

The summation of the forces imparted to the proximal joint gave:

$$Fxpj_L = Fxdj_L + IFxpj_L \tag{171}$$

$$Fypj_L = Fydj_L + IFypj_L \tag{172}$$

$$Fzpj_L = Fzdj_L + IFzpj_L \tag{173}$$

The calculation of the moments at the proximal joint centre caused by the external forces imparted to the distal end (with attention given to the fact that no moment will be produced about the y-axis since the y component of the distal force acts through the proximal joint centre) required:

Figure 10: Free body diagram for segment B (X-Y plane of the ground frame of reference)

$$Mxextpj_L = Fzdj_L * Y \tag{174}$$

$$Mzextpj_L = Fxdj_L * Y \tag{175}$$

The calculation of the moment due to inertial forces required:

$$IMxpj_L = IFzpj_L * Y * C2 \tag{176}$$

$$IMzpj_L = IFxpj_L * Y * C2 \tag{177}$$

The calculation of the inertial torque imparted to the proximal joint centre due to the segmental inertia, estimated from the moment of inertia, IYY, was carried out using the body segment parameters:

$$ITx_L = -IYY * AAx \tag{178}$$

$$ITz_L = -IYY * AAz \tag{179}$$

The summation of the moments imparted to the proximal joint centre in the local frame required:

$$Mxpj_L = Mxextpj_L + IFxpj_L + ITx_L \tag{180}$$

$$Mypj_L = 0.0 \tag{181}$$

$$Mzpj_L = Mzextpj_L + IFxpj_L + ITz_L \tag{182}$$

Therefore the net loading information, i.e. forces and moments imparted to the proximal joint centre are defined. This information had to be converted back to the ground frame of reference with the use of the inverse matrix $[B]^{-1}$ *so that it could be the input into the next segmental calcualtions. For the swinging phase the externally applied forces and moments were equal to zero. For the foot during the stance phase the external forces (Fxcp, Fycp, Fzcp) were measured as acting at the centre of pressure (Xcp, Ycp, Zcp) which suggested that the calculation ought to take this fact into consideration. The first step was to convert the centre of pressure coordinates into the foot local frame of reference:*

$$\begin{bmatrix} Xcp_L \\ Ycp_L \\ Zcp_L \end{bmatrix} = [B] * \begin{bmatrix} Xcp \\ Ycp \\ Zcp \end{bmatrix} \tag{183}$$

The calculation of the moments due to external forces, equations (6.174) and (6.175) was replaced by:

$$Mxpj_L = (Fycp_L * Zcp_L) - (Fzcp_L * Ycp_L) \tag{184}$$

$$Mypj_L = (Fzcp_L * Xcp_L) - (Fxcp_L * Zcp_L) \tag{185}$$

$$Mzpj_L = (Fxcp_L * Ycp_L) - (Fycp_L * Xcp_L) \tag{186}$$

Equation (6.169) representing the inertial force component in the y- axis of the foot was also changed due to the definition on the foot local axes system to:

$$IFypj_L = mass * (gy_L + Axcg_L) \tag{187}$$

The calculation of the moments due to inertial forces of the foot (equations 6.176 and 6.176) was also changed to take into accound the axes definition of the foot:

$$IFxpj_L = (IFypj_L * Zdj_L) - (IFzpj_L * Ydj_L) \tag{188}$$

$$IFypj_L = (IFzpj_L * Xdj_L) - (IFxpj_L * Zdj_L) \tag{189}$$

$$IFzpj_L = (IFxpj_L * Ydj_L) - (IFypj_L * Xdj_L) \tag{190}$$

The definition of the foot allows in theory the inertial moment to have components about each of the three axes. However, lack of body segment data to enable the calculation of inertia about the transverse axis of the foot, made the determination of the latter impossible. It ought to be pointed out though that the inertial torque has the smallest contribution to the total moment about the proximal joint. During the stance phase the inertial torque approaches zero due to the fact that the angular acceleration becomes zero. All the above facts suggest that the inertial torque about the transverse axis of the foot could be ignored.

The listings of the algorithms and the command file that run the analysis can be found in the discette that accompanies the thesis. The calculations about each joint were performed by a series of algorithms. These were: LANKLE.FOR, LKNEE.FOR, LHIP.FOR, RANKLE.FOR, RKNEE.FOR, RHIP.FOR which referred to the calculation of the forces and moments at the ankle, knee and hip joints for the left and right sides of the body respectively.

0.7 Calculation of joint angles

As discussed earlier the method used to calculate joint angles was that suggested by Grood et al. [1983]. The floating axis involves three directional cosines (F1, F2, F3) which are calculated from the cross-product of the directional cosines of y-axis of the distal segment (D21, D22, D23) and those of the z-axis (P31, P32, P33) of the proximal segment:

$$F1 = D22 * P33 - D23 * P32 \tag{191}$$

$$F2 = D23 * P31 - D21 * P33 \tag{192}$$

$$F3 = D21 * P32 - D22 * P31 \tag{193}$$

The angle of abduction-adduction (AA) was defined as the angle between the z-axis of the proximal segment and the y-axis of the distal segment as shown in the next equation:

$$AA = \eta * ((cos^{-1}(P31 * D21 + P32 * D22 + P33 * D23)) - 90^o) \tag{194}$$

where η was a qualifier to represent the side of the body. Adduction is in opposite directions for the two sides of the body, just as in any axes system. The 90 degree offset meant that the calculated angles resembled those used in the clinical setting.

The flexion-extension angle was defined to lie between the y-axis of the proximal segment and the floating axis as shown in the next calculation:

$$Fe = \zeta * sin^{-1}(F1 * P21 + F2 * P22 + F3 * P23) \tag{195}$$

where ζ again is a qualifier because flexion is not in the same direction at all joints. In the axis systems, flexion at the hip is opposite to flexion of the knee.

The internal-external angle was defined by the angle between the z-axis of the distal segment and the floating axis as shown in the next equation:

$$IE = \eta * sin^{-1} * (F1 * D31 + F2 * D32 + F3 * D33) \tag{196}$$

with η being again a qualifier to account for the difference in axes derived angles for the two sides of the body. The three angles with their clinical applicability were calculated using algorithm FLAXIS.FOR which can be found in the discette that accompanies the thesis.

0.8 MODEL GAIT-2

Model Gait-2 uses most of the techniques presented in Gait-1. The differences between Gait-1 and Gait-2 refer to the determination of the knee joint centre which caused the introduction in Gait-2 of the Dynamic coordinate system. The test protocol had to change to take into account the new marker positions in the lower limb (FIGURE 11 on page 38) and during the static trial (trial for the determination of the several joint centres -see protocol) both the Dynamic and segmental coordinate systems were evaluated. When the directional cosine relationships of Dynamic and segmental coordinate systems were established with respect to the ground frame of reference, the segmental system was expressed with respect to the dynamic coordinate system. This relationship was used for the recovery of the segmental marker system during the actual Dynamic trials for the necessary calculations. The calculations referred to both right and left lower limbs.

If the Dynamic and segmental coordinate systems' directional cosine matrices with respect to the ground frame of reference are D_{D-g} (to be used for dynamic to ground conversion) and S_{S-g} (to be used for segment to ground conversion) respectively and S_D the directional cosine matrix of the segment system expressed with respect to dynamic systrem then in the static trial to relate the systems we need:

$$\{x,y,z\}_D = D_{D-g} * (\{x,y,z\}_g - \{x,y,z\}_{DO_g}) \tag{197}$$

where $\{x,y,z\}_D$ and $\{x,y,z\}_g$ are the marker coordinates expressed in the dynamic and segmental coordinate systems respectively and $\{x,y,z\}_{DO_g}$ is the origin of the dynamic system expressed in the ground system.

In the dynamic trial the reverse takes place to recover the marker which now is missing:

$$\{x,y,z\}_g = D_{g-D} * (\{x,y,z\}_D) + \{x,y,z\}_{DO_g} \tag{198}$$

In each dynamic trial the segmental system was reproduced and used in the calculations. Example calculations are shown in the next sections.

0.8.1 Thigh segment coordinate system

The new segment (local) coordinate system of the thigh was calculated to allow the application of origin and insertion data from Brand [1992]. The new thigh segment coordinate system was based on the previously calculated hip joint centre and the two new markers placed on medial and lateral epicondyles.

The system origin was the new knee joint centre calculated to lie in the midpoint of the line joining the two epicondyles. For the left knee the calculation of the knee joint centre involved markers 18 and 19, (the right knee refers to markers 20 and 21) (ϵ is the direction qualifier indicator (+1, -1):

$$ez = (R18 - R19)/P \tag{199}$$

where

$$P = ((X18 - X19)^2 + (Y18 - Y19)^2 + (Z18 - Z19)^2)^{1/2} \tag{200}$$

Using the scalar form to calculate the cosines for the z-axis:

$$T31 = (X18 - X19)/P \tag{201}$$

$$T32 = (Y18 - Y19)/P \tag{202}$$

$$T33 = (Z18 - Z19)/P \tag{203}$$

$$EP = \epsilon * (EPI * 0.5) + H18 \tag{204}$$

Where EPI is the distance between the two epicondyles as measured during the anthropometric measurements and H18 the height of marker 18.

And the midpoint is Lkj i.e. the knee centre in the scalar form:

$$XLkj = X18 + \epsilon * (T31 * EP) \tag{205}$$

$$YLkj = Y18 + \epsilon * (T32 * EP) \tag{206}$$

$$ZLkj = Z18 + \epsilon * (T33 * EP) \tag{207}$$

Therefore, the new thigh segment coordinate system calculation of the y-axis was carried out using the hip and knee joint centres:

$$ey = (Rhj - Rkj)/P \tag{208}$$

Using the scalar form:

$$T21 = (Xhj - Xkj)/P \tag{209}$$

$$T22 = (Yhj - Ykj)/P \tag{210}$$

$$T23 = (Zhj - Zkj)/P \tag{211}$$

where

$$P = ((Xhj - Xkj)^2 + (Yhj - Ykj)^2 + (Zhj - Zkj)^2)^{1/2} \tag{212}$$

Calculation of the first approximation of the z-axis between Lkj and marker 18 requires in the scalar form:

$$TA31 = (X18 - Xkj)/PQ \tag{213}$$

$$TA32 = (Y18 - Xkj)/PQ \tag{214}$$

$$TA33 = (Z18 - Xkj)/PQ \tag{215}$$

where:

$$PQ = ((X18 - Xkj)^2 + (Y18 - Xkj)^2 + (Z18 - Xkj)^2)^{1/2} \tag{216}$$

applying cross-product to estimate the x-axis:

$$T11 = T22 * TA33 - T23 * TA32 \tag{217}$$

$$T12 = T23 * TA31 - T21 * TA33 \tag{218}$$

$$T13 = T21 * TA32 - T22 * TA31 \tag{219}$$

The above calculations of the first approximation of the thigh z-axis will not necessarily establish orthogonality of the z-axis to the calculated thigh y-axis . This is a result to the more medial location of the hip joint and therefore, the true z- axis of the thigh was calculated by cross-product to ensure orthogonality:

$$T31 = T12 * T23 - T13 * T22 \tag{220}$$

$$T32 = T13 * T21 - T11 * T23 \tag{221}$$

$$T33 = T11 * T22 - T12 * T21 \tag{222}$$

Which concludes the direction cosine matrix for the thigh segment coordinate system.

0.8.2 Thigh Dynamic coordinate system

In Gait-2 the segment thigh axes system was only evaluated during the static trial. In the Dynamic trial as seen in Figure 11 on page 38 the segmental axes system markers are not present. That means that the two systems, Dynamic and segmental ought to be related in terms of direction cosine matrices in the static trial so that the segment system markers will be reproduced with the help of the cosine relationships during the dynamic trial calculations.

But first, the Dynamic system had to be calculated in the static trial calculations. The Dynamic axes system was based on markers 22 and 23 for the left thigh and markers 24 and 25 for right thigh as well as the hip joint centre as calculated before (see FIGURE 11 on page 38):

$$ez = (R22 - R23)/PS \tag{223}$$

where:

$$PS = ((X22 - X23)^2 + (Y22 - Y23)^2 + (Z22 - Z23)^2)^{1/2} \tag{224}$$

Using the scalar form to calculate the z-axis:

$$T31_D = (X22 - X23)/PS \tag{225}$$

$$T32_D = (Y22 - Y23)/PS \tag{226}$$

$$T33_D = (Z22 - Z23)/PS \tag{227}$$

The first approximation of y-axis is evaluated from marker 22 and the hip joint centre Hj:

$$TSA = (X22 - Xhj) * T31_D + (Y22 - Yhj) * T31_D + (Z22 - Zhj) * T31_D \tag{228}$$

$$XA = X22 - (T31_D) * TSA \tag{229}$$

$$YA = Y22 - (T32_D) * TSA \tag{230}$$

$$ZA = Z22 - (T33_D) * TSA \tag{231}$$

with:

$$TSA2 = ((XA - Xhj)^2 + (YA - Yhj)^2 + (ZA - Zhj)^2)^{1/2} \tag{232}$$

Y-axis is calculated in scalar form:

$$T21_D = (XA - Xhj)/TSA2 \tag{233}$$

$$T22_D = (YA - Yhj)/TSA2 \tag{234}$$

$$T23_D = (ZA1 - Zhj)/TSA2 \tag{235}$$

applying cross-product to estimate the x-axis:

$$T11_D = T22 * T33 - T23 * T32 \tag{236}$$

$$T12_D = T23 * T31 - T21 * T33 \tag{237}$$

$$T13_D = T21 * T32 - T22 * T31 \tag{238}$$

which concludes the direction cosine matrix of the left thigh Dynamic system.

When both the Dynamic and Segmental directional cosine matrixes were calculated in the static trial the relation between the two systems had to be evaluated. The following procedure allowed all the markers missing from the dynamic trials to be expressed in the dynamic axes system as explained further down in the section. This expression could be tranferred whenever and wherever needed in the dynamic trials.

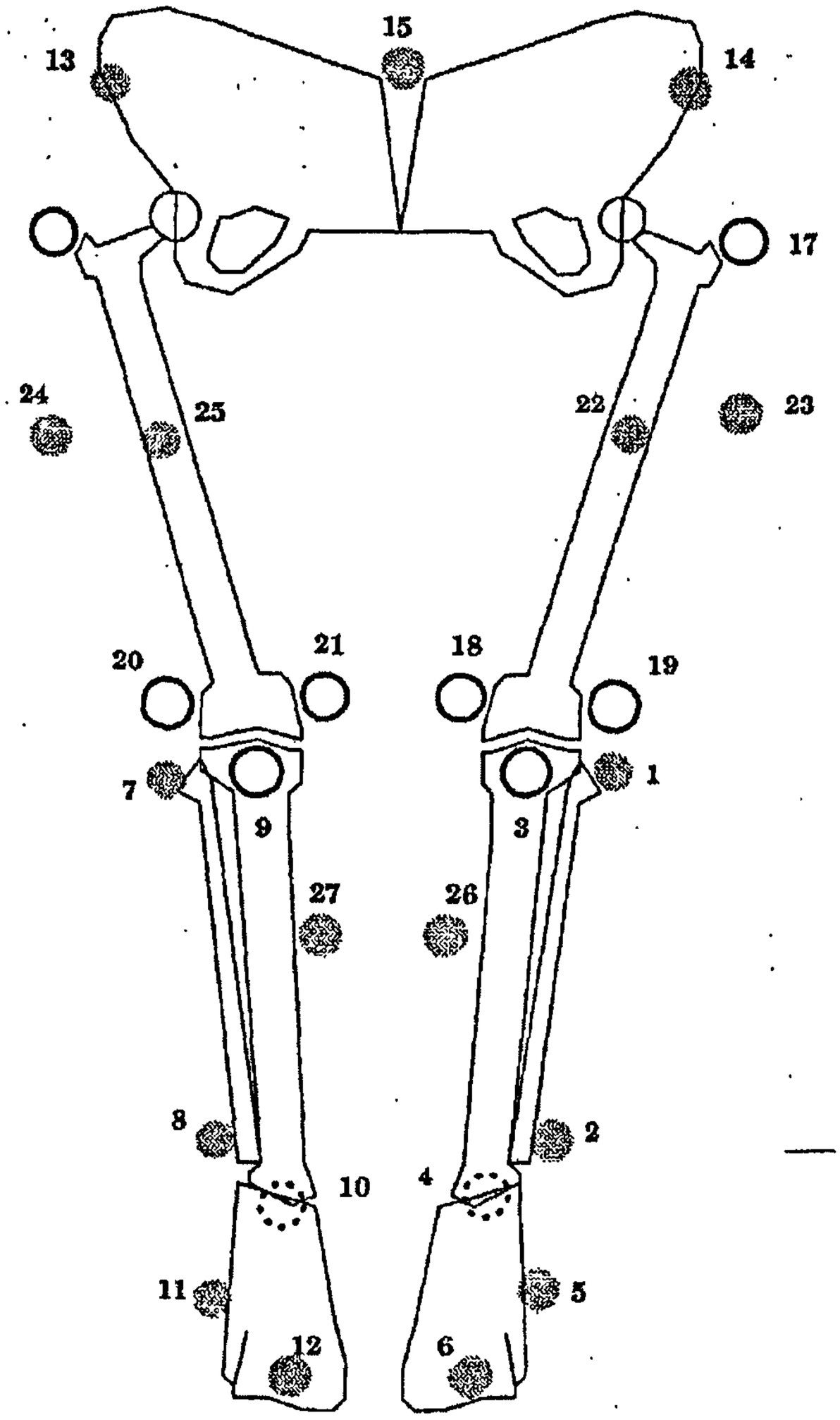

Static trial markers

9: Right tibial tuberosity

20: lateral epicondyle of right femur
21: medial epicondyle of rigth femur
16: greater trochanter of right femur
markers 3, 19, 18, 17, respectively for left lower limb and left side of pelvis

Dynamic markers:

15: posterior superior iliac spine

13: right anterior superior iliac spine
24: right thigh side marker
25: right thigh front marker
7: right fibula head

27:right shank marker
8: lateral malleolus of right lower limb
11: lateral to the 5th metatarsal joint
12: mid -toe of right foot

10; mid-heel of right foot

markers 14, 23, 22, 1, 26, 2, 5, 6, 4
are the respective markers of the left

Figure 6.10: Marker positioning for both the dynamic trials and the static tri-

To express the three markers and origin of the left thigh segment coordinate system (X18, X19, hip joint center hj), with respect to the Dynamic coordinate system the following steps were required:

Firstly, the markers previously expressed with respect to the ground frame of reference are expressed in the dynamic frame of reference using equation (6.194):

$$\begin{bmatrix} X18^1_D \\ Y18^1_D \\ Z18^1_D \end{bmatrix} = [T]_D * \begin{bmatrix} X18_g \\ Y18_g \\ Z18_g \end{bmatrix} \tag{239}$$

Where 18_g and 18_D the expressions of marker 18 in the ground and dynamic coordinate systems respectively, and

$$[T]_D = \begin{bmatrix} TD11 & TD12 & TD13 \\ TD21 & TD22 & TD23 \\ TD31 & TD32 & TD33 \end{bmatrix} \tag{240}$$

is the dynamic to ground directional cosine matrix.

To finish the procedure the origin of the dynamic system (o_D) needs to be substracted from the previous calculation according to equation (6.195) :

$$X18_D = X18^1_D - Xo_D \tag{241}$$

$$Y18_D = Y18^1_D - Yo_D \tag{242}$$

$$Z18_D = Z18^1_D - Zo_D \tag{243}$$

The same procedure is followed for marker 19 and the hip joint i.e. all three markers-points needed to define the segment axis.

Therefore, whenever in the dynamic trials the reproduction of the missing segmental marker system was required the reverse procedure to the one employed in the static trials was applied after the calculation of the dynamic coordinate system:

$$\begin{bmatrix} X18^t_D \\ Y18^t_D \\ Z18^t_D \end{bmatrix} = [T]^{-1}_D * \begin{bmatrix} X18_D \\ Y18_D \\ Z18_D \end{bmatrix} \tag{244}$$

Where 18_g and 18_D the expressions of marker 18 in the ground and dynamic coordinate systems respectively, and

$$[T]^{-1}_D = \begin{bmatrix} TD11 & TD21 & TD31 \\ TD12 & TD22 & TD32 \\ TD13 & TD23 & TD33 \end{bmatrix} \tag{245}$$

is the ground to dynamic directional cosine matrix.

Figure 11: Marker positioning for both the dynamic trials and the static trials i.e. the markers that are used to determine the segmental coordinate systems; Markers used at GAIT-1:1,2,3,4,5,6,7,8,9,10,11,12,13,14,15,16,17 for the static trial and without 16,17 for the dynamic trial; Markers used at GAIT-2:1,2,3,4,5,6,7,8,9,10,11,12,13,14,15,16,17,18,19,20,21, 22,23,24,25,26,27 for the static trial and without 3,9,16,17,18,19,20,21 for the dynamic trial;

To finish the procedure the origin of the dynamic system (o_D) needs to be added to the previous calculation according to equation (6.195):

$$X18_g = X18_D^t + Xo_D \tag{246}$$

$$Y18_g = Y18_D^t + Yo_D \tag{247}$$

$$Z18_g = Z18_D^t + Zo_D \tag{248}$$

Therefore 18_g represents the segmental system's marker in the ground frame of reference. The same procedure was followed for every marker that was used to define the segmental coordinate system.

0.9 Shank dynamic coordinate system

The same procedure as with the thigh axes described above, was followed in the shank segment for left and right lower limb. The segmental coordinate system was the one used in Gait-1. However, the dynamic coordinate system was introduced since it allowed for a better measurement of the rotational behaviour with respect to the Y-axis. The latter was possible with the use of a longer marker to replace the tibial one. The new marker was placed approximately in the midpoint of the whole length of the bony part of shank segment as shown in Figure 11 on page 38 . The dynamic coordinate system of the left shank was calculated using markers 1, 2 and 26 (right shank dynamic markers are 7, 8 and 27):

$$ez = (R2 - R1)/PSA \tag{249}$$

where:

$$PSA = ((X2 - X1)^2 + (Y2 - Y1)^2 + (Z2 - Z1)^2)^{1/2} \tag{250}$$

Using the scalar form to calculate the y-axis:

$$S21_D = (X2 - X1)/PSA \tag{251}$$

$$S22_D = (Y2 - Y1)/PSA \tag{252}$$

$$S23_D = (Z2 - Z1)/PSA \tag{253}$$

The first approximation of z-axis is evaluated from marker 2 and marker 26:

$$SS = (X2 - X26) * S31_D + (Y2 - Y26) * S31_D + (Z2 - Z26) * S31_D \tag{254}$$

$$XA1 = X22 - (S21_D) * SS \tag{255}$$

$$YA1 = Y2 - (S22_D) * SS \tag{256}$$

$$ZA1 = Z2 - (S23_D) * SS \tag{257}$$

with:

$$SS2 = ((XA1 - X26)^2 + (YA1 - Y26)^2 + (ZA1 - Z26)^2)^{1/2} \tag{258}$$

z-axis is calculated in scalar form:

$$S31_D = (XA1 - X26)/SS2 \tag{259}$$

$$S32_D = (YA1 - Y26)/SS2 \tag{260}$$

$$S33_D = (ZA1 - Z26)/SS2 \tag{261}$$

applying cross-product to estimate the x-axis:

$$S11_D = S22 * S33 - S23 * S32 \tag{262}$$

$$S12_D = S23 * S31 - S21 * S33 \tag{263}$$

$$S13_D = S21 * S32 - S22 * S31 \tag{264}$$

which concludes the direction cosine matrix of the left shank Dynamic coordinate system.

The only "difference" between the the shank segment and the shank dynamic systems is the new marker (26 for the left shank and 27 for the right shank -Figure 11 on page 38). Exactly the same procedure with the one applied to the thigh segment was adopted here. The new marker had to be expressed in dynamic terms in the static trial and then reproduced in the dynamic trials as explaned in equations (6.194) and (6.195). The foot and pelvis calculations were identical to Gait-1. The discette that accompanies the thesis includes listings for most of the above algorithms and the corresponding command files.

Bibliography

Andriacchi, T.P., and Strickland A.B. "Gait Analysis as a tool to Assess Joint Kinetics ". Proceedigs of NATO Advanced Study Institute Biomechanics of Normal and Pathological Articulating Joints, *1:82–102, 1982.*

Bell, A.L., Douglas, P.R., and Brand R.A. " A comparison of the accuracy of several hip center location prediction methods ". Journal of Biomechanics, *23(6):617–621, 1990.*

R.A. Brand. "PERSONAL COMMUNICATION ". MUSCLE INSERTION AND ORIGIN DATA, *Lower limbs:15, 1992.*

A. Cappozzo. "Gait Analysis Methothology ". Human Movement Science, *3:27–50, 1984.*

Crownshield, R.D., Johnston, R.C., Andrews, J.G., and Brand R.A. "A Biomechanical Investigation of the Human Hip ". Journal of Biomechanics, *11:75–85, 1978.*

Eberhart, H., Inman, V.T., and Saunders J.B. "Fundamental Studies of Human Locomotion and other information relating to Artificial limbs". Report of National Research Council on Artificial Limbs, University of California, Berkeley, *112:4–13, 1947.*

Grood, E.S., and Suntay W.J. "A Joint Coordinate Sytem for the Clinical Description of Three Dimensional Motions: Application to the Knee ". Journal of Biomechanical Engineering, Transactions of the ASME, *105:136–144, 1983.*

G.A. Ishai. "Whole body gait kinetics". *PhD thesis, Bioengineering Unit, University of Strathclyde, 1975.*

Johnson, R., and Charnley .J. "Treatment of pulmonary embolism in total hip replacement". Clinical Orthopaedics, *247:149–154, 1977.*

J.P. Paul. Bioengineering Studies of the Forces Transmitted by Joint. II. *London : Pergamon Press, Biomechanics and Related Bioengineering Topics:Editor R.M. Kenedi, 1965.*

J.P. Paul. Forces transmitted by joints in the human body. In Proceedings of the institution of mechanical engineers, *volume 181, pages 8–15, 1966.*

J.P. Paul. The effect of walking speed on the force actions transmitted at the hip and knee joints. In Proceedings of the Royal Society of Medicine, *volume 63, pages 200–204, 1970.*

A. Pedotti. "Simple equipment used in clinical practice for evaluation of locomotion". IEEE Transactions in Biomedical Engineering, *24(5):456–461, 1977.*

Procter, P., and Paul J.P. "Ankle joint biomechanics ". Journal of Biomechanics, *15(9):627–634, 1982.*

Small, C.F., Bryant, J.T., and Pichora D.R. "Rationalisation of Kinematic descriptions for Three-Dimensional Hand and Finger Motion ". Journal of Biomedical Engineering, *14:133–141, 1992.*

R. Tooth. "The Biomechanics of Arthrodesis and Arthroplasty in the Human Leg". *PhD thesis, University of Strathclyde U.K., 1976.*

Tylkowski, C.M., Simon, S.R., and Mansour J.M. "Internal Rotation Gait in spastic Cerebral Palsy ". The Hip, Proceedings of the 10th Open Scientific meeting of the hip Society. St. Louis: C.V Mosby; Editor J.P. Nelson, *1:89–125, 1982.*

D.A. Winter. "The biomechanics and motor control of human gait". Waterloo: University of Waterloo Press, *pages 161–280, 1987.*

Appendix B

WRAPPING MOMENT ARMS CALCULATION

A short review of the "WRAPPING AROUND THE JOINT" muscles calculation technique.

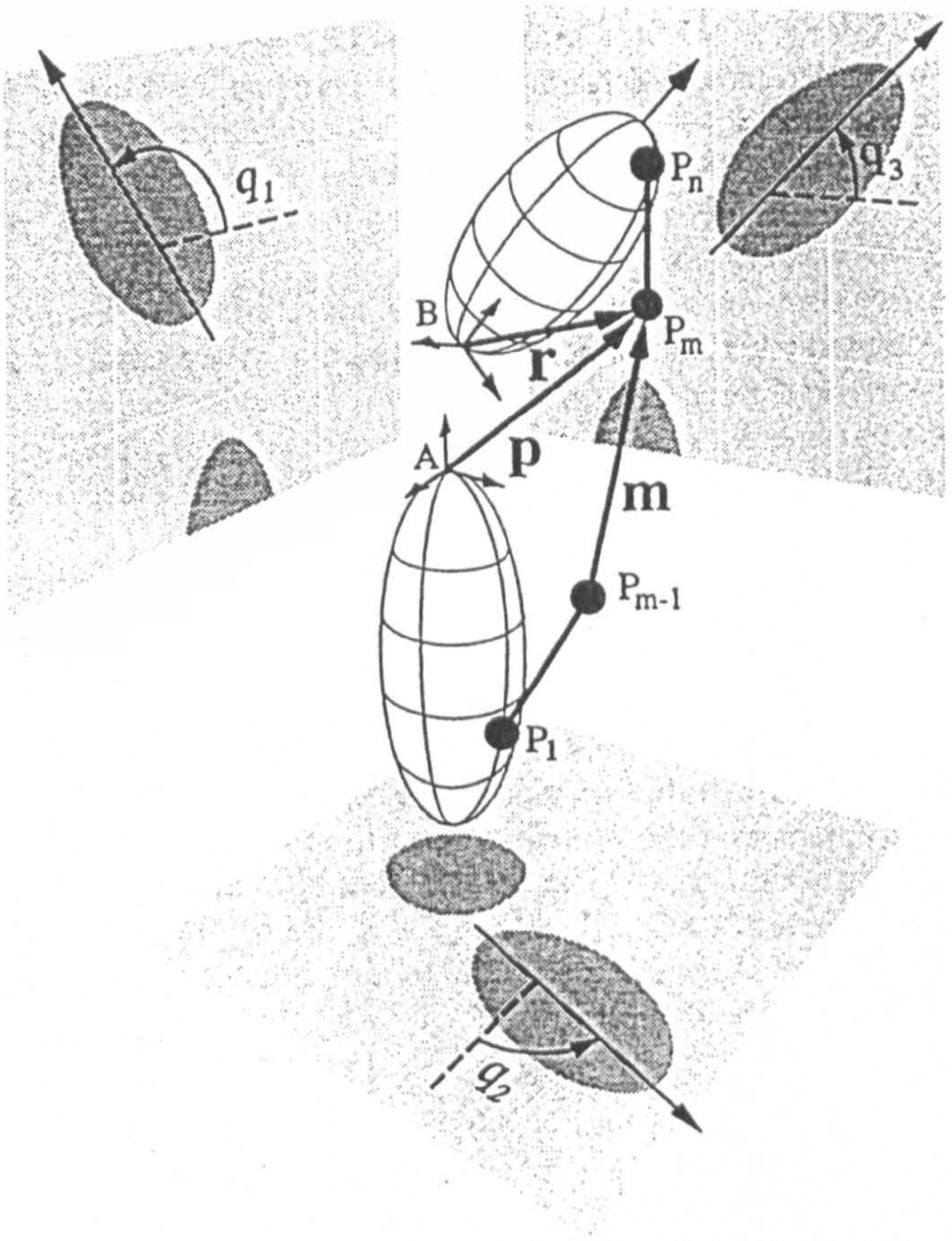

Definition of terms used in moment arm calculations. Points P_1–P_n define the muscle path. P_1–P_{m-1} are fixed in body A. P_m–P_n are fixed in body B. m is the vector from point P_{m-1} to P_m. P expresses point P_m in reference frame A. r expresses P_m in B. In general, six generalized coordinates (three rotations angles: q_1, q_2, q_3, and three translation coordinates, not shown) are needed to characterize the orientation and position of body B relative to body A. The moment arm for each generalized coordinate (q_i) is given by $\partial p/\partial q_i \cdot m$.

FIGURE 1APB

The calculation of moment arm and musculotendon length for a muscle crossing a revolute joint. Coordinates P_1 through P_M define the muscle path. P_1 through P_M are fixed in body A; P_1 through P_{M+1} are fixed in body B. Thus, $\vec{V}$ (where $\vec{v} = P_{M+1} - P_M$) is the only muscle segment that

changes length as the joint is flexed. In general, three angles, theta θ_i (i=1,2,3) are needed to characterise the orientation of the body A relative to body B. Only one angle, θ_1 , is needed for a revolute joint. The moment arm, (ma) for each orientation angle is given by:

$$ma = \partial l / \partial \theta_i \quad \text{where} \quad l = | \vec{v} |$$

Musculotendon length (l^{ML}) is given by:

$$l^{ML} = \sum_{i=0}^{n-1} | P_{n+1} - P_n |$$

JOINT MODELS

The lower limb was modelled as seven rigid-body segments: 1) pelvis, 2) femur, 3)patella, 4) tibia/fibula, 5)talus, 6) foot (comprising the calcaneus, navicular, cuboid, cuneiforms, and metatarsals), and 7)toes (phalanges) (see FIGURE 3.13, 3.14), with reference frames fixed in each segment. The relative motion of these segments is defined by models of the hip, knee, ankle, subtalar, and metatarsophalangeal joints.

We characerised the hip as a ball-and-socket joint. The transformation between the pelvic and femoral reference frames is thus determined by successive rotations of femoral frame about three orthogonal axes in femoral head.

Similarly the following FIGURES describe the kinematics of knee and angle joints.

Appendix C

EMG CALCULATION

A short review of the classical EMG to FORCE calculation problem with a full example of gait analysis.

Using of EMG in the biomechanical analysis

Muscle activity and the corresponding EMG-activity are not the only factors which determine muscle force. The length of the muscle, the type of contraction (concentric, isometric, eccentric) and the velocity of the contraction play an important role in the relation between EMG and muscle force. Since the joint movements are affected by the joint torque rather than muscle forces, the lever arm of these forces is an important factor as well. This means that joint torque, joint angle (in relation to muscle length), angular velocity (in relation to velocity of shortening or lengthening of the muscle) and the lever arm of the muscle (to produce joint torque) have to be combined with EMG-data in order to estimate forces produced by the muscles. For this reason, the amplitude of the EMG-signal or -activity in two measurements can only be compared within the same test subject, the same muscle and the same electrode position, on the condition that the angle joint, angular velocity and motion pattern (because of pre-stretch) are equal in the two conditions.

1. Relation between muscle force and the EMG-signal.

Since the EMG-signal is the only tool currently available to provide information concerning the neuromuscular control of movement in a non-invasive way, several authors have tried to establish a relation between muscle force and the electromyographic signal.
We will not discuss the basic principles of EMG-measurement, since this is dealt with in other chapters of the book. We will, however, use these principles in order to explain some of the algorithms which have been applied to find a relation between the measured EMG-signal and the corresponding muscle force.

1.1. From EMG-signal to muscle activity.

The raw bipolar EMG signal only provides limited and inaccurate information. By visual inspection of a graphical representation of the signal the onset of muscular activity can be estimated. In addition, a rough impression of the activity of the muscle involved can be derived from the amplitude of the signal and the number of maxima and minima per time unit. However, more precise quantitative methods are needed to allow systematic study of the EMG-force relationship. Some of these methods are explained below.

1.1.1. Linear envelope.

Calculation of the "Linear Envelope" provides a profile of the myoelectric activity of the muscle over time. A linear envelope detector (either hard- or software) is applied to the raw EMG signal. This detector consists of a combination of a full-wave rectifier followed by a low pass filter. The specifications of the filter can largely influence the results of the signal processing. For this reason, filter characteristics should meet two requirements: the time constant should be short enough to follow changes in Motor Unit Potentials, but also long enough to produce an effective averaging of the signal (25-300 ms). The Linear Envelope is an indicator of the number of firing motor units, their firing rate and the area of active motor units. Information derived, includes the onset of muscle activity, the instantaneous activity of the muscle and the pattern of muscle contraction during different phases in movement.

1.1.2. Root Mean Square.

The Root Mean Square (RMS) is an instantaneous measure of the power output of the myoelectrical signal and provides a moving average over time. A close relation between the RMS value, and the area under the spectral curve is to be expected.
Mathematically, the RMS value of an EMG voltage is defined as follows:

$$RMS\,EMG(t) = \sqrt{\frac{\int_t^{t+T} EMG^2(t)dt}{T}}$$

Unlike integration (see below), the RMS method requires no full-wave rectification, because the time varying EMG signal is squared. The unit of the RMS EMG is mV or ìV.
The RMS value depends on the number of activated motor units, their firing frequency and the area covered by the activated motor unit. An inverse relationship between the signal amplitude and the conduction velocity could be established. Additionally, RMS is not affected by cancellation caused by the superposition of motor unit action potential trains.

1.1.3. Integrated EMG-signal (IEMG).

The total amount of muscular activity occurring during any given time interval is represented by the area under the curve. Integration is performed (in hardware or software) after passing the raw EMG signal through a full wave rectifier. In some cases this procedure is then followed by a low pass filter. In both cases the same term "integrated EMG" is used. We will limit our discussion to the pure integration of the rectified signal (without low pass filtering), since the results of the low pass filtered signal are dependent on the cut-off frequency and slope of the filter.
The integration technique consists of a continuous evaluation of the area under the curve. Therefore, the amplitude of the IEMG at time t equals the summed values of the rectified signal from the beginning of the activity up to the time t. Consequently, the IEMG-value will increase in time.
In practical integrator designs, the time period must be limited because of the limited dynamic range of the integrator circuit. Typically, this is accomplished by integrating over fixed time intervals. In such cases, the operation is expressed as follows:

$$I\,EMG(t) = \int_t^{t+T} |\,EMG(t)\,|\,dt$$

For the choice of the time interval T, two procedures may be distinguished: the time reset, in which the amplitude line is set to zero at constant time intervals, and the level reset, where the integrated EMG value is set to zero whenever its value exceeds a predefined level.
Any change in the raw EMG signal is reflected in the shape of the integrated EMG curve. High myoelectrical activity in the raw signal is reflected by a steep slope in the integrated EMG curve, whereas with lower myoelectrical activation, the curve is more plateau like. The integrated EMG is proportional to the Motor Unit amplitude, the firing rate, but is independent of the conduction velocity.
It should be noted that all the calculation methods mentioned above and especially the integration technique, do not discriminate between artefacts and myoelectrical activity. A shift of the baseline of the EMG-signal is one of the most common artefacts caused by displacements of

electrodes relative to the muscle and leading to a complete distortion of the integrated signal. During long periods of low force levels, long window sampling duration may also detect an unacceptable amount of noise. Furthermore, the techniques cannot be applied easily to EMG-signals with rapidly changing activity, since time constants of filters or reset procedures need to be adapted according to the characteristics of the measured signal.

In studies concerning the relation between EMG and Force, however, IEMG is probably the most frequently used technique.

1.1.4. Differentiated EMG (DEMG).

A differential equation has been developed by Spaepen (1986), to overcome some of the difficulties mentioned above, based on findings of Van Leemputte et al. (1984).
Hence, the technique is based on three observations:

1) The activation of muscle fibres corresponds to a change in the value of the EMG signal, and not to a specific level of electrical signal.
2) If several muscle fibres of the same motor unit are activated simultaneously, a synchronous set of electrical signals will reach the electrodes, thus leading to a signal with a larger amplitude.
3) Sudden increases or decreases in the amplitude of the EMG signal do not relate to immediate and proportional changes in muscle force. Typical exponential increases or decreases have been reported in literature quite frequently. These changes in force are often characterised by time constants.

A value of the muscle activity which directly relates to muscle force can therefore be calculated from the following differential equation (Spaepen et al., 1986):

$$A_{t_{n+1}} = p \cdot A_{t_n} + q \cdot \sqrt{| E_{t_{n+1}} - E_{t_n} |}$$

where $A(t_{n+1})$: the muscle activity at time t_{n+1};
$A(t_n)$: the muscle activity at time t_n;
$E(t_{n+1})$: raw EMG-signal at time t_{n+1};
$E(t_n)$: raw EMG-signal at time t_n;
p : constant value, equal to 0.9875 for an EMG-signal sampled at 500 Hz
q : constant value, converting the electrical units to mechanical units.

Muscle activity at time t_{n+1} is the sum of two parts:

- one part which remains from the activity at time t_n ($p^*A(t_n)$), with $p < 1$ and indicating the exponential decrease in force;
- one part which is added by new EMG-activity and related to the change in the EMG-signal (Et_{n+1}-Et_n) of which the absolute value is taken, since increases and decreases in the signal are considered equally important. The square root of this difference has been taken, since it has been proven experimentally that the highest changes in amplitude do not relate to proportional increases in isometric muscle force.

Least squares methods can be used to define the value for q for a given experimental situation in which both the EMG-signal and the torque output have been measured.
The calculation procedure requires a given value for the muscle activity at the first time interval. In most cases, this value is not known, so a rough approximation is used. After approximately 0.5 s the effect of the initial value on the calculation of the muscle activity is cancelled out. If the researcher intends to use this procedure, EMG-measurements need to begin at least half a second before the point in time when muscle activity is to be determined, in this way overcoming the problem of the unknown initial value. The procedure leads to Pearson correlation coefficients of a linear regression between isometric force and calculated activity of typically 0.98.
Since the DEMG takes the time characteristics of force production into account, it can also be applied in dynamic analyses. Furthermore, results of the calculations are hardly influenced at all by artifacts such as the shift of the base line, caused by moving electrodes.

1.2. Relation between muscle force and calculated EMG-activity.

Several authors have studied the relationship between calculated EMG-activity and muscle force. The importance of finding a reliable and steady relation between these parameters has been explained in the introduction above. Some of the factors of major importance in biomechanics analyses were also explained, e.g. kinematics of the movement, co-contraction of synergists or agonist and antagonist muscles, processing methods and parameters related to data acquisition.

1.2.1 Temporal aspects.

The first factor to be taken into account when addressing the relation between quantified EMG and muscle force is the time difference between the onset and cessation of myoelectrical activity and the production of muscle force.
Ralston et al (1976) studied the delay in the rectus femoris muscle using the raw EMG signal. A time delay of 30-40 msec was found between the onset of EMG and muscle force. Time delays of 200-300 msec occurred between the cessation of the electrical activity and muscle force. The study of Redfern (1984) on the triceps brachii reports a time delay between EMG and force onset from rest of about 50 msec and cessation delays of 180 msec. Time delays seem to be muscle dependent. However, the time delays at the onset are much shorter then the delay times at the cessation of EMG activity.
The delay time observed at the onset is influenced by the initial tension level in the muscle.Decreased delay has been reported in situations where the muscle is held at a baseline tension prior to a stepwise increase in force, which can be explained by the absence of mechanical slack. Based on the previous findings, it may be concluded that in the interpretation of quantified EMG and force, the influence of the time delay at onset as well as the delay at cessation of tension development needs to be considered.

1.2.2. Isometric force and calculated EMG.

In a study by Lippold (1952) on the isometric force production of the triceps surae muscle, a linear relationship between force production and the IEMG signal was demonstrated. Determination coefficients ranging from .95 to .99 were reported. Nevertheless, slight changes in the slope of the IEMG-force curve were observed.
In contrast to this highly linear relationship, several other authors showed the force-IEMG relationship to be curvilinear. Table 1 presents an overview.
Several studies have tried to resolve these discrepancies. Moritani and de Vries (1978), stressed the importance of electrode configuration: Unipolar detection of the EMG signal, was more likely to result in a linear relationship, while bipolar detection tended to present a curvilinear relationship.
On the other hand, Bawa and Stein (1976) presented a more physiological explanation for the non linearity of the relationship, by arguing that for increasing force output a non linearity between the neural firing rate and force output could be demonstrated.

Woods and Bigland (1983), examined the possible influence of muscle fibre composition on the force-EMG relationship. The type of relationship seemed to depend on the fibre composition: in muscles with uniform fibre type, a linear relationship could be established, while in muscles with mixed fibre types the relationship tended to be more curvilinear.

LINEAR	CURVILINEAR
Innman et al (1952)	Zuniga and Simons (1969)
Lippold (1952)	Komi and Buskirk (1970)
Close et al (1960)	Bouisset (1973)
de Jong and Freund (1967)	Kuroda et al (1970)
de Vries (1968)	Lawrence and De Luca (1983)
Woods and Bigland-Ritchie (1983)	Woods and Bigland-Ritchie (1983)

Table 1: References to some of the authors reporting Linear and Curvilinear Relationships Between Processed Emg and Muscle Force.

The relation between the RMS value and force output has also been studied. Lawrence and De Luca (1983) concluded from their studies using normalised RMS and force values, that this relation primarily depends on the muscle under consideration, and is generally independent of the subject. Confirmation of this conclusion can be found in the work of Woods and Bigland-Ritchie (1983).
In a study focusing on the relation between the mechanical load and EMG-activity of trunk extensor en flexor muscles under isometric conditions (Spaepen et al, 1986), the mean correlation calculated by means of a linear regression of the muscular activity of M. rectus abdominis and M. erector spinae, and the resulting moment at L5 registered by means of a force platform, was 0.951 (limits of 0.88-0.98). Later, the relation between the moment at the knee joint and the isometric muscular activity of the three extensor muscles was studied, in which case a Pearson correlation coefficient varying from 0.94 to 0.99 was found (Mermans,1986; Spaepen et al, 1987).

1.2.3 EMG-torque relation for different joint angles and angular velocities.

From the summary of the biomechanical principles above, it is clear that both muscle length and contraction velocity should be taken into account when discussing the EMG-torque relationship in dynamic muscle work. Grieves and Pheasant (1976) measured the torque produced by M. gastrocnemius and M. soleus at different joint angles. They demonstrated a clear relation between the IEMG and muscle length, at different contraction levels. Vredenbregt and Rau (1973) showed similar findings in their study on the Biceps Brachii, indicating that the slope of the IEMG-force curve output varies with the joint angle.
Similar results, based on the DEMG-method are reported by Mermans (1986), using a combined registration of muscular activity and the net joint moment produced by the quadriceps muscle. In her study, test subjects were asked to perform a maximum static extension of the knee at different joint angles. The smaller values for the torque at small and large knee angles are caused by three factors: a change in moment arm of the muscle, a decrease in muscle force for short and long muscles and an additional decrease because of a smaller muscle activity which is observed towards the extreme of the motion range. The highly linear correlation between DEMG and force (cfr. suppra) is used to normalise the measured torque values to an equal (maximal) level of muscle activity for all joint angles. In this case, changes in the length of the moment arm and muscle length are the only remaining factors to explain the changes in net torque as a function of the joint angle.
As stated above, the contraction velocity has a tremendous effect on tension output, especially during concentric contractions. In discussing the relation between the quantified EMG and muscle tension, two distinct situations, i.e. concentric versus eccentric contractions, need to be

addressed. In a study concerning the relationship between force, velocity and the integrated EMG during concentric plantar flexion, Bigland and Lippold (1954) obtained a classic force-velocity curve (Hill's equation). In a study on forearm rotation, Zahalak et al. (1976) reported a similar relationship for the biceps brachii.
The results are quite different for eccentric contractions.
Asmussen (1956) reported higher EMG levels during eccentric contraction, than during concentric contractions with the same tension level.
Information regarding the force-velocity relationship for eccentric contractions, is contradictory. Some authors report no increase in the IEMG level, as velocity of the eccentric contraction increases. Others report a slight increase in force as eccentric velocity is increased, similar to the classical tension-velocity curve described above. In a study on elbow flexion, Komi (1973) reported that the IEMG-force relation for the biceps brachia and brachioradialis muscles is influenced by both the direction of the movement (i.e. concentric versus eccentric contraction) and the level of contraction velocity.
We studied the relation between the activity of the three extensor muscles and the knee torque during knee movement. Eccentric and concentric contractions were performed at angular velocities of 50, 100, 150 and 200 degrees/s, and joint angles ranging from 60 to 175 degrees. The regression coefficients obtained from the maximal isometric contractions were used to normalise maximum voluntary contraction to an equal level of maximum muscle activity. Negative values of angular velocity indicate eccentric contractions, whereas positive values are related to concentric contractions. The isometric torque is indicated at the angular velocity of 0 degrees/s. Because all later mentioned values are registered at the same joint angle, muscle length and moment arm of the muscle force are equal and hence do not affect the following discussion.
Eccentric forces are clearly smaller than the isometric ones. It is seen that eccentric torques at the same joint angle exceed the isometric moment by 13 % at the maximum and that concentric torques are considerably lower than the isometric torque, even at low angular velocities.

2. Conclusions.
Human movement is accomplished through a coordinated activation of groups of muscles around the joints. The way this muscle coordination is performed is not yet well defined.
A first step to solve this complex problem is to find the relation between muscle activity, muscle force and the movements produced by those forces. Numerous mathematical models exist which allow simulation of movements of body segments on which muscle forces are imposed. The same segmental movement, however, can be obtained by forces in different muscles, since an important redundancy in muscle forces exists. Mechanical and mathematical laws alone will not determine coordination activities.
Hypotheses on the coordination of muscle contraction may be proposed and their verification requires observation of the relevant muscle activity. Furthermore, it should be possible to translate those activities into muscle forces. Simulation techniques can then be applied to determine the resultant movement and to test and modify the original hypotheses.
Although the results give a better insight in the EMG-force relationship, and are valuable and promising, they do not solve the above mentioned problem. We strongly recommend further research in this area, to answer basic questions such as what are the forces in the muscles, the stresses in the bones and the joints, how can we control this large set of motors which allow movement in extremely different situations?
Unless new measurement techniques are developed to measure muscle forces in vivo during movement, advances in the biomechanics of human movement will be determined above all by progress in the measurement and analysis of the electromyographic signal.

References:

Asmussen E,
1956, Observations on experimental muscle soreness, *Acta rheumatologica Scandinavica* 2: 109-116.

Basmajian JV; De Luca CJ,
1985, *Muscles alive, Their functions revealed by electromyography*, Baltimore: ed5, Wiliams & Wilkins.

Bawa P; Stein J,
1976, Frequency response of the human soleus muscle, *J neurophysiol* 39: 788-793.

Bigland B; Lippold OCJ,
1954, The relationship between force, velocity and integrated electrical activity in human muscles, *J physiol (London)* 123:214-224.

Bouisset S,
1973, EMG and muscle force in normal motor activities, in Desmedt JE (ed),*New concepts of the motor unit, neuromuscular disorder, electromyographickinesiology (New Developments in electromyography and clinical neurophysiology 1)* Basel: Krager, 547-583.

Cavagna GA; Dusman B; Margaria R,
1968, Positive work done by previously stretched muscle, *Journal of applied physiology* 24 (1): 21-32.

Close JR; Nickel ED; Todd FN,
1960, Motor unit action potential counts, *J bone joint surg (Am)* 42: 1207-1222.

de Jong RH; Freund FG,
1967, Relation between electromyogram and isometric twitch tension in human muscle, *Am j physiol* 15: 479-482.

De Vries HA,
1968, Efficiency of electrical activity as a physiological measure of the functional state of muscle tissue, *Am j physiol*, 47:10-22.

Gordon AM; Huxley AF; Julian FJ,
1966, The variation in isometric tension with sarcomere length in vertebrate muscle fibers, *J Physiol*, 184: 170-192.

Grieves DW; Pheasant ST,
1976, Myoelectric activity, posture and isometric torque in man, *Electromyogr clinneurophysiol* 16:3-21.

Inman VT; Ralstone HJ; Saunders JB,
1952, Relationship of human electromyogram to muscular tension, *Electroencephalogr clin neurophysiol* 4: 187-194.

Komi PV; Buskirk ER,
1970, Reproducibility in electromyographic measurements with inserted wire electrodes and surface electrodes, *Electromyography* 4:357-367.

Komi PV,
1973, Relationship between muscle tension, EMG and velocity of contraction under concentric and eccentric work, in Desmedt JE (ed): *New Developments in electromyography and clinical neurophysiology*, vol 1, Basel: p 596-606.

Kuroda E; Klissouras V; Milsum JH,
1970, Electrical and metabolic activities and fatigue in human isometric contraction, *J appl physiol* 29: 358-367.

Lawrence JH; De Luca CJ,
1983, Myoelectric signal versus force relationship in different human muscles, *J appl physiol*, 54: 1653-1659.
Lieber RL; Boakes JL,
1988, Sarcomere length and joint kinematics dyring torque production in the frog hindlimb, *Am j physiol* 254: C759-Cc768.
Lippold OJC,
1952, The relationship between integrated action potentials in the human muscle and its isometric tension, *J physiol (London)* 117: 492-499.
Magid A; Law DJ,
1985, Myofibrils bear most of the resting tension in frog skeletal muscle, *Science*, 230: 1280-1282.
Mermans E,
1986, *Study van het resulterend moment tijdens statische en dynamische inspanningen van de kniestrekkers*, 68p. (Leuven: KULeuven;licentiaatsverhandeling lichamelijke opleiding).
Moritani T; De Vries HA,
1978, Reexamination of the relationship between the surface integrated electromyogram (iEMG) and force of isometric contraction, *Am j phys med* 57: 263-277.
Ralston HJ; Todd FN; Innman VT,
1976, Comparison of electrical activity and duration of tension in the human rectus femoris muscle, *Electroencephalogr clin neurophysiol*, 16: 271-279.
Redfern MS,
1984, *Time delays between the onset of the EMG and tension in the triceps brachii,* Technical Report Ann Arbor, MI, Center for Ergonomics, University of Michigan.
Spaepen AJ; Baumann W; Maes H,
1986, Relation between mechanical load and EMG activity of selected muscles of the trunk under isometric conditions, *Proceedings of the Vth meeting of the European Society of Biomechanics,* Berlin, 595-600.
Spaepen AJ; Wouters M; Sansen W; Steyaert M,
1987, An integrated system for muscle strength testing and exercise, *Proceedings of the ninth annual conference of the IEE engineering in medicine anf biology society* 2: 1069-1070.
Van Ingen Schenau GJ; De Boer RW; Vergroesen I,
1984, Kracht en snelheid 3: De counterbeweging, *Geneeskunde en sport* 17: 44-48.
Van Leemputte MF; Spaepen AJ; Willems EJ,
1984, Quantification of EMG using a differentiation technique, in Ducheyne P; Van der Perre G; Aubert AE (eds), *Biomaterials and biomechanics* 5: 103-107.
Vredenbregt J; Rau G,
1973, Surface electromyography in relation to force, muscle length and endurance, in Desmedt JE (ed): *New developments in electromyography and clinical neurophysiology*,vol1, Basel.
Woods JJ; Bigland-Ritchie B,
1983, Linear and non-linear EMG/Force relationships in human muscles, *Am j phys med* 62: 287-299.
Zahalak GI; Duffy J; Steward PA,
1976, Partially activated human skeletal muscle: An experimental investigation of force, velocity and EMG, *J of applied mechanics* 98:81.
Zajac FE,
1993, Muscle coordination of movement: a perspective, *J. Biomechanics* 26: 109-124
Zuniga NE; Simons DG,
1969, Nonlinear relationship between averaged electromyogram potential and muscle tension in normal subjects, *Arch phys med* 50: 61-63.

Appendix D

GAUSSIAN ELIMINATION METHOD

The GAUSSIAN ELIMINATION method is used to check the rank of the augmented matrix for the system of equations given in Equations (7.8) to (7.13). The procedure is as follows:

$$\left[\begin{array}{cccccc|c} 1 & 0 & 0 & 1 & 0 & 0 & Fr_{1'}— \\ 0 & 1 & 0 & 0 & 1 & 0 & Fr_{2'}— \\ 0 & 0 & 1 & 0 & 0 & 1 & Fr_{3'}— \\ 0 & -R_{13} & R_{12} & 0 & -R_{23} & R_{22} & Mr_{1'}— \\ R_{13} & 0 & -R_{11} & R_{23} & 0 & -R_{21} & Mr_{2'}— \\ -R_{12} & R_{11} & 0 & -R_{22} & R_{21} & 0 & Mr_{3'}— \end{array}\right] \begin{array}{c} row(1) \\ row(2) \\ row(3) \\ row(4) \\ row(5) \\ row(6) \end{array} \tag{D.1}$$

$R_{13}(row(2)) \div row(4), equals$

$$\left[\begin{array}{cccccc|c|c}
1 & 0 & 0 & 1 & 0 & 0 & Fr_{1'}— & row(1) \\
0 & 1 & 0 & 0 & 1 & 0 & Fr_{2'}— & row(2) \\
0 & 0 & 1 & 0 & 0 & 1 & Fr_{3'}— & row(3) \\
0 & 0 & R_{12} & 0 & R_{13}-R_{23} & R_{22} & Mr_{1'}+R_{13}Fr_{2'}— & row(4) \\
R_{13} & 0 & -R_{11} & R_{23} & 0 & -R_{21} & Mr_{2'}— & row(5) \\
-R_{12} & R_{11} & 0 & -R_{22} & R_{21} & 0 & Mr_{3'}— & row(6)
\end{array}\right] \tag{D.2}$$

$$-R_{12}(row(3))+row(4), leadsto$$

$$\left[\begin{array}{cccccc|c}
1 & 0 & 0 & 1 & 0 & 0 & Fr_{1'}— \\
0 & 1 & 0 & 0 & 1 & 0 & Fr_{2'}— \\
0 & 0 & 1 & 0 & 0 & 1 & Fr_{3'}— \\
0 & 0 & 0 & 0 & R_{13}-R_{23} & R_{22}-R_{12} & Mr_{1'}+R_{13}Fr_{2'}-R_{12}Fr_{3'}— \\
R_{13} & 0 & -R_{11} & R_{23} & 0 & -R_{21} & Mr_{2'}— \\
-R_{12} & R_{11} & 0 & -R_{22} & R_{21} & 0 & Mr_{3'}—
\end{array}\right]\begin{array}{l}(1)\\(2)\\(3)\\(4)\\(5)\\(6)\end{array} \quad \text{(D.3)}$$

-$R_{13}(row(1)row(5)), resultsin$

$$\left[\begin{array}{cccccc|c}
1 & 0 & 0 & 1 & 0 & 0 & Fr_{1'}— \\
0 & 1 & 0 & 0 & 1 & 0 & Fr_{2'}— \\
0 & 0 & 1 & 0 & 0 & 1 & Fr_{3'}— \\
0 & 0 & 0 & 0 & R_{13}-R_{23} & R_{22}-R_{12} & Mr_{1'}+R_{13}Fr_{2'}-R_{12}Fr_{3'}— \\
0 & 0 & -R_{11} & R_{23}-R_{13} & 0 & -R_{21} & Mr_{2'}-R_{13}Fr_{1'}— \\
-R_{12} & R_{11} & 0 & -R_{22} & R_{21} & 0 & Mr_{3'}—
\end{array}\right]\begin{array}{l}(1)\\(2)\\(3)\\(4)\\(5)\\(6)\end{array}$$

(D.4

-$R_{11}(row(3)row(5)), equals$

$$\left[\begin{array}{cccccc|c} 1 & 0 & 0 & 1 & 0 & 0 & Fr_{1'}— \\ 0 & 1 & 0 & 0 & 1 & 0 & Fr_{2'}— \\ 0 & 0 & 1 & 0 & 0 & 1 & Fr_{3'}— \\ 0 & 0 & 0 & 0 & R_{13}-R_{23} & R_{22}-R_{12} & Mr_{1'}+R_{13}Fr_{2'}-R_{12}Fr_{3'} \\ 0 & 0 & 0 & R_{23}-R_{13} & 0 & -R_{21}-R_{11} & Mr_{2'}-R_{13}Fr_{1'}+R_{11}Fr_{3'} \\ -R_{12} & R_{11} & 0 & -R_{22} & R_{21} & 0 & Mr_{3'}— \end{array}\right]$$

after manipulation with the above augmented matrix, the final matrix is

$$\left[\begin{array}{cccc|c} 1 & 0 & 0 & 1 & 0 \\ 0 & 1 & 0 & 0 & 1 \\ 0 & 0 & 1 & 0 & 0 \\ 0 & 0 & 0 & 1 & (R_{11}-R_{21})/(R_{23}-R_{13}) \\ 0 & 0 & 0 & 0 & 1 \\ 0 & 0 & 0 & 0 & 0 \end{array}\right] \left[\begin{array}{c} 0 \\ 0 \\ 1 \\ (Mr_{2'}+R_{13}Fr_{1'}+R_{11}Fr_{3'})/(R_{23}-R_{13} \\ (R_{22}-R_{12})/(R_{13}-R_{23}) \\ 0 \end{array}\right]$$

Thus the rank of the augmented matrix is five.

$$
\left[\begin{array}{cccc|c|c|c|c}
1 & 0 & 0 & 1 & 0 & 0 & & Fr_{1'} \\
0 & 1 & 0 & 0 & 1 & 0 & & Fr_{2'} \\
0 & 0 & 1 & 0 & 0 & 1 & & Fr_{3'} \\
0 & 0 & 0 & 1 & (R_{11}-R_{21})/(R_{23}-R_{13}) & (Mr_{2'}+R_{13}Fr_{1'}+R_{11}Fr_{3'})/(R_{23}-R_{13} & & \\
0 & 0 & 0 & 0 & 1 & (R_{22}-R_{12})/(R_{13}-R_{23}) & (Mr_{1'}+R_{13}Fr_{2'} & -R_{12}Fr_{3'})/(R_{13}-R_{23} \\
0 & 0 & 0 & 0 & 1 & (R_{22}-R_{12})/(R_{13}-R_{23}) & (Mr_{1'}+R_{13}Fr_{2'} & 0- \\
0 & 0 & 0 & 0 & 0 & 0 & & (6)
\end{array}\right]
$$

(1.6)

Thus the rank of the augmented matrix is five.